AFFDL-TR-73-42
Part II, Volume I

DEVELOPMENT AND EVALUATION OF METHODS OF PLANE STRESS FRACTURE ANALYSIS
Part II. Volume I. A Technique for Predicting Residual Strength of Structure

M. M. RATWANI
D. P. WILHEM

NORTHROP CORPORATION
AIRCRAFT DIVISION

AUGUST 1977

TECHNICAL REPORT AFFDL-TR-73-42, PART II, VOLUME I
Report for Period January 1973 – December 1974

AIR FORCE FLIGHT DYNAMICS LABORATORY
AIR FORCE SYSTEMS COMMAND
WRIGHT-PATTERSON AIR FORCE BASE, OHIO 45433

NOTICE

When Government drawings, specifications, or other data are used for any purpose other than in connection with a definitely related Government procurement operation, the United States Government thereby incurs no responsibility nor any obligation whatsoever; and the fact that the Government may have formulated, furnished, or in any way supplied the said drawings, specifications, or other data, is not to be regarded by implication or otherwise as in any manner licensing the holder or any other person or corporation, or conveying any rights or permission to manufacture, use, or sell any patented invention that may in any way be related thereto.

This report has been reviewed by the Office of Information (OI) and is releasable to the National Technical Information Service (NTIS). At NTIS, it will be available to the general public, including foreign nations.

This technical report has been reviewed and is approved for publication.

George P. Sendeckyj

G.P. SENDECKYJ
Project Engineer

R.M. Bader

ROBERT M. BADER, Chief
Structural Integrity Branch
Structural Mechanics Division

FOR THE COMMANDER

HOWARD L. FARMER, Colonel, USAF
Chief, Structural Mechanics Division

Copies of this report should not be returned unless return is required by security considerations, contractual obligations, or notice on a specific document.

AIR FORCE/56780/17 October 1977 — 500

Unclassified

SECURITY CLASSIFICATION OF THIS PAGE *(When Data Entered)*

REPORT DOCUMENTATION PAGE

READ INSTRUCTIONS BEFORE COMPLETING FORM

1. REPORT NUMBER AFFDL-TR-73-42, Part II, Volume I	2. GOVT ACCESSION NO.
3. RECIPIENT'S CATALOG NUMBER	
4. TITLE *(and Subtitle)* Development and Evaluation of Methods of Plane Stress Fracture Analysis, Part II, Volume I, A Technique for Predicting Residual Strength of Structure	5. TYPE OF REPORT & PERIOD COVERED Part II (Phase II) Final Report--Jan. 1973 - Dec. 1974
	6. PERFORMING ORG. REPORT NUMBER NOR 74-309
7. AUTHOR(s) M. M. Ratwani and D. P. Wilhem	8. CONTRACT OR GRANT NUMBER(s) F33615-72-C-1796
9. PERFORMING ORGANIZATION NAME AND ADDRESS Northrop Corporation Aircraft Division 3901 West Broadway, Hawthorne, California 90250	10. PROGRAM ELEMENT, PROJECT, TASK AREA & WORK UNIT NUMBERS Project 486U Task 0204
11. CONTROLLING OFFICE NAME AND ADDRESS Air Force Flight Dynamics Laboratory Wright-Patterson Air Force Base Ohio 45433	12. REPORT DATE August 1977
	13. NUMBER OF PAGES 285
14. MONITORING AGENCY NAME & ADDRESS *(if different from Controlling Office)* SAME	15. SECURITY CLASS. *(of this report)* Unclassified
	15a. DECLASSIFICATION/DOWNGRADING SCHEDULE

16. DISTRIBUTION STATEMENT *(of this Report)*
Approved for Public Release; Distribution Unlimited

17. DISTRIBUTION STATEMENT *(of the abstract entered in Block 20, if different from Report)*

18. SUPPLEMENTARY NOTES

19. KEY WORDS *(Continue on reverse side if necessary and identify by block number)*

Structural Residual Strength	J-integral	Plane Stress Fracture
Fracture Mechanics Analysis	$\sqrt{J_R}$ Resistance Curve	Mixed Mode Fracture
Elastic-Plastic Analysis	Crack Opening Displacement	Crack Growth Resistance
Dugdale Model	Finite Element Modeling	
Prandtl-Reuss Material Behavior	Fastener Modeling	Crack Line Wedge Loaded Specimen

20. ABSTRACT *(Continue on reverse side if necessary and identify by block number)*

A procedure for residual strength analysis of complex structure has been outlined and tested in predicting failure stresses for several complex, riveted, bolted and adhesively bonded structural panels. This new method makes use of the material crack growth resistance curve incorporating both elasto-plastic and slow stable tear in the fracture criterion for skin critical structure. Comparisons were made with assumed Dugdale, Prandtl-Reuss, and elastic material

DD FORM 1 JAN 73 1473 EDITION OF 1 NOV 65 IS OBSOLETE

Unclassified

SECURITY CLASSIFICATION OF THIS PAGE *(When Data Entered)*

behavior for both skin and stiffener critical structure using a J integral approach. The role of material slow tear has been examined for both linear elastic and elastic-plastic behavior and compared with the analysis which indicates the superiority of the elasto-plastic analysis to the point of stringer failure at ultimate strength.

The importance of finite element modeling of attachment and stiffener has been determined and the use of a flexible fastener model for riveted and bolted structure verified. A shear spring model was demonstrated for use with adhesively bonded stringers with excellent correlation with measured panel failure stress.

Several material crack growth resistance curves have been developed using the crack line wedge loaded specimen geometry for two aluminum and titanium alloys and one high strength steel. The requirements necessary to develop the fracture criterion data for both plane stress and mixed mode fracture have been examined and good repeatability of materials fracture data have been obtained.

FOREWORD

This report was prepared by Northrop Corporation, Aircraft Division, Hawthorne, California, under Air Force Contract F33615-72-C-1796. The project was initiated under Project Number 486U, "Advanced Metallic Structures," Advanced Development Program. The work reported herein was administered under the direction of the Air Force Flight Dynamics Laboratory, Air Force Systems Command, Wright-Patterson Air Force Base, Ohio, by Captain George F. Zielsdorff (FBR, currently ASD) and Dr. George Sendeckyj (FBEC), Project Engineers.

The research was conducted between January 1973 and December 1974 as a conclusion to Phase II. This report was submitted by the authors M. M. Ratwani and D. P. Wilhem, February 1974 for AFFDL review. The report has been assigned NOR 74-309 for internal control at Northrop Corporation.

The authors wish to acknowledge the constructive discussion regarding the development of the recommended procedure with Captain Zielsdorff (ASD) and his invaluable assistance in its formation. The secretarial assistance of Lessie Speciale and Peggy Souther is also acknowledged. The aforementioned program was under the technical supervision of C. Rosenkranz of the Structures Research and Technology Department.

CONTENTS

CONTENTS (Continued)

CONTENTS (Continued)

CONTENTS (Continued)

ILLUSTRATIONS

ILLUSTRATIONS (Continued)

ILLUSTRATIONS (Continued)

ILLUSTRATIONS (Continued)

ILLUSTRATIONS (Continued)

ILLUSTRATIONS (Continued)

TABLES

TABLES (Continued)

I. INTRODUCTION

This report describes the research conducted during Phase II of a three phase investigation into the development of an improved method of thin section residual strength prediction of cracked aircraft structure (where conditions of plane stress or mixed mode fracture prevail). Phase I (AFFDL-TR-73-42) examined the current state-of-the-art of structural, residual strength prediction and assessed the potential of each method. Based on this survey it was found that certain elements of a sound residual strength prediction technique exist, but in fragmented forms. In addition a suitable failure criterion was deemed necessary to treat an elasto-plastic fracture behavior so that ultraconservative designs might be avoided. To address these problems the research of Phase II was directed in two parallel areas; development of suitable analytical tools and a compatible, supporting fracture criteria. The problems addressed in this report are common to typical, critical aircraft structure which has been previously sized based on strength and fatigue requirements. The proposed method of analysis is not intended for use in performing parametric studies (stiffener spacing, rivet pitch, etc.) which can be more cheaply accomplished using linear elastic assumptions and closed form solutions. It does however represent a major advancement in the ability to predict residual strength of a structure which is accompanied by large amounts of slow tear and plasticity prior to structural failure. Two types of residual strength behavior were examined-skin critical and stiffener critical conditions. Which type prevails is governed primarily by crack length to stiffener spacing ratios and to a lesser degree by material crack growth resistance.

To present this method in light of others currently available, Section II of the report presents a summary of those predictive methods detailed in the Phase I report. In addition those factors known to affect residual strength prediction and therefore deemed necessary to consider in the prediction scheme are also outlined. An examination of elastic and elasto-plastic failure criterion is also reported in Section II with emphasis on the current elastic-plastic criteria and their relationship to the proposed criterion.

In Section III is described the rudiments of the selection process for the analysis method to be used with the developed failure criterion. Since in both plane stress and mixed mode fracture, residual strength predictions cannot be based solely on elastic analysis, the emphasis has been placed on modeling the structure to account for fastener flexibility and comparisons made with those predictions of COD, stringer stress and fastener stresses using elastic assumptions. The Bueckner/Hayes approach (see e.g., Reference 1) to Dugdale type elastic-plastic analysis and Prandtl-Reuss material behavior are compared to one another and to the elastic results for a riveted, wing channel stiffened panel. Values of J integral for this panel configuration are compared for the three assumed material behaviors, i.e., elastic, Dugdale, and Prandtl-Reuss. As a conclusion to Section III those factors influencing residual strength prediction which are structural, loading, and material sensitive are described and suggestions made on how they may be treated in the overall, residual strength predictive method. Section IV describes the correlation of test and analytical data for a three wing channel stiffened, riveted panel.

Comparison is made on the basis of stiffener, rivet and skin strain for various crack lengths. Crack displacement data are also compared with those measured under elastic loading indicating the importance of fastener modeling in the overall finite element analysis. Using an assumed Dugdale plastic zone model and calculated stiffener stresses a prediction of failure stress was made for this stringer critical case which is within seven percent of the actual fracture stress.

Using the skin and stiffener critical assumptions for a given structure those materials data required to establish either fracture criterion are described in Section V. Included is a short description of the method and specimens employed in obtaining crack growth resistance data and the materials information required for development of either the analysis and/or failure criterion.

Section VI includes the analytical and experimental data obtained from crack growth resistance studies using the crack line wedge loaded (CLWL) specimen geometry. The essential details of an elastic and elastic-plastic analysis of this geometry are presented and compared with the experimental results and with each other assuming Prandtl-Reuss and Dugdale material behavior. A comparison of crack growth resistance data based on stress intensity (K_R) and J integral assumptions is made for the materials tested in this study. The features of specimen independency of K_R data is explored for two geometries. The detailed steps required to obtain a $\sqrt{J}_R$ crack growth resistance curve are outlined and materials data compared on this basis. This forms the foundation of the skin critical failure criterion.

Using a two bay, zee stiffened panel configuration the effect of method of attachment on residual strength prediction is both analytically and experimentally studied in Section VII for a complex, landed aluminum panel configuration. Two crack length to stiffener spacing ratios were examined for riveted, bolted, and adhesively bonded stiffeners which represented both skin and stiffener critical conditions. An intercomparison of both analytical and experimental data are presented in this Section.

Section VIII provides a detailed general description of the analysis method and the procedures required to obtain a structural residual strength prediction. Utilizing this procedure the residual strength predictions are compared with those experimental data obtained from the zee stiffened panels. In addition the application of the proposed procedure to the more complex structural panels to be analyzed and tested during Phase III of this program will be discussed. Possible refinements and additions to the procedure are also discussed in Section VIII which will shorten computational time and produce greater accuracy.

Finally, in Section IX those conclusions based on the studies of Phase II are itemized including a short summary of the pertinent results of Phase II.

1.1 PURPOSE

Damage tolerance requirements as outlined in MIL-A-83444 specify that a residual strength analysis be performed on all structure critical to flight safety. If a given arrangement is known to have a propensity to fracture in a plane strain mode the tools of linear elastic fracture mechanics can be used with a high degree of confidence and success. However, once material thickness, toughness or structural arrangements are such that prior to fracture extensive amounts of slow tear occur with plasticity (both crack tip and structural) modifications to or extensions of existing analyses must be formulated. This new method must be such that designers and stress analysts can take advantage of tougher materials and be able to predict not only critical stress but also crack size at fracture. None of the currently available methods can accomplish this requirement, therefore a search for a new method was undertaken as part of this study. A full discussion of the limitations of current residual strength prediction schemes is given in Reference 1. The proposed procedure fulfills the requirement of bridging the gap between gross yielding (structural collapse) on one hand and plane strain fracture in the other extreme.

1.2 BACKGROUND

In the development of fail safe aircraft structures it was evident that advantage could be taken of slow tear and structural arrangement to prevent catastrophic failure. By judicious structural arrangement it was found possible to contain long structural crack sizes through crack arrest at either free boundaries, bonded tear straps or skin splices. First attempts at analyzing these structures were based on "go no-go", trial and error procedure heavily oriented to experimentally derived constants, usually obtained from the structure itself.

With the success of linear elastic fracture mechanics in treating fatigue crack growth and fracture of part-through thickness surface flaws in rocket tankage, a natural extension was toward the residual strength problems of through-flawed aircraft fuselage structure. However, the predictions of both critical crack size and residual strength were much less than the actual structure would tolerate. A search was then instituted for a fracture criterion for thin sections. Modifications to existing criterion were proposed, but found to be heavily dependent on geometric variables unlike those used so successfully for plane strain fracture prediction. Extreme amounts of lateral (through the thickness) contraction accompanied by slow, stable tear of the crack were observed prior to fracture. In order to take advantage of this behavior it was necessary to treat the problem as it actually occurred, i.e., by an elasto-plastic fracture analysis incorporating both material crack tip plasticity and slow tear. With this tool it would then be possible to predict not only strength at failure but accompanying slow tear or critical crack size. Through use of an elastic-plastic analysis one could also distinguish between those structures which are skin or stiffener fracture critical, a most important consideration heretofore not adequately covered in other proposed residual strength schemes.

With this background the requirements of a new procedure were clear and well defined and should incorporate all possible affecting parameters in the developed method.

1.3 TESTING PHILOSOPHY

The requirements for residual strength testing can be separated into either structural or materials oriented and will be examined in turn so that the rationale for each is readily apparent.

Although three structural materials (aluminum, titanium, and steel) were examined in Phase II, along with the several other parameters, the intent of the accomplished materials evaluation was to illustrate the usefulness of the method proposed herein and not strictly for data generation.

Development of the fracture criterion necessitated testing in both the strong and weak crack orientations, employing a sufficient number of specimens to obtain repeatable crack growth resistance data.

During selection of the structural test panels of Phase II it was felt that initially a relatively simple geometry should be examined so that several iterations of the finite element model could be accomplished at reasonable cost. Based on these analytical-experimental comparisons the next step in panel complexity was addressed - that of a variable thickness skin with several methods of stiffener attachment. Two crack lengths were selected for each of the three attachment variables - one representing a skin critical structure and the other a stiffener critical situation. Thus the residual strength data (including strain, crack opening displacement, or COD, etc.) could be compared with the results from the developing analysis as well as intercompared with other panel data. A maximum amount of information was obtained from each panel so that those areas in need of modification in the analysis could be identified.

This same philosophy has been employed in selection of the structural tests of Phase III. In these panels, an even greater degree of aircraft structural realism is the basis for both design and crack location.

1.4 OUTLINE OF PHASE II

During this program phase an analytical procedure has been developed which can be used to predict the fracture response of a complex structural component. This has been accomplished in two tasks: (1) by careful examination of all structural characterization parameters and (2) development of a compatible fracture criterion. A review of all currently available fracture criteria is presented in Section II. Sections III through VIII of this report elaborate on the development, application, and limitations of this procedure.

II. METHODS OF STRUCTURAL RESIDUAL STRENGTH PREDICTION

2.1 SUMMARY OF AVAILABLE TECHNIQUES

In References 1 and 2 a comprehensive review of structural residual strength techniques was presented. Reference 1 concluded that the "ideal" residual strength analysis method should be amenable to some existing computational stress analysis method--i.e., finite element. This tie is advisable since it must treat structural problems which cannot be accurately represented by the simplification involved in mathematical assumptions required for analytical stress intensity solutions.

The basic methods of residual strength analysis can be separated into two categories: Notch strength and fracture mechanics. The former is restrictive in usage in other than as a material failure criterion. Also falling into this category is the effective width concept which is now considered to be equivalent to the notch or crack strength analysis method (see e.g., Kuhn, Reference 3). Fracture mechanics based methods on the other hand have shown promise due to their success in predicting residual strength in plane strain or small scale yielding problems. Attempts have been made to extend the linear elastic fracture mechanics methods to treat large scale yielding problems. A summary of these methods is given in References 1 and 2. It was concluded that an accuracy of ± 5% was possible in obtaining the required fracture criterion data. However, the available mathematical tools (e.g., References 4 and 5) were not as accurate as the finite element method using either special cracked elements or the procedure described in Reference 6. In order to treat the problem of slow, stable tear associated with high toughness thin section fracture, the crack growth resistance curve (K_R) showed good promise (Reference 7) but difficulties in estimating crack tip plasticity have led to an alternate failure criterion.

The alternate criterion employs Rice's J integral (Reference 8) in combination with slow tear or a $\sqrt{J_R}$ versus Δa curve (for skin critical structure). This criterion (incorporating slow tear) was proposed in both References 9 and 10 for other than plane strain fracture. Its application to structural problems was proposed in References 1 and 9. The analysis involves computation of J values for the structure of interest for successive crack sizes and a tangency condition similar to the K_R curve approach. This approach has been employed in this study with good success. It has the current capability to consider the majority of structural, loading and material parameters which were given in Table I of Reference 1 (see Table VIII) for the "ideal" residual strength prediction technique. This technique represents a major step forward in analyzing residual strength of through cracked complex structural arrangements where slow stable tear and large plastic zones prevail.

2.2 FACTORS AFFECTING RESIDUAL STRENGTH PREDICTIONS

In the analysis of any structure the assumptions made in the analysis should be consistent with the actual behavior of the structure under load. If the analysis does not account for proper boundary conditions, load transfer

effects, etc., it will not be able to accurately predict the behavior of the structure. These factors are particularly important in cracked structures because of the presence of singular stresses ahead of the cracked tip. In predicting structural strength accurately, it is necessary that various factors affecting residual strength be carefully considered and their influence on predictions studied. Those factors considered important to residual strength predictions are discussed in this Section.

2.2.1 Effect of Failure Criteria

The selection of a failure criteria is perhaps the most important factor influencing the residual strength prediction. Several failure criteria have been suggested by various investigators. The most commonly suggested failure criteria are based on modification to linear elastic fracture mechanics - critical stress intensity factor, K_c (References 11 and 12), crack opening displacement δ, or COD (Reference 13), strain energy density, or S (Reference 14), and those based on J integral studies or J critical (References 1 and 15). Some of these failure criteria have been reported on in Reference 1 and others are discussed in Sections 2.3 and 2.4.

2.2.2 Effect of Analytical Technique

The analysis method used will play an important part in structural residual strength prediction. The most commonly used analytical techniques are either based on mathematical techniques or finite element methods. Mathematical techniques have restricted use in residual strength prediction of stiffened panels due to the complicated boundary conditions and load transfer effects involved.

The advantage of the analytical method is that the solutions are either available in closed form or they can be obtained using numerical analysis. The numerical analysis techniques generally require small computer run times, however certain simplified assumptions must be made to account for load transfer effects, fasteners, etc., and hence the results obtained must be considered approximate and may not predict residual strength accurately. Mathematical analysis does permit parametric variations as well as generalized solutions. An example of the use of mathematical techniques in parametric studies is shown in Reference 16.

Finite element methods are also a very versatile tool for residual strength analysis. Various load transfer effects, fastener flexibility, stiffener geometries, lands in the structure, etc., can be easily accounted for and the results obtained have a high degree of accuracy. However, the major disadvantages are: large computer run times, solutions are not closed form, and therefore cannot be easily generalized. If finite element techniques were used to do parametric studies of any nature, the cost would perhaps be prohibitive and hence this technique is not well suited for parametric residual strength studies. In this program finite element methods were used and are recommended for use in residual strength predictions since in most cases those structures requiring residual strength analysis have already been modeled and hence readily adapted to the proposed analysis method. In the finite element analysis the method of modeling the structure will have considerable influence on the predicted

residual strength. The finite element model used should be such that it accounts for detailed structural geometry, i.e., lands in the structure, stiffeners and flexibility of the fastener system. The major factors influencing finite element results are discussed in the following subsections.

2.2.2.1 Effect of Fastener Modeling on Residual Strength Predictions

Using a finite element technique for cracked, stiffened structure requires that the method of fastener modeling match the structural behavior as close as possible since it has considerable effect on the stresses and displacements obtained in the analysis. Crack surface displacements or openings and consequently stress intensity factors are dependent on the assumed analytical flexibility of the fasteners. The stress intensity factors can vary as much as 25 percent and crack surface displacements 50 percent, depending on the assumed fastener flexibility. Similar effects have been observed in studies reported in Reference 16. These factors will have considerable influence on residual strength predictions if either K_c or crack opening displacements were to be used as criterion for skin critical fracture cases.

In finite element analysis, fasteners are generally modeled as shear elements, therefore these shear elements should be so proportioned that they have the same flexibility as the actual structural fasteners. Two different fastener models examined in the present study are discussed in Section 3.1.

2.2.2.2 Effect of Fastener Modeling on Load Carried by Stiffeners

In through-the-thickness cracked structure, fastener flexibility plays a very important role. Fastener flexibility influences load transfer to the stringer when the skin is cracked or load shedding to the skin when a stringer is cracked. Analytical calculations of loads transferred to stiffeners may show a variation of five to fifteen percent depending on the applied load and assumed flexibility of the fastener (refer to Section 3.2.2). Accurate estimates of load transfer to the stiffeners are of particular importance for the case of long, through-the-thickness (skin) cracks where the failure is essentially governed by a stiffener critical situation. The effect of finite element modeling of the fastener on load transferred to intact stringer for the cracked skin condition is discussed in detail in Section 3.2 with specific examples.

2.2.3 Effect of Analysis Method

Currently there are two methods of analysis - elastic and elastic-plastic. The elastic techniques (based on strict, linear elasticity) have been found to give ultra conservative residual strength predictions for higher toughness materials which make their use extremely limited. This is particularly true for materials and thickness involving plane stress fracture behavior where slow, stable crack extension plays an important role in determining residual strength.

Most of the current failure criteria proposed in the literature are based on elastic-plastic analysis. The results of elastic-plastic analysis are affected by the size and shape of plastic zone assumed ahead of the crack tip. The most commonly used elastic-plastic analysis is based on the assumption of a Dugdale (Reference 17) type, strip plastic zone ahead of the crack tip (see e.g., Reference 18). Justification for the wide spread use of this model lies not in the soundness of the physical arguments but in the fact that in most fracture analysis cases it appears to work rather well. Another advantage of this model is the simplicity of analysis. In the proposed method the Dugdale model has been used for structural residual strength predictions and these results have been compared with analysis assuming Prandtl-Reuss material behavior. The results of using these two methods of elastic-plastic analysis to predict residual strength are discussed at length in Sections 3.3 and 7.1.

2.3 ELASTIC APPROACHES AS FAILURE CRITERIA

For over a decade linear elastic fracture mechanics (LEFM) has been used successfully as a tool in studying fatigue crack propagation and brittle fracture in solids. However the role of linear elastic fracture mechanics is restricted to brittle and semi-brittle materials and low stress levels where plasticity is confined to a very small region ahead of the crack tip. Another imposing condition is that the crack tip plasticity does not significantly alter the behavior of the material ahead of the crack tip. In LEFM the most widely used single factor to study fatigue and fracture phenomena is the stress intensity factor (K). For elastic material behavior, the relationship between stress intensity factor K, strain energy release rate ($\mathcal{G}$) and J integral is well known (see e.g., Reference 8). Thus all elastic approaches to residual strength prediction essentially use as a failure criterion critical stress intensity (K_c) or modification to K_c to account for plasticity. Stress intensity factors are available in the literature for various crack shapes and geometries. Some stress intensities factors have been reported for stiffened panels in References 4, 5, and 19. These References have employed mathematical approaches based on certain simplified assumptions about fastener flexibility and stiffener geometries. In Reference 19 the problem of an infinite plate with equally spaced stringers and cracks located in alternate bays was considered. The stiffener was assumed to be an integral part of the structure and has its area concentrated at one point. The problem of a continuously bonded stringer was examined in Reference 4 and no allowance was made for fastener flexibility. Poe (Reference 5) studied the problem of a cracked sheet with riveted, attached stringer. Analytical solutions for various symmetric crack locations, percentages of stiffening, and stiffener and rivet pitch were obtained. It was also assumed that the rivets were fixed (i.e., rigid). In References 4, 5, and 19 it was assumed that the stringers were attached to a sheet along a line and no allowance for the flexibility of the fastener was made. In Reference 16 a mathematical technique was developed which accounted for fastener flexibility. It is essentially a modification to the Reference 5 technique and has been used to obtain stress intensity factors for various crack lengths and stiffener spacings.

In References 6 and 11 the finite element method was used to obtain stress intensity factors for built-up structures with skin cracks. In Reference 6 a unique empirical method of fastener modeling was used to account for fastener flexibility. Swift also used a similar method of accounting for fastener flexibility in the mathematical techniques of

Reference 16. The flexibility of fastener was not considered in the finite element analysis of Reference 11.

2.3.1 The Critical Plane Stress, Stress Intensity (K_c) Approach

Vlieger and Broek (Reference 2) in a report prepared for AGARD presented a summary of the then state-of-the-art of structural residual strength analysis. The consensus was that there were two basic methods of analysis: finite element and mathematical analysis. With these methods they found that the difference in residual strength prediction using the two were slight for simple panel geometries and loading.

The failure criterion used with the various methods is based on critical stress or stress intensity data. These data are usually obtained from large, center cracked tensioned sheets of the same material, thickness and width of the planned structure. For tougher, aircraft alloys this can require fracture testing of unreinforced, center cracked panels of extremely large width in an attempt to keep net section stress below yield strength. Sullivan and Freed (Reference 20) and Feddersen (Reference 21) have suggested a minimum width greater than 27 times the anticipated plastic zone size for the expected crack size. By testing a series of crack lengths a material residual strength (in the presence of a given crack length) diagram can be made. Based on these data either an envelope of crack initiation, slow tear and fracture or values of critical stress intensity K_c can be established for a given crack size. These values then become the basis for the skin critical failure criteria. These criteria can be modified to include plasticity effects (see Section 2.4) but difficulty in incorporating slow tear behavior becomes a major problem. Using standard compliance measurements to determine crack size and plasticity-to-fracture during the fracture test is not conducive to separation of the two unless other means of crack length measurement are employed concurrently, i.e., photographic coverage. Under increasing load testing this type of measurement becomes both expensive and tedious and is not a readily repeatable quantity.

Once the failure envelope (critical stress versus crack size) or so-called plane stress fracture toughness (K_c) value is determined they are then compared to analytical solutions for either stress in a skin with attached stringer or stress intensity (to be elaborated on in Section 8). The use of these fracture data in the overall analysis scheme is summarized in References 1 and 2 and will not be repeated here. In order to treat the slow, stable tear situation the original concept of crack growth resistance (K_R) first introduced in 1960 (Reference 22) has been proposed to estimate the residual strength of simple, reinforced panels (see e.g., Reference 12) using a tangency condition between the crack driving force (K) curve and the basic material K_R curve. Here again in the presence of large loads and plastic zones the correction to be added to the structurally derived K's is open to question since estimates of plastic zone size can be in considerable error (see discussions in Section 2.4 and Section 4) for some materials and thicknesses.

In summary the use of a strict, elastic approach (assuming small scale yielding) as a failure criterion for materials and thicknesses where other

than plane strain fracture occur would result in extremely conservative designs. Therefore, the emphasis has been placed in this study on attempting to "marry" the two influencing parameters, plasticity and slow tear into one, workable fracture criterion for skin fracture critical structure. This research has resulted in a resistance curve--crack driving force curve based on Rice's J integral (Reference 8) to account for plasticity and modified resistance curve $\sqrt{J_R}$, to account for both plasticity and slow stable tear. This method of analysis will be described briefly in Section 2.4.4 and its usage shown in analyzing the zee stiffened structural panels of Section 7. It is further recommended that the procedure developed in this report be used for all residual strength determinations particularly in light of the interrelationship between K and J in the elastic case, i.e.,

$J = \frac{K^2}{E}$ for plane stress conditions.

2.3.2 The Critical Plane Strain Stress Intensity K_{Ic} Approach

The use of plane strain fracture toughness (K_{Ic}) as a failure criterion for other than plane strain conditions is incorrect. The so-called mixed mode (mode here meaning stress state at crack tip) or thickness dependent fracture condition is caused by increased plasticity due to reduction in triaxiality of stress at the crack tip with decreasing thickness. This problem can be treated with the method described in this report whereas any modification to the plane strain K_{Ic} value will have little utility and generally lead to an overdesign (heavier structure) of a given fracture critical structure.

2.4 ELASTIC-PLASTIC APPROACHES AS FAILURE CRITERIA

Elastic approaches as failure criteria have found only limited use in failure predictions mainly because of its restricted application in failure predictions. Elastic approaches have been determined to be useful only in cases where plasticity is restricted to a small zone ahead of a crack tip, more commonly known as small-scale yielding. However, in the presence of moderately large and large plastic zones with accompanying slow tear the elastic approach has been found to be inadequate. In all such cases some type of plasticity analysis is required. Plastic deformations in a structure are dependent on the loading history of the structure and hence an ideal plastic analysis should be based on the incremental theory of plasticity. Such an analysis will incorporate effects of unloading and cyclic plasticity under fatigue loading, however most of the plasticity solutions available in the literature are based on deformation theory of plasticity. Because of the complicated nature of the plasticity problem elastic analysis with some form of plasticity correction is generally used to account for plasticity ahead of a crack tip. Most of the available techniques used in accounting for crack tip plasticity are based on elastic-perfectly plastic behavior of the material. In References 23 and 24 an elastic-plastic analysis was presented which accounted for material strain hardening. Some of the more commonly used fracture criterion based on elastic-plastic analysis are discussed in the following subsections.

2.4.1 Critical Stress Intensity Factor Based on Irwin Correction for Plasticity

The simplest method to account for plasticity ahead of a crack tip has been suggested by Irwin (Reference 25). He suggested that the plastic zone may be taken into account by assuming in the analysis an effective crack size equal to the physical crack length plus one-half of the plastic zone size. McClintock and Irwin (Reference 26) suggested that the plastic zone correction r_y may be taken as

$$r_y = \frac{1}{2\pi}\left(\frac{K_I}{F_{ty}}\right)^2 \qquad \text{for plane stress}$$

and

$$r_y = \frac{1}{4\sqrt{2\pi}}\left(\frac{K_I}{F_{ty}}\right)^2 \qquad \text{for plane strain}$$

where K_I is the elastic stress intensity factor and F_{ty} is the 0.2% offset yield strength of the material.

This estimate of plastic zone is based on Mode III loading, which predicts a circular plastic zone of radius r_y. In this form the plastic zone correction is a function of stress intensity factor. If closed form, elastic solutions for K_I in terms of crack length are available, then r_y can be computed in terms of K_I and substituted in the appropriate equation and a plastic zone corrected value of K_I obtained. If the stress intensity factors are not available in closed form, then the plastic zone correction must be obtained by an iteration procedure. Fracture initiation is assumed to take place when the computed stress intensity factor based on effective crack length reaches the critical value of stress intensity K_c.

2.4.2 Plastic Stress Intensity Factors

In References 23 and 24 the concept of plastic stress intensity factors was introduced. In conventional linear elastic fracture mechanics the coefficient of the singularity ahead of the crack tip is defined as a stress intensity factor. This definition was extended in References 23 and 24 to the case of realistic materials which exhibit strain hardening under increasing load. The plastic stress intensity factor is associated with the dominant singularity in the plastic zone. The stress-strain relationship used in the analysis is of the Ramberg-Osgood form

$$\epsilon = \sigma + \alpha\sigma^n$$

where σ is the uniaxial tensile stress nondimentionalized by initial yield stress σ_i and ϵ is the uniaxial strain nondimensionalized by the corresponding yield strain ϵ_i, where $\epsilon_i = \sigma_i/E$. E is the initial (elastic) slope of the

stress-strain curve, and α and n are material constants.

For plane stress, plane strain, and anti-plane shear the dominant stress field (σ_{ij}) and strain field (ϵ_{ij}) may be written as

$$\sigma_{ij} = K_\sigma \, r^{-1/(n+1)} \, \bar{\sigma}_{ij} \, (\theta)$$

$$\epsilon_{ij} = K_\epsilon r^{-n(n+1)} \, \bar{\epsilon}_{ij} \, (\theta)$$

where K_σ is the stress intensity factor nondimensionalized with respect to initial yield stress σ_i, K_ϵ is the strain intensity factor nondimensionalized with respect to initial yield strain ϵ_i and σ_{ij} (θ) and ϵ_{ij} (θ) are dimensionless functions of the angle θ.

The plastic stress intensity factors are dependent on strain-hardening exponent "n". In Reference 24, plastic stress intensity factors for various values of strain hardening exponent "n" have been obtained using a finite element method. Reference 27 discusses plastic stress intensity factors for cracked plates subjected to biaxial loading. Failure is assumed to initiate when the plastic stress intensity factor reaches a critical value $K_\sigma{}^c$.

For small-scale yielding the plastic stress intensity factors are directly related to elastic stress intensity factors through the following relationship

$$K_\sigma = C_n \left(\frac{K_I}{\sigma_i \sqrt{\pi}} \right)^{\frac{2}{n+1}}$$

$$K_\epsilon = (K_\sigma)^n$$

The coefficient C_n depends on the strain hardening coefficient and is given for a number of cases for both plane stress and plane strain in Reference 23.

2.4.3 Crack Opening Displacement (COD)

Wells in 1963 (Reference 28) suggested a fracture criterion based on the finite opening displacement δ of the crack tip. The fracture is assumed to initiate when the crack opening reaches a critical value δ_c, independent of of crack length. Wells proposed this criterion to study fracture phenomenon in nonhardening materials.

Consider an infinite plate with a crack loaded as shown in Figure 1(a). Under applied loads local yielding occurs at the crack tips (even for brittle materials) as shown in Figure 1(b). The size of the plastic zone depends on

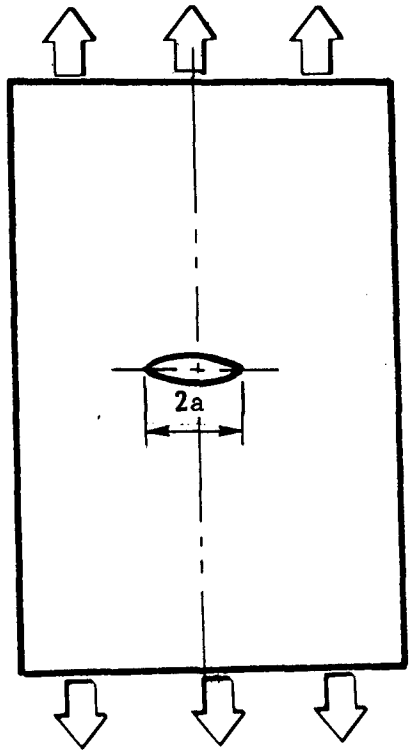

(a.) Plate in Tension with Central Crack

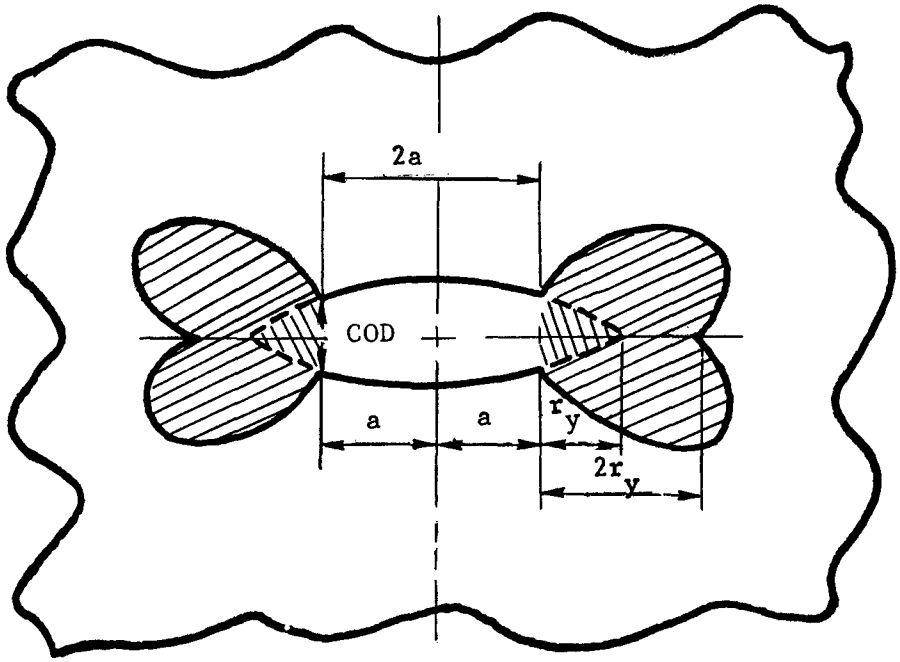

(b.) Plastic Zone Ahead of Crack Tip

Figure 1. Center Cracked Tension Panel and Associated Plastic Zone Geometry

the applied stress, crack length and yield strength of the material. Crack opening displacement (better known as COD) is defined as the relative displacement between the opposite surfaces of the crack at the location corresponding to the physical crack tip as shown in Figure 1(b). In the analysis the effective crack tip is assumed to be at the center of the plastic zone.

2.4.3.1 Dugdale Model

In a cracked structure, the plastic zone generally is fan shaped as indicated in Figure 1(b). From an analytical point of view, it is rather difficult to account for this shape of plastic zone. A simplified plastic zone model based on a strip shaped zone was suggested by Dugdale in Reference 17. In the Dugdale Model the plastic zone ahead of the crack tip is assumed to have the form of a strip with constant stress applied to the strip equal to the materials uniaxial yield strength (F_{ty}). The length of the plastic zone is such that there are no stress singularities at the end of a fictitious crack tip which is assumed to be at the end of the plastic strip.

Consider the through-the-thickness cracked plate of Figure 2(a). The plastic zone is assumed to be of size P having a constant yield stress F_{ty} acting in opposition to the applied stress, σ. Thus the material behavior is assumed to be elastic-perfectly plastic. The size of the plastic zone is such that under applied external loads and stresses equal to F_{ty} within the plastic zone, there are no stress singularities at the fictitious crack tips A and B. (The physical crack size is 2a). The solution to the problem of Figure 2(a) is obtained by superposing solutions as shown in Figure 2(b). The size of the plastic zone P can be determined directly if closed form solutions for stress intensity factors can be determined. However, if numerical techniques or finite element methods are used for the analysis, the size of the plastic zone is determined by indirect means as discussed in Section 3.3.3.1. Dugdale's plastic zone model is mathematically similar to Barenblatt's cohesive force model (References 29 and 30) though conceptually different. Barenblatt suggested that the singular stresses ahead of a crack tip are not physically possible. However, there are certain intermolecular forces (cohesive forces) acting in that region such that there are no stress singularities. Based on this concept Barenblatt proposed a theory of brittle fracture. A detailed version of Barenblatt's theory is given in Reference 31. The Dugdale model provides a very suitable analytical model to obtain crack opening displacements for cracked structures. The COD will be given by the opening of crack surfaces at the physical crack tip, C or D (Figure 2) under the loading system indicated. Knowing the size of the plastic zone, COD can be easily obtained by superposing the two solutions of Figure 2(b).

Crack opening displacement has been used as a failure criterion to study rupture due to cracks in pipes and cylinders, under plane stress conditions. This failure criterion had found limited utility in failure analysis mainly due to experimental difficulties arising in measurement of small crack openings close to the crack tip. Other drawbacks of this failure criterion are that the value of COD at failure is not a material property due to its thickness dependency. Also this failure criterion is not consistent with the local stress-strain criterion ahead of the crack since this criterion does not

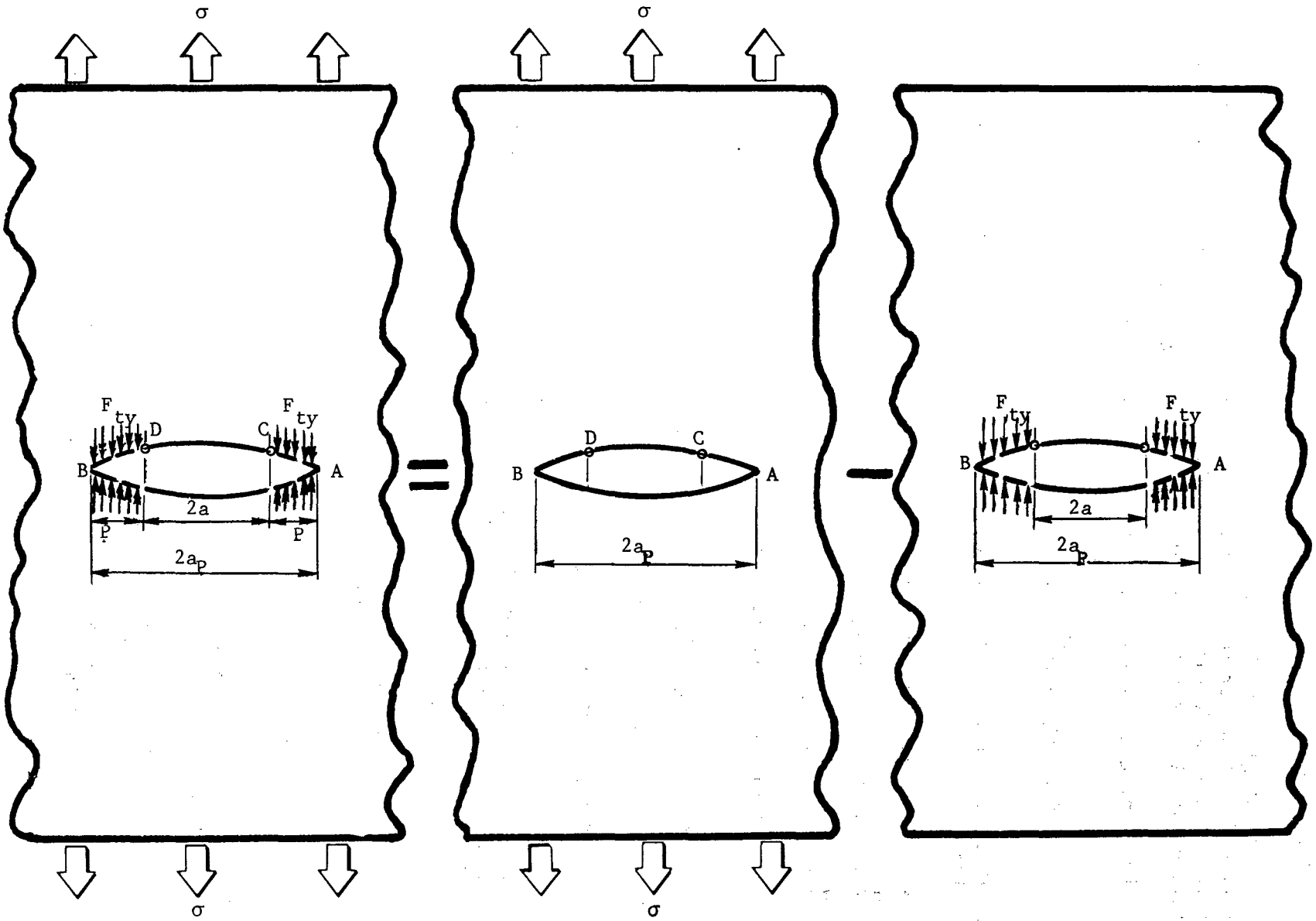

(a.) Dugdale Plastic Zone Model (b.) Superposition for Dugdale Model Analysis

Figure 2. Dugdale Model Plastic Zone and Superposition

specify the region in which fracture displacements are concentrated.

2.4.4 J Integral

The J integral has been investigated by several researchers as a failure criterion for plane strain fracture (References 15, 32, and 33). In Phase I of this program (Reference 1) the suitability of the J integral as a failure criterion for plane stress fracture was described.

The J integral is defined by Rice (Reference 8) as

$$J = \int_{\Gamma} \left(W dy - \vec{T} \cdot \frac{\partial \vec{u}}{\partial x} ds\right)$$

where Γ is any contour surrounding the crack tip, traversing in a counter clockwise direction.

W is the strain energy density

$\vec{T}$ is the traction on Γ, and

$\vec{u}$ is the displacement on an element along arc s.

The strain energy density W is given by

$$W = \int [\sigma_x \, d\epsilon_x + \tau_{xy} \, dr_{xy} + \tau_{xz} \, dr_{xz} + \sigma_y \, d\epsilon_y + \tau_{yz} \, dr_{yz} + \sigma_z \, d\epsilon_z]$$

and for generalized plane stress

$$W = \int [\sigma_x \, d\epsilon_x + \tau_{xy} \, dr_{xy} + \sigma_y \, d\epsilon_y] \, .$$

For elastic material behavior, J is equivalent to Irwin's strain energy release rate $\mathcal{G}$. For Mode I, the relation between $\mathcal{G}$ and stress intensity factor K_I is given by

$$\mathcal{G} = \frac{1-\nu^2}{E} K_I^2 \quad \text{for plane strain}$$

$$\mathcal{G} = \frac{K_I^2}{E} \quad \text{for plane stress}$$

Thus for elastic material behavior J can be related to stress intensity factor K. Contrary to K or $\mathcal{G}$, the use of J is not restricted to small scale yielding. J can be used as a generalized fracture parameter even for large scale yielding, (see e.g., Reference 15). For an elastic-perfectly plastic material (materials exhibiting Dugdale type plastic zones - see References 1 and 34), J is directly related to crack opening displacement, COD and for such a material the relationship is given by

$$\delta = \frac{J}{F_{ty}} \, .$$

The application of the J integral as a fracture criterion has been mainly restricted to plane strain fracture and its application to plane stress fracture has not been studied in any extensive manner. This perhaps is due to slow stable tear that normally accompanies plane stress fracture. The J integral can be used to predict plane stress fracture if a J_R resistance curve similar to the recently proposed K_R resistance curve can be obtained. In practice it is perhaps desirable to plot square root of J_R ($\sqrt{J_R}$) since for elastic cases it is directly related to stress intensity factor versus crack extension. This curve will have the form shown in Figure 3.

In Reference 22, Kraft, et al, first introduced a failure criterion based on crack growth resistance concepts, or K_R. They suggested that a crack will grow stably if the increase in resistance as the crack grows is greater than the increase in applied stress intensity. If these conditions are not met, unstable fast fracture will occur. This fast fracture occurs when

$$K = R, \quad \text{and} \quad \frac{\partial K}{\partial a} \geq \frac{\partial R}{\partial a}$$

This concept has been used in Reference 12 to predict residual strength of simple strap stiffened panels. The procedure is explained in Section 5.2.

The method of employing stress intensity factors along with a K_R curve has several disadvantages, however, which are associated with estimates of crack tip plasticity as previously discussed in Section 2.3. This concept can be extended to incorporate plasticity effects by using J in place of the stress intensity factor K. The use of J has several advantages as discussed in References 1 and 9. A brief outline of the procedure involves the following steps.

- Obtain $\sqrt{J_R}$ curve for the skin material of the structure using a suitable specimen (e.g. crack line wedge loaded or center cracked tension).
- Obtain J values for the stiffened structure for various crack lengths and applied stresses using a suitable plasticity model (e.g. Dugdale Model).
- Determine the point of instability from the $\sqrt{J}$ curves of the structure and $\sqrt{J_R}$ curves of the material as shown schematically in Figure 4.

The square root of J versus crack length are plotted for various applied stresses. The $\sqrt{J_R}$ resistance curve is superimposed on the diagram at some physical crack length under consideration, say a_o. The corresponding failure stress is given by the point of tangency between $\sqrt{J_R}$ curve and $\sqrt{J}$ curve at point A. Thus fracture stress is given by σ_4 in Figure 4 with associated slow tear of the amount Δa.

This technique is employed in this report to analyze skin critical, cracked structure. The details of the method with appropriate examples and corresponding experimental data are given in Section 8.

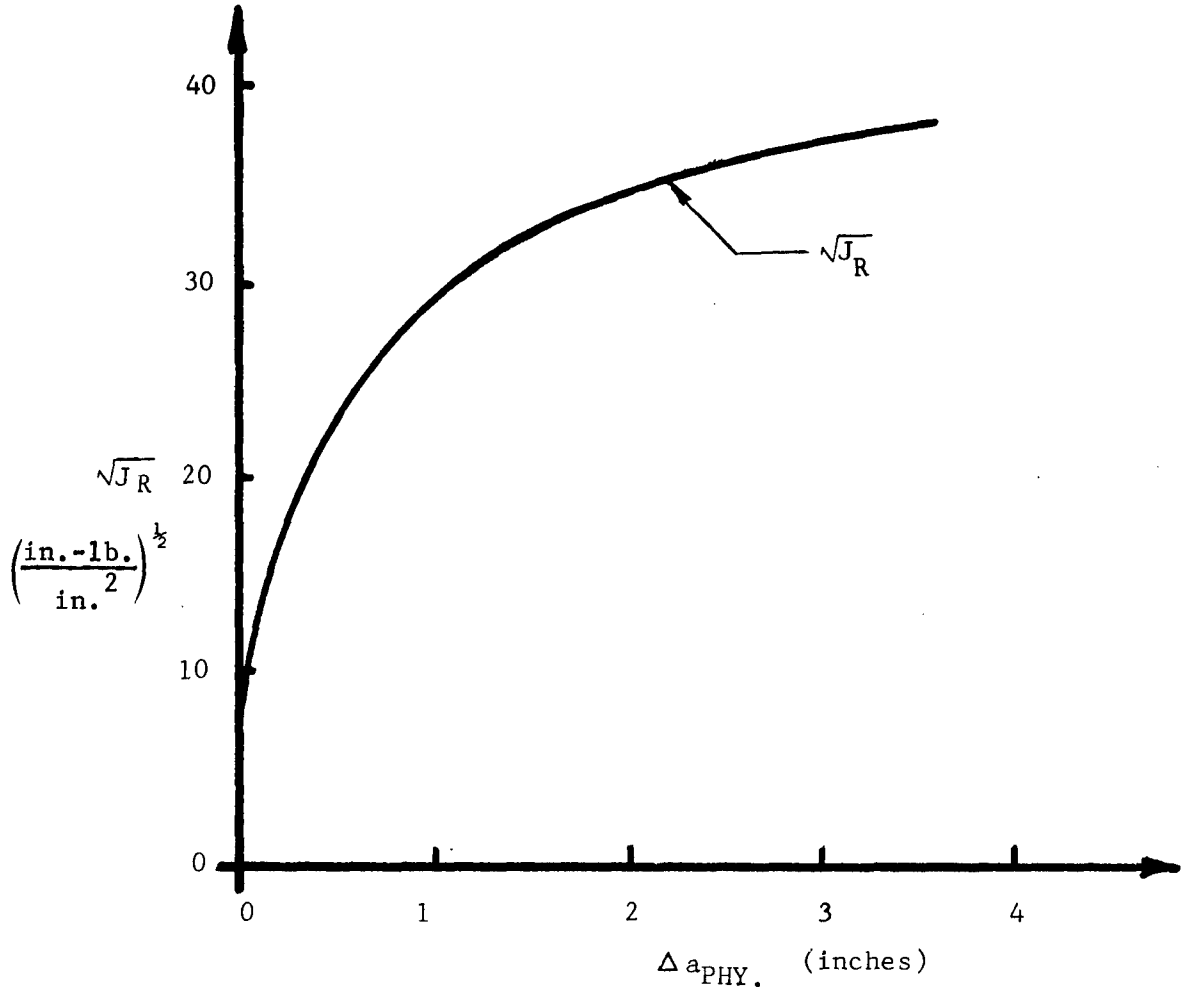

Figure 3. Square Root of J_R Resistance Curve

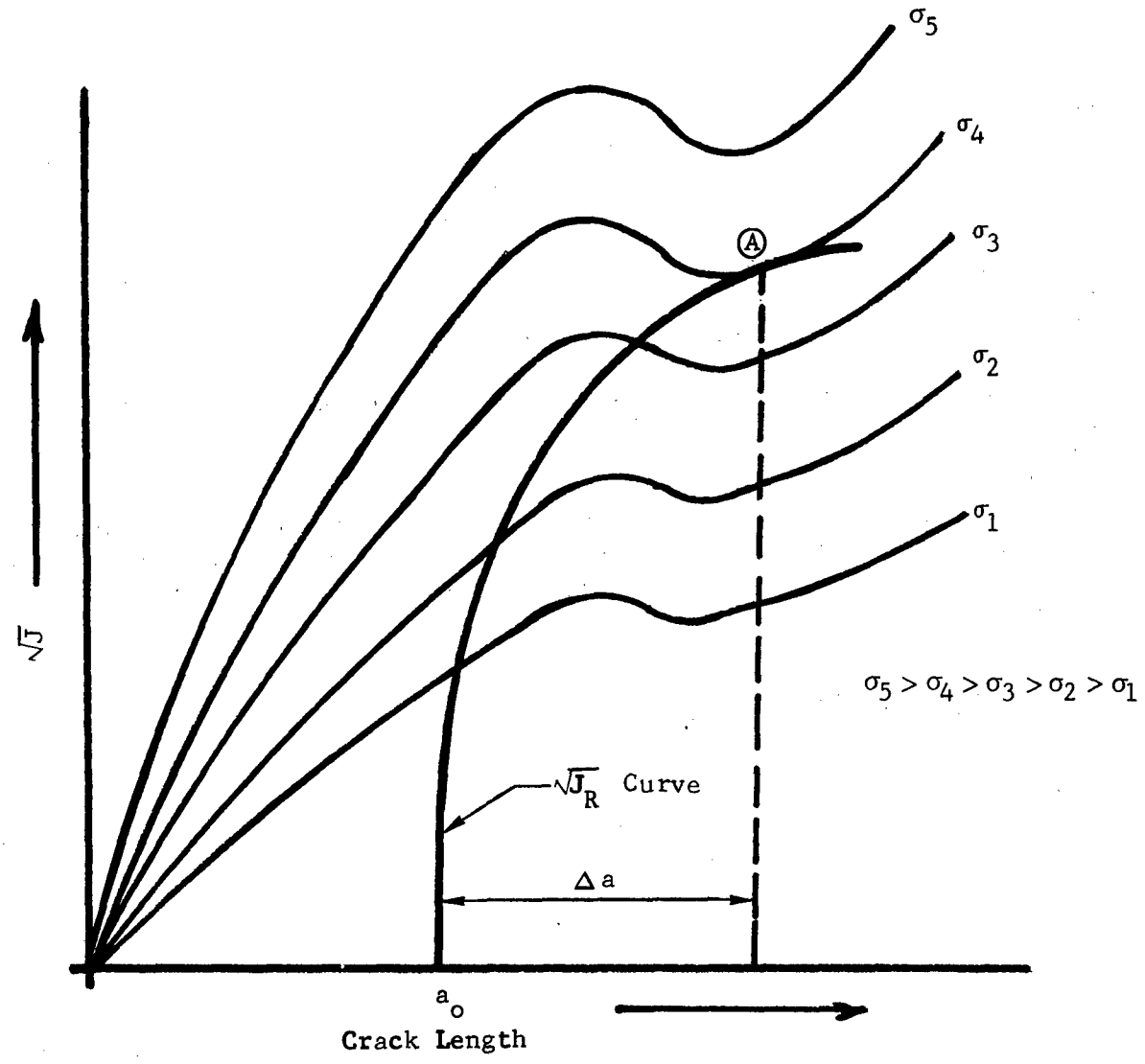

Figure 4. Failure Analysis Based on $J_{CRITICAL}$ Curve

III. STRUCTURAL CHARACTERIZATION

As discussed in Section 2.2 many factors influence residual strength prediction of a structure. These factors must be carefully considered in order to make reasonable estimates of residual strength. The first step is to select a suitable analysis method, which should be reasonable from the point of accuracy desired and cost. In the present program the finite element method is recommended for residual strength prediction since most critical to flight structures are normally analyzed using finite element analysis. Those factors considered to be important in the finite element modeling of a cracked, stiffened structure are discussed in Section 3.1. In both plane stress and mixed mode fracture the residual strength predictions cannot be based solely on elastic analysis and suitable plasticity effects must be incorporated to produce accurate estimates of residual strength. The method used to account for plasticity will depend on the type of materials employed in the structure. In the present program the Dugdale model is used to account for plastic zones and was found to give good correlation with the experimental data. These elastic and elastic-plastic analytical techniques are discussed in detail in Sections 3.2 and 3.3.

Finally, if a structure is of complicated geometry, has nonuniform material properties, is layered or subjected to biaxial loading then certain simplified assumptions may have to be made in the analysis. Some of these factors are discussed in Section 3.4.

3.1 STRUCTURAL IDEALIZATION

Due to the presence of singular stresses ahead of the crack tip the finite element analysis requires more care than usually exercised. If linear elastic stress intensities are required, there are two finite element based methods; one is to use a very fine mesh size to treat the large stress gradient ahead of the cracked tip and the other is to use special elements or so-called cracked elements. These special elements have been developed to take into account the singularity ahead of a crack tip thus avoiding use of a fine mesh in that area. Considerable reduction in computer run time is possible by using a cracked finite element. In the proposed technique residual strength predictions are based on elastic-plastic analysis and the J integral is used in the failure prediction scheme. The elastic-plastic analysis uses the Bueckner-Hayes approach (References 18 and 34) for Dugdale type plastic zone calculations, where the energy is computed from the resulting displacements. Hence, in the present analysis it is not considered necessary to use a cracked element or fine mesh.

A finite element study of a complex structure should be able to incorporate flexibility of fasteners as well as modeling the sub-structure in such a way that when one member is cracked load transfer in the remaining structure can be conveniently studied. A complete finite element model should also be able to account for lands in the skin and be convenient for elastic-plastic studies.

In any residual strength study careful consideration must be given to the modeling of skin (sheet), substructure and attachments. These factors are discussed in the following subsections where a riveted, wing channel stiffened panel is analyzed. In addition finite element modeling of a more complex-landed, Zee-stiffened panel with riveted, bolted and bonded stiffeners is discussed in Section 7. The finite element program used in these analyses is NASTRAN.

3.1.1 Modeling of Skin or Sheet

Rectangular or triangular plate elements may be used in the finite element modeling of the structural skin. For an elastic analysis of cracked structure, triangular plate elements have been used by various investigators. In most cases when a special cracked element is not available very fine grid must be used in the vicinity of the crack tip. The grid or mesh size is gradually increased further away from the tip. In Reference 35, it was shown that an element or mesh size to half crack length ratio of 0.01 gave results very close to the exact, elastic stress intensity solution. In the finite element model of a riveted wing channel stiffened panel (to be discussed in Section 3.1.2) an element size of 0.2 inches was used for various crack lengths. This element size was considered sufficiently small for the present study since the Dugdale type elastic-plastic analysis is based on the Bueckner-Hayes energy approach and not on computing elastic stress intensity factors.

If the skin structure is landed (pocketed) special care must be taken in modeling those portions containing the lands. It may be assumed for analytical purposes that the land is symmetrical about the center-line of the thickness. With this assumption the finite element modeling is considerably simplified and allows the use of the plate elements in the landed portions of the structural skin. These plate elements are provided with the same thickness as the thickness of the land. The rest of the plate elements have the same thickness as the skin. This method of modeling a structure with lands or pockets is discussed further in Section 7. As mentioned previously symetrically lumping the land thickness with the skin material does not consider the effect of asymmetry due to the presence of the land on only one side of the skin as in the actual structure. This did not appear to be a limitation in the analysis as will be shown in the data of Sections 7 and 8.

3.1.2 Modeling of Substructure

The stiffeners are known to affect the crack tip environment primarily by virtue of their cross sectional area and their moment of inertia (i.e., the disposition of the stiffener material away from the skin). The placement of stiffener material to either side of the attachment line is of secondary importance; hence, the finite element idealization will concentrate all the stiffener material in the planes defined by the loci of the attachment centerlines. This method of modeling the substructure is referred to as a lumped parameter technique, which has been used by Swift (Reference 6) in the analysis of cracked, stiffened fuselage panels.

The wing channel panel shown in Figure 5 was modeled as illustrated in Figure 6. The total structure (Figure 6(a)) is looked upon as consisting of skin and stringer connected by rivets as shown in Figure 6(b). The skin or sheet is idealized as plate elements and the connecting fasteners as shear elements

Young's Modulus - Sheet = 10.3×10^6 psi

Young's Modulus - Rivets = 10.2×10^6 psi

NOTES: Wing Channels
Area = 1.57 square inches
I_{x-x} = 0.778
I_{y-y} = 2.53
Thickness = 0.1875 inches
Young's Modulus = 10.3×10^6 psi

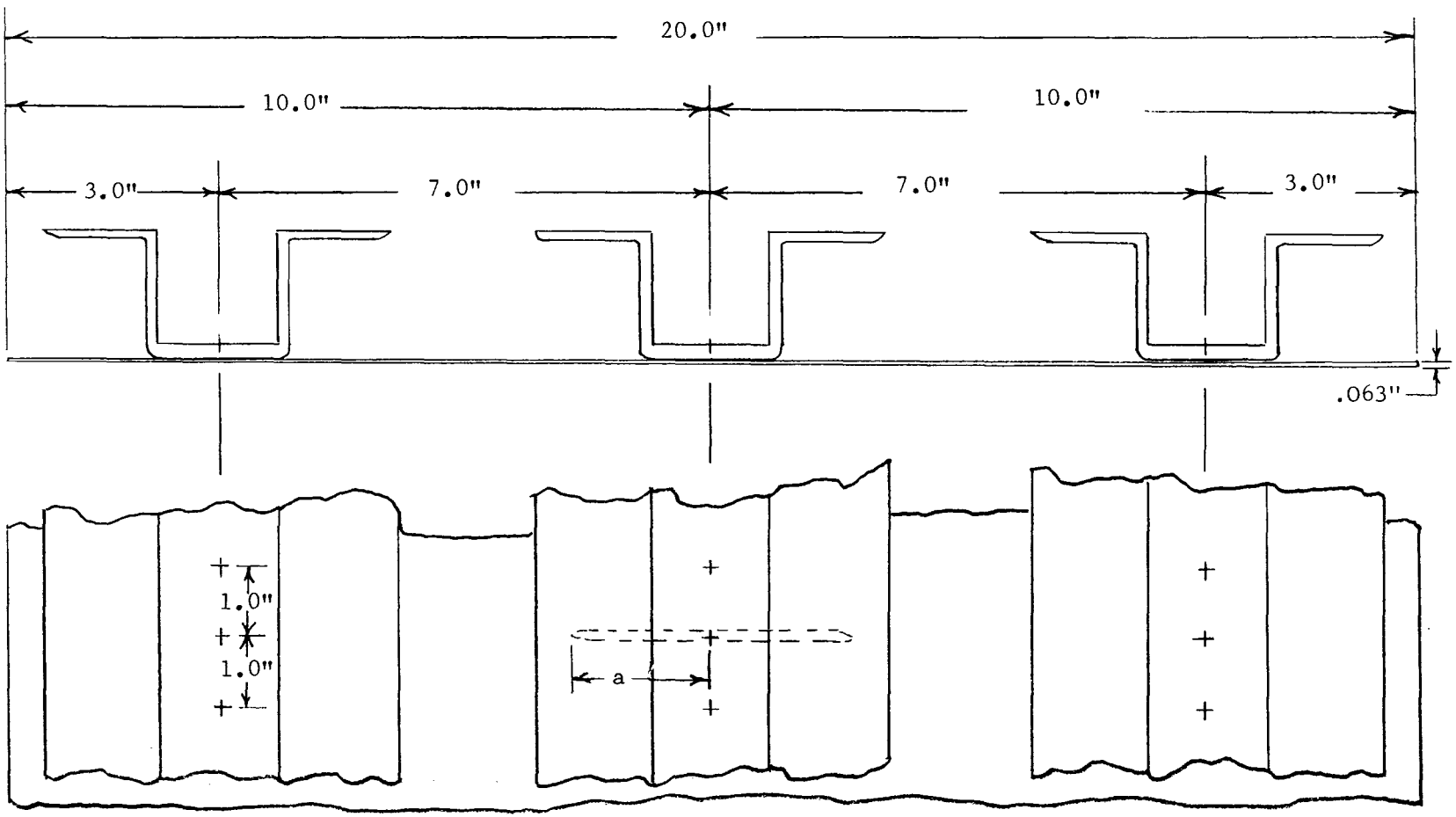

Figure 5. Wing Channel Stiffened Panel - Heavily Stiffened

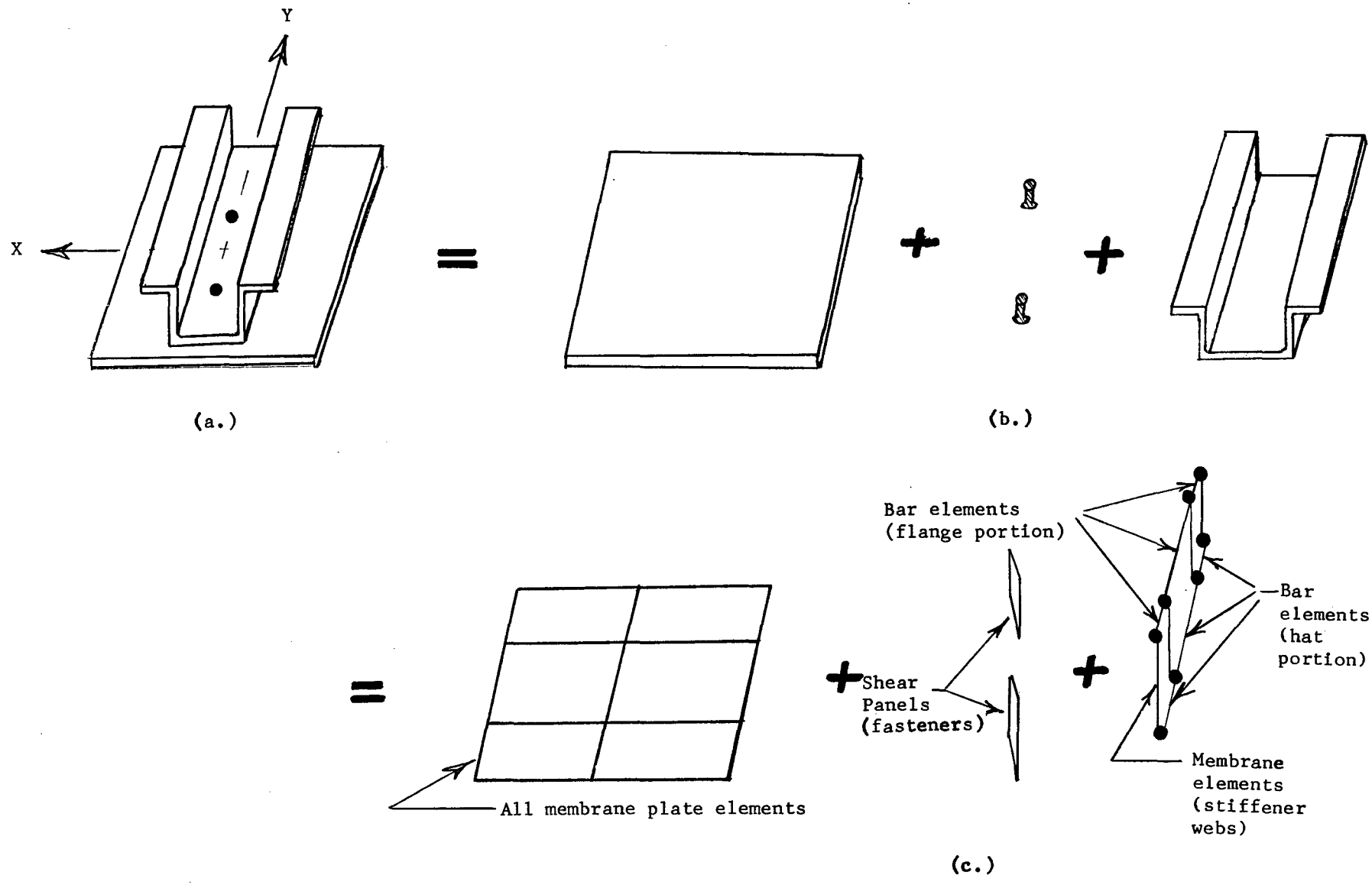

Figure 6. Sheet-Rivet-Channel Finite Element Idealization

(see Figure 6(c)). As noted the connected portion of the structure (i.e. hat portion and flange) are idealized as bar or rod elements. In this case the stiffener webs were idealized as membrane elements. The rod elements are considered to have the same cross-sectional area as that of the two flanges. The membrane elements in the model have the same thickness as the thickness of two webs.

One row of attachments (rivets) was assumed in this wing channel panel example. If two rows of fasteners or staggered fasteners are used, the modeling of the structure must change to more realistically model the problem. In the case of multiple fastener rows, the hat portion of the stiffener should not be idealized using bar elements since there will be two or more rows of connecting shear elements. The hat portion must then be idealized as a membrane element. This way of modeling the connected leg of the stiffener is illustrated for the case of a bonded zee-stiffened panel in Section VII. If a multiple row of attachments with staggered pitch is used in a structure, the hat portion may be idealized as bar elements if it is assumed that there is only one continuous row of attachments. However, the more realistic approach would be to idealize the connected portion of the substructure as membrane elements such that grid points are provided in the model at all attachment points.

In the finite element analysis the lateral displacement (in the Z direction) for both stiffener and skin is restricted. This restriction considerably reduces computer run times without significantly affecting the analytical results.

3.1.3 Modeling of Attachments

As discussed in Section 2.2.2.1 the assumed stiffness of a fastener in a cracked structure has considerable effect on load transfer, crack openings and stress intensity factors. In Reference 5, Poe analyzed cracked stiffened panels using a mathematical technique assuming rigid attachment conditions. Swift (Reference 16) studied similar problems using the Poe technique but assumed flexible fasteners. He found that stress intensity factors and stiffener stresses may differ by as much as 50% from Poe's results, depending on crack length. In the present study two different fastener flexibility models were considered. In both, the fastener is modeled as a shear element and these shear elements are provided at the same locations as the actual fasteners. In the first model it was assumed that the shear element had the same area as the area of the attachment. For example in Figure 6(c) the shear panels have the same area as the area of the fasteners. In the second attachment model it was assumed that the deflection of the shear element was same as the experimentally determined deflection of a similarly attached joint. In Reference 36 Swift has presented the following empirical equation for the rivet shear deflection in riveted aluminum alloy sheets:

$$\delta = \frac{Pf}{E_a d} \qquad (1)$$

where

δ = deflection

P = applied load

E_a = modulus of aluminum, and

d = rivet diameter

and, for aluminum alloy rivets,

$$f = 5.0 + 0.8 \left(\frac{d}{t_1} + \frac{d}{t_2}\right)$$

where t_1 and t_2 are the thicknesses of the joined sheets.

In the idealized shear element, the deflection is given by

$$\delta = \frac{P\,h}{A_s\,G_a} \tag{2}$$

where

A_s = the area of the shear element

G_a = shear modulus of aluminum

h = distance between the centers of the sheets which are connected together.

By equating the two deflections (Equations 1 and 2),

$$\frac{Pf}{E_a d} = \frac{Ph}{A_s G_a} \quad .$$

The area of the shear element, A_s is given by

$$A_s = \frac{h}{G_a} \quad \frac{E_a d}{f} \quad . \tag{3}$$

If the material connected by the attachments have different moduli the empirical constant in the fastener deflection formula (Reference 36) is given by:

$$f = 5.0 + 0.8 \left(\frac{d}{t_1} + \frac{d}{t_2} \quad \frac{E_1}{E_2}\right) \tag{4}$$

where E_1 and E_2 are Young's moduli of the two connected sheets. The fastener models discussed above are referred to as an equivalent area model and attachment or fastener flexibility model. These two models are used in the elastic-plastic analysis of a lightly stiffened wing channel panel. The geometry of this panel is shown in Figure 7. The wing channel is attached by a

NOTES:

Young's Modulus - Sheet = 10.3×10^6 psi

Young's Modulus - Rivets = 10.3×10^6 psi

Wing Channels

Area = 0.44 square inches

I_{x-x} = 0.038

I_{y-y} = 0.484

Thickness = 0.09375 inches

Young's Modulus = 10.3×10^6 psi

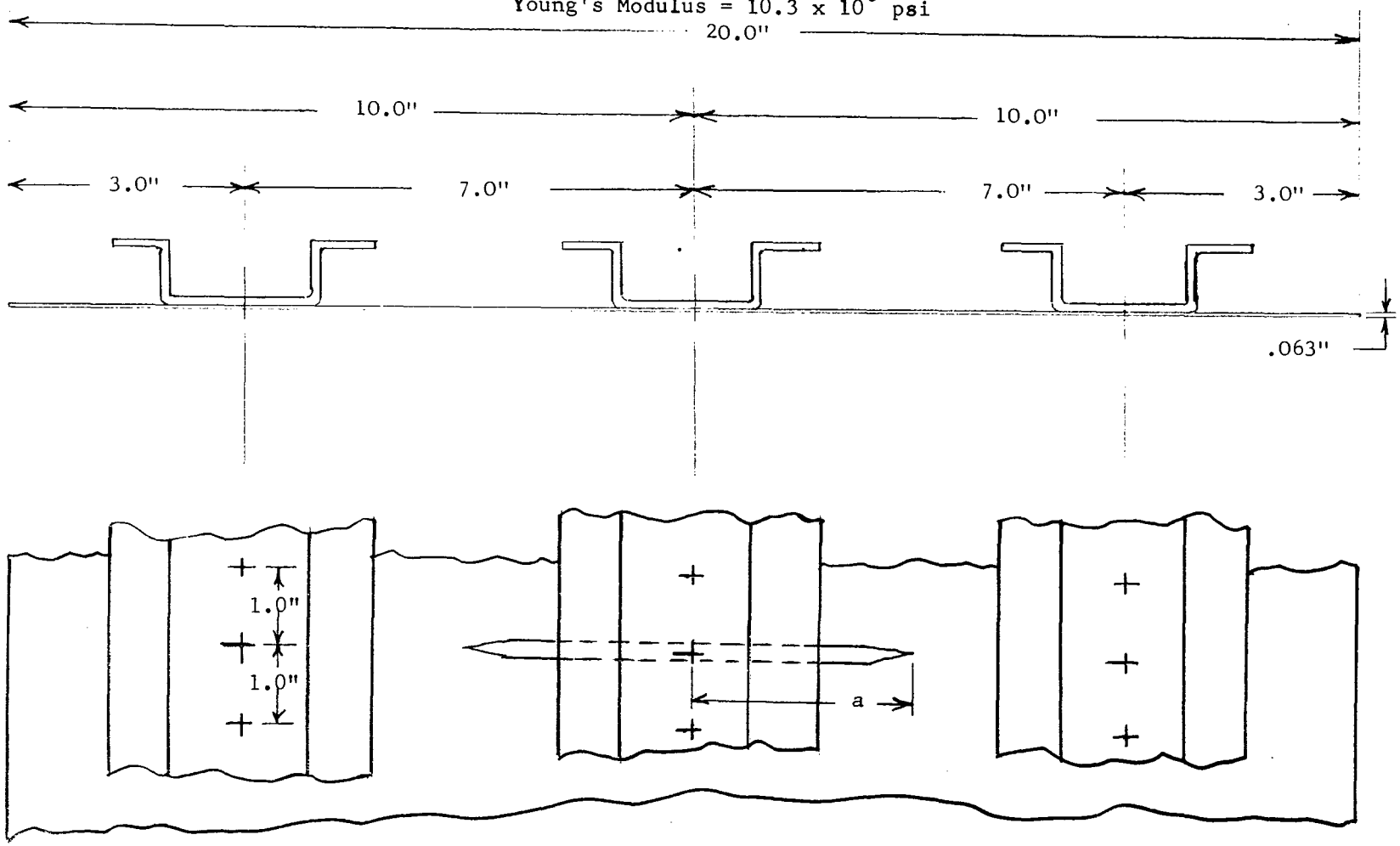

Figure 7. Wing Channel Stiffened Panel - Lightly Stiffened

single row of 1/4-inch diameter rivets with 1-inch pitch. In the finite element model of this panel the area of the idealized shear element was calculated as follows:

Taking

t_1 = the thickness of sheet = 0.063 inch,

t_2 = the thickness of hat portion of the wing channel = 0.09375 inch,

d = the diameter of rivets = 0.250 inch and the constant f defined by Equation (4) with ($E_1 = E_2$), is

$$f = 5.0 + 0.8 \left(\frac{d}{t_1} + \frac{d}{t_2} \right)$$

$$= 5.0 + 0.8 \left[0.250" \left(\frac{1}{0.063"} + \frac{1}{0.09375"} \right) \right]$$

$$= 10.308 .$$

The distance between the center of the connected sheets is

$$h = 1/2 \ (0.063" + 0.90375")$$

$$= 0.0784".$$

Area of shear element is

$$A_s = \frac{h}{G_a} \ \frac{E_a d}{f} \text{ (Equation 3)}$$

$$= 2(1 + \nu)\frac{hd}{f}$$

$$= 2(1 + 0.33) \times \frac{0.0784" \ (0.25")}{10.308}$$

$$= 0.00506 \text{ inches.}$$

If h_1 is the distance between node points in the finite element model where a shear element is provided, then the thickness of the shear element in the model is given by $t = A_s/h_1$. Note that h_1 should be the diameter of the rivets for rivets near the crack location. The actual stresses in the attachment, σ (stress in shear element) are determined from the finite element analysis. The force transferred through the shear element is given by:

$$P = A_s \sigma \qquad (5)$$

Equation 5 represents the force transferred through the attachment. The stress in the attachment or rivet is given by:

$$\text{Stress in Rivet} = \frac{P}{\text{Area of Rivet}} = \frac{P}{\frac{\pi}{4}d^2} \qquad (6)$$

The influence of these two attachment models on both elastic and elastic-plastic analysis of this wing channel panel are discussed in Section 3.3 and 3.4. The finite element model of this riveted, wing channel panel is shown in Figure 8.

3.2 ELASTIC ANALYSIS OF CRACKED STRUCTURE

As discussed in Section 2.3, elastic analysis is not adequate for prediction of residual strength. For parametric studies, for example, to determine the effects of percentage stiffening, stringer spacing, fastener spacing, fastener flexibility, etc., on residual strength and crack propagation under fatigue loads, elastic analysis is a very useful tool. Currently the computer times involved in performing elastic-plastic parametric studies are prohibitive. In the present program both elastic and elastic-plastic analyses are used to study the effect of percentage stiffening for the case of a riveted wing channel stiffened panel. The effect of rivet modeling has been examined for the case of a lightly stiffened wing channel panel.

The effect of percentage stiffening and rivet modeling on stiffener stresses and crack opening displacements is discussed in the following sections using elastic analysis.

3.2.1 Effect of Percentage Stiffening on Stresses in Stringer

Figure 9 shows the stresses in the central and outer channels (stringers) for both heavily and lightly stiffened wing channel panels with a skin half crack length of 2.8 inches. The geometries of these panels are shown in Figures 5 and 7. It is seen that for these stiffening ratios (wing channel areas) the stresses in the central stringer are affected by the area of the stiffener. However, the stresses in the outer stringers are only slightly dependent on the cross section area of the stiffener.

For an applied stress of 30 ksi, the influence of crack length on the stresses in the stringers is shown in Figure 10. It is seen that the stresses in the central stringer increase with crack size until the crack tip is very near the outer stringer. With further increase in crack length, the stress in the central stringer increases only slightly.

The stresses in the outer stringers are slightly affected by the presence of the crack up to a half crack length of about 3.5 inches, or ratio of crack length to stringer spacing, a/s of 0.5. Beyond this point the outer stringer starts picking up the load and the stress in the outer stringer is strongly dependent on the stiffener area.

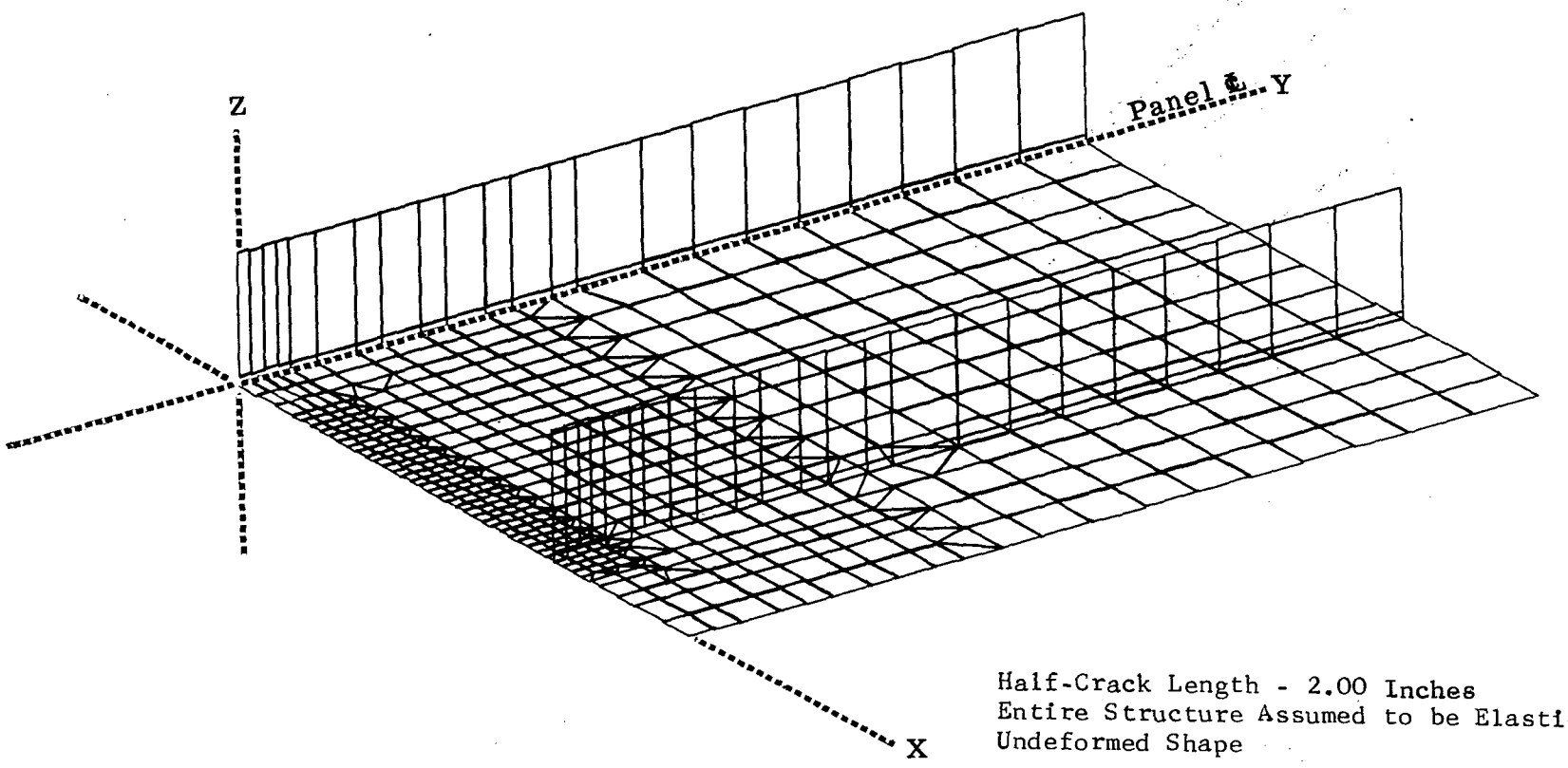

Figure 8. Finite Element Model of Riveted, Wing Channel Stiffened Panel

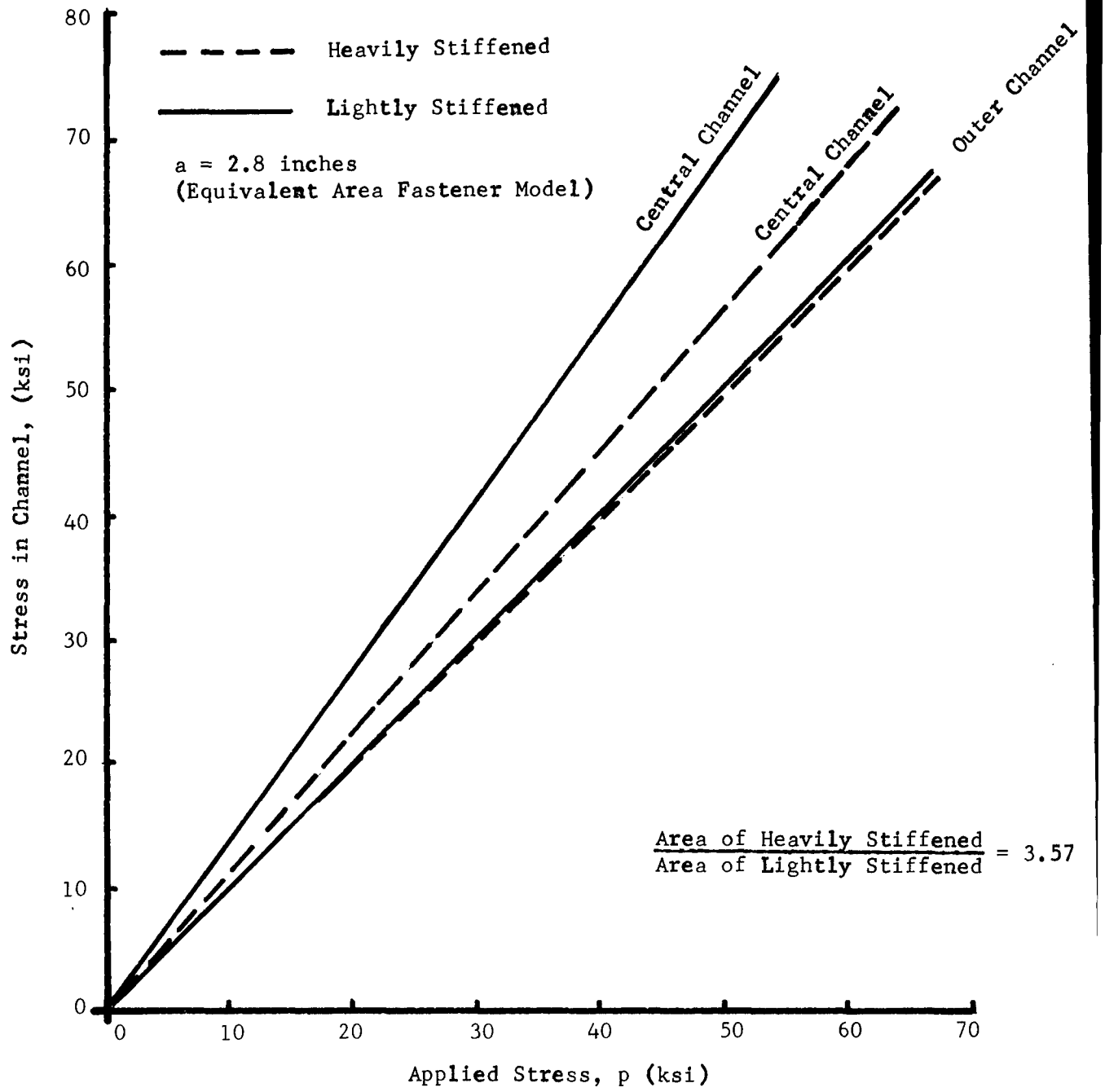

Figure 9. Elastic Stresses in Central and Outer Channels - Lightly and Heavily Stiffened Wing Channel Panels - a = 2.8 Inches

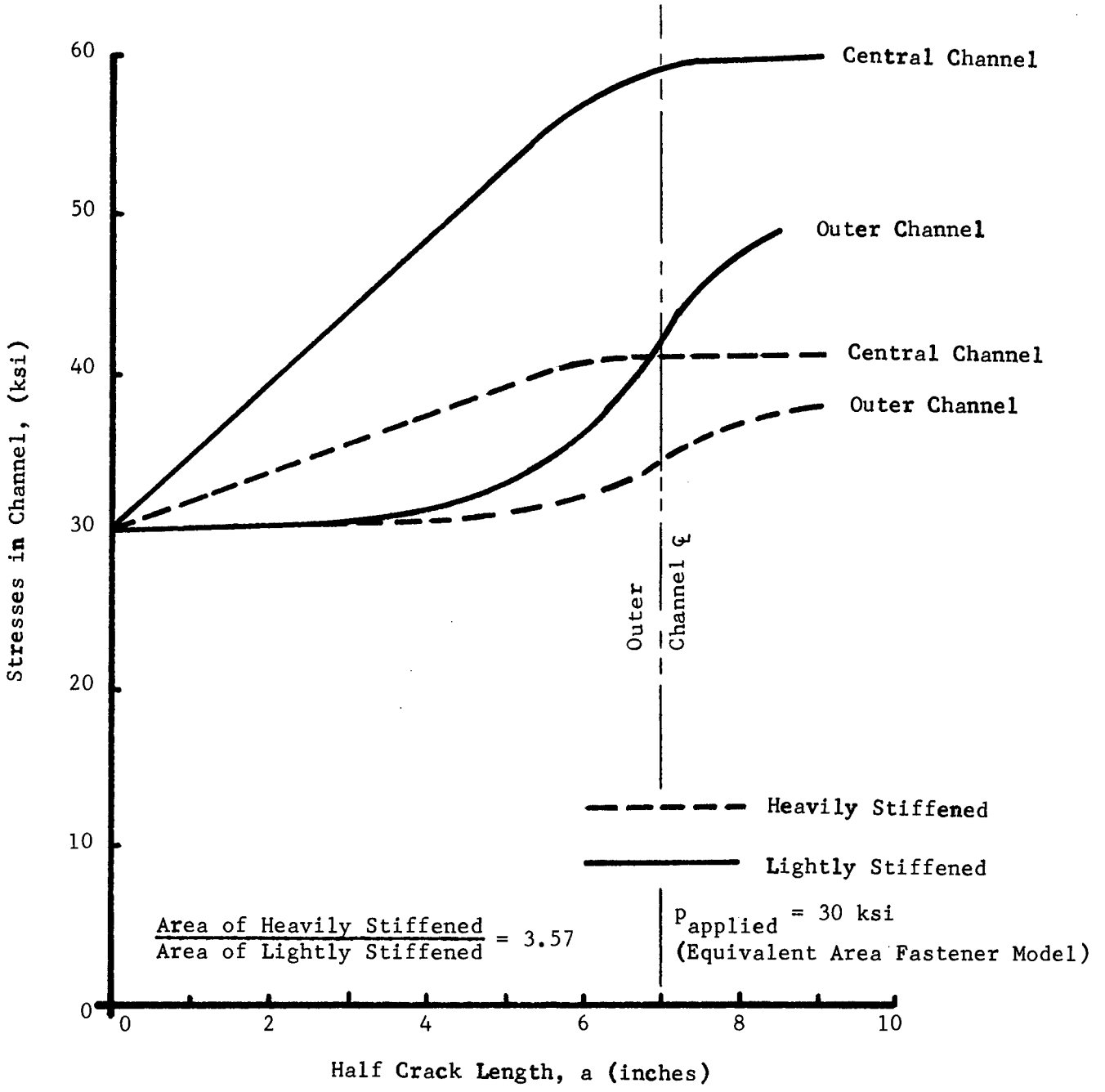

Figure 10. Stresses in the Central and Outer Wing Channels as a Function of Crack Length - Applied Stress = 30 ksi

3.2.2 Effect of Fastener Modeling on Crack Openings and Stresses

Two fastener models, the equivalent area and flexible fastener model, were used to study the effect of fastener modeling for the case of a lightly stiffened wing channel panel. Figure 11 shows analytical crack surface displacements for the two fastener models at half crack lengths of 2.8 inches and 5.4 inches. It is seen that for the flexible fastener model, crack surface displacements are more than fifty percent higher than corresponding displacements for the equivalent area model. These crack surface displacements have considerable effect when computing the stress intensity factors, since in finite element analysis, the stress intensity factors are generally obtained from the crack surface displacements. Thus the elastic stress intensity factors will depend on the assumed flexibility of the fastener. Normalized elastic stress intensity factors $\frac{K}{\sigma\sqrt{\pi a}}$ for the two physical crack lengths are,

$$\frac{K}{\sigma\sqrt{\pi a}} = 0.667, \; a = 2.8 \text{ inches, Flexible Fastener Model}$$

$$\frac{K}{\sigma\sqrt{\pi a}} = 0.587, \; a = 2.8 \text{ inches, Equivalent Area Rivet Model}$$

$$\frac{K}{\sigma\sqrt{\pi a}} = 0.678, \; a = 5.4 \text{ inches, Flexible Fastener Model}$$

$$\frac{K}{\sigma\sqrt{\pi a}} = 0.620, \; a = 5.4 \text{ inches, Equivalent Area Rivet Model}$$

These values of normalized stress intensity factor show a variation of about 12 percent for a physical half crack length of 2.8 inches and 9 percent for a physical half crack length of 5.4 inches.

The effect of fastener modeling on the stress in the outer and central stringer is shown in Figure 12 for the 2.8 and 5.4 inch crack lengths. It is seen that the stresses in the outer stringer are only slightly influenced by the type of fastener used, since the crack has not yet reached the outer stringer, and there are no crack surface displacements at the outer stringer. However, when the crack tip is beyond the outer stringer, the crack surface displacements at the location of the outer stringer and stresses in the outer stringer are affected by the fastener modeling. In Figure 12, it is seen that the stresses in the central stringer are significantly affected by the fastener modeling. Values for the flexible fastener model are about nine percent lower than those obtained for the equivalent area model.

The influence of two fastener models on stresses in the central channel fastener for the same two crack lengths is shown in Figure 13. It is seen that the stresses given by the equivalent area model are extremely high and unrealistic. For example, at an applied stress of 30 ksi the equivalent area model gives stresses almost twice as high as those given by the flexible fastener model. At 30 ksi applied stress and a 5.4 inch half crack length the equivalent area model gives stresses above ultimate strength. Also for a 2.8

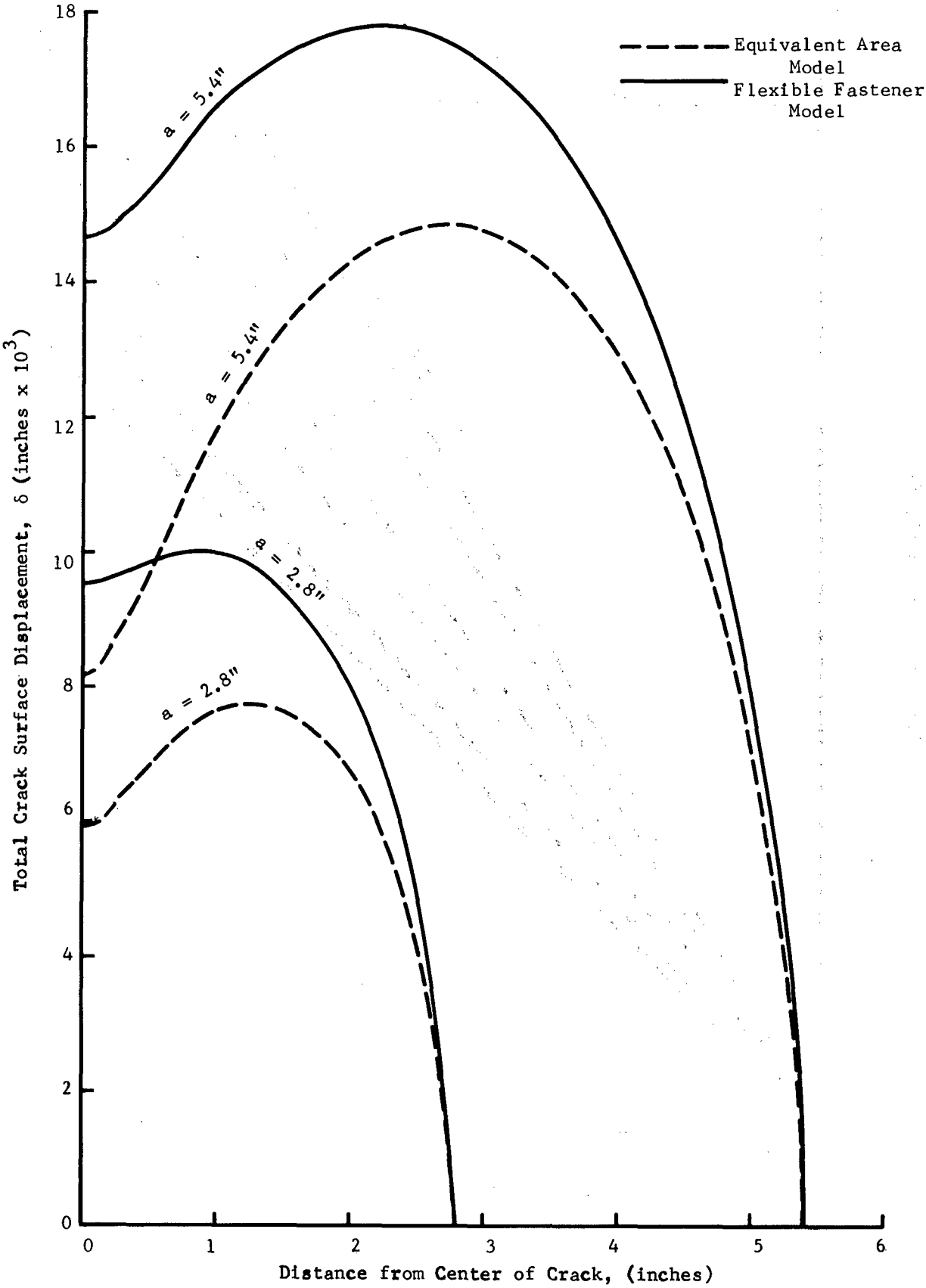

Figure 11. Crack Surface Displacement for Lightly Stiffened Panel for Two Crack Sizes

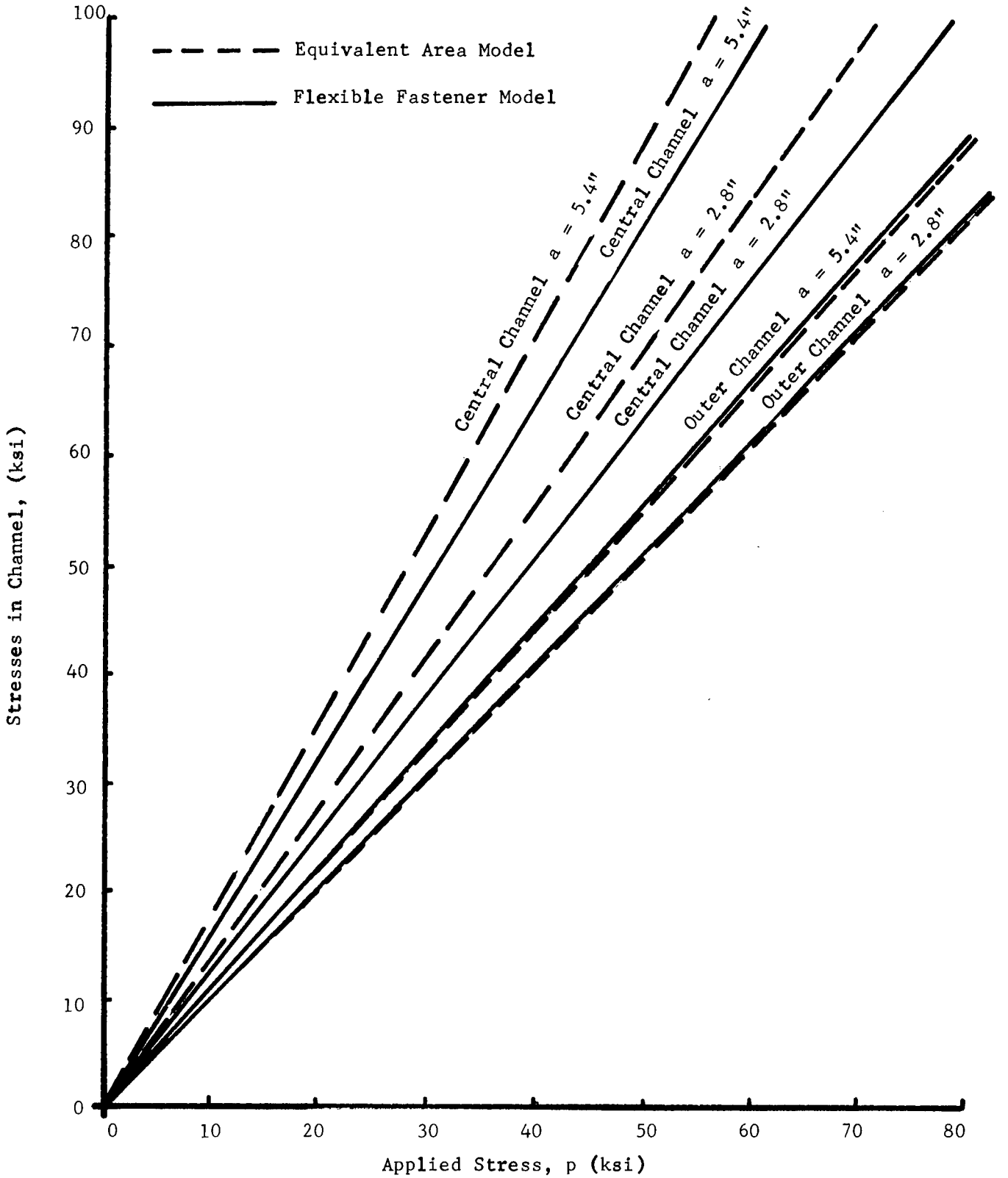

Figure 12. Stresses in Lightly Stiffened Channels as a Function of Applied Stress

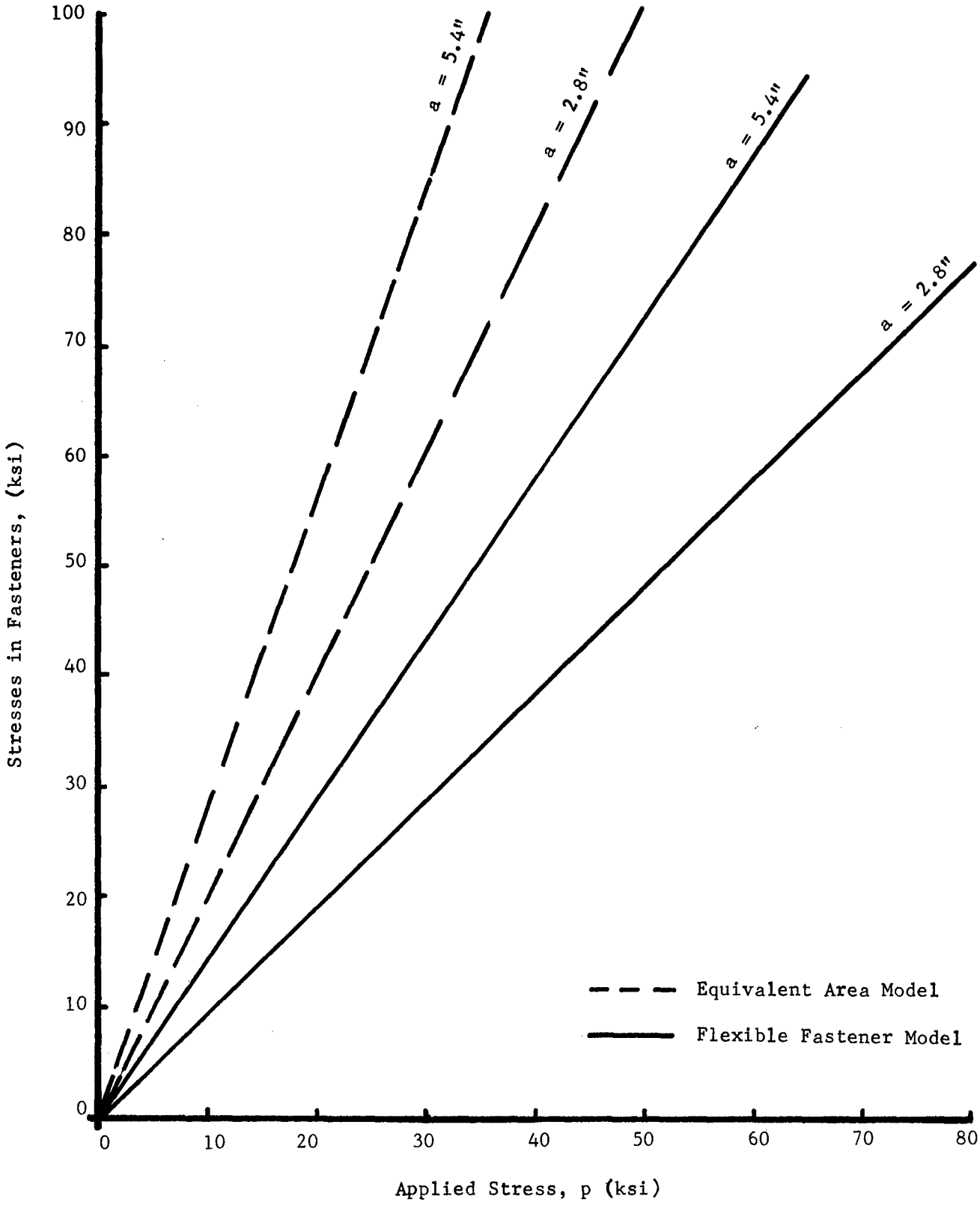

Figure 13. Stresses in the Center Channel Fasteners for Two Crack Lengths - Lightly Stiffened Panel

inch half crack length and an applied stress of 40 ksi the calculated fastener stress is close to ultimate stress. It is unrealistic to assume that these values of stresses could be reached in an actual structure without total failure. In Section 4.4 the testing of this particular wing channel panel will be discussed and it was shown to sustain much higher loads without fastener failure. The experimental data and analytical correlation are discussed in Section 4 using the two fastener models.

3.2.3 Effect of Fastener Modeling on J Integral Calculations

The fastener modeling affects both elastic and elasto-plastic residual strength predictions. The plot of $\sqrt{J}$ versus applied stress (again for the wing channel panel) for an elastic analysis is shown in Figure 14. For both heavily and lightly stiffened cases the value of $\sqrt{J}$ depends on the assumed stiffness of the fastener at both long and short crack lengths. The two fastener models show a variation of about 13 percent in $\sqrt{J}$ values at a half crack length of 2.8 inches and about a 10 percent variation at a half crack length of 5.4 inches. The percentage variation in square root of J obtained from the two models is of the same order of magnitude as the percentage variation in stress intensity.

3.3 ELASTIC-PLASTIC ANALYSIS OF CRACKED STRUCTURES

As discussed in Section 2.4, the elastic-plastic analysis represents a more realistic approach to structural residual strength prediction. However elastic-plastic analysis represents an additional complexity compared to a simple elastic analysis. One of the major factors to be considered is the size and shape of plastic zone ahead of the crack tip. In the present study a Dugdale type plastic zone is proposed for the elastic-plastic analysis. For Dugdale type plastic zones the values of the J integral are directly related to COD and hence values of J can be easily computed. In order to develop confidence in the Dugdale type plastic zone, the analysis of stiffened panels was also carried out assuming Prandtl-Reuss material behavior. Values of J were compared for the two cases. The path independence of J was established by taking several contours. The elastic-plastic analysis will also influence the stresses in the reinforcing members of the structure. These factors including the influence of fastener modeling on elastic-plastic analysis are discussed in following subsections.

3.3.1 Dugdale Model Type Elastic-Plastic Analysis

As mentioned in Section 2.4.3.1, the elastic-plastic analysis of a cracked structure (based on Dugdale type plastic zone assumptions) can be carried out directly if the closed form solutions for stress intensity factors can be obtained. However, if these closed form solutions are not available some iteration method must be used to determine the size of plastic zone. In Reference 18, a method has been suggested for Dugdale model type elastic-plastic analysis. This method has been used in the analysis of this study.

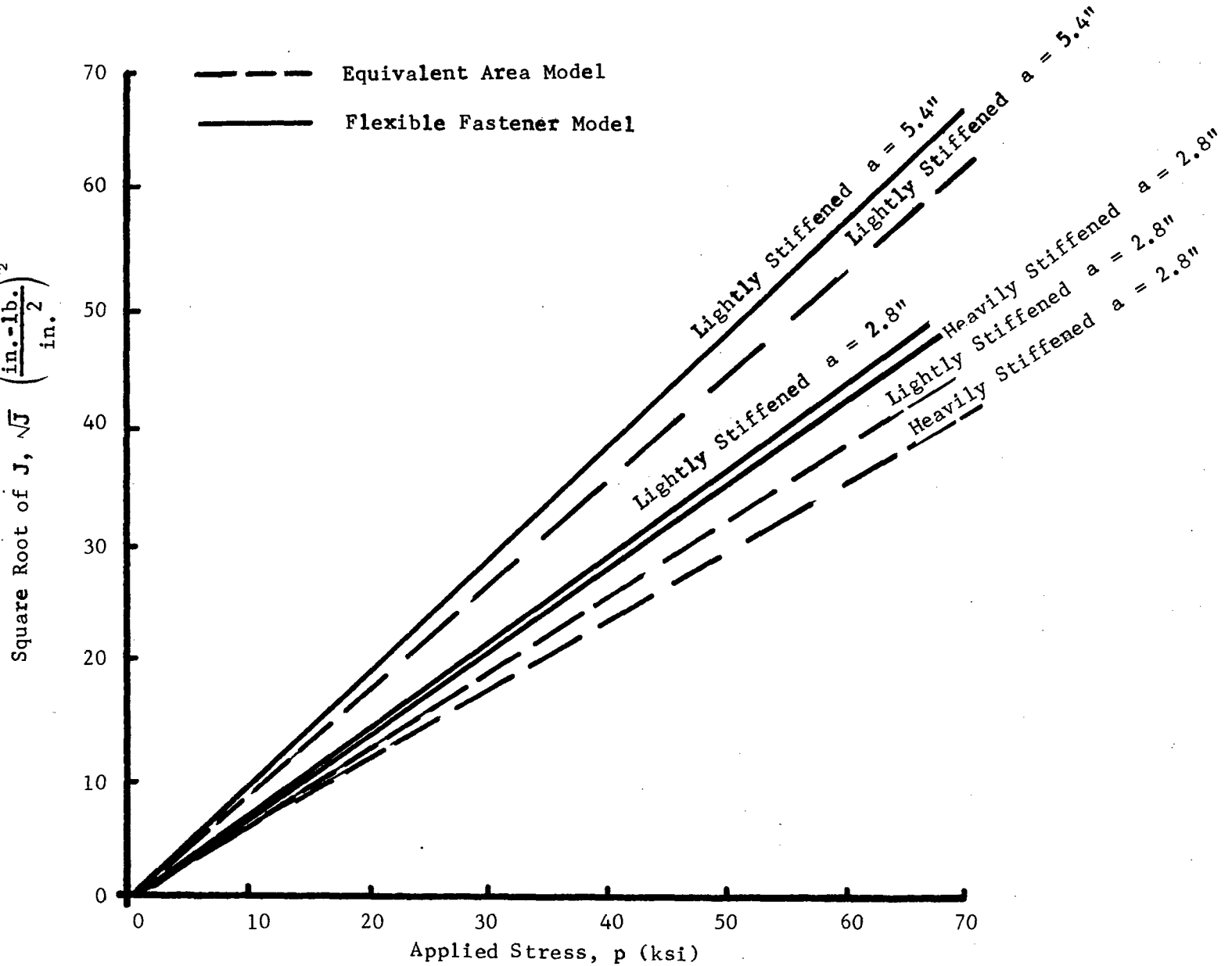

Figure 14. Elastic J Integral Values for Heavily and Lightly Stiffened Wing Channel Panels

3.3.1.1 Bueckner-Hayes Approach for Dugdale Model Analysis

A cracked structure, shown in Figure 15(a), is subjected to stress p. Under this applied load, there is a plastic zone built-up ahead of each crack tips. The plastic zone is assumed to be a Dugdale type, strip zone and the zone is subjected to yield stress F_{ty} opposite to the applied boundary stress as shown in Figure 15(b). The solution to this problem can be obtained by superposition of the cases shown in Figure 15(c-e). Case (c) of Figure 15 gives no singularities and the solution to the original problem (Figures (a) and (b)) essentially consists of obtaining solutions to the cases of Figures 15(d) and (e). It was shown in Reference 18 that the ratio of applied stress (p) to yield stress (F_{ty}) is given by

$$\left(\frac{p}{F_{ty}}\right) = \left[\frac{\left(\frac{\partial U_d}{\partial a_e}\right)_P}{\left(\frac{\partial U_d}{\partial a_e}\right)_F}\right]^{\frac{1}{2}} \qquad (7)$$

where $\left(\frac{\partial U_d}{\partial a_e}\right)_P$ is the derivative of strain energy for the case when the plastic zone is subjected only to yield stress as shown in Figure 15(e), and $\left(\frac{\partial U_d}{\partial a_e}\right)_F$ is the derivative of strain energy for the case when the crack is fully loaded with stress p as shown in Figure 15(d).

The elastic-plastic analysis based on the Bueckner-Hayes approach consists of the following steps:

1. For a particular physical crack length 2a, select various plastic zone lengths and effective crack lengths (i.e. physical crack length + plastic zone) a_e, a_{e1}, a_{e2}, etc.

2. Perform a finite element analysis of the structure with crack lengths a_1, a_2, etc. such that the crack surfaces are loaded with uniform stress σ (e.g. 30 ksi).

3. Perform the finite element analysis of the structure with crack lengths a_{e1}, a_{e2}, etc., containing only plastic zone lengths a_{e1}-a, a_{e2}-a, etc., loaded with the same stress σ.

4. Obtain the strain energy U_d of the system for each partially and fully loaded case. The strain energy associated with the presence of a crack is then given by

$$U_d = \int_0^{a_e} \sigma\, v(x)\, dx \qquad \text{(fully loaded case)} \qquad (8)$$

$$U_d = \int_a^{a_e} \sigma\, v(x)\, dx \qquad \text{(partially loaded case).} \qquad (9)$$

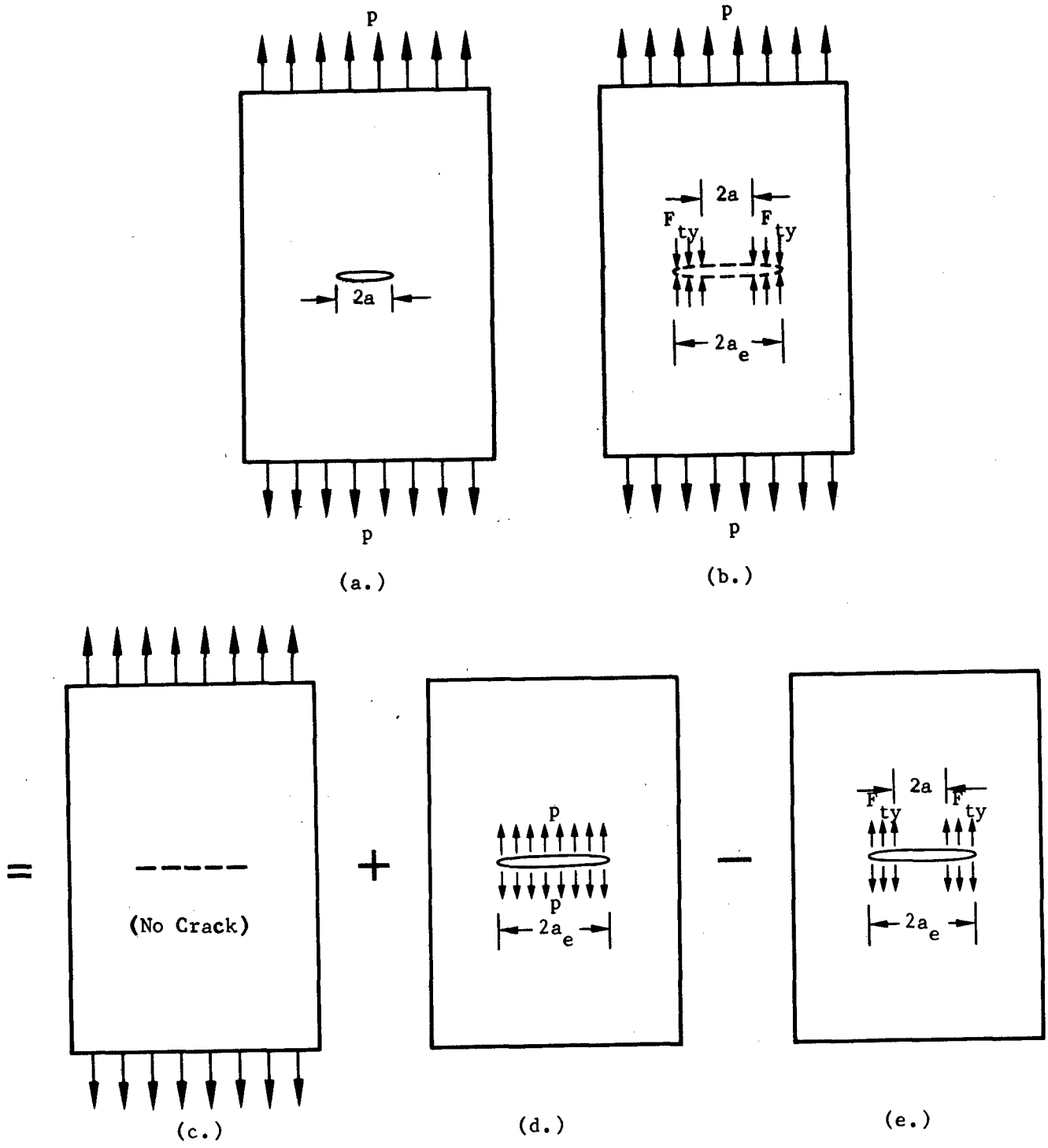

Figure 15. Superposition Technique for Dugdale Type Analysis

5. Obtain the rate of change in strain energy with respect to crack length for fully and partially loaded cases. Corresponding to a given plastic zone size, the ratio of applied stress to yield stress is determined by solving Equation 7. The details of this procedure are discussed in References 1 and 34.

Reference 34 recommends that the derivative of strain energy with respect to crack length be determined by central difference formulas. However this procedure works only for the case of unstiffened panels where the strain energy U_d is a smooth function of crack length. For a stiffened panel U_d is a continuous function of crack length but the function is not smooth when plastic zones are in the vicinity of the stiffeners. Hence the strain energy derivative obtained by using strict central difference methods tends to give erroneous results for stiffened panel geometries. Good results are obtained by plotting a curve between strain energy (U_d) and crack length (a_e) and determining the strain energy derivative directly from the curve.

6. Obtain the crack opening displacement (COD) by using

$$\delta = 2\left[\frac{P}{\sigma} v_F - \frac{F_{ty}}{\sigma} v_p\right]$$

or

$$\delta = 2\,\frac{F_{ty}}{\sigma}\left[\frac{P}{F_{ty}} v_F - v_p\right] \qquad (10)$$

where δ = crack opening displacement at the end of the physical crack tip

v_F = crack surface opening at the location of the physical crack for a fully loaded case with an effective crack length a_e and

v_p = crack surface opening at the location of the physical crack for a partially loaded case with effective crack length a_e. σ is the constant applied stress on the crack surface in the finite element analysis (Reference 34).

For a Dugdale type plastic zone the relationship between the J integral and crack opening displacement is

$$J = F_{ty}\delta \,. \qquad (11)$$

The values of J integral are obtained from Equation (1) for each value of δ.

3.3.1.2 Dugdale Model Type Elastic-Plastic Analysis of Heavily Stiffened Wing Channel Panel

Both the heavily and lightly stiffened wing channel panel described in Section 3.1 were analyzed using the Bueckner-Hayes approach just described in Section 3.3.1.1. For the heavily stiffened wing channel panel (see Figure 5) physical crack lengths of 2, 2.8, 4, 5.4, 6.6, 7.2, and 7.8 were investigated using an equivalent area fastener model. Strain energy (U_d) for various effective crack lengths for both partially and fully loaded cases were calculated and the results are shown in Table I. The procedure of Section 6.1.2.1 of Reference 1 was followed in calculating the values of U_d, $\frac{\partial U_d}{\partial a_e}$, $\frac{p}{F_{ty}}$, δ, and the stress required to produce the given plastic zone, p.

The relation between $\sqrt{J}$ and applied stress p, for various physical half crack lengths 'a' is shown in Figure 16. These data are cross plotted in Figure 17 for constant stress levels for the seven physical crack lengths investigated. The following trends are observed:

1. For a constant physical crack size, the values of $\sqrt{J}$ increase with applied stress, p, as shown in Figure 16.

2. For the same applied stress, the values of $\sqrt{J}$ increase with physical crack length up to a crack length of 5.4 inches. With increasing crack length the values of $\sqrt{J}$ decrease as seen in Figure 17.

3. If the center wing channel is broken the $\sqrt{J}$ increases drastically over that for the same crack length with the center stringer intact.

In Figure 16 the initial portion of the $\sqrt{J}$ versus p curve is established from an elastic calculation of $\frac{\partial U}{\partial a}$ since $\frac{\partial U}{\partial a} \approx G$ in the elastic case. The significance of these calculations can be seen in Figure 17 which indicates the large load transfer (at the edge wing channels) as the crack approaches the channel. These results are reminiscent of the elastic, closed form solutions for K reported by Poe for reinforced structure (Reference 5); however, in this case the effect of plasticity has been included in $\sqrt{J}$ through the Dugdale (Bueckner-Hayes method) plastic zone calculation. For this panel configuration the skin area is about 27% of the channel area and would thus represent an extreme case of a heavily stiffened panel. The data of Figure 17 verify this statement and indicate limited nonlinear behavior due to the presence of the large stiffener areas available for load transfer.

The computer time involved in solving for the $\sqrt{J}$ for these seven crack lengths on an IBM 370/165 computer are shown in Table II.

TABLE I. DUGDALE ZONE CALCULATIONS

Physical Crack Length (inches)	Crack + Plastic Zone (inches)	U_d (F) (in.-lb./in.)	$\left(\frac{\partial U_d}{\partial a_e}\right)_{(F)}$ (lb./in.)	$V_f \times 10^{-2}$ (inches)	U_d (P) (in.-lb./in.)	$\left(\frac{\partial U_d}{\partial a_e}\right)_{(p)}$ (lb./in.)	$V_p \times 10^{-2}$ (inches)	p (ksi)	δ_c (inches)	$\left(\frac{\sqrt{J}}{\left(\frac{\text{in.-lb.}}{\text{in.}^2}\right)^{\frac{1}{2}}}\right)$
2.0	2.2	10162	8407	1.705	147.6	2226	.465	36.4	.0037	16.2
	2.6	13525	9024	3.056	1038	3149	.986	42.0	.0073	22.8
	3.0	17381	10526	3.967	2667	4401	1.547	46.0	.0092	25.5
	3.6	24051	12110	4.983	6457	7550	2.293	56.0	.0146	32.2
	4.2	31893	14163	5.774	11730	10128	2.938	60.0	.0175	35.2
	5.0	43842	15870	6.612	20637	12713	3.677	63.5	.0201	37.8
2.0	6.0	60460	16618	7.392	34615	13978	4.373	65.0	.0215	39.2
2.8	3.0	17381	10526	1.941	148.9	2742	.469	36.2	.0047	18.2
	3.6	24051	12110	4.122	1794	4178	1.317	41.7	.0099	26.5
	4.2	31893	14163	5.460	5163	6500	2.165	48.1	.0137	31.2
	5.0	43842	15870	6.751	10894	10348	3.147	57.4	.0206	38.3
	6.0	60460	16140	7.891	23789	12662	4.083	62.9	.0260	43.0
	6.4	67037	15542	8.215	28896	12315	4.368	63.2	.0263	43.2
	6.8	72894	13417	8.451	33641	11150	4.580	64.8	.0280	44.6
2.8	7.0	75087	10965	8.529	35586	9725	4.651	66.9	.0303	46.4
2.8	3.0	251042	97343	8.637	153.6	3011	.484	12.5	.0093	25.7
Center	3.6	309448	97732	20.599	1961	4865	1.519	15.8	.0275	44.2
Wing	4.2	368321	107102	28.305	5991	9232	2.756	20.8	.0496	59.4
Channel	5.0	495391	105074	36.314	14886	13778	4.538	25.7	.0770	74.0
Broken	6.0	557454	85364	43.422	30792	15826	6.435	30.6	.1099	88.4
	6.4	594670	79240	45.400	37723	16542	7.083	32.45	.1222	93.2
	6.8	620846	59082	46.762	44026	14693	7.577	35.4	.1405	99.9
2.8	7.0	630119	46365	47.184	46539	12565	7.744	36.9	.1502	103.3
4.0	4.2	31893	13964	2.240	149.8	1308	.472	21.7	.0019	11.65
	4.6	37673	14936	4.104	1066	3270	1.031	33.2	.00795	23.8
	5.0	43842	15870	5.403	2766	5543	1.653	42.0	.0138	31.3
	6.0	60460	15622	7.461	10128	8274	2.980	51.7	.0219	39.45

Table I (continued)

Physical Crack Length (inches)	Crack + Plastic Zone (inches)	U_d (F) (in.-lb./in.)	$\left(\frac{\partial U_d}{\partial a_e}\right)_{(F)}$ (lb./in.)	$V_f \times 10^{-2}$ (inches)	U_d (P) (in.-lb./in.)	$\left(\frac{\partial U_d}{\partial a_e}\right)_{(p)}$ (lb./in.)	$V_p \times 10^{-2}$ (inches)	p (ksi)	δ_c (inches)	$\sqrt{J}$ $\left(\frac{\text{in.-lb.}}{\text{in.}^2}\right)^{\frac{1}{2}}$
↓	6.4	67037	15542	8.001	13926	9461	3.385	55.45	.0256	42.6
	6.8	72894	13417	8.382	17697	8980	3.689	58.1	.0283	44.8
4.0	7.0	75087	10965	8.505	19314	8085	3.791	61.0	.03145	47.2
5.4	6.0	60460	--	4.518	1056	--	1.019	--	--	--
↓	6.4	67037	15542	5.759	2678	4674	1.593	38.9	.0140	31.5
	6.8	72894	13417	6.535	4795	5292	2.043	44.6	.0184	36.2
	7.0	75087	6780	6.770	5855	3070	2.197	47.8	.0211	38.7
	7.2	75606	2918	6.809	6023	1765	2.220	55.2	.0275	44.2
	7.6	76838	3445	6.858	6914	2719	2.259	63.1	.0343	49.3
	8.0	78362	4639	6.891	8198	4215	2.289	67.7	.0383	52.1
5.4	8.4	80549	5468	6.924	10286	5220	2.320	69.4	.0398	53.1
6.6	6.8	72894	--	2.237	144	--	.455	--	--	--
↓	7.0	75087	6780	3.088	474	1052	.640	28.0	.0052	19.1
	7.2	75606	2918	3.190	565	1303	.643	47.45	.0133	30.8
	7.6	76838	3445	3.304	1256	2132	.717	55.9	.0168	34.6
	8.0	78362	4639	3.370	2271	3840	.770	64.6	.0205	38.2
	8.4	80549	5708	3.433	4328	5189	.827	67.7	.0219	39.4
6.6	8.8	82928	5948	3.479	6422	5235	.869	66.6	.0214	39.0
7.2	7.4	78584	--	1.666	138	--	.434	--	--	--
↓	7.6	79815	5788	2.209	454	2050	.589	42.25	.0065	21.5
	8.0	82057	6766	2.783	1368	3631	.9055	52.0	.0101	26.8
	8.4	85228	7555	3.197	3359	5078	1.227	58.2	.0125	29.8
	8.8	88101	9381	3.451	5430	7381	1.433	63.0	.0146	32.2
7.2	9.4	94609	10847	3.827	10740	8850	1.767	64.1	.0151	32.8
7.8	8.0	82057	--	1.333	124	--	.391	--	--	--
↓	8.4	85228	7550	2.591	1185	3215	1.023	46.3	.0056	19.8
	8.8	88101	9381	3.201	2696	5874	1.383	56.2	.0103	27.0
	9.4	94609	13197	4.044	7059	9657	2.046	60.7	.0126	30.0
7.8	10.0	103937	15546	4.929	14284	12042	2.805	62.5	.0137	31.2

NOTES - Applied Stress Corresponding to U_d Values is 158,730 psi Fty = 71,000 psi
(P), p = Partially Loaded Crack
(F), f = Fully Loaded Crack

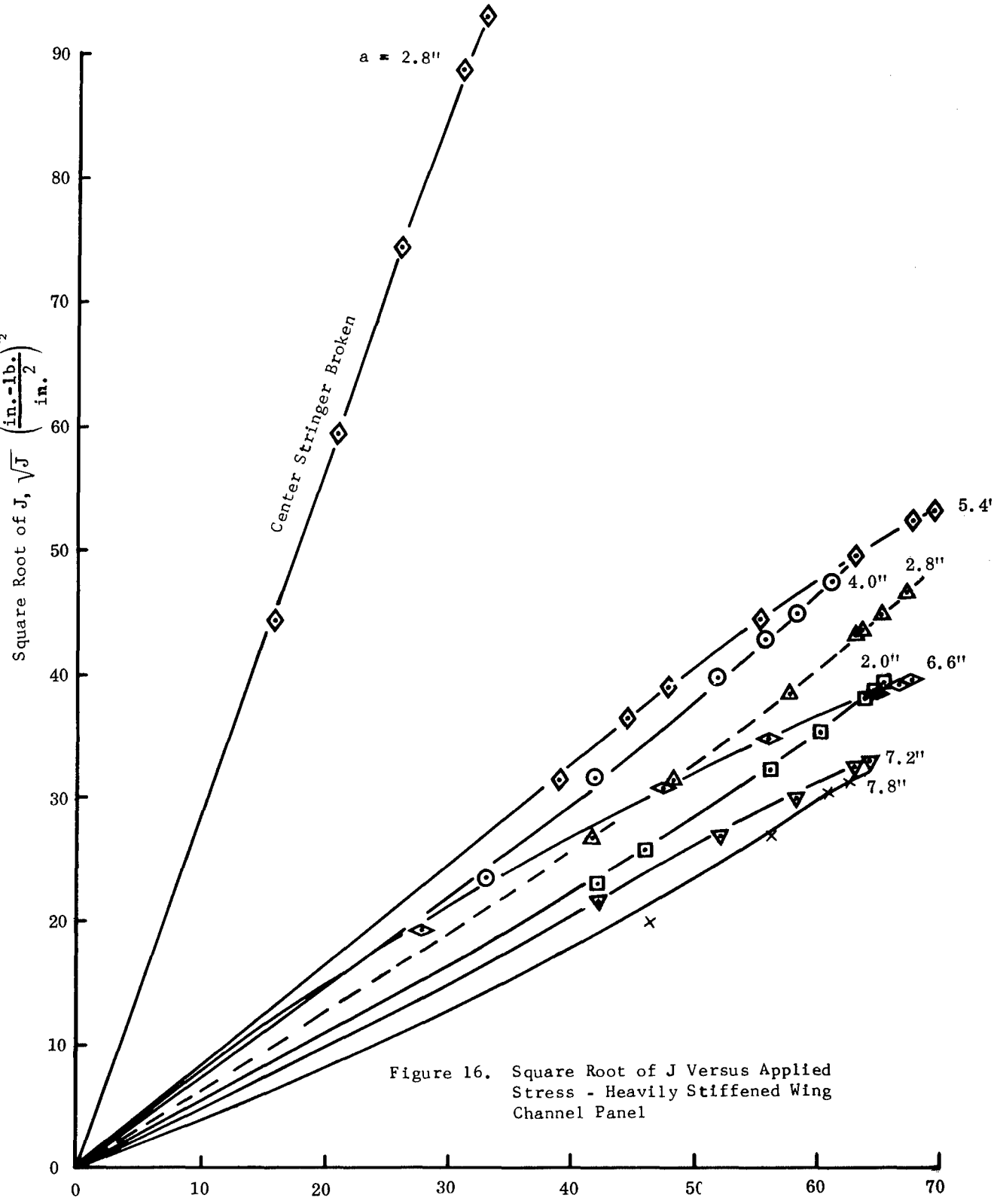

Figure 16. Square Root of J Versus Applied Stress - Heavily Stiffened Wing Channel Panel

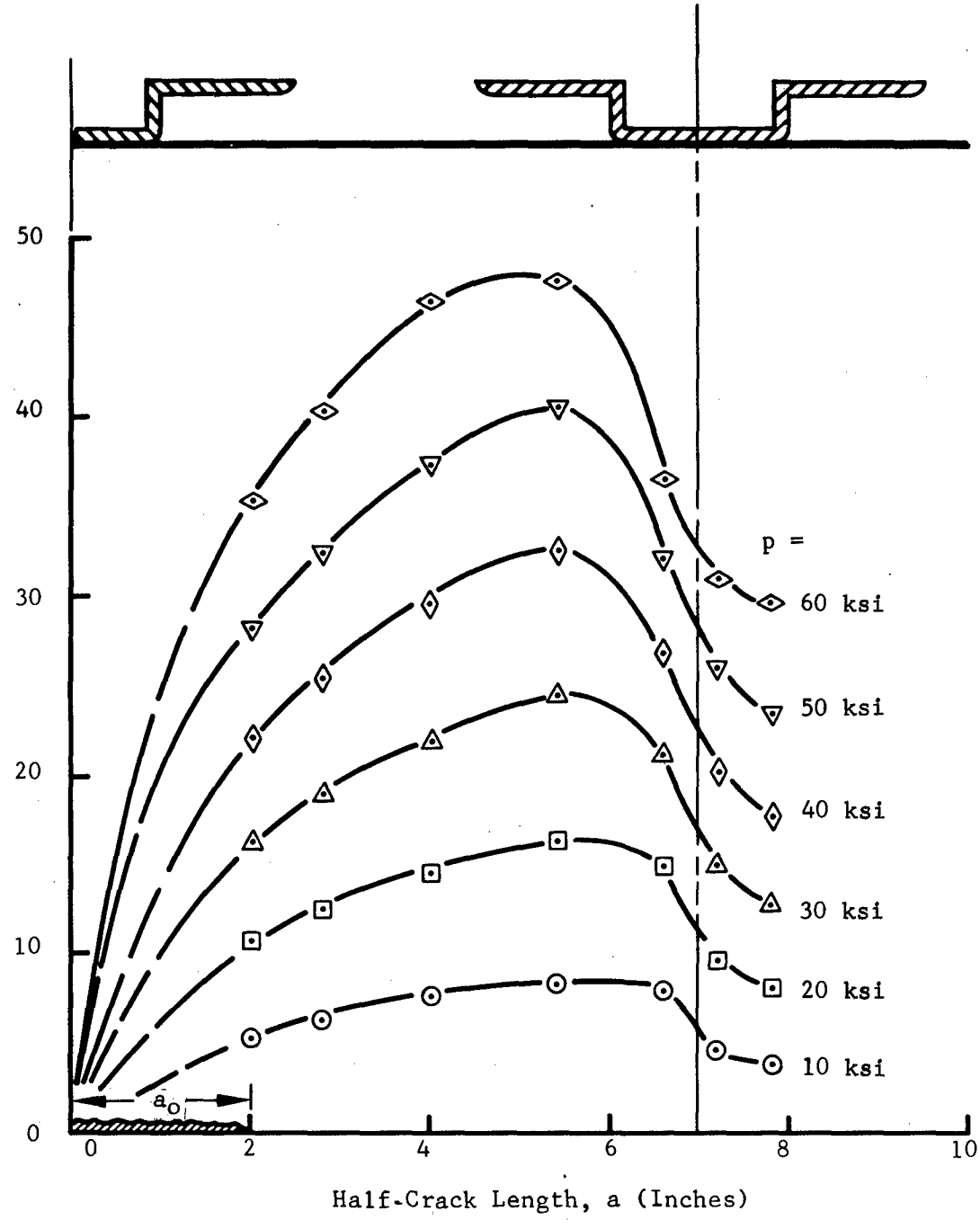

Figure 17. Square Root of J as Function of Crack Size at Constant Stress, Heavily Stiffened Wing Channel Panel

TABLE II. IBM 370/165 RUN TIME FOR DUGDALE SOLUTIONS - WING CHANNEL INTACT

CRACK LENGTH, a (INCHES)	LOAD CASES EXAMINED	TIME (MIN.)	
		CPU	I/O
2.0	14	11.52	5.89
2.8	11	8.14	4.07
4.0	8	6.17	2.54
5.4	13	8.44	3.28
6.6	8	6.48	2.55
7.2	12	5.70	2.46
7.8	6	5.65	2.05
	TOTALS:	52.10	22.84

At first glance the total run times appear excessive. However, the trend of Figure 17 is not unexpected and could have been established from Dugdale calculations for only four crack lengths without loss of accuracy. This would have reduced CPU and I/O time by about 40%. In other words once the general trend of $\sqrt{J}$ versus crack length is established for a given substructure/skin configuration, variations in substructure parameters (I, $\bar{y}$, etc.) can be treated with ease. This would require calculations at relatively few crack lengths to observe trends over those of any previously examined structural configuration.

3.3.1.3 Dugdale Model Type Elastic-Plastic Analysis of a Lightly Stiffened Wing Channel Panel

The Dugdale model (Bueckner-Hayes) type elastic-plastic analysis of a lightly stiffened wing channel panel (see Figure 7), was carried out for physical half crack lengths (a) of 2.8, 5.4, 6.6, and 7.8 inches. The same plastic zone sizes were used as employed for the heavily stiffened wing channel panel. The calculations of J used the same finite element idealization as in the heavily stiffened case with appropriate changes to account for differences in wing channel geometry.

The square roots of the J integral for the heavily stiffened and lightly stiffened cases for inelastic behavior as functions of applied stress are compared in Figure 18 for discrete values of physical half crack length. Once again, J has been computed from the relation $J = F_{ty}\,\delta$, where δ is the crack opening displacement (COD). The differences in J between the two cases amounts to approximately 20% to 25% for crack lengths greater than 2.8 inches with the heavily stiffened panels requiring a higher stress to obtain a given value of $\sqrt{J}$ at the same physical crack length with increasing plastic zone size. This trend is more evident in Figure 19 where a cross plot of the data of Figure 18 has been superimposed on the heavily stiffened case at constant stress. Two distinct trends are evident from Figure 19.

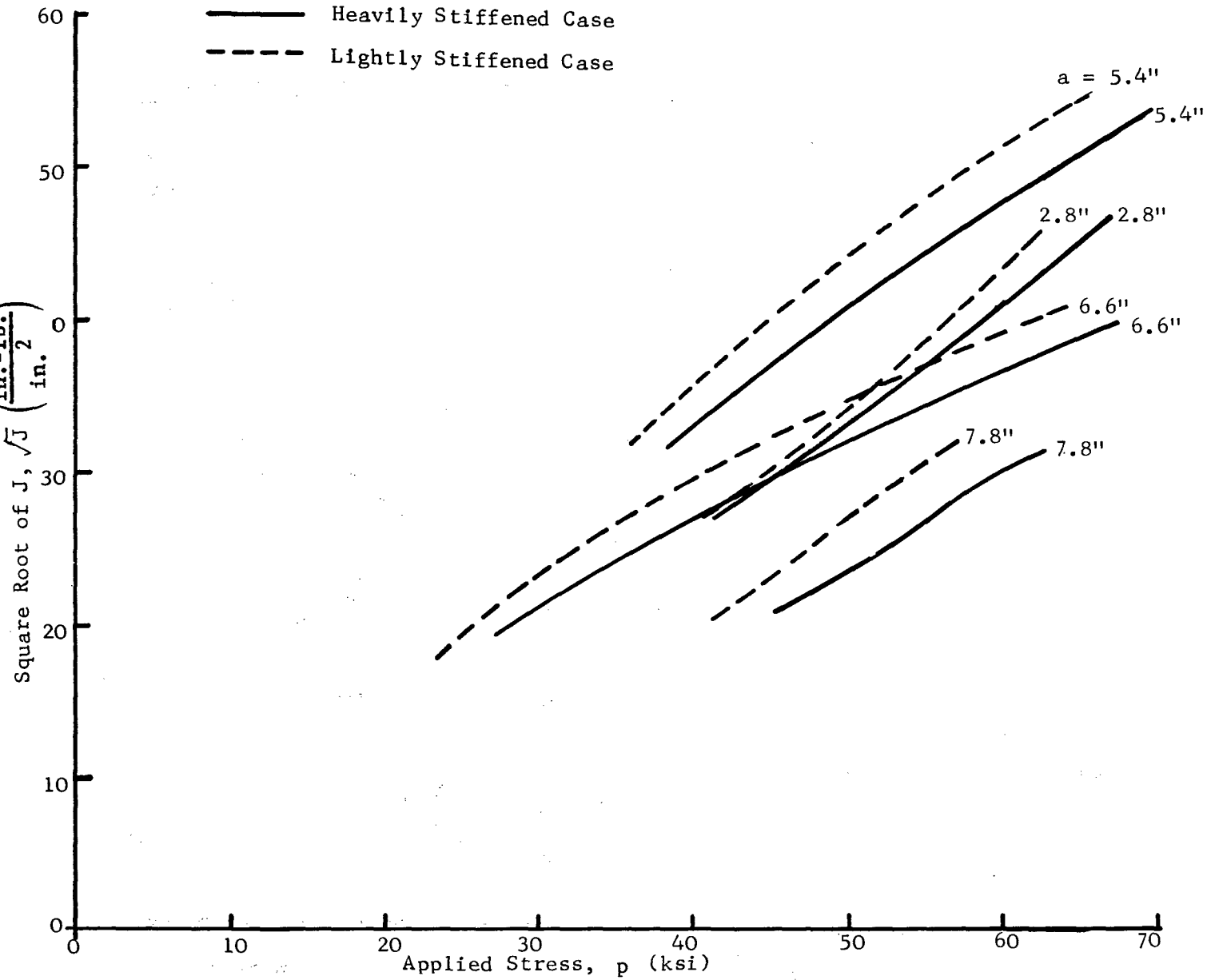

Figure 18. Comparison of Heavily and Lightly Stiffened Computed J Values Using the Dugdale, Bueckner-Hayes Approach

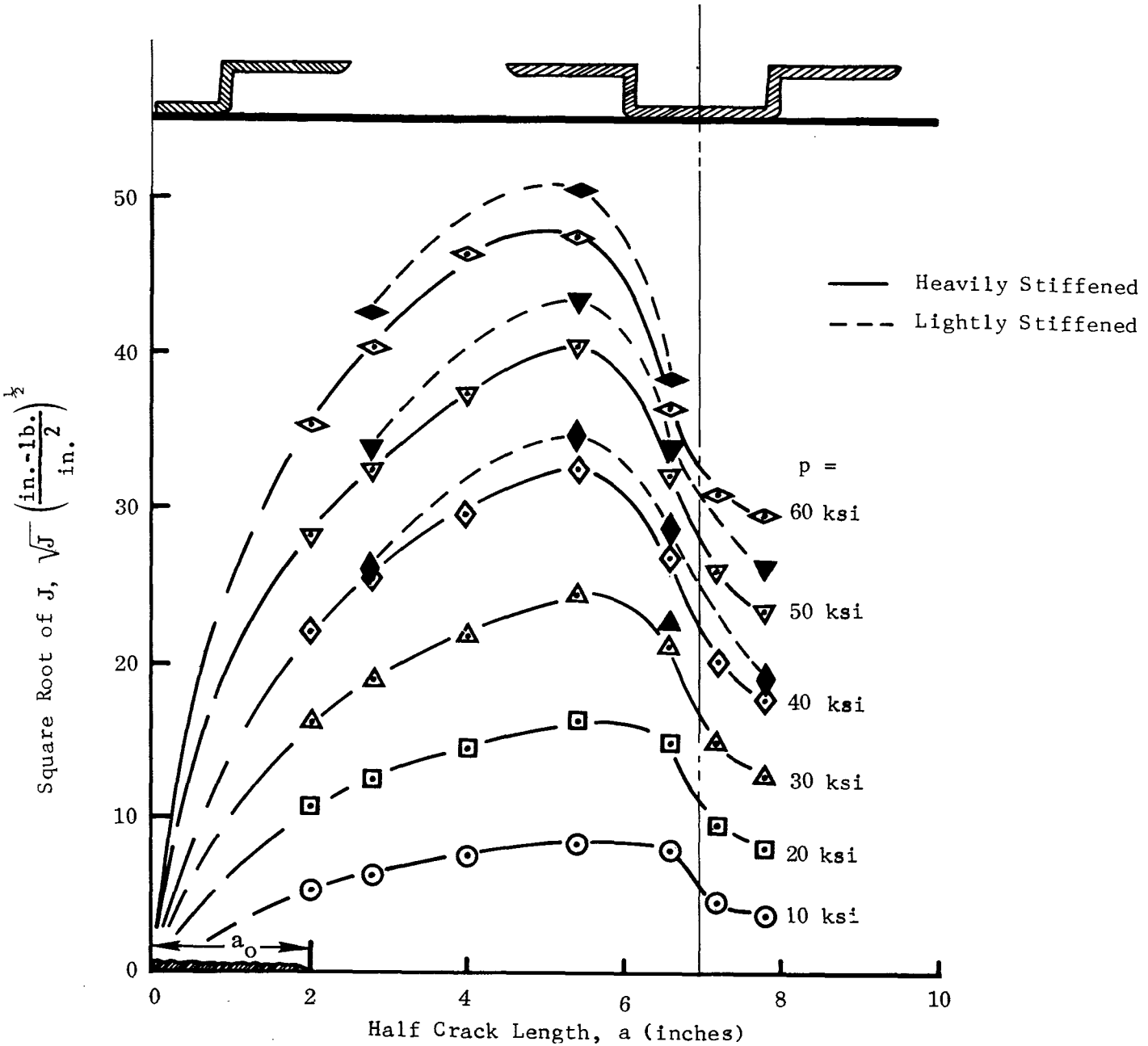

Figure 19. Comparison of Square Root of J Values at Constant Stress for Heavily and Lightly Stiffened Wing Channel Stiffened Panels

1. Increasing stress produces larger differences in $\sqrt{J}$ for any given crack size--the lightly stiffened panels having the higher value of J.

2. Smaller crack size (or crack length to stringer spacing ratios) result in small differences (<10%) in J for applied stress levels up to 86% of F_{ty}.

In addition, load transfer to the edge wing channels also occurs for the lightly stiffened case as the crack approaches the channel. The extent of this load transfer is smaller, as would be expected, than in the heavily stiffened case.

Figures 20(a) and 20(b) show the plot of plastic zone size versus p/F_{ty} for lightly and heavily stiffened wing channel panels with various crack lengths. It is observed that for the same crack length and normalized applied stress (p/F_{ty}) the plastic zone size for the lightly stiffened panel is larger than that for the heavily stiffened case.

The crack opening displacement (COD) at the center of the crack for physical crack lengths of 5.4 inches and 6.6 inches is shown in Figure 21 as a function of ratio of applied stress to yield stress. As anticipated, the COD at the center of crack for the heavily stiffened panel is smaller than that for the lightly stiffened panel. It can also be seen that the crack openings are almost a linear function of applied stress between p/F_{ty} ratios of 0.4 and 0.9.

3.3.2 Analysis Based on Prandtl-Reuss Material Behavior

In Section 3.3.1 the elastic-plastic analysis of cracked stiffened panels based on Dugdale type strip plastic zones assumptions ahead of the crack tips were examined. The Dugdale type elastic-plastic analysis is based on elastic-perfectly plastic material behavior assuming constant stress equal to the material yield stress in the plastic zone. This assumption may seem presumptious in light of the application here to a work-hardening metal such as aluminum alloys. However, elastic-plastic analysis based on Dugdale plasticity has shown good agreement with experimental data. In this program analytical results obtained by Dugdale type analysis have been compared with those based on Prandtl-Reuss material behavior. In the Prandtl-Reuss theory, the total strain in the plastic range is considered to be the sum of the elastic strain and the plastic or permanent strain. Here the elastic strain is defined as the decrease in strain during unloading and the plastic or permanent strain is the strain observed after complete unloading. The mathematical details for Prandtl-Reuss material behavior are discussed fully in Reference 37, and the mathematical details applicable to J integral calculations are discussed in References 34 and 1.

In order to establish the suitability of the J integral as a failure criterion for structural residual strength it is necessary to show that this integral is path independent for stiffened structures. Rice, Reference 8, showed the path independence of J based on the unique relationship of strain energy density (W) and strain state for a material deforming according to the Hencky theory of plasticity. The path independence for J for Prandtl-

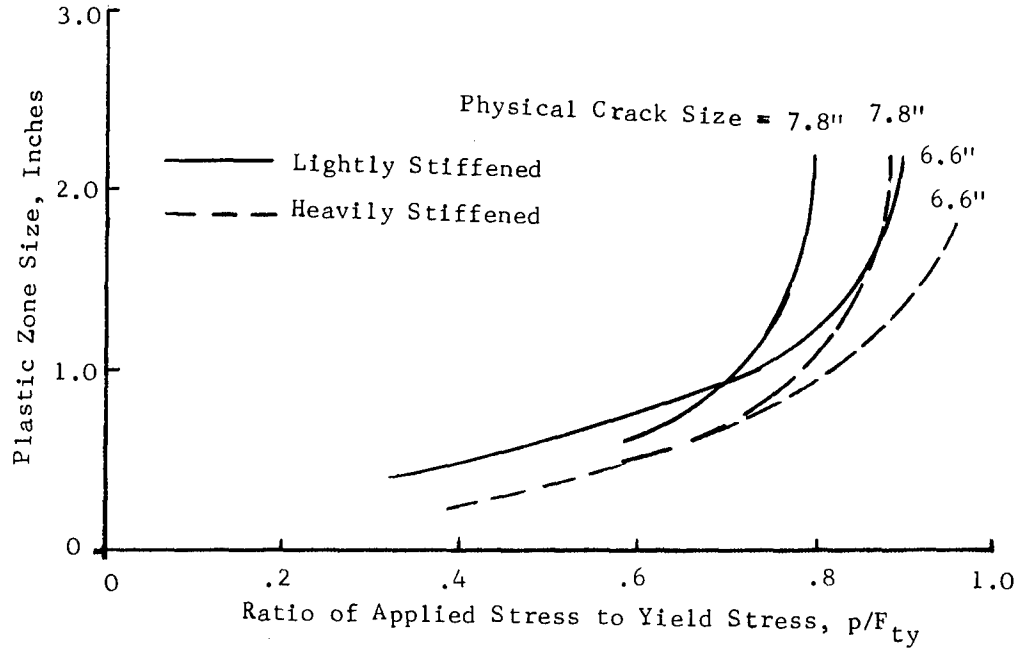

(a.)

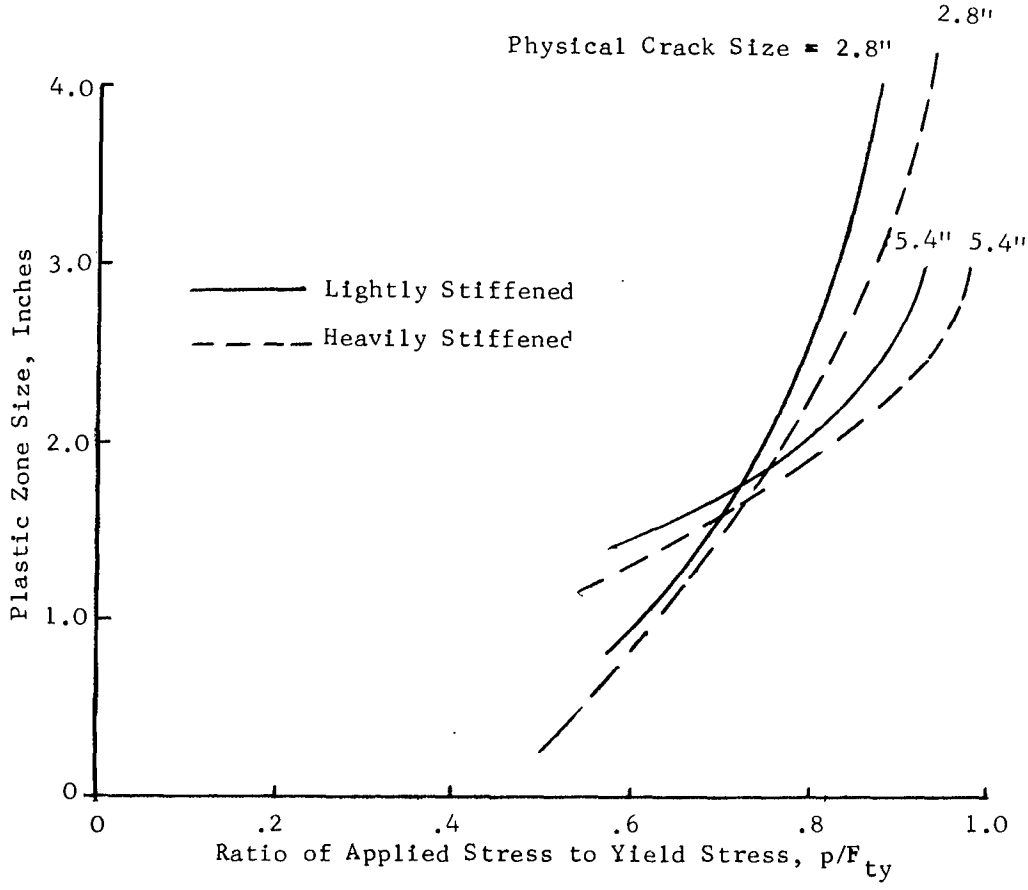

(b.)

Figure 20. Plastic Zone Size for Lightly and Heavily Stiffened Wing Channel

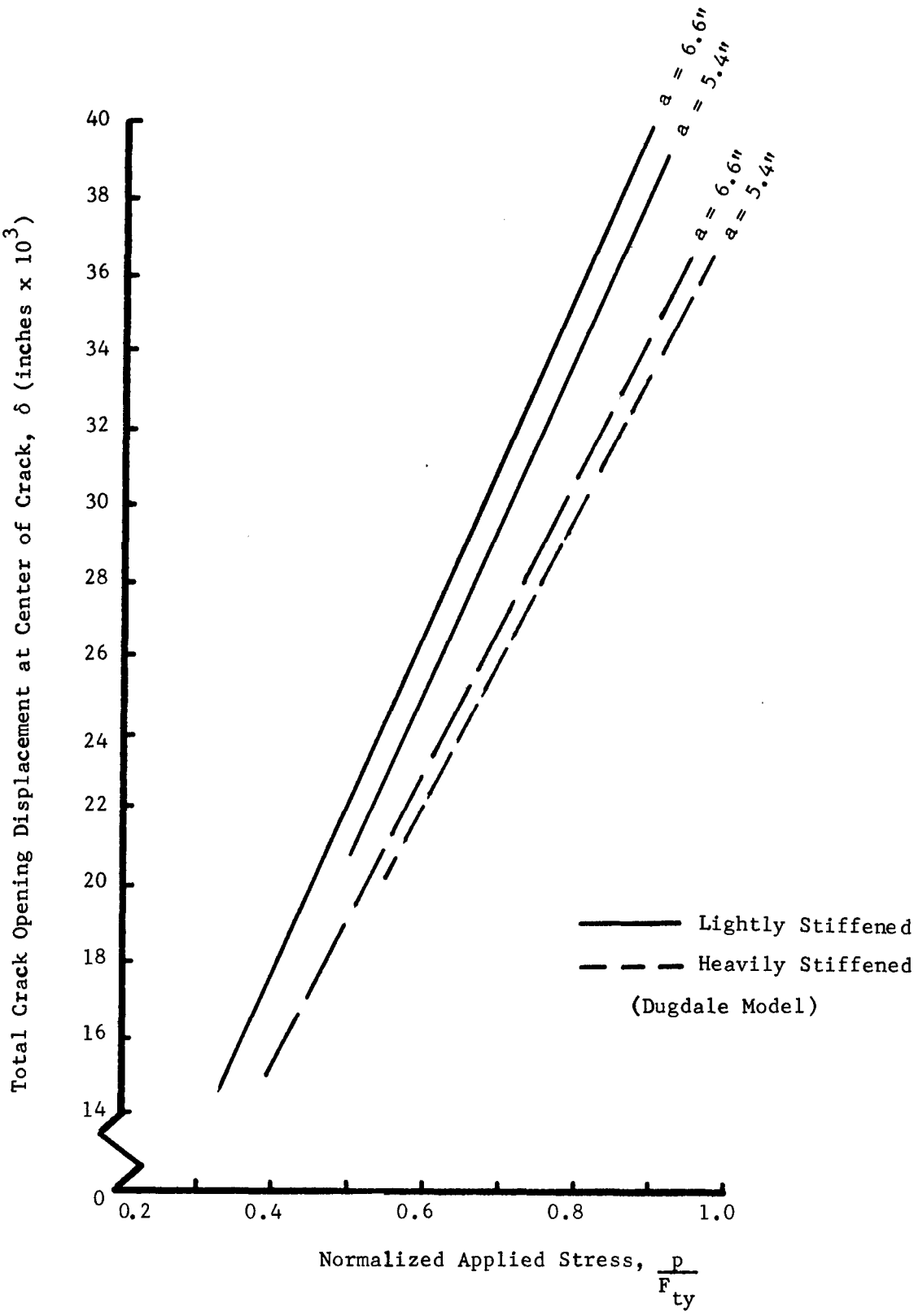

Figure 21. Crack Opening Displacement for Lightly and Heavily Stiffened Wing Channel Panel - Dugdale Analysis

Reuss material behavior has not been shown mathematically. The path independence of the J integral and the effect of Prandtl-Reuss material behavior on J are discussed in the following subsections.

3.3.2.1 Path Independence of J Integral

The J integral has been shown to be path independent for simple unreinforced panels. In Reference 34 Hayes showed the path independence of the J integral for Prandtl-Reuss material behavior using finite element analysis. Although the "proof" of path independence of J for such materials was later shown to be incorrect it has been shown that numerical path independence can be maintained up to net section yield if care is taken with the numerical solutions (Reference 38). In this study the path independence of the J integral is shown for stiffened panels by taking contours in several different paths.

The J integral is defined as:

$$J = \int_{\Gamma} \{W(\epsilon)\, dy - \vec{T} \cdot \frac{\partial \vec{u}}{\partial x}\, ds\} \tag{12}$$

where W is defined as the strain energy density and given by:

$$W = \int [\sigma_x d\epsilon_x + \tau_{xy} d\gamma_{xy} + \tau_{xz} d\gamma_{xz} + \sigma_y d\epsilon_y + \tau_{yz} d\gamma_{yz} + \sigma_z d\epsilon_z] \; . \tag{13}$$

For plane stress conditions:

$$W = \int [\sigma_x d\epsilon_x + \tau_{xy} d\gamma_{xy} + \sigma_y d\epsilon_y] \tag{14}$$

The contour integral J is evaluated along the curve Γ which is, in principle, any curve surrounding the crack tip. The positive direction of s in traversing Γ is counterclockwise. For ease in evaluation of J, the curve Γ can be taken in a rectangular path. Then dy will be nonzero only for those portions of Γ which parallel the y (i.e., loading) axis. Thus W need be evaluated only for those portions of Γ for which dy is nonzero, which simplifies the computation of J.

Following the details of calculations given in Reference 1, Equation (14) reduces to:

$$W = \frac{1}{2E} [\sigma_x + \sigma_y]^2 + \frac{1+\nu}{E} [(\tau_{xy})^2 - \sigma_x \sigma_y] + \int \bar{\sigma} d\bar{\epsilon}_p$$

where $\bar{\sigma}$ and $\bar{\epsilon}_p$ are equivalent stress and equivalent plastic strain, respectively, and the equivalent stress is given as:

$$\bar{\sigma} = [\sigma^2_x - \sigma_x \sigma_y + \sigma^2_y + 3\tau_{xy}{}^2]^{\frac{1}{2}} \tag{15}$$

To illustrate the steps involved in numerical evaluation of the J integral, the cracked, wing channel stiffened panel (see Figure 7) used in earlier Dugdale-type analysis with the equivalent area fastener model was

considered. The skin material is assumed to be 7075-T6 and its stress-strain behavior is shown in Figure 22 and has been obtained from 0.063 inch material tested in this program. The finite element idealization is the same as that employed for the Dugdale-model calculations. Two contours are selected to calculate J for various load increments. Contour I is selected away from the outer stringer and Contour II a little beyond the outer stringer, as shown in Figure 23. For Contour I, J is given by:

$$J_I = 2\int_{31}^{149} \{[\frac{1}{2E}(\sigma_x + \sigma_y)^2 + \frac{1+\nu}{E}(\tau_{xy}^2 - \sigma_x\sigma_y) - \sigma_x(\frac{\partial u}{\partial x}) - \tau_{xy}(\frac{\partial v}{\partial x})] + \int_o^{\bar{\epsilon}_p} \bar{\sigma}\, d\bar{\epsilon}_p\}dy$$

$$+ 2\int_{149}^{137} [\tau_{xy}(\frac{\partial u}{\partial x}) + \sigma_y(\frac{\partial v}{\partial x})]dx$$

$$- \sigma_x(\frac{\partial u}{\partial x}) - \tau_{xy}(\frac{\partial v}{\partial x})] + \int_o^{\bar{\epsilon}_p} \bar{\sigma}\, d\bar{\epsilon}_p\}dy$$

For Contour II J is given by:

$$J_{II} = 2\int_{73}^{112} \{[\frac{1}{2E}(\sigma_x + \sigma_y)^2 + \frac{1+\nu}{E}(\tau_{xy}^2 - \sigma_x\sigma_y)$$

$$- \sigma_x(\frac{\partial u}{\partial x}) - \tau_{xy}(\frac{\partial v}{\partial x})] + \int_o^{\bar{\epsilon}_p} \sigma\, d\bar{\epsilon}_p\}\, dy$$

$$+ 2\int_{112}^{108} [\tau_{xy}(\frac{\partial u}{\partial x}) + \sigma_y(\frac{\partial v}{\partial x})]\, dx$$

$$+ 2\int_{108}^{149} \{[\frac{1}{2E}(\sigma_x + \sigma_y)^2 + \frac{1+\nu}{E}(\tau_{xy}^2 - \sigma_x\sigma_y) - \sigma_x(\frac{\partial u}{\partial x})$$

$$- \tau_{xy}(\frac{\partial v}{\partial x})] + \int_o^{\bar{\epsilon}_p} \bar{\sigma}\, d\bar{\epsilon}_p\}\, dy$$

$$+ 2\int_{149}^{137} [\tau_{xy}(\frac{\partial u}{\partial x}) + \sigma_y(\frac{\partial v}{\partial x})]\, dx$$

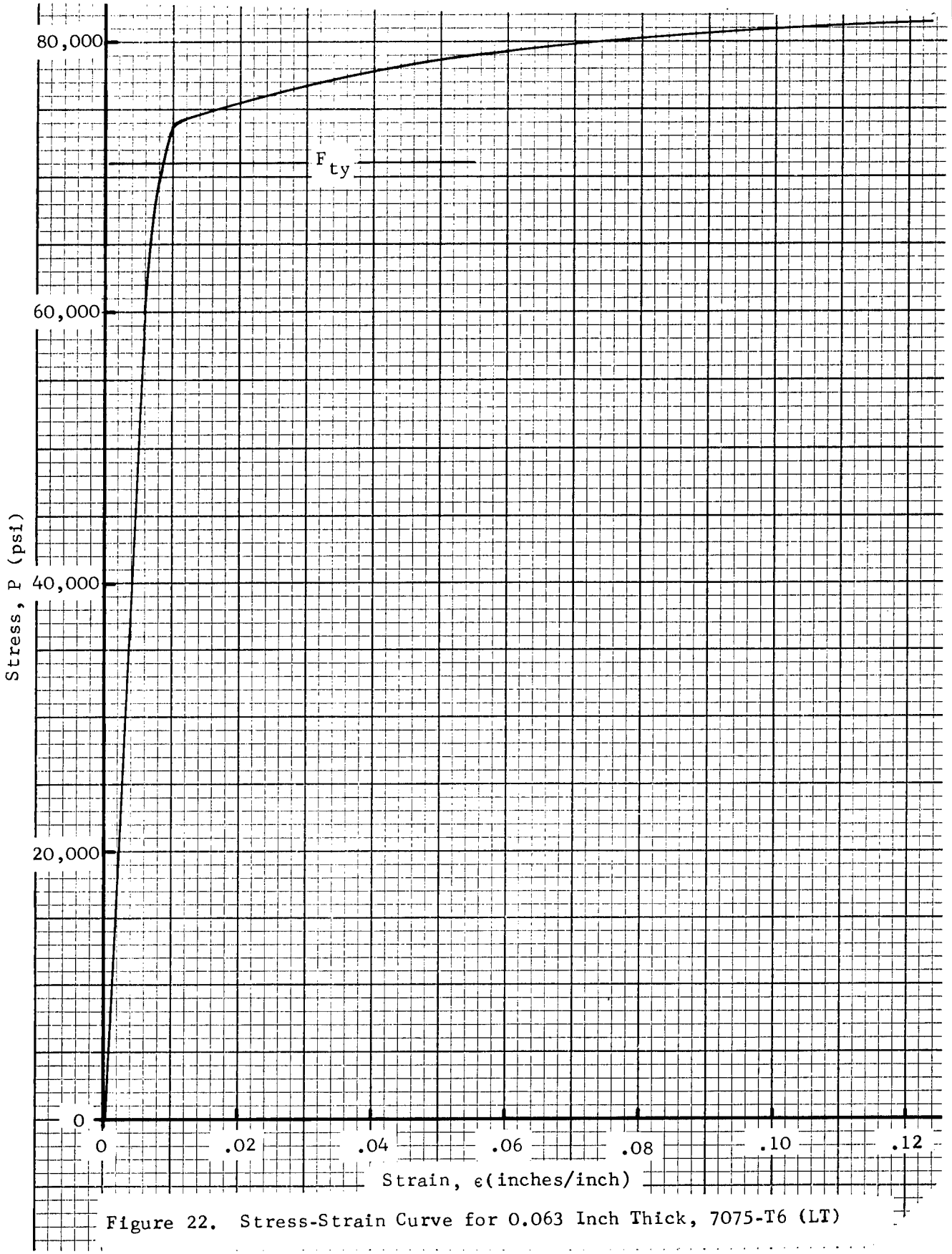

Figure 22. Stress-Strain Curve for 0.063 Inch Thick, 7075-T6 (LT)

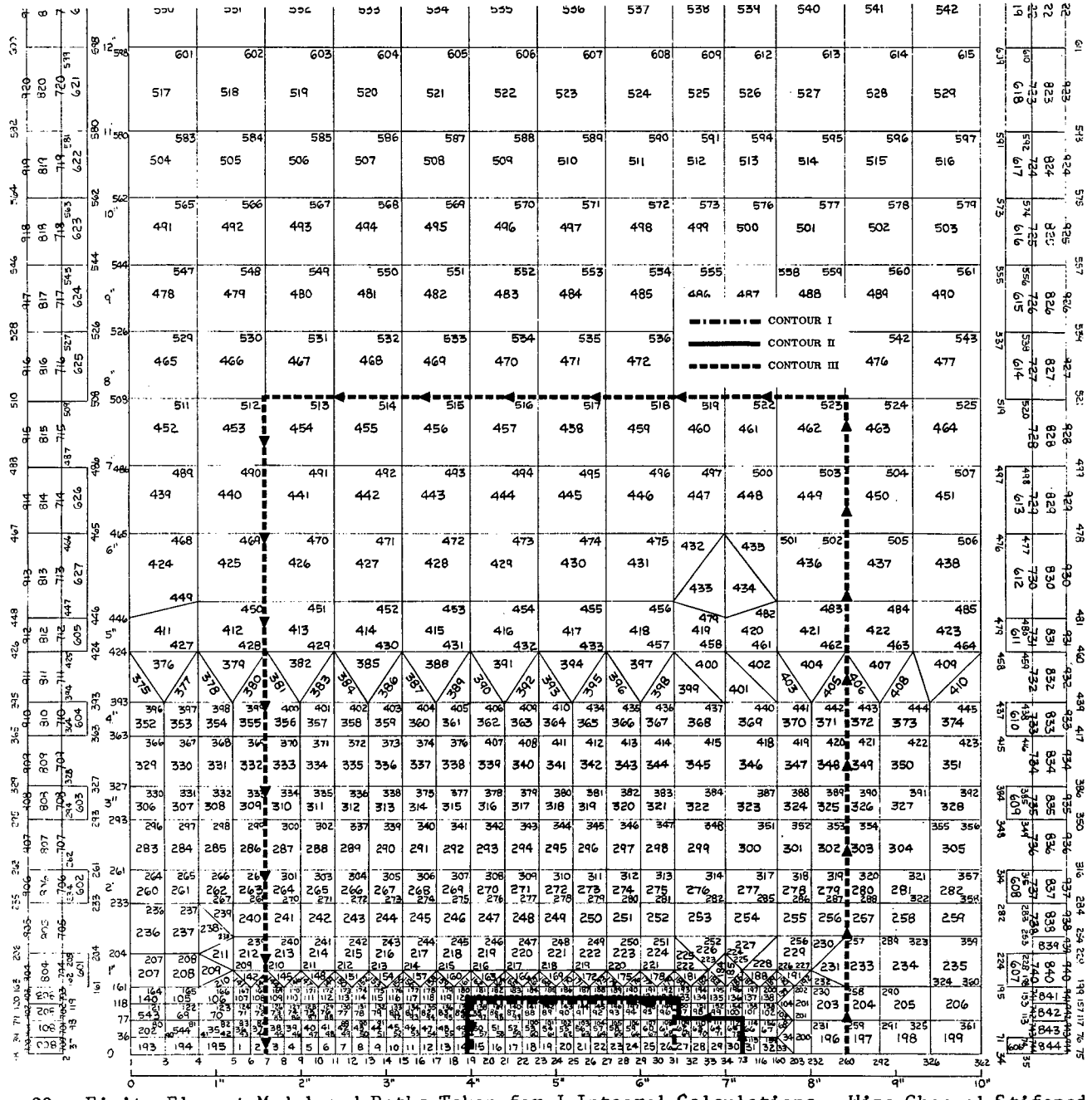

Figure 23. Finite Element Model and Paths Taken for J Integral Calculations - Wing Channel Stifened Panel

$$+ 2 \int_{137}^{19} \{[\frac{1}{2E} (\sigma_x + \sigma_y) + \frac{1+\nu}{E} (\tau_{xy} - \sigma_x \sigma_y) - \sigma_x (\frac{\partial u}{\partial x})$$

$$- \tau_{xy} (\frac{\partial v}{\partial x})] + \int_{o}^{\bar{\epsilon}_p} \bar{\sigma} \, d\bar{\epsilon}_p \} \, dy$$

For purposes of calculation, J is considered to consist of two parts. Part J_1 is that part of J which does not involve a plastic part and Part J_2 is the plastic part, which is:

$$\int_{o}^{\bar{\epsilon}_p} \bar{\sigma} d\bar{\epsilon}_p \, . \tag{16}$$

Table III shows the values of σ_x, σ_y, τ_{xy}, $\frac{\partial u}{\partial x}$, $\frac{\partial v}{\partial x}$, $\bar{\sigma}$, J_1, J_2 and J for the various segments of Contour I, for an applied stress of 50 ksi. For the segments for which $\bar{\sigma}$ is greater than the proportional limit of the material (55,379 psi) and dy is nonzero, a value of $\bar{\epsilon}_p$ is obtained from the stress strain curve. (Figure 22) and the value of the plastic part of J calculated from Equation (16). Similar sets of calculations for Contour II are shown in Table IV for the same applied stress.

Table V shows the values of $\sqrt{J}$ for the two contours for various load increments. It is seen that up to an applied stress of 60 ksi, the values of $\sqrt{J}$ for both contours are the same. However, for stresses above 60 ksi, the values of $\sqrt{J}$ for Contour II are less than the values of $\sqrt{J}$ for Contour I.

A similar set of calculations were done for the lightly stiffened wing channel panel (see Figure 7) with half crack length of 5.4 inches using the flexible fastener model. In this case three different contours shown in Figure 23 were used to compute the J integral values. Contours I and II were the same as discussed for the earlier case, however, Contour III was taken remote from the crack. In this case most of the elements around the contour are elastic and small contribution of the plastic part is involved along the path. Thus the results of J integral values based primarily on elastic contributions (along Contours III) can be compared with those with heavy plastic contributions to J (along contours I and II). The results of J integral calculations along these three contours are shown in Table VI.

TABLE III. CONTOUR I, J CALCULATIONS FOR 5.4 INCH PHYSICAL CRACK, LIGHTLY STIFFENED PANEL ASSUMING PRANDTL-REUSS MATERIAL BEHAVIOR - (50,000 PSI STRESS)

Grid Points at ends of Γ_I Segment	Stresses at Midpoint of Segment			$\frac{\partial u}{\partial x} X10^3$	$\frac{\partial v}{\partial x} X10^3$	d_x (inch)	d_y (inch)	$\bar{\sigma}$ (ksi)	J_1 $\left(\frac{\text{in-lb}}{\text{in}^2}\right)$	$J_2 = \int_0^{\bar{\epsilon}_p} \int \bar{\sigma} d\bar{\epsilon}_p dy$ $\left(\frac{\text{in-lb}}{\text{in}^2}\right)$	$J = J_1 + J_2$ $\left(\frac{\text{in-lb}}{\text{in}^2}\right)$
	σ_x (ksi)	σ_y (ksi)	τ_{xy} (ksi)								
31 - 68	23.9584	77.6194	2.3946	-0.4206	-0.4236	0.0	0.2	68.9662	108.7924	20.41	129.2024
68 - 108	19.2326	78.5194	4.2500	-1.0001	-1.3658	0.0	0.2	71.2688	118.2990	30.04	148.3390
108 - 149	12.907	77.3794	3.7684	-1.5997	-2.4071	0.0	0.2	72.0973	119.1923	38.812	158.0043
149 - 148	9.3852	77.814	2.0107	-2.2666	-3.5574	-0.2	0.0	73.6541	112.5502	0.0	112.5502
148 - 147	6.9888	78.1487	-0.8348	-2.9756	-5.032	-0.2	0.0	74.9132	156.3041	0.0	156.3041
147 - 146	4.6782	76.5795	-4.613	-3.8049	-6.9141	-0.2	0.0	74.7789	204.7724	0.0	204.7724
146 - 145	1.0101	74.3157	-8.4361	-4.6621	-9.4229	-0.2	0.0	75.2481	264.3767	0.0	264.3767
145 - 144	-5.0167	67.616	-15.610	-5.0189	-13.079	-0.2	0.0	75.2816	322.4016	0.0	322.4016
144 - 143	-6.9668	48.827	-31.762	-4.0639	-15.1152	-0.2	0.0	76.1528	243.5812	0.0	243.5812
143 - 142	-5.5546	37.9501	-27.060	-2.4342	-13.3104	-0.2	0.0	62.2783	175.7048	0.0	175.7048
142 - 141	-6.0255	25.047	-24.195	-1.5314	-11.0543	-0.2	0.0	50.7028	95.9296	0.0	95.9296
141 - 140	-10.1255	13.7995	-17.9623	-1.4045	-9.8077	-0.2	0.0	37.4247	44.0456	0.0	44.0456

TABLE III. CONTOUR I, J CALCULATIONS FOR 5.4 INCH PHYSICAL CRACK, LIGHTLY STIFFENED PANEL ASSUMING PRANDTL-REUSS MATERIAL BEHAVIOR - (50,000 PSI STRESS) (CONTINUED)

Grid Points at ends of Γ_I Segment	Stresses at Midpoint of Segment			$\frac{\partial u}{\partial x} X10^3$	$\frac{\partial v}{\partial x} X10^3$	d_x (inch)	d_y (inch)	$\bar{\sigma}$ (ksi)	J_1 $\left(\frac{\text{in-lb}}{\text{in}^2}\right)$	$J_2 = \int_0^{\epsilon_p}\int \bar{\sigma} d\bar{\epsilon}_p dy$ $\left(\frac{\text{in-lb}}{\text{in}^2}\right)$	$J = J_1 + J_2$ $\left(\frac{\text{in-lb}}{\text{in}^2}\right)$
	σ_x (ksi)	σ_y (ksi)	τ_{xy} (ksi)								
140 - 139	-13.6948	7.8779	-13.4432	-1.5470	-8.4828	-0.2	0.0	29.9942	18.4118	0.0	18.4118
139 - 138	-17.7434	4.6122	-9.2457	-1.7898	-7.1089	-0.2	0.0	25.9692	6.4959	0.0	6.4959
138 - 137	-20.6199	2.9576	-6.9500	-2.0398	-5.9700	-0.2	0.0	25.2946	1.3922	0.0	1.3922
137 - 96	-24.8123	1.4755	-4.5054	-2.4563	-5.5139	0.0	-0.2	26.4570	20.7940	0.0	20.7940
96 - 56	-32.5930	0.2041	-1.8133	-3.1710	-5.4672	0.0	-0.2	32.8460	24.4222	0.0	24.4222
56 - 19	-42.2604	-0.0410	0.1133	-4.1005	-5.4170	0.0	-0.2	42.2404	34.4132	0.0	34.4132
										ΣJ =	2161.1412
										$\sqrt{J}$ =	46.488

TABLE IV. CONTOUR II, J CALCULATIONS FOR 5.4 INCH PHYSICAL CRACK, LIGHTLY STIFFENED PANEL ASSUMING PRANDTL-REUSS MATERIAL BEHAVIOR - (50,000 PSI STRESS)

Grid Points at ends of Γ_{II} Segment	Stresses at Midpoint of Segment			$\frac{\partial u}{\partial x} \times 10^3$	$\frac{\partial v}{\partial x} \times 10^3$	d_x (inch)	d_y (inch)	$\bar{\sigma}$ (ksi)	J_1 $\left(\frac{\text{in-lb}}{\text{in}^2}\right)$	$J_2 = \int\int \frac{\bar{\epsilon}_p}{\bar{\sigma} d\bar{\epsilon}_p} dy$ $\left(\frac{\text{in-lb}}{\text{in}^2}\right)$	$J = J_1 + J_2$ $\left(\frac{\text{in-lb}}{\text{in}^2}\right)$
	σ_x (ksi)	σ_y (ksi)	τ_{xy} (ksi)								
73 - 72	16.8674	64.2883	1.20037	-0.5503	-0.1021	0.0	0.2	57.7706	75.5761	3.919	79.4951
72 - 112	13.5789	61.6564	2.9781	-0.6768	-0.3079	0.0	0.2	56.3497	71.0605	0.1584	71.2189
112 - 111	13.1769	62.9014	3.8038	-0.7679	-0.5324	-0.2	0.0	57.8341	14.5648	0.0	14.5648
111 - 110	14.3079	65.3318	3.7071	-0.7892	-0.8027	-0.2	0.0	59.8283	22.1473	0.0	22.1473
110 - 109	15.3373	68.9869	3.9269	-0.8862	-1.1264	-0.2	0.0	63.1079	32.4772	0.0	32.4772
109 - 108	16.0393	75.5569	4.2934	-1.0987	-1.5926	-0.2	0.0	69.3507	50.0198	0.0	50.0198
108 - 149	12.907	77.3794	3.7684	-1.5997	-2.4071	0.0	0.2	72.0973	119.1923	38.812	158.0043
149 - 148	9.3852	77.814	2.0107	-2.2666	-3.5574	-0.2	0.0	73.6541	112.5502	0.0	112.5502
148 - 147	6.9888	78.1487	-0.8348	-2.9756	-5.032	-0.2	0.0	74.9132	156.3041	0.0	156.3041
147 - 146	4.6782	76.5795	-4.613	-3.8049	-6.9141	-0.2	0.0	74.7789	204.7724	0.0	204.7724
146 - 145	1.0101	74.3157	-8.4361	-4.6621	-9.4229	-0.2	0.0	75.2481	264.3767	0.0	264.3767
145 - 144	-5.0167	67.616	-15.610	-5.0189	-13.079	-0.2	0.0	75.2816	322.4016	0.0	322.4016
144 - 143	-6.9668	48.827	-31.762	-4.0639	-15.1152	-0.2	0.0	76.1528	243.5812	0.0	243.5812
143 - 142	-5.5546	37.9501	-27.060	-2.4342	-13.3104	-0.2	0.0	62.2783	175.7048	0.0	175.7048
142 - 141	-6.0255	25.047	-24.195	-1.5314	-11.0543	-0.2	0.0	50.7028	95.9296	0.0	95.9296
141 - 140	-10.1255	13.7995	-17.9623	-1.4045	-9.8077	-0.2	0.0	37.4247	44.0456	0.0	44.0456

TABLE IV. CONTOUR II, J CALCULATIONS FOR 5.4 INCH PHYSICAL CRACK, LIGHTLY STIFFENED PANEL ASSUMING PRANDTL-REUSS MATERIAL BEHAVIOR - (50,000 PSI STRESS) (CONTINUED)

Grid Points at ends of Γ_{II} Segment	Stresses at Midpoint of Segment			$\frac{\partial u}{\partial x} \times 10^3$	$\frac{\partial v}{\partial x} \times 10^3$	d_x (inch)	d_y (inch)	$\bar{\sigma}$ (ksi)	J_1 $\left(\frac{\text{in-lb}}{\text{in}^2}\right)$	$J_2 = \int_0^{\bar{\epsilon}_p}\int \bar{\sigma} d\bar{\epsilon}_p dy$ $\left(\frac{\text{in-lb}}{\text{in}^2}\right)$	$J = J_1 + J_2$ $\left(\frac{\text{in-lb}}{\text{in}^2}\right)$
	σ_x (ksi	σ_y (ksi)	τ_{xy} (ksi)								
140 - 139	-13.6948	7.8779	-13.4432	-1.5470	-8.4828	-0.2	0.0	29.9942	18.4118	0.0	18.4118
139 - 138	-17.7434	4.6122	-9.2457	-1.7898	-7.1088	-0.2	0.0	25.9692	6.4959	0.0	6.4959
138 - 137	-20.6199	2.9576	-6.950	-2.0397	-5.97	-0.2	0.0	25.2947	1.3922	0.0	1.3922
137 - 96	-24.8123	1.4755	-4.5054	-2.4563	-5.5139	0.0	-0.2	26.4570	20.7940	0.0	20.7940
96 - 56	-32.5930	0.2041	-1.8133	-3.1710	-5.4672	0.0	-0.2	32.8460	24.4222	0.0	24.4222
56 - 19	-42.2604	0.0410	0.1133	-4.1005	-5.4170	0.0	-0.2	42.2404	34.4132	0.0	34.4132
										ΣJ =	2153.5229
										$\sqrt{J}$ =	46.406

TABLE V. COMPUTED VALUES OF $\sqrt{J}$ FOR CONTOURS I AND II OF FIGURE 23

LIGHTLY STIFFENED WING CHANNEL PANEL

a = 5.4 inches

EQUIVALENT AREA FASTENER MODEL

STRESS (psi)	$\sqrt{J}$ CONTOUR I $\left(\frac{\text{in.-lb.}}{\text{in.}^2}\right)^{\frac{1}{2}}$	$\sqrt{J}$ CONTOUR II $\left(\frac{\text{in.-lb.}}{\text{in.}^2}\right)^{\frac{1}{2}}$
10,000	8.647	8.647
15,000	13.009	13.021
20,000	17.465	17.486
25,000	21.754	21.770
30,000	25.935	25.959
35,000	30.422	30.452
45,000	40.000	39.790
50,000	46.488	46.406
60,000	77.002	77.045
65,000	103.925	102.420

TABLE VI. COMPUTED VALUES OF $\sqrt{J}$ FOR CONTOURS I, II AND III OF FIGURE 23
LIGHTLY STIFFENED WING CHANNEL PANEL
a = 5.4 inches

FLEXIBLE FASTENER MODEL

STRESS (psi)	$\sqrt{J}$ CONTOUR I $\left(\frac{\text{in.-lb.}}{\text{in.}^2}\right)^{\frac{1}{2}}$	$\sqrt{J}$ CONTOUR II $\left(\frac{\text{in.-lb.}}{\text{in.}^2}\right)^{\frac{1}{2}}$	$\sqrt{J}$ CONTOUR III $\left(\frac{\text{in.-lb.}}{\text{in.}^2}\right)^{\frac{1}{2}}$
15,000	14.399	14.397	14.395
30,000	28.715	28.706	28.733
40,000	38.574	38.508	38.432
50,000	51.538	51.343	51.324

To further show the path independence of J another set of J calculations was made for the heavily stiffened wing channel panel (see Figure 5) with a half crack length of 2.8 inches using the flexible fastener model. In calculating J the two contours shown in Figure 24 were used and the values of J integral for these two contours are shown in Table VII.

The Prandtl-Reuss calculations of J for the heavily and lightly stiffened wing channel panel in Tables V, VI and VII indicate the following trends.

1. The heavily stiffened panel with small crack length (a = 2.8 inches) shows the J integral is path independent to an applied stress of 0.85 of the yield strength (Table VII). The difference in J values for the two contours is less than 0.2 percent.

2. For a lightly stiffened panel with long crack length (half crack length = 5.4 inches) the J integral is path independent to an applied stress of over 0.7 of the yield strength.

3. The three contours examined showed a maximum variation of less than 0.5 percent in the value of $\sqrt{J}$. However, for an applied stress of 0.85 of yield stress, the J integral showed a variation of about four percent.

   NOTE: At this applied stress the outer stringers have yielded and the stresses in the finite elements around the crack-tip are higher than the ultimate strength of the material. Some of the members along Contours I and II have stresses about 8 percent higher than the ultimate strength of the material. Using non-linear analysis in the NASTRAN program if the stresses in the members exceed the ultimate strength, the stresses are linearly extrapolated from the stress-strain curve. It is perhaps for these reasons that the four percent variation in $\sqrt{J}$ occurs along the two contours at high applied stresses. For large crack lengths

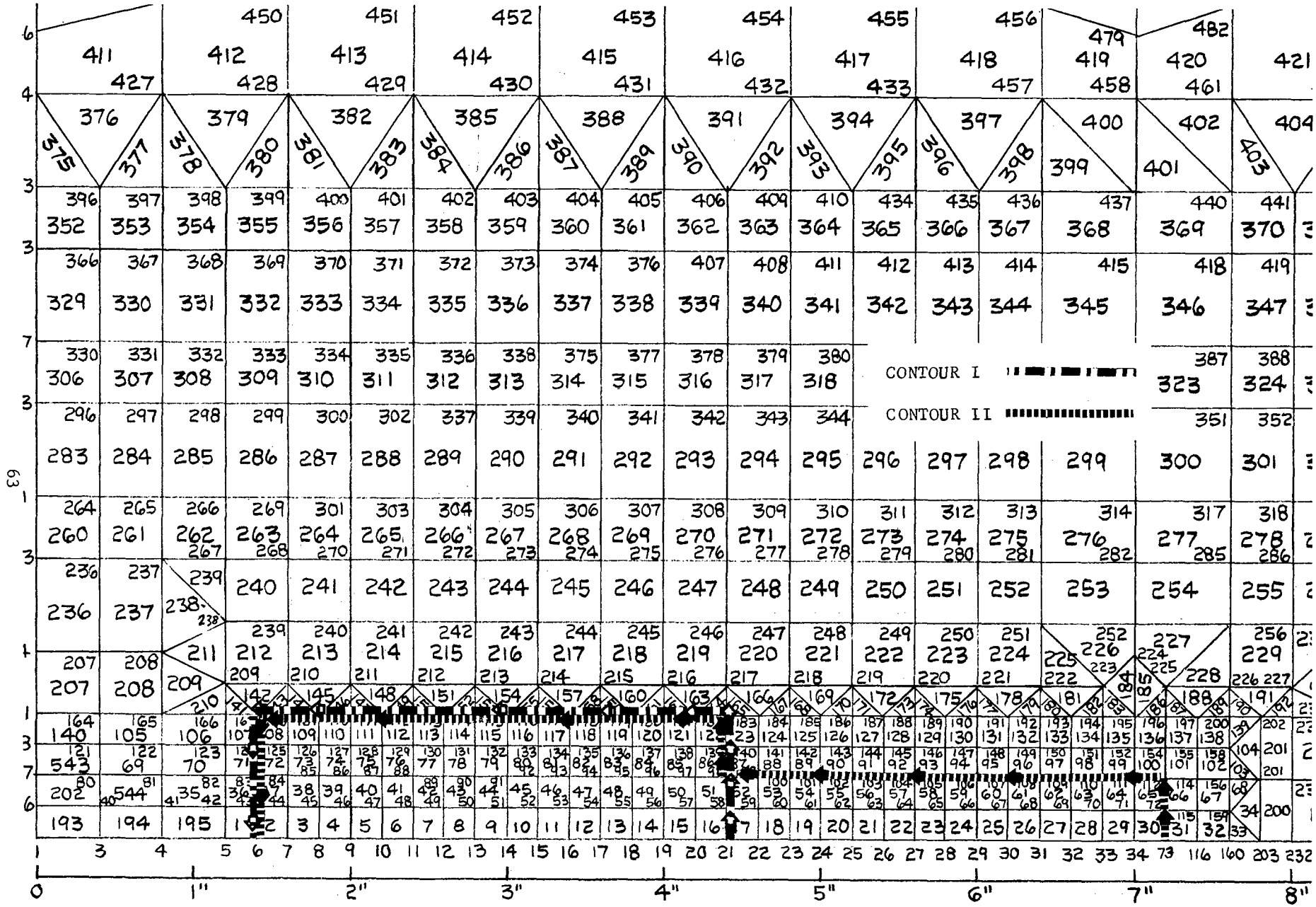

Figure 24. J Integral Contour for Heavily Stiffened Panel (a = 2.8 Inches)

and high applied stress there is considerable contribution of the plastic part of J. Therefore a small error associated with stress in the plastic range will contribute significantly to J integral values due to large plastic strains.

From these observations it is evident that the Prandtl-Reuss calculated J integral is path independent irrespective of whether the contour is taken beyond the outer stringers or not. However, for large crack lengths and high stresses extreme care must be taken in calculating the plastic part of the J integral.

TABLE VII. COMPUTED VALUES OF $\sqrt{J}$ FOR CONTOURS I AND II OF FIGURE 24
HEAVILY STIFFENED WING CHANNEL PANEL
a = 2.8 inches

FLEXIBLE RIVET MODEL

STRESS (psi)	$\sqrt{J}$ CONTOUR I $\left(\frac{\text{in.-lb.}}{\text{in.}^2}\right)^{\frac{1}{2}}$	$\sqrt{J}$ CONTOUR II $\left(\frac{\text{in.-lb.}}{\text{in.}^2}\right)^{\frac{1}{2}}$
15,000	11.272	11.268
30,000	21.144	21.144
40,000	28.335	28.336
50,000	35.913	35.914
60,000	44.861	44.945

3.3.2.2 An Analytical Comparison of Elastic, Dugdale and Prandtl-Reuss Material Behavior

The plastic zones developed ahead of a crack tip will be of a different size depending on plastic zone assumptions. Figure 25 shows the plot of stresses in the grid elements ahead of the crack tip versus p/F_{ty}, for a 5.4 inch physical crack assuming Prandtl-Reuss material behavior, where F_{ty} corresponds to the normal 0.2 percent offset yield stress. It can be seen that the stresses in individual elements are fairly constant after a certain applied stress. If one assumes that the individual elements yield at a stress of F_{ty} (71 ksi for this aluminum material), then the number of elements reaching this yield stress will indicate the size of the plastic zone which will depend on the applied stress, p which can be determined from Figure 26. For Prandtl-Reuss and Dugdale models, Figure 26 shows the plot of plastic zone size versus p/F_{ty} based on the assumption that the element reaching yield stress becomes plastic, for the lightly stiffened aluminum wing channel stiffened panel. The data in Figure 26 shows that for the same applied stress (up to $p/F_{ty} = 0.8$), the Dugdale model gives larger plastic zone sizes than the Prandtl-Reuss material behavior.

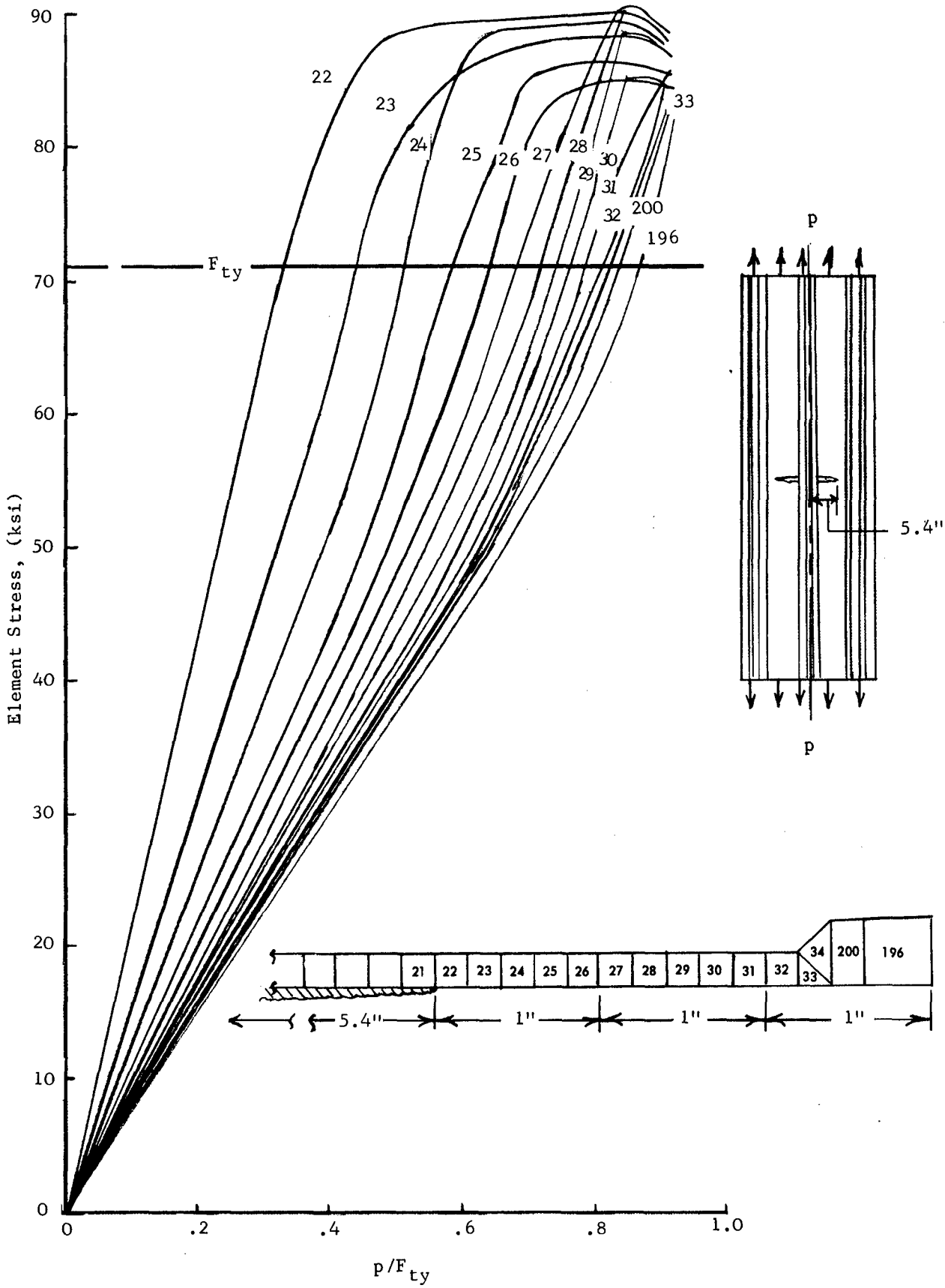

Figure 25. Stresses in Elements Ahead of the Crack as a Function of Normalized Applied Stress, Lightly Stiffened Wing Channel Panel

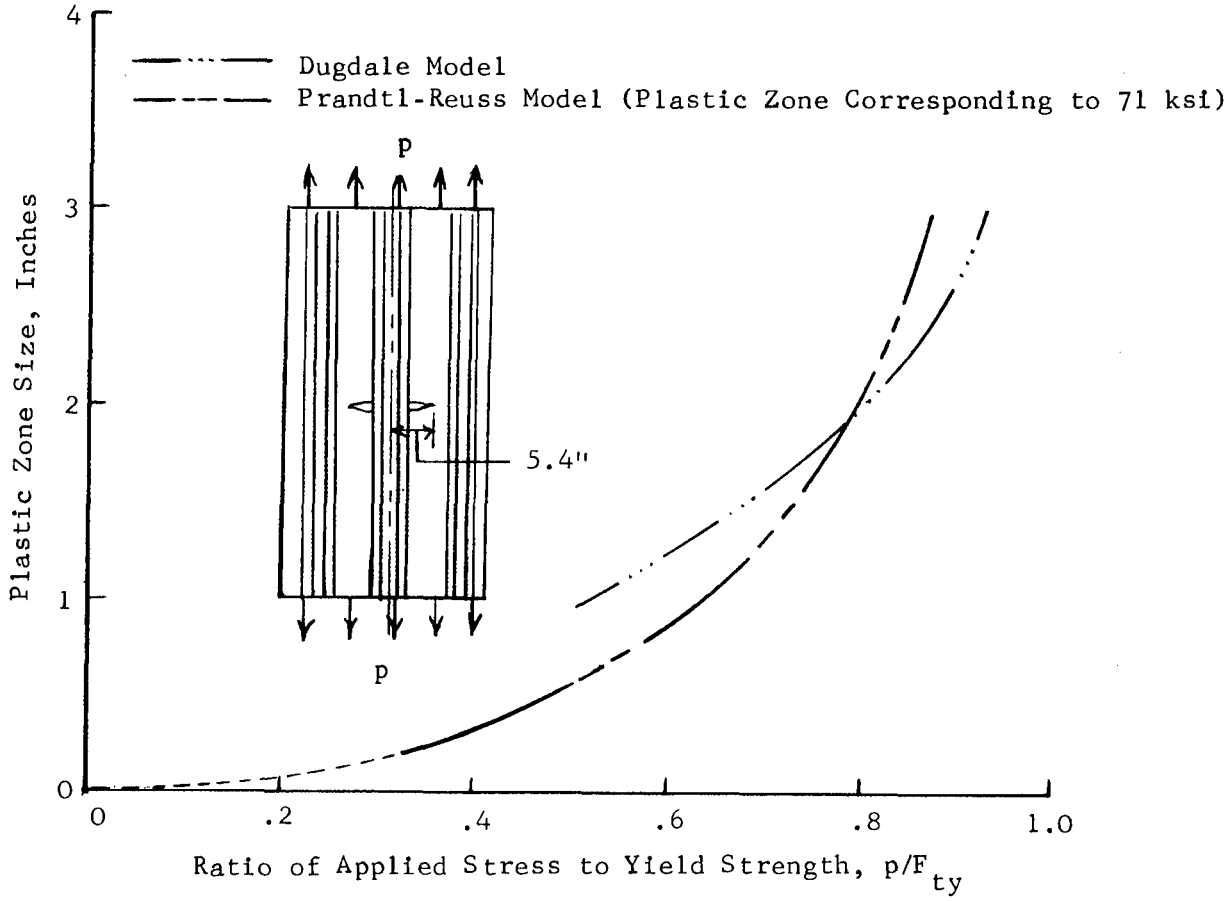

Figure 26. Plastic Zone Size for Lightly Stiffened Wing Channel Panel for Two Plastic Zone Models at Constant Physical Crack Size

The comparison of crack opening at the center of the crack for the lightly stiffened wing channel panel (half crack length of 5.4 inches) using Prandtl-Reuss, Dugdale, and elastic analysis is shown in Figure 27. To an applied stress of 0.6 of yield the central crack opening given by the Dugdale model and from the assumed Prandtl-Reuss material behavior are almost the same. However, at higher applied stresses, crack openings given by assuming Prandtl-Reuss material behavior are greater than those given by Dugdale type material behavior. At 80 percent of yield the crack openings calculated by assuming Dugdale behavior are 13 percent higher than those given by elastic material behavior. For the heavily stiffened wing channel panel, Figure 28 shows the variation of square root of J with applied stress for Prandtl-Reuss and elastic material behaviors for a half crack length of 2.8 inches. The values of $\sqrt{J}$ for Prandtl-Reuss behavior are similar to the elastic results up to an applied stress of 50 ksi; beyond this stress Prandtl-Reuss values are larger than those for the elastic case. This very small difference in $\sqrt{J}$ for the two cases is primarily due to the very high percentage stiffening (stringer area four times skin area) for this wing channel panel. The comparison between Dugdale and elastic behavior for the same heavily stiffened panel with the same crack length and an equivalent area fastener model is shown in Figure 29. It is seen that up to an applied stress of 40 ksi the Dugdale and elastic values are similar. For larger applied stresses the Dugdale values are higher than the elastic values. For an applied stress of 60 ksi ($p/F_{ty} = 0.845$), Dugdale model values of $\sqrt{J}$ are about 11 percent higher than the elastic values (see Figure 29).

A comparison of $\sqrt{J}$ values for a lightly stiffened panel having a half crack length of 2.8 inches assuming Dugdale, Prandtl-Reuss and elastic material behavior and the equivalent area fastener model are shown in Figure 30. The $\sqrt{J}$ values for elastic and Prandtl-Reuss material behaviors are similar up to an applied stress of approximately 40 ksi ($p/F_{ty} = 0.56$) whereas the values for assumed Dugdale material behavior are slightly higher. For stresses greater than 40 ksi Dugdale and Prandtl-Reuss material behaviors give $\sqrt{J}$'s considerably larger than computed elastic values. At an applied stress of 60 ksi ($p/F_{ty} = 0.845$) the $\sqrt{J}$ values given by Dugdale and Prandtl-Reuss material behaviors are about 18 percent higher than those assuming elastic material behavior. For the heavily stiffened panel, at the same applied stress, the difference between Dugdale and elastic assumptions is approximately 11 percent. As the applied stress increases the difference in $\sqrt{J}$ given by Dugdale and Prandtl-Reuss material behavior decreases.

To compare $\sqrt{J}$ values for a longer crack length the same lightly stiffened panel was studied at a half crack length of 5.4 inches using the same assumptions, i.e., elastic, Dugdale, and Prandtl-Reuss material behaviors. Figure 31 shows this comparison. For this large crack length the Dugdale values are higher than the elastic values even for small applied stresses, i.e., less than 50 percent of yield stress. However, for higher stresses, the difference between elastic and Dugdale $\sqrt{J}$ values is less than those encountered at a smaller crack length (see Figure 30). This is primarily due to the crack tip being close to the stiffener. Up to an applied stress of 45 ksi Prandtl-Reuss determined $\sqrt{J}$ values are noted to be between the elastic and Dugdale values. For higher stress the Prandtl-Reuss values are larger than those obtained from Dugdale plastic zone assumptions.

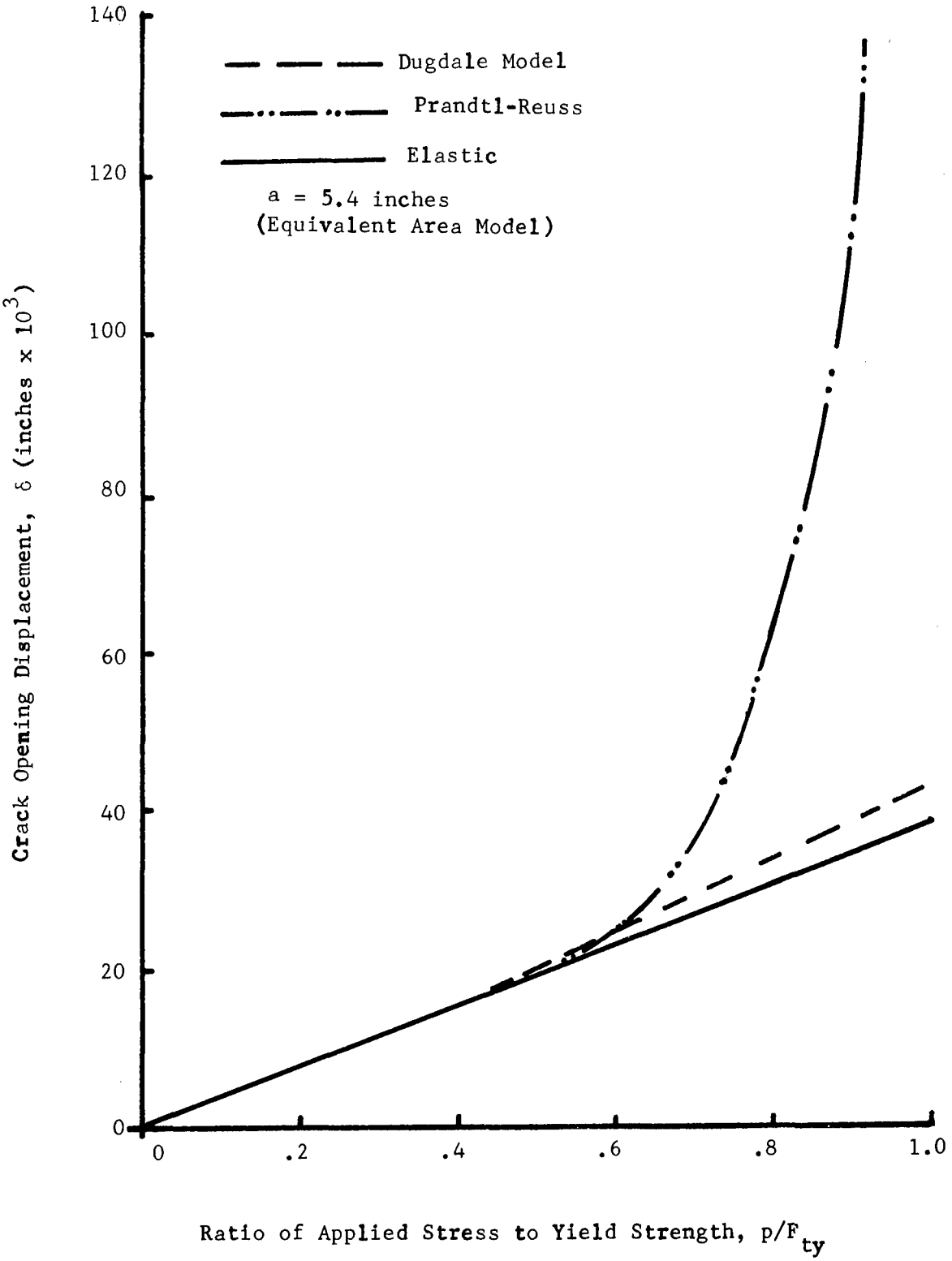

Figure 27. Crack Opening Displacements for Lightly Stiffened Wing Channel Panel for Three Assumed Material Behaviors

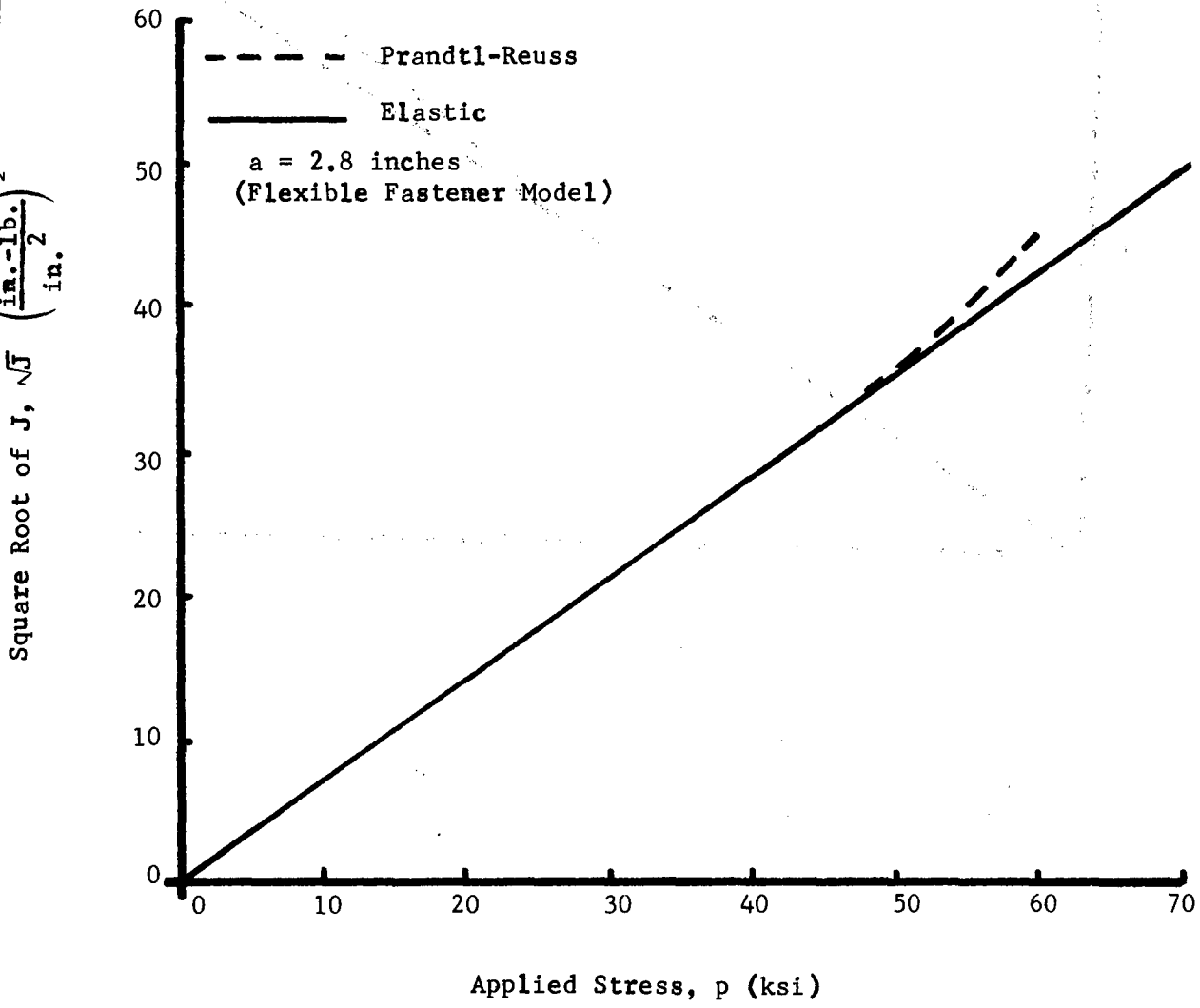

Figure 28. Comparison of Prandtl-Reuss and Elastic $\sqrt{J}$ Values for Heavily Stiffened Wing Channel Panel - a = 2.8 Inches

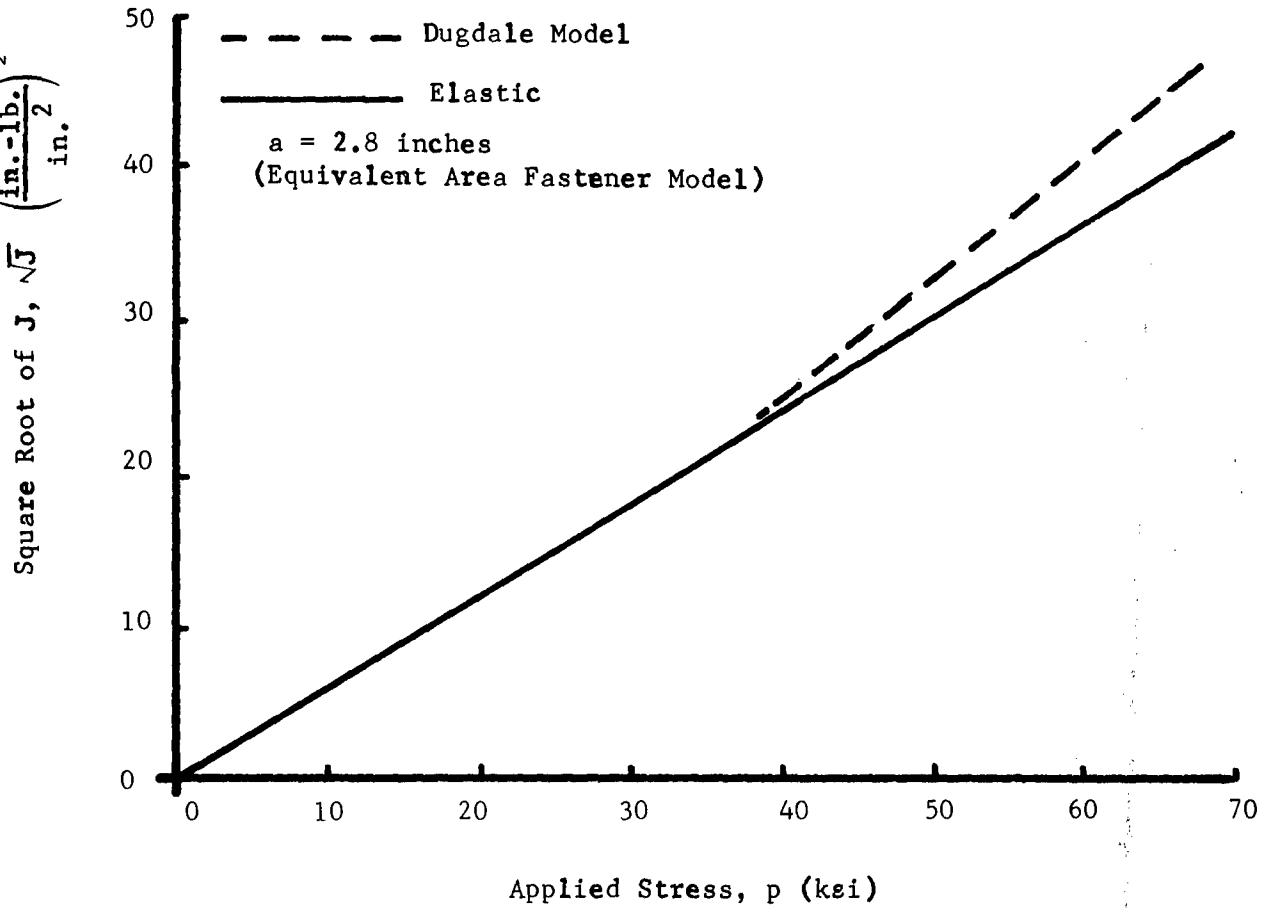

Figure 29. Comparison of Dugdale and Elastic $\sqrt{J}$ Values for Heavily Stiffened Wing Channel Panel - a = 2.8 Inches

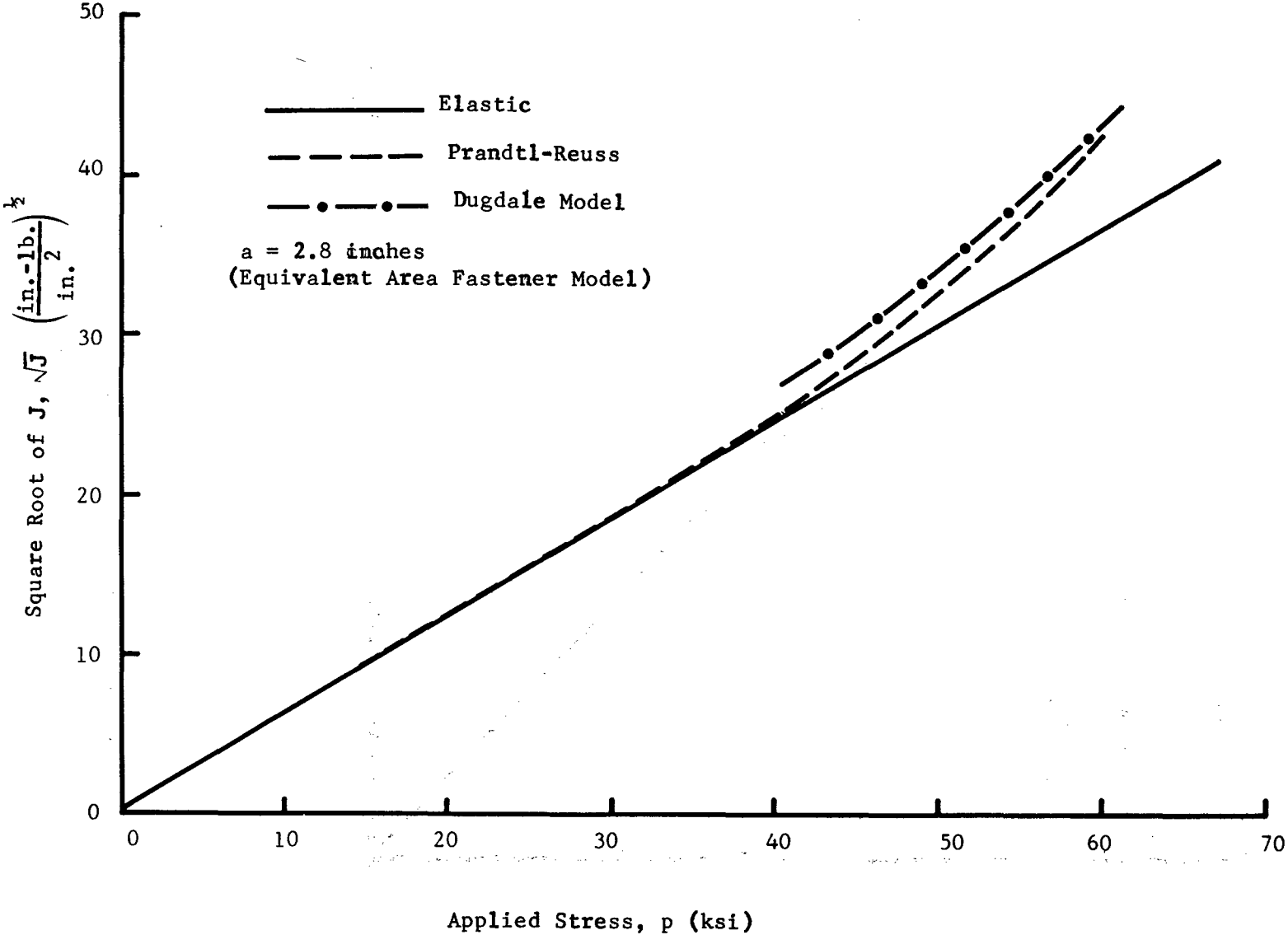

Figure 30. Comparison of Square Root of J for Elastic, Prandtl-Reuss and Dugdale Model Material Behavior, Lightly Stiffened Wing Channel Panel - a = 2.8 Inches

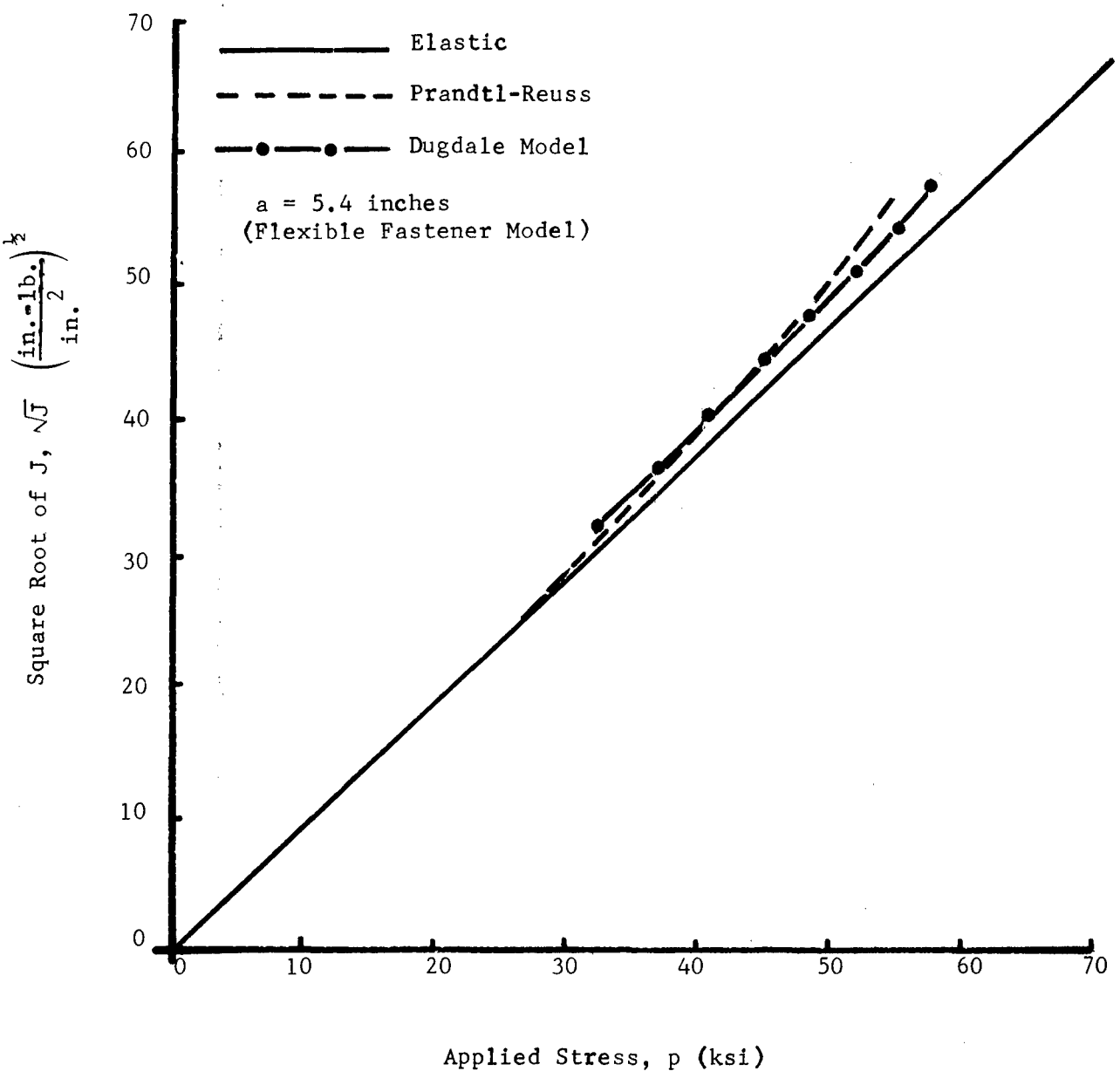

Figure 31. Comparison of Elastic, Prandtl-Reuss and Dugdale $\sqrt{J}$ Values for Lightly Stiffened Wing Channel Panel - a = 5.4 Inches

Based on these results it is evident that in stiffened panels with small and/or medium crack lengths a linear elastic analysis is likely to overestimate the residual strength of a structure. For large crack lengths (or crack length to stiffener spacing ratios) a linear elastic analysis and elastic-plastic analysis may differ by less than ten percent in square root J values. However, it is likely that at such large crack lengths the failure is likely to be governed by a stringer critical case rather than as a skin critical case. It has also been shown that a Dugdale type analysis results in $\sqrt{J}$ values which differ only slightly from those obtained from Prandtl-Reuss material behavior for both the heavily and lightly stiffened wing channel panels.

3.3.3 Effect of Elastic-Plastic Analysis on Stresses in Fasteners and Stiffeners

Section 3.2 discussed the stresses in fasteners and stiffeners for a wing channel stiffened panel based on linear elastic analysis. However, it is known that plasticity developed ahead of a crack tip will influence these stresses. Dugdale model elastic-plastic analysis of stiffened panels assumes that the fasteners and stiffeners behave elastically throughout the analysis and that the plasticity is confined to a region ahead of the crack tip in the skin only. This assumption is justified if the stresses in the stiffeners and fasteners remain elastic. If prior to failure the stiffeners yield, the analysis does not represent a realistic case. This is particularly true for stiffener critical structure. However, the assumption of fasteners and stiffeners remaining elastic can be used for skin critical structures. For a stringer critical structure it is more realistic to use the elastic-plastic analysis based on Prandtl-Reuss material behavior.

3.3.3.1 Effect of Dugdale Analysis on Stresses in Fasteners

The effect of Dugdale model type elastic-plastic analysis on stresses in the fastener just above the crack in the central stringer of the lightly stiffened wing channel panel is shown in Figure 32. It will be noted that the stresses are higher than those based on elastic assumptions. The difference in stresses between elastic-plastic and elastic analysis increases with applied stress as noted. However, the variation of stresses in the fastener with applied stress is essentially linear.

3.3.3.2 Effect of Dugdale Analysis on Stresses in Stiffener

The stresses in central and outer stiffeners for both lightly and heavily stiffened wing channel panels at the crack line are shown in Figure 33 for various physical crack lengths. These stresses were computed using the superposition principles outlined in Section 3.3.1.1. In this case the stresses are obtained by superposing the cases shown in Figures 15(c), (d), and (e).

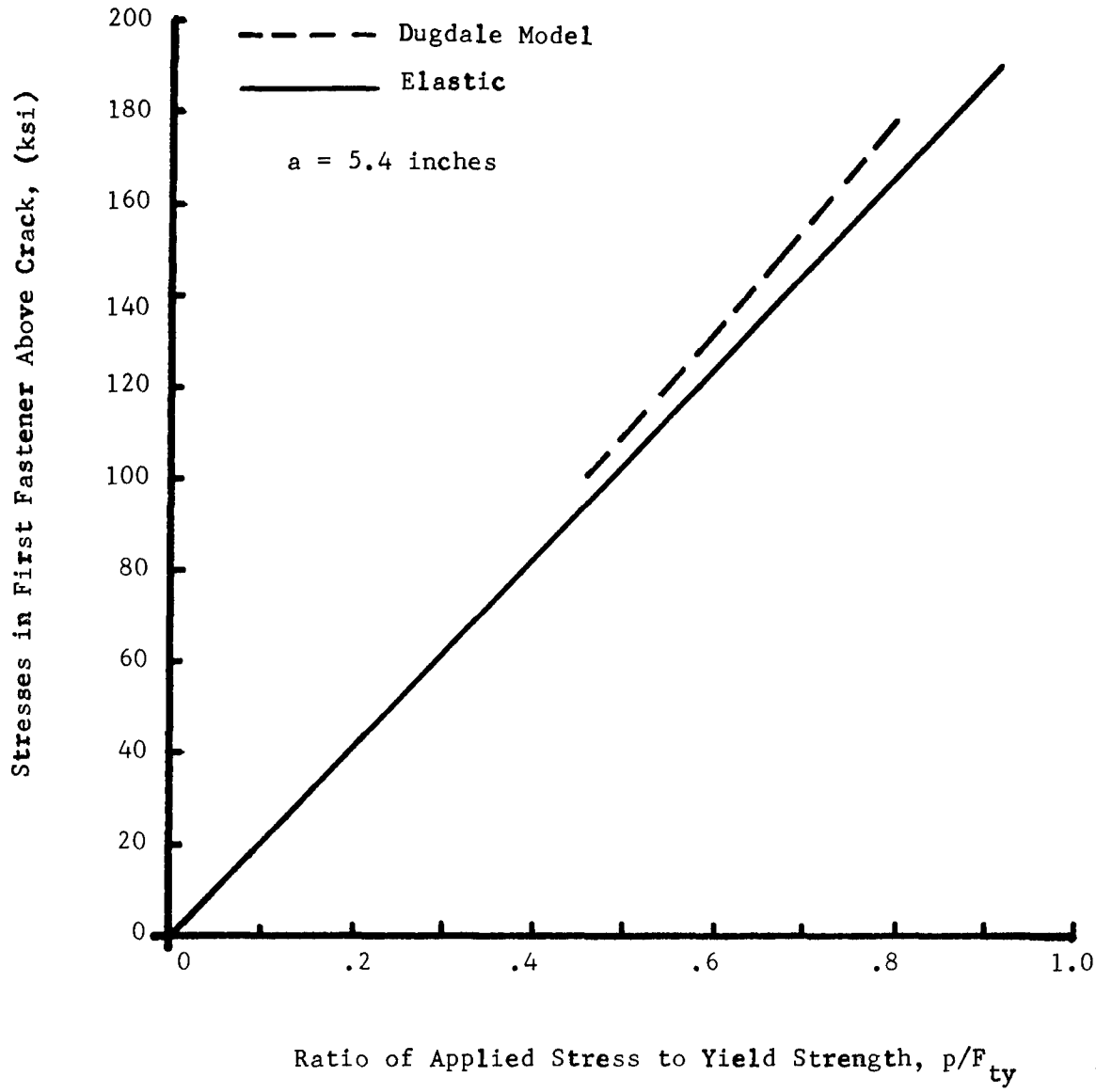

Figure 32. Stresses in Fastener, Lightly Stiffened Wing Channel Panel - a = 5.4 Inches

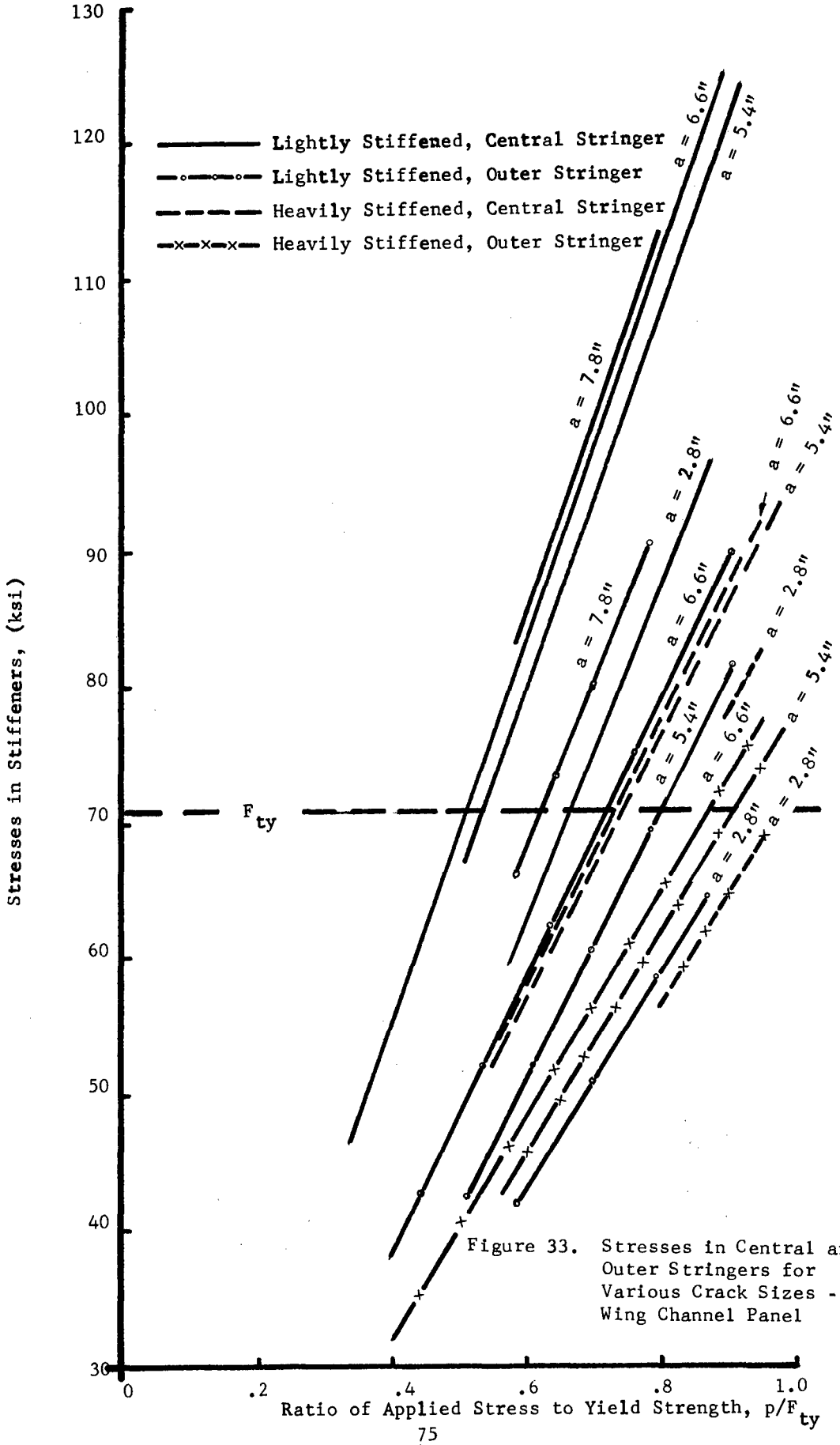

Figure 33. Stresses in Central and Outer Stringers for Various Crack Sizes - Wing Channel Panel

The plots of stress in the stringer versus applied load is almost linear in the stress range shown in Figure 33. At the same physical crack length and applied stress the lightly stiffened panel stringer has considerably higher stress than those for the heavily stiffened case. As anticipated, the stresse in both stringers increase with physical crack size.

Finite element member stresses for the lightly stiffened wing channel flanges (center and edge wing channel) have been computed for various Dugdale plastic zone sizes at constant values of physical crack length and are shown i Figure 34. These stresses are shown for locations near the crack and at some distance away. It is evident from the plots of Figure 34 that the bottom flan stresses reach a material yield (F_{ty}) at very small plastic zone sizes for both the center and edge channel flanges. One exception is for the short (2.8 inch) physical crack length at the edge stiffener flange which does not yield for plastic zones extending to the flange centerline. Rather large reductions in member stress occur at positions further removed from the crack (e.g., the one inch location compared to 0.3 or 0.1 inch positions) for all crack lengths.

To better understand the magnitude of the local stresses (i.e., member stresses) in relationship to gross panel stress (p) required to produce increasing plastic zones, the data of Figure 34 has been cross plotted and normalized to F_{ty} for various physical crack lengths. Figure 35 shows this comparison for the lightly stiffened case center stiffener elements (channel flange) and Figure 36 for the edge stiffener flange. Ordering is as would be anticipated, i.e., the applied stresses increase with decreasing crack length in order to reach a full member yield (member stress = F_{ty}) for each element position. It appears from the 2.8 inch curve of Figure 36 that full member yield would be reached at an applied stress of approximately 90% of yield. This condition is not evident from the member stress plot of Figure 34.

It appears that such plots as shown in Figures 35 and 36 provide further insight into the governing conditions for selection of a skin versus stiffener failure criterion.

The analysis of the lightly stiffened wing channel panel described above was for an all aluminum panel. A similar analysis was carried out assuming an all titanium, heavily stiffened and lightly stiffened panel. Figures 37 and 38 show the stresses in outer and central wing channels for this all titanium panel as a function of a_e, where a_e is the effective crack length i.e., physical crack length plus plastic zone.

For this particular titanium wing stiffened panel configuration, the following points can be observed:

1. For small crack lengths, the cross sectional area of the outer stringer (1.57 and 0.44 square inches) does not have a significant effect on the stresses (see Figure 33) in the outer stringer.

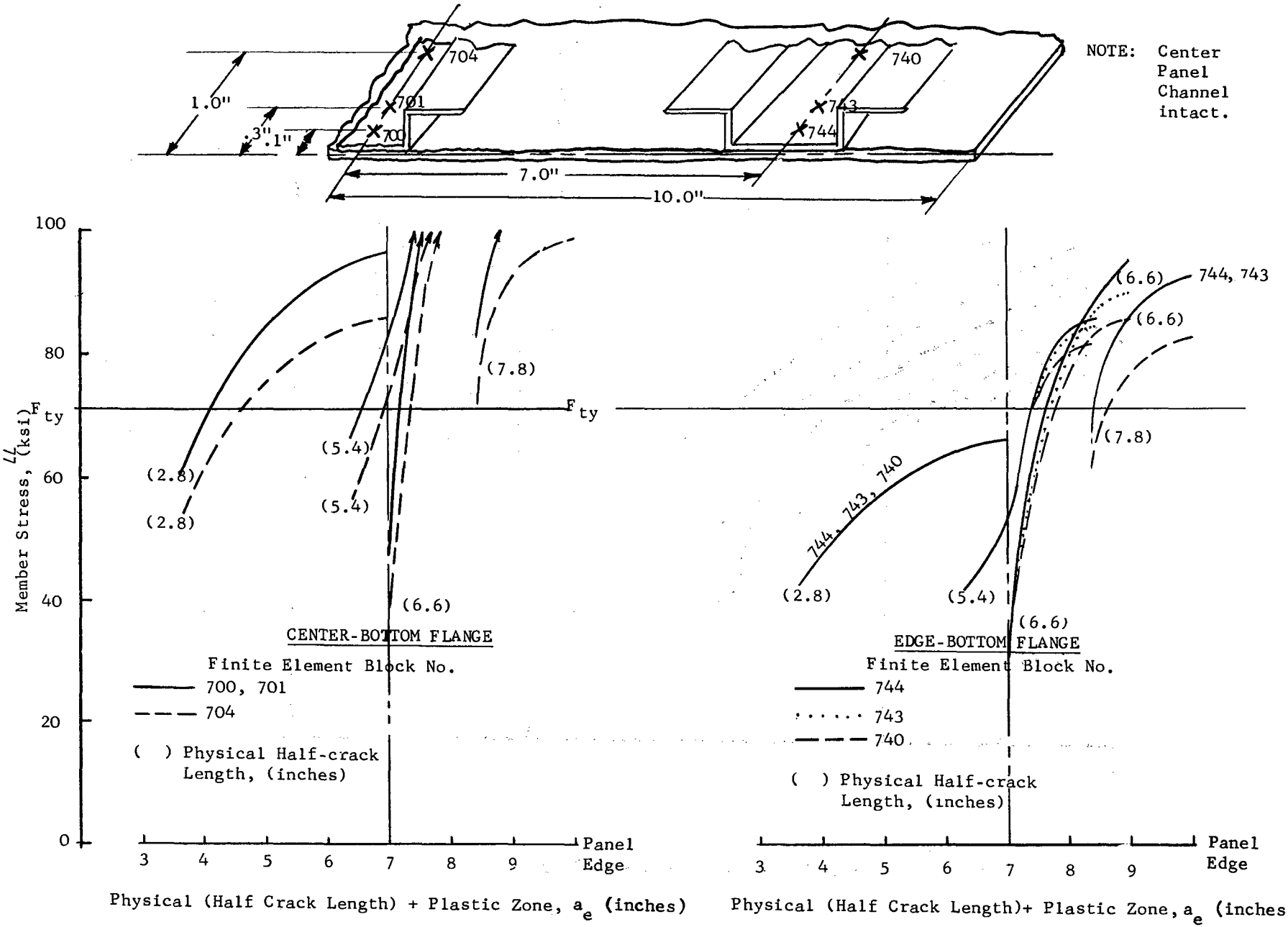

Figure 34. Member Stresses - Lightly Stiffened Panel

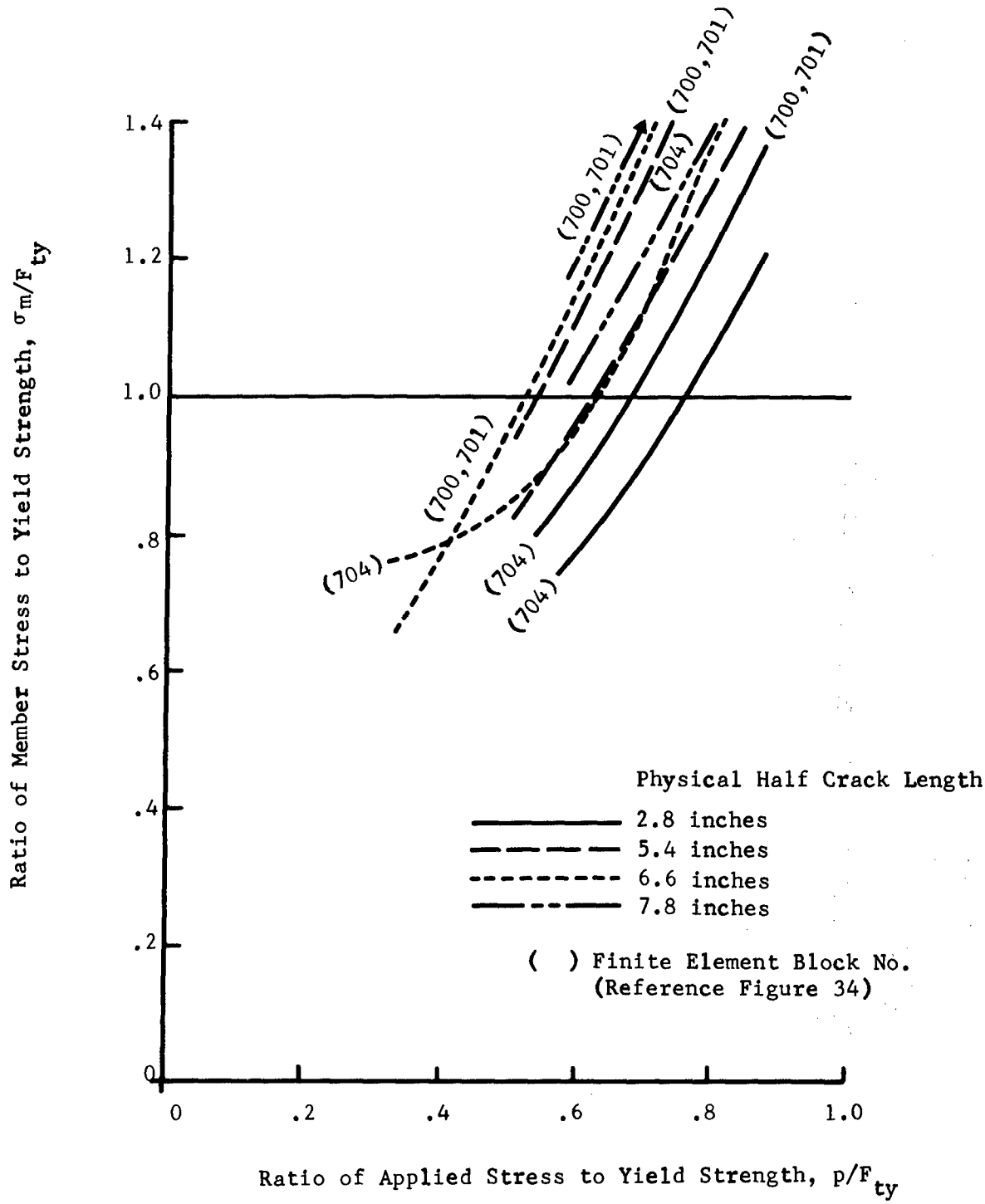

Figure 35. Normalized Stresses in Bottom Flange of Lightly Stiffened Wing Channel Panel - Central Stringer

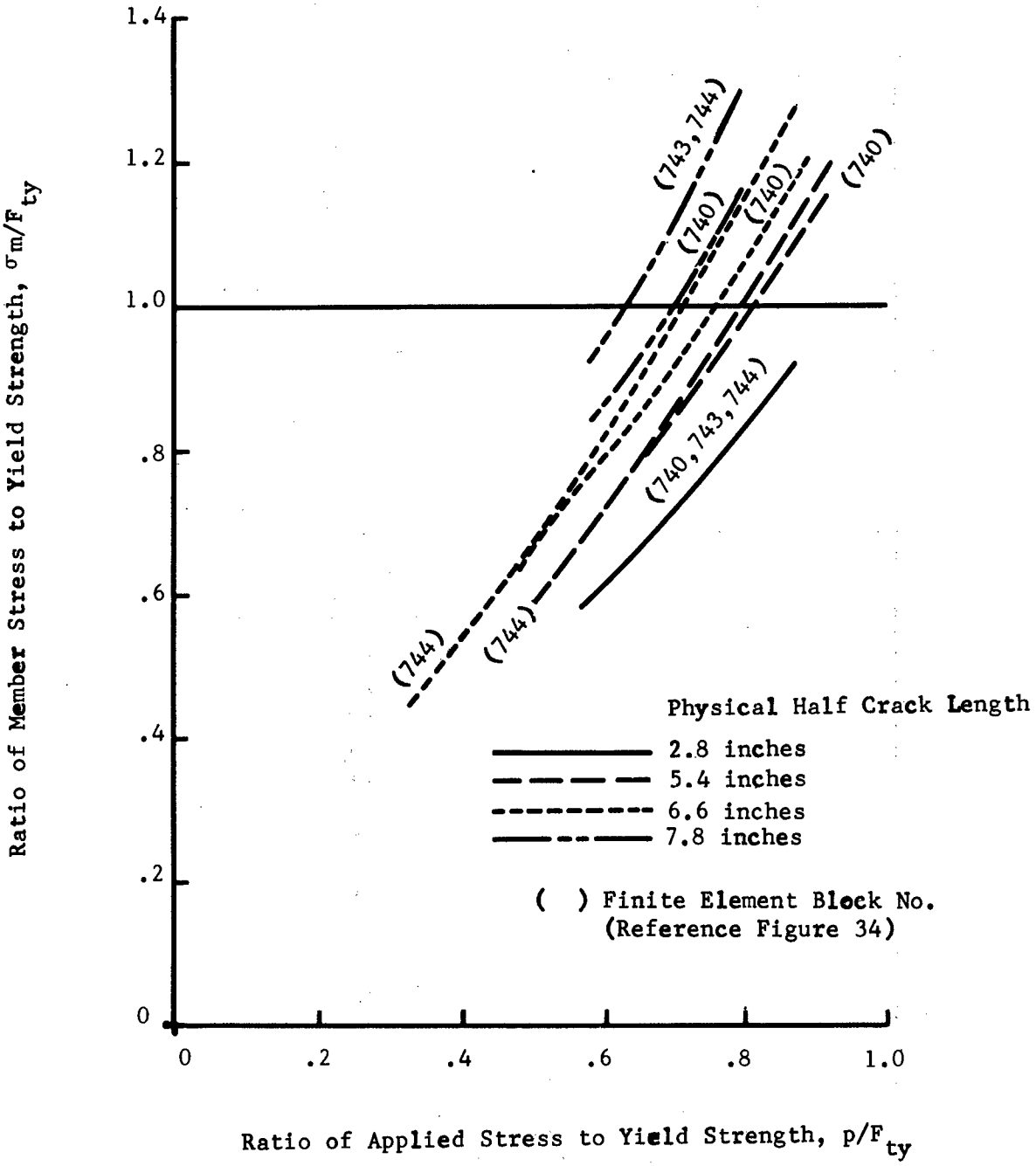

Figure 36. Normalized Stresses in Bottom Flange of Lightly Stiffened Wing Channel Panel - Outer Stringer

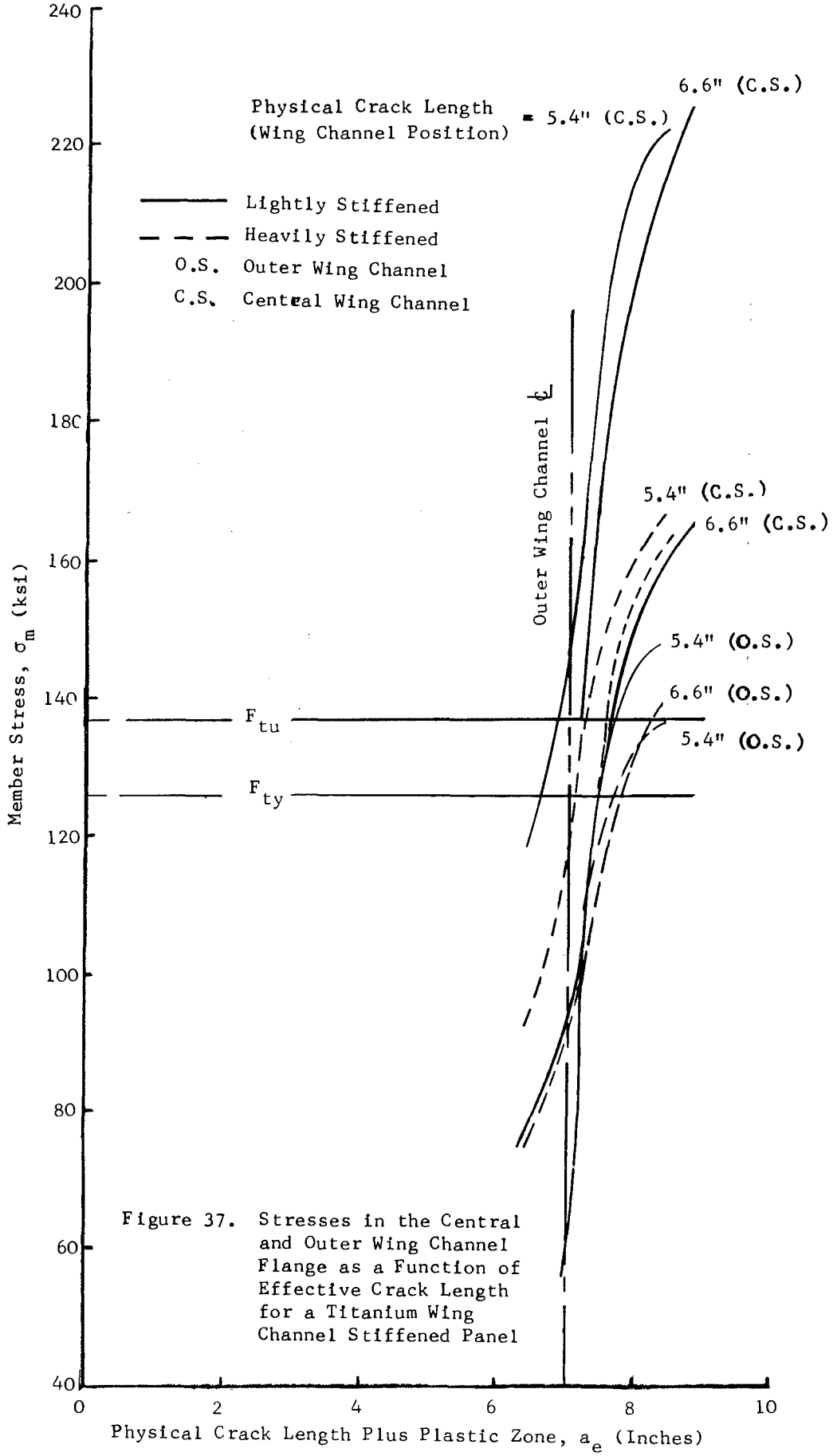

Figure 37. Stresses in the Central and Outer Wing Channel Flange as a Function of Effective Crack Length for a Titanium Wing Channel Stiffened Panel

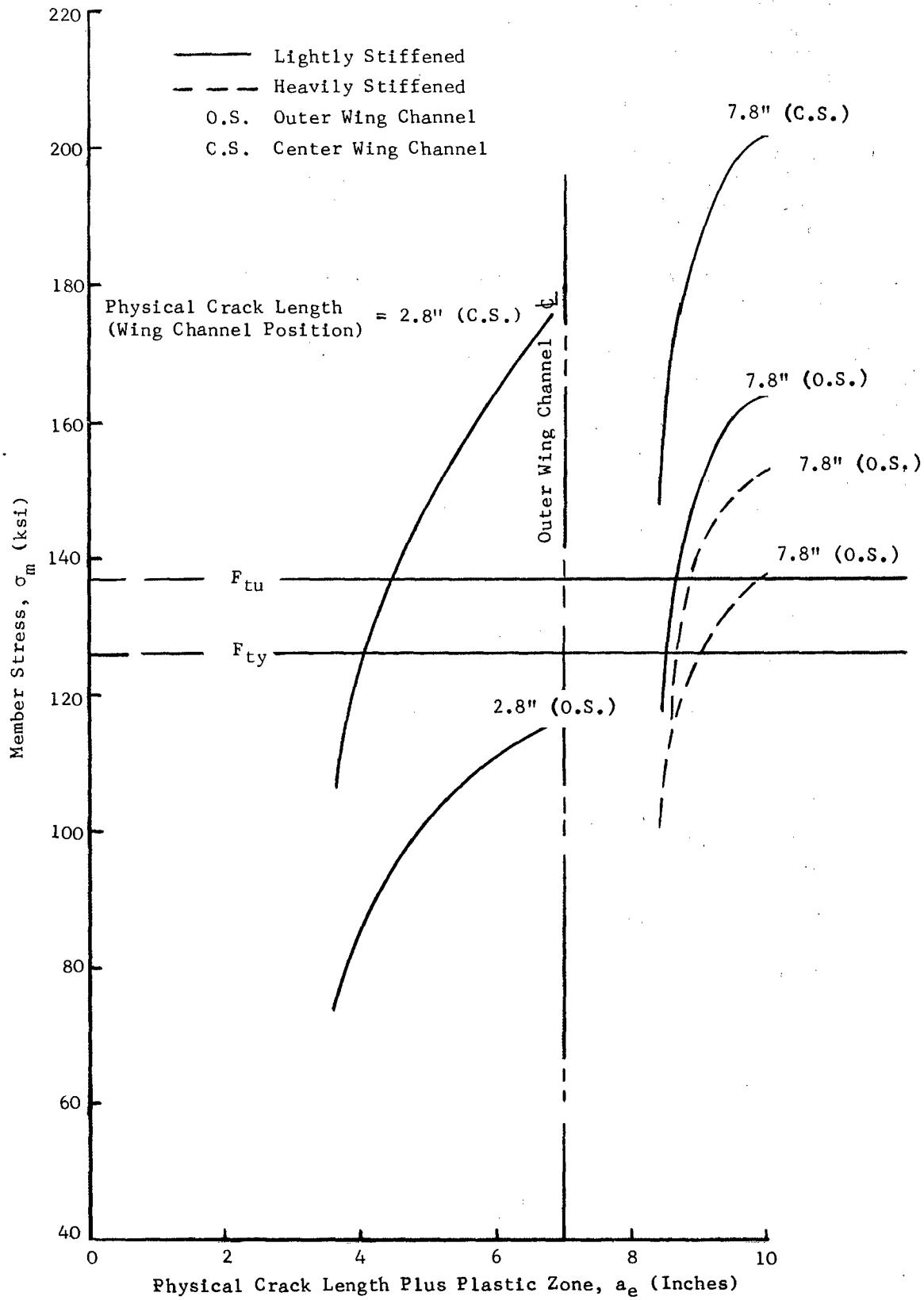

Figure 38. Stresses in the Central and Outer Wing Channel Flange as a Function of Effective Crack Length for a Titanium Wing Channel Stiffened Panel

2. The outer stringer reaches yield when the plastic zone is some distance ahead of the centerline of the outer stringer (see Figures 34 and 37). The distance of the plastic zone from the centerline of the stringer will depend on the area of the stringer. For the lightly stiffened case this distance will be small; the reverse is true for the heavily stiffened wing channel panel.

3. For very large physical crack lengths, the stresses in the central stringer are only slightly dependent on the crack size for the same applied load (see Figure 33 - This is also evident from the elastic analysis of Figure 10.)

3.3.3.3 Comparison of Elastic, Dugdale, and Prandtl-Reuss Material Behavior - Analyses of Stresses in Stiffeners

The stresses in central and outer stiffeners based on elastic, Dugdale, and Prandtl-Reuss material behavior are shown in Figure 39 for a physical half crack length of 2.8 inches. The stresses in the outer stringer appear to be independent of the type of analyses employed. For the central stringer the Dugdale analysis gives higher stresses than those obtained from elastic and Prandtl-Reuss assumptions. Prandtl-Reuss and elastic behavior are similar up to 70 percent of F_{ty}; however, at stresses beyond this value, Prandtl-Reuss values become lower than corresponding elastic values.

Figures 40 and 41 show the stresses in central and outer stringers, respectively, for elastic, Dugdale and Prandtl-Reuss type of material behavior, for a 5.4 inch half crack size in a lightly stiffened wing channel panel. For the same applied stress, p, the stresses for the three types of material behavior are almost the same up to yielding of both the outer and central stringers. The failure stresses predicted for the central stringer by Dugdale model and Prandtl-Reuss behavior are different. From Figure 41 the applied stress p required for yielding of the outer stringer is within ten percent for the two types of assumed material behavior (Dugdale and Prandtl-Reuss). Correspondingly, the size of the plastic zone at onset of outer stringer yielding is also within ten percent for these two types of assumed material behavior.

Based on the analytical results for the heavily and lightly stiffened wing channel panel configuration, the following observations can be made for this panel geometry:

1. The outer stringers may be assumed to yield when the plastic zone is a little beyong the centerline of the outer stringer.

2. The applied stress p required to cause stiffener yielding in the Dugdale model and Prandtl-Reuss cases is only slightly different from the applied stress causing stringer yielding using elastic assumptions. Thus, the stiffeners may be assumed to yield at the stresses obtained assuming elastic structural behavior.

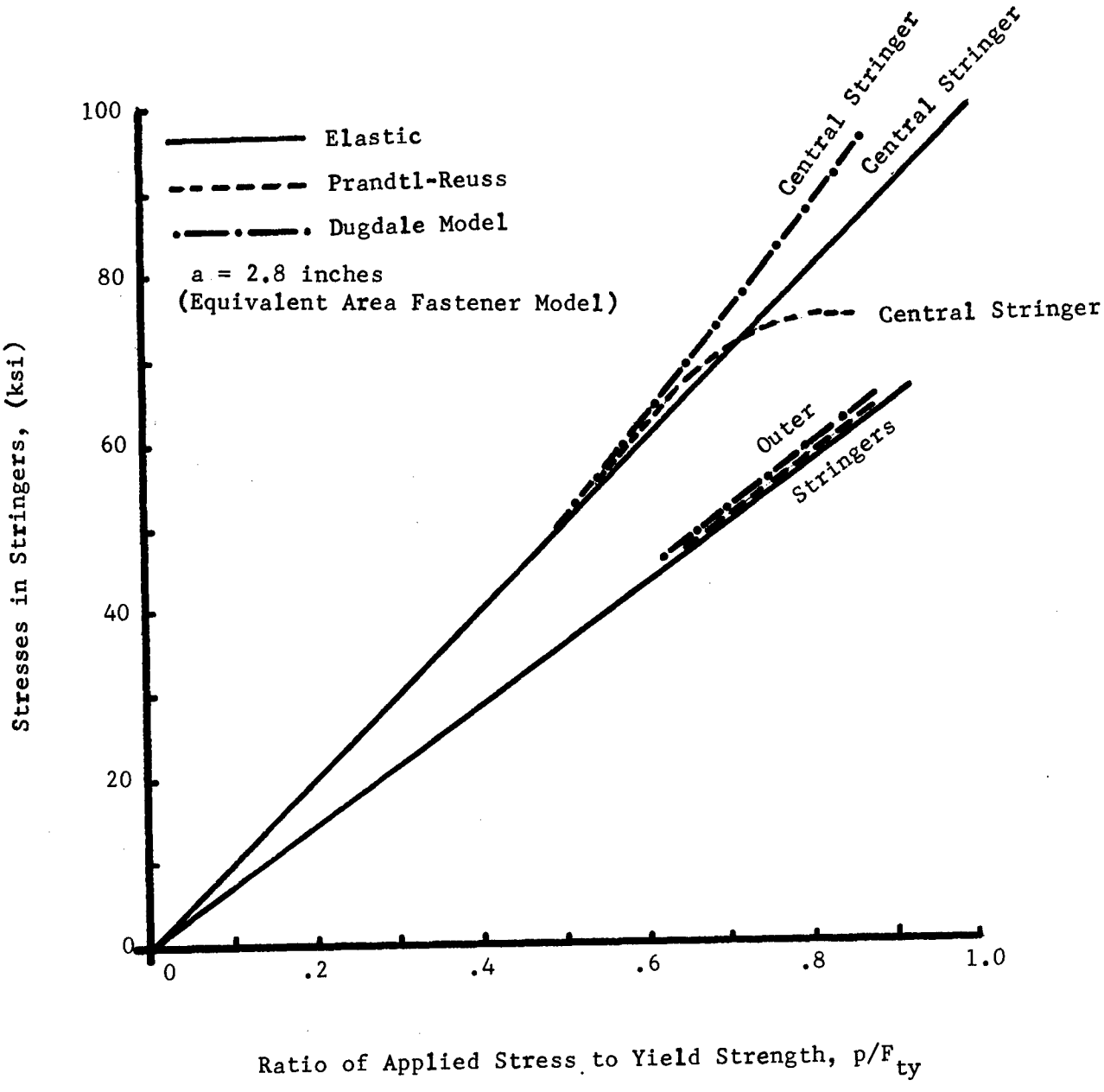

Figure 39. Stresses in Stiffeners for Assumed Elastic, Prandtl-Reuss and Dugdale Model Behavior - Wing Channel Panel a = 2.8 Inches

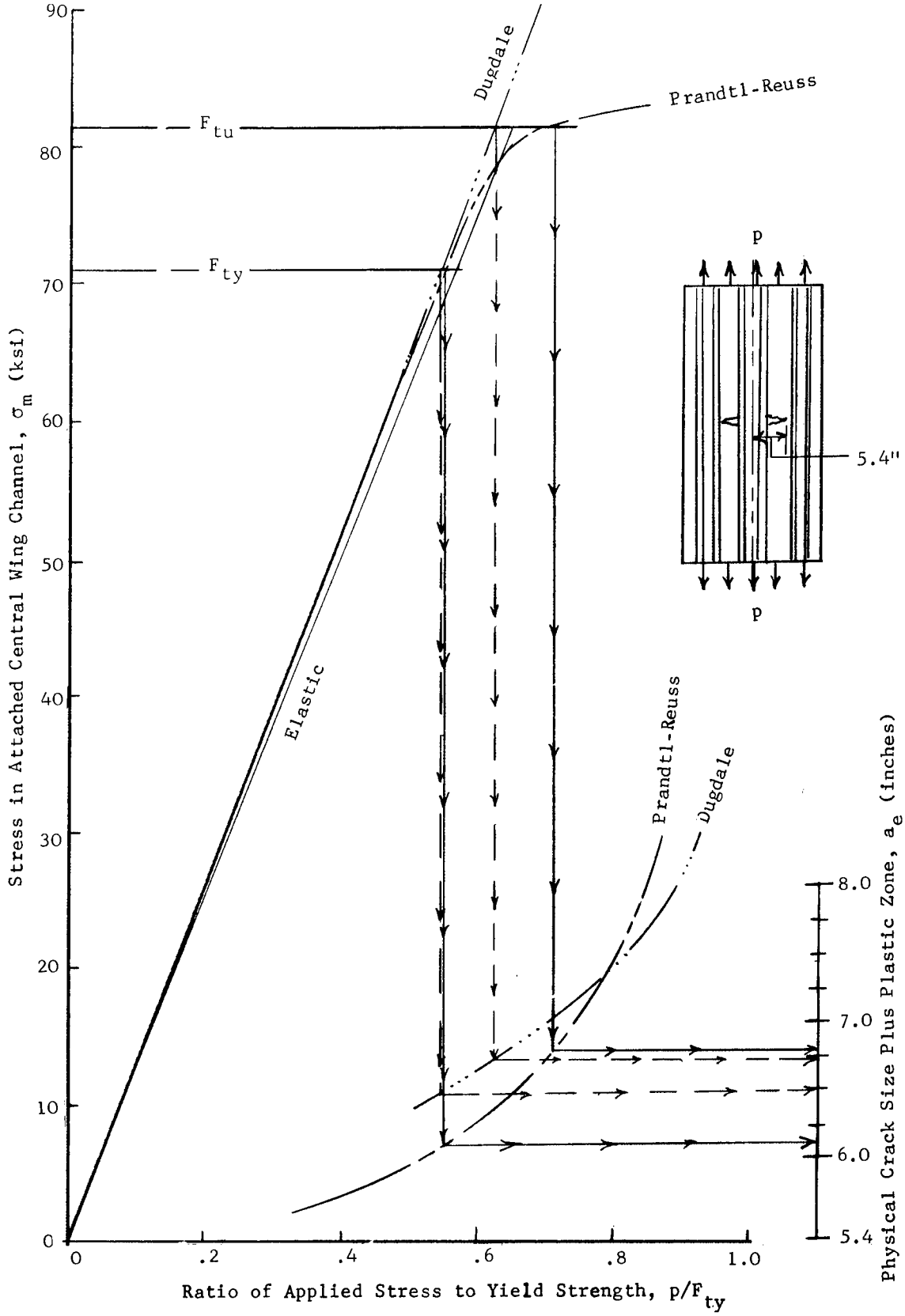

Figure 40. Stress in Central Stringer for Dugdale, Prandtl-Reuss, and Elastic Material Behavior Assumptions

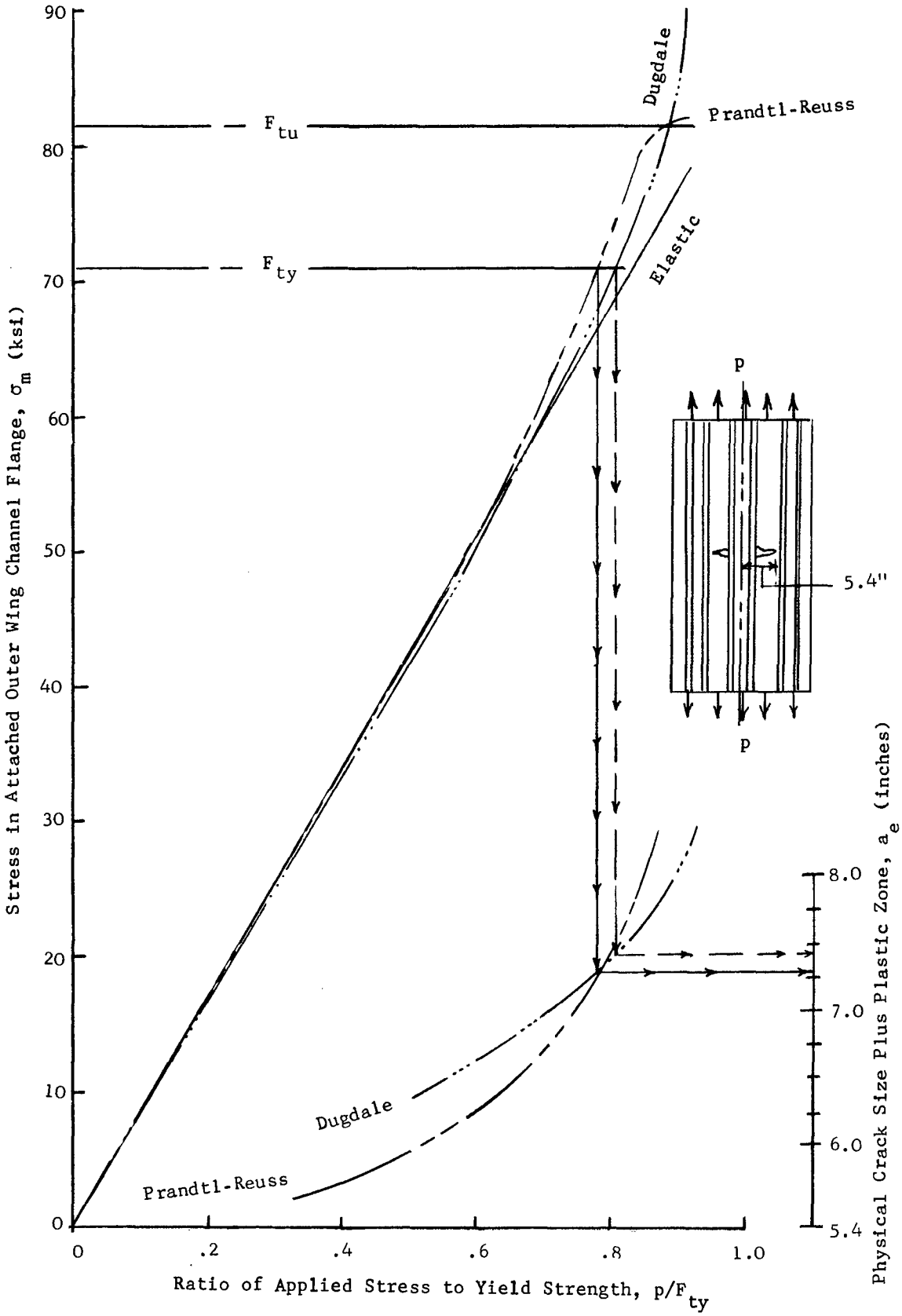

Figure 41. Stress in the Outer Stringer for Dugdale, Prandtl-Reuss, and Elastic Material Behavior Assumptions

3. For stiffener yielding and failure the Dugdale model gives stresses which are very close to those stresses obtained by assuming Prandtl-Reuss material behavior. Hence, the Dugdale model may be used to study both yielding and ultimate strength failure of the stringers.

4. For the lightly stiffened panel case, the central stringer may be assumed to be broken when the outer stringer yields (see Figures 37 and 38).

5. The failure of the stringers will be governed by the critical strain reached in the stringer.

3.3.4 Effect of Fastener Modeling on Elastic-Plastic Analysis of Stiffened Structure

In Section 3.1.3 two different methods of modeling fasteners (equivalent area and flexible fastener) were discussed, and in Section 3.3 the effect of these fastener models on elastic analysis of the crack structure was examined. The fastener modeling will also affect the elastic-plastic analysis of stiffened panels. Therefore, in this section the influence of fastener modeling on fastener stresses, stiffener stresses and square root of J calculations is considered.

3.3.4.1 Effect of Fastener Modeling on Stresses in Rivets

The effect of the two fastener models on stress in the rivet in the central stringer immediately above the crack for the lightly stiffened wing channel is shown in Figures 42 and 43 for half crack lengths of 2.8 inches and 5.4 inches, respectively. For both crack lengths and fastener models the stresses given by the Dugdale type analysis are higher than those given by the elastic analysis. The percentage increase in stress due to an elastic-plastic analysis is similar for the two fastener models. At a 2.8 inch half crack length the stresses obtained from an elastic-plastic analysis are approximately 12 percent higher than the elastic case at 70 percent of the yield stress. For both small and large crack lengths, the equivalent area fastener model results in calculated stress nearly twice as high as those given by the flexible fastener model. These higher stresses are observed for both elastic and elastic-plastic analysis. For example, the equivalent area model will predict fastener failure at very low applied stresses for either elastic behavior or Dugdale plastic zone assumptions. Fastener failure here has been defined as an ultimate strength failure (see Figures 42 and 43) although in actual practice it is known that the fastener will fail at some critical value of shear strength. These predicted stresses appear to be rather unrealistic since it is known that fastener failure would not be expected at such low applied stresses. The stresses given by the flexible fastener model appear to be more realistic for both crack lengths.

3.3.4.2 Effect of Fastener Modeling on Displacements

The effect of fastener modeling on the crack opening at the center of the crack (panel centerline) for the lightly stiffened wing channel panel is

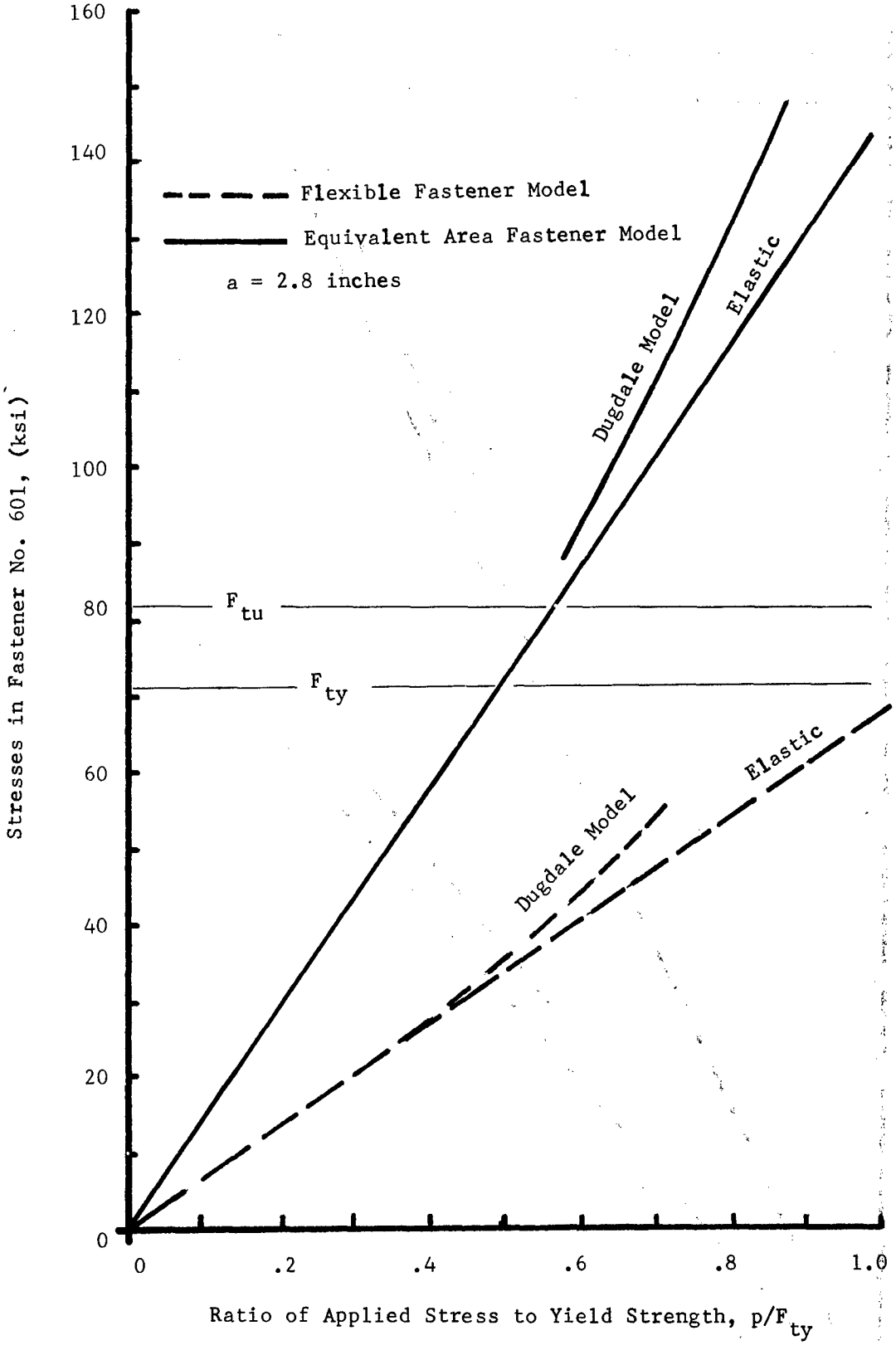

Figure 42. Stresses in Fastener for Two Fastener Models - Lightly Stiffened Wing Channel Panel - a = 2.8 Inches

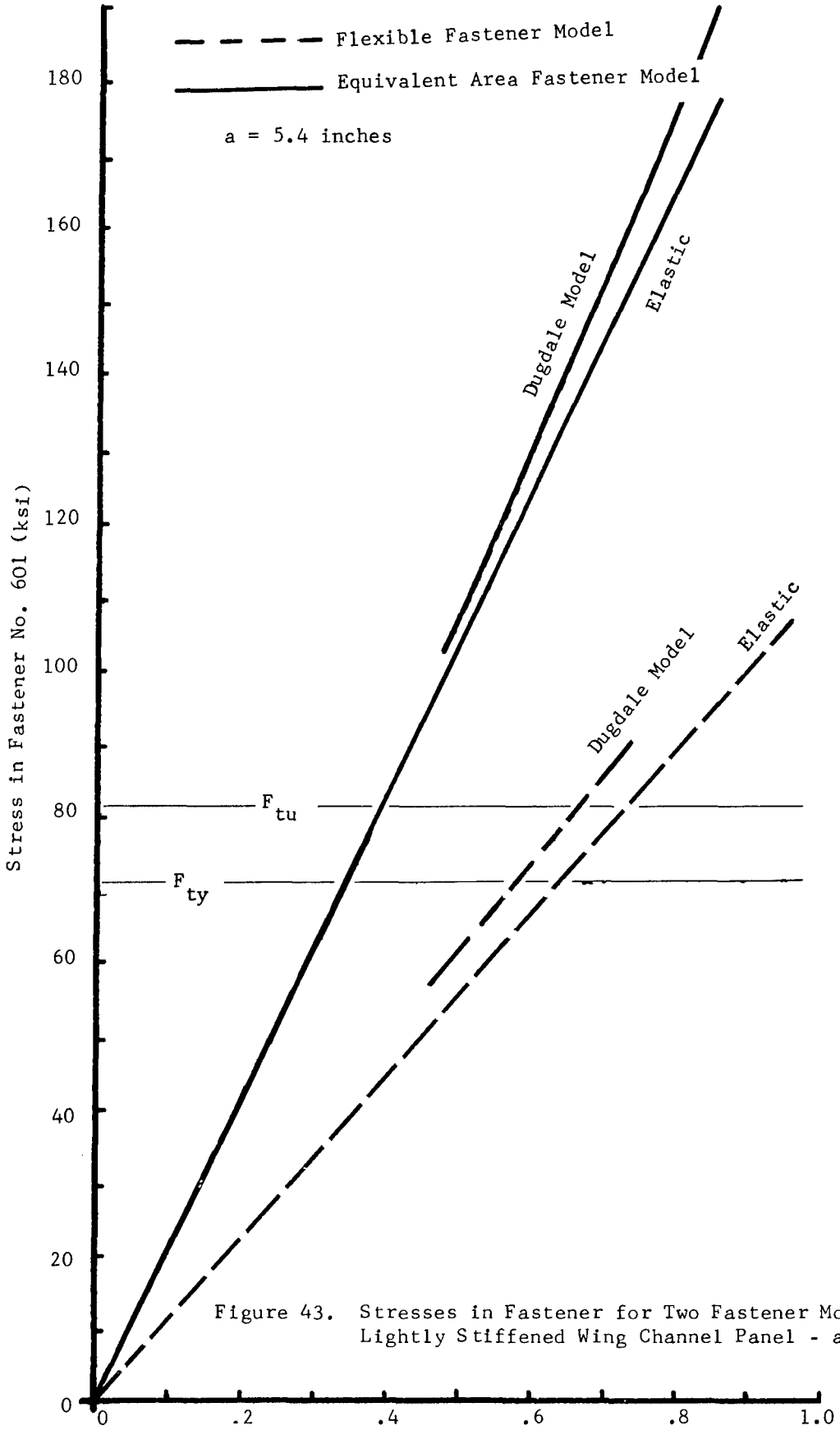

Figure 43. Stresses in Fastener for Two Fastener Models - Lightly Stiffened Wing Channel Panel - a = 5.4 Inches

shown in Figure 44 assuming Prandtl-Reuss material behavior. Up to 45 percent of yield, Prandtl-Reuss deflections are similar to those given by elastic behavior. However, at higher applied stresses assumed Prandtl-Reuss behavior gives extremely large crack openings compared to elastic behavior. The crack openings given by the flexible fastener model are much larger than those given by the equivalent area model. At an applied stress of 60 percent of yield the flexible fastener model gives deflections 75 percent higher than the equivalent area model. However, the difference between crack openings given by the two models decreases with increasing load caused primarily by large plastic deformations at higher stresses.

3.3.4.3 Effect of Fastener Modeling on Stresses in Stringers

The effect of fastener modeling on stresses in stringers for assumed Prandtl-Reuss and Dugdale material behaviors are compared in Figures 45 and 46. For this lightly stiffened panel (a_{PHY} = 5.4 inches) there is little difference in the outer stringer stresses for the two fastener models for both Prandtl-Reuss and Dugdale material behavior. However, the stresses in the central stringer are higher for the two fastener models for both Prandtl-Reuss and Dugdale material behavior. The difference in stringer stresses is larger for Dugdale than for Prandtl-Reuss behavior. For assumed Prandtl-Reuss material behavior, either fastener model gives almost identical stringer stresses at applied stresses greater than 70 percent of yield.

3.3.4.4 Effect of Fastener Modeling on J Integral Values

Section 3.3.3 discussed the effects of two fastener models on J integral values for elastic material behavior; fastener modeling will influence an elastic-plastic analysis in a similar manner. Figure 47 shows the influence of fastener modeling on $\sqrt{J}$ for a 5.4 inch physical half crack and assumed Prandtl-Reuss material behavior. The flexible fastener model results in higher values of $\sqrt{J}$ than those of the equivalent area model. The flexible fastener based square root of J values are 12 percent higher than corresponding values based on the equivalent area fastener at an applied stress of 70 percent of yield.

The influence of these fastener models on Dugdale type elastic-plastic analysis is shown in Figure 48. The flexible rivet model produces higher values of $\sqrt{J}$ for both short and long crack lengths. At a half crack length of 5.4 inches the flexible fastener model produces values of $\sqrt{J}$ which are 12 percent higher than the values from the equivalent area based model. At 70 percent of yield similar differences were observed for Prandtl-Reuss material behavior. At the same crack length the two fastener models show a smaller difference in square root at J at a 2.8 inch half crack length compared to the 5.4 inch half crack size. For example the two models show a difference of 10 percent (in $\sqrt{J}$) at an applied stress of 70 percent of yield for the 2.8 inch half crack length. Based on the results of these models it appears that the difference in square root of J increases as

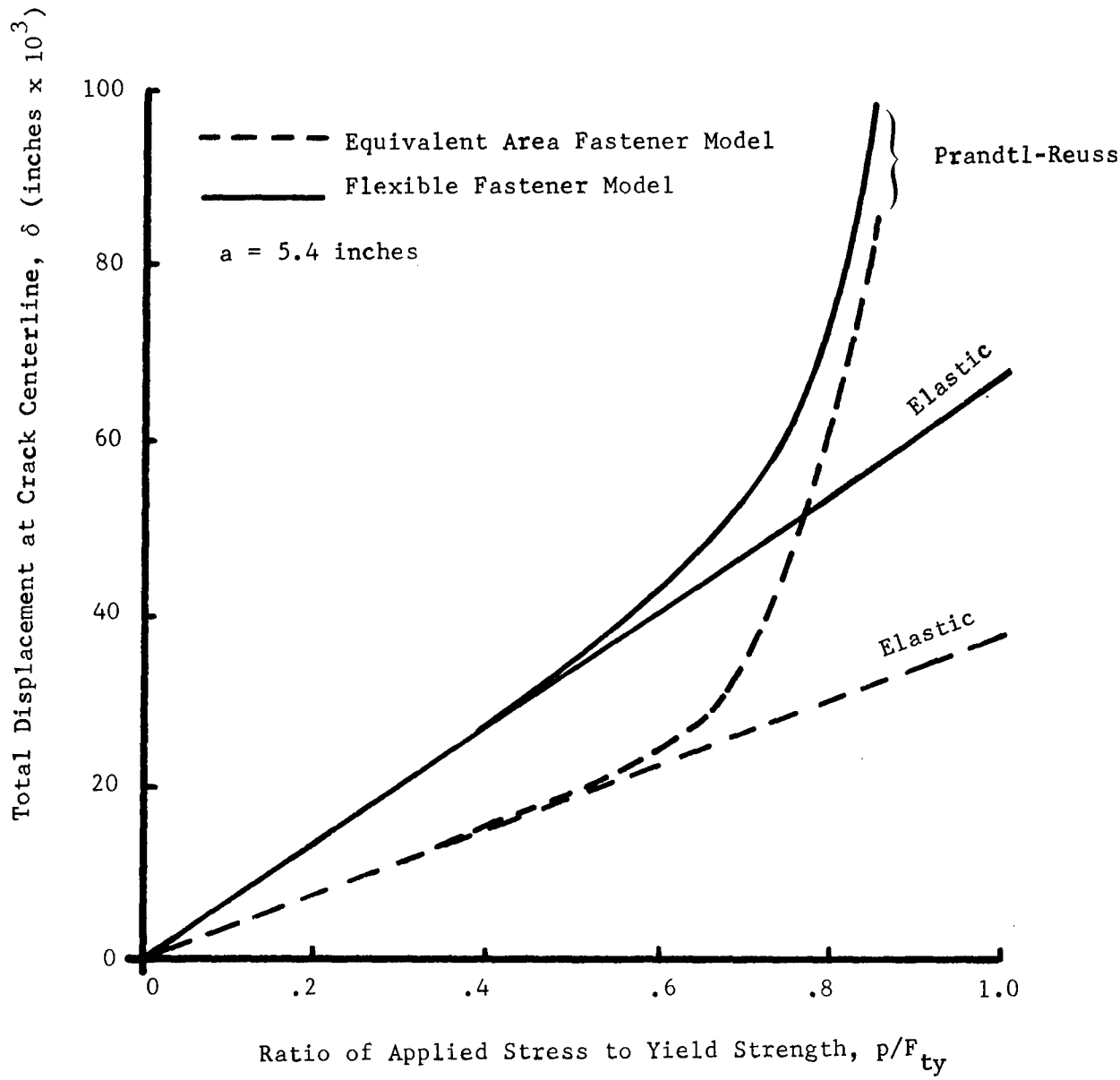

Figure 44. Crack Opening Displacement for Two Fastener Models for Lightly Stiffened Wing Channel Panel - a = 5.4 Inches

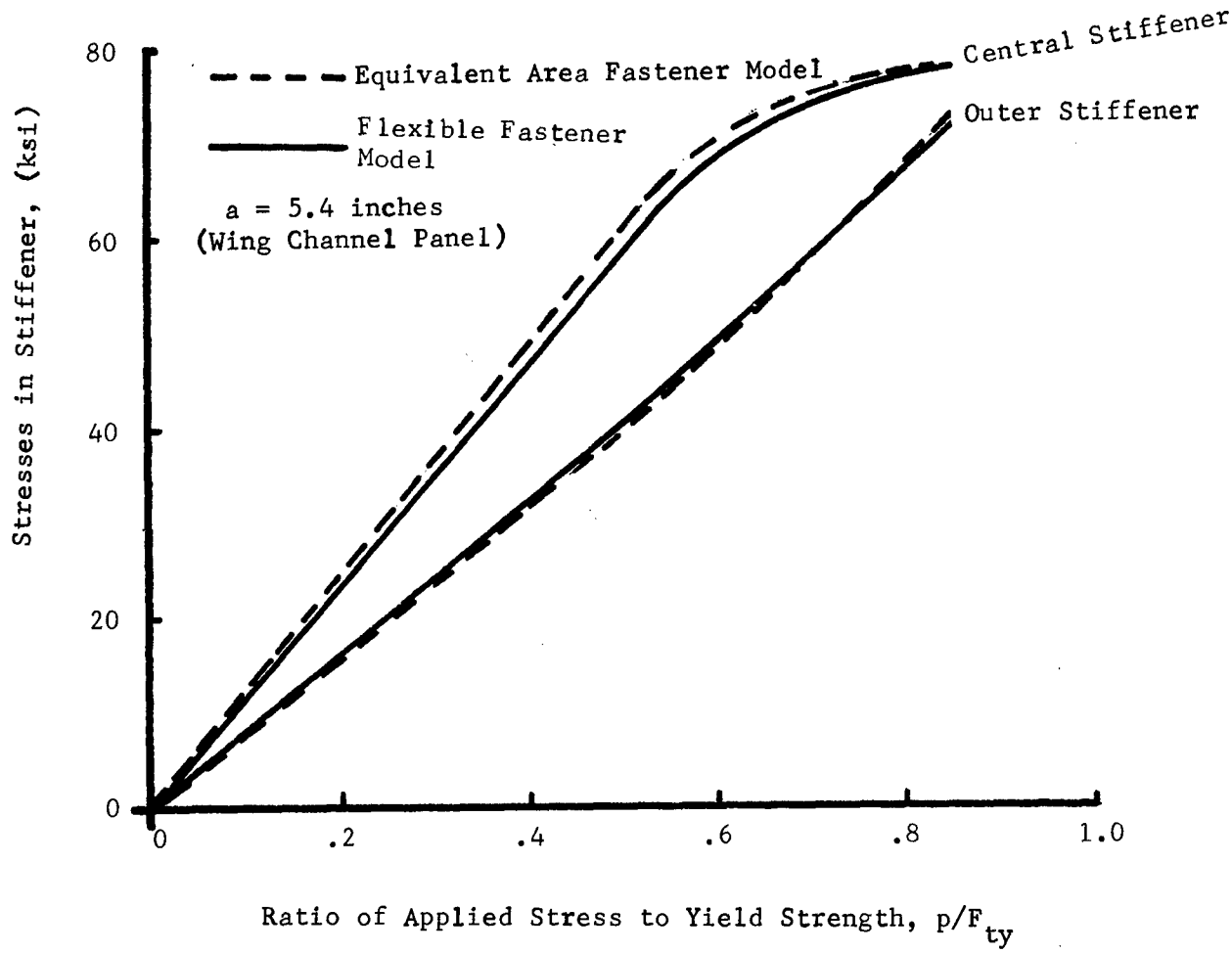

Figure 45. Stresses in Central and Outer Stiffeners for Two Fastener Models Using Prandtl-Reuss Material Behavior - a = 5.4.Inches

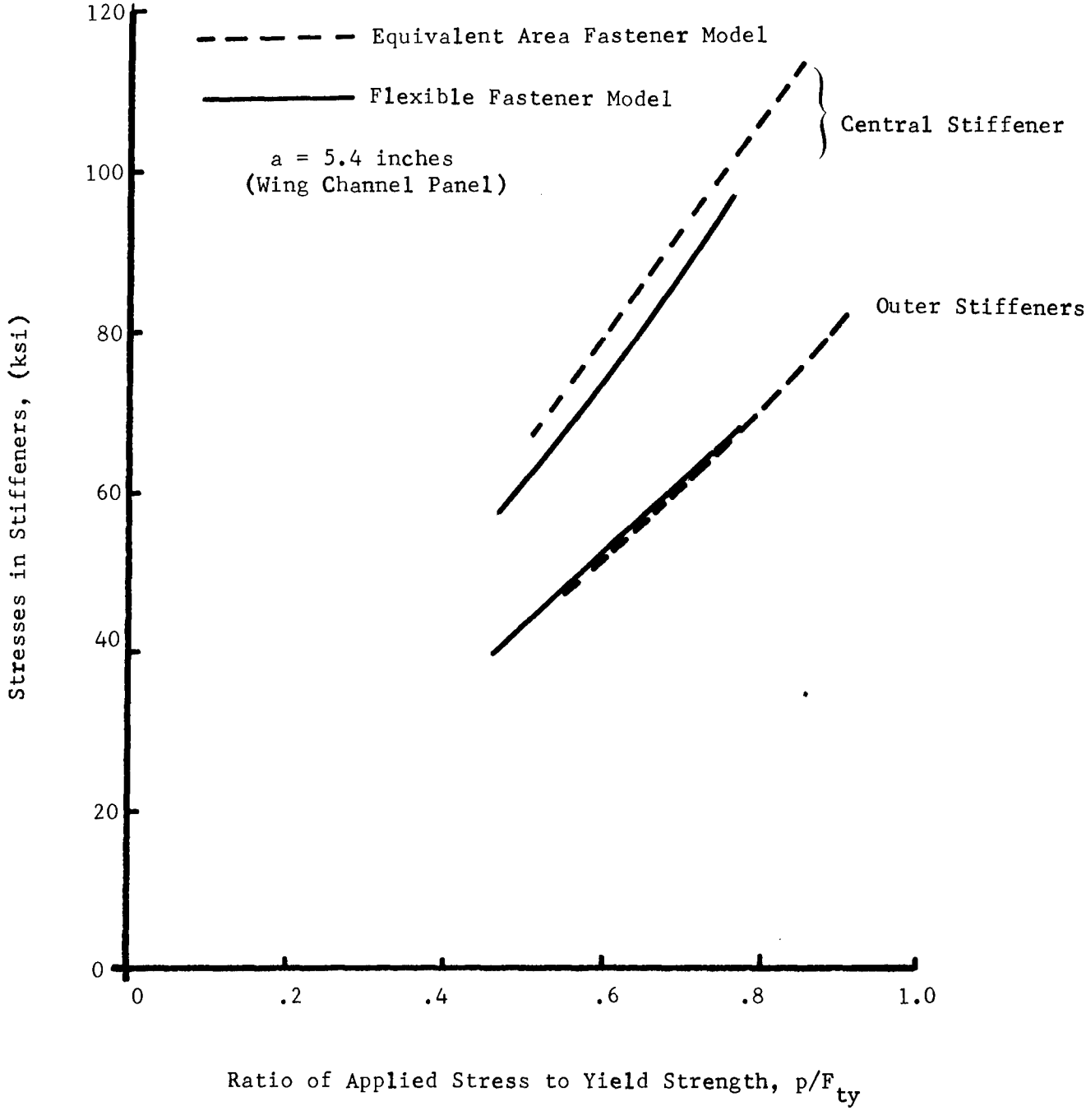

Figure 46. Stresses in Central and Outer Stiffeners for Two Fastener Models Using Dugdale Model Assumptions - a = 5.4 Inches

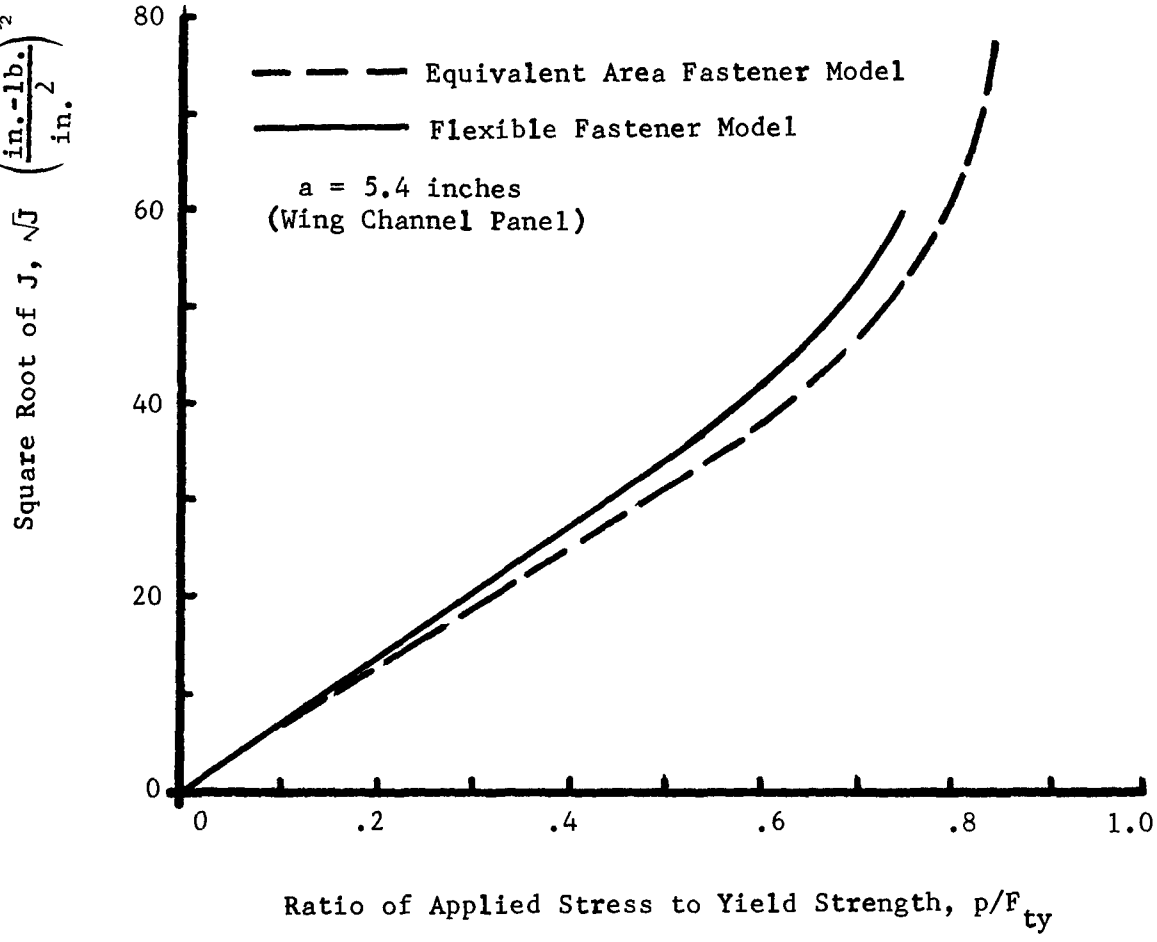

Figure 47. Square Root of J Values for Two Fastener Models Using Prandtl-Reuss Material Behavior - a = 5.4 Inches

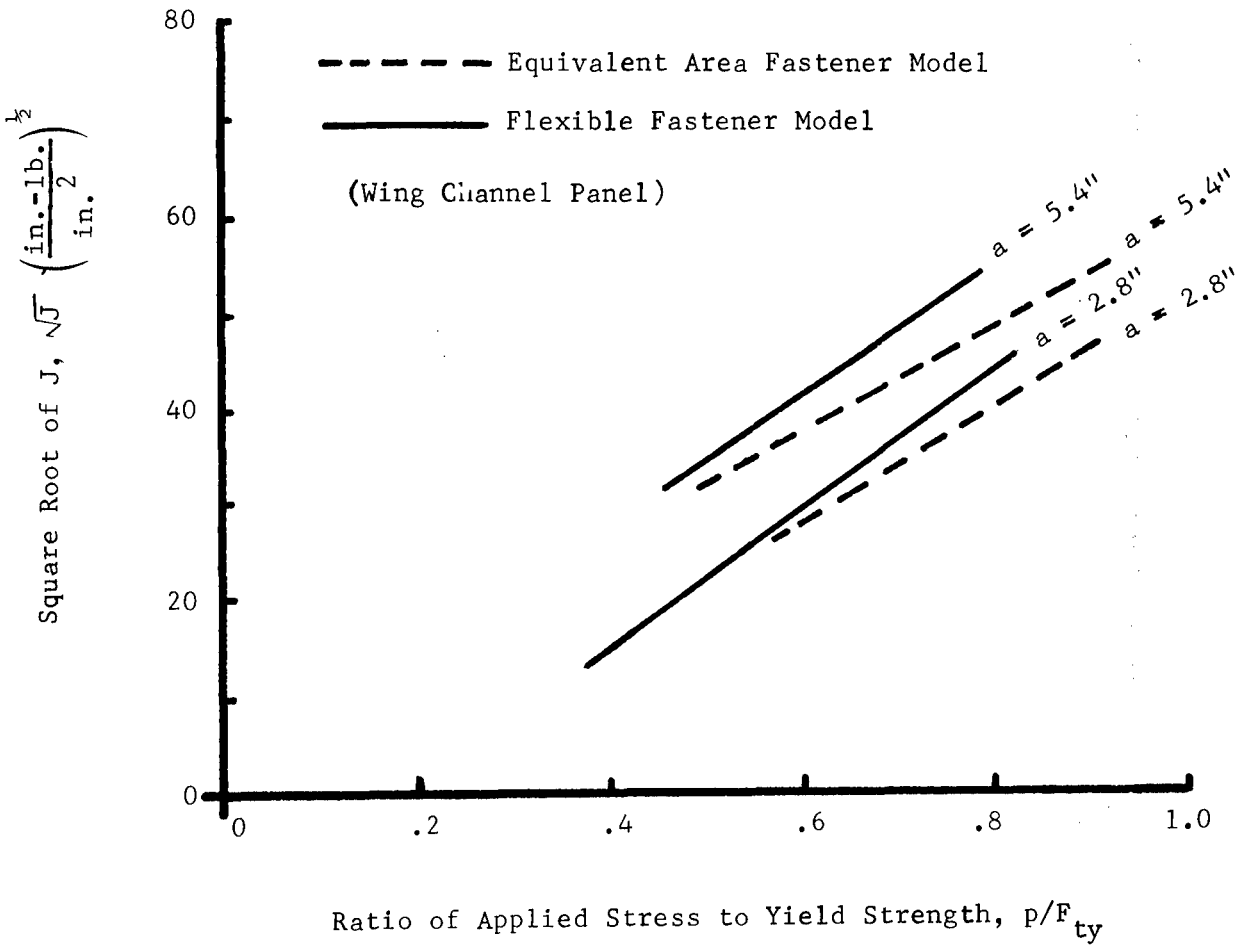

Figure 48. Influence of Fastener Model on Dugdale Model - Square Root of J for Long and Short Crack Lengths

crack length increases. The higher $\sqrt{J}$ value from the flexible fastener model is caused primarily by the flexible model accounting for fastener flexibility hence larger crack openings. The equivalent area rivet model on the other hand will tend to give lower values of $\sqrt{J}$ thus overestimating the residual strength of a crack structure. Similar trends of influence of the two fastener models were noted for elastic stress intensity factors as discussed in Section 3.2.2.

3.4 OTHER FACTORS INFLUENCING RESIDUAL STRENGTH

In the "ideal" residual strength prediction technique outlined in Reference 1, there were particular parameters (structural, loading and material) which would be accounted for in the "ideal" method. These parameters are repeated here in Table VIII. These parameters have been reviewed in light of the proposed technique developed during this program. Those parameters of Table VIII which have not been investigated thus far in the proposed analysis/fracture criterion have been marked with an asterisk. It is these parameters and means of treating them which will be addressed in this section. It will become apparent in the discussions of this report how finite element modeling, testing technique, and other factors can be utilized to treat the specific parameters of Table VIII which have been or are addressed directly.

3.4.1 Layered Construction

In a layered structure (e.g., laminated) failure may propagate through individual layers or through the whole structure. For example, a layered structure could be metallurgically or adhesively bonded and consist of many layers. In such construction flaws or cracks could exist in one or more layers or in the bond. If a linear elastic approach is used then it is necessary to know the stress intensity factors for flaws in individual layers and the fracture would then be governed by the critical stress intensity factor. In such a structure the realistic case involves plastic zones at the crack tips. An elastic-plastic analysis is necessary to determine the plastic zones in each individual layer. The use of the J integral as a failure criterion for such a structure will be suitable if J values can be computed for each individual layer. The values of J will be different depending on flaw or crack location, size, etc., in each layer and J will be path independent for each layer. Dugdale type analysis with the Bueckner-Hayes approach cannot be applied directly if more than one layer is cracked and several iteration processes would be required. The problem can be treated directly by using Prandtl-Reuss material behavior in conjunction with a finite element model for a cracked, layered structure. Assuming Prandtl-Reuss material behavior, J values can be computed for each of the individual layers. The procedure described in Section VIII can then be used for residual strength prediction. The results thus obtained are based on the assumption that the fracture is governed by the dominant crack in one of the layers. The effect of stable tear of other cracks on the dominant crack is assumed to be negligible. The procedure will not be applicable if the cracks in all of the layers are of the same order or magnitude. If this

TABLE VIII. PARAMETERS TO BE ACCOUNTED FOR IN AN "IDEAL" RESIDUAL STRENGTH PREDICTION TECHNIQUE

STRUCTURAL PARAMETERS

- Overall structural arrangement
  - Type of Construction
    - Skin stiffened (e.g., stringers, longerons, etc.)
    - Monolithic (thick skin/unreinforced)
    - *Layered - (e.g., core stabilized honeycomb)
    - Planked
    - Integrally stiffened (e.g., waffle pattern)
  - Panel Geometry
    - Planform shape (e.g., rectangular, trapezoidal, etc.)
    - Panel curvature
    - Boundary conditions - (e.g., attachment to spars, ribs, frames, etc.)
    - Orientation of stiffening with respect to panel boundaries and stiffener spacing
- Detailed structural considerations
  - Skin thickness changes (e.g., taper or abrupt)
  - Reinforcement geometry (e.g., rectangular, hat section, channel, Z, etc.)
  - Attachment details (e.g., bolted, riveted, screwed, bonded, welded, etc.)
  - Fastener Flexibility
  - Eccentricity

LOADING PARAMETERS

- Uniaxial Tension
- *Biaxial
- *Biaxial + Shear

MATERIAL PARAMETERS

- Crack Tip Plasticity (not necessarily small with respect to crack length)
- Slow Tear (i.e., stable crack extension)
- *Crack Tip Buckling
- *Load/Strain Rate Sensitivity
- Thermal Effects
- Environmental Effects
- Thickness/Property Variation
- *Anisotropy
- Stiffener Yielding
- Strain Hardening

* Discussed in Section 3.4

is so, the analysis can be carried out by assuming that all the cracks are of the same length. The $\sqrt{J_R}$ curve approach is applicable to layered structures irrespective of the number of layers of crack lengths. In order to account for slow tear of cracks in different layers, several iterations would be required.

3.4.2 Effect of Biaxial and Biaxial Plus Shear Loading

Biaxial stress is known to have a significant effect on fracture initiation. It has been pointed out (Reference 39) that analytically the effect of biaxial stress is of second order and is negligible if purely elastic analysis is considered. However, biaxial stresses show considerable effect if elastic-plastic analysis is considered. This is mainly due to the fact that the stress applied parallel to the crack affects the plastic zone size ahead of the crack tip. In Reference 27, plastic stress intensity factors for plates subjected to a biaxial state of stress have been obtained. It was shown that for applied normal loads beyond the limit for small scale yielding, the biaxial tensile loading decreases both plastic strain intensity factors and the plastic zone. Compressive loading parallel to the crack exhibit opposite effects. Thus, the failure strength of a structure is increased if the applied biaxial loading is tensile and is decreased if applied biaxial loading is compressive. Similar effects have been observed in the experimental work of Reference 39. In Reference 27, a fracture criterion based on critical plastic strain intensity is recommended for uniaxial and biaxial state of stress. It has been shown in Reference 27 that there is a one-to-one correspondence between J integral and the plastic stress (or strain) intensity factors for deformation theory of plasticity with no unloading. Hence, theoretically J critical can be used to predict failure under a biaxial state of stress. The major difficulty involved in the biaxial analysis will perhaps be a suitable plasticity model to account for biaxial stresses since the Dugdale model used in the present analysis will not be suitable. However, J calculations assuming Prandtl-Reuss material behavior under a biaxial state of stress can be readily made. It should be noted that the effect of biaxial tensile loading to increase the residual strength is applicable to unreinforced structure only. For reinforced panels the influence of tensile, biaxial loading may be entirely different since the biaxiality will influence the load transferred to or carried by the stiffeners. This influence is to be examined, and will be reported in the Phase III report.

If shear loads are present in addition to biaxial loads, the crack tip is subjected to both Mode I and Mode II type of loading. Under such a loading system a crack will grow at an angle which for elastic analysis is a function of K_I and K_{II} (see e.g. Reference 40). For elastic analysis it has been suggested that energies for the two modes of loading ($\mathscr{G}_I$ and $\mathscr{G}_{II}$) may be added to govern fracture. In a similar manner Rice has recommended (Reference 8) that J_1 and J_2 under two modes of loading may also be added; thus fracture would be governed by the sum of J_1 and J_2. Plasticity models for biaxial and shear loading are presently not available; hence, the use of J as a failure criterion under this type of loading (biaxial + shear) is presently not feasible for plane stress fracture. A more realistic approach to the problem is perhaps the strain energy density function suggested by Sih (Reference 14). However, this theory is still in an exploratory stage and its utility to elastic-plastic problems has not as yet been established.

3.4.3 Crack Tip Buckling

In-plane buckling of the crack is known to affect the residual strength of center cracked tension panels. In structural arrangements (stiffened skin) the crack located between stiffeners, and sufficiently long cracks at stiffeners can cause a 20 to 25 percent loss in residual strength. The proposed analysis method does not permit crack tip buckling. However, the fracture or failure criterion can include this parameter by causing a reduction in the $\sqrt{J_R}$ curve over that of the unbuckled state.

For example in developing the $\sqrt{J_R}$ curves from the crack line wedge loaded specimen geometry significant care is taken to prevent crack buckling or any in-plane specimen buckling. The effect of crack buckling on critical stress or strain intensity has been primarily studied on the unstiffened center crack tension specimen (see e.g., Reference 41 - 43). In reinforced (stiffened skin) structure the magnitude of crack tip buckling is not usually severe for typical aircraft structure. Therefore, in most cases it can be neglected in the analysis without causing undue inaccuracies. If buckling is anticipated due to inefficient reinforcement, large stiffener spacing and/or a crack between stiffeners, then a reduction in the $\sqrt{J_R}$ curve would be advisable to adequately treat the problem. The amount that the $\sqrt{J_R}$ curve should be reduced can be established by testing the CCT specimen geometry, without buckling restraint, for the same material and thickness. $\sqrt{J}$ integral values can be calculated for this geometry using the method given in Reference 44 and compared with the CLWL specimen data. The difference between the buckled and unbuckled $\sqrt{J_R}$ values can then be used to determine the most critical, buckled condition. Some confidence can then be placed in a percentage reduction to apply to the overall $\sqrt{J_R}$ curve for the particular cracked, structural geometry.

3.4.4 Load/Strain Rate Sensitivity

During the course of this investigation the effect of loading rate on crack growth resistance was examined on one CLWL specimen. The specimen was a 0.195 inch thick, 7075-T651 aluminum, loaded at a crosshead speed of 10 inches per minute or 50 times faster than the normal CLWL test speed used during this program. No difference in the K_R data was noted for this higher rate. Based on the results of this simple test it cannot be concluded that load or strain rate effects are not important. It is believed that of the materials investigated in this program the one which would show the greatest tendency for strain rate sensitivity would be the 9 nickel steel. However, the finished condition of this material was such that studies of its rate sensitivity were abandoned.

If one is concerned with the possibility of a high loading rate environment for a particular structural arrangement, and it is known that the chosen material is load or strain rate sensitive to any large degree (indicated by changes in tensile properties, for example) then it can be treated in the following manner:

Obtain the normal $\sqrt{J_R}$ data for the material and thickness of interest and plot these data as a function of effective crack extension (plasticity included), a_e. Using the CCT specimen, fracture test two or three specimens with the same initial crack aspect ratio (2a/width) at radically different loading rates with buckling restrained. From the load-compliance data compute vaues of $\sqrt{J_R}$ for assumed crack extensions, Δa's. Remembering in this case the Δa's will be effective crack extensions (includes plastic zones) the data can be compared with the normal rate data and any significant changes accounted for by shifting the $\sqrt{J_R}$ curve an appropriate amount.

As an alternate approach it is also possible to determine the effect of strain rate on the material stress-strain curve. If Prandtl-Reuss material behavior is assumed then this strain rate developed stress-strain curve can be included directly in the analysis (see Section 3.3 and 7.1). It should also be acceptable to alter the material yield strength used in the Dugdale model and determine modified values of $\sqrt{J}$ for given crack size and load. Irwin (Reference 45) has suggested such an approach to account for strain hardening effects on plastic zone sizes. With the resulting analytical data the normal load rate $\sqrt{J_R}$ curve can then be used to determine skin critical stress.

3.4.5 Anisotropy

3.4.5.1 Metallurgical Anistropy

The influence of metallurgical properties on crack growth resistance has been discussed in Volume II of this report. Those materials which exhibit extreme prefered rolling tendencies, metallurgical banding of through-the-thickness structures, etc., will require great care in obtaining the necessary fracture criterion data.

The analysis presented for obtaining $\sqrt{J}$ values in Section VI, for example, for the CLWL specimen would require that the actual values of Modulus, yield strength, etc.,would have to be included in the analysis method to compute meaningful J integral values.

3.4.5.2 Structural Anisotropy

For certain structural arrangements the use of crack arrestor strips has been employed or proposed for new designs. These strips may consist of a bonded or integral layer of material other than that used in the basic skin. There are also arrangements which may have different skin/reinforcement material. From this structural anisotropy standpoint calculations of J integral for the various combinations is possible as long as the structure is modeled accurately. If the proper material properties are employed along with suitable flexibility for the bond materials in the finite element analysis (for those which use adhesive or metallurgical bonds) then fairly accurate computation of J should be possible. This will be possible as long as the crack tip is assumed to be in one or the other material. When the crack approaches the boundary of the arrestor strip other methods of analysis may have to be employed.

IV. COMPARISON OF PREDICTED AND EXPERIMENTAL DATA FOR WING CHANNEL STIFFENED PANEL

As discussed in Section 3.3 a panel with three wing channel stiffeners was employed as a trial panel for both analytical and experimental studies of residual strength prediction. In this section the comparison of analytical COD's, strains and load transfer will be made with those experimentally obtained values for the lightly stiffened panel geometry. The term "lightly stiffened" used here does not imply a thin skinned, small area stiffener geometry since the ratio of channel to skin cross sectional area is 1.05 for the fabricated geometry. However, the term "lightly stiffened" panel is used here to distinguish it from the "heavily stiffened" panel of Section 3.3 which has a ratio of channel to skin cross sectional area of 3.74.

A detailed comparison of the data obtained from this lightly stiffened panel will be given in this Section as well as a prediction of residual strength.

Figure 49 is the detailed drawing of the test panel. The only deviation from this drawing was the cross sectional area of the wing channel (See Section A-A). The undercut indicated (to 0.100" thickness on top flanges) was not attempted on the 3 wing channels due to machining difficulties. The finite element modeling of the channel assumed a 0.44-square inch cross sectional area. With the undercut the area would have been 0.444 square inches, without the undercut it was 0.508 square inches. It is felt that this difference in area was not as important as any difference which might occur in the area of the bottom (attached) flange.

The finite element model has 0.211 square inches of bottom flange attachment area (modeled as a rod element) compared to 0.244 square inches in the actual channel, a difference of approximately 10 percent which is not believed to be significant since the thicknesses are identical. Hence the actual panel stresses could be obtained through a multiplying factor equal to the ratio of tested panel area to the panel area used in the analysis. The initial slot length (skin slotted only) was 4.30 inches in overall length.

Figure 50 is a photo of the complete test setup. Details of the channel and skin sides of the wing channel panel are noted in Figures 51 and 52. MTS type clip gages were mounted on the skin side of the specimen, on the panel center line, and three inches on either side of the panel center line, (see Figure 52) to measure crack opening displacements (deflection).

4.1 CRACK OPENING DEFLECTIONS (COD's)

As noted in Figure 52, three MTS, clip type deflection gages were used to record COD at the panel center line and three inches to either side of center on the skin side. Two x-y plotters (Figure 50) were used to record load versus total clip gage deflection, δ.

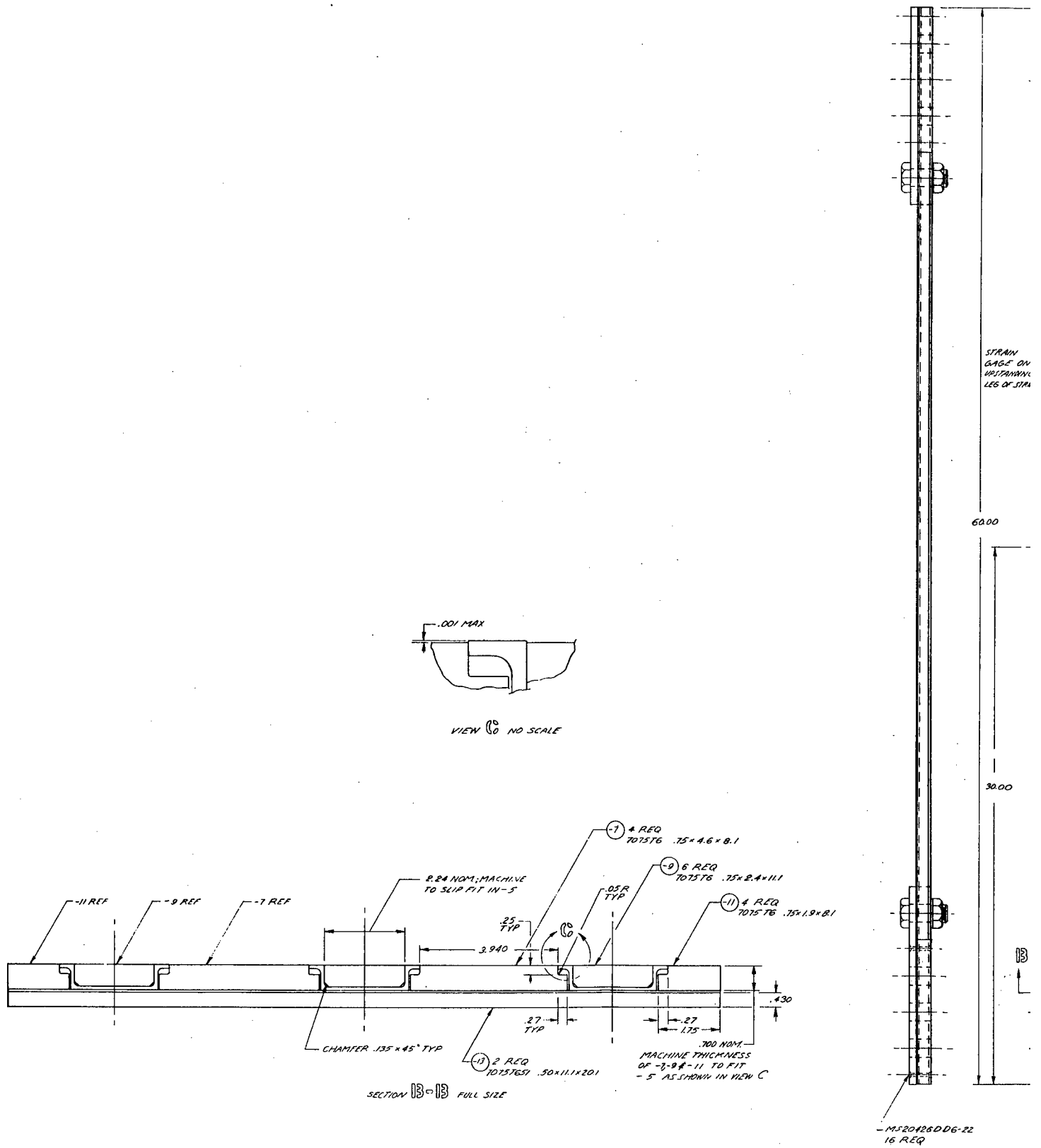

Figure 49. Wing Channel Panel

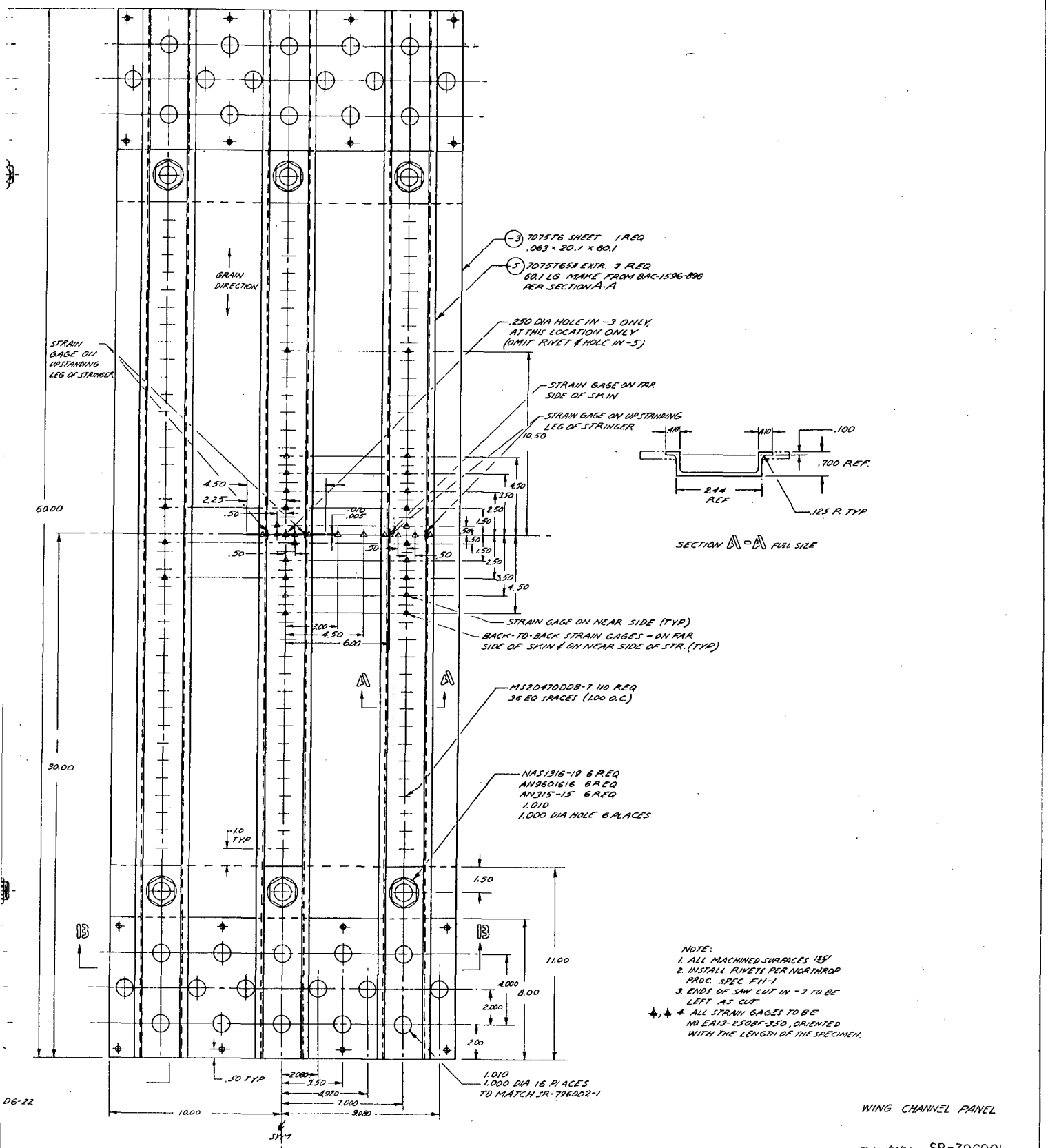

06-22

WING CHANNEL PANEL

FGJ 1/29/74 SR-796001

2

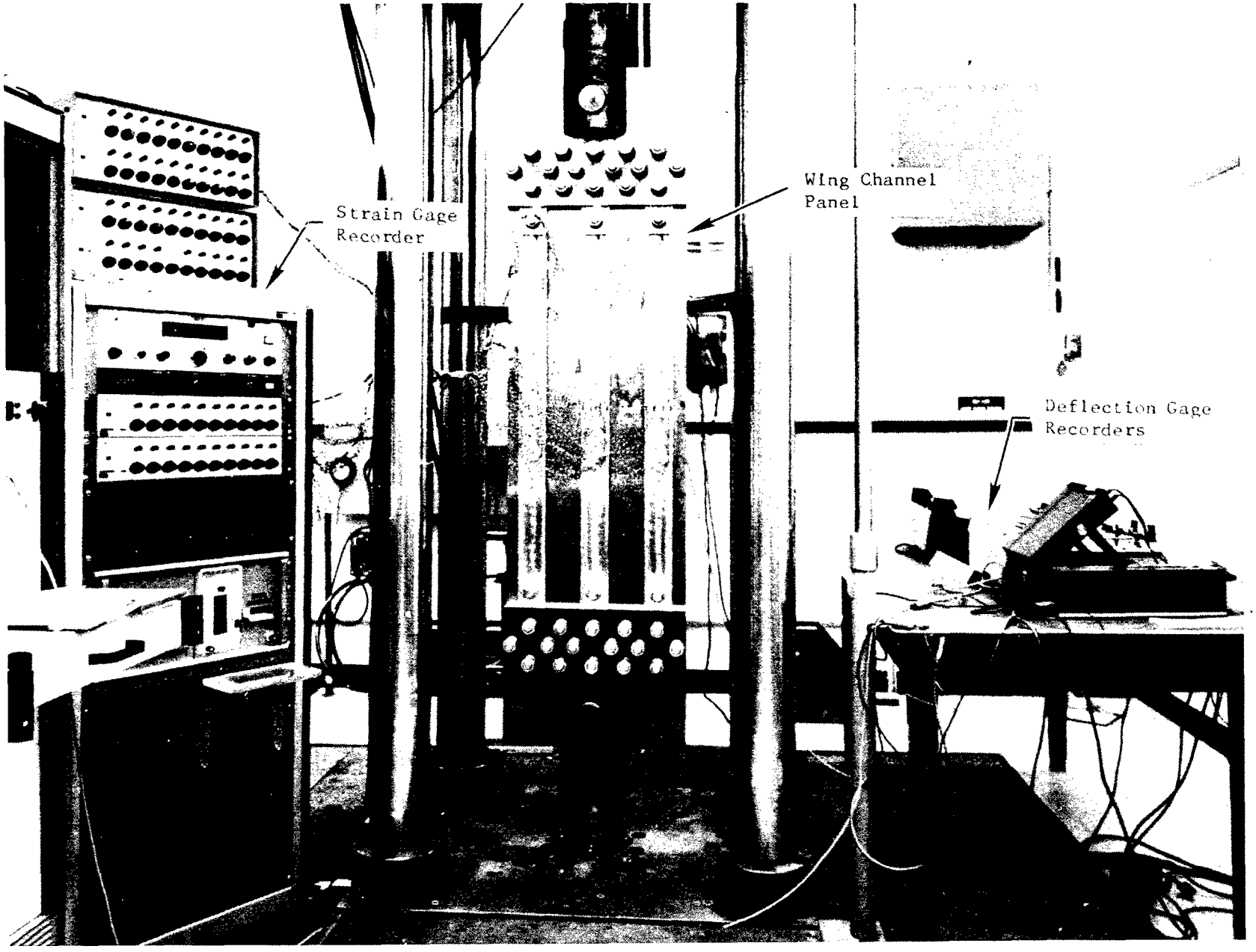

Figure 50. View of Wing Channel Panel Test Set-up in 200 kip MTS Test Frame

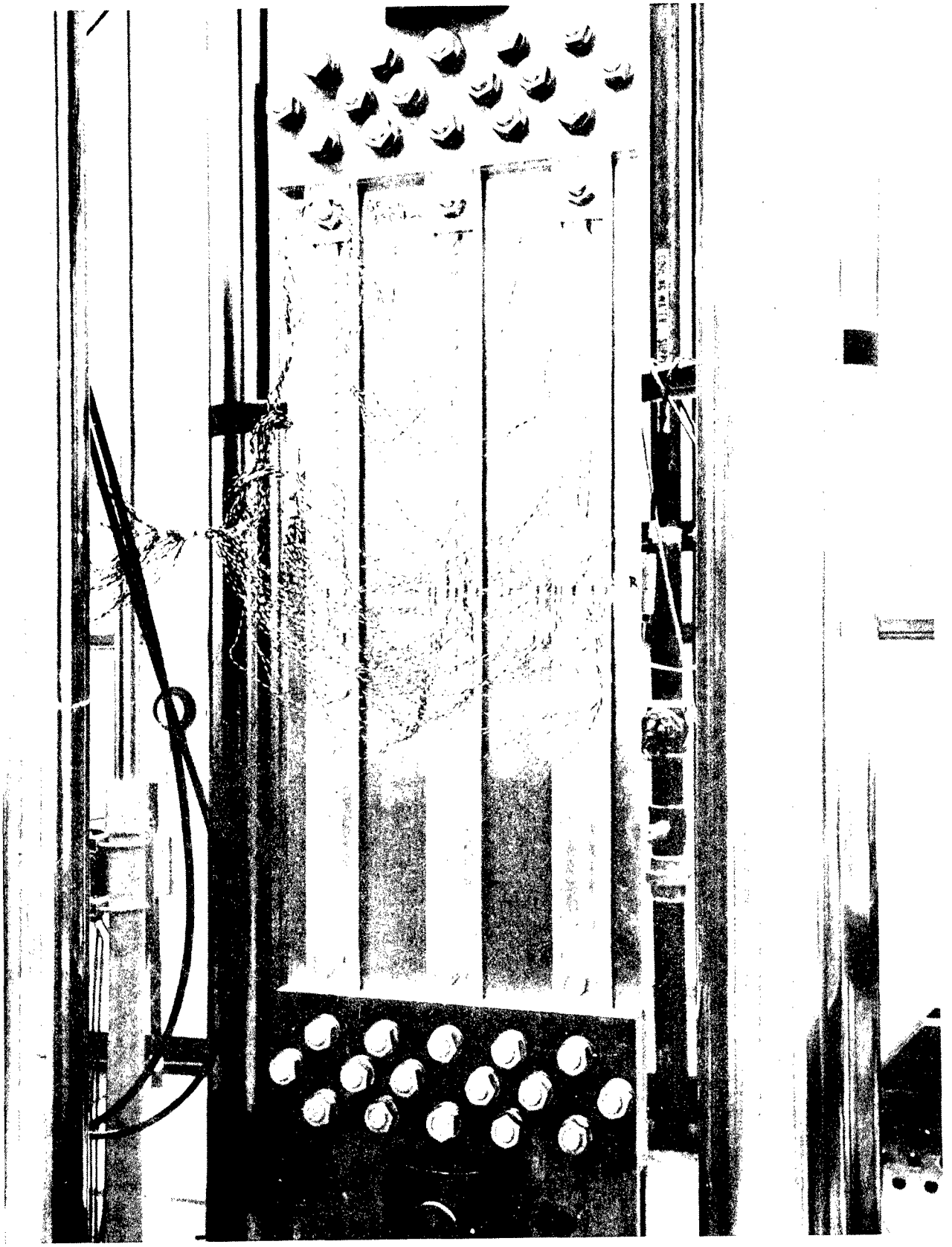

Figure 51. View of Test Panel - Wing Channel Side

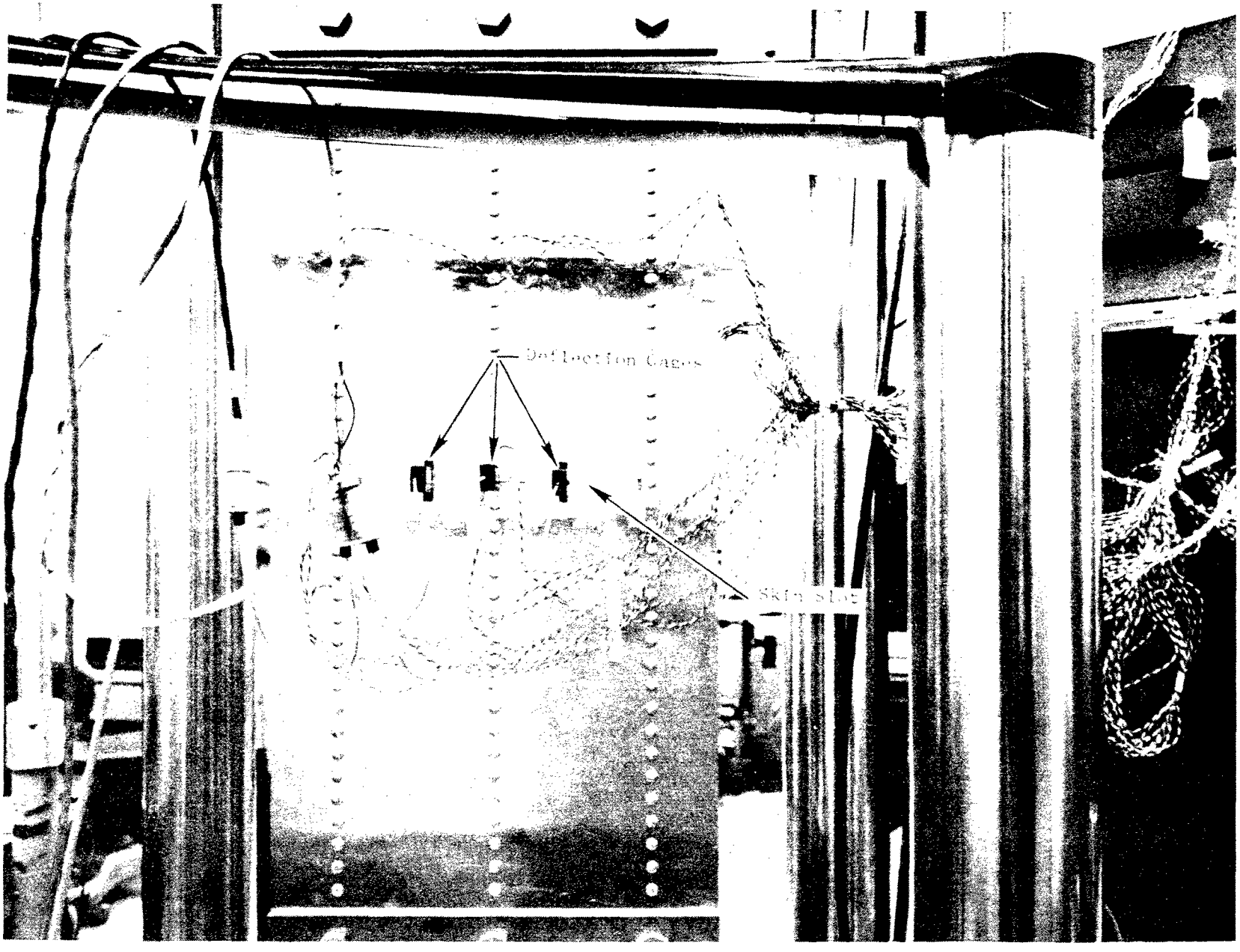

Figure 52. View of Wing Channel Test Panel - Skin Side - Deflection Gages in Place

The test procedure involved loading the panel in increments for a succession of jeweler's saw slot lengths (total slot lengths), 4.3, 5.6, 7.0, 8.0, 9.0, and 10.8 inches.

From the finite element model of the lightly stiffened wing channel panel a succession of elastic analyses were run for the six slot lengths and values of COD obtained for the three clip gage locations. In this case the values of COD for the gages located 3 inches from the panel centerline were assumed equal due to panel symmetry. The comparison of the experimentally obtained COD's for the outer gages (average of the two gages) and the analytical results using the two fastener models is shown in Figure 53. It is obvious that the flexible fastener model agrees quite well with the experimental data (within 13 percent at the longest crack length). Here again the limitations of a fastener model based on equivalent area are apparent. This limitation is even more apparent if the comparison of the centerline COD's are examined. These data are shown in Figure 54 where an excellent correlation between experimental COD and the flexible fastener model results are indicated. The equivalent area fastener model is seen to be approximately 75 percent below the measured data and flexible fastener COD trend.

Based on these data the decision was made to model all subsequent structural panels using the flexible fastener model. A complete description of this finite element model is contained in Section 3.1.

4.2 PANEL STRAIN DATA

The location of the fifty-eight strain gages attached to the lightly stiffened wing channel is noted in Figure 55. In addition to strain gages located on the bottom (attached) flange and skin there were gages positioned on the upstanding legs of the channel (gage numbers 27, 31, 36 and 40) and in the crack path, on the skin material. These gages are numbered 33 and 34 on the channel side and 37 on the skin side. The respective distance of these gages were 3, 4½ and 6 inches from the panel center line along the crack path.

Strain gage readings were recorded on a DATRAN recording unit at specific units of load during a load holding process for each increment of crack (slot) length. Re-zeroing of the gages was accomplished at zero load prior to testing at a new value of crack or slot length. These data are shown for the eight values of slot or crack half length, "a" in Table IX.

The strain data from several gage locations on both skin and channel have been plotted as a function of applied load, p in Figures 56 and 57 for gages along the panel centerline for "a" of 2.8 and 5.4 inches. Linear elastic behavior of both skin and channel are evident.

Figures 58 and 59 show results of the strain survey for the 2.8 and 5.4 inch-long half-slot lengths along the edge channel centerline. Once again linear elastic behavior predominates for an "a" of 2.8 inches. Some nonlinear effects are noted for the 5.4 inch slot in Figure 59 at load levels beyond 16 kips.

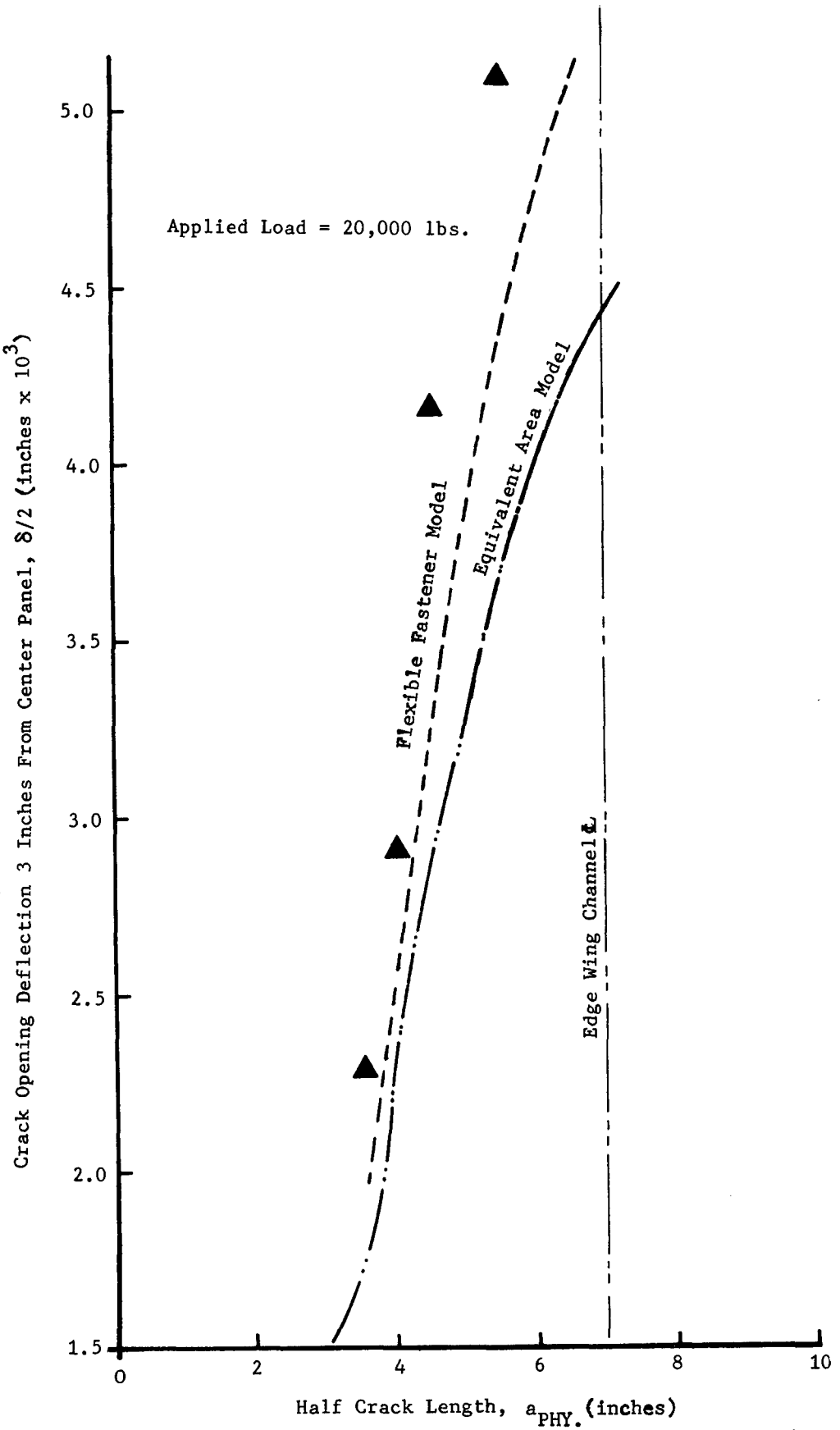

Figure 53. Wing Channel COD as a Function of Crack Length for Two Fastener Models - Gage 3 Inches from Panel Centerline

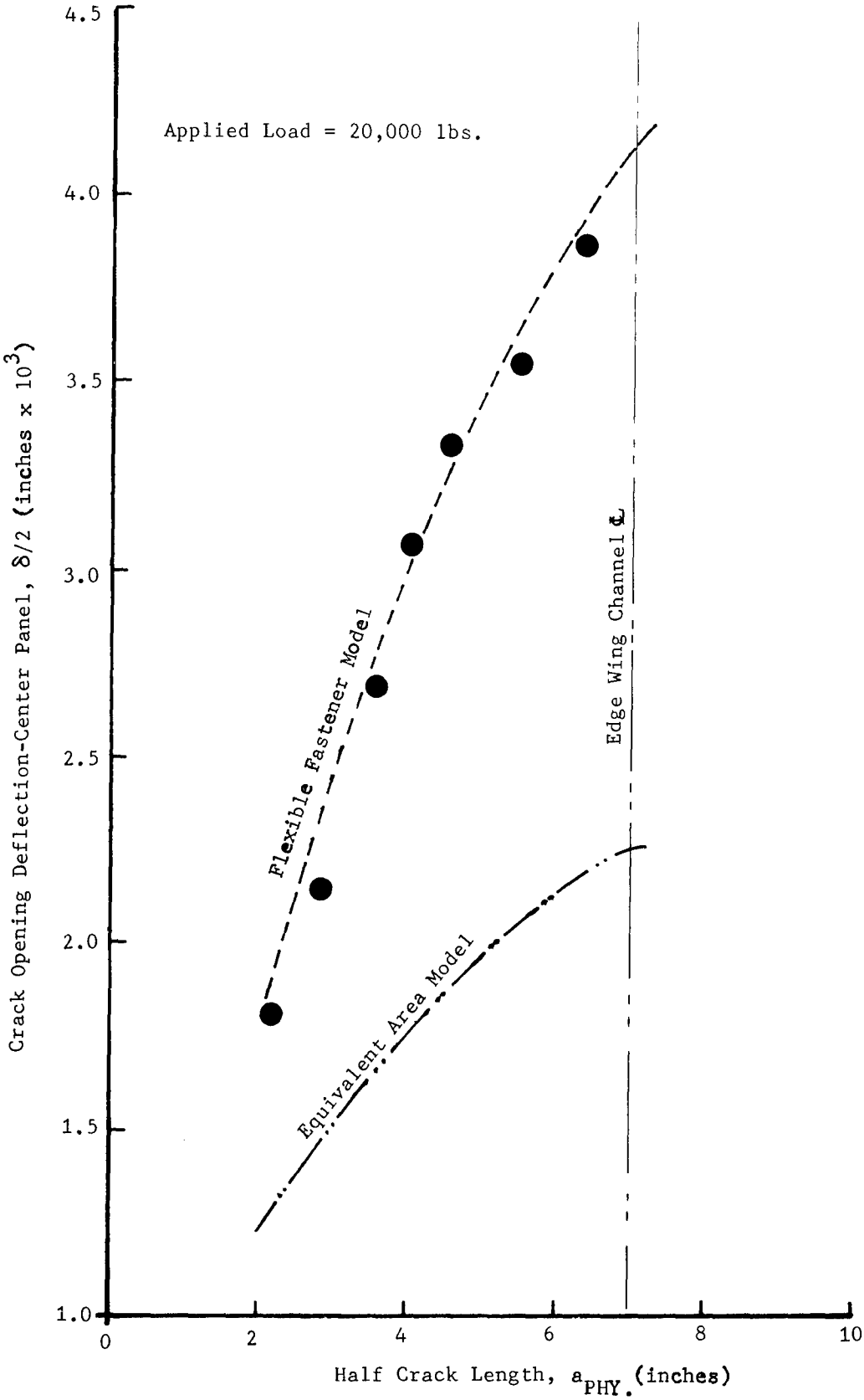

Figure 54. Wing Channel Panel COD as a Function of Crack Length for Two Fastener Models - Gage on Panel Centerline

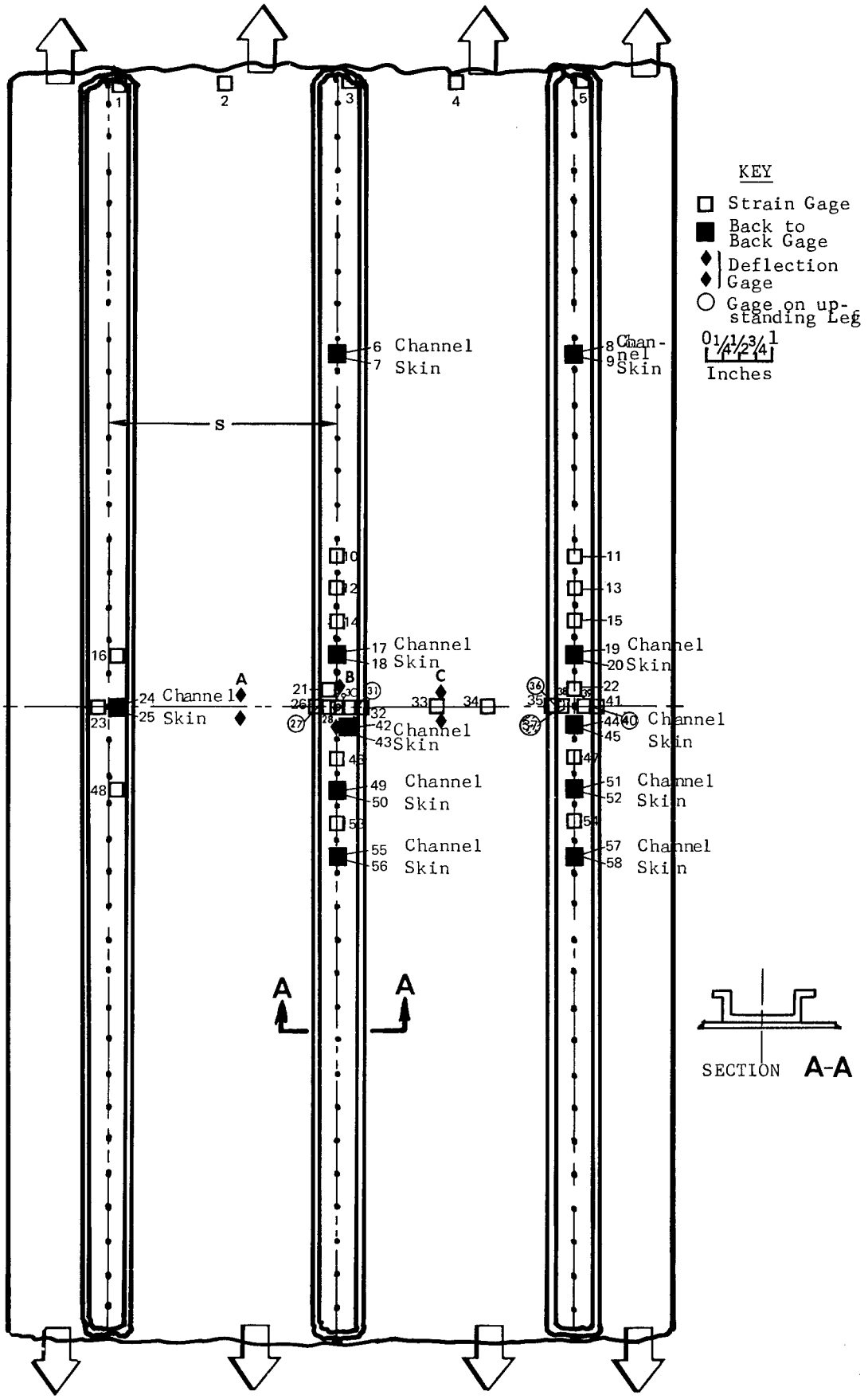

Figure 55. Strain Gage and Deflection Gage Locations on Wing Channel Panel

TABLE IX. WING CHANNEL PANEL STRAIN GAGE DATA

SLOT OR CRACK HALF LENGTH, a (inches)	MACHINE LOAD (kips)	GAGE LOCATION (STRAIN x 10^{-3} inches/inch)																
		(1)	(2)	(3)	(4)	(5)	(6)	(7)	(8)	(9)	(10)	(11)	(12)	(13)	(14)	(15)	(16)	(17)
2.15	10	.43	.24	.435	.25	.44	.355	.32	.36	.30	.35	.375	.33	.38	.36	.38	.36	.48
	20	.815	.50	.865	.52	.855	.71	.62	.72	.56	.70	.75	.68	.765	.73	.755	.73	.915
	30	1.18	.76	1.27	.79	1.26	1.06	.91	1.08	.79	1.05	1.13	1.025	1.14	1.11	1.13	1.09	1.355
	40	1.52	1.045	1.67	1.09	1.67	1.42	1.195	1.44	1.025	1.41	1.51	1.38	1.53	1.495	1.51	1.47	1.80
	50	1.83	1.38	1.975	1.44	1.985	1.75	1.455	1.77	1.22	1.77	1.88	1.72	1.90	1.85	1.87	1.84	2.165
2.15	53	1.92	1.49	2.07	1.56	2.08	1.85	1.53	1.88	1.27	1.88	1.99	1.83	2.015	1.96	1.985	1.96	2.27
2.8	10	.42	.24	.445	.26	.45	.36	.32	.37	.30	.36	.38	.34	.395	.37	.39	.37	.51
	20	.81	.495	.88	.515	.87	.71	.61	.73	.555	.70	.76	.695	.78	.755	.77	.735	.97
	30	1.17	.76	1.30	.79	1.28	1.06	.90	1.09	.79	1.05	1.14	1.04	1.165	1.14	1.15	1.11	1.44
2.8	32	1.24	.81	1.38	.85	1.36	1.13	.95	1.16	.83	1.12	1.215	1.11	1.24	1.22	1.23	1.18	1.53
3.5	10	.435	.24	.45	.25	.45	.35	.305	.36	.30	.35	.39	.355	.40	.39	.39	.38	.55
	20	.825	.495	.88	.51	.87	.69	.595	.73	.545	.705	.77	.715	.79	.80	.78	.76	1.05
	25	1.01	.62	1.09	.64	1.075	.86	.74	.91	.665	.88	.97	.90	.99	1.00	.975	.95	1.305
3.5	30	1.19	.76	1.30	.78	1.28	1.04	.88	1.085	.78	1.06	1.16	1.08	1.19	1.21	1.17	1.14	1.56
4.0	5	.22	.11	.22	.12	.215	.16	.145	.17	.15	.17	.19	.17	.20	.19	.195	.19	.29
	10	.43	.23	.44	.24	.44	.34	.295	.36	.29	.35	.39	.355	.40	.40	.395	.39	.565
	15	.63	.36	.66	.37	.645	.51	.44	.535	.42	.52	.58	.54	.60	.61	.595	.58	.83
	20	.825	.485	.875	.50	.855	.68	.58	.72	.535	.70	.78	.73	.80	.83	.79	.78	1.10
4.0	25	1.01	.62	1.085	.64	1.065	.85	.72	.90	.65	.89	.975	.92	1.005	1.05	.995	.98	1.37
4.5	5	.215	.115	.22	.12	.22	.17	.15	.18	.16	.18	.19	.175	.21	.21	.21	.20	.315
	10	.43	.235	.44	.245	.45	.34	.30	.37	.30	.355	.40	.37	.42	.415	.41	.395	.60
	15	.62	.35	.65	.37	.66	.50	.43	.545	.42	.53	.59	.55	.615	.62	.61	.58	.86
	20	.82	.48	.875	.51	.88	.68	.58	.735	.55	.71	.80	.75	.825	.86	.82	.785	1.16
4.5	25	1.01	.61	1.09	.65	1.095	.85	.72	.925	.67	.90	1.00	.95	1.035	1.08	1.03	.99	1.44
5.4	5	.22	.12	.215	.12	.22	.17	.14	.175	.16	.18	.20	.19	.21	.22	.215	.215	.33
	10	.425	.23	.425	.24	.435	.33	.28	.355	.29	.36	.395	.39	.415	.44	.425	.42	.63
	15	.63	.36	.65	.37	.66	.505	.43	.54	.42	.55	.61	.60	.63	.69	.65	.645	.95
5.4	20	.83	.49	.865	.50	.86	.67	.56	.725	.54	.74	.805	.80	.84	.93	.86	.86	1.26

TABLE IX. WING CHANNEL PANEL STRAIN GAGE DATA (CONTD.)

SLOT OR CRACK HALF LENGTH, a (inches)	MACHINE LOAD (kips)	GAGE LOCATION (STRAIN x 10^{-3} inches/inch)																
		(18)	(19)	(20)	(21)	(22)	(23)	(24)	(25)	(26)	(27)	(28)	(29)	(30)	(31)	(32)	(33)	(34)
2.15	10	.19	.38	.33	.465	.37	.35	.36	.35	.275	.38	.485	.542	.50	.385	.29	.425	.37
	20	.28	.76	.64	.93	.74	.695	.71	.695	.59	.765	.97	1.07	.98	.78	.62	.86	.74
	30	.30	1.13	.92	1.39	1.105	1.04	1.06	1.035	.92	1.155	1.44	1.59	1.46	1.17	.965	1.29	1.10
	40	.30	1.51	1.195	1.87	1.48	1.39	1.415	1.38	1.26	1.55	1.94	2.115	1.96	1.57	1.315	1.74	1.475
	50	.27	1.87	1.43	2.33	1.84	1.735	1.76	1.725	1.60	1.945	2.40	2.59	2.43	1.96	1.67	2.185	1.84
2.15	53	.25	1.99	1.50	2.47	1.95	1.84	1.87	1.83	1.71	2.07	2.54	2.73	2.57	2.09	1.78	2.32	1.96
2.8	10	.17	.39	.34	.50	.38	.355	.36	.36	.27	.39	.53	.59	.53	.395	.28	.66**	.39
	20	.21	.765	.645	.99	.75	.69	.715	.70	.575	.78	1.03	1.145	1.04	.79	.605	1.26**	.765
	30	.19	1.15	.93	1.48	1.12	1.04	1.07	1.04	.90	1.18	1.54	1.70	1.56	1.195	.95	1.905**	1.15
2.8	32	.195	1.22	.98	1.58	1.20	1.11	1.14	1.11	.965	1.26	1.645	1.81	1.66	1.28	1.01	2.03**	1.23
3.5	10	.17	.39	.345	.53	.375	.36	.375	.36	.26	.41	.57	.645	.58	.41	.285		.425
	20	.18	.75	.655	1.06	.75	.70	.74	.71	.565	.82	1.12	1.25	1.13	.83	.60	O	.845
	25	.17	.97	.80	1.33	.94	.88	.92	.885	.72	1.02	1.40	1.56	1.41	1.04	.77	U	1.06
3.5	30	.145	1.17	.95	1.60	1.13	1.055	1.11	1.06	.885	1.23	1.685	1.87	1.70	1.25	.94		1.27
																	T	
4.0	5	.11	.195	.18	.27	.18	.17	.185	.18	.12	.20	.29	.33	.295	.20	.13		.24
	10	.17	.395	.35	.55	.375	.35	.38	.36	.26	.41	.59	.67	.595	.42	.275		.495
	15	.18	.59	.51	.82	.56	.53	.57	.54	.40	.62	.88	.99	.89	.63	.43		.75
	20	.16	.79	.67	1.10	.76	.71	.76	.72	.55	.83	1.18	1.315	1.18	.84	.59		1.00
4.0	25	.13	.99	.82	1.39	.96	.885	.95	.90	.71	1.045	1.48	1.64	1.48	1.06	.76		1.26
4.5	5	.12	.205	.19	.29	.195	.18	.20	.19	.11	.21	.31	.355	.31	.21	.125		.54
	10	.17	.41	.365	.57	.39	.35	.39	.37	.24	.42	.62	.70	.62	.43	.265		1.075
	15	.175	.61	.53	.85	.58	.52	.58	.54	.38	.62	.905	1.02	.91	.63	.41		1.61
	20	.145	.82	.70	1.155	.79	.70	.78	.73	.53	.84	1.225	1.38	1.23	.855	.58		2.22
4.5	25	.115	1.03	.86	1.455	.99	.88	.98	.915	.69	1.07	1.545	1.73	1.56	1.085	.75		2.88
5.4	5	.125	.22	.21	.31	.21	.185	.22	.215	.08	.20	.33	.38	.33	.205	.09		
	10	.16	.43	.40	.60	.41	.365	.44	.42	.20	.41	.65	.74	.66	.42	.22		
	15	.145	.65	.59	.93	.63	.55	.66	.64	.34	.64	1.00	1.13	1.005	.655	.38		
5.4	20	.10	.87	.77	1.25	.84	.73	.88	.85	.48	.865	1.34	1.50	1.35	.88	.53		

**At Slot Tip

TABLE IX. WING CHANNEL PANEL STRAIN GAGE DATA (CONTD.)

SLOT OR CRACK HALF LENGTH, a (inches	MACHINE LOAD (kips)	GAGE LOCATION (STRAIN x 10^{-3} inches/inch)																
		(35)	(36)	(37)	(38)	(39)	(40)	(41)	(42)	(43)	(44)	(45)	(46)	(47)	(48)*	(49)	(50)	(51)
2.15	10	.34	.35	.36	.35	.35	.35	.345	.40	.07	.37	.315	.44	.37	.345	.36	.27	.37
	20	.695	.70	.715	.71	.70	.70	.70	.81	.17	.34	.595	.86	.74	.70	.725	.49	.74
	30	1.05	1.05	1.065	1.06	1.045	1.06	1.06	1.22	.27	1.105	.86	1.27	1.105	1.08	1.075	.69	1.11
	40	1.42	1.42	1.425	1.42	1.395	1.42	1.42	1.65	.35	1.48	1.13	1.68	1.48	1.44	1.435	.87	1.48
	50	1.77	1.77	1.775	1.77	1.73	1.77	1.77	2.07	.42	1.83	1.365	2.02	1.835	1.80	1.78	.98	1.845
2.15	53	1.88	1.88	1.885	1.88	1.84	1.88	1.88	2.205	.44	1.94	1.435	2.12	1.945	1.91	1.88	1.00	1.96
2.8	10	.345	.35	.37	.365	.36	.36	.35	.42	.08	.38	.32	.46	.39	.40	.37	.26	.38
	20	.70	.705	.73	.72	.705	.71	.71	.84	.18	.75	.60	.89	.76	.73	.74	.46	.75
	30	1.07	1.07	1.09	1.085	1.06	1.07	1.075	1.28	.27	1.12	.865	1.32	1.135	1.09	1.10	.64	1.13
2.8	32	1.14	1.14	1.16	1.155	1.13	1.14	1.145	1.37	.285	1.20	.92	1.405	1.21	1.175	1.17	.67	1.205
3.5	10	.35	.36	.375	.38	.355	.36	.35	.45	.08	.38	.32	.49	.39	.36	.39	.255	.38
	20	.71	.72	.74	.745	.71	.72	.72	.91	.18	.76	.60	.955	.77	.75	.77	.45	.765
	25	.895	.90	.92	.93	.885	.90	.90	1.135	.22	.95	.74	1.18	.96	.95	.955	.535	.96
3.5	30	1.085	1.09	1.11	1.115	1.06	1.08	1.08	1.37	.25	1.14	.875	1.42	1.16	1.15	1.14	.61	1.15
4.0	5	.17	.18	.19	.19	.18	.18	.185	.22	.02	.19	.17	.25	.19	.11		.15	.19
	10	.35	.36	.38	.38	.355	.365	.368	.465	.07	.385	.32	.51	.39	.39	O	.25	.39
	15	.53	.54	.57	.57	.535	.55	.55	.70	.13	.58	.465	.75	.58	.59	U	.355	.58
	20	.72	.73	.76	.76	.715	.73	.73	.94	.18	.775	.61	1.00	.78	.76		.45	.78
4.0	25	.905	.92	.955	.96	.89	.91	.92	1.185	.21	.97	.745	1.24	.98	.98	T	.53	.98
4.5	5	.175	.18	.205	.20	.185	.18	.19	.24	.02	.20	.175	.27	.20	.035		.15	.20
	10	.36	.37	.405	.40	.365	.37	.37	.485	.07	.40	.3[illegible]	.53	.405	.31		.26	.40
	15	.53	.55	.60	.59	.54	.55	.55	.72	.125	.59	.48	.785	.61	.335		.36	.60
	20	.725	.74	.80	.795	.73	.74	.74	.97	.165	.80	.62	1.03	.81	.54		.45	.80
4.5	25	.92	.94	1.01	1.00	.91	.94	.935	1.24	.19	1.00	.77	1.29	1.01	.945		.53	1.005
5.4	5	.145	.17	.28	.22	.19	.18	.16	.26	.02	.21	.19	.29	.215	.02		.16	.21
	10	.315	.35	.525	.43	.36	.36	.34	.51	.07	.42	.35	.56	.425	.09		.27	.41
	15	.50	.55	.80	.655	.55	.56	.53	.79	.12	.64	.52	.845	.65	.335		.37	.625
5.4	20	.69	.75	1.065	.88	.74	.75	.72	1.055	.135	.86	.67	1.12	.865	.64		.46	.84

*Drifting Gage

TABLE IX. WING CHANNEL PANEL STRAIN GAGE DATA (CONTD.)

SLOT OR CRACK HALF LENGTH, a (inches)	MACHINE LOAD (kips)	GAGE LOCATION (STRAIN x 10^{-3} inches/inch)																
		(52)	(53)	(54)	(55)	(56)	(57)	(58)										
2.15	10	.32	.35	.37	.345	.32	.36	.345										
↓	20	.595	.70	.74	.69	.60	.725	.67										
	30	.84	1.05	1.10	1.04	.87	1.085	.97										
	40	1.065	1.42	1.465	1.39	1.135	1.45	1.27										
↓	50	1.26	1.77	1.81	1.735	1.34	1.795	1.515										
2.15	53	1.315	1.88	1.92	1.84	1.38	1.905	1.58										
2.8	10	.32	.355	.38	.345	.32	.38	.355										
↓	20	.595	.70	.75	.69	.585	.74	.675										
↓	30	.84	1.06	1.12	1.04	.84	1.11	.98										
2.8	32	.89	1.13	1.19	1.11	.895	1.18	1.04										
3.5	10	.33	.36	.385	.34	.31	.37	.35										
↓	20	.61	.72	.76	.69	.57	.74	.68										
↓	25	.735	.90	.95	.87	.69	.925	.83										
3.5	30	.86	1.09	1.14	1.05	.82	1.11	.99										
4.0	5	.18	.18	.19	.17	.155	.18	.18										
↓	10	.33	.36	.385	.34	.295	.37	.35										
↓	15	.48	.55	.58	.52	.43	.56	.52										
↓	20	.62	.74	.77	.70	.55	.75	.68										
4.0	25	.755	.93	.96	.875	.68	.94	.85										
4.5	5	.185	.185	.20	.175	.16	.19	.18										
↓	10	.345	.37	.40	.35	.30	.385	.36										
↓	15	.50	.56	.595	.522	.425	.57	.53										
↓	20	.64	.745	.79	.70	.55	.76	.695										
4.5	25	.78	.945	.99	.89	.68	.96	.865										
5.4	5	.20	.19	.21	.175	.16	.19	.18										
↓	10	.36	.38	.41	.35	.30	.38	.36										
↓	15	.53	.585	.62	.54	.43	.58	.535										
5.4	20	.68	.785	.82	.73	.56	.775	.71										

TABLE IX. WING CHANNEL PANEL STRAIN GAGE DATA (CONTD.)

SLOT OR CRACK HALF LENGTH, a (inches)	MACHINE LOAD (kips)	GAGE LOCATION (STRAIN x 10^{-3} inches/inch)																
		①	②	③	④	⑤	⑥	⑦	⑧	⑨	⑩	⑪	⑫	⑬	⑭	⑮	⑯	⑰
5.85***	1	.04	.02	.03	.025	.04	.03	.04	.035	.045	.035	.05	.035	.05	.045	.05	.05	.08
	2	.08	.04	.075	.05	.085	.06	.07	.07	.08	.07	.09	.07	.095	.09	.095	.09	.15
	3	.12	.065	.12	.07	.13	.10	.10	.11	.11	.11	.13	.115	.14	.13	.14	.14	.215
	4	.16	.09	.16	.095	.17	.13	.125	.14	.14	.145	.17	.155	.18	.175	.18	.18	.28
	5	.20	.11	.205	.12	.22	.16	.15	.18	.17	.18	.21	.19	.225	.22	.225	.22	.35
	8	.33	.18	.34	.19	.355	.26	.24	.29	.26	.29	.33	.32	.355	.35	.365	.36	.545
	10	.41	.225	.43	.24	.445	.33	.295	.36	.315	.37	.41	.395	.44	.44	.45	.44	.67
5.85	12	.50	.27	.52	.29	.54	.40	.35	.44	.375	.44	.49	.475	.53	.535	.54	.53	.80
6.3***	5	.21	.11	.215	.12	.22	.165	.15	.185	.16	.18	.21	.20	.225	.22	.23	.24	.36
	10	.425	.23	.43	.24	.445	.33	.285	.36	.31	.37	.41	.40	.435	.46	.455	.47	.69
	15	.64	.35	.65	.36	.665	.50	.42	.54	.45	.56	.61	.62	.655	.71	.68	.70	1.04
	20	.83	.47	.865	.49	.875	.67	.56	.73	.57	.77	.82	.84	.87	.98	.905	.94	1.37
	25	1.02	.61	1.075	.63	1.085	.84	.70	.915	.69	.98	1.03	1.05	1.085	1.24	1.135	1.18	1.70
	30	1.205	.74	1.275	.77	1.295	1.01	.825	1.10	.80	1.19	1.24	1.27	1.31	1.49	1.365	1.43	2.015
	35	1.39	.875	1.48	.91	1.51	1.18	.96	1.29	.90	1.40	1.45	1.495	1.53	1.74	1.60	1.68	2.29
	40	1.54	1.00	1.65	1.04	1.69	1.33	1.07	1.45	.99	1.575	1.635	1.67	1.725	1.92	1.80	1.89	2.50
	45	1.73	1.15	1.86	1.20	1.91	1.52	1.21	1.665	1.11	1.79	1.865	1.88	1.975	2.13	2.05	2.17	2.73
	50	1.895	1.23	2.045	1.34	2.115	1.69	1.33	1.855	1.22	1.98	2.075	2.07	2.185	2.30	2.275	2.43	2.92
	55	2.06	1.44	2.23	1.51	2.29	1.86	1.44	2.03	1.31	2.145	2.28	2.23	2.40	2.435	2.49	2.69	3.06
	60	2.21	1.61	2.38	1.69	2.45	2.015	1.51	2.205	1.39	2.34	2.465	2.41	2.585	2.57	2.69	2.995	3.22
	65	2.36	1.77	2.54	1.88	2.62	2.19	1.60	2.375	1.50	2.51	2.66	2.57	2.77	2.70	2.88	3.515	3.36
	70	2.515	1.945	2.70	2.08	2.785	2.35	1.69	2.54	1.59	2.64	2.86	2.69	2.95	2.77	3.045	3.88	3.47
	75	2.67	2.12	2.87	2.285	2.96	2.50	1.77	2.68	1.69	2.755	3.04	2.80	3.12	2.83	3.18	4.11	3.545
	80	2.82	2.28	3.03	2.47	3.115	2.64	1.85	2.82	1.77	2.86	3.20	2.88	3.255	2.88	3.31	4.42	3.63
	85	2.98	2.47	3.20	2.66	3.285	2.79	1.925	2.96	1.87	2.95	3.37	2.95	3.39	2.93	3.435	4.75	3.71
	90	3.13	2.635	3.36	2.835	3.43	2.90	1.99	3.08	1.95	3.02	3.51	2.995	3.49	2.945	3.51	5.05	3.77
	95	3.27	2.80	3.52	3.015	3.61	3.035	2.07	3.21	2.04	3.095	3.65	3.05	3.60	2.965	3.61	5.395	3.85
	100	3.41	2.97	3.65	3.195	3.74	3.12	2.095	3.30	2.105	3.09	3.73	3.025	3.65	2.93	3.64	5.75	3.895
UNLOAD TO 0	kips	-.13	.10	-.05	.22	-.14	-.08	-.09	-.09	-.095	-.14	-.11	-.265	-.14	-.60	-.17	.42	-.055
	25	.89	.705	1.01	.84	.945	.74	.565	.84	–	–	–	–	–	.80	1.015	1.69	1.215
	50	1.80	1.39	2.015	1.56	1.99	1.59	1.16	1.80	1.11	1.82	2.00	1.77	2.08	1.60	2.10	3.05	2.16
	75	2.61	2.15	2.845	2.355	2.88	2.40	1.63	2.62	1.60	2.47	2.935	2.40	2.94	2.29	2.92	4.36	3.06
	100	3.43	2.975	3.66	3.22	3.78	3.135	2.10	3.33	2.12	3.085	3.76	2.99	3.68	2.905	3.67	5.755	3.88
	110	3.71	3.29	3.95	3.55	4.10	3.33	2.22	3.53	2.28	3.175	3.96	3.06	3.83	2.96	3.79	6.45	4.10
6.3	120	4.00	3.63	4.23	3.92	4.44	3.50	2.31	3.73	2.43	3.25	4.135	3.12	3.94	3.01	3.87	7.18	4.27

***Natural Crack - Induced by Fatigue

TABLE IX. WING CHANNEL PANEL STRAIN GAGE DATA (CONTD.)

SLOT OR CRACK HALF LENGTH, a (inches)	MACHINE LOAD (kips)	GAGE LOCATION (STRAIN x 10^{-3} inches/inch)																
		(18)	(19)	(20)	(21)	(22)	(23)	(24)	(25)	(26)	(27)	(28)	(29)	(30)	(31)	(32)	(33)	(34)
5.85	1	.04	.05	.055	.07	.05	.04	.055	.06	.02	.03	.06	.07	.07	.03	.02		
	2	.06	.10	.10	.13	.09	.08	.10	.11	-.001	.08	.135	.15	.14	.075	.01	O	O
	3	.09	.145	.14	.20	.13	.11	.14	.155	.02	.12	.20	.235	.21	.12	.03	U	U
	4	.11	.19	.19	.26	.175	.15	.19	.20	.04	.16	.27	.315	.275	.17	.055		
	5	.135	.23	.23	.32	.22	.185	.24	.25	.065	.21	.34	.39	.34	.21	.08	T	T
	8	.19	.37	.36	.51	.35	.295	.38	.395	.14	.34	.55	.63	.56	.345	.16		
	10	.22	.46	.44	.63	.435	.37	.47	.49	.19	.43	.69	.79	.70	.44	.21		
5.85	12	.25	.555	.53	.77	.525	.44	.56	.59	.24	.52	.83	.955	.84	.53	.27		
6.3	5	.145	.25	.24	.335	.23	.20	.26	.42	.01	.22	.355	.41	.36	.225	.10		
	10	.23	.48	.46	.66	.46	.38	.51	.825	.20	.445	.71	.82	.72	.45	.22	O	O
	15	.275	.71	.67	.99	.70	.565	.77	1.27	.33	.68	1.075	1.23	1.09	.685	.37	U	U
	20	.215	.96	.87	1.33	.94	.745	1.02	1.76	.47	.91	1.44	1.63	1.46	.93	.53		
	25	.125	1.21	1.07	1.68	1.19	.915	1.27	2.315	.63	1.16	1.81	2.03	1.82	1.175	.71	T	T
	30	.02	1.455	1.26	2.03	1.43	1.09	1.52	2.955	.80	1.41	2.17	2.42	2.18	1.43	.89		
	35	-.11	1.70	1.43	2.37	1.66	1.28	1.76	3.75	1.00	1.67	2.53	2.79	2.54	1.70	1.09		
	40	-.23	1.91	1.56	2.67	1.86	1.44	1.98	4.68	1.155	1.90	2.825	3.09	2.84	1.925	1.27		
	45	-.37	2.17	1.72	3.06	2.12	1.64	2.27	6.575	1.38	2.20	3.21	3.47	3.22	2.22	1.50		
	50	-.50	2.42	1.85	3.405	2.35	1.83	2.53	9.345	1.59	2.47	3.55	3.80	3.58	2.495	1.71		
	55	-.65	2.65	1.915	3.76	2.61	2.03	2.815		1.815	2.76	3.89	4.10	3.92	2.78	1.94		
	60	-.86	2.96	1.32	4.215	3.17	2.29	3.16	O	2.07	3.09	4.305	4.50	4.375	3.15	2.23		
	65	-1.03	3.14	1.385	4.635	3.35	2.85	3.68	U	2.33	3.43	4.70	4.84	4.735	3.44	2.46		
	70	-1.17	3.32	1.41	5.04	3.55	3.125	3.98		2.60	3.75	5.055	5.15	5.09	3.765	2.73		
	75	-1.30	3.465	1.41	5.40	3.71	3.39	4.28	T	2.85	4.055	5.37	5.41	5.42	4.07	2.995		
	80	-1.42	3.60	1.41	5.755	3.87	3.64	4.55		3.12	4.37	5.685	5.67	5.73	4.375	3.26		
	85	-1.54	3.72	1.39	6.16	4.03	3.925	4.85		3.405	4.71	6.02	5.94	6.07	4.72	3.55		
	90	-1.64	3.795	1.325	6.47	4.145	4.16	5.09		3.65	4.995	6.25	6.09	6.30	5.01	3.805		
	95	-1.75	3.895	1.28	6.84	4.305	4.44	5.39		3.94	5.35	6.54	6.295	6.595	5.36	4.10		
	100	-1.82	3.94	1.12	7.11	4.41	4.73	5.68		4.24	5.72	6.69	6.37	6.76	5.71	4.40		
UNLOAD TO 0	kips	-1.00	-.03	-1.06	.35	.24	.315	.30		-.15	.13	-.08	-.425	-.05	.115	-.125		
	25	-.955	1.20	-.375	1.93	1.53	1.41	1.48		.75	1.36	1.45	1.13	1.54	1.35	.82		
	50	-1.33	2.33	.16	3.635	2.63	2.605	2.77		1.86	2.77	3.125	2.75	3.215	2.77	1.97		
	75	-1.59	3.17	.70	5.325	3.52	3.64	4.15		3.005	4.21	4.875	4.54	4.96	4.21	3.14		
	100	-1.83	3.97	1.145	7.16	4.45	4.72	5.675		4.26	5.75	6.72	6.39	6.79	5.75	4.425		
	110	-1.99	4.12	.965	7.73	4.74	5.28	6.31		4.86	6.72	7.00	6.65	7.11	6.66	5.05		
6.3	120	-2.04	4.28	.70	8.595	5.08	6.055	7.38		5.915	8.24	7.185	6.81	7.28	8.265	6.10		

TABLE IX. WING CHANNEL PANEL STRAIN GAGE DATA (CONTD.)

SLOT OR CRACK HALF LENGTH, a (inches)	MACHINE LOAD (kips)	GAGE LOCATION (STRAIN x 10^{-3} inches/inch)																
		(35)	(36)	(37)	(38)	(39)	(40)	(41)	(42)	(43)	(44)	(45)	(46)	(47)	(48)*	(49)	(50)	(51)
5.85	1	.002	.02	.10	.06	.045	.03	.01	.055	.02	.05	.05	.07	.05	.62		.05	.05
	2	.04	.06	.18	.105	.08	.07	.045	.11	-.02	.09	.09	.12	.10	.495		.08	.095
	3	.07	.10	.255	.15	.12	.11	.08	.16	-.02	.14	.135	.18	.14	.67		.11	.135
	4	.10	.14	.34	.20	.16	.15	.12	.21	-.01	.18	.17	.23	.185	.72		.14	.18
	5	.13	.17	.42	.245	.20	.18	.155	.26	.001	.22	.21	.285	.23	.735		.17	.22
	8	.24	.29	.68	.385	.31	.31	.27	.43	.03	.36	.33	.455	.36	.86		.25	.345
	10	.31	.36	.84	.48	.38	.38	.35	.54	.05	.45	.405	.57	.45	.20		.30	.43
5.85	12	.38	.44	1.015	.57	.46	.46	.42	.66	.07	.54	.48	.68	.545	.93		.34	.52
6.3	5	.14	.19		.27	.20	.195	.18	.28	.001	.25	.25	.30	.24	.385		.175	.22
	10	.305	.38	O	.525	.39	.39	.36	.56	.045	.48	.47	.59	.48	.565		.30	.43
	15	.48	.58	U	.785	.58	.59	.55	.85	.085	.72	.70	.89	.72	.555		.41	.65
	20	.67	.79		1.05	.76	.80	.74	1.14	.095	.96	.92	1.20	.98	1.11		.50	.885
	25	.86	1.00	T	1.32	.93	1.01	.915	1.44	.11	1.20	1.14	1.49	1.23	1.415		.54	1.125
	30	1.06	1.22		1.60	1.105	1.22	1.12	1.755	.13	1.44	1.365	1.78	1.49	1.65		.54	1.37
	35	1.27	1.445		1.87	1.28	1.425	1.32	2.07	.13	1.685	1.58	2.03	1.74	1.89		.52	1.61
	40	1.45	1.64		2.105	1.44	1.61	1.51	2.35	.14	1.90	1.78	2.19	1.96	2.095		.48	1.815
	45	1.69	1.91		2.395	1.65	1.84	1.74	2.72	.14	2.16	2.07	2.385	2.23	2.36		.43	2.065
	50	1.90	2.14		2.67	1.84	2.05	1.91	3.07	.14	2.40	2.375	2.535	2.46	2.585		.36	2.275
	55	2.12	2.40		2.97	2.05	2.27	2.11	3.425	.15	2.65	2.77	2.65	2.70	2.84		.25	2.50
	60	2.32	2.78		3.57	2.60	2.615	2.32	3.92	.16	3.155	1.60	2.775	3.00	3.14		.105	2.71
	65	2.55	3.03		3.835	2.81	2.805	2.49	4.30	.15	3.335	1.62	2.88	3.16	3.57		.012	2.87
	70	2.81	3.32		4.135	3.08	3.06	2.74	4.74	.175	3.56	1.65	3.00	3.35	3.765		-.12	3.065
	75	3.06	3.61		4.41	3.325	3.27	2.93	5.10	.21	3.72	1.63	3.08	3.48	4.11		-.22	3.20
	80	3.31	3.885		4.69	3.57	3.485	3.12	5.48	.25	3.895	1.61	3.145	3.60	4.38		-.32	3.33
	85	3.60	4.205		4.98	3.85	3.73	3.325	5.90	.30	4.085	1.60	3.24	3.72	4.625		-.44	3.45
	90	3.845	4.48		5.22	4.08	3.93	3.51	6.25	.355	4.22	1.555	3.29	3.805	4.90		-.525	3.54
	95	4.13	4.80		5.52	4.35	4.17	3.69	6.63	.43	4.38	1.525	3.37	3.90	5.23		-.645	3.64
	100	4.415	5.12		5.80	4.63	4.41	3.91	6.97	.525	4.52	1.42	3.43	3.93	4.37		-.76	3.695
UNLOAD TO 0	kips	-.22	.05		.445	.23	.11	-.11	.30	.11	.26	-2.185	-.39	.08	.40		-.09	-.51
	25	.79	1.20		1.65	1.34	1.23	.99	1.81	.23	1.51	-1.02	.87	1.28	1.11		-.48	1.07
	50	1.94	2.475		2.93	2.54	2.335	2.02	3.50	.03	2.605	-.05	1.83	2.28	2.845		-.68	2.13
	75	3.14	3.765		4.30	3.60	3.375	2.99	5.16	.36	3.555	.83	2.61	3.13	3.32		-.72	2.96
	100	4.45	5.16		5.82	4.66	4.445	3.97	7.015	.54	4.545	1.46	3.41	3.94	5.60		-.78	3.72
	110	5.04	5.835		6.435	5.20	4.92	4.375	8.01	.74	4.86	1.38	3.675	4.09	6.145		-.92	3.85
6.3	120	5.82	6.86		7.595	5.96	5.54	4.885	OUT	1.02	5.21	1.29	3.94	4.27	6.805		-1.01	3.93

*Drifting Gage

TABLE IX. WING CHANNEL PANEL STRAIN GAGE DATA (CONTD.)

SLOT OR CRACK HALF LENGTH, a (inches)	MACHINE LOAD (kips)	GAGE LOCATION (STRAIN x 10^{-3} inches/inch)																
		(52)	(53)	(54)	(55)	(56)	(57)	(58)										
5.85	1	.055	.05	.05	.04	.05	.045	.05										
	2	.10	.08	.095	.07	.08	.08	.09										
	3	.14	.12	.14	.11	.12	.12	.13										
	4	.175	.16	.18	.145	.15	.16	.16										
	5	.21	.19	.22	.18	.175	.20	.20										
	8	.33	.31	.35	.29	.27	.32	.31										
	10	.40	.385	.43	.37	.325	.40	.38										
5.85	12	.47	.465	.51	.44	.38	.48	.45										
6.3	5	.21	.20	.215	.18	.175	.20	.20										
	10	.38	.395	.42	.365	.32	.40	.37										
	15	.55	.605	.63	.56	.46	.60	.545										
	20	.69	.82	.85	.76	.595	.80	.715										
	25	.82	1.045	1.08	.95	.71	1.00	.875										
	30	.94	1.265	1.30	1.155	.81	1.22	1.04										
	35	1.055	1.49	1.52	1.36	.86	1.43	1.18										
	40	1.15	1.68	1.72	1.53	.89	1.62	1.28										
	45	1.26	1.915	1.955	1.75	.915	1.85	1.40										
	50	1.35	2.115	2.17	1.94	.93	2.06	1.495										
	55	1.415	2.28	2.345	2.11	.91	2.235	1.55										
	60	1.14	2.48	2.555	2.32	.87	2.43	1.51										
	65	1.20	2.63	2.73	2.48	.83	2.595	1.59										
	70	1.26	2.76	2.915	2.64	.805	2.77	1.67										
	75	1.29	2.84	3.06	2.75	.75	2.91	1.72										
	80	1.32	2.92	3.20	2.85	.69	3.05	1.78										
	85	1.335	2.98	3.33	2.94	.615	3.18	1.82										
	90	1.33	3.02	3.44	3.01	.55	3.30	1.875										
	95	1.33	3.07	3.55	3.075	.45	3.41	1.90										
	100	1.28	3.06	3.62	3.09	.29	3.49	1.89										
UNLOAD TO 0	kips	-.17	-.04	-.105	-.22	-.045	-.10	-.42										
	25	.065	1.06	1.06	.95	-.01	1.00	.57										
	50	.46	1.88	2.115	1.81	.015	2.02	.995										
	75	.875	2.46	2.92	2.47	.145	2.805	1.43										
	100	1.285	3.07	3.65	3.11	.29	3.515	1.89										
	110	1.21	3.16	3.815	3.22	.145	3.69	1.92										
6.3	120	1.05	3.23	3.94	3.30	-.03	3.84	1.89										

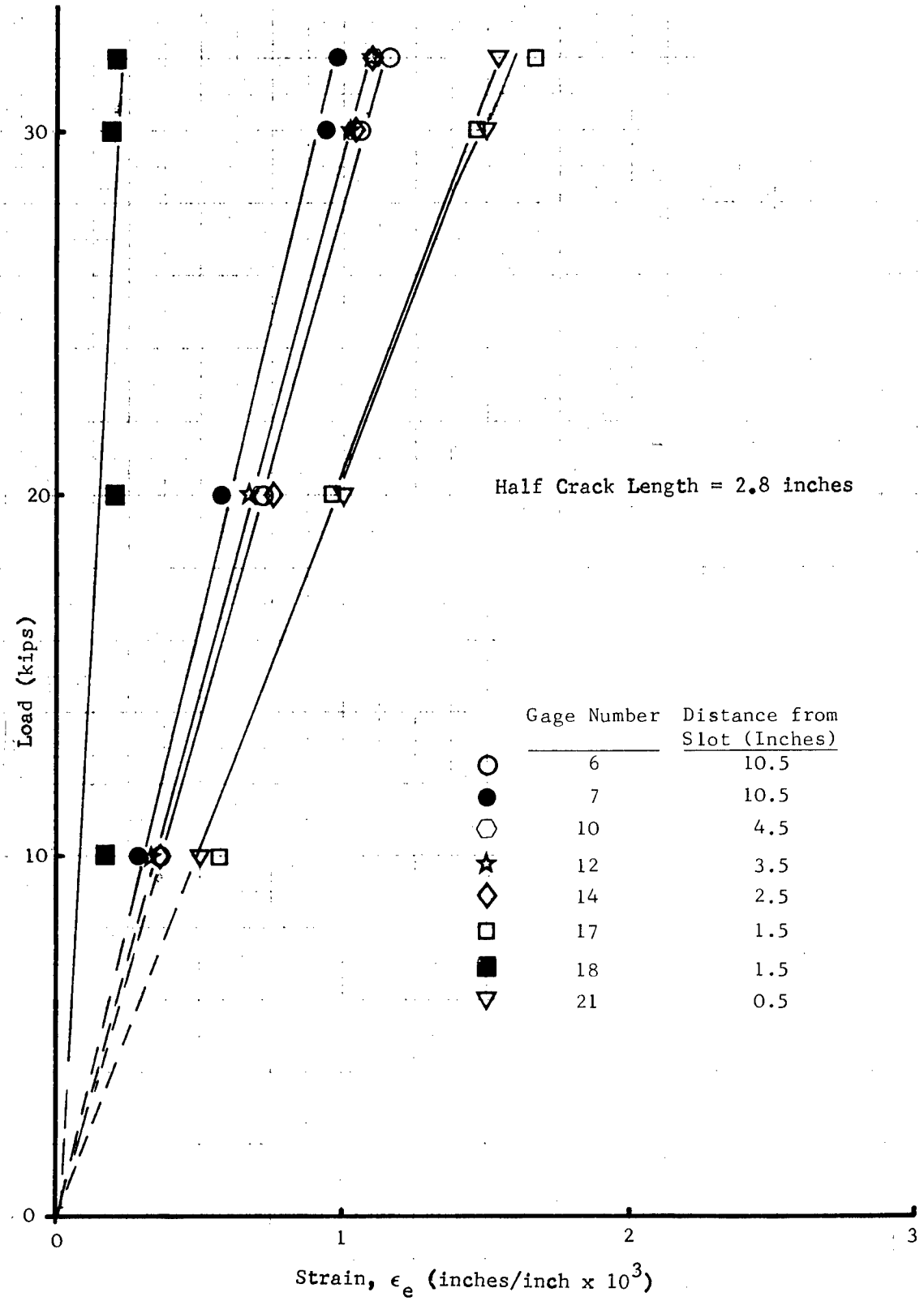

Figure 56. Strain Gage Data - Wing Channel Panel - Center Channel, a = 2.8 Inches

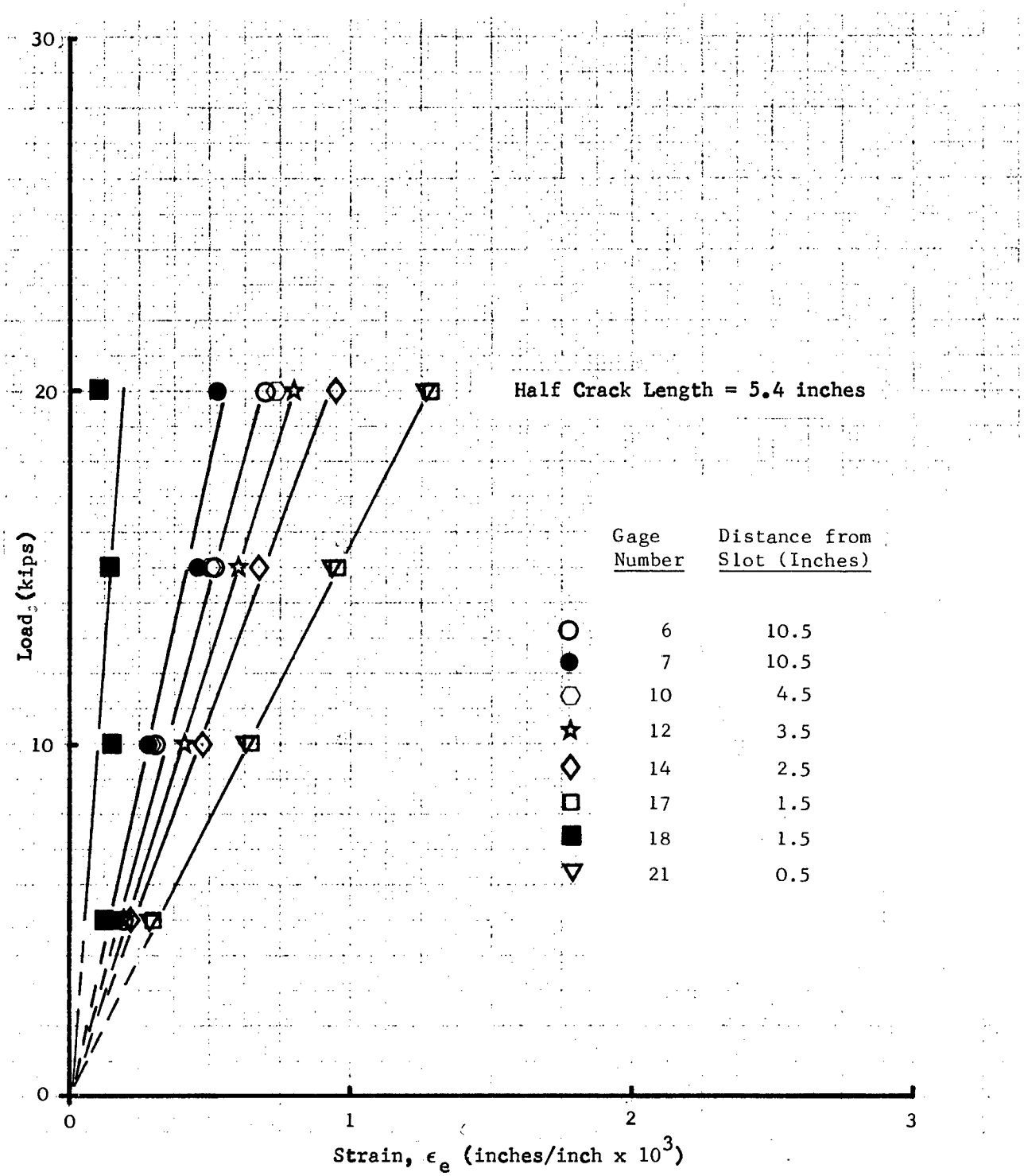

Figure 57. Strain Gage Data - Wing Channel Panel - Center Channel, a = 5.4 Inches

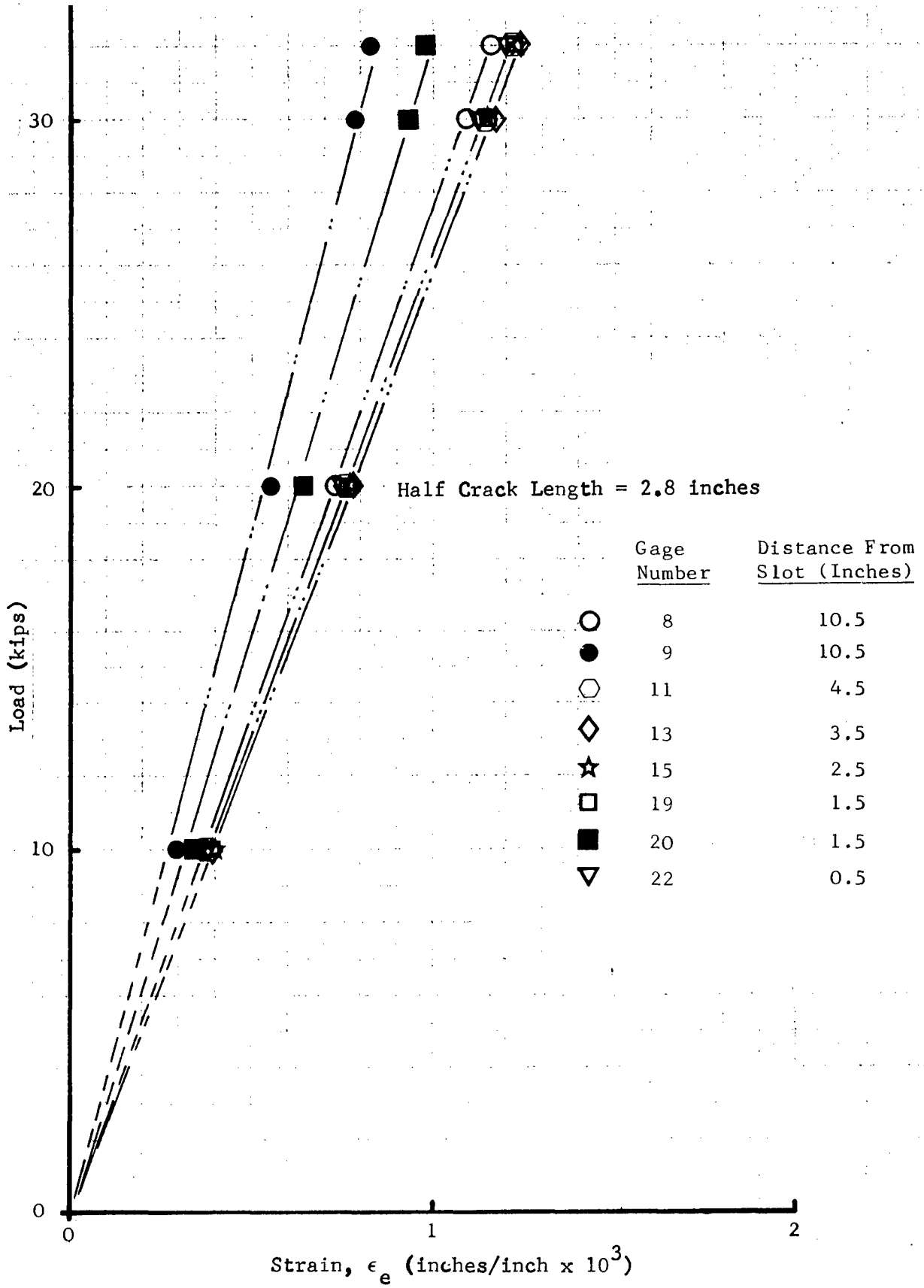

Figure 58. Strain Gage Data - Wing Channel Panel - Edge Channel, a = 2.8 Inches

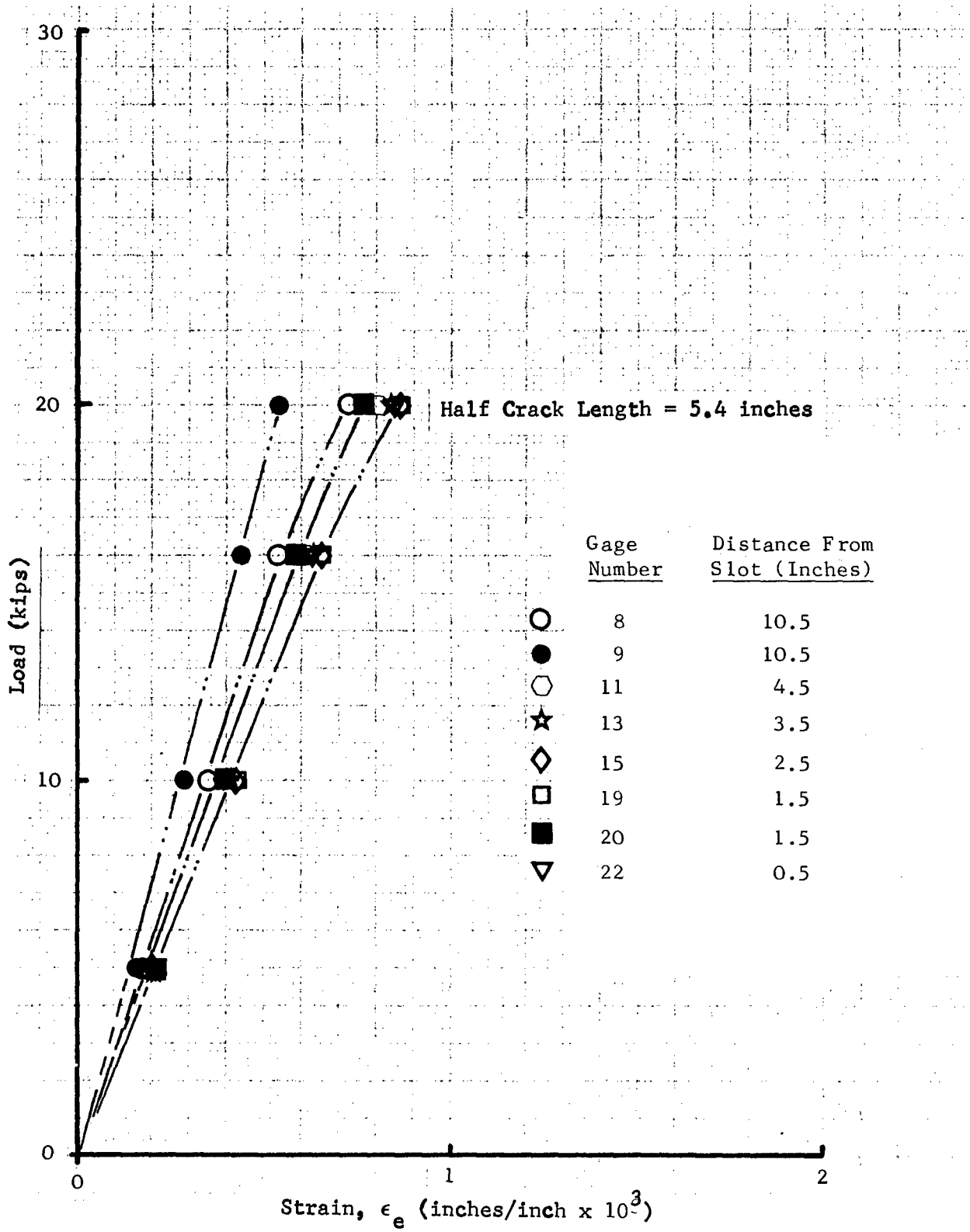

Figure 59. Strain Gage Data - Wing Channel Panel - Edge Channel, a = 5.4 Inches

The strain data (from Table IX) for the skin and channel gages (center and edge channels) adjacent to the slot at a constant load of 20 kips are shown in Figures 60 and 61. The strains in gage 17 (Figure 60) located on the central stringer are almost a linear function of crack length. It is apparent from these data that somewhere beyond a half crack length of 3.5 inches or at crack length to channel span ratio a/s of 0.5 and beyond, nonlinear behavior of the edge channel occurs (e.g., gages 19, 20 of Figure 60 and 44, 45 of Figure 61) as a function of crack length. A similar behavior was observed for stresses in the central and outer stringers in the elastic analysis of this wing channel panel (see Figure 10, and related discussion in Section 3.2.1). It may be noted that the strains indicated by gages 18 and 43 on the skin are very small as these gages are located just above the crack surface at the centerline of the crack (see Figure 55).

These data (Figures 60 and 61) have been extrapolated back to a zero crack length (dashed lines) based on the following assumptions:

1. The stringer cross sectional area = 0.508 square inches.

2. Total cross sectional stringer area = 0.508 square inches x 3 = 1.524 square inches.

3. Total cross sectional sheet area = 0.063 inches x 20 inches = 1.260 square inches.

4. Total Panel Cross Sectional Area = 2.784 square inches.

For a 20,000 pound force at the grip the average gross area panel stress $\left(\overset{\infty}{\sigma}_g\right)$ is,

$$\overset{\infty}{\sigma}_g = \frac{20{,}000 \text{ pounds}}{2.784 \text{ square inches}} = 7{,}184 \text{ psi}$$

and strain, $\epsilon = \frac{\overset{\infty}{\sigma}_g}{E} = \frac{7{,}184 \text{ psi}}{10.07 \times 10^6 \text{ psi}} = 0.7134 \times 10^{-3}$ inches/inch .

A survey plot of strain data from center and edge channel at the 6.3 inch half crack length are shown in Figures 62 and 63 up to a load of 120 kips. The trend in these data are not unexpected with channel strain increasing at constant load as you get close to the crack. The behavior of the gages on the skin side 18 (Figure 62) and 20 (Figure 63) was also anticipated. For example, compressive strain immediately above the crack prior to the first rivet (the center rivet was missing) and decreasing strain with load for the edge channel position as the skin plastic zone size increases.

A comparison of the elastic strains from the finite element model was made for two half-crack lengths (2.8 and 5.4 inches) for the channel gages up the center channels from the crack line. Figure 64 compares these data with both the equivalent area and flexible fastener models. It is seen that the flexible fastener model provides a better fit to both data sets.

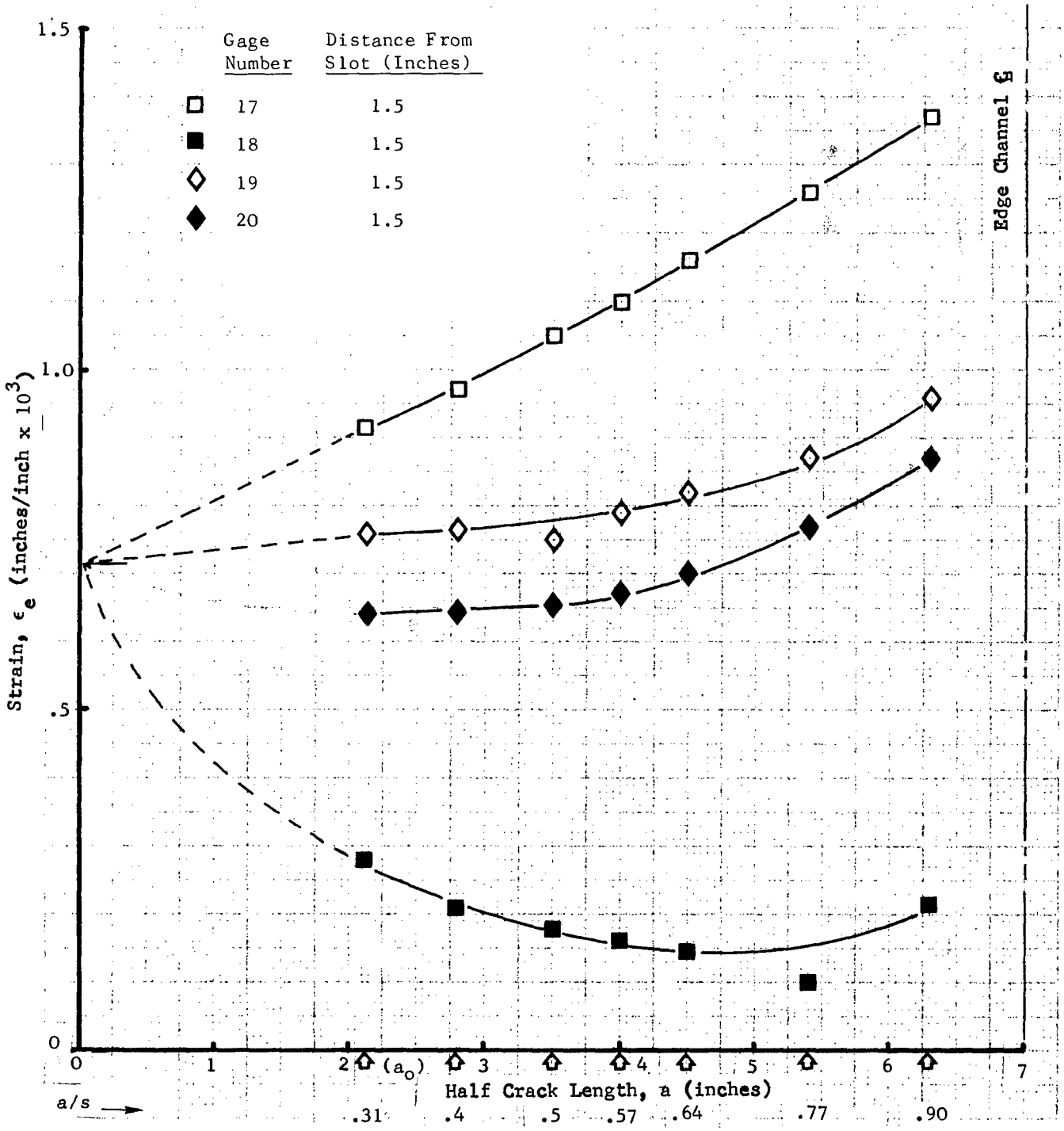

Figure 60. Center-Edge Wing Channel and Skin Strain as a Function of Crack Length, Load = 20 kips

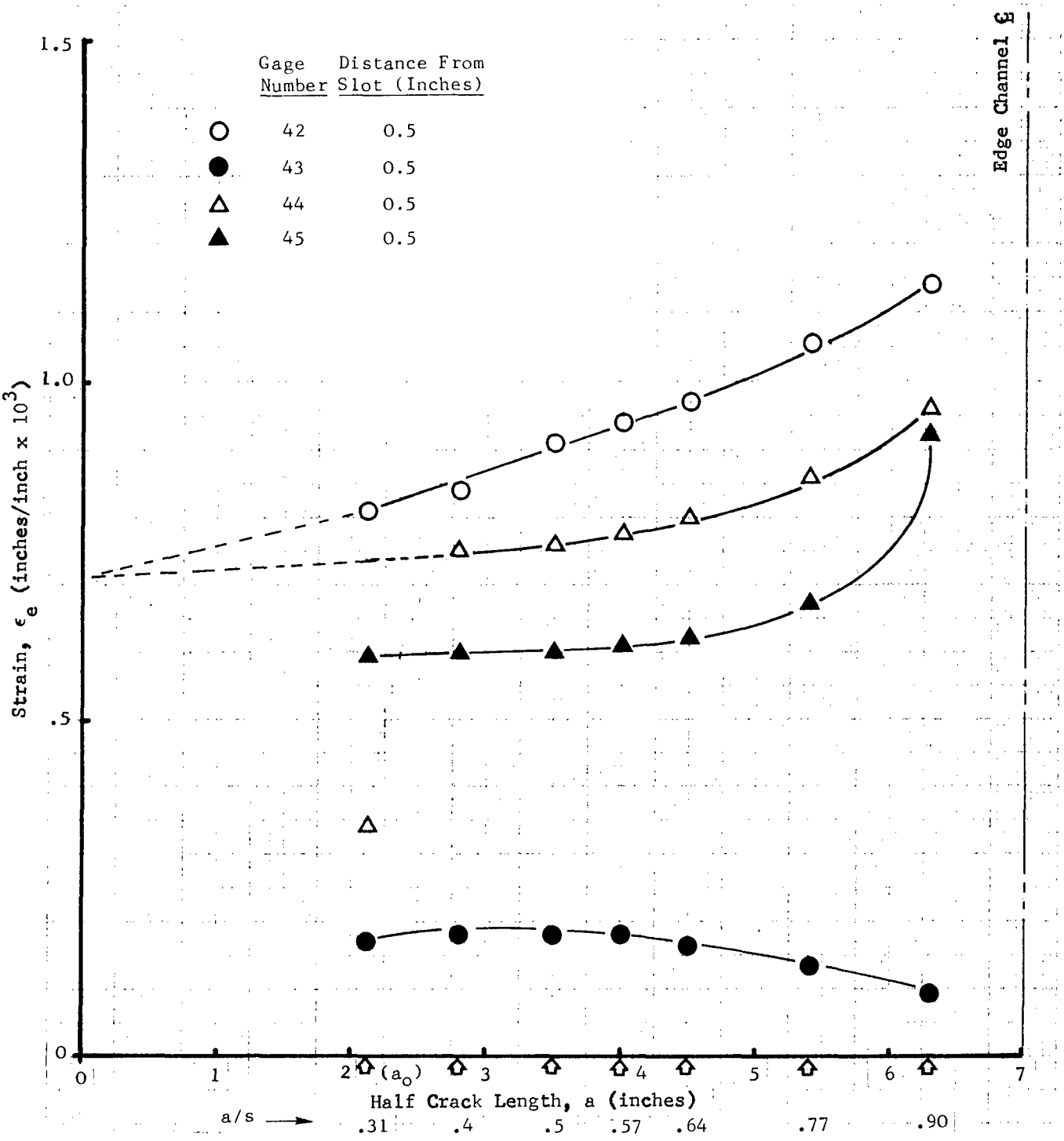

Figure 61. Center-Edge Wing Channel and Skin Strain as a Function of Crack Length, Load = 20 kips

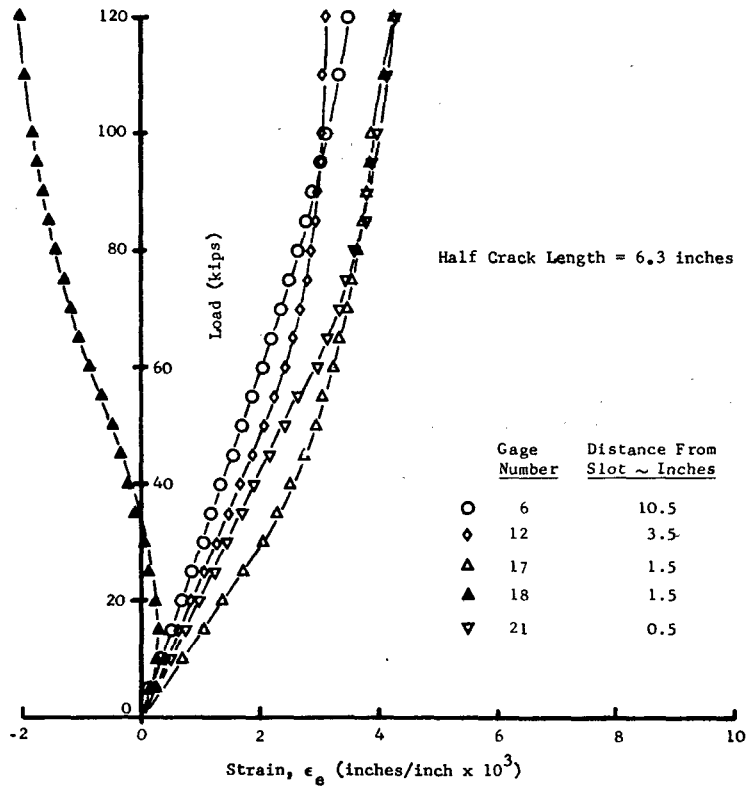

Figure 62. Strain to Fracture-Center Wing Channel-a = 6.3 Inches

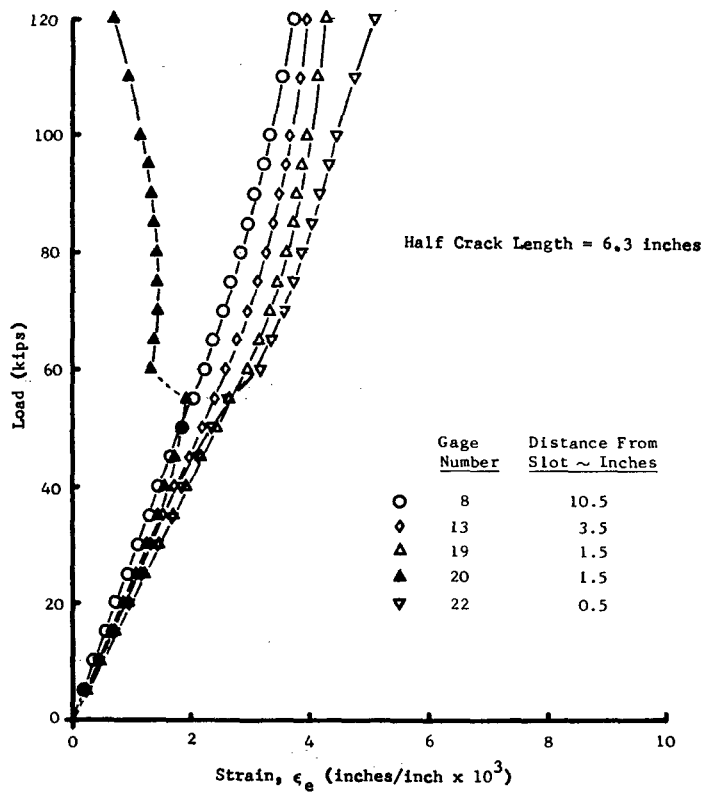

Figure 63. Strain to Fracture-Edge Wing Channel-a = 6.3 Inches

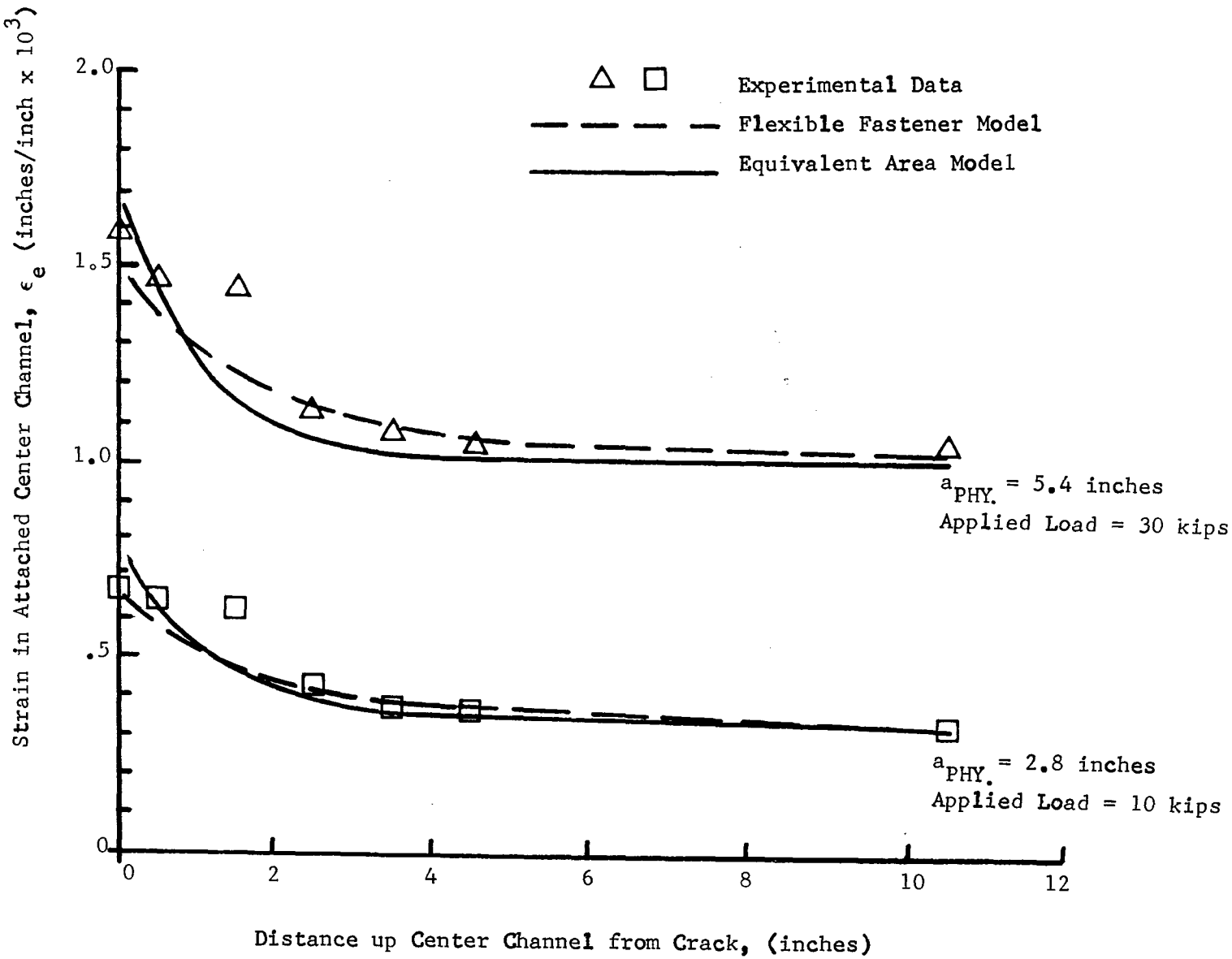

Figure 64. Comparison of Center Channel Strain - Two Fastener Models - Lightly Stiffened Wing Channel Panel

By altering the fastener model it is possible to produce a better fit to the strain data of Figure 64 closer to the crack. However, this alteration results in an undersirable compromise with COD, i.e., attempting to remodel the fasteners would have led to greater differences in COD. For the J integral approach it is desirable to maintain a closer relationship between deflections rather than strain since the calculation of J involves differences in deflection (in the Dugdale model) rather than local strain conditions.

4.3 LOAD TRANSFER

Some indication of the amount of load transferred to the wing channels due to the presence of the crack can be seen in Figures 55 through 59. The back to back gages (17 and 19 on the channel side and 18 and 20 on the skin side) show large strains on the channel side for any given load.

As a preliminary check of the rivet modeling effects on load transfer to the flange the linear elastic strain data for both the flexible fastener and equivalent area models are compared in Table X. These are data for the rod elements (700, 705, and 711) representing the bottom flange of the wing channel for a half slot length of 2.8 inches and a load of 20 ksi. Additional comparison of finite element analytical and experimental values of strain for the membrane element 800 representing the upstanding leg and top flange (900) rod element are also given in Table X for the same slot length.

The data of Table X is inconclusive as to the accuracy of the rivet modeling on finite element calculated strains for this short crack condition. This was also shown for another load level (10 kips) in Figure 64 for the same 2.8 inch crack. However, at the longer (5.4 inch) crack length the superiority of the flexible fastener model is indicated in Figure 64. In examining the load transfer data of Table X it should be noted that the experimental values agree for the most part within 20 percent of those obtained from the finite element model. It must again be emphasized that greater accuracy in predicted strain could be achieved by altering the fastener model but only at the expense of reducing accuracy of the computed J integral values, particularly in the vicinity of the stiffeners where load transfer is most important.

4.4 FAILURE PREDICTION

The lightly stiffened wing channel panel was fatigue cracked ($\Delta K < 10$ ksi$\sqrt{\text{inch}}$) from the saw slot of half length 5.4 inches to 5.85 inches at which time strain and deflection data were taken at ten load levels. The crack was subsequently grown to a half length of 6.3 inches. The panel was then loaded, in increments to 100 kips, unloaded and subsequently loaded to fracture from a load of 120 kips. Fracture of this panel took place at approximately 124 kips which would correspond to a gross area stress of 44.5 ksi or a net area stress of 62.3 ksi.

It was possible to predict the stringer critical failure of the panel from previous analytical considerations. Figure 65 shows variation of stresses in the central stringer as a function of applied stress for physical half crack lengths of 5.4, 6.3, and 6.6 inches based on elastic, Prandtl-Reuss and Dugdale assumptions. For a 5.4 inch half crack length the Dugdale model would predict

TABLE X. COMPARISON OF EXPERIMENTAL AND FINITE ELEMENT STRAINS – WING CHANNEL PANEL – CENTER CHANNEL – 20,000 POUNDS LOAD

Element Number	Strain Gage Number	Distance From Slot (Inches)	Rivet Model	Half Crack Length (Inches)	Experimental Strain, ϵ_e ($\times 10^{-3}$ in./in.)	Analytical Strain, ϵ_a ($\times 10^{-3}$ in./in.)	ϵ_e/ϵ_a
711	10	4.5	Flexible Fastener	2.8	0.70	0.72	0.97
705	17	1.5	↕	↕	0.97	0.82	1.18
700	29	0.1	↕	↕	1.07	0.92	1.16
800	27 & 31	0.1	↕	↕	0.785*	0.90	0.872
900	26 & 32	4.5	Flexible Fastener	↕	0.59*	0.74	0.76
711	10	4.5	Equivalent Area	↕	0.70	0.70	1.00
705	17	1.5	↕	↕	0.97	0.79	1.22
700	29	0.1	↕	↕	1.07	1.01	1.06
800	27 & 31	0.1	↕	↕	0.785*	0.957	0.820
900	26 & 32	4.5	Equivalent Area	2.8	0.59*	0.715	0.825
711	10	4.5	Flexible Fastener	4.5	0.74	0.80	0.925
705	17	1.5	↕	↕	1.26	1.01	1.25
700	29	0.1	Flexible Fastener	4.5	1.40	1.17	1.20

*Average of the two gages – less than 5% difference in readings (See Table IX).

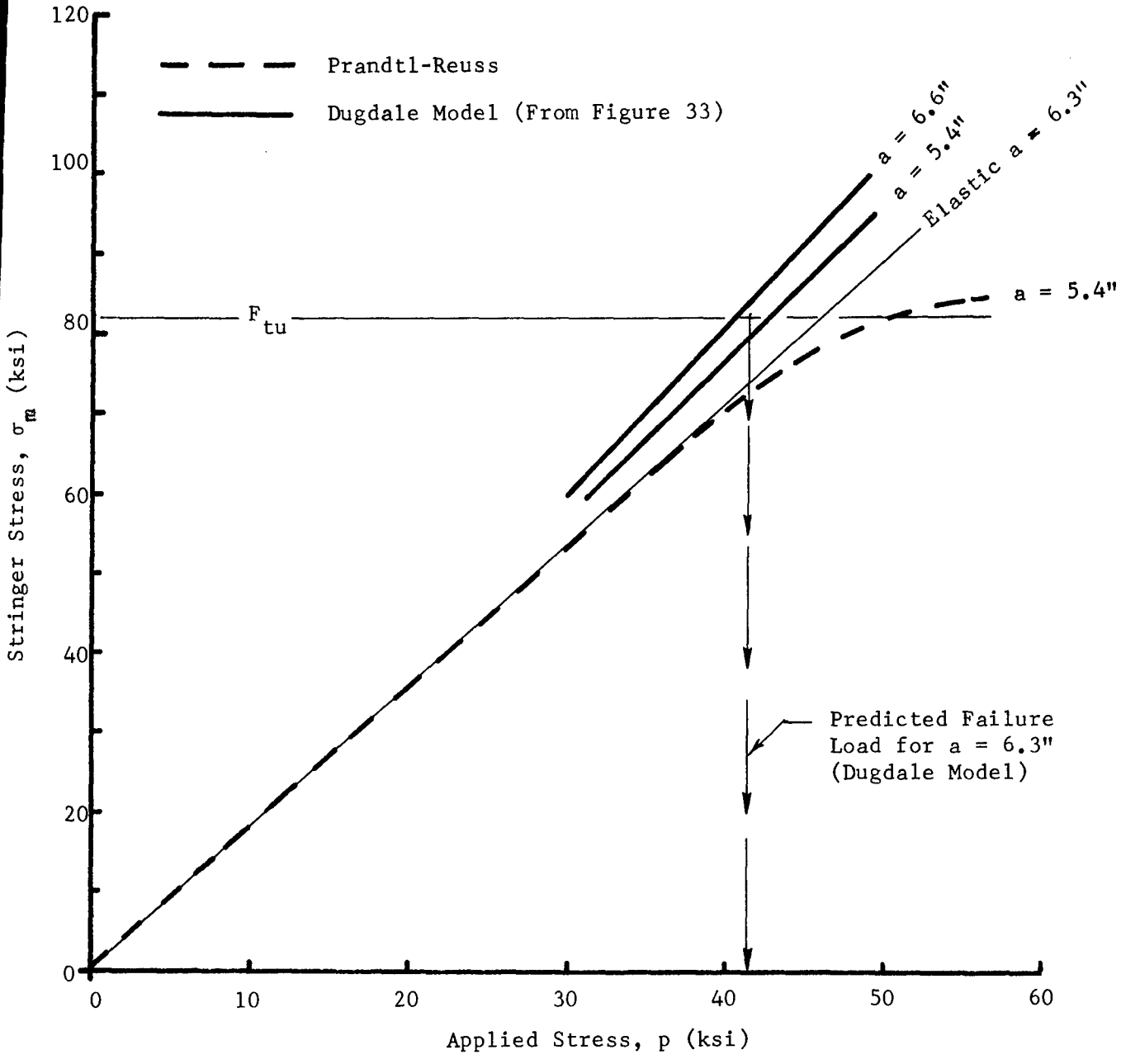

Figure 65. Predicted Failure Stress for Wing Channel Panel - a = 6.3 Inches

stringer failure (assuming failure at ultimate stress) at an applied stress of 43 ksi. Prandtl-Reuss behavior would predict failure at 51 ksi. Thus it can be assumed that for this lightly stiffened panel at a half crack length of 5.4 inches failure would probably be bounded between these two stresses (i.e., 50 ksi $> \sigma_{critical} >$ 43 ksi). From Figure 65, the stringer failure stress for the half crack length of the tested panel (6.3 inches - by interpolation between a = 5.4 inches and a = 6.6 inches) is 41.5 ksi. Since the actual failure stress for the panel was 44.5 ksi, the Dugdale model analysis has predicted a stringer critical failure within 6.8 percent of the actual failure stress. The elastic analysis would predict stringer failure at an applied stress of 46 ksi for a half crack length of 6.3 inches. This stress is 3.4 percent higher than the actual failure stress of 44.5 ksi. Thus the experimental residual strength of the wing channel panel lies between the stresses given by an elastic and Dugdale type analysis.

There are indications from the data of Figure 62 that the center channel is reaching a nonlinear behavior at approximately 60 kips. A similar observation can be made for the edge channel (Figure 63). Examination of the panel during loading to failure did not indicate any slow stable tear of the skin prior to fracture. Hence, it was concluded that fracture was due to net section yielding of the intact wing channels.

Another observation of interest was the inplane buckling of the panel, within the bays, for half crack lengths greater than 1/2 the bay width. This was an unexpected trend for the heavy stiffening of this panel geometry where the skin and stringer areas are approximately equal. This behavior was also quite prevalent in the Zee stiffened panels to be discussed in Section VII, but did not result in any large influence on residual strength. Extreme care was taken in the gripping arrangement, and grip shims were fabricated along with the panel (see Figure 49) so that the least amount of bending would take place at mid-panel. This uniformity of inplane loading is noted in the strain data of Table IX.

Figures 66 and 67 show the fractured wing channel panel. It will be noticed that the skin crack ran to and through the outer channel rivet holes during the rapid fracture sequence.

Since the wing channel panel geometry was chosen as a preliminary model for the finite element analysis it was not selected to be either skin or stiffener critical. Both the light and heavily stiffened panel configurations, were considerably heavy in stiffened area therefore it was not unexpected that net section yield would govern the fracture of this panel. The use of the 0.063 inch thick 7075-T6 skin material also would preclude any large amounts of slow tear prior to fracture. Thus the fracture of this lightly stiffened panel could be predicted from the analysis to be a stringer critical case where fracture would be governed by stringer ultimate strength. In the panels of Section VII both skin and stiffener critical fracture conditions are examined for a zee stiffened panel geometry.

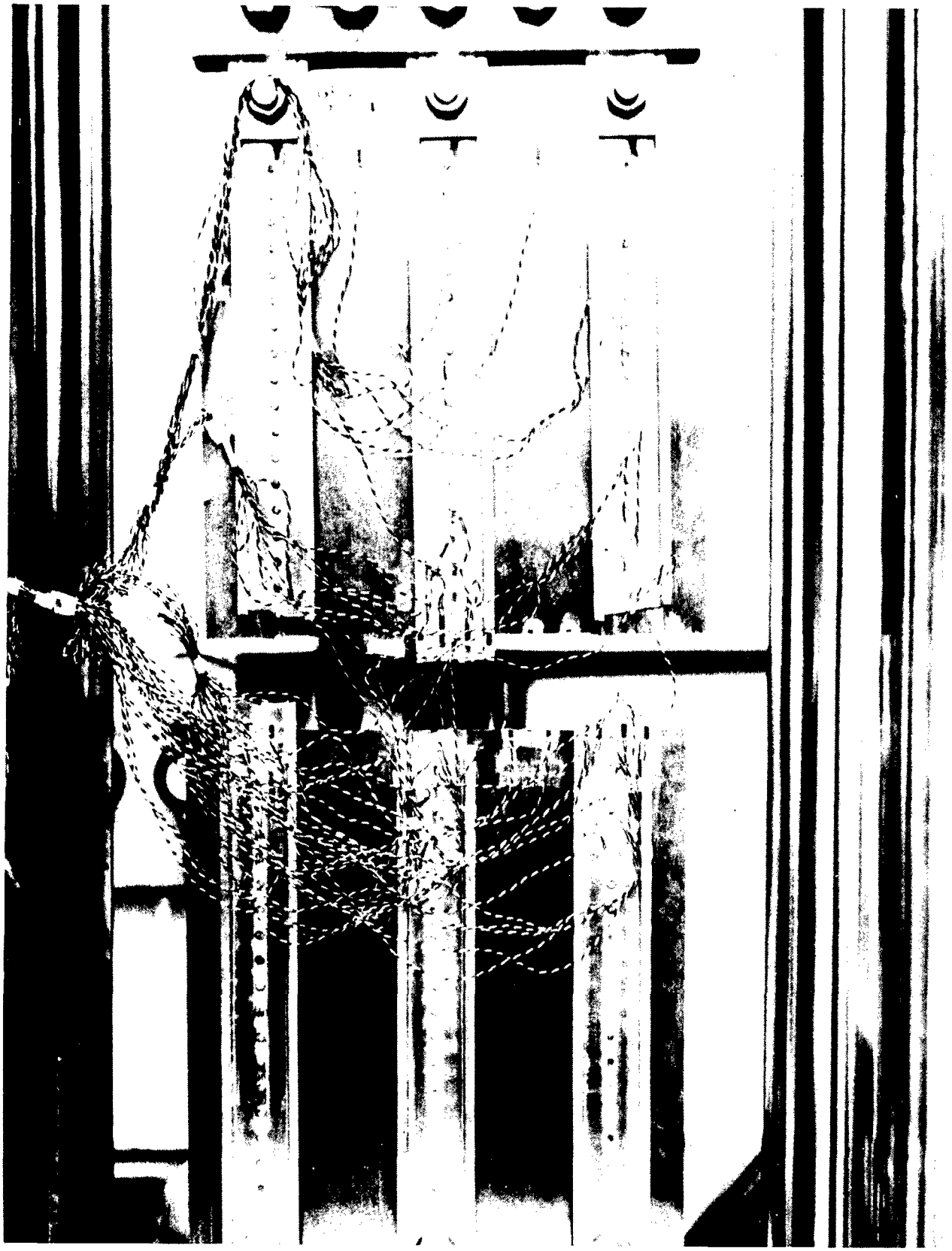

Figure 66. Wing Channel Panel Fracture - Channel Side

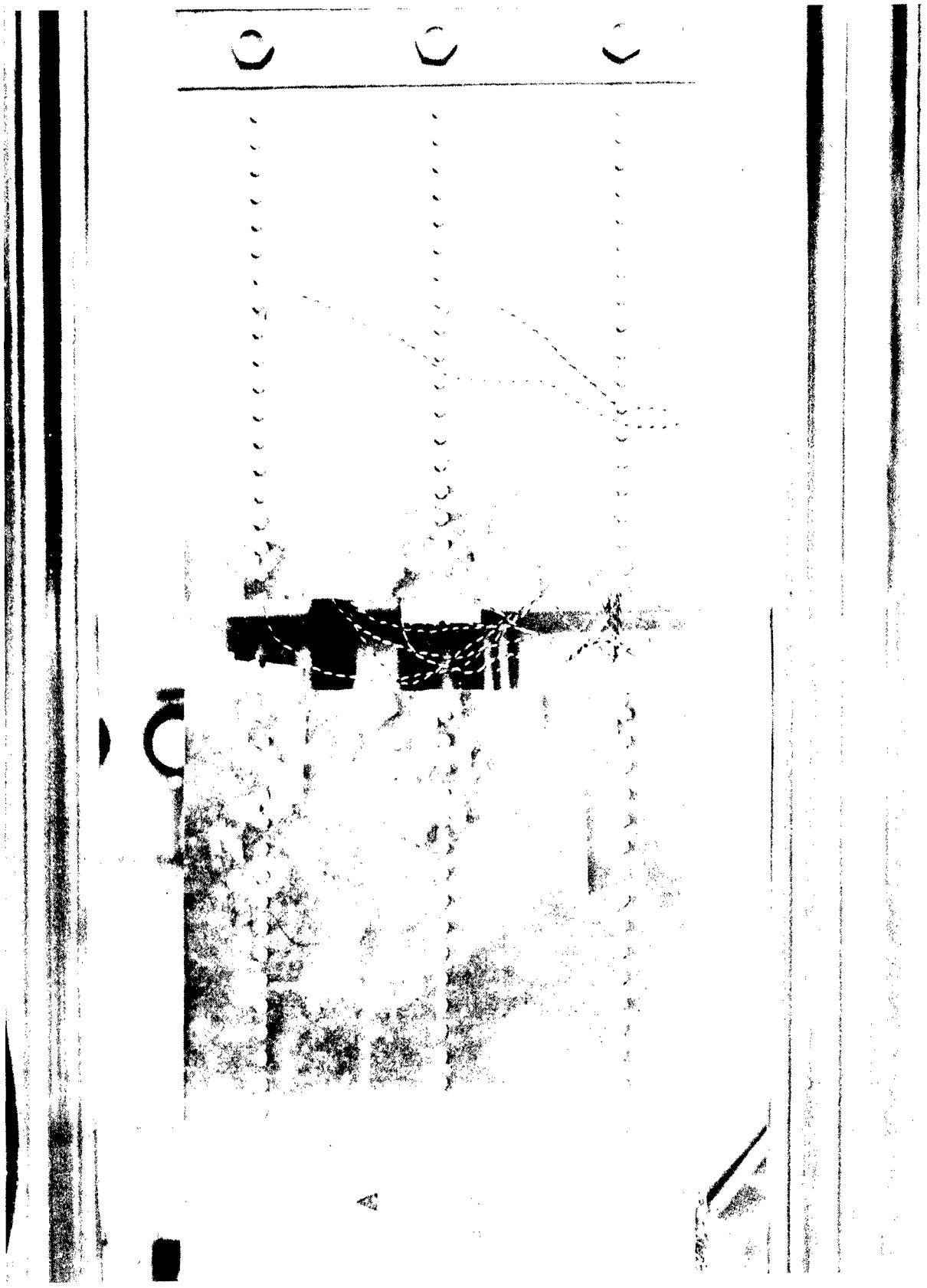

Figure 67. Wing Channel Panel Fracture - Skin Side

V. MATERIALS CHARACTERIZATION

5.1 REQUIRED MATERIALS DATA

Important to the development of any materials fracture criterion are those environments or material properties which affect the determination of a given fracture parameter. This is equally important in the development of any structural fracture criteria. In a given aircraft structure there can be two types of fracture criteria - so-called skin critical and stiffener critical cases. The emphasis in this study has been placed primarily in the skin critical case, although the data of Section VII for the zee stiffened panel geometry indicate both skin and stiffener critical structure. It is important to consider both criterion in any complete fracture or residual strength analysis. However, in the absence of any fatigue cracks in the stiffener the more important problem deals with obtaining the necessary data to assess if a skin or stiffener critical case governs.

5.1.1 Stiffener Data

In the stiffener critical case the 0.2% offset yield strength (F_{ty}) and ultimate strength (F_{tu}) of the stiffening material must be accurately known so that the stiffener stress can be monitored during the finite element computational procedure. This situation is particularly true for the skin crack at stiffener configuration and/or the long crack between stiffener problem, i.e., when crack length 2a approaches the stiffener spacing, s, ($2a/s \longrightarrow 1.0$).

The value of Young's Modulus for the stiffening material should also be chosen to reflect as accurately as possible the material planned for use in the structure of interest. For example it could be possible to have a 3 to 8 percentage difference in Modulus between skin and stiffener which could become significant in computing stiffener stresses in the overall analytical procedure.

It is believed that handbook (e.g. MIL-HDBK-5) values of F_{ty}, F_{tu} and E will be sufficient--particularly if the product form is similar, i.e., use extrusion values for extruded angles, tee's, etc. However, when a new material or differently formed section shape is planned for the stiffening structure it is imperative that the basic materials property data be included in the proposed analysis for that section and material. Since these data are not difficult nor costly to obtain they should be included as part of the overall material's data gathering scheme, when warranted.

5.1.2 Structural Skin Data

In the proposed plane stress, residual strength analysis method the cover material or skin fracture criterion is based on development of $\sqrt{J_R}$ versus physical crack extension (Δa) values. The details of generalizing these data are contained in Section VI and for obtaining the materials data in Volume II. In this section those material properties necessary to meet first, the analysis procedure and secondly the skin fracture criterion will be described.

In the analysis method it is required to obtain accurate determinations of material yield strength and Young's Modulus. Modulus should preferably be obtained from the actual material (and thickness) planned or sized for the structure. The reason thickness is important is that the skin material in many cases will be landed or pocketed. This milling procedure (be it chemical or mechanical) is known to have some influence on crack growth resistance, K_R - hence also $\sqrt{J_R}$. From those specimen geometries tested to obtain K_R or $\sqrt{J_R}$ (CLWL, CCT, etc.) using compliance techniques it is necessary to obtain accurate, Young's Modulus values in the direction of initial crack orientation, i.e., LT or TL from the undeformed broken half of the particular specimen geometry utilized. Two flat tensile specimens are usually sufficient. Modulus values should be confirmed using strain gage specimens with readings taken in conjunction with standard extensometer readings since the value of Young's Modulus plays an important role in the determination of crack size, during slow stable crack growth. The value of E used in the specimen compliance relationship should be an average of the strain gage Moduli obtained from the two tensile coupons.

In the analytical technique (see Section VIII) it is also necessary to have an accurate measure of the material 0.2 percent offset yield strength, F_{ty} since the value of the J integral (in the Dugdale sense) is computed from the product of crack opening displacement and F_{ty}. Here again the chosen value of yield strength should represent an average value from the thickness and direction of anticipated crack extension. Within the finite element technique these data are also necessary.

NOTE: It must be remembered that irregardless of the method of analysis the skin failure criterion dictates that Modulus and yield strength as a minimum be determined parallel to expected direction of crack growth in the most accurate possible manner. Data from the particular material and thickness expected in service is preferable.

5.2 GENERAL DISCUSSION OF CRACK GROWTH RESISTANCE, K_R

As noted in Section 2.3.1 the original concept of constant critical energy release rate proposed in Reference 46 was changed to an energy balance concept by the research of Reference 22. The modification of this original concept was brought about by the experimental observation by Krafft and co-workers that the geometric effect (i.e., crack length, specimen width, etc.) could be explained by a resistance type curve rather than a single value of strain energy release. Just such a curve was developed for 1/8 inch thick 7075-T6 aluminum in Reference 22.

The concept of crack growth resistance is shown in Figure 68. As a crack in a panel extends under increasing load the amount of slow tear prior to fracture is a function of panel thickness which in turn influences crack tip plasticity. Several investigators have recently examined the crack growth resistance concept (see e.g. References 7, and 47 through 53) in an attempt to shed some additional light onto the mechanisms influencing crack resistance. Interest has also led to the formation of a Task

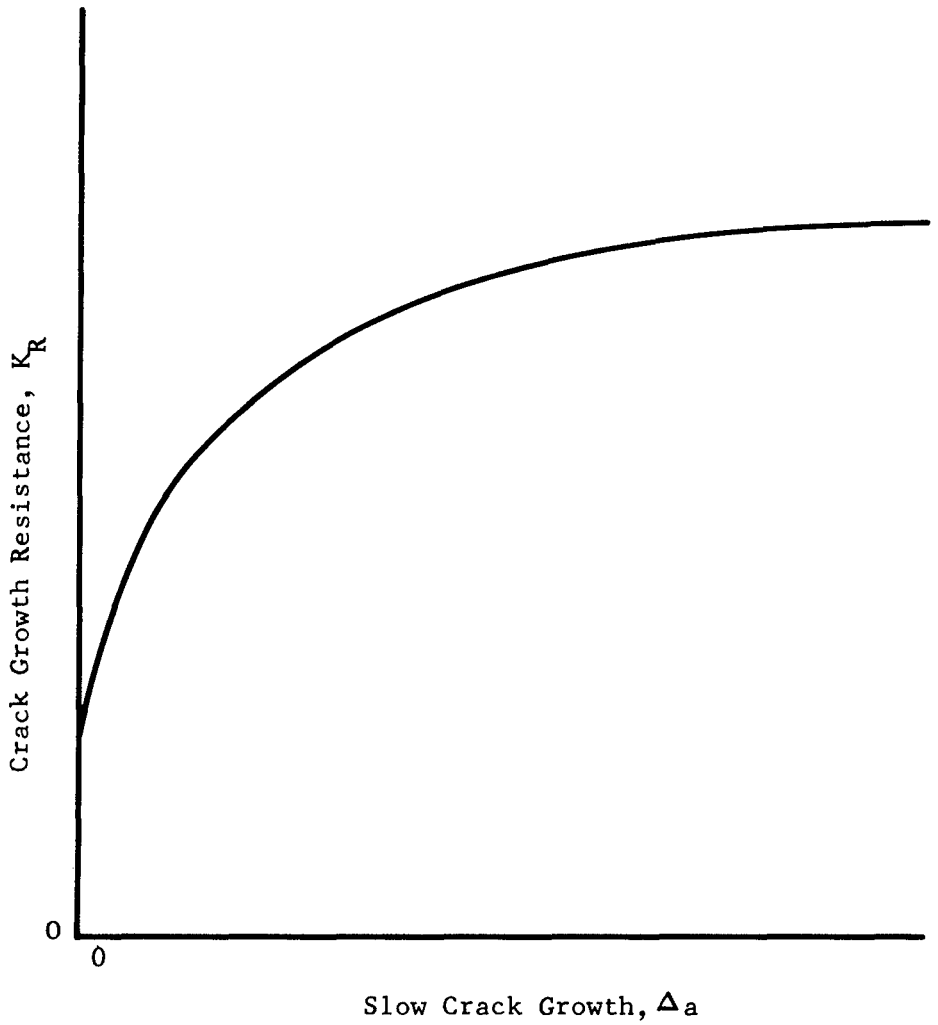

Figure 68. Schematic of Crack Growth Resistance

Group within the American Society of Testing and Materials (Committee E-24 on Fracture Testing of Metals) and the preparation of a Proposed Recommended Practice for R - curve determination (Reference 54).

In general the crack growth resistance curve can be used in conjunction with the crack driving force curve, for a given specimen geometry, to predict fracture based on a critical K for that specimen geometry. An example of this behavior is shown in Figure 69. For a given initial crack size ($2a_o$ or a_o) under increasing stress (σ_n) a family of curves (dashed) can be established for the given geometry. At some point (X in this case) the following conditions are met between the resistance curve K_R and the driving force curves, K

$$K = K_R \text{ and}$$

$$\frac{\partial K}{\partial a} \geq \frac{\partial K_R}{\partial a} \tag{17}$$

At that point there is a tangency between the applied driving force and resistance curve (point X of Figure 69) and instability takes place for the given specimen geometry. Associated with this point is the amount of slow stable crack growth (cross hatched) prior to instability.

In the CCT specimen geometry the amount of stable tear is a function of specimen width as well as applied stress and is the reason for the specific comments relating to a given specimen geometry. Therefore, to develop the full range of K_R data a rather wide CCT specimen is required to limit net section yielding and to maintain limited plasticity (with respect to crack size) particularly for the tougher materials. A width equal to or greater than

$$W \geq \frac{27}{2\pi}\left(\frac{K_c}{F_{ty}}\right) \tag{18}$$

has been suggested to provide general elastic conditions at the crack tip. For those materials which have high toughness (K_c) it can be seen that widths in excess of 48 inches would be required. Therefore, the development of the K_R curve was proposed and has been accomplished through testing the crackline wedge loaded (CLWL) specimen geometry. The crack driving force curves (for displacement controlled testing) for these specimens are decreasing functions of K^2/E or load (stress) since once the wedge load is applied and the crack runs then loading drops off - hence K decreases. With this particular specimen geometry quite large increments in slow crack growth, Δa, can be observed and development of a plateau value of K_R is often possible for some materials. It is currently thought that the plateau value of K_R is the maximum toughness possible for a given material and thickness.

The general shape of the K_R curve is reflected by the material toughness. Those materials exhibiting extensive plasticity (at the crack tip) and large amounts of slow tear have the appearance shown schematically in

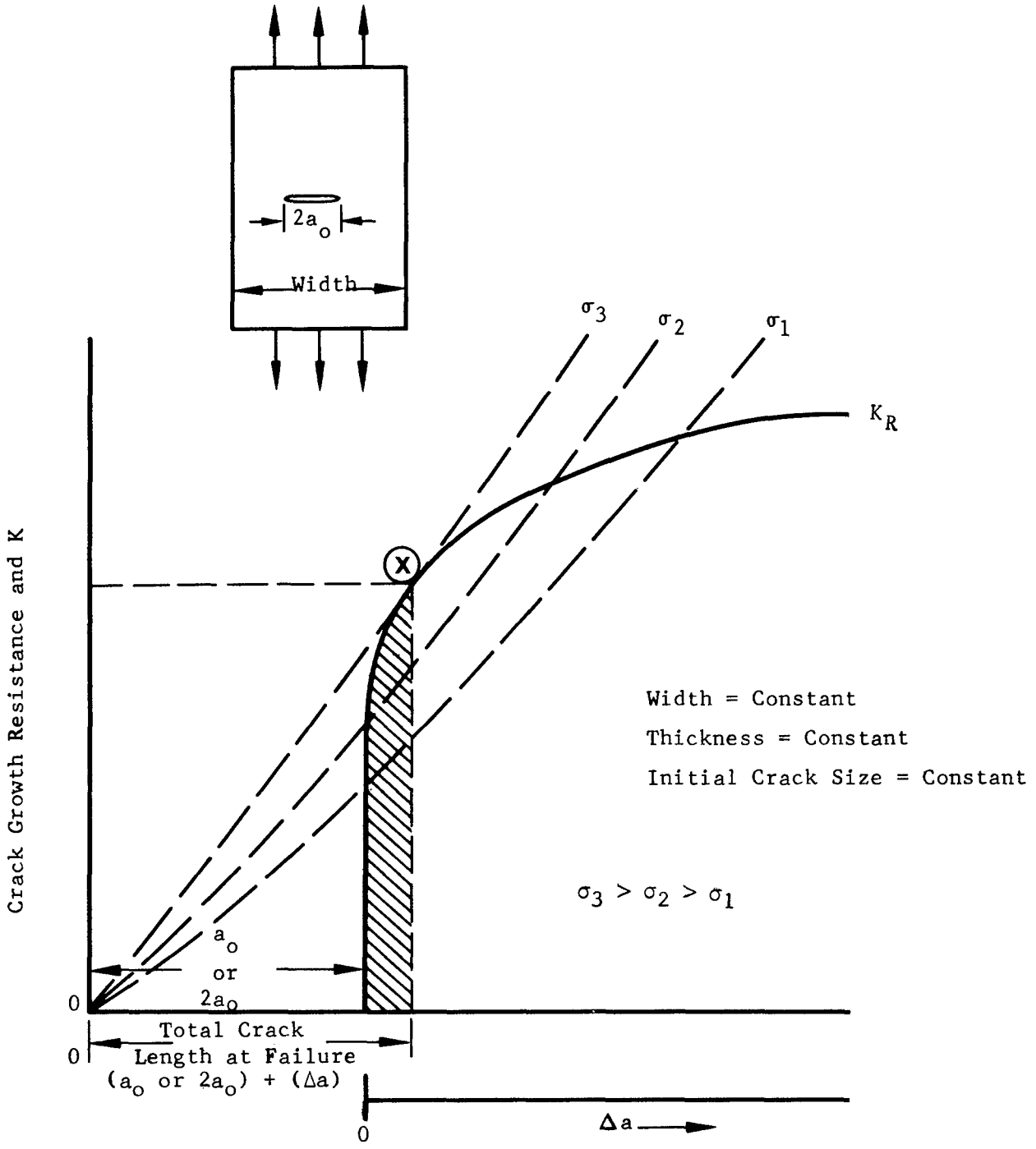

Figure 69. Fracture Instability as Predicted from K_R Curve and Crack Driving Force - Load Control Test

Figure 70 (a). Those materials with moderate or low toughness have K_R curves shaped like those in Figure 70 (b). The actual comparison of the K_R curves for the materials tested during this program are shown in Section 6.2.1.

Since the method described in this report uses the $\sqrt{J_R}$ curve (which is established in a manner similar to that used in obtaining the K_R curve) it is believed that this general background information on the development of crack growth resistance would be useful. How one obtains the basic K_R data will be described next, the procedure used in converting these data to a $\sqrt{J_R}$ curve is given in Section 6.3.

5.3 TEST(S) TECHNIQUE

A detailed description of how crack growth resistance data are obtained is given in Volume II of this report. A short description of the test technique employed during this program will be presented next.

The test method using the CLWL specimen closely follows that given in Reference 54. In this method a specimen with the dimensions shown in Figure 71 is loaded through a tapered wedge and split clevis arrangement through the large loading hole. All specimens were previously fatigue precracked by tension-tension loading using a split, D shaped loading clevis at the large hole. A compliance relationship is established for the specimen (loaded in tension) for a series of slot lengths. Double compliance is used (see measurement points V_1 and V_2, Figure 71) to calculate applied wedge load (P) for a given crack size. The testing of this CLWL geometry provides information on both physical and effective crack size based on return slope relationships with specimen compliance. In addition to having more stable behavior during slow crack extension the CLWL geometry permits values of both effective (includes crack tip plasticity) as well as physical crack size to be readily determined.

In the CLWL test the wedge is driven through the split clevis (at the large hole) until small crack extension takes place. The specimen is restrained from out of plane buckling by being sandwiched between retainer plates which have rollers on top and bottom surfaces. Therefore, the specimen is forced to rotate within its own plane but restrained from any out of plane motion. As the crack runs and becomes arrested a trace of displacements V_1 versus V_2 are obtained. After arrest the loading wedge is partially removed and a trace of a return slope (of V_1 vs. V_2) is obtained as well as a visual measurement of crack size. The same process is repeated until an overall value of $a/W \gtrsim 0.6$ is obtained in crack growth.

For additional discussion of interpretations and analysis of data, Volume II of this report is recommended.

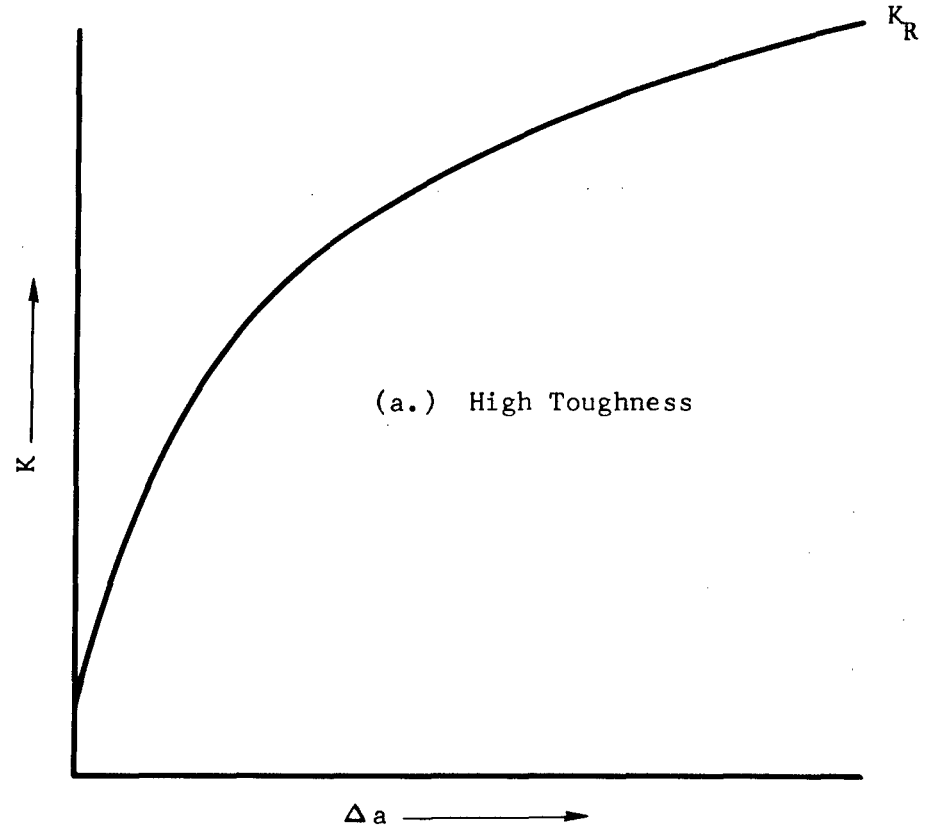

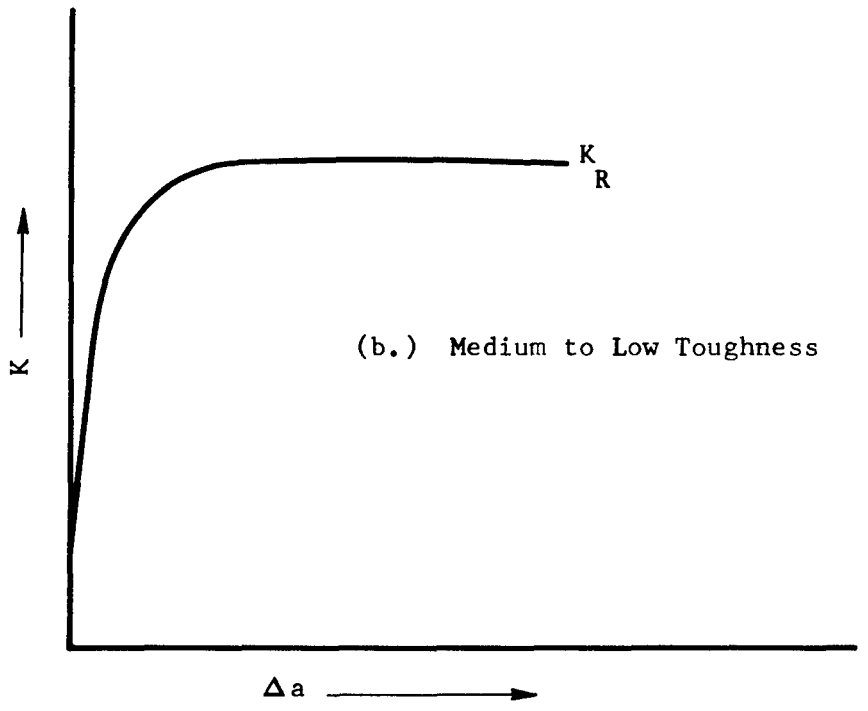

Figure 70. Comparison of Crack Growth Resistance Curve for Various Material Toughness

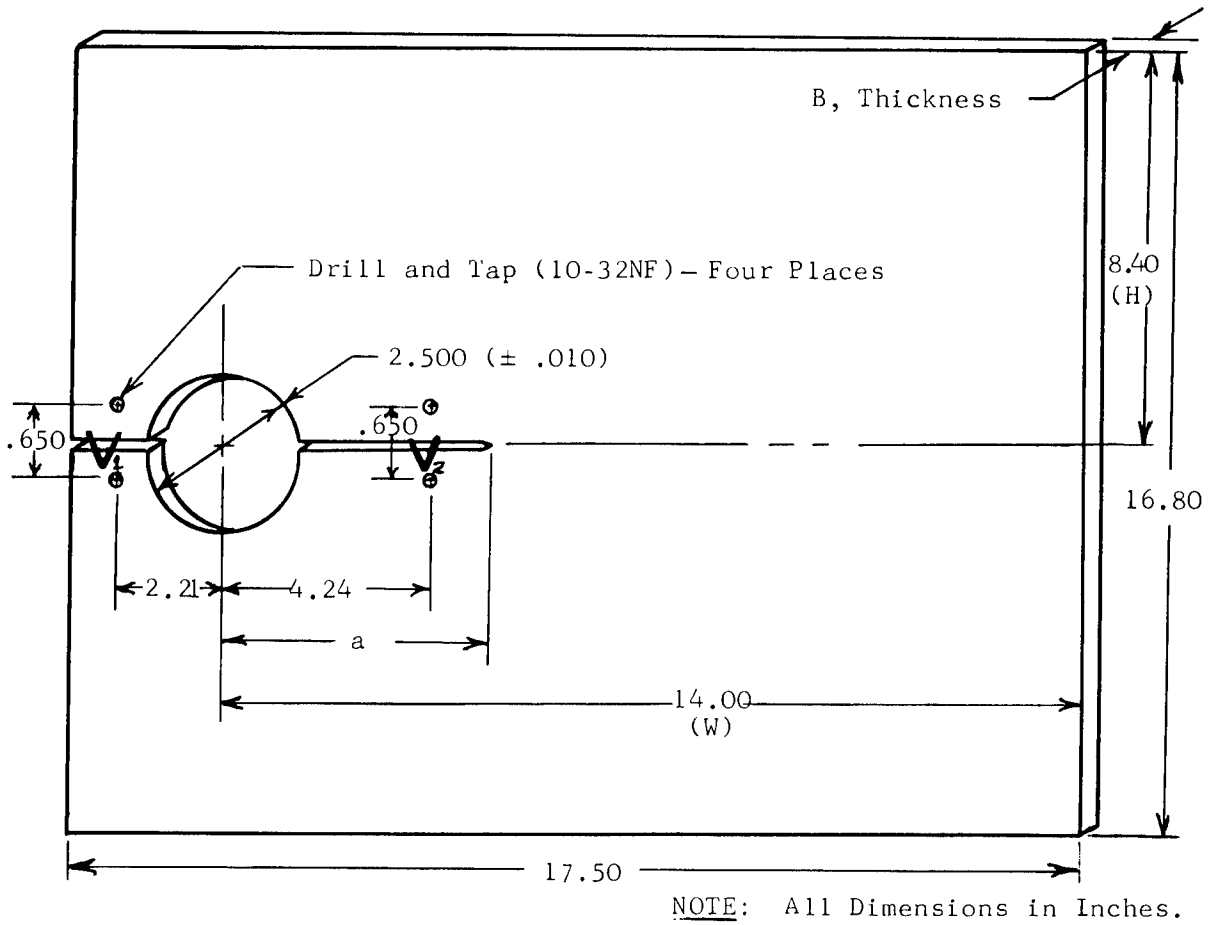

TL - Specimens have rolling direction parallel to slot.

LT - Specimens have rolling direction perpendicular to slot.

Figure 71. Crack Line Wedge Loaded (CLWL), CS Type Specimen (H/W = .6)

VI. CRACK GROWTH RESISTANCE

The failure criterion proposed in the residual strength analysis procedure outlined in this report is based on the skin material's resistance to crack growth. In order to obtain these data the crack line wedge loaded (CLWL) specimen is used in conjunction with a combination of analytical and experimental results to obtain a crack growth resistance curve based on J integral results. In this Section a description of the elastic and elastic-plastic analysis of the CLWL specimen is presented. Comparisons of both linear elastic (K_R) and elastic-plastic ($\sqrt{J_R}$) materials data are given along with the results of changing specimen geometry on K_R for the CLWL and center cracked tension (CCT) geometries. In addition the results of a series of tests at small crack extension ($\Delta a < 0.05$ inch) and low K_R are reported which can form the basis for initial values of crack growth resistance. A complete description of the procedure required to obtain J integral values from the CLWL data is given and the resulting $\sqrt{J_R}$ vs. Δa_{PHY} curves presented for the materials tested.

6.1 THE CLWL SPECIMEN

The crack line wedge loaded specimen (CLWL) is currently being used for crack growth resistance curve determination. Analytical work on this specimen has been primarily based on the results obtained for the compact specimen. The applicability of compact specimen results to the CLWL specimen geometry has not been fully established. In addition, an elastic-plastic analysis of this specimen is not known to be available in the literature. Thus an elastic-plastic analysis of this specimen was deemed necessary and an analysis was performed using finite element methods. Essential features of this analysis are discussed below.

6.1.1 Finite Element Modeling of CLWL Specimen

Triangular membrane elements have been used to model the crack-line wedge-loaded specimen. Due to symmetry only one-half of the specimen was modeled as shown in Figure 72. An element size of 0.1 inch was used in the region ahead of the crack tip. This corresponds to an element size to crack length ratio of 0.02 for the smallest crack length considered (4.9 inches) and 0.011 for the longest crack length examined (8.9 inches). Of primary concern was the elastic-plastic analysis so that values of the J integral could be computed on certain paths, hence, the element size of 0.1 inch was considered to be sufficiently small for this analysis. The grid size is gradually increased to about 1.75 inches near the specimen boundaries.

During the modeling of this specimen it was found that an important consideration was the point or points of application of the wedge loading force (P) and the constraints to be provided to the loaded points. By applying constraints so that all the loaded points on the circular hole have the same displacement along the y-y axis (Figure 73) the analytical displacements in the y-direction at the clip gage points V_1 and V_2 were considerably smaller than those observed from the experimental data.

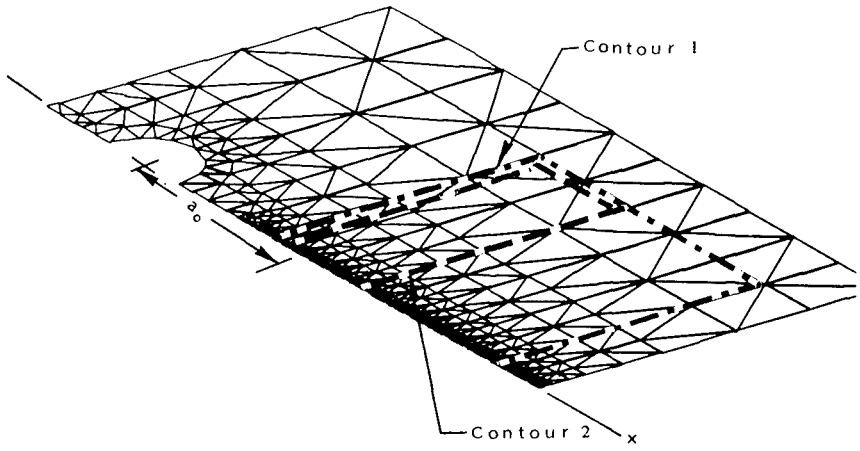

Figure 72. Finite Element Model and J Integral Paths for CLWL Specimen

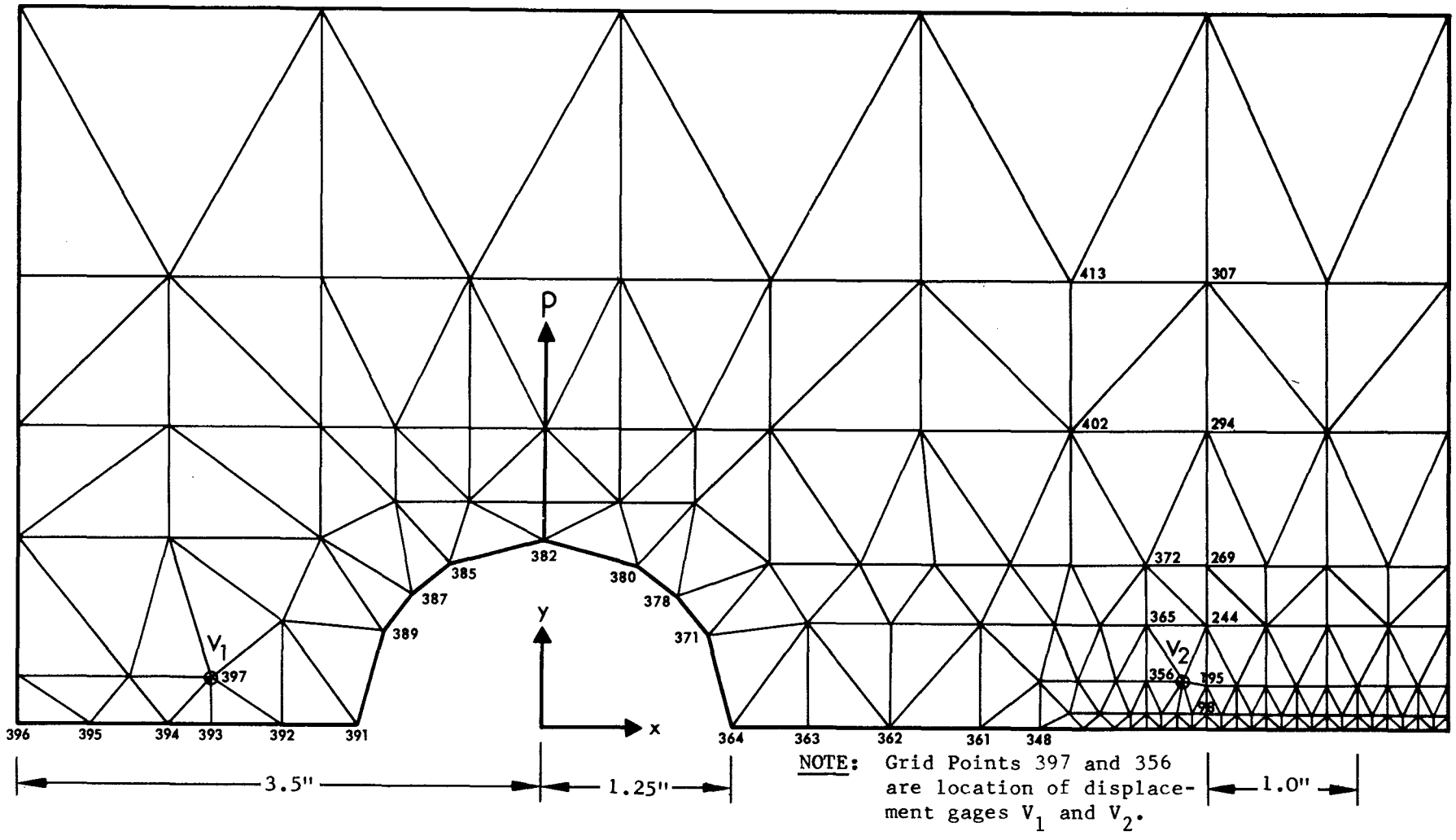

Figure 73. Enlarged View of Finite Element Modeling at Loading Hole - CLWL Specimen

The following three cases of load application were considered.

Case I. Grid points 378, 380,382,385 & 387 (see Figure 73) were loaded with total load P such that P/3 is applied at grid point 382, P/4 is applied at grid points 380 and 385, and P/12 applied at points 378 and 387. It is also assumed that all loaded grid points have the same displacement in the y-y direction.

Case II. Grid points 380, 382, and 385 loaded with total P such that a P/2 load is applied at grid point 382 and P/4 applied at each of the points 380 and 385. It is also assumed that the displacement of grid points 380, 382 and 385 is the same in the y-y direction.

Case III. Grid point 382 is loaded with load P and it is assumed that all the grid points on the circumference of the circle have no displacement constraints.

These three loading cases gave total displacements at grid points 397 and 356 (see Figure 73) at clip gauge locations V_1, V_2 as shown in Table XI.

TABLE XI. TOTAL DISPLACEMENTS AT POINTS V_1 AND V_2 FOR CLWL SPECIMEN AT APPLIED LOAD OF P = 1000 LBS

Position	CASE I (inches x 10^3)	CASE II (inches x 10^3)	CASE III (inches x 10^3)
V_1	27.126	29.364	32.851
V_2	6.082	6.296	6.637

The data of Table XI indicates that the method of load application has a considerable influence on the analytical displacements. Comparisons with the experimental elastic displacement data showed that Case III loading produced very good correlation with analytical results. This correlation will be shown later in Section 6.1.2. Hence it was assumed in the subsequent analysis that the specimen is loaded with point loads as shown in Figure 73 and that there are no displacement constraints on the node points around the periphery of the circular hole. This method of load application is consistent with the shape of the rocker wedges used in loading the hole experimentally.

6.1.2 Elastic Analysis of CLWL Specimen

An elastic analysis of the CLWL specimen geometry was performed for several crack length to specimen width ratios (a/W). These analytical displacements were then compared with experimentally observed displacements for the specimen loaded by wedge loading. Figure 74 shows a comparison of the finite element model and experimentally measured displacements. The correlation between experimental and analytical results appears to be extremely good.

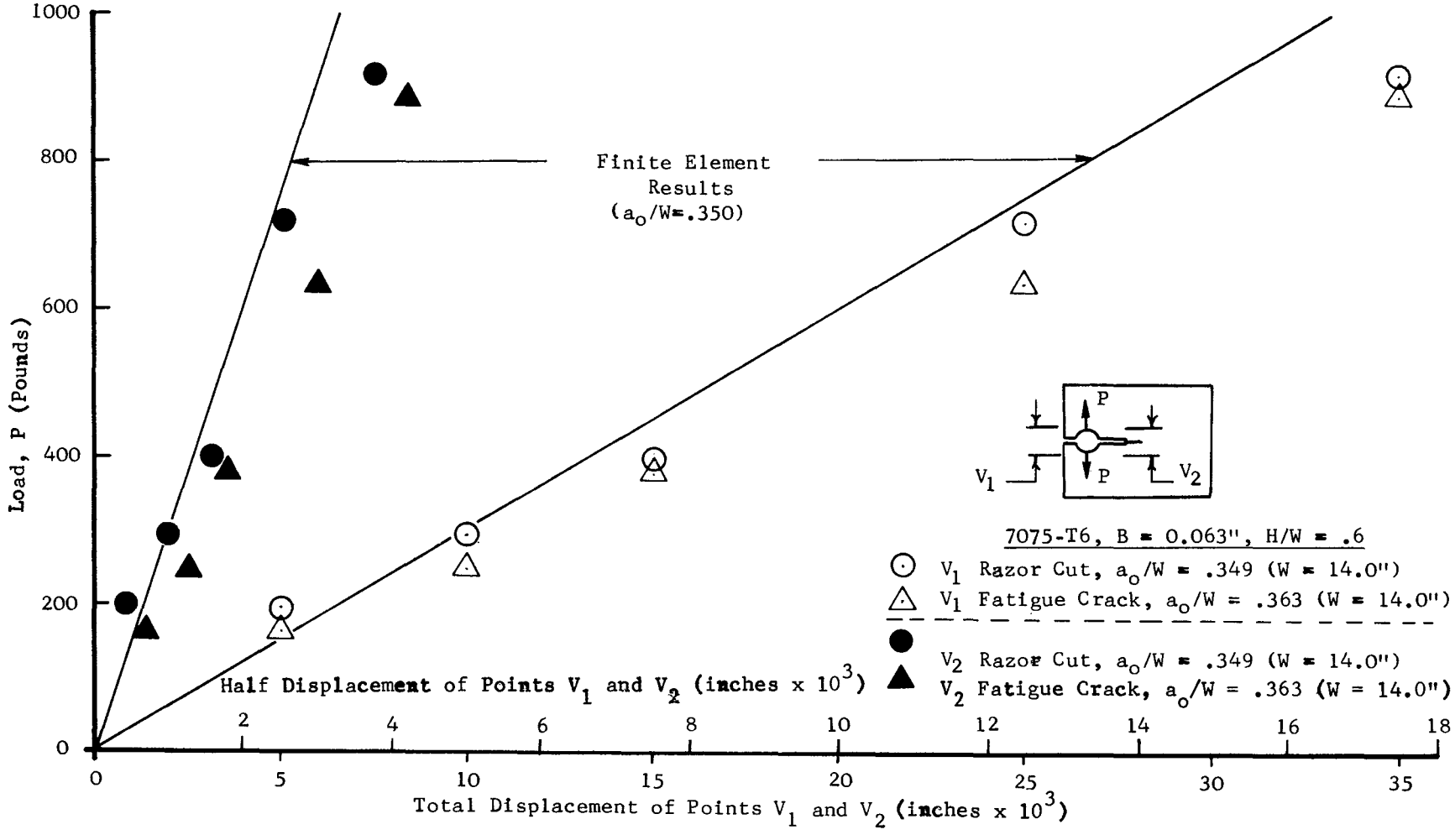

Figure 74. Comparison of Experimental Deflection Data with Finite Element Results for CLWL Specimen

The elastic stress intensity factors computed from this analysis were from 7 to 9 percent lower than those proposed for use with this CLWL specimen geometry (Reference 54). The larger differences occurred for the shorter crack lengths.

Elastic J integral values were computed for several a/W ratios. For a 4.9 inch crack (a/W = 0.35) two different paths (see Figure 72) were used to compute J integral values. The two values of square root of J were within one percent of each other, hence for additional crack lengths it was only necessary to use one path for subsequent computations of J. Values of elastic J integral were computed for crack lengths of 4.9, 5.4, 5.9, 6.4, 6.9, 7.4, 7.9, 8.4 and 8.9 inches and are shown in Figure 75 plotted as a function of applied stress. The data of Figure 75 was cross plotted in Figure 76 at constant load (1000 lbs) as a function of crack length. This plot (Figure 76) indicates a linear function between $\sqrt{J}$ and "a" to a crack length of about 6 inches. At larger crack lengths the values of square root of J increase very rapidly with crack length.

6.1.3 Elastic-Plastic Analysis of CLWL Specimen

Elastic-plastic analysis of the CLWL specimen geometry was performed assuming both Dugdale plastic zone model and Prandtl-Reuss material behaviors. The results of these two analyses and their comparison are discussed in the following Subsections.

6.1.3.1 Dugdale Model Type Elastic-Plastic Analysis

A Dugdale type elastic-plastic analysis was carried out using the Bueckner-Hayes energy approach described in Section 3.3.1.1. In addition the original Dugdale approach was employed which is based on removing singularities ahead of the crack tip. The results obtained by these two approaches showed excellent agreement. Figure 77 shows the comparison of $\sqrt{J}$ values for the elastic case and Dugdale type analysis at a fixed physical crack length of 4.9 inches (a/W = 0.35). The material was assumed to be 7075-T6 aluminum sheet, 0.063 inches thick. From Figure 77 it can be seen that for values of $\sigma_{app.}/F_{ty}$ (where $\sigma_{app.} = P/BW$) less than 5 percent the values of $\sqrt{J}$ for the elastic and Dugdale type analysis are similar. At higher values of applied stress (>10 percent of yield) considerable differences are noted in $\sqrt{J}$ values for the two cases.

Figure 78 shows the variation of $\sqrt{J}$ as a function of applied stress for various physical crack lengths. Here the material was assumed to be 0.0784 inch thick 2024-T3 aluminum. For the same applied stress (load) the value of $\sqrt{J}$ increases with crack length.

In Figure 79 the variation of plastic zone size as a function of applied stress is shown for the CLWL specimen. Several observations can be made from the data of Figures 78 and 79. Large plastic zones and square root of J values are obtained for applied stresses which are relatively small percentages of the 2024-T3 yield strength, e.g., a two-inch long plastic zone at less than

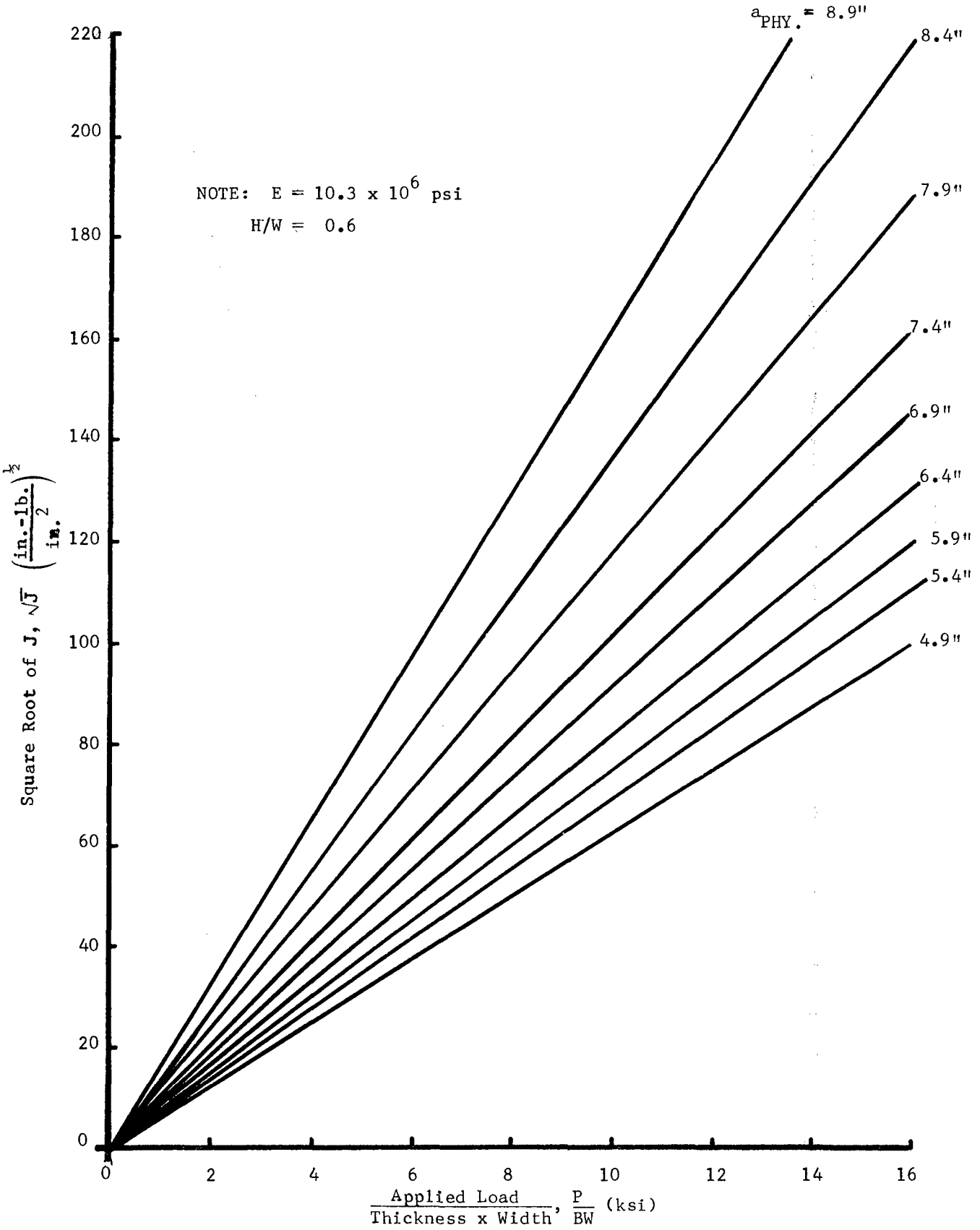

Figure 75. CLWL Elastic Square Root of J Values for Various Crack Sizes and Applied Stress

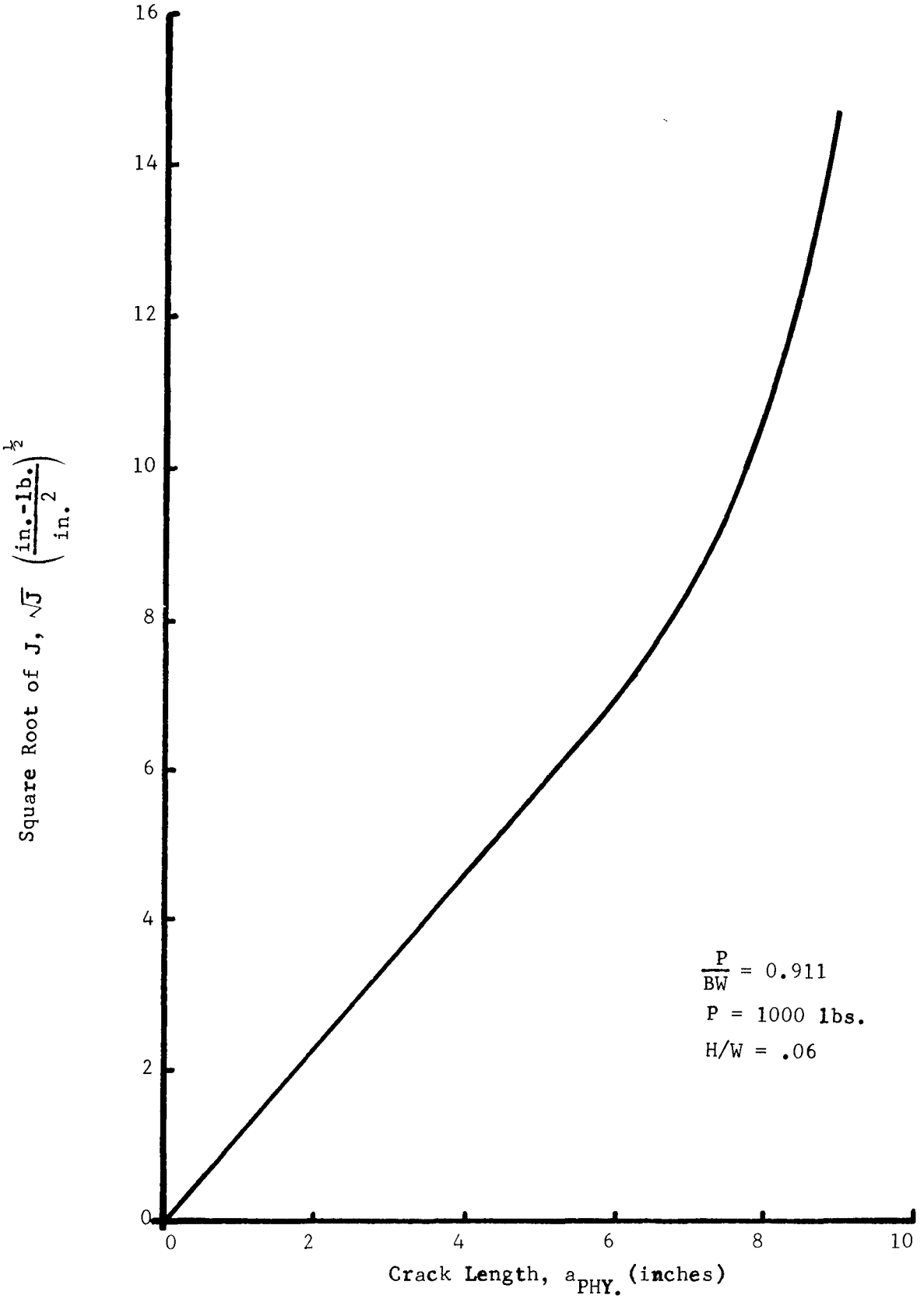

Figure 76. Square Root of J as a Function of Crack Size at Constant Load - CLWL Specimen

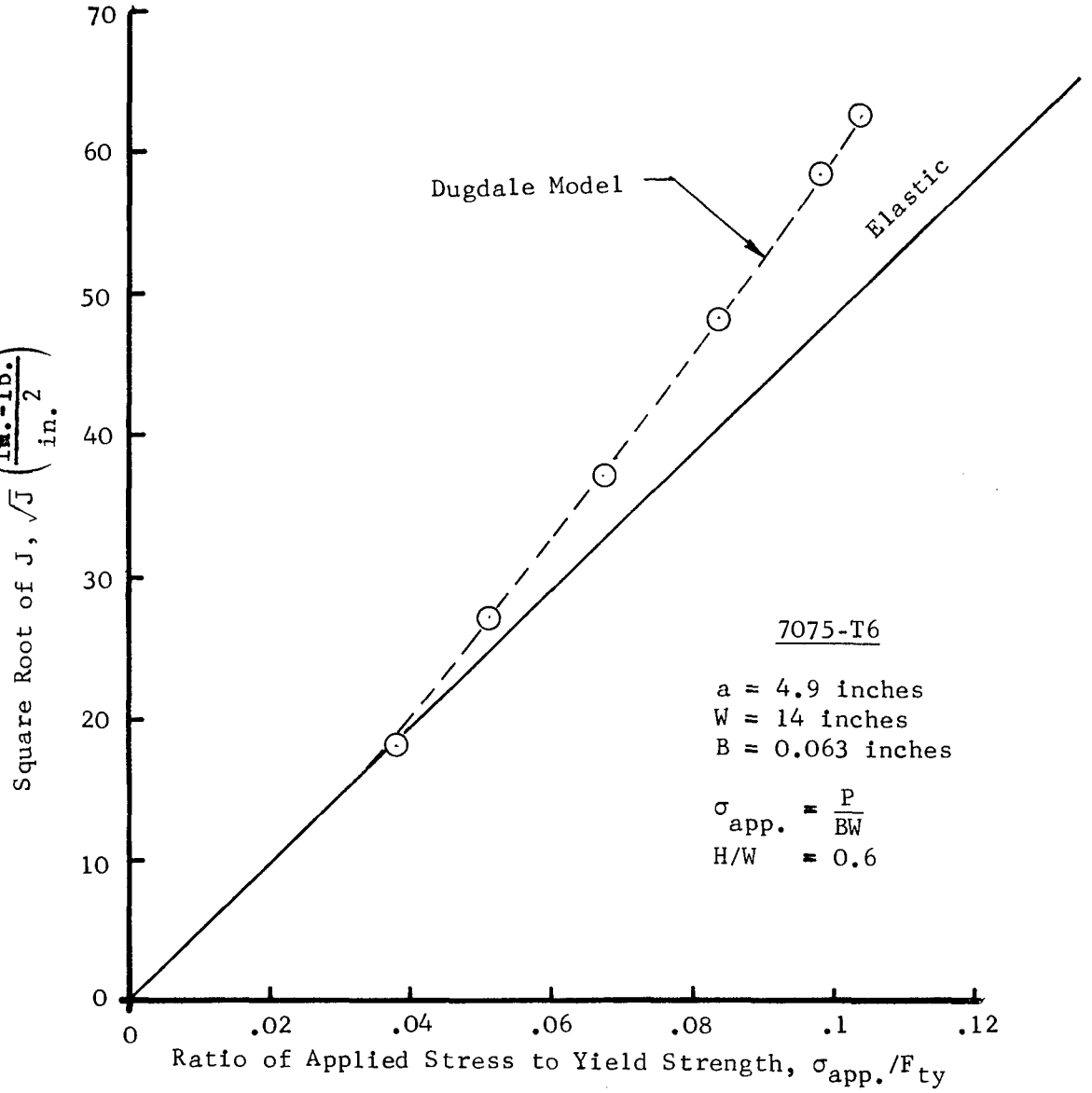

Figure 77. Square Root of J as a Function of Applied Stress for 7075-T6, CLWL Specimen

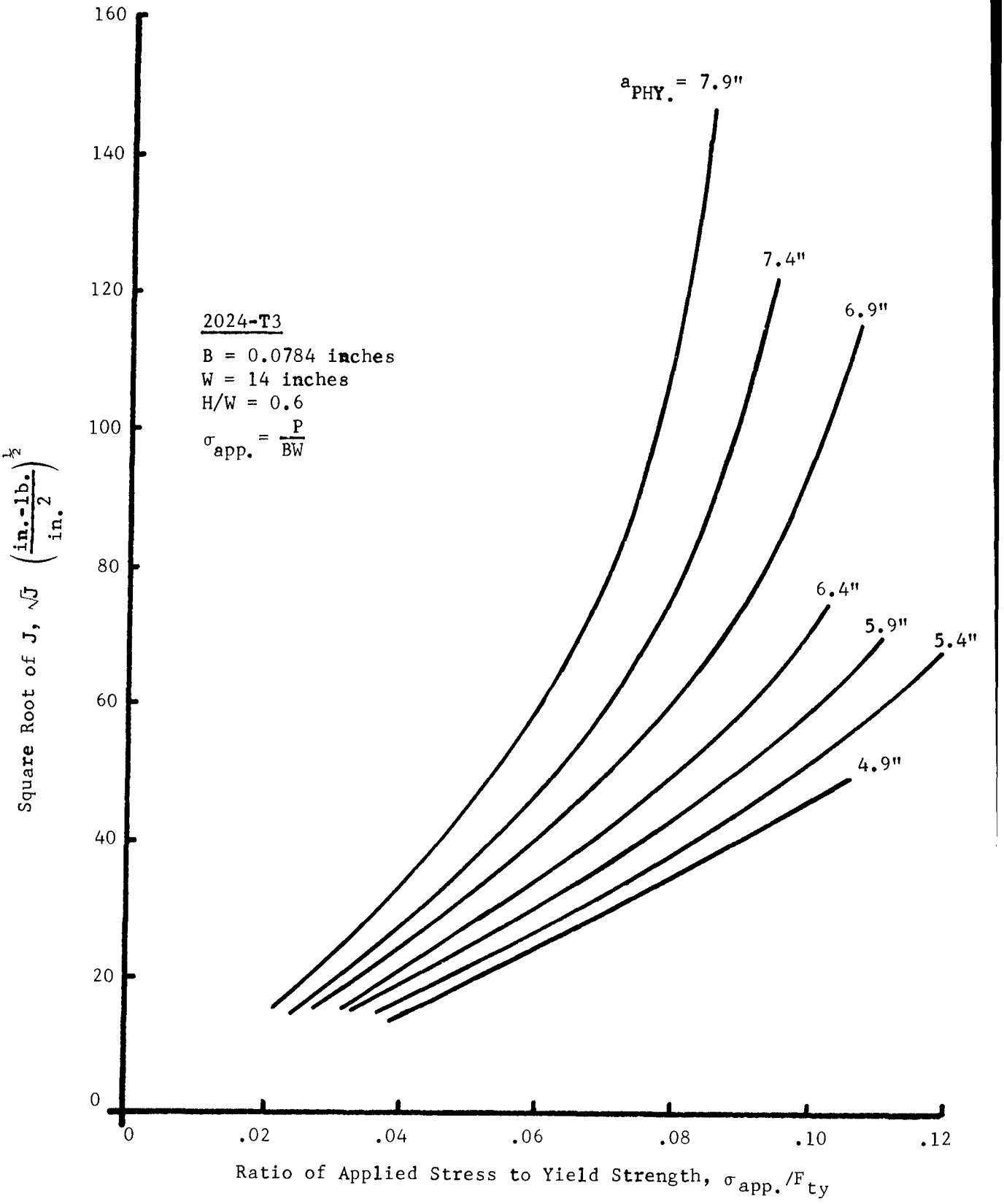

Figure 78. Dugdale Analysis of CLWL Specimen - 2024-T3, B = 0.0784 Inches

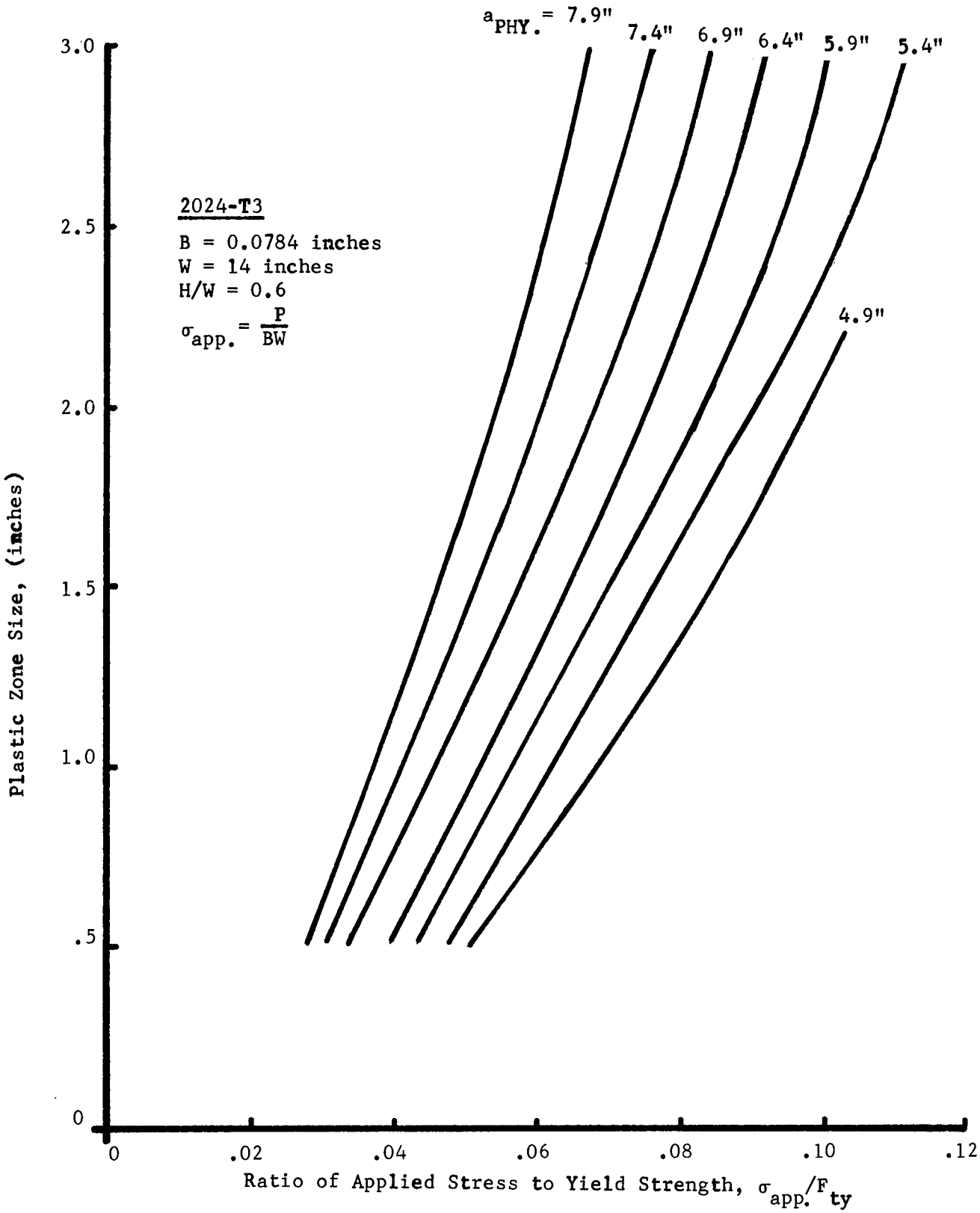

Figure 79. Dugdale Model Plastic Zone Size as a Function of Applied Stress - CLWL Specimen

ten percent of the yield strength. Since the J integral values in the Dugdale sense are calculated from crack opening displacements it is obvious that large crack opening displacements are obtained at low applied stresses.

6.1.3.2 Analysis Based on Prandtl-Reuss Material Behavior

The Prandtl-Reuss elastic-plastic analysis of the CLWL specimen was performed for two different crack lengths. A plot of Prandtl-Reuss $\sqrt{J}$ values versus P/BWF_{ty} for physical crack lengths of 4.9 and 6.9 inches is shown in Figure 80. Also shown for comparison are $\sqrt{J}$ values assuming elastic and Dugdale material behaviors. To a P/BWF_{ty} ratio of 0.02, the $\sqrt{J}$ values are similar for the three types of material behavior. For a 4.9 inch physical crack length, Prandtl-Reuss values are only slightly larger than elastic values, however Dugdale values are higher than both. At the 6.9 inch crack length the effect of large plasticity is observed, with Prandtl-Reuss values higher than elastic values. A considerable increase in the values of $\sqrt{J}$ are given by assuming Dugdale behavior. This trend in the Dugdale type analysis is in contrast to that observed for stiffened panel geometries where a close correlation was obtained between Dugdale and Prandtl-Reuss material behaviors. It can also be noted that for the same applied load (stress) Prandtl-Reuss behavior results in $\sqrt{J}$, values between the elastic and Dugdale, this ordering was also observed in the stiffened panel analysis.

Using the assumptions described in Section 3.3.2, plastic zone lengths were calculated for assumed Prandtl-Reuss material behavior. A comparison of Dugdale and Prandtl-Reuss type plastic zones is shown in Figure 81. Except for extremely small applied loads the Dugdale analysis gives larger plastic zone sizes than those based on Prandtl-Reuss material behavior. It should be noted that for the stiffened panels good correlation was obtained between the plastic zone sizes resulting from the two material behaviors. From this comparison of Dugdale and Prandtl-Reuss behavior it would appear that a Dugdale analysis would result in unrealistic values of $\sqrt{J}$. If this is true a $\sqrt{J_R}$ based resistance curve obtained from a Dugdale type analysis would appear unrealistic. It could be concluded that the correct method required to obtain a J_R curve would be based on Prandtl-Reuss material behavior. This would involve several Prandtl-Reuss computer analyses with correspondingly large computer runtimes.

To overcome this problem a method is described in Section 6.3 to obtain a $\sqrt{J_R}$ resistance curve, accounting for plasticity, from experimental crack growth resistance data combined with the elastic analysis described in Section 6.1.2.

6.2 RESISTANCE CURVES

The individual specimen crack growth resistance data (K_R) based on physical crack extension are given in Volume II of this report. Since the failure criterion of the recommended analysis uses J_R rather than K_R, a comparison of material K_R data trends will be summarized in this section. Average curves have been drawn through the data to indicate the trends between materials and crack direction.

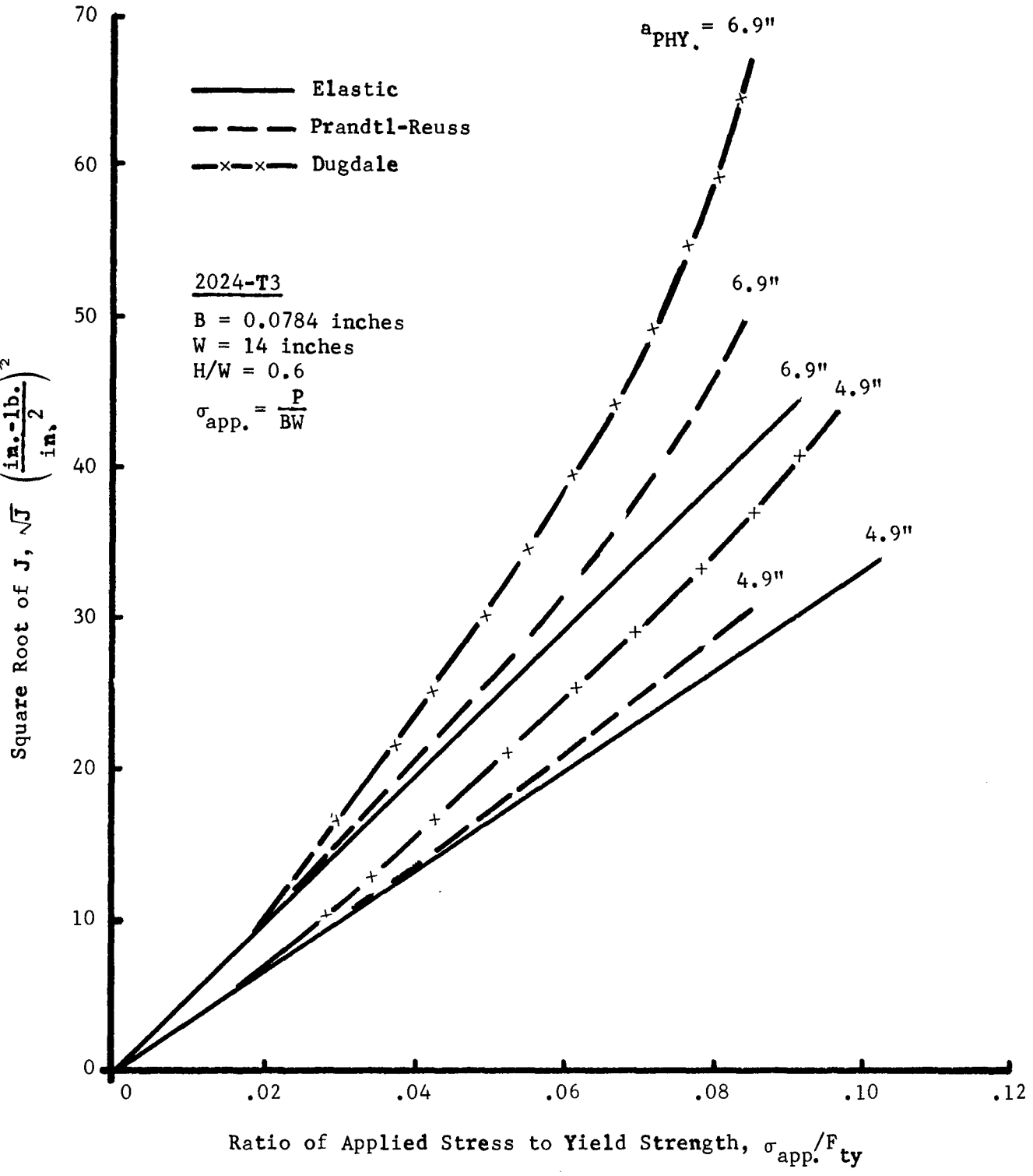

Figure 80. Analytical Comparison of Elastic, Prandtl-Reuss and Dugdale Material Behavior of CLWL Specimen

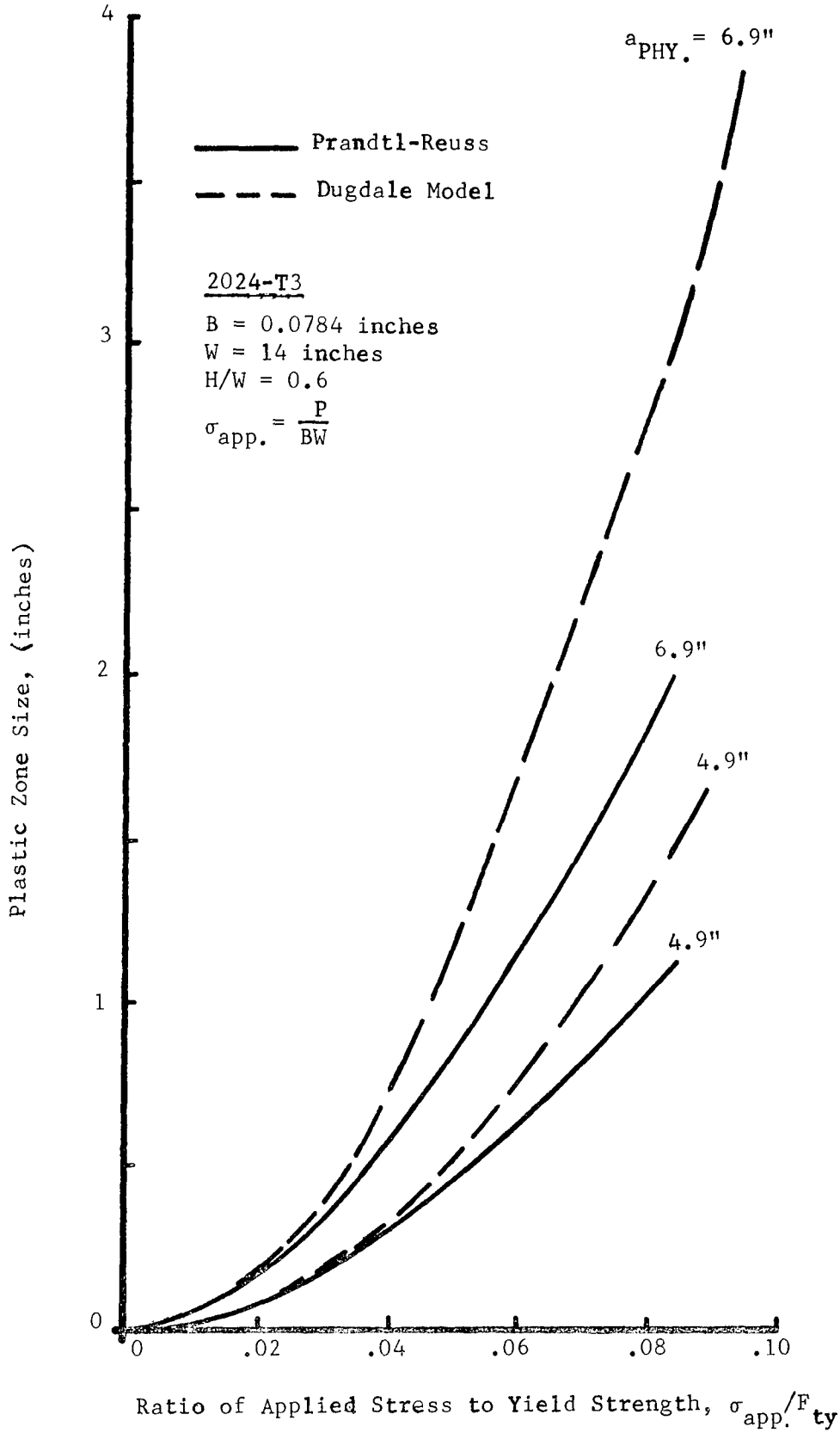

Figure 81. Comparison of Dugdale and Prandtl-Reuss Material Behavior Plastic Zone Sizes - CLWL Specimen

6.2.1 K_R Data

The K_R versus physical crack extension $\Delta a_{PHY.}$ curves are shown in Figures 82 through 93 for the materials tested during this program. Physical crack extension is defined here as $\Delta a_{PHY.} = (a_{PHYSICAL} - a_o)$ where $a_{PHYSICAL}$ is the return slope determined crack size (see Volume II for definition) from the CLWL specimen test and a_o is the initial (physical) crack size for the same specimen geometry.

Some general observations can be made about these data prior to discussing material groups. It will be noted that all materials except 2024-T3 show a widespread difference between the so-called strong (LT) and weak (TL) crack orientations. The toughest material (highest K_R data) is the 9 Ni steel (see Figure 93) with K_R values in excess of 600 ksi $\sqrt{\text{inch}}$, the least tough is 7075-T6 (e.g., see Figure 82 or 83). A plateau level of K_R could not be reached in this specimen width (14 inches) for several of the materials and the plateau was usually observed in the TL direction only. The only exception to this was for the thin, LT direction Ti-6Al-4V alloy (see Figure 91) which was in the mill annealed condition.

Only a small portion of the K_R curve could be obtained for the thicker, 7075-T6 and Ti-6Al-6V-2Sn due to out-of-plane crack extension during loading of the CLWL specimen. (See Volume II for a complete description of this problem.)

Some specific observations concerning these K_R data curves follow: the heat treatment of the 7075-T6 material to the overaged T7 condition does not show a significant increase in the TL, K_R plateau properties (< 10 ksi $\sqrt{\text{inch}}$) for the thick material (compare Figures 83 and 85), a large increase in toughness was noted for both thicknesses in the LT direction for the T7 over the T6 condition (see Figures 82-85), only small differences in K_R (<10 ksi $\sqrt{\text{inch}}$) were noted for the 2024-T3 material in all thicknesses, the largest difference in crack growth resistance for LT and TL properties occurs for the 0.21 inch, Ti-6Al-6V-2Sn (see Figure 92); the smallest difference was in the 1/4-inch thick 2024-T3 alloy (Figure 87).

6.2.1.1 K_R and Specimen Independency

The question has been raised on several occasions as to the possibility of a dependency of crack growth resistance on specimen geometry. Several studies have shown that there is a good correlation between those K_R data obtained from the CLWL specimen and those obtained from other specimen geometries (see References 7 and 49).

Four center cracked tension (CCT) specimens were tested as part of this program to determine if any differences were apparent between the K_R data for the two geometries. The CCT test specimen was 20 inches wide and 60 inches long in all cases. An elastic compliance curve was developed for this specimen configuration and is shown in Figure 94. Clip gages were mounted on the front and back surfaces in all cases and crack buckling restrained by two sets

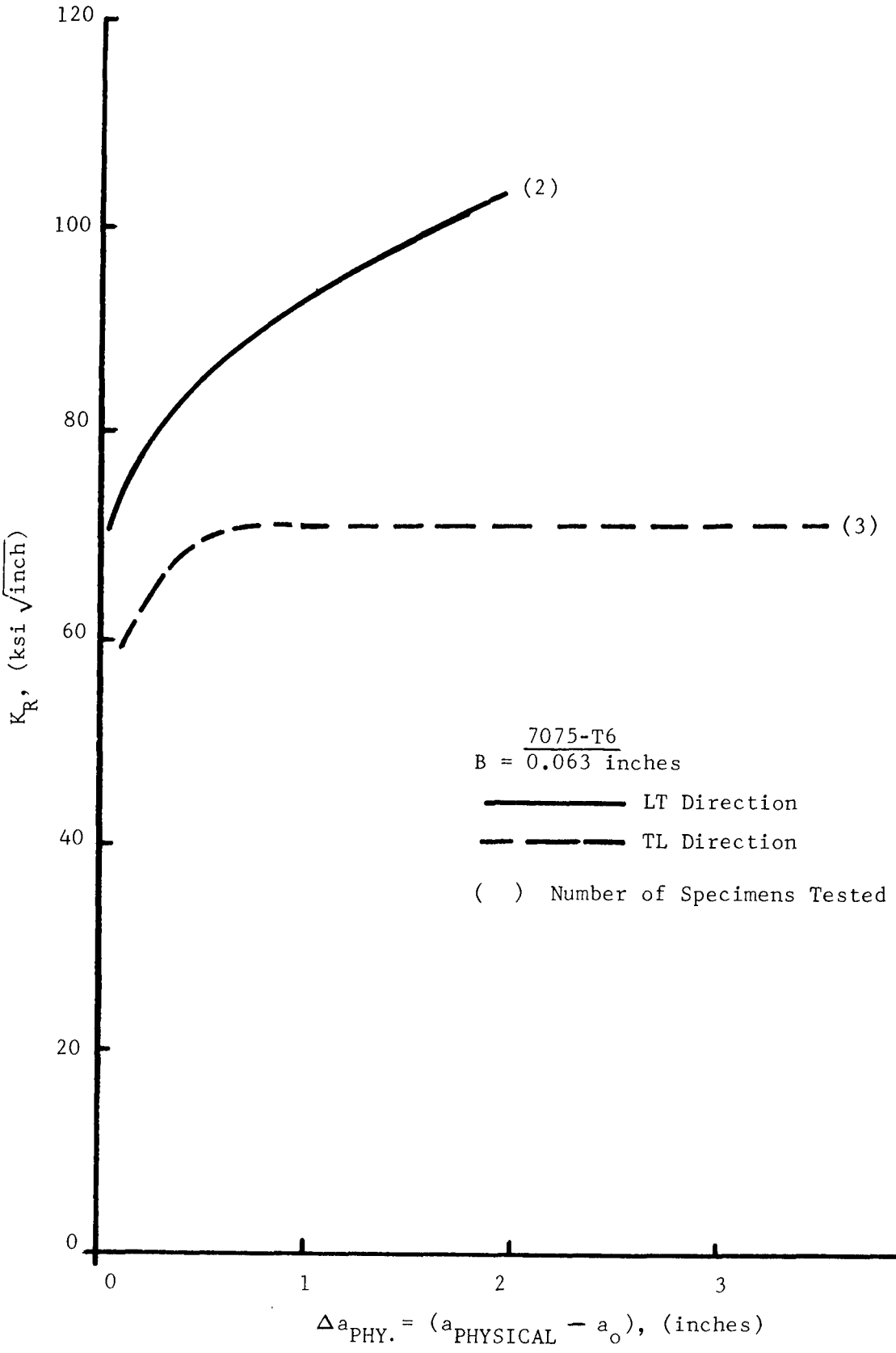

Figure 82. Average Crack Growth Resistance Curves - 0.063 Inch, 7075-T6

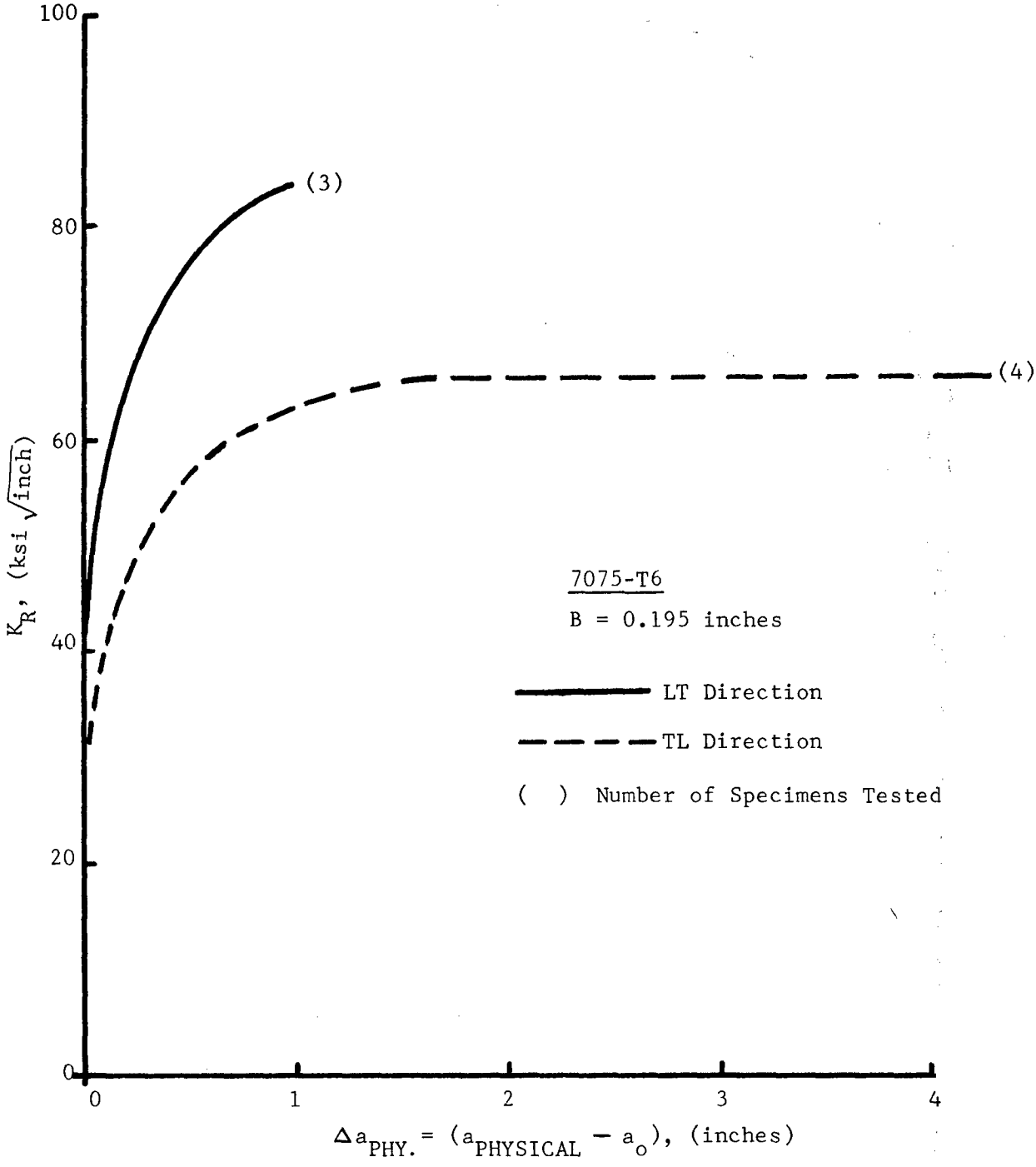

Figure 83. Average Crack Growth Resistance Curves - 0.195 Inch, 7075-T6

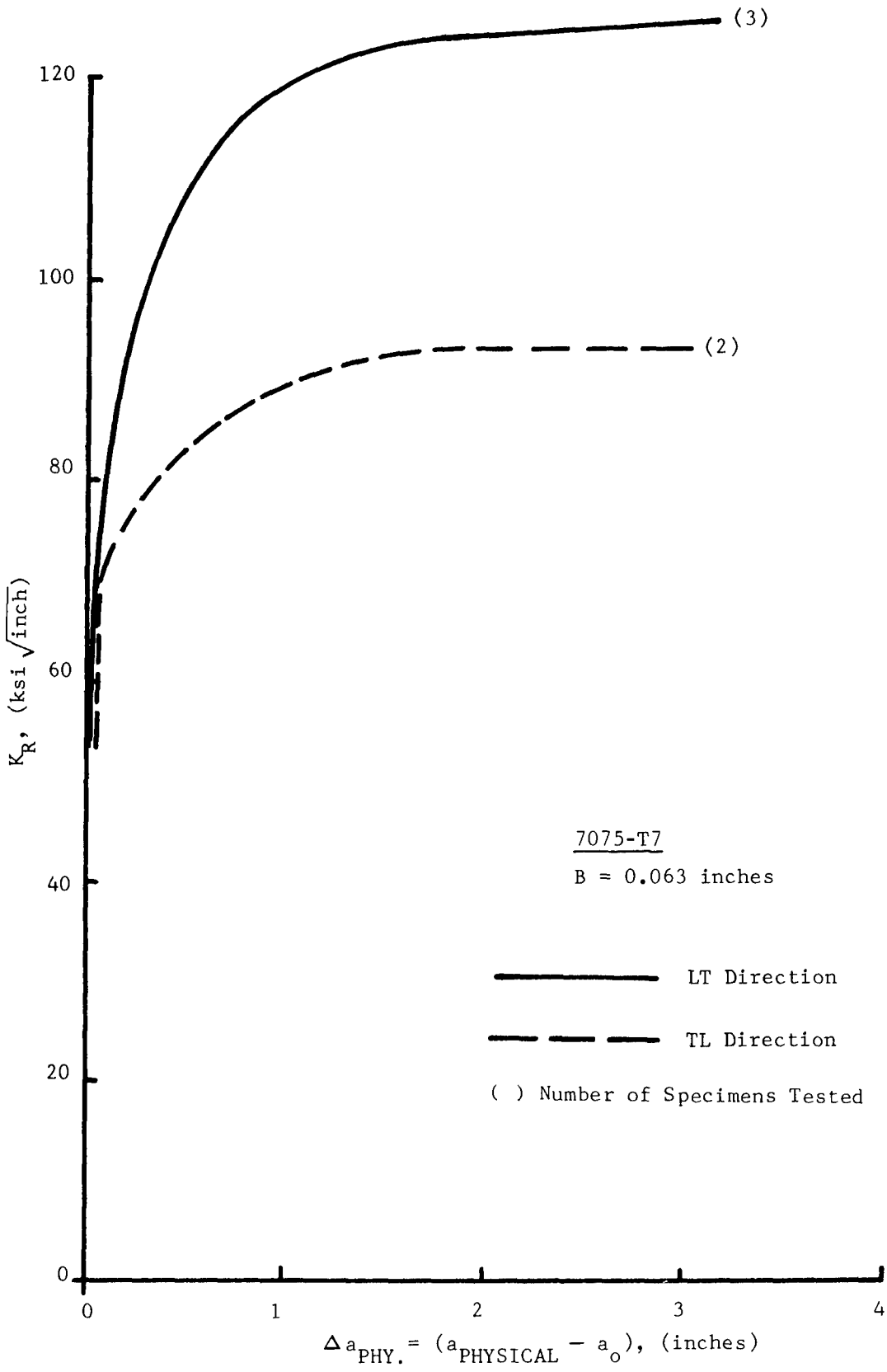

Figure 84. Average Crack Growth Resistance Curves - 0.063 Inch, 7075-T7

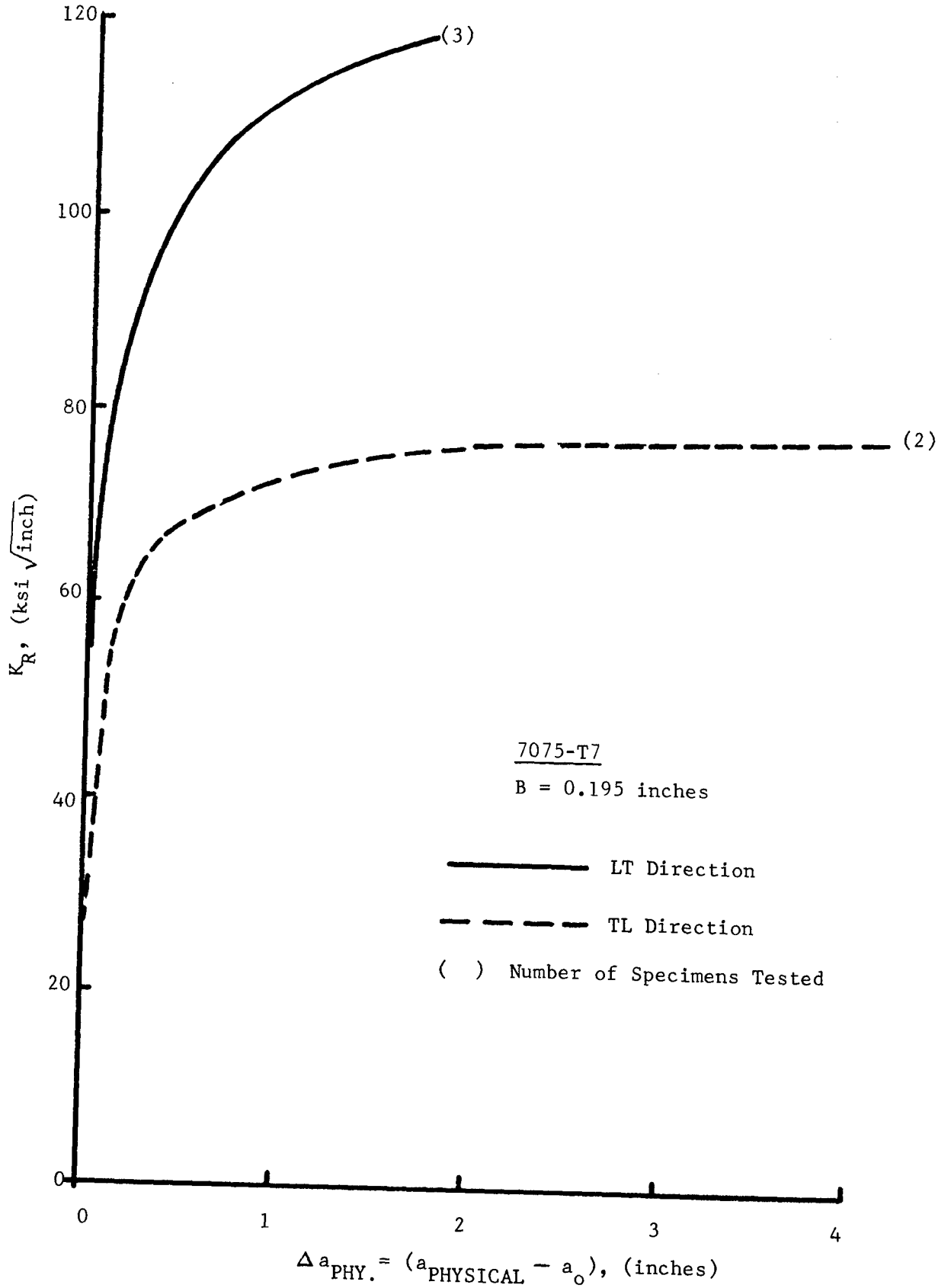

Figure 85. Average Crack Growth Resistance Curves - 0.195 Inch, 7075-T7

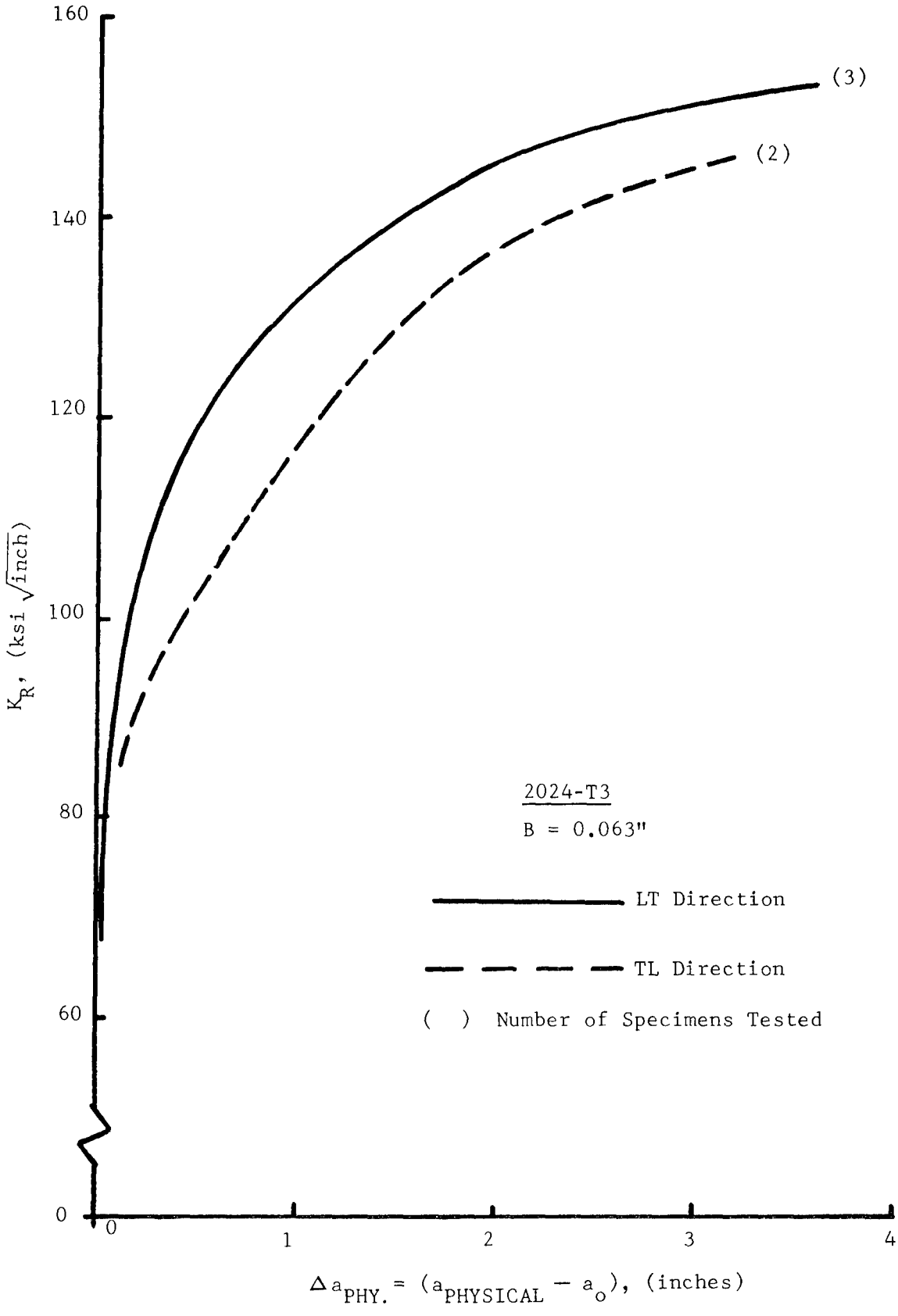

Figure 86. Average Crack Growth Resistance Curves - 0.063 Inch, 2024-T3

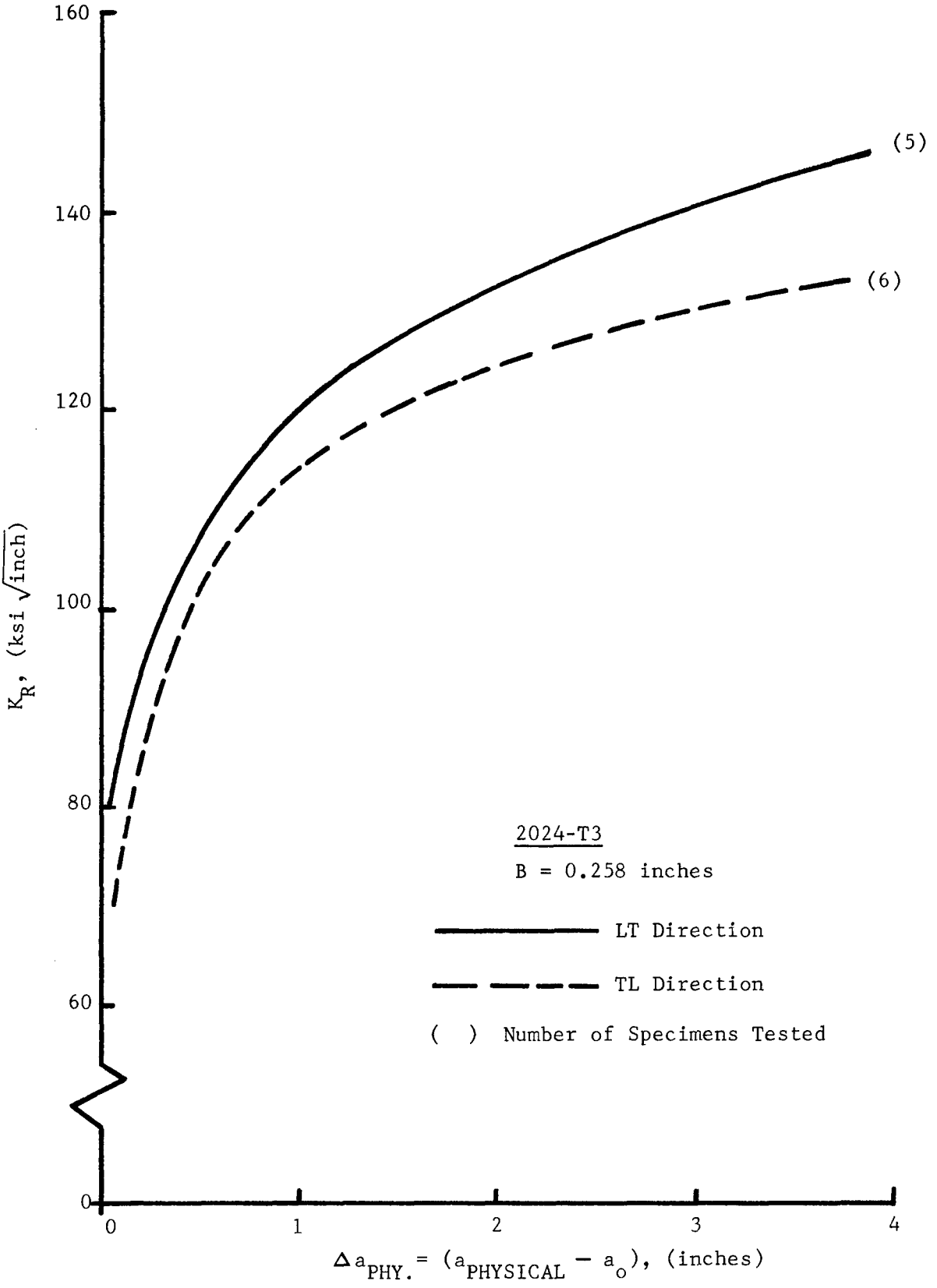

Figure 87. Average Crack Growth Resistance Curves - 0.258 Inch, 2024-T3

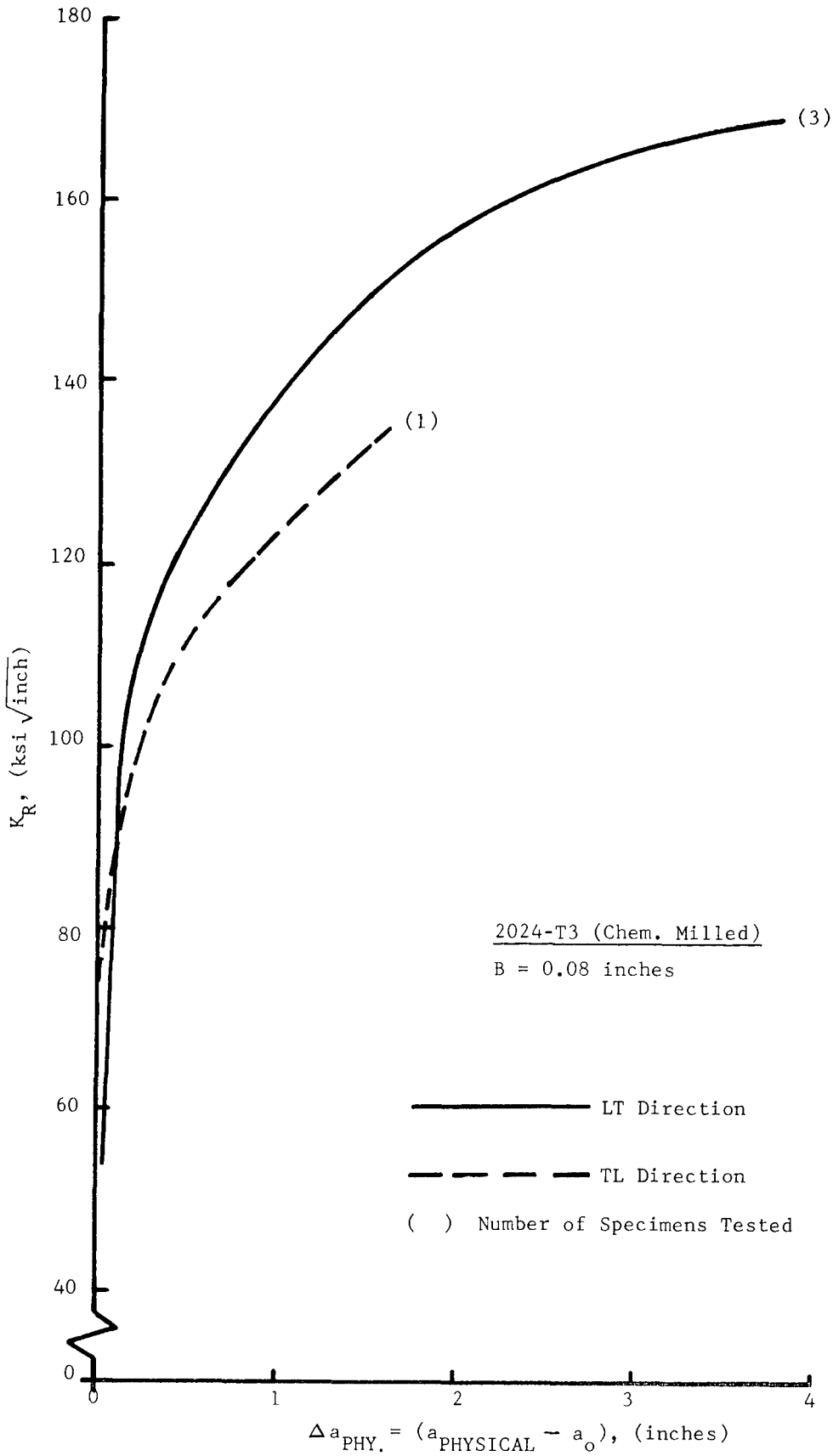

Figure 88. Average Crack Growth Resistance Curves - 0.08 Inch, Chem. Milled 2024-T3

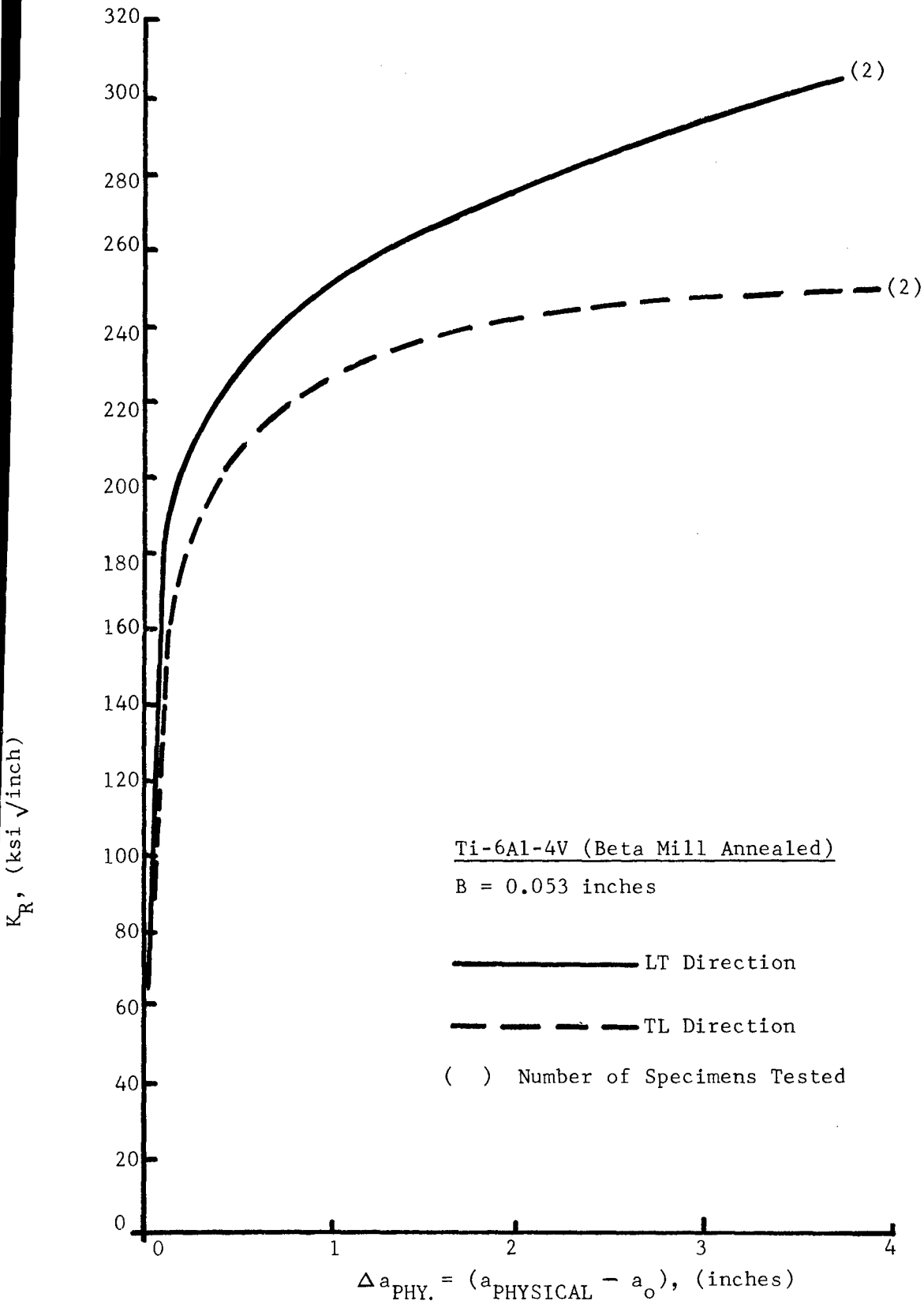

Figure 89. Average Crack Growth Resistance Curves - 0.053 Inch, Beta Mill Annealed Ti-6Al-4V

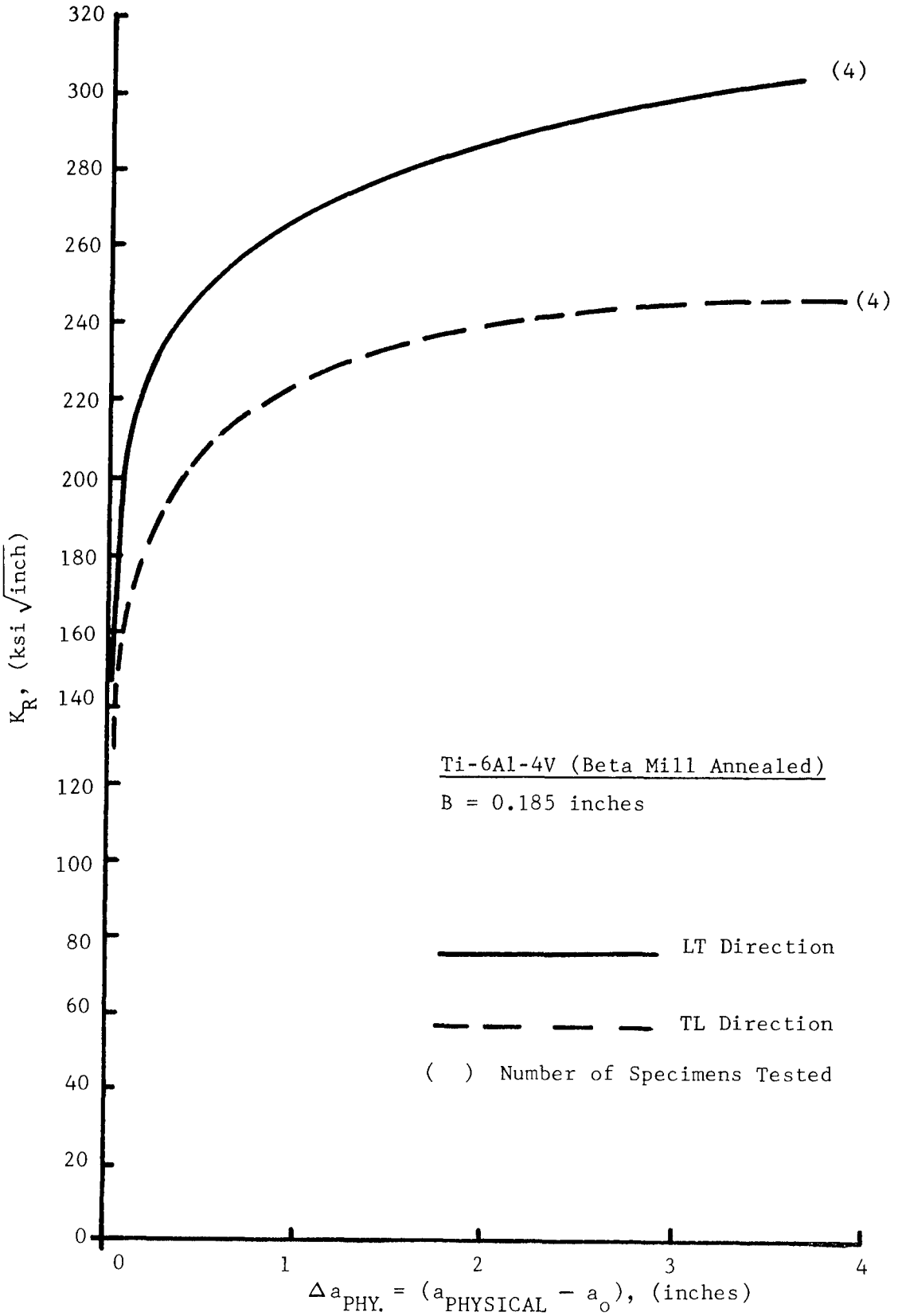

Figure 90. Average Crack Growth Resistance Curves - 0.185 Inch, Beta Mill Annealed Ti-6Al-4V

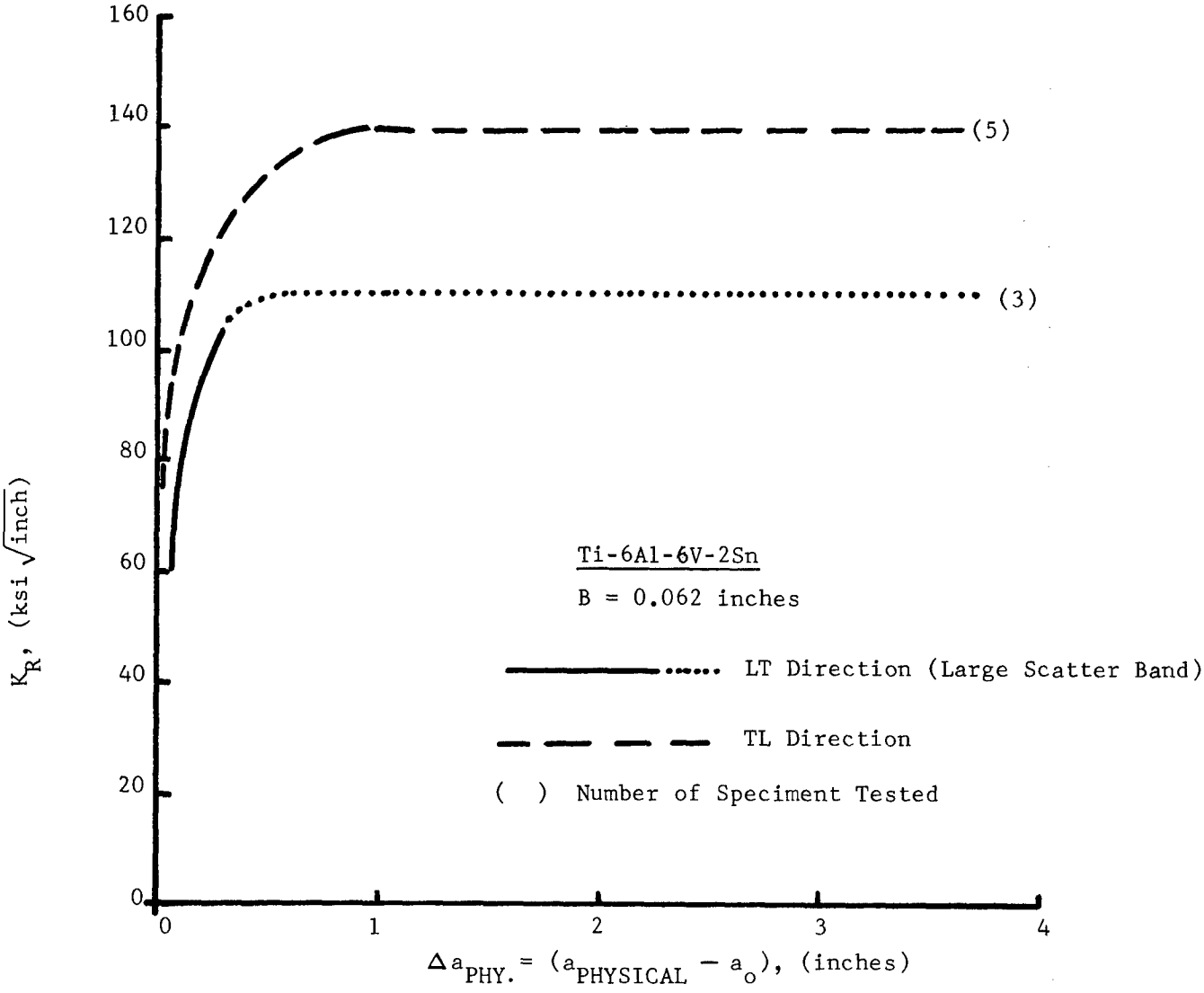

Figure 91. Average Crack Growth Resistance Curves - 0.062 Inch, Ti-6Al-6V-2Sn

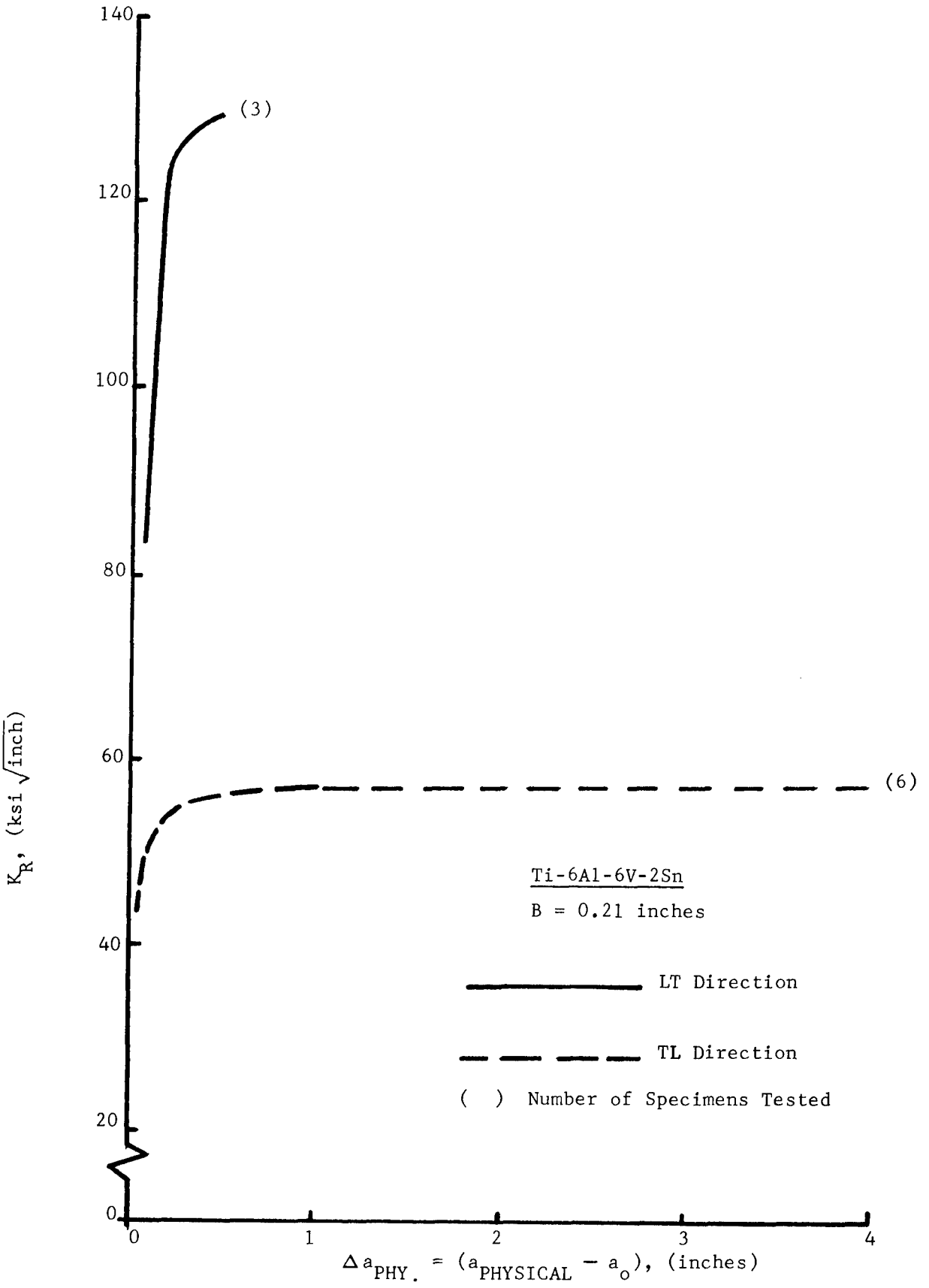

Figure 92. Average Crack Growth Resistance Curves - 0.21 Inch, Ti-6Al-6V-2Sn

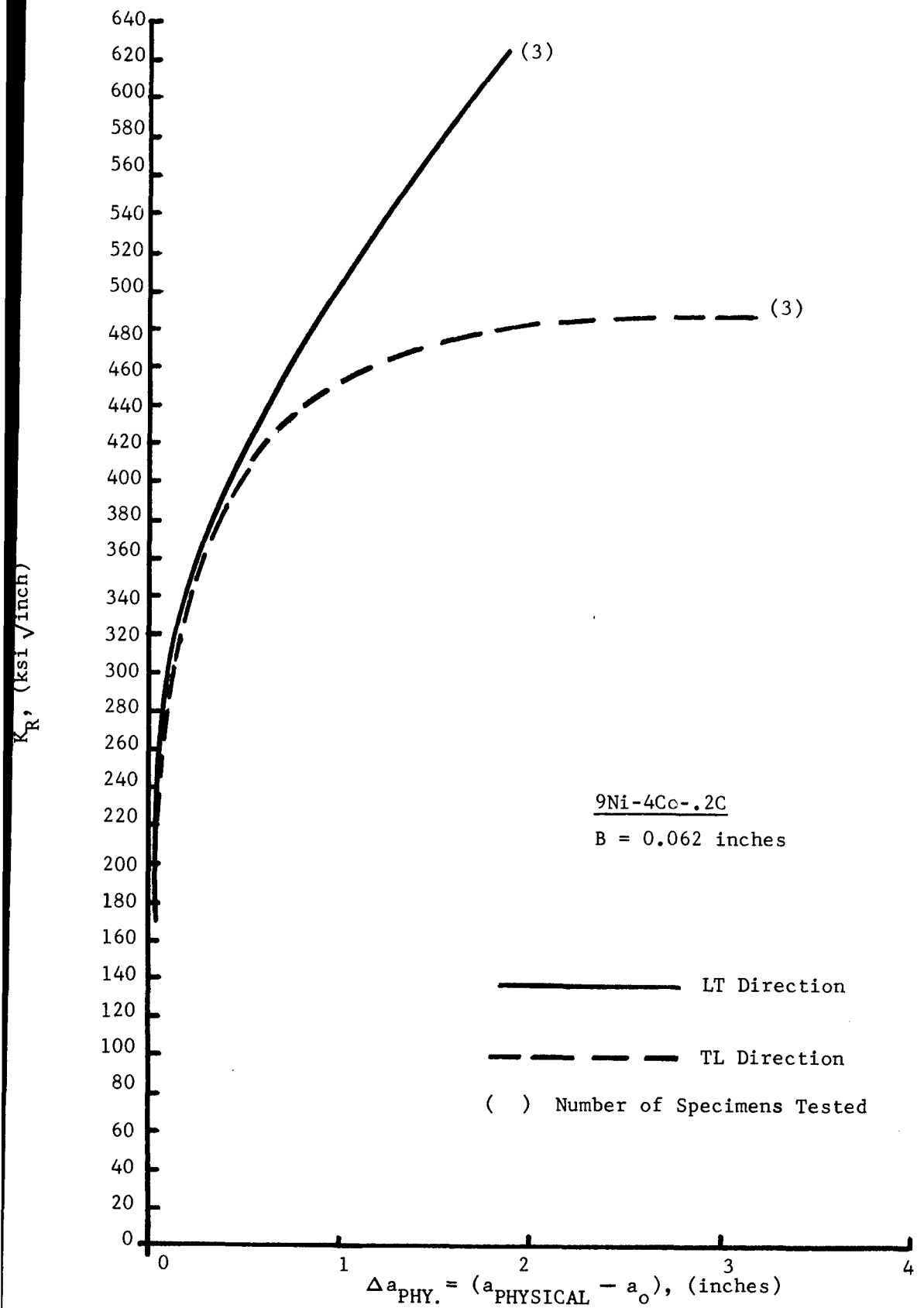

Figure 93. Average Crack Growth Resistance Curves - 0.062 Inch, 9Ni-4Co-.2C Steel

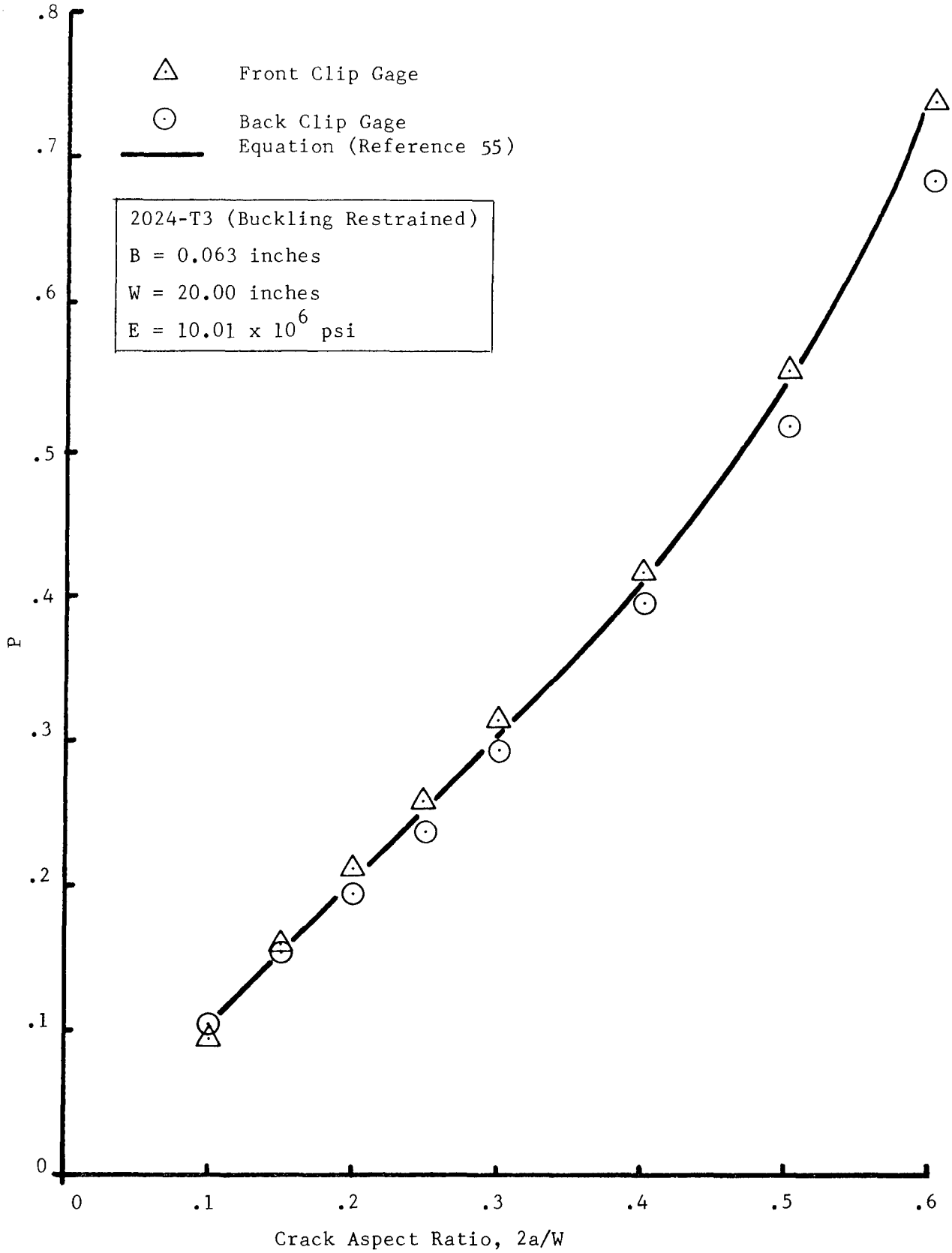

'igure 94. Compliance Calibration Curve for Center Cracked Tension Specimen Geometry

of guide plates both during calibration and fracture testing. The agreement with the analytical solution of Reference 55 (based on Westegaard function) is quite good as noted in Figure 94. The CCT test data were obtained under displacement control after initial fatigue precracking. The data were analyzed as recommended in Reference 54 and are shown in Figures 95 through 98. It will be noted that the crack extension is based on effective crack size, Δa_e, for both the CLWL as well as CCT data. A comparison on this basis is required since it was not possible to visually measure the CCT crack extension. Thus all of these data include some measure of crack tip plasticity both in the value of $a_{effective}$ as well as K_R.

It can be seen that the agreement between the CLWL and CCT data is quite good ($\leq$ 10 ksi$\sqrt{\text{inch}}$, 10 percent or less) for all cases except the thick, 7075-T6 (Figure 96). Note that an expanded crack extension scale has been used for these data. As discussed in Volume II of this report this material experienced crack turning (toward the rolling direction) for CLWL specimens tested in the LT crack orientation. This turning would occur almost immediately after loading from the precrack, but here again the CCT data are within 10 ksi $\sqrt{\text{inch}}$ (approximately 10 to 15 percent) of the CLWL data curve.

The CCT data are higher in most cases than the CLWL data since both the CCT and CLWL compliance relationships assume straight line (perpendicular to loading direction) crack progression. This was not the case for the 7075-T6 (LT) nor the Ti-6Al-6V-2Sn (LT) material tested in the CLWL geometry. As noted in Volume II of this report the crack progressed in a saw-tooth fashion for the titanium alloy thus any off-angle crack progression is going to result in higher COD's, hence indications of larger crack sizes than those realized from the CLWL data. For this reason the CLWL curves are shifted to the right in those cases of off-angle crack progression (see Figures 95 and 96). No difficulty was experienced with out of plane crack progression for the 2024-T3 material except at the longest crack lengths and the data of Figure 97 reflect this normal behavior.

In all cases the fracture progression for the CCT, LT specimens was normal to the loading and rolling direction. At first crack extension the thicker 7075-T6 (specimen T6-55HLT-001) showed a tendency to deviate at a 45-degree angle to the original fatigue crack direction but returned to its original state after a small (<0.2 inch) crack extension.

It appears from these K_R data and those of other investigators that have used different specimen geometries that a good correlation exists between slow crack growth and K_R. This verification in itself is encouraging and indicates that the CLWL geometry can be used to obtain either K_R or J_R data. Preliminary indications are that these data will usually be on the low side of the data band developed from an increasing load type test configuration.

6.2.2 Crack Resistance at Very Small Crack Extensions

In determining the crack growth resistance characteristics of a material it becomes important to have an indication of the early part of the slow crack growth phase where large increases in either K_R or J_R occur with small amounts

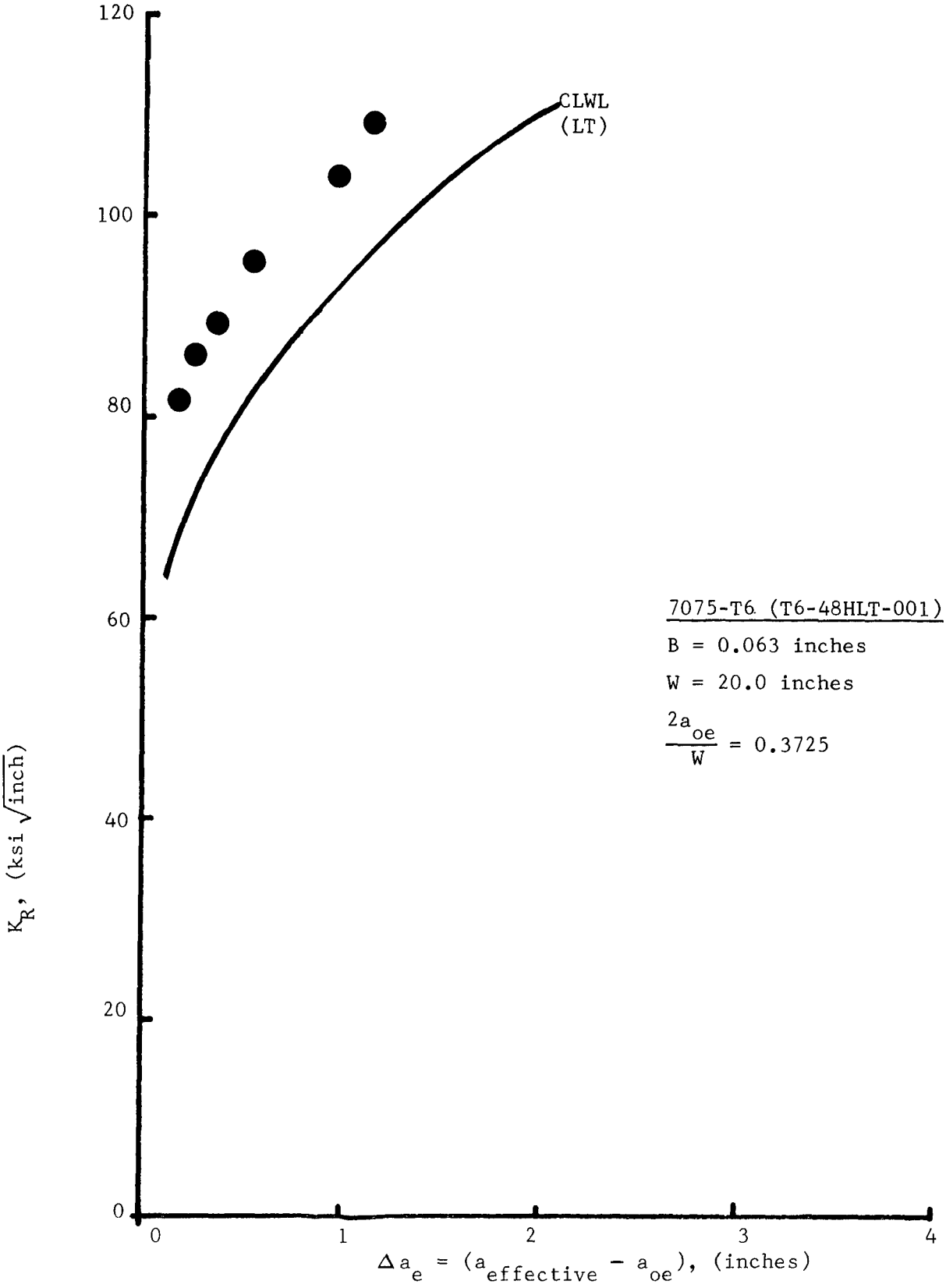

Figure 95. Comparison of CLWL and CCT Resistance Data - 0.063 Inch, 7075-T6

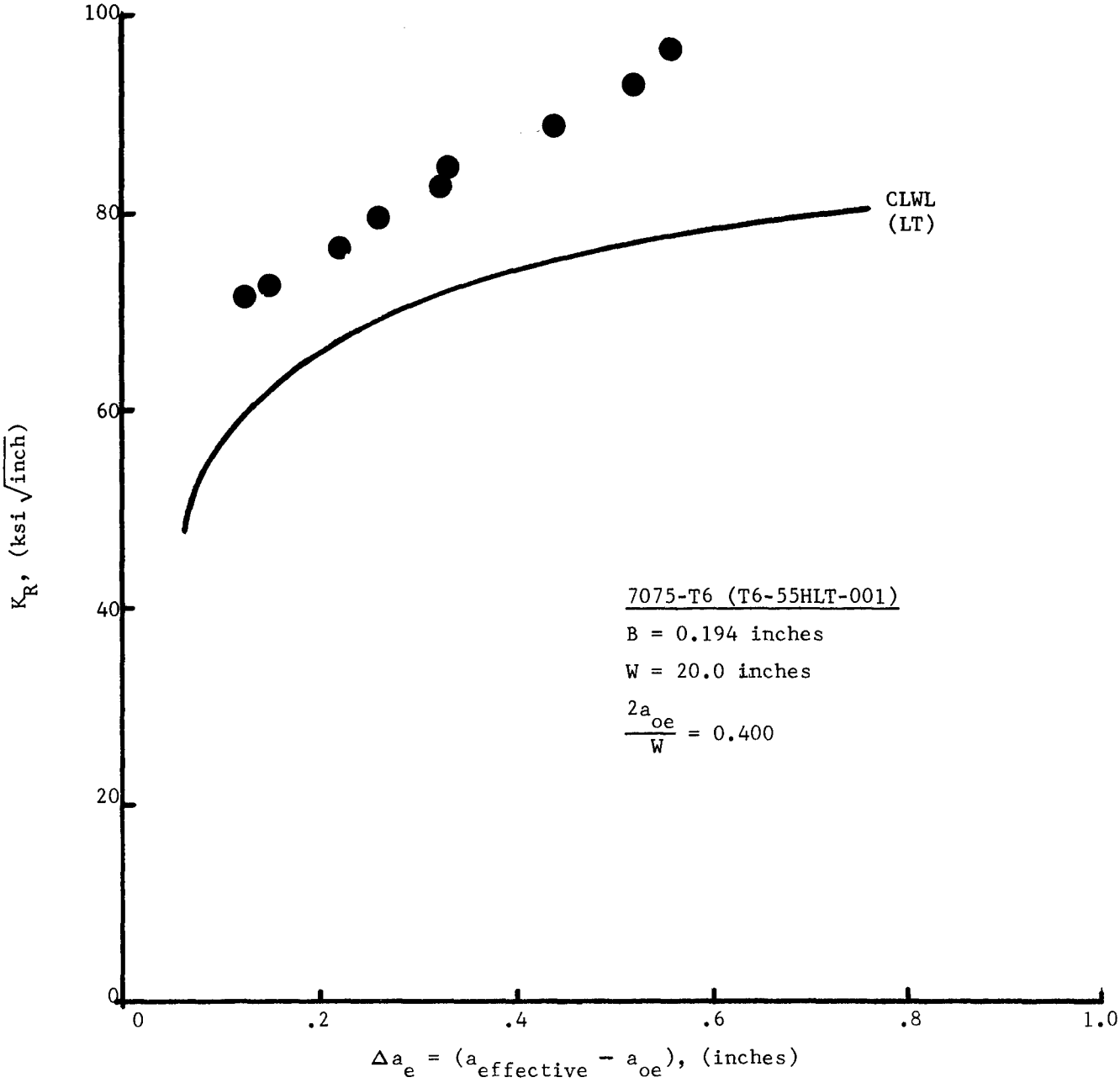

Figure 96. Comparison of CLWL and CCT Resistance Data - 0.194 Inch, 7075-T6

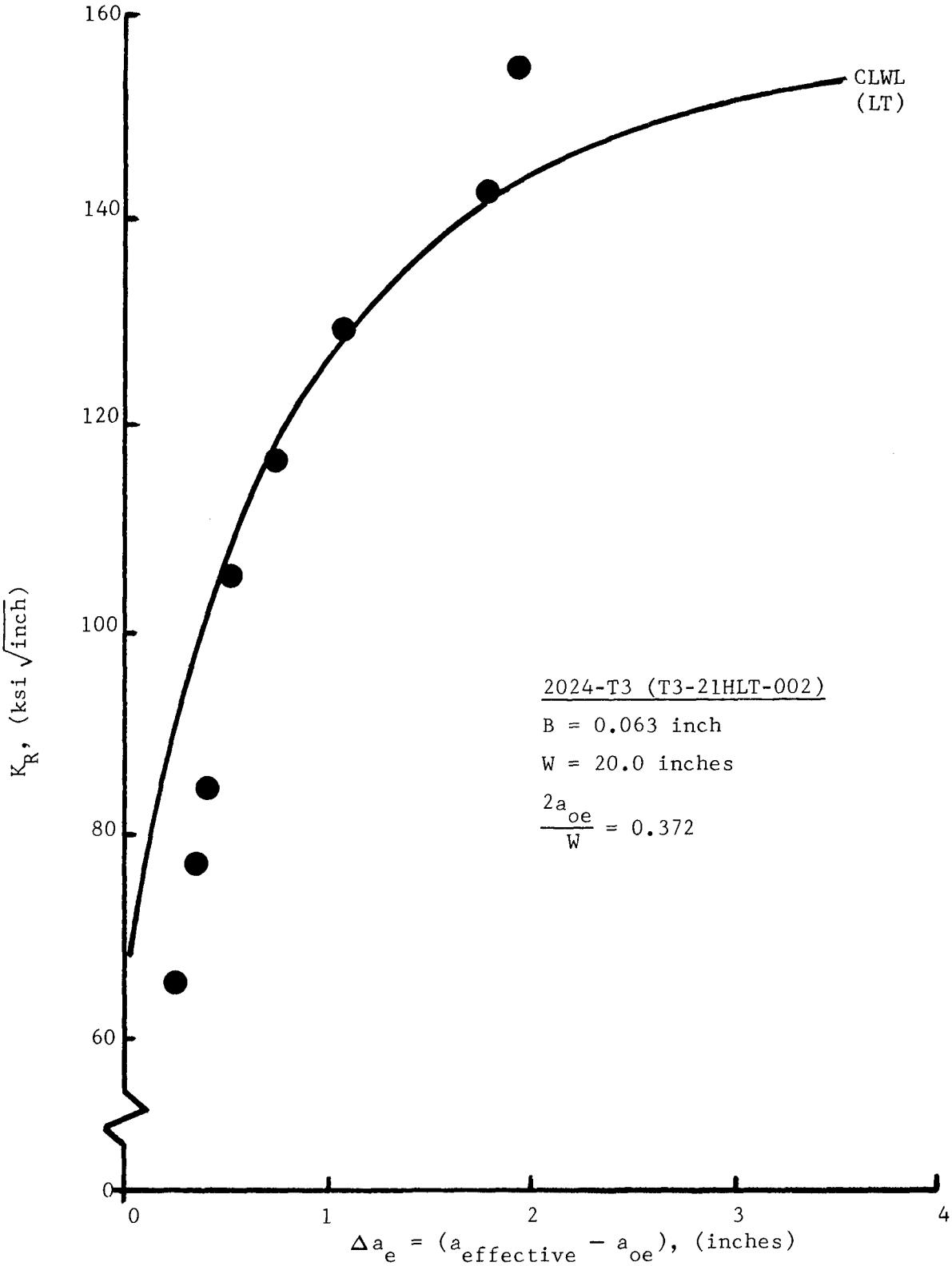

Figure 97. Comparison of CLWL and CCT Resistance Data - 0.063 Inch, 2024-T3

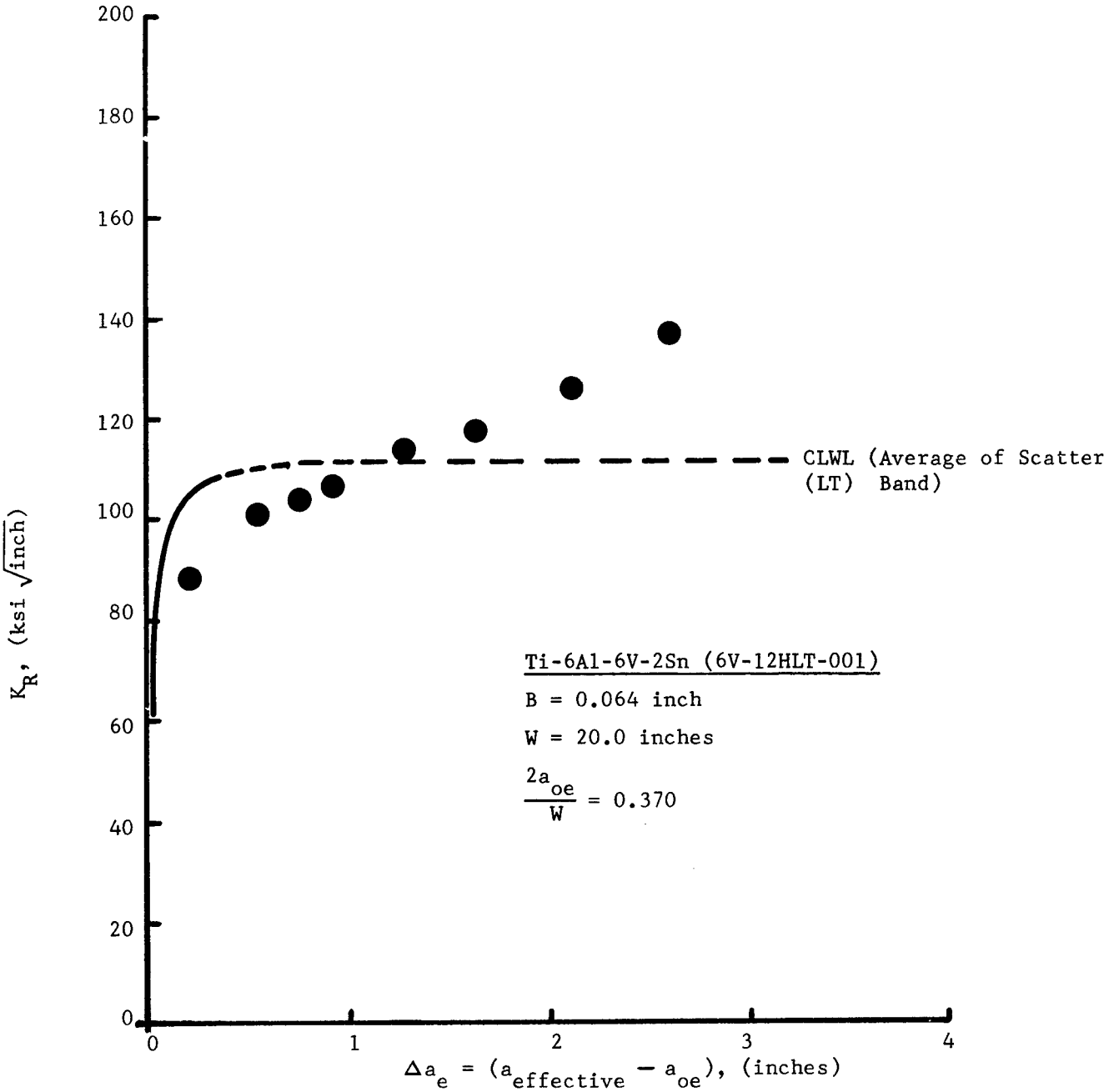

Figure 98. Comparison of CLWL and CCT Resistance Data - 0.064 Inch, Ti-6Al-6V-2Sn

of $\Delta a_{PHY.}$ or Δa_e. Since the skin critical fracture criterion outlined in this report employs a tangency condition with these curves the initial slopes or better yet a starting point for K_R, J_R should be established. A special test series examined this early phase of crack extension and will be reported on next.

6.2.2.1 Low K_R Test Series

The results of a special test series will be reported here which involved the determination of crack growth resistance values (K_R) at very small, physical crack extensions (Δa (measured) < 0.05-inch). The low K_R test series was prompted by several factors but primarily to establish a basic value of K_R for very small crack extension ($\Delta a_{PHY.}$ < 0.02 inch) and to verify its value in both wedge and tension loading for the CLWL specimen geometry.

A 2024-T3, CLWL specimen (T3-32CLT-011), 0.258-inches thick, was alternately fatigue cycled and either wedge or tension loaded until small amounts of crack extension occurred. Values of K_R and $\Delta a_{PHY.}$ were then evaluated. Table XII shows the sequence of events and relevant test data.

By examining the macrophotograph of Figure 99 the procedure of Table XII can be readily indicated. At points 1, 3, 5, 7, 9 and 11 fatigue precracking was accomplished between points of K_R data (2, 4, 6, 8, 10, and 12).

From trial experiments on another specimen the fatigue marking process (as indicated in Table XII) provides an excellent delineation of the prior and post statically induced slow tear behavior. These are noted as areas 2, 4, etc., on Figure 99. Care was exercised to fatigue crack to a sufficient distance beyond the prior (statically induced) plastic zone to prevent plastic hinging influences. The extent of the surface plastic zone can be noted from the side view of Figure 99. Tunneling of the statically induced crack front is evident for each slow tear region. This observation along with the consistency in K_R data for these small values of slow tear as noted from Table XII, have led to the following:

1. For very small amounts of slow crack growth (< 0.05-inch) the value of K_R appears to be in the range of 40 to 50 ksi $\sqrt{\text{inch}}$ with an average value of $\approx$47 ksi $\sqrt{\text{inch}}$ for this 2024-T3 material.

2. The mode of loading (tension or CLWL) does not appear to influence the shape of the crack front nor the value of associated K_R.

3. The data range of 40-50 ksi $\sqrt{\text{inch}}$ with an average value of 47 ksi $\sqrt{\text{inch}}$ for small crack extension is extremely close to reported plane strain fracture toughness values (K_{Ic}) for 2024-T3. K_{Ic} values of 30-45 ksi have been reported for thick (<3 inches) sections of this material. The tunneling action points to development of plane strain fracture modes at these low stress intensities for this thickness of material.

The last observation has resulted in the following proposed construction of the typical K_R versus Δa curves.

TABLE XII. TEST SEQUENCE AND FATIGUE CRACK GROWTH AND K_R DATA FOR LOW K_R TEST

STEP	CONDITION	FATIGUE CRACKING DATA				STATIC LOADING DATA		
		$K_{min.}$ (ksi/inch)	$K_{max.}$ (ksi/inch)	FREQ. (HZ)	NO. OF CYCLES	AVERAGE CRACK* LENGTH (INCH)	MEAS. Δa* (INCHES)	RETURN SLOPE K_R (ksi/inch)
1	Pre-cracking	Normal pre-cracking conditions				5.222		
②	CLWL					5.266	.028	40.52
3	Fatigue Crack	17.9 14.6 11.1	35.8 29.1 22.2	5 12 15	5,000 8,500 9,000	5.466		
④	TENSION					5.507	.041	49.66
5	Fatigue Crack	18.7 15.1 11.5 9.4	37.3 30.2 22.9 18.8	5 12 14 16	3,000 5,000 5,000 8,000	5.768		
⑥	CLWL					5.807	.039	48.465
7	Fatigue Crack	15.75 12.1 9.9	31.5 24.15 19.8	10 12 17	16,300 26,000 20,000	6.047		
⑧	CLWL					6.086	.039	50.51
9	Fatigue Crack	16.6 12.9 10.7	33.2 25.8 21.4	10 12 14	11,900 36,800 15,500	6.463		
⑩	TENSION					6.541	.078	53.24
11	Fatigue Crack	17.2 14.1 11.7	34.4 28.1 23.3	8 10 12	12,000 9,000 9,000	~6.864		
⑫	TENSION	(CRACK LENGTH TOO LONG - SPECIMEN TWISTING)						

* Measurements Taken at Mid-Thickness, Before and After Crack Extension.

SPECIMEN NO. T3-32CLT-011

B = .258"

W = 14"

H/W = .6

◯ Indicates where K_R data were obtained.

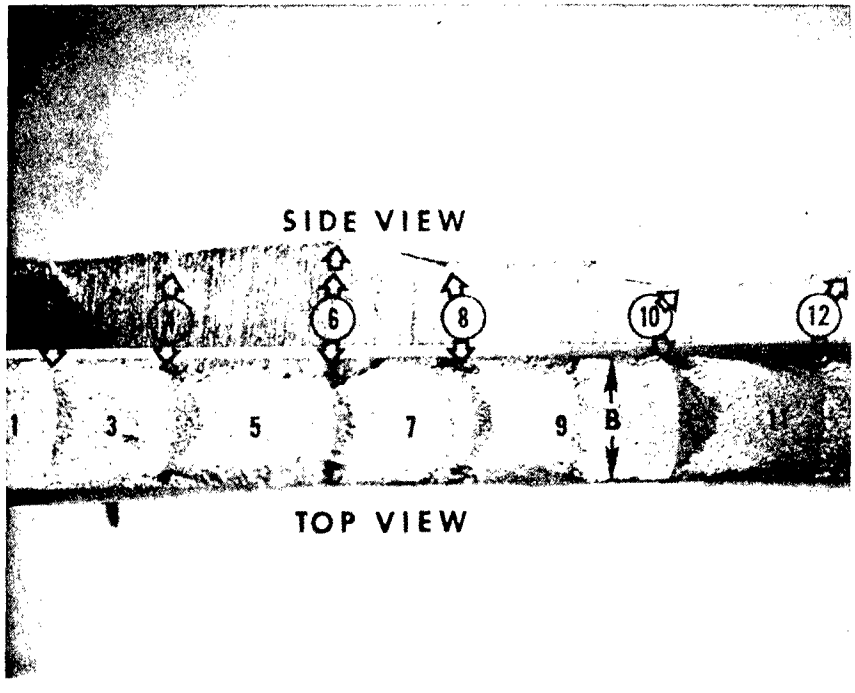

Figure 99. Macrophotograph of Fracture Surface of Low K_R Test Specimen

The exact starting point of the K_R versus Δa curve would be at zero K_R for zero slow crack growth as shown by the dashed line in Figure 100. After small, initial crack extension (< 0.10 inch) the curves become layered above a value of K_{Ic} as indicated, with thickness. (NOTE: There can be exceptions to this trend as indicated in Volume II where the 0.08-inch thick chem milled 2024-T3, K_R data was above that of 0.063-inch thick sheet material). Prior to the appearance of thickness influences on the K_R curve (at low values of Δa) it was observed that the initial part of the K_R curve was not affected by side grooving. (See Volume II of this report for a complete discussion of side grooving). This evidence combined with the values of K_R approaching K_{Ic} for small crack extension led to the following postulation for the region of low K_R (i.e., zero to K_{Ic}).

A crack in a material, regardless of thickness, will under increasing load experience an increasing stress intensity. At some threshold K_R (call it K_{th}) the microscopic slow tear process begins in the mid-thickness region. At this point the internal (mid-thickness) slow crack growth predominates and increasing load increases both internal crack growth but more importantly plastic zone development. The plastic zone aids in dissipating energy built up by the mid-thickness crack growth until visual crack extension occurs on the surface. The extent of the visual crack extension is again independent of material thickness but does depend on plastic zone development. In other words (referring to Figure 100), with increasing thickness, B, the extent of mid-thickness crack extension can result in specimen fracture (at K_{Ic}) under rising load test conditions.

The significance of the data of Table XII and the proposed small Δa (slow tear) behavior is that simplification of the K_R or $\sqrt{J_R}$ curve is now possible. Some linear relationship is apparently valid for construction of the K_R curve up to the K_{Ic} value for a given material. Beyond that point the influence of specimen thickness predominates and the K_R or $\sqrt{J_R}$ curve can be evaluated by conventional means. Additional confirmative testing would be required on other materials and thicknesses to see if these trends are repeatable.

Figure 101 compares the early slow tear, K_R data from Table II with those data previously obtained for this 2024-T3 material in the LT direction. It is seen that these data are consistent with that developed during routine R-curve testing. Once again the emphasis on small scale slow tear behavior is established.

6.3 J_R RESISTANCE CURVE

As discussed in Section 2.4 the J integral approach was proposed to predict residual strength of a structure. Therefore it is necessary to obtain the crack growth resistance of a material in terms of J as a failure criterion. The crack growth resistance of a material in terms of stress intensity factor, commonly known as the K_R concept, has been fully discussed in Section 6.2, where the K_R resistance curves obtained from the CLWL specimen were presented. In this section the procedure for obtaining a J_R resistance curve from experimental data is outlined.

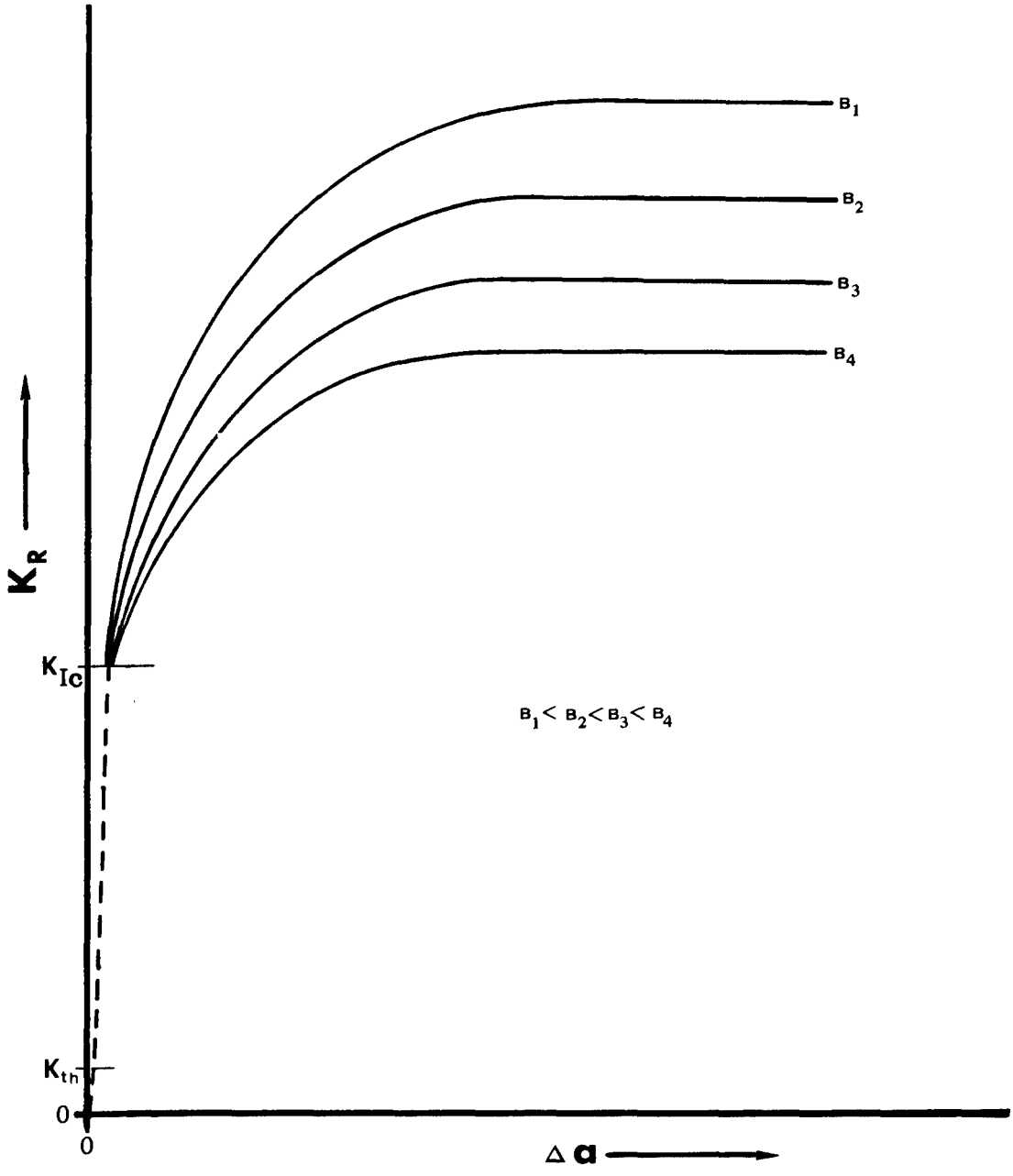

Figure 100. Postulated R-Curve Behavior Based on Low K_R Test Series

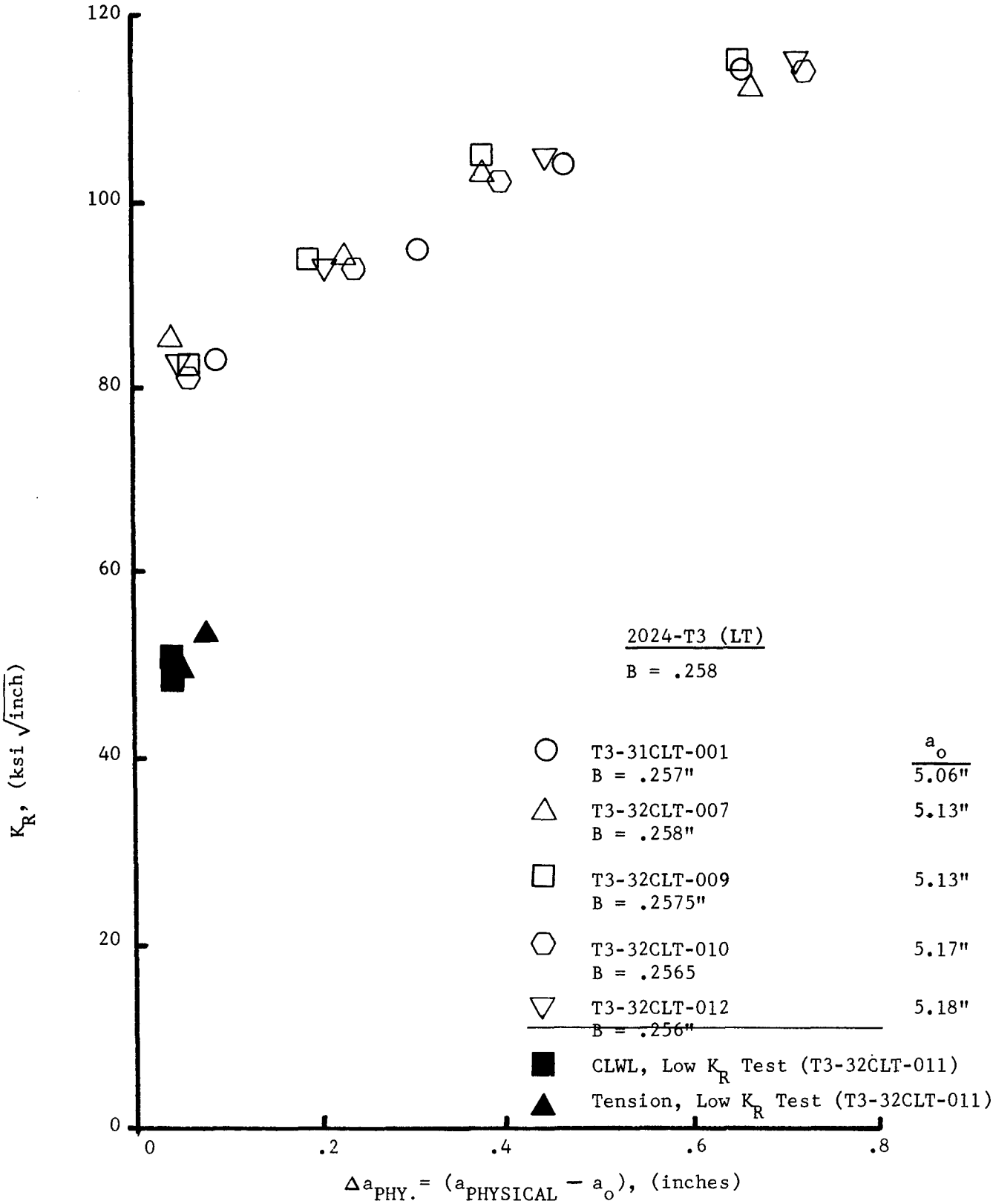

Figure 101. Comparison of Early Slow Tear Behavior and Routine Crack Growth Resistance Data

Section V of Volume II of this report shows the detailed procedure followed in obtaining a K_R curve from experimental, CLWL data. The procedure is summarized here for convenience, it is:

1. Obtain a double displacement curve (for displacements V_1 and V_2) at every crack extension and for unloading after every crack extension.

2. Obtain effective crack length (a_e) and physical crack length ($a_{PHY.}$) at every crack extension using the ratios of V_1 and V_2 obtained in Step 1 and an elastic calibration curve between a/W and V_1/V_2.

3. Obtain the load at every crack extension using a/W, corresponding to effective crack length, and the compliance relationship between $\frac{EBV_1}{P}$ and a/W.

4. Using the load from Step 3. and effective crack length (a_e) obtained in Step 2. determine the value of stress intensity factors from the suitable stress intensity formula for this specimen geometry.

5. From the physical crack length obtained in Step 2. and stress intensity factors obtained in step 4, plot the K_R curve as a function of physical crack extension ($\Delta a_{PHY.}$).

It may be noted that in computing K_R the elastic stress intensity factors (K_R) obtained in this manner take into consideration the plasticity ahead of the crack tip by using effective crack length (effective crack length = physical crack length + plastic zone correction or $a_e = a_{PHY.}$ + Plastic Zone Correction).

The advantage of this method is that the plasticity is accounted for through use of experimentally determined plastic zones. This same principal is used to obtain the $\sqrt{J_R}$ resistance curve. The experimentally determined effective crack length (see Step 2) and load (see Step 3) are used to determine the values of $\sqrt{J_R}$ from elastic solutions presented in Figure 75 for the CLWL specimen geometry.

For example a 2024-T3 material, 0.064 thick will be analyzed for $\sqrt{J_R}$ versus $\Delta a_{PHY.}$. From Steps 1, 2 and 3 calculate the values of applied load P, physical crack extension $\Delta a_{PHY.}$ and effective crack length a_e. The values from one test are shown in Columns 1-3 of Table XIII. From the applied load (P), specimen thickness (B) and width (W) the values of P/BW are obtained as shown in Column 4 of Table XIII. Using these values of P/BW and a_e corresponding values of $\sqrt{J}$ are obtained from Figure 75. (NOTE: The elastic modulus is 10.3×10^6 psi in the analysis performed in Figure 75). Thus for an applied load of 3.006 kips and an effective crack length of 5.41 inches a value of the square root of J is obtained by linearly interpolating between crack lengths of 5.4 and 5.9 inches in Figure 75. This value is seen to be $23.2 \left(\frac{\text{in-lb}}{\text{in}^2}\right)^{1/2}$. In a similar fashion linear interpolation is used to

TABLE XIII. $\sqrt{J_R}$ CALCULATIONS - W = 14 INCHES AND B = 0.0638 INCHES

P* (kips)	$a_{PHY.}$ (inches)	a_e (inches)	$\frac{P}{BW}$ (ksi)	$\left(\frac{\sqrt{J_R}}{\frac{in.-lb.}{in.^2}}\right)^{\frac{1}{2}}$
3.006	0.06	5.410	3.365	23.2
3.318	0.15	5.512	3.715	25.9
3.523	0.31	5.799	3.944	29.0
3.606	0.55	6.097	4.037	31.34
3.740	0.88	6.319	4.187	33.2
3.619	1.18	6.668	4.051	35.33
3.566	1.385	6.885	3.992	36.1
3.462	1.745	7.144	3.876	37.35
3.378	2.03	7.353	3.782	38.0
3.146	2.29	7.716	3.522	39.3
3.009	2.62	7.964	3.369	39.8
2.860	2.91	8.236	3.202	41.76
2.662	3.14	8.589	2.980	43.53

*2024-T3, Specimen T3-21CLT-003 (Figure 110)

obtain $\sqrt{J_R}$ values for other effective crack lengths and P/BW values as shown in Table XIII. Similar calculations are performed for additional CLWL tests and on other materials. Results of the single specimen test given in Table XIII and two additional resistance curve tests are plotted in Figure 110. Here $\sqrt{J_R}$ is plotted versus physical crack extension since physical crack length has more meaning in the failure prediction scheme. Table XIV shows the materials, thickness and fracture plane orientation for which $\sqrt{J_R}$ curves have been obtained. These $\sqrt{J_R}$ curves are shown in Figures 102 through 119.

TABLE XIV. LISTING OF MATERIAL, THICKNESS AND CRACK ORIENTATION FOR WHICH $\sqrt{J_R}$ VALUES HAVE BEEN OBTAINED

MATERIAL	THICKNESS (inches)	CRACK ORIENTATION	REFERENCE FIGURE
7075-T6	0.063	LT	102
7075-T6	0.063	TL	103
7075-T6	0.195	LT	104
7075-T6	0.195	TL	105
7075-T7	0.064	LT	106
7075-T7	0.064	TL	107
7075-T7	0.195	LT	108
7075-T7	0.195	TL	109
2024-T3	0.064	LT	110
2024-T3	0.064	TL	111
2024-T3	0.080	LT	112
2024-T3	0.258	LT	113
2024-T3	0.258	TL	114
Ti-6Al-6V-2Sn*	0.062	LT	115
Ti-6Al-6V-2Sn*	0.062	TL	116
Ti-6Al-6V-2Sn*	0.210	TL	117
9Ni-4Co-0.2C*	0.063	LT	118
9Ni-4Co-0.2C*	0.063	TL	119

*In obtaining a $\sqrt{J}$ curve for these materials from Figure 75 a correction must be made to account for the difference in Young's Modulus. The curves of Figure 75 are based on the Young's Modulus of 10.3×10^6 psi. The data in Figures 115-119 take into consideration the Young's Moduli of the individual materials.

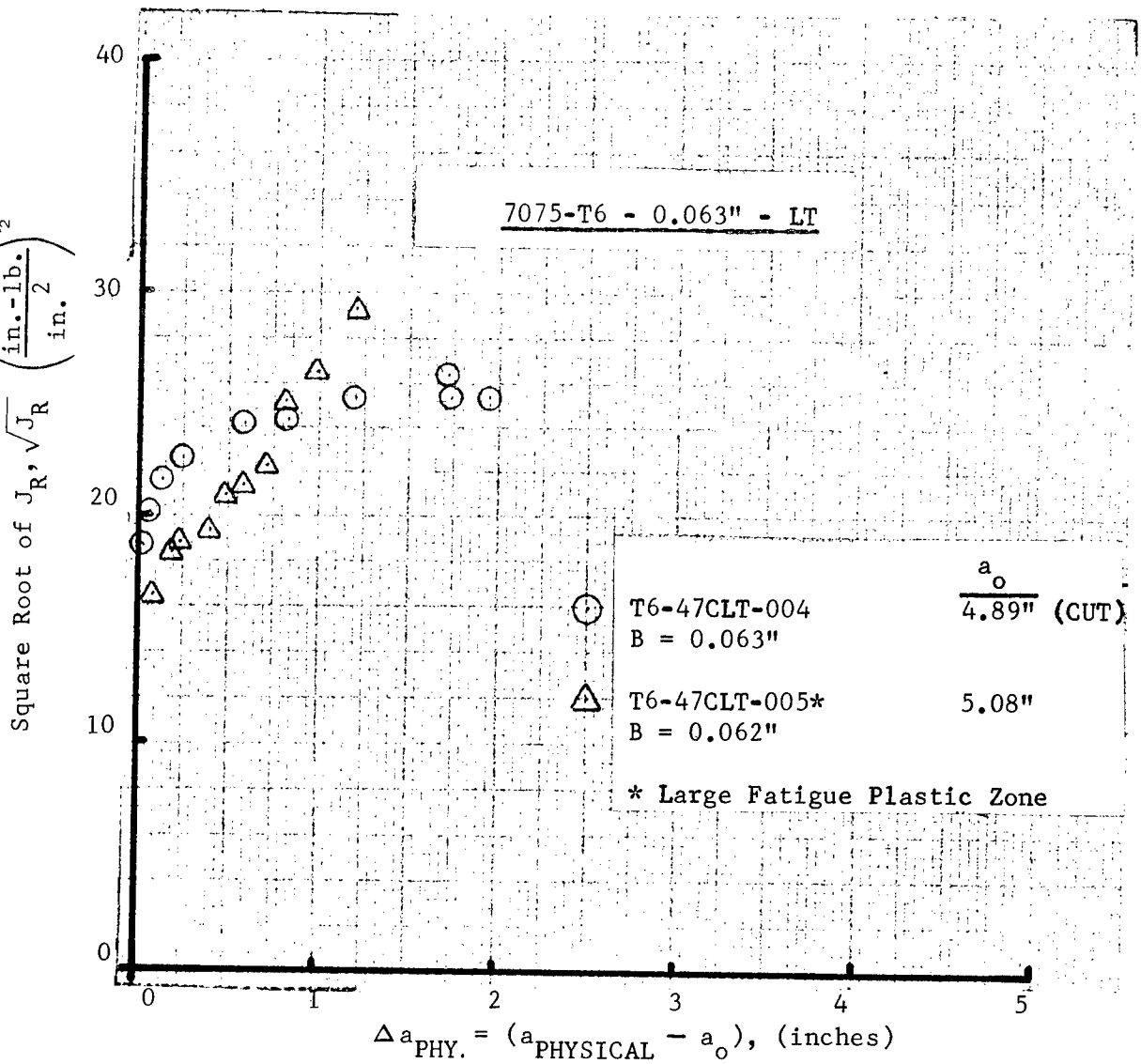

Figure 102. $\sqrt{J_R}$ Crack Growth Resistance Data - 7075-T6-.063 Inch, LT

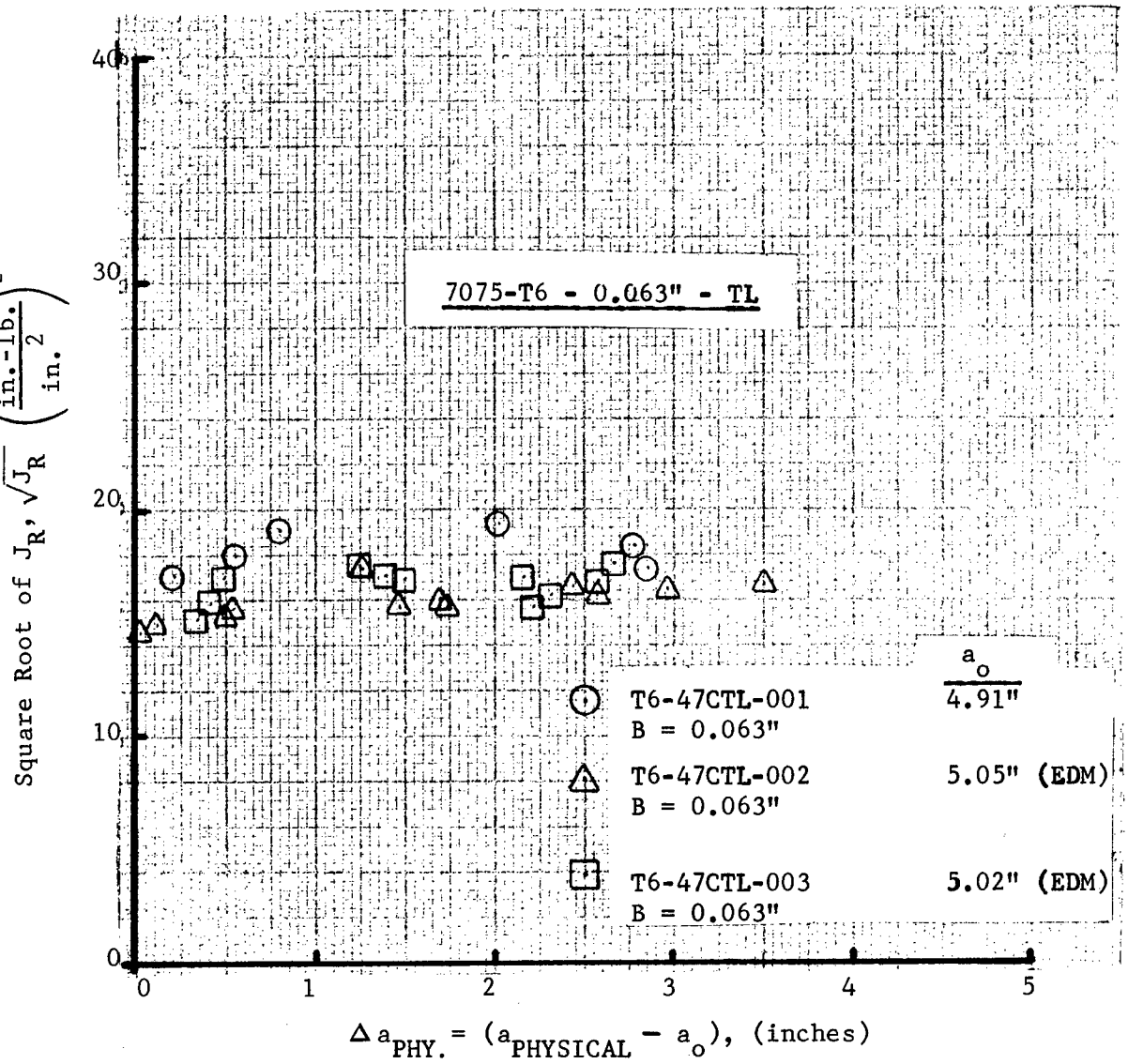

Figure 103. $\sqrt{J_R}$ Crack Growth Resistance Data - 7075-T6 - .063 Inch, TL

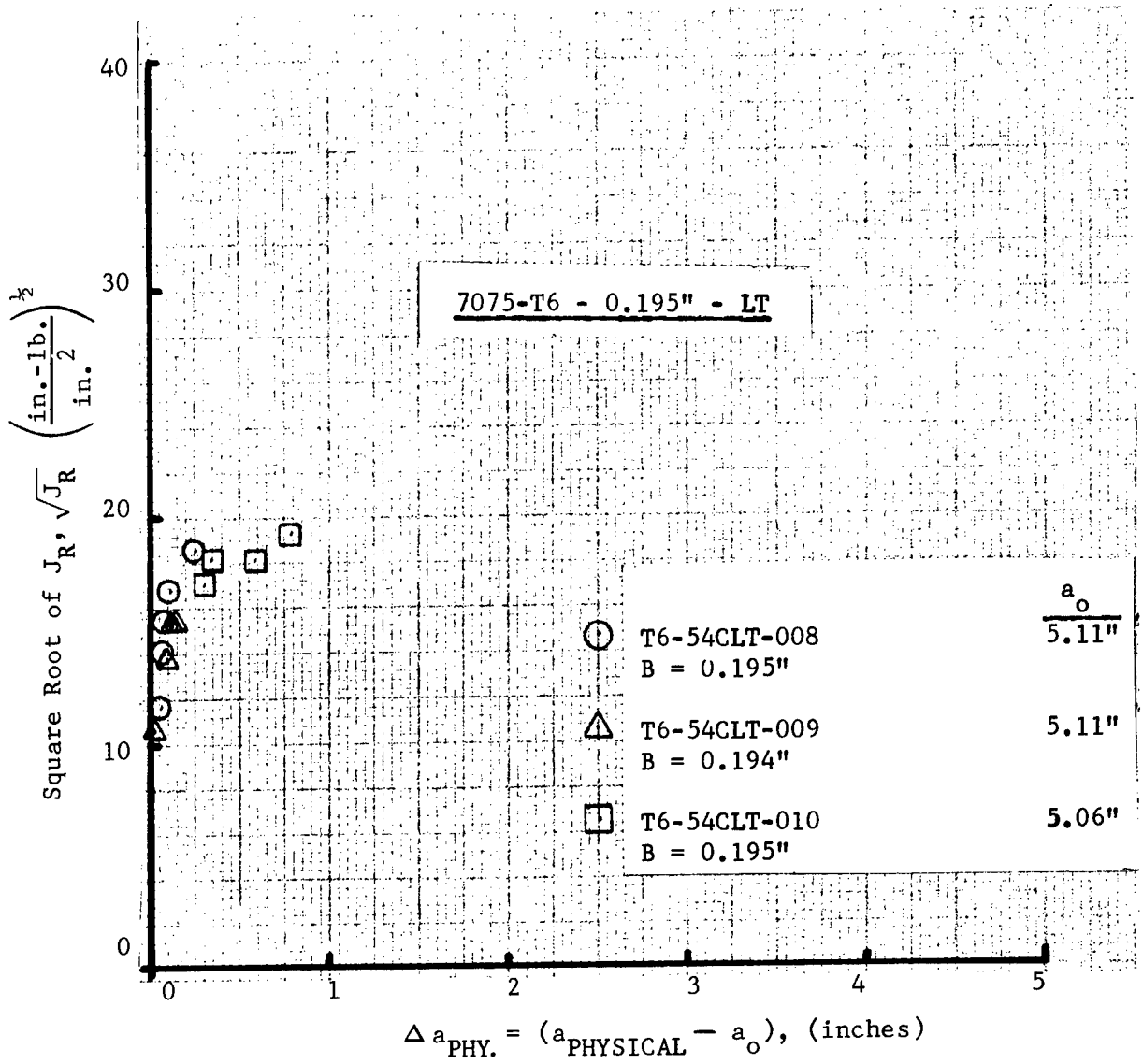

Figure 104. $\sqrt{J_R}$ Crack Growth Resistance Data - 7075-T6 - .195 Inch, LT

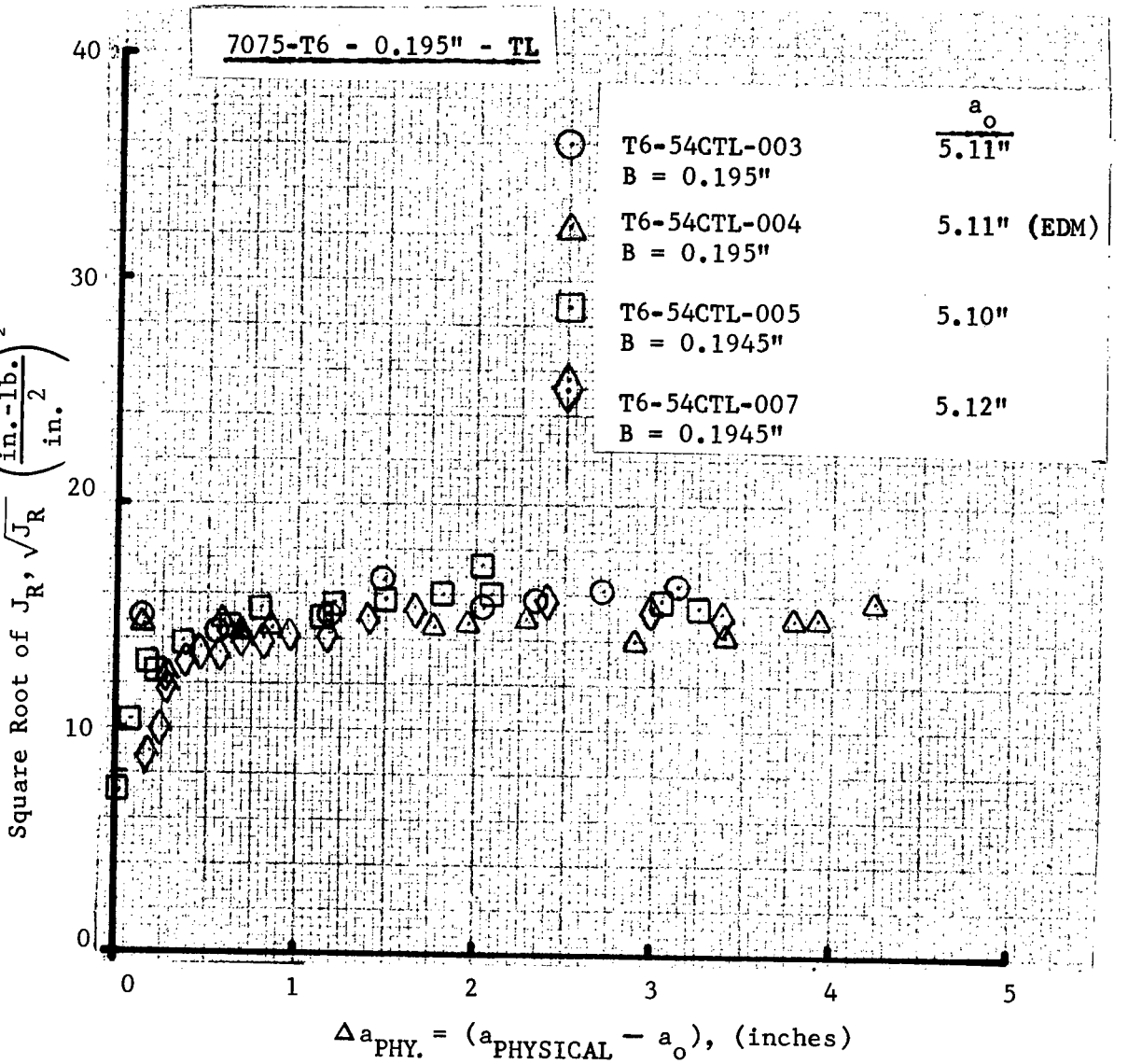

Figure 105. $\sqrt{J_R}$ Crack Growth Resistance Data - 7075-T6 - .195 Inch, TL

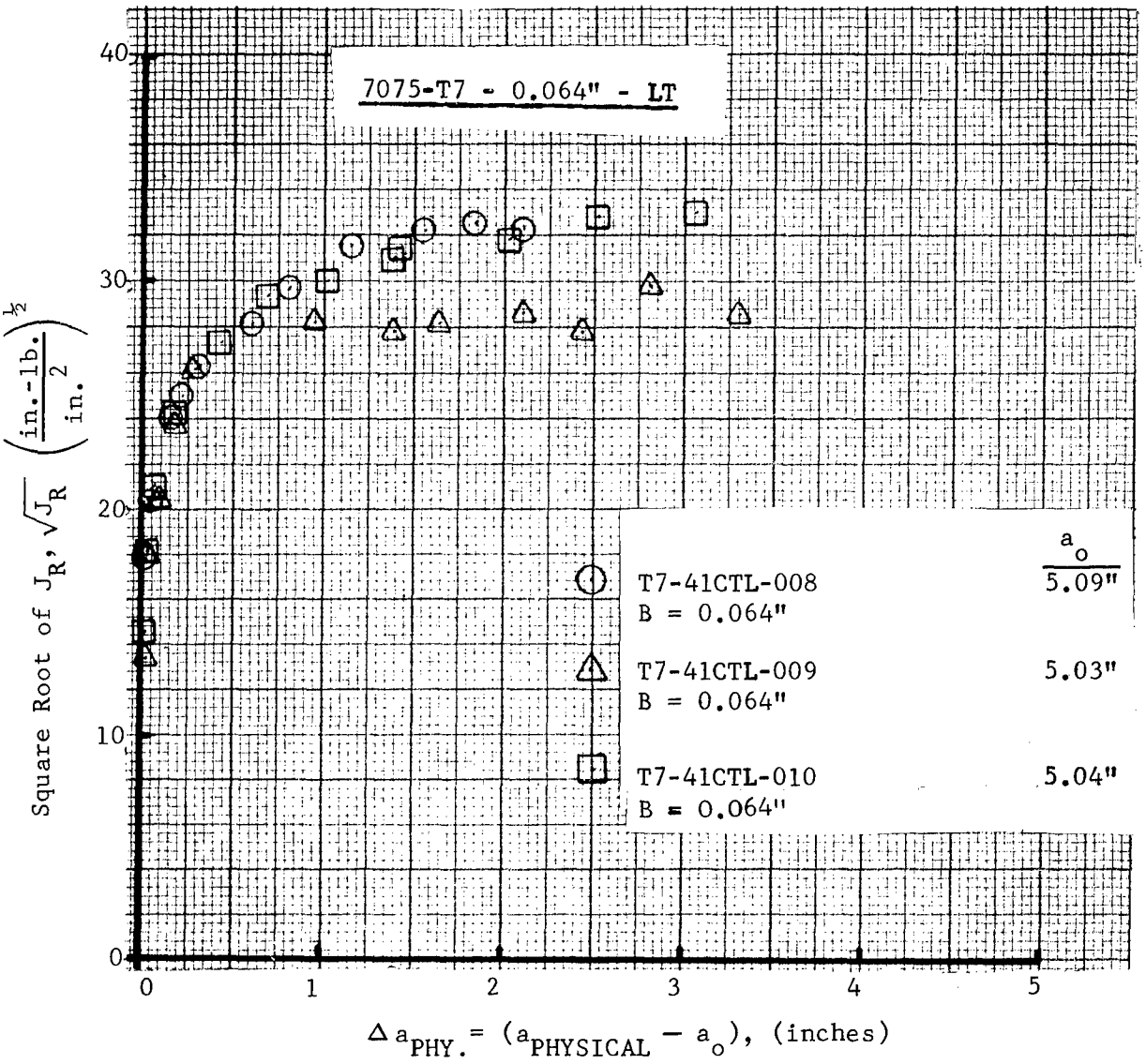

Figure 106. $\sqrt{J_R}$ Crack Growth Resistance Data - 7075-T7 - .064 Inch, LT

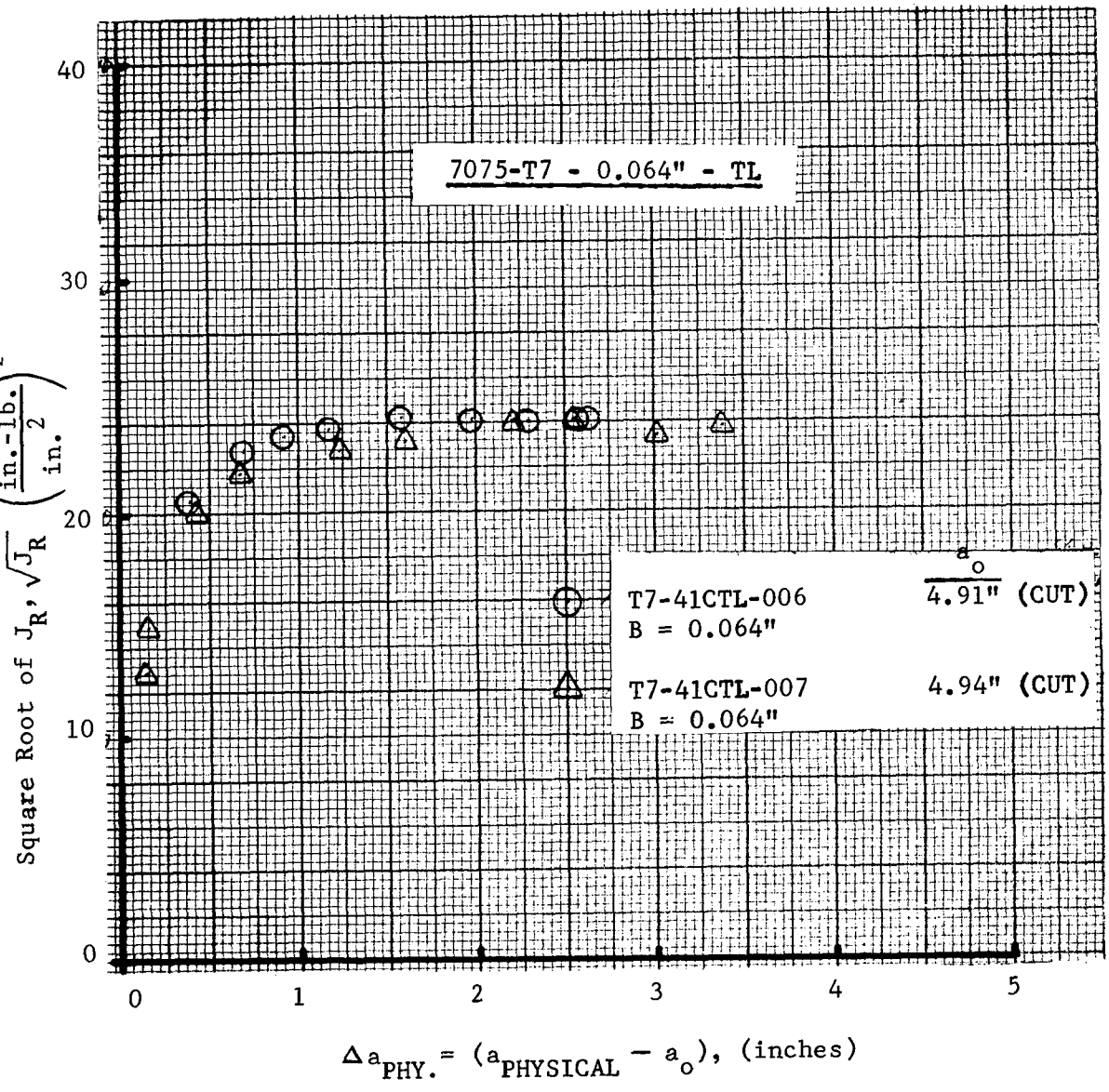

Figure 107. $\sqrt{J_R}$ Crack Growth Resistance Data - 7075-T7 - .064 Inch, (TL)

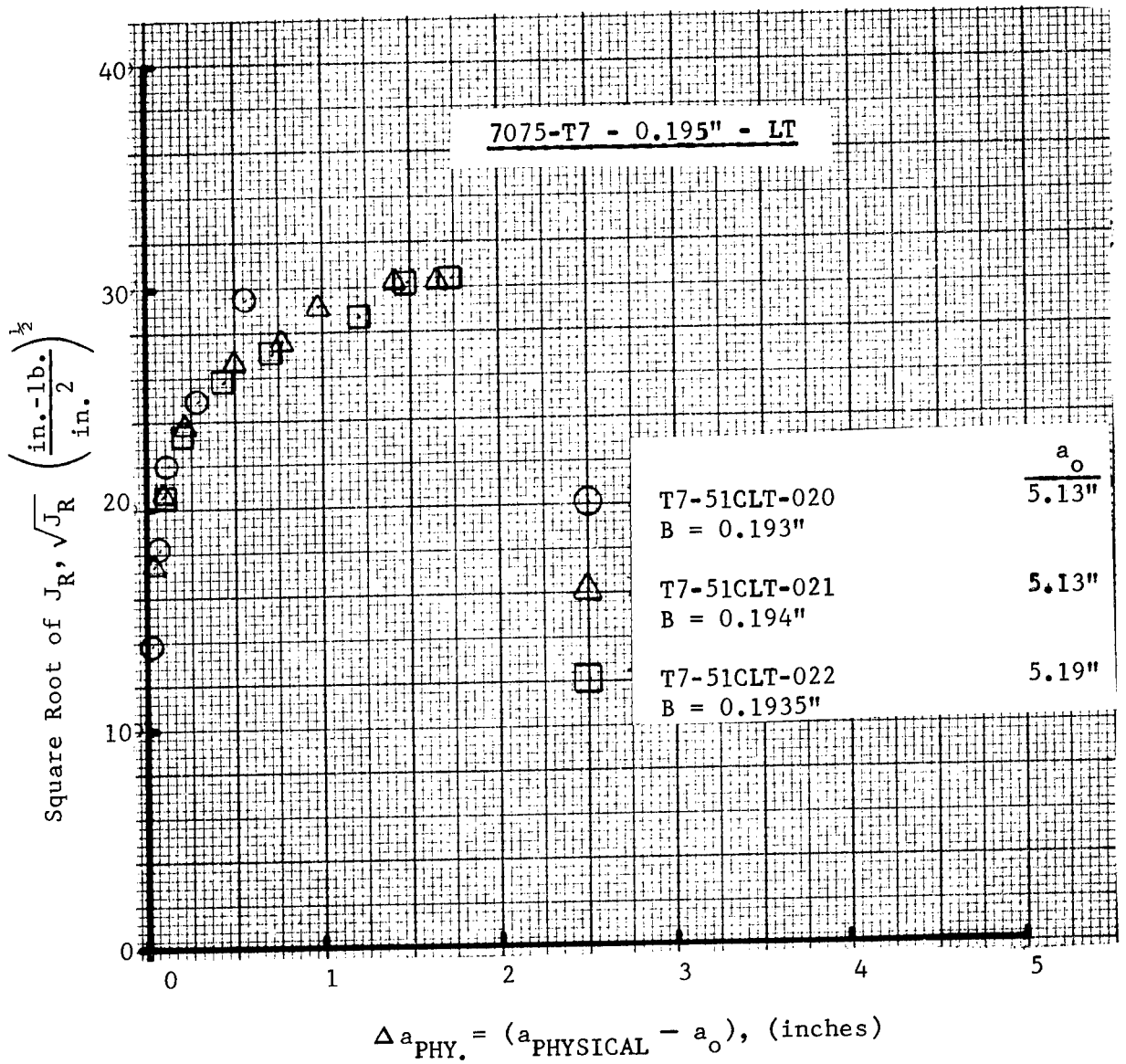

Figure 108. $\sqrt{J_R}$ Crack Growth Resistance Data - 7075-T7 - .195 Inch, LT

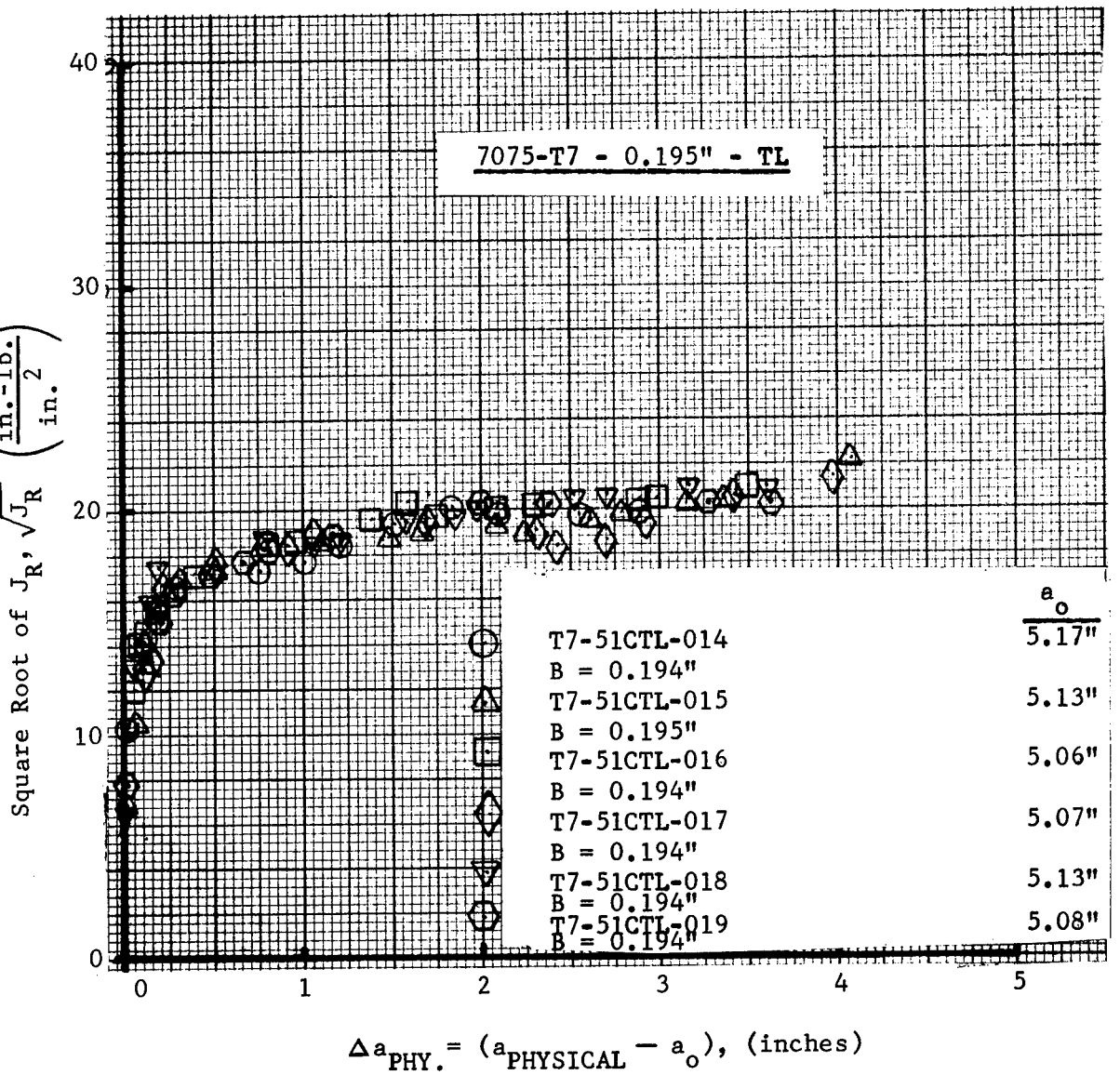

Figure 109. $\sqrt{J_R}$ Crack Growth Resistance Data - 7075-T7 - .195 Inch, TL

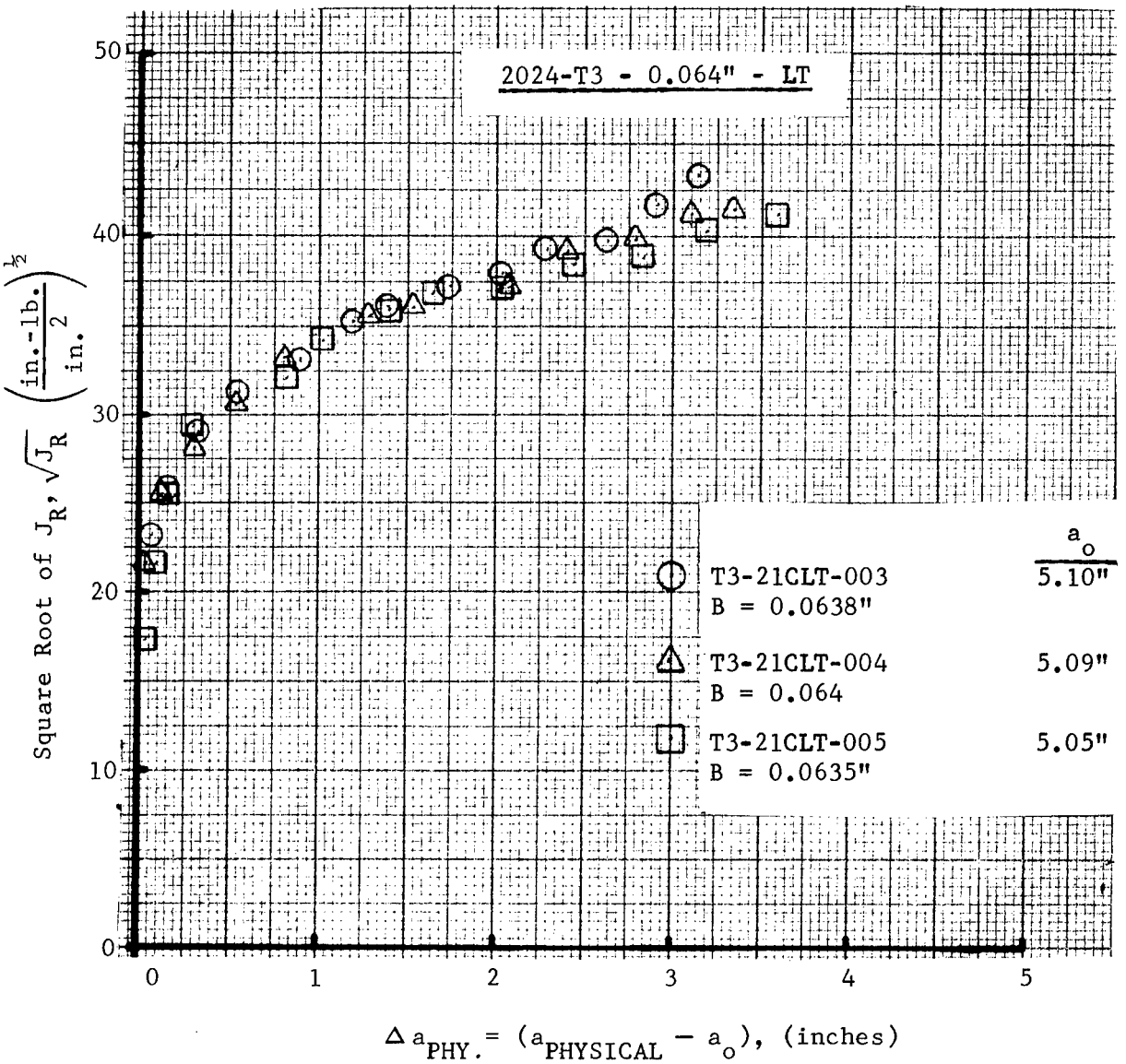

Figure 110. $\sqrt{J_R}$ Crack Growth Resistance Data - 2024-T3 - .064 Inch, LT

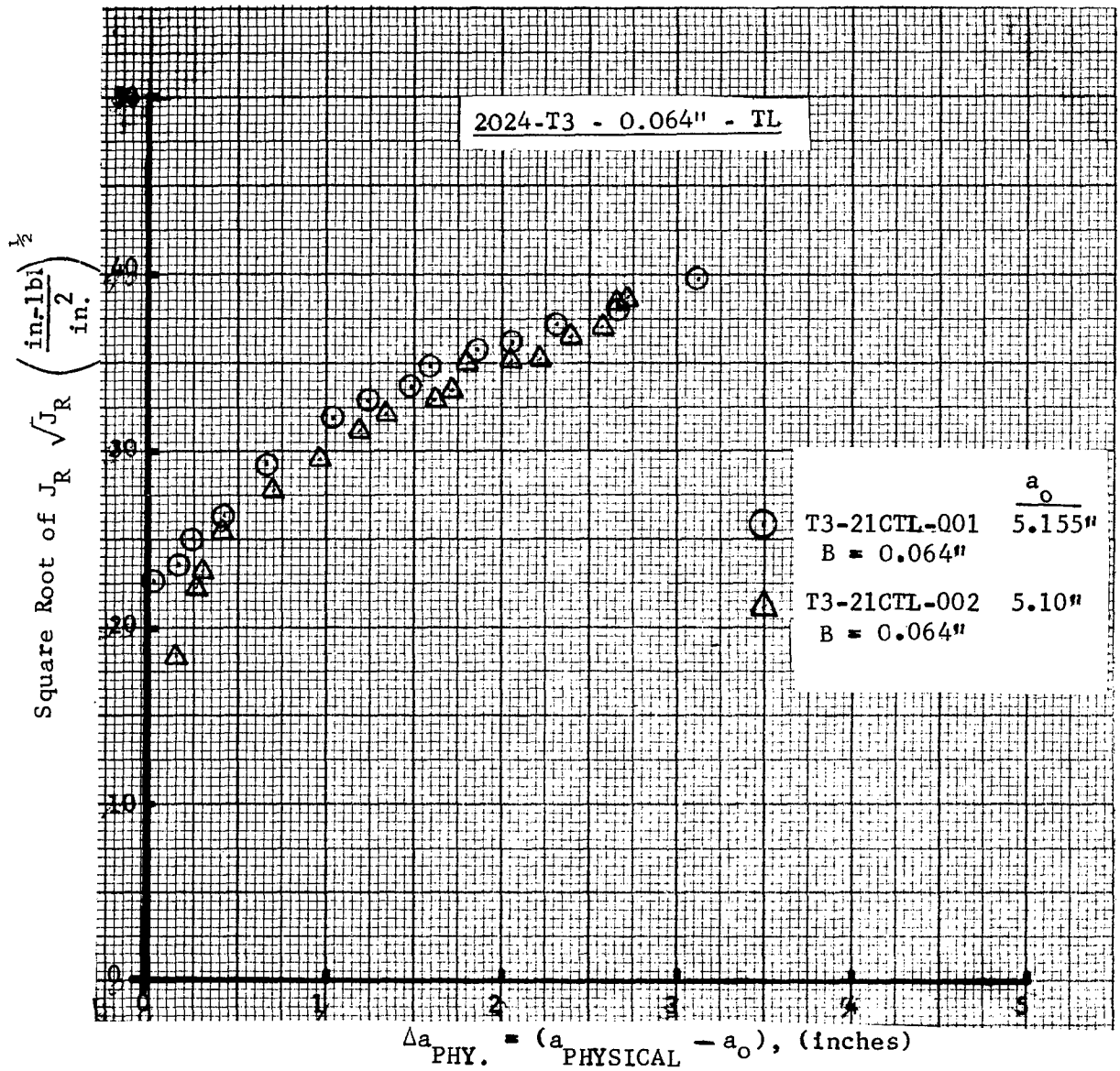

Figure 111. $\sqrt{J_R}$ Crack Growth Resistance Data - 2024-T3 - .064 Inch, TL

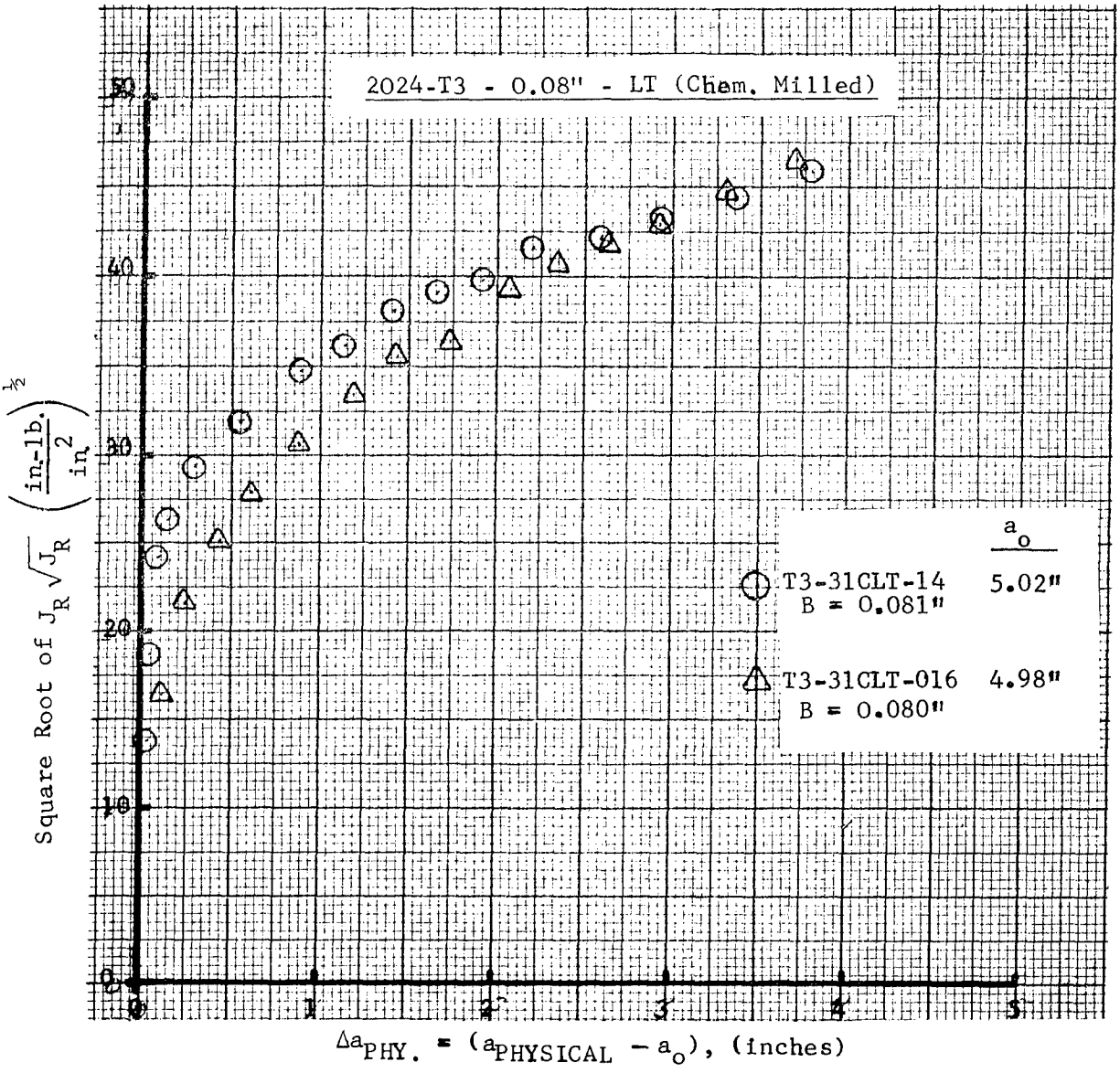

Figure 112. $\sqrt{J_R}$ Crack Growth Resistance Data - 2024-T3 - .08 Inch - LT (Chem. Milled)

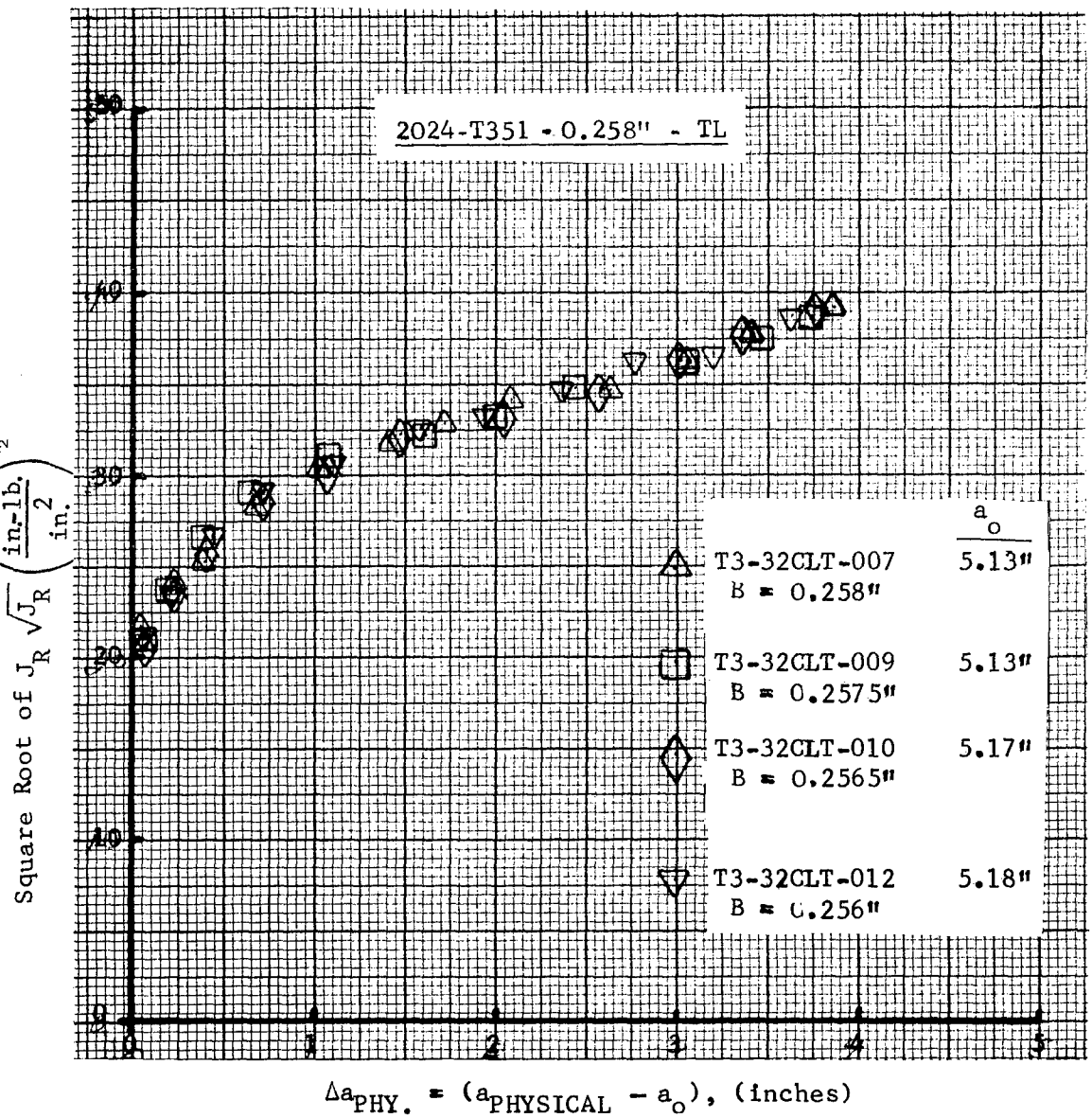

Figure 113. $\sqrt{J_R}$ Crack Growth Resistance Data - 2024-T351 - .258 Inch, LT

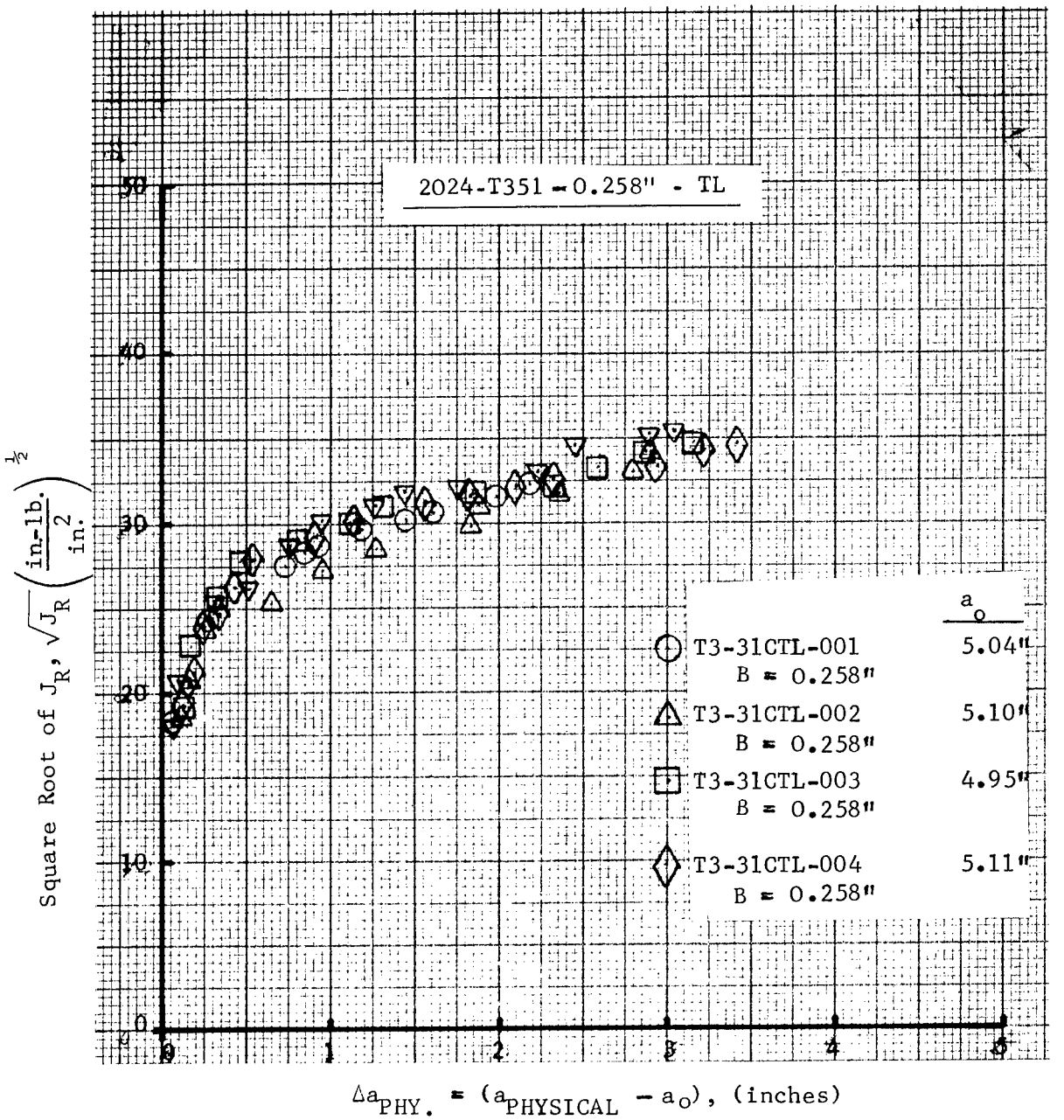

Figure 114. $\sqrt{J_R}$ Crack Growth Resistance Data - 2024-T351 - .258 Inch, TL

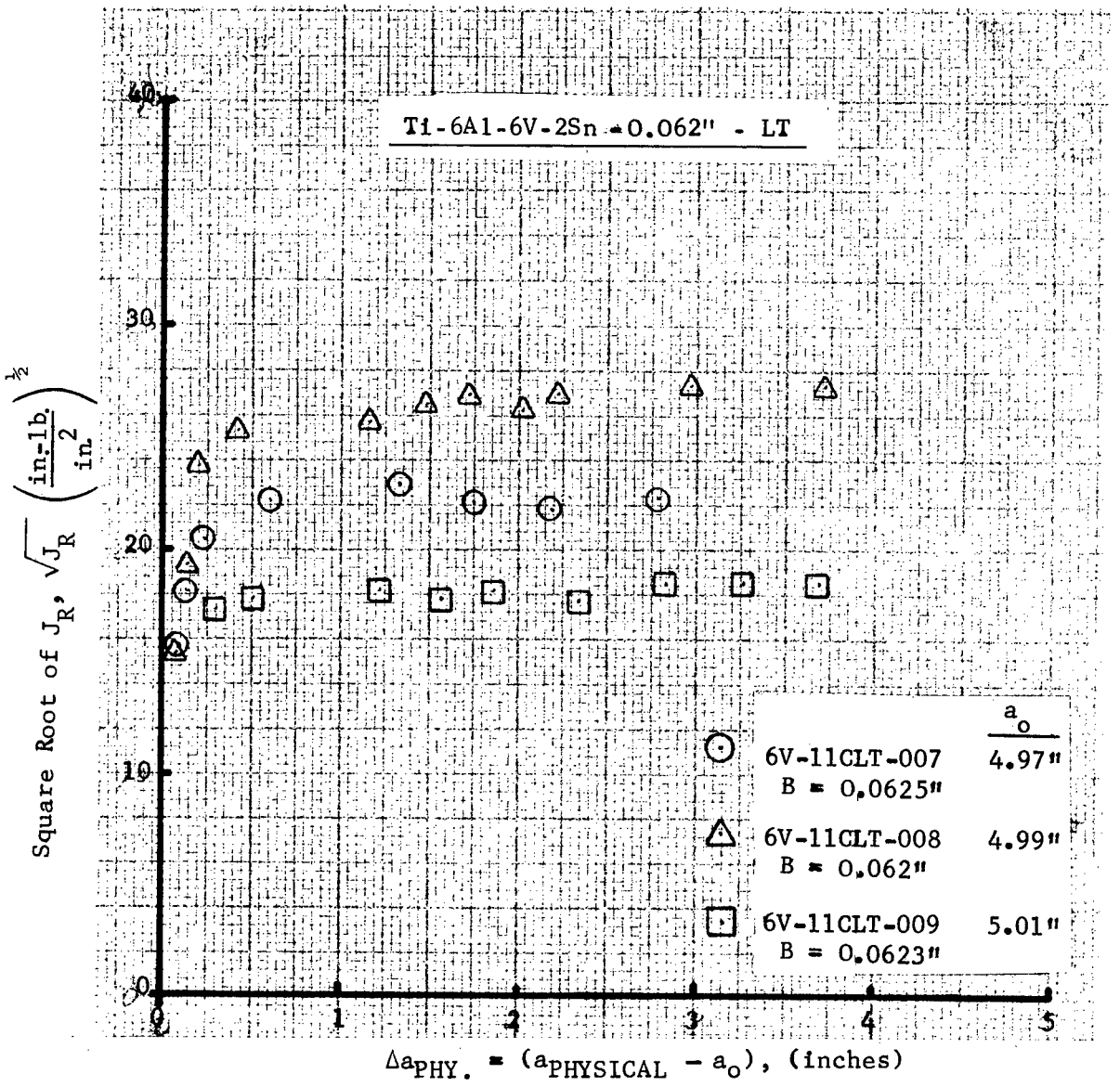

Figure 115. $\sqrt{J_R}$ Crack Growth Resistance Data - Ti-6A1-6V-2Sn - .062 Inch, LT

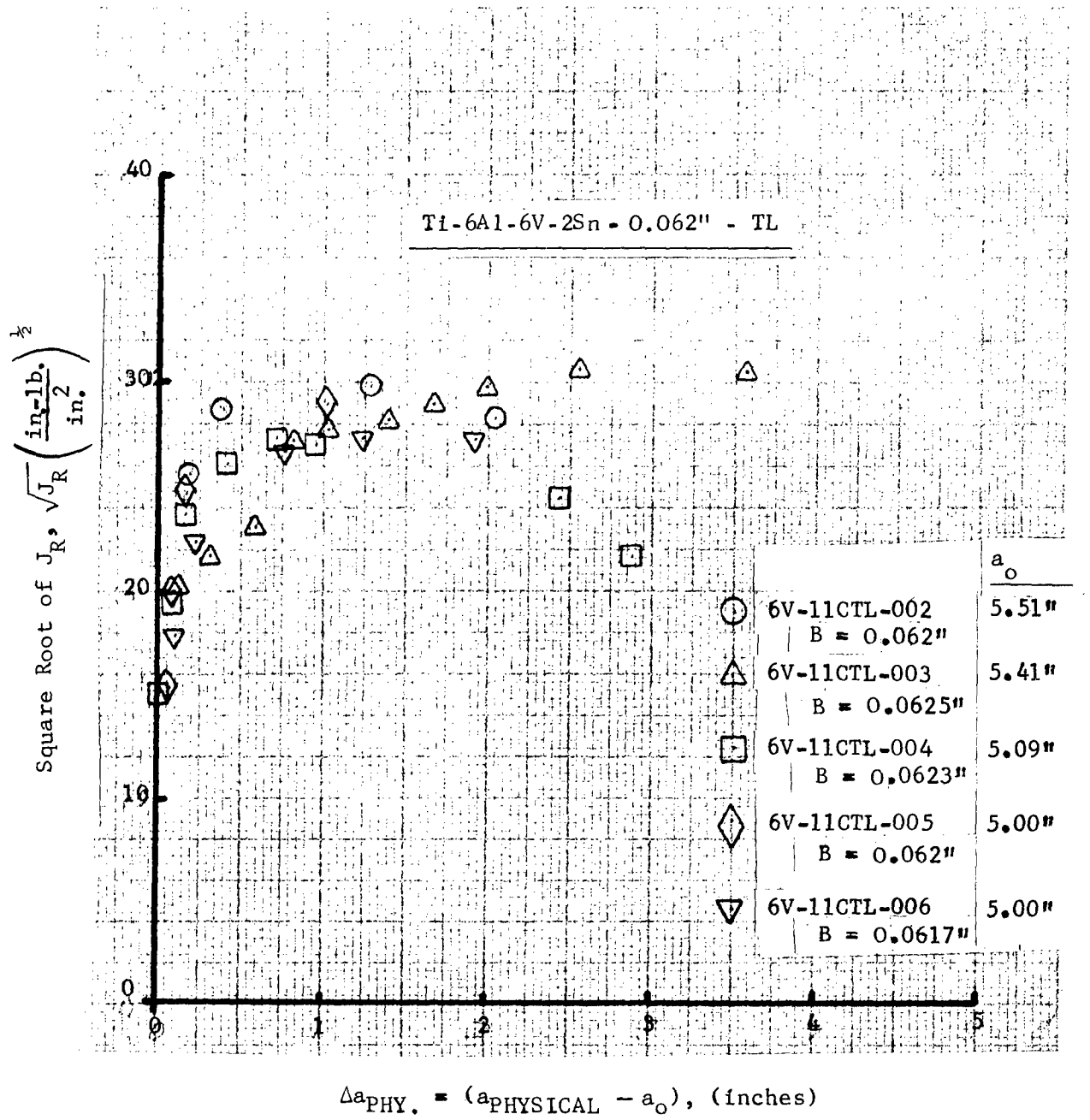

Figure 116. $\sqrt{J_R}$ Crack Growth Resistance Data - Ti-6Al-6V-2Sn - .062 Inch, TL

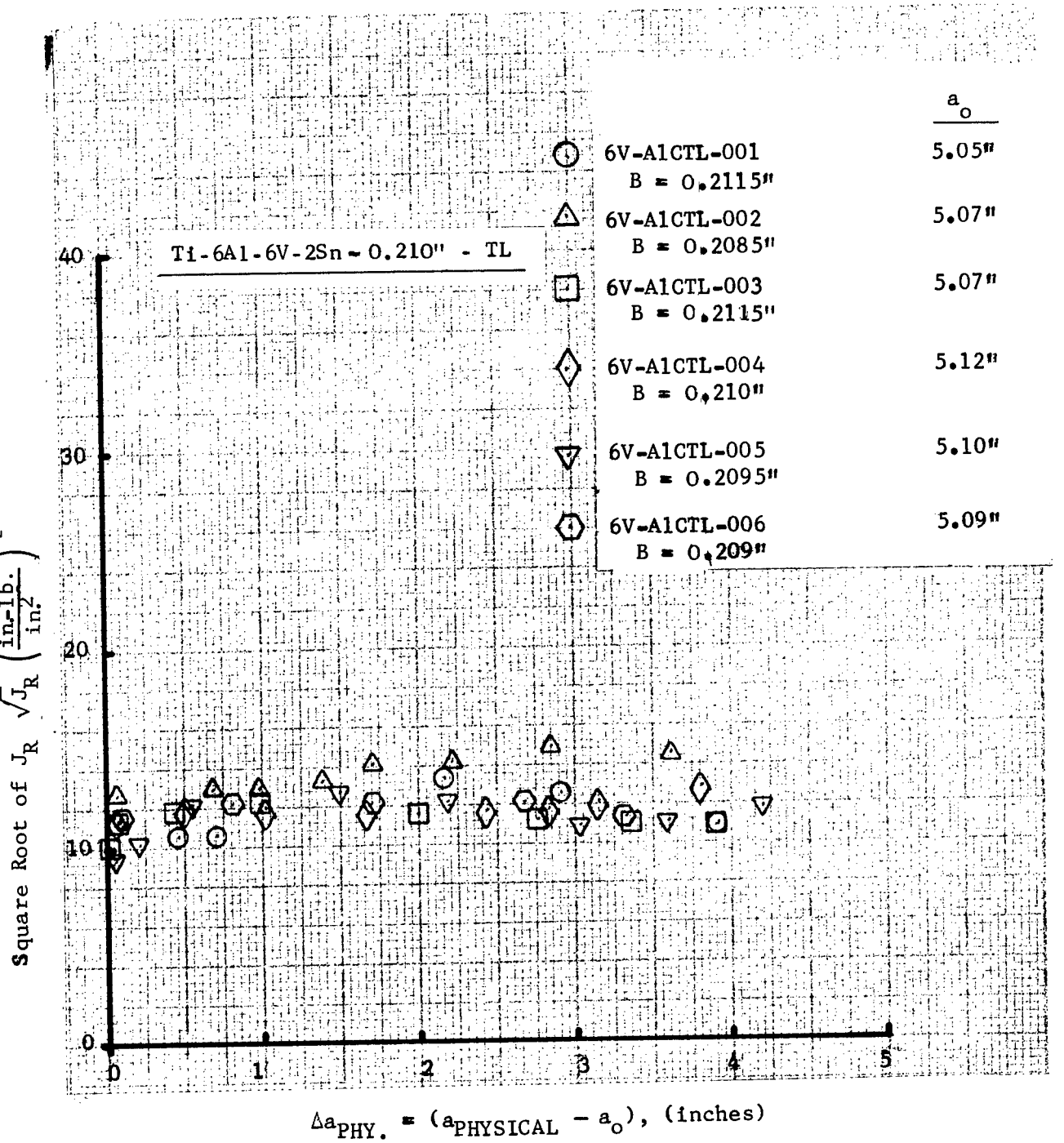

Figure 117. $\sqrt{J_R}$ Crack Growth Resistance Data - Ti-6Al-6V-2Sn - .210 Inch, TL

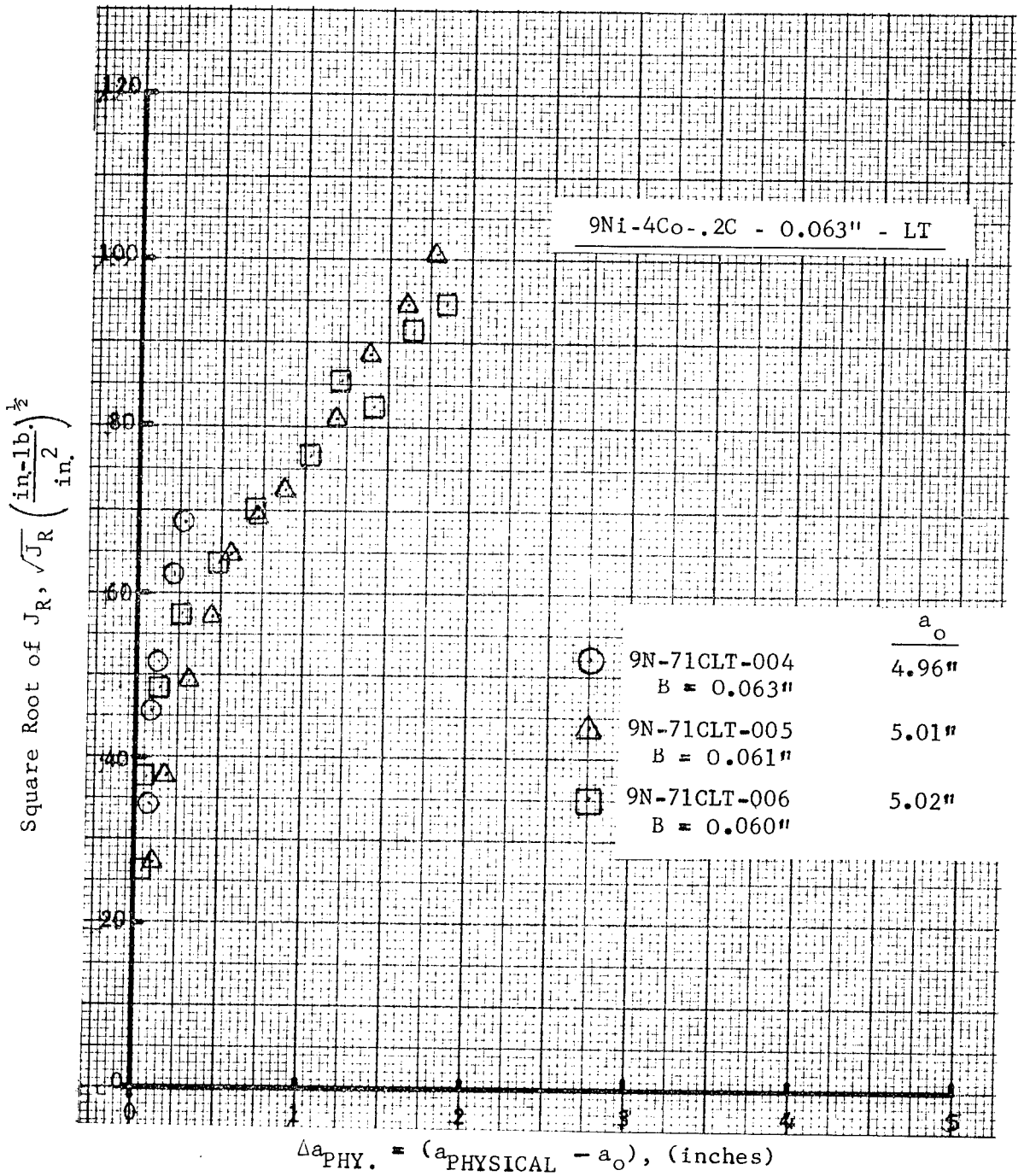

Figure 118. $\sqrt{J_R}$ Crack Growth Resistance Data - 9Ni Steel - .063 Inch, LT

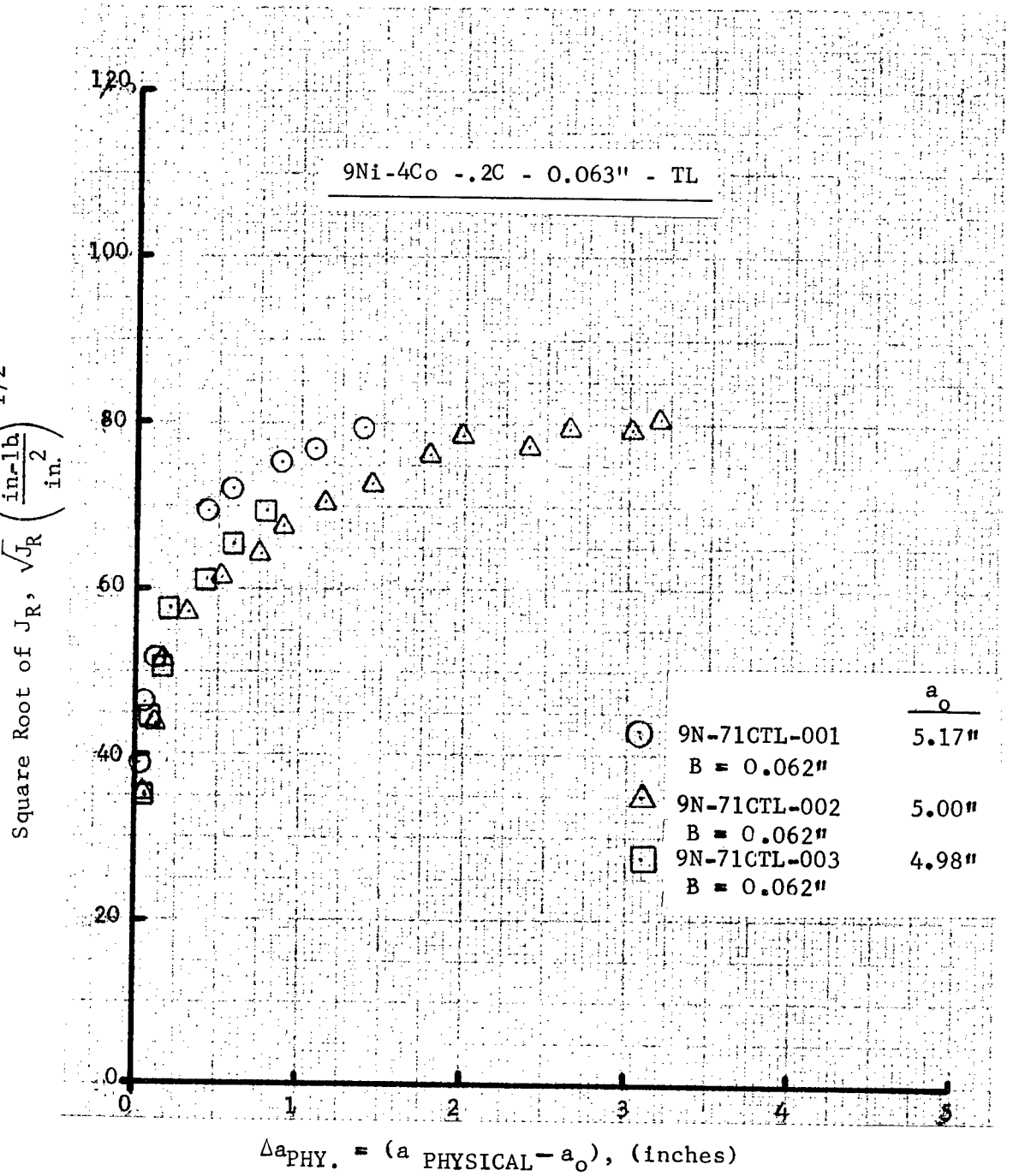

Figure 119. $\sqrt{J_R}$ Crack Growth Resistance Data - 9Ni Steel - .063 Inch, TL

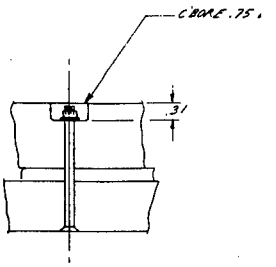

SECTION C-C FULL SIZE

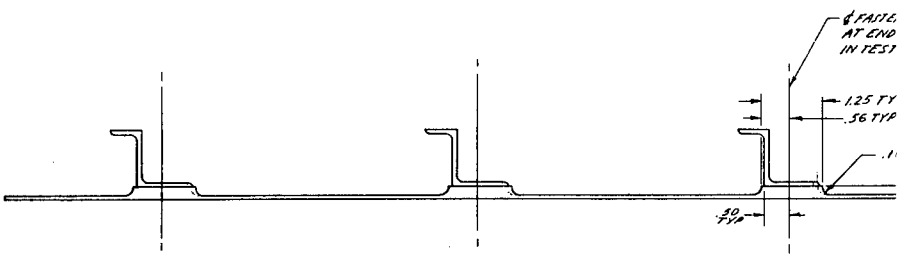

SECTION B-B FULL SIZE

Ⓐ

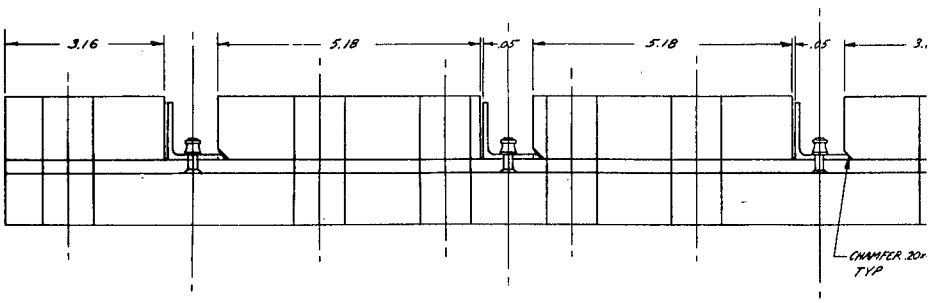

SECTION A-A FULL SIZE

Figure 120. Wing Panel Zee Stiffened

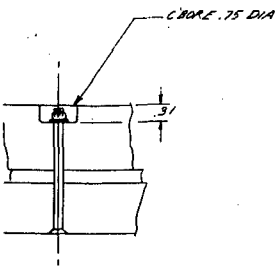

SECTION C₀-C₀ FULL SIZE

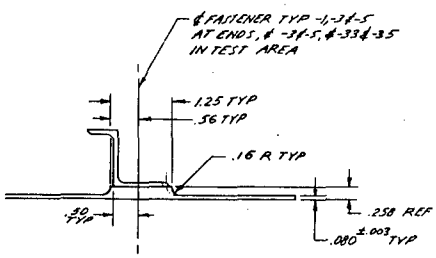

Ⓐ

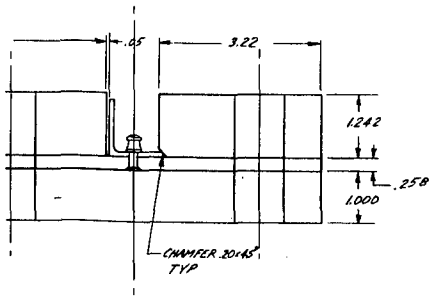

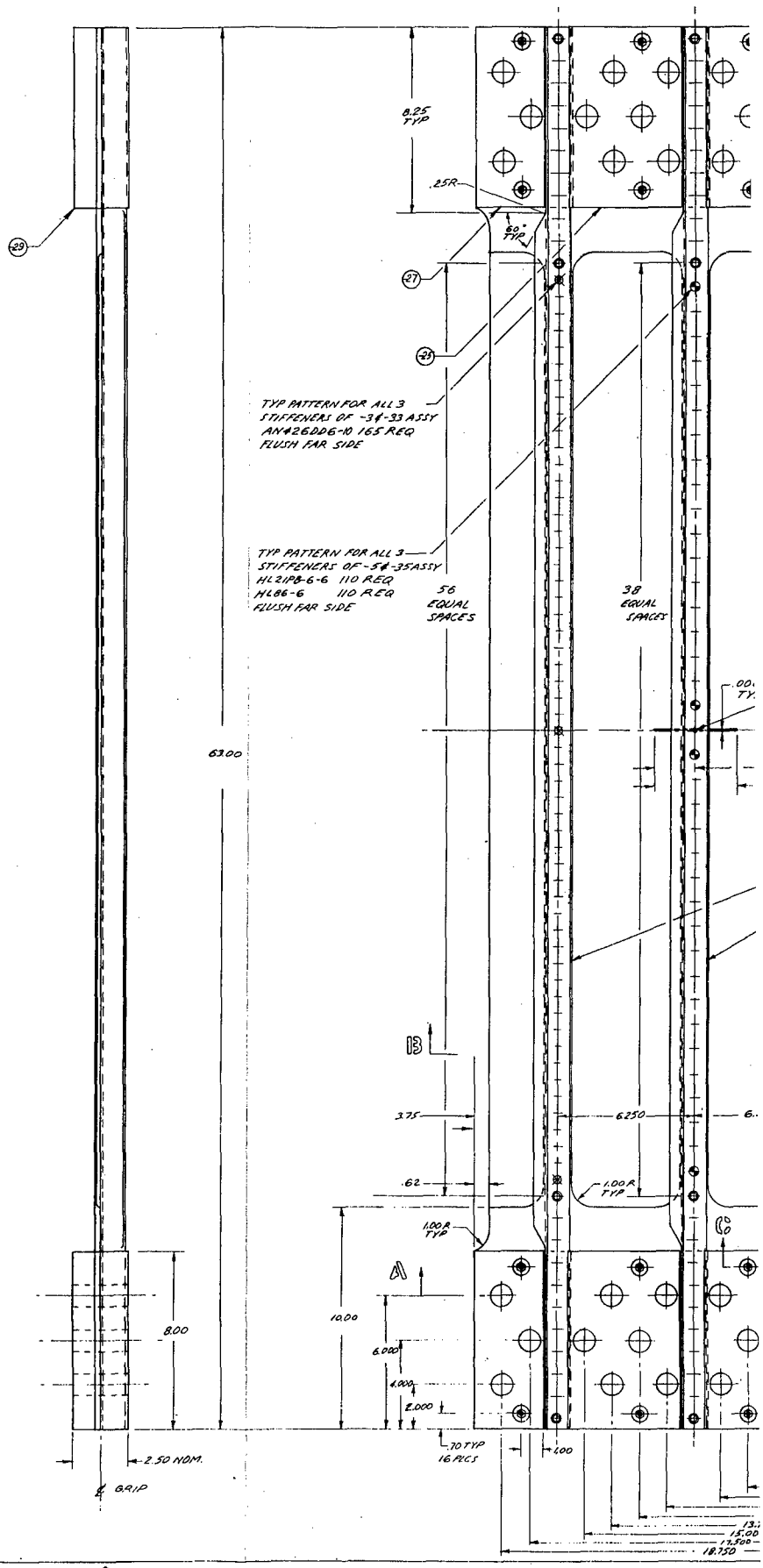

REVISIONS		
LTR	DESCRIPTION	DATE
A	STR. WIDTH "TOCK" NOM 1.00 THRU LAND 1.25 NOM 1.12 CHAMFER .20 X 45° NOM .15 X 45°	4/10/74 AM

SKIN SLIT DIMENSIONS		
DASH NO.	A	B
-7	1.90	3.80
-9	1.90	3.80
-11	1.90	3.80
-37	4.15	8.30
-39	4.15	8.30
-41	4.15	8.30

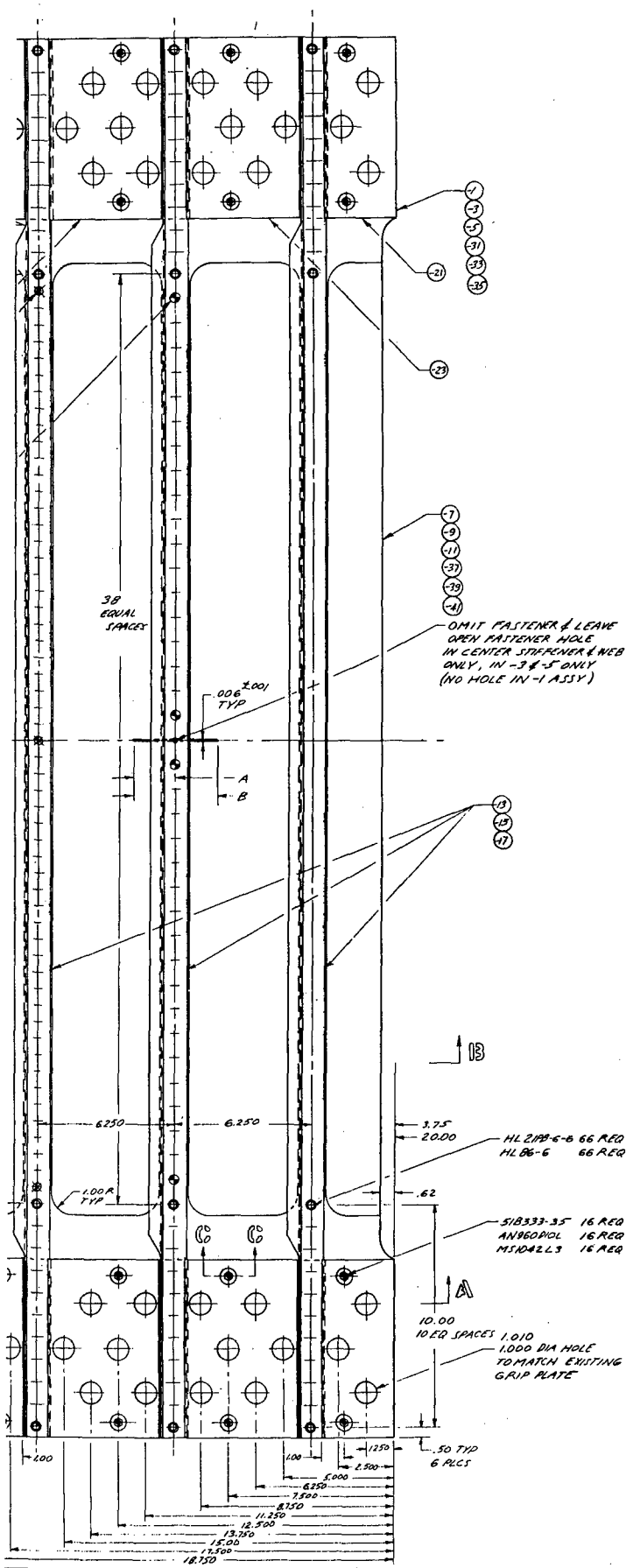

3. CENTER GRIP ENDS WITH MACHINE & WITHIN .010
2. BOND -13 TO -7 & -13 TO -37 PER PROC SPEC MA-108. INSTALL HI-LOK FASTENERS AFTER BOND IS COMPLETED.
1. USE PROC. SPEC: FH-1, FH-6.2, FH-21 & MA-108

NOTE -

-35	-33	-31	-5	-3	-1	PART OR IDENTIFYING NO.	SEE NOTES	NOMENCLATURE OR DESCRIPTION	MATERIAL & FINISH NO.	SIZE UNTRIMMED	SPECIFICATION OR PART DATA	ZONE	ITEM
NO. REQ.													
176	66	66	176	66	66	HL86-6		HI-LOK COLLAR					
176	66	66	176	66	66	HL21188-6-6		HI-LOK PIN					
	165			165		MS20426DD6-10		RIVET					
16	16	16	16	16	16	AN960D10L		WASHER					
16	16	16	16	16	16	MS21042L3		NUT					
16	16	16	16	16	16	5/8B333-35		SCREW					
1						-41		WEB	PLATE AL 2024 T3511	.359×10.2 ×63.2			
	1					-39		WEB	PLATE AL 2024 T3511	.298×10.2 ×63.2			
		1				-37		WEB	PLATE AL 2024 T3511	.238×10.2 ×63.2			
						-35		HI-LOK PANEL					
						-33		RIVETED PANEL					
						-31		BONDED PANEL					
2	2	2	2	2	2	-29		BLOCK	PLATE AL 2024 T351	1.18×8.2 ×20.2			
2	2	2	2	2	2	-27		↕	↕	1.50×3.3 ×8.2			
2	2	2	2	2	2	-25				1.50×5.5 ×8.2			
2	2	2	2	2	2	-23				1.30×5.5 ×8.2			
2	2	2	2	2	2	-21		BLOCK	PLATE AL 2024 T351	1.50×3.4 ×8.2			
3			3			-17		STIFFENER	AND10139-1108 EXT 2024 T3511	63.2 LG			
	3			3		-15		STIFFENER	AND10139-1108 EXT 2024 T3511	63.2 LG			
		3			3	-13		STIFFENER	AND10139-1108 EXT 2024 T3511	63.2 LG			
			1			-11		WEB	PLATE AL 2024 T351	.238×10.2 ×63.2			
				1		-9		WEB	PLATE AL 2024 T351	.238×10.2 ×63.2			
					1	-7		WEB	PLATE AL 2024 T351	.238×10.2 ×63.2			
						-5		HI-LOK PANEL					
						-3		RIVETED PANEL					
						-1		BONDED PANEL					

PARTS LIST

UNLESS OTHERWISE NOTED
LINEAR .X = ±.1
TOLERANCES .XX = ±.04
.XXX = ±.010
LINEAR DIM. ARE IN INCHES
ANGULAR TOL EXCEPT SHEET METAL FLG ± 0° 30'
MFG ACCEPTANCE TOL PER NORTHROP STD 10Y201
FINISH PER
ODD DASH NO. SHOWN
EVEN DASH NO. OPPOSITE

CONTRACT NO.

DRAWN R.JEFFRIES 4/10/74
DESIGN
CHECKED
PROGRAM
NORTHROP APPROVAL
OTHER APPROVAL

Northrop Corporation Aircraft Division Hawthorne, California

WING PANEL, ZEE STIFFENED

SIZE J | CODE IDENT NO. 80126 | SR-796003

SCALE 1/2 & WHITE | SHEET 1 OF 1

SR-796003 A

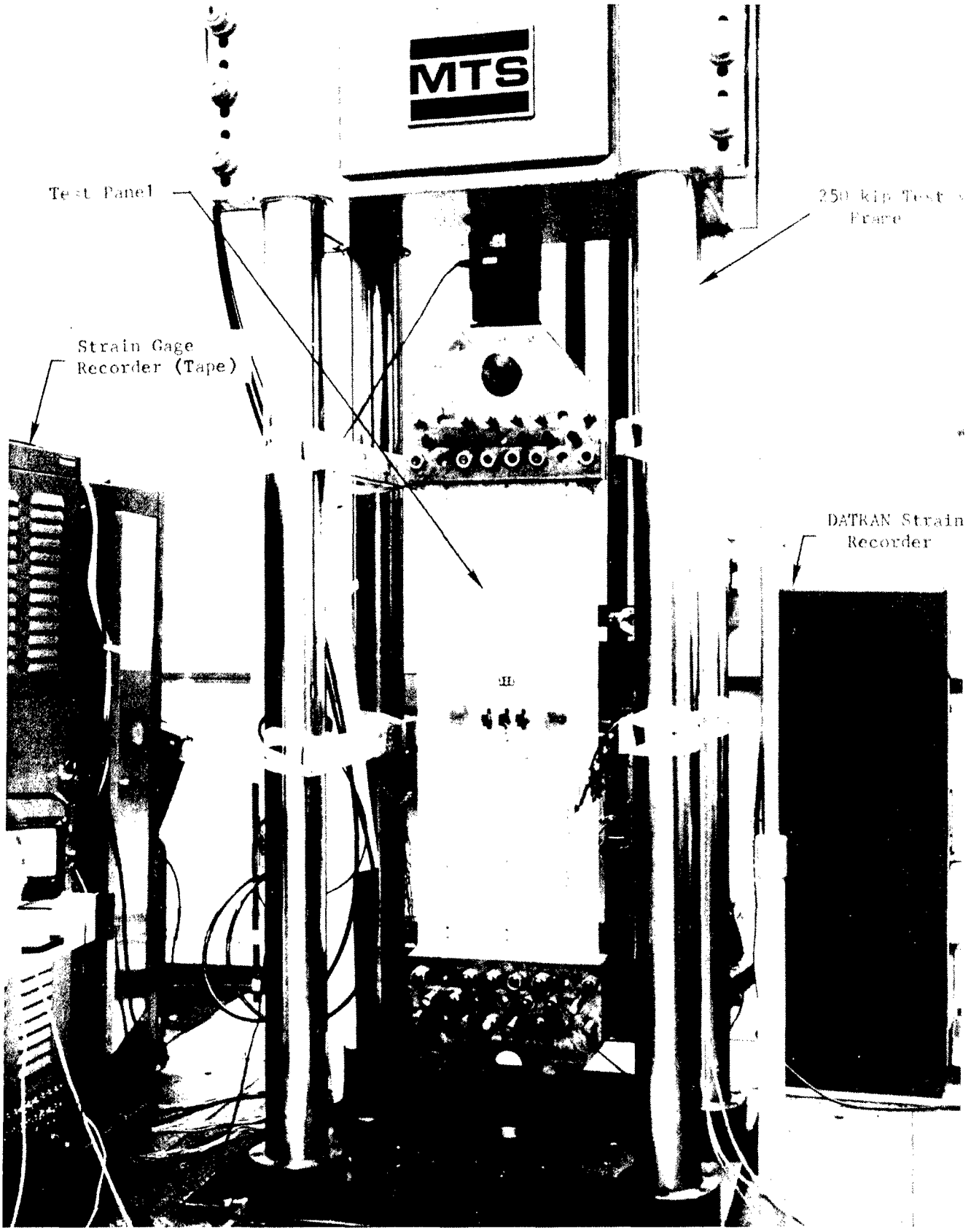

Figure 121. Zee Stiffened Panel Test Arrangement

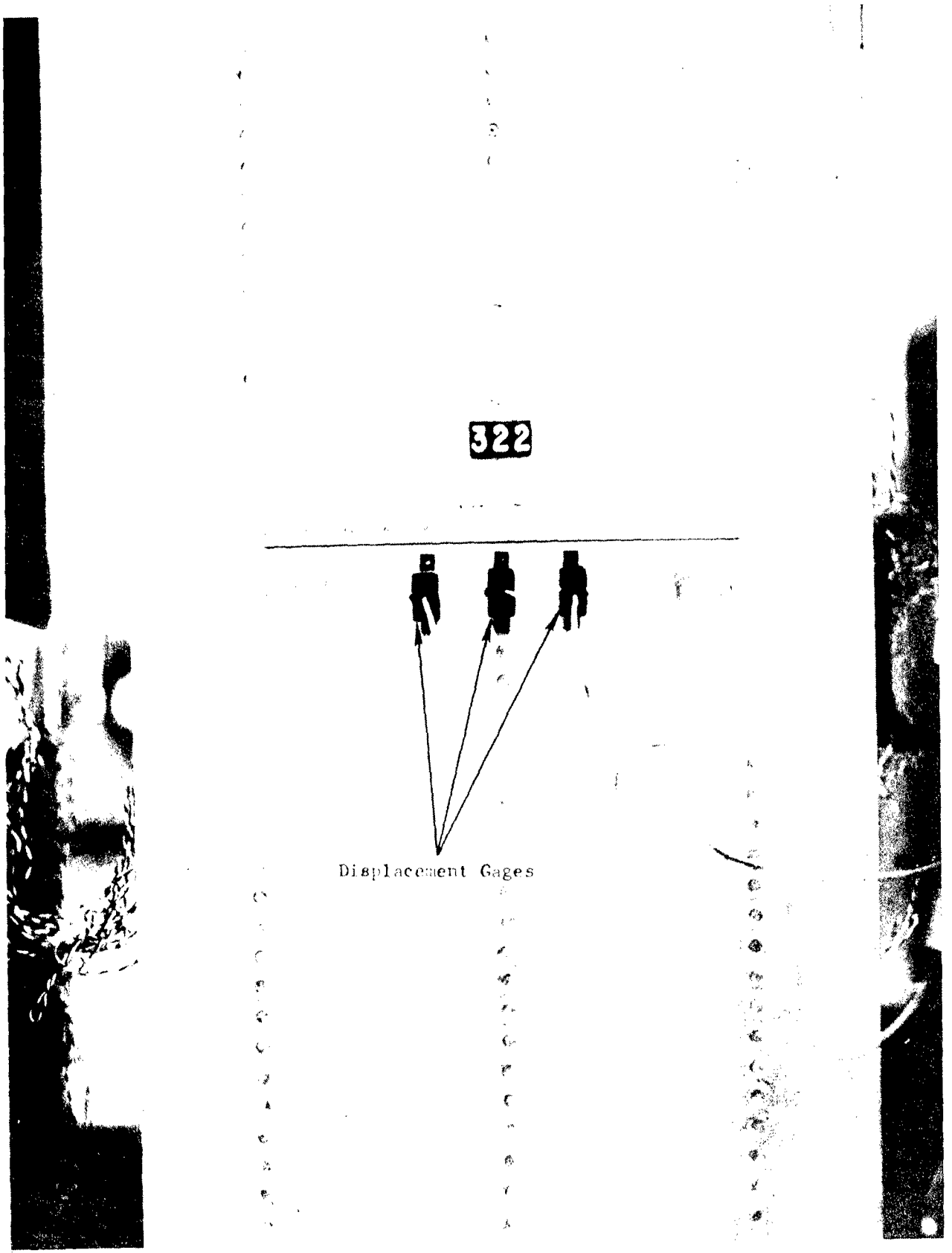

Figure 122. Typical Displacement Gage Locations - Zee Stiffened Panel

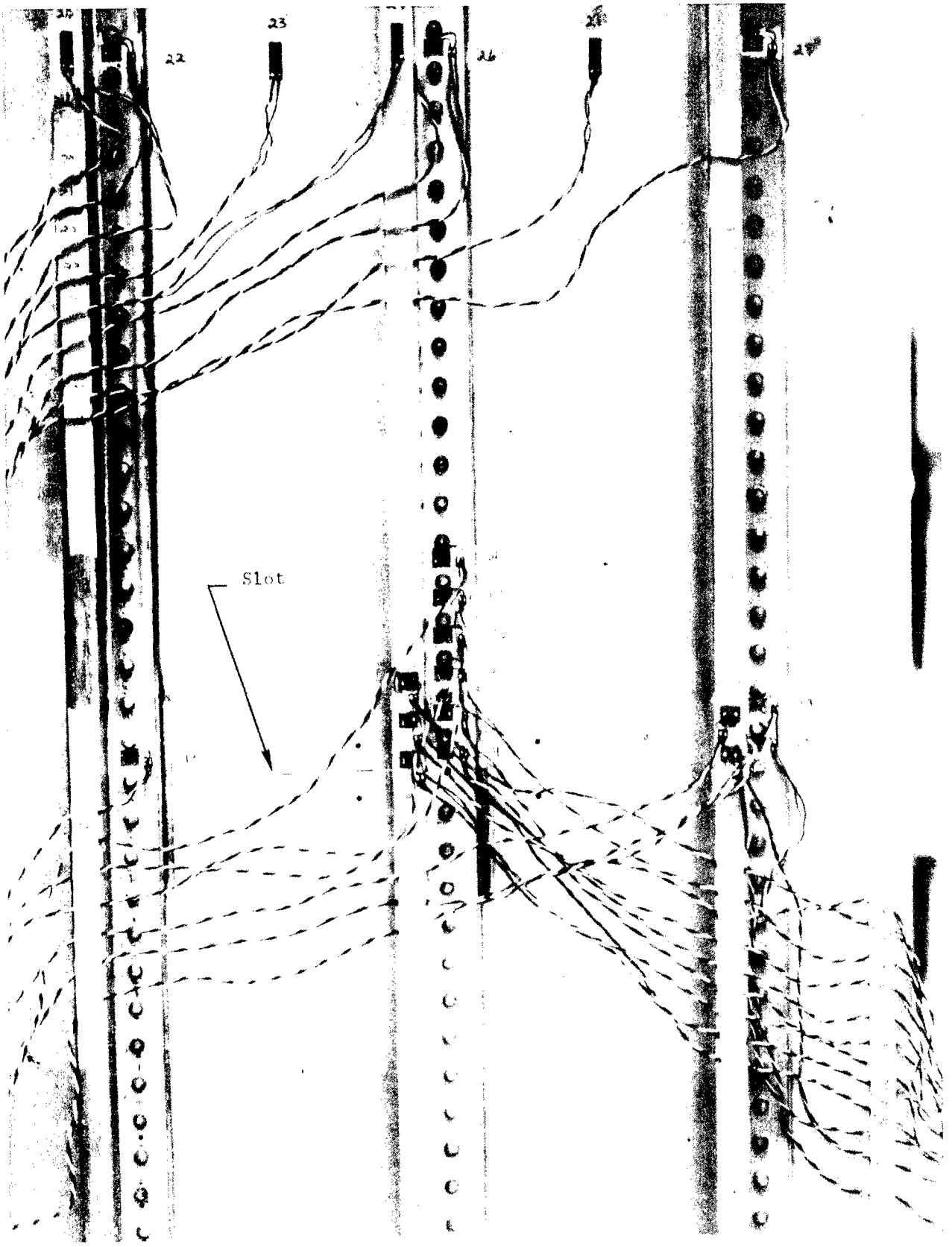

Figure 123. Typical Strain Gage Layout - Zee Stiffened Panel

TABLE XV. CROSS SECTIONAL AREAS FOR CHEM MILLED 2024-T3 ZEE STIFFENED PANELS

PANEL NUMBER	AVERAGE AREA LANDS ($inches^2$)				AVERAGE AREA POCKETS ($inches^2$)					TOTAL SKIN AREA ($inches^2$)	TOTAL STRINGER AREA ($inches^2$)	TOTAL PANEL AREA ($inches^2$)	RATIO STRINGER AREA/ SKIN AREA
	LEFT	RIGHT	CENTER	TOTAL	LEFT EDGE	LEFT	RIGHT	RIGHT EDGE	TOTAL				
3-2-1*	.3210	.3264	.3143	.9617	.2255	.3906	.3996	.2069	1.223	2.185	.768	2.953	.3515
3-2-2*	.3178	.3215	.3290	.9682	.2104	.4033	.3986	.2156	1.228	2.196	.768	2.964	.350
3-3-1**	.3213	.3244	.3231	.9687	.2079	.3995	.3887	.2070	1.203	2.172	.768	2.940	.354
3-3-2**	.3277	.3182	.3175	.9634	.2055	.3887	.3888	.2006	1.184	2.147	.768	2.915	.358
3-3-3†	.3215	.3210	.3272	.9697	.2079	.3837	.3886	.1977	1.178	2.148	.768	2.916	.358
3-3-3†	.3160	.3200	.3251	.9611	.2006	.3791	.3838	.2104	1.174	2.135	.768	2.903	.360

* Riveted

** HI-LOK

† Adhesively Bonded

sectional area. Any calculations of stress for the individual panels used the areas listed in Table XV. The greatest variation in total skin area in the test section was less than three percent for all panels.

2. After initiating and growing the fatigue cracks 1/4-inch beyond the starter slot length the deflection and strain gages were balanced out with the panel hanging free in the test machine. Of the 28 strain gages 12 were monitored by recording on tape and in some cases 3 gages were monitored on both tape and through the DATRAN strain gage monitor. With the exception of the first test panel (3-2-1) tape recordings of strain gage output from selected gages and the machine load cell were monitored simultaneously to fracture.

3. At specified increments of load, the load was held constant and both strain and COD data obtained. This was essentially the same procedure followed for the wing channel stiffened panel of Section IV. However, in this case the load was not reduced to zero prior to obtaining the next load increment but went in successive, increasing steps until some indication of crack tip plasticity occurred. At that time the panel was loaded to fracture from the last steady state load condition. (The exception to this procedure was panel 3-3-2 where a series of unloadings to zero load preceded fracture).

4. During the loading to fracture continuous recording of the 12 strain gages plus load occurred on tape in conjunction with separate load/deflection traces for the three deflection gages. High speed motion picture coverage ($\sim$ 700 frames/second) was employed in an attempt to record panel fracture. A digital VTVM was in the film field of view to correlate load with crack extension. However, it was determined that these films were useful only in determining the arrest or non-arrest of the crack. Of the six panels tested two successful recordings were made to panel fracture. These films confirmed those observations which could have been made visually - i.e., if crack arrest did or did not occur prior to catastrophic failure.

5. After panel failure all strain gages were again surveyed under zero load conditions prior to removing the panel from the test machine.

In the following three subsections the detail data obtained from these three panel geometries will be presented and comparisons made with the analytical results.

7.1 RIVETED PANEL

The analysis of the riveted zee stiffened panel was carried out in a manner similar to that performed on the wing channel panel. Both elastic and elastic-plastic analyses were carried out for various crack lengths. The finite element modeling, elastic, elastic-plastic analysis, and experimental data of this panel are discussed in the following subsections.

7.1.1 Finite Element Modeling of Zee-Stiffened, Riveted Panel

The finite element modeling is similar to that used for the wing channel stiffened-panel configuration. The panel is essentially modeled as a two-dimensional structure. The bending stiffness of the sheet (skin) is neglected. Membrane elements are used to model the panel skin. All membrane elements of the skin are modeled as triangular elements. The thickness of the land is assumed to be symmetrically placed about the centerline of the sheet thickness. The portion of the panel having lands are modeled as triangular membrane elements like the "pocketed" portions, except in this case the thickness of the triangular finite elements is equal to the thickness of the land. The zee stiffeners are modeled in a manner similar to the wing channel stiffened panel. The top and bottom (attached) flanges of the zee section are modeled as rod elements and the vertical web as a membrane element as shown in Figure 124. The effect of unsymmetry caused by the zee cross-sectional shape of the stringer is not considered. In this case only a quarter panel need be modeled for finite element analysis due to panel symmetry.

As mentioned in section 3.4, very good correlations were obtained between experimental and analytical results using the flexible fastener model. Thus, the flexible fastener model, slightly modified to account for the lands in the structure, was used for these panels. In the finite element modeling shear elements are provided at every rivet location. The depth of shear elements is made equal to the diameter of the rivet hole. In Section 3.1.3, (see Equation (1)) the formula for rivet deflection was given as:

$$\delta = \frac{pf}{E_a d}$$

and (see Equation (4) the constant f as:

$$f = 5.0 + 0.8\left(\frac{d}{t_1} + \frac{d}{t_2}\right)$$

where t_1 and t_2 are the thicknesses of the joined sheets. No data were available for rivet deflection for landed structure hence it was necessary to modify these formulas. The cross section of the actual structure is shown in Figure 125 (a). The structure is idealized (neglecting the curved portions of the land) as shown in Figure 125 (b).

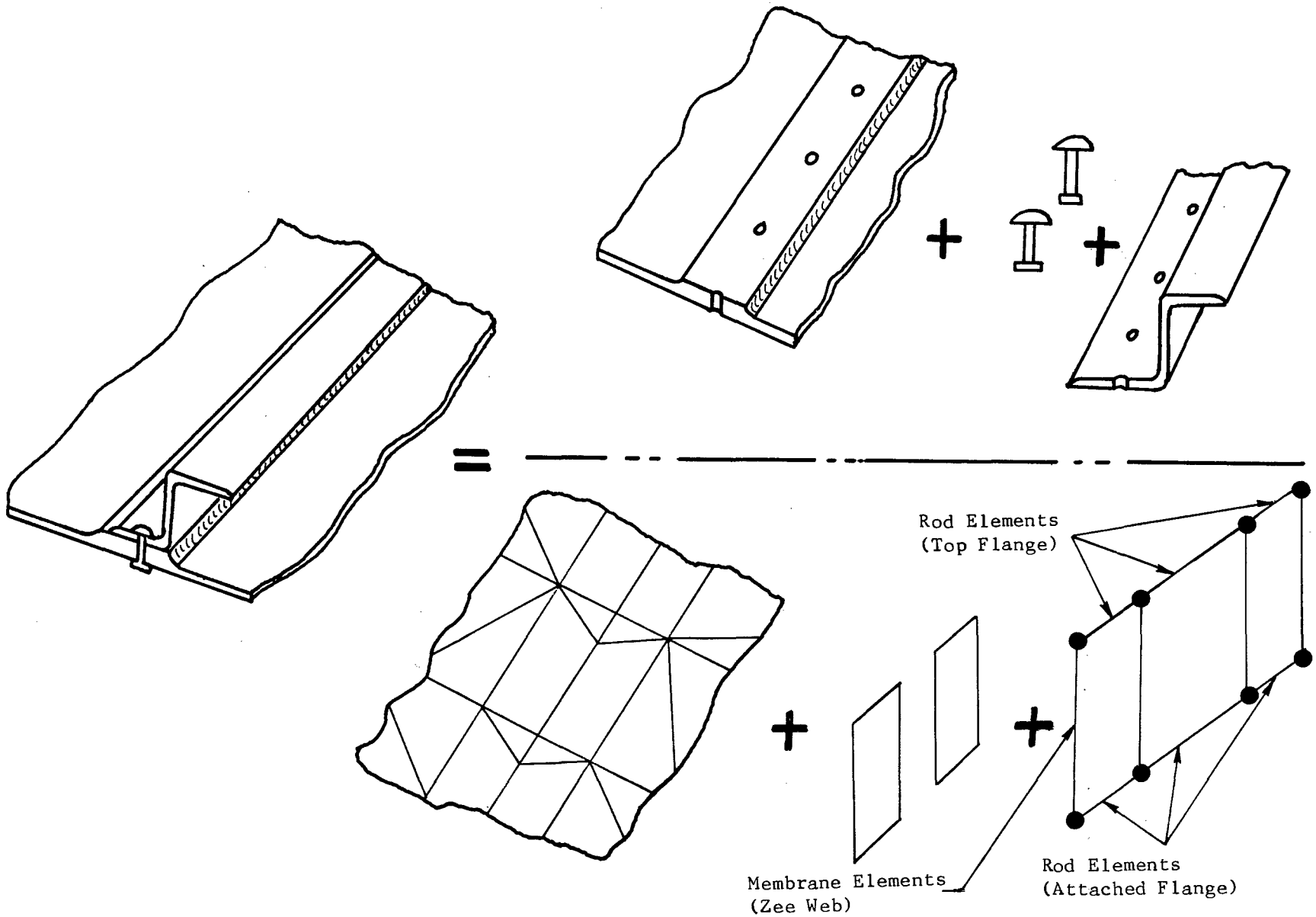

Figure 124. Finite Element Representation of Riveted Wing Panel, Zee Stiffened

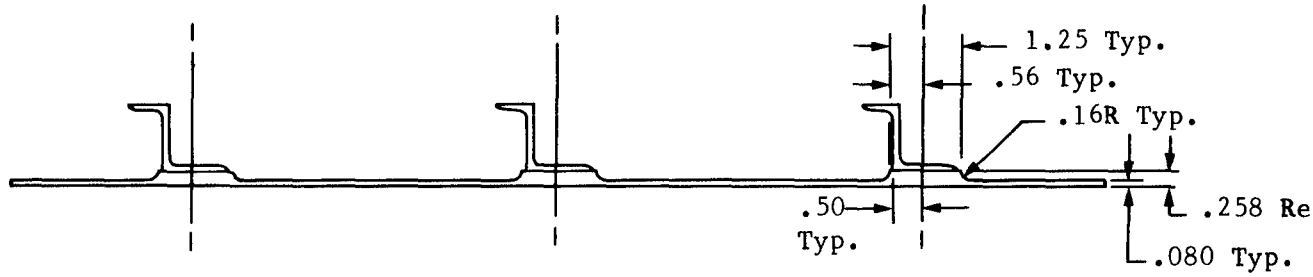

(a) Actual Structure

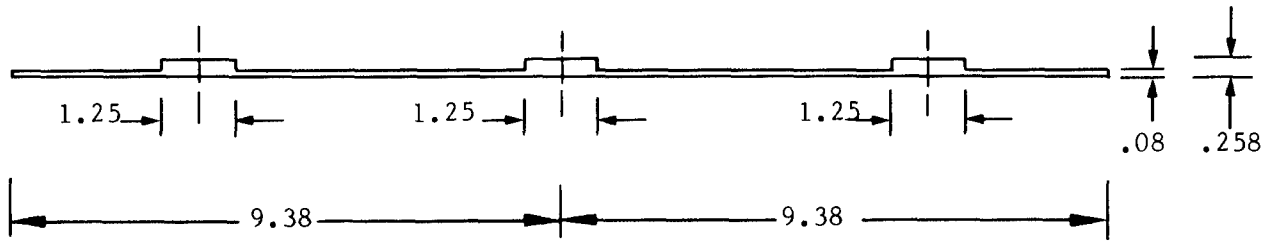

(b) Idealized Skin Structure

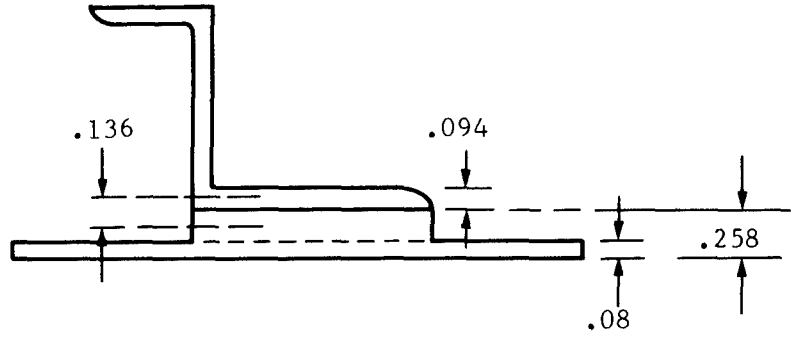

(c) Idealized Skin/Zee Structure

NOTE: All Dimensions in Inches

Figure 125. Cross Sectional Views of Zee Stiffened Panel for Structural Idealization

The thickness of the sheet, t_1 in Equation (4), is replaced by the average thickness of the panel where average thickness $t_{avg.}$ is given by:

$$t_{avg.} = \frac{\text{Skin area of the panel}}{\text{Width of the panel}}$$

$$= \frac{2(9.38") \times 0.08" + 3 \times 1.25" \ (0.258"-0.08")}{2(9.38")} = 0.11558".$$

From Figures 120 and 125(c) the thickness of connecting leg of the stiffener, $t_2 = 0.094$ inches and the rivet diameter used is 3/16 inches.

Substituting these values in Equation (4) results in the constant f being:

$$f = 7.8435.$$

The distance (h) between the centers of the sheets connected together is in this case the distance between the center lines of the attached stiffener leg thickness and thickness of the land extending from the sheet. Thus, for this landed case (see Figure 125(c))

$$h = \frac{0.094"}{2} + \tfrac{1}{2} (0.258" - 0.08")$$

$$= 0.136".$$

And the area of the shear element is given by Equation (3):

$$A_s = \frac{h}{G_a} \frac{E_a d}{f}$$

$$= \frac{0.136"}{7.8435} \ 2.66 \times \frac{3}{16}" D$$

where $E_a/G_a = 2.66$

$$A_s = 0.00864 \text{ inches}^2.$$

The depth of the shear element = 0.2 inch (approximately equal to the diameter of the rivet hole) and the thickness of the shear element is equal to:

$$\frac{A_s}{0.2"} = \frac{0.00864 \text{ inches}^2}{0.2"} = 0.0432".$$

The finite element grid actually used to model one-quarter of the panel is shown in Figure 126. The computer run time for one elastic run with a crack length of 4.25 inches was 6 minutes. A complete Dugdale model type elastic-plastic analysis with the same crack length and 8 load (or plastic zone) cases required approximately 35 minutes.

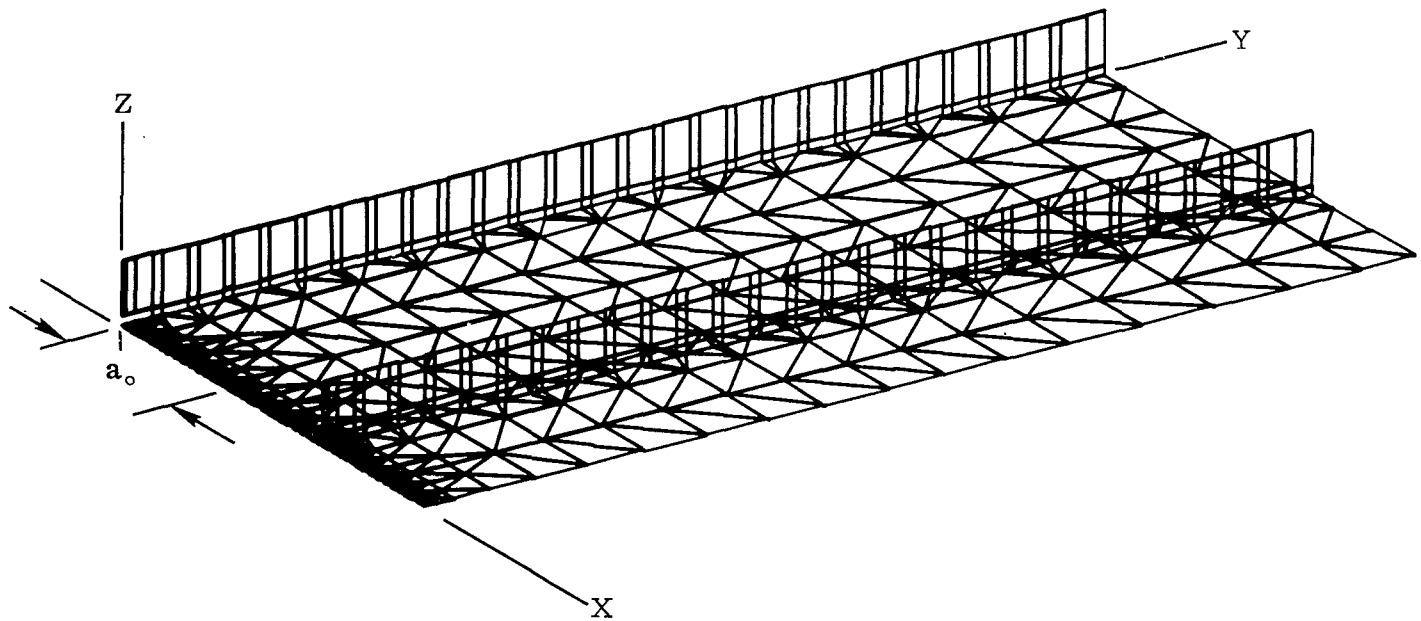

Figure 126. Finite Element Model of Riveted Zee Stiffened Panel

7.1.2 Elastic Analysis of Riveted Zee Stiffened Panel

An elastic analysis of the riveted panel was performed for various crack lengths. For comparative purposes stress intensity factors were obtained at these crack lengths using the crack surface displacements from the finite element analysis. These values will be used later for predictive purposes with the K_c failure criterion. The plane stress state of displacement in the vicinity of the crack tip under Mode I loading can be expressed as (Reference 56):

$$u = \frac{K_I}{G}\sqrt{\frac{r}{2\pi}}\ \frac{\cos\theta}{2}\left[\frac{1-\nu}{1+\nu} + \sin^2\frac{\theta}{2}\right]$$
$$v = \frac{K_I}{G}\sqrt{\frac{r}{2\pi}}\ \frac{\sin\theta}{2}\left[\frac{2}{1+\nu} - \cos^2\frac{\theta}{2}\right] \qquad (19)$$

where r and θ are local polar coordinates at the crack tip, u and v are displacements along the x and y axis, G is the shear modulus and ν Poisson's ratio.

Crack surface displacements can be determined within a reasonable degree of accuracy from the finite element analysis. Using these displacements the values of K_I are computed at various values of r. A curve is then plotted between K_I and r/a. The value of K_I is obtained by extrapolating this curve to r = 0. The stress intensity factors computed in this manner are shown in Figure 127, where elastic stress intensity factors are plotted as a function of crack length for various values of applied stress to yield strength ratio. It is seen that, for a fixed applied stress, the stress intensity factors increase as the crack length increases up to a half-crack length of approximately 4.75 inches. With further increase in crack length the stress intensity factors decrease since the crack surface displacements are influenced by the stiffener and the land. This decrease in stress intensity factors occurs to the point where the crack tip reaches the land (a = 5.625 inches) where with further increase in crack length the stress intensity factors increase once again. This elastic analysis has been performed so that predictions of residual strength could be made based on elastic behavior and to compare those results with predictions based on elastic-plastic analysis and experimental data.

7.1.3 Elastic-Plastic Analysis of Riveted Zee Stiffened Panel

The riveted, zee stiffened panel was analyzed assuming a Dugdale type plastic zone ahead of the crack tip using the Bueckner-Hayes energy approach discussed in Section 3.3.1.1. Figures 128 and 129 show the variation of square root of J with applied stress to yield strength ratio (p/F_{ty}) for various crack lengths. These curves have been cross plotted in Figure 130, where the variation of square root of J is shown with physical crack length for constant applied stresses. The trend of these curves is quite similar to the elastic stress intensity factors curves shown in Figure 127. At a constant applied load the values of square root of J increase with crack length up to a physical half crack-length of approximately 4.5 inches. Further increase in crack length results in decreasing values of square root of J due

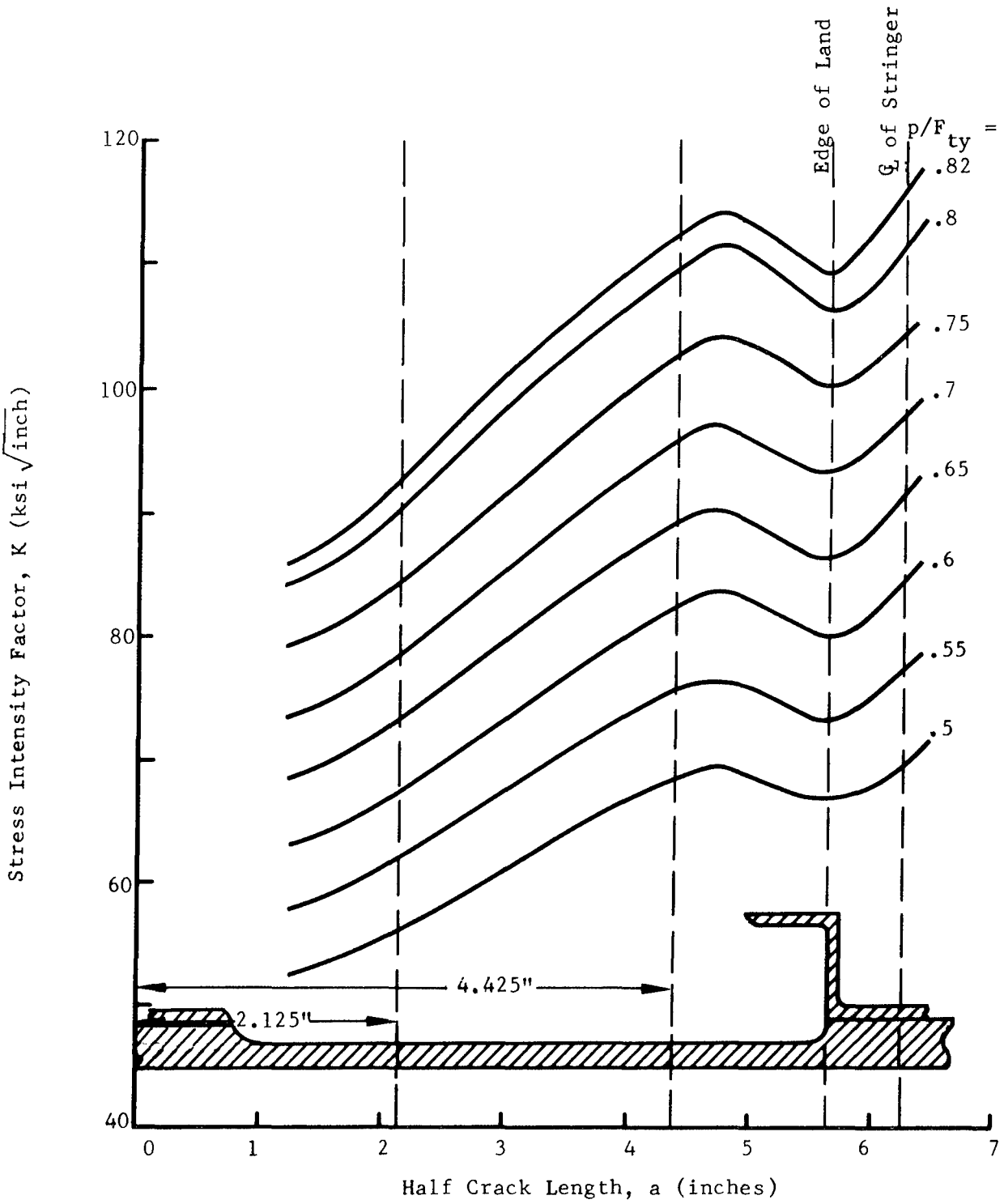

Figure 127. Stress Intensity Factor Analysis for Riveted Zee Stiffened Panel

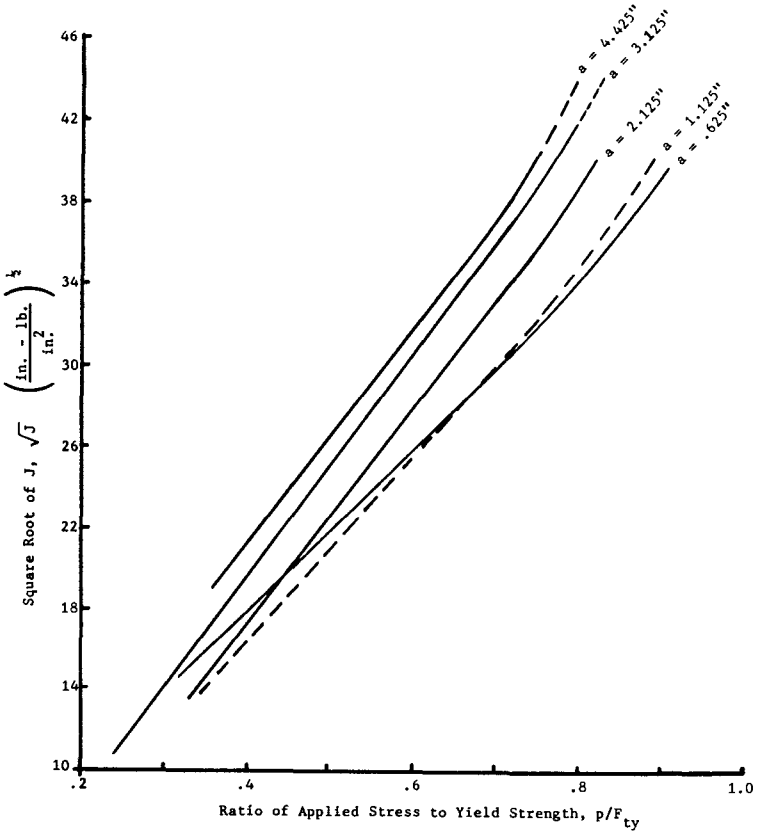

Figure 128. Square Root of J for Riveted Zee Stiffened Panel as a Function of Applied Stress a = .625 to 4.425 Inches

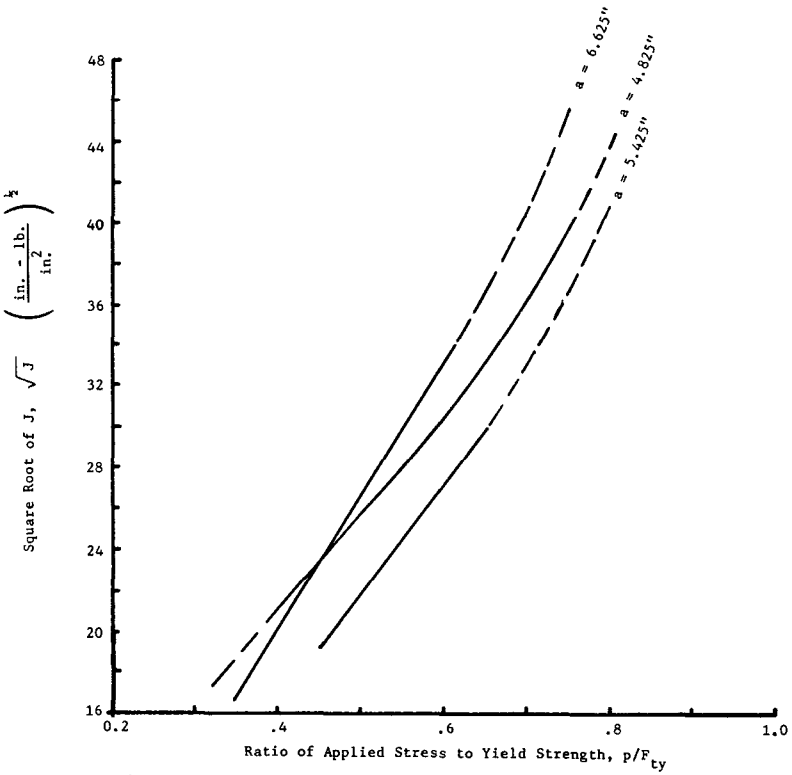

Figure 129. Square Root of J for Riveted Zee Stiffened Panel as a Function of Applied Stress a = 5.425 to 6.625 Inches

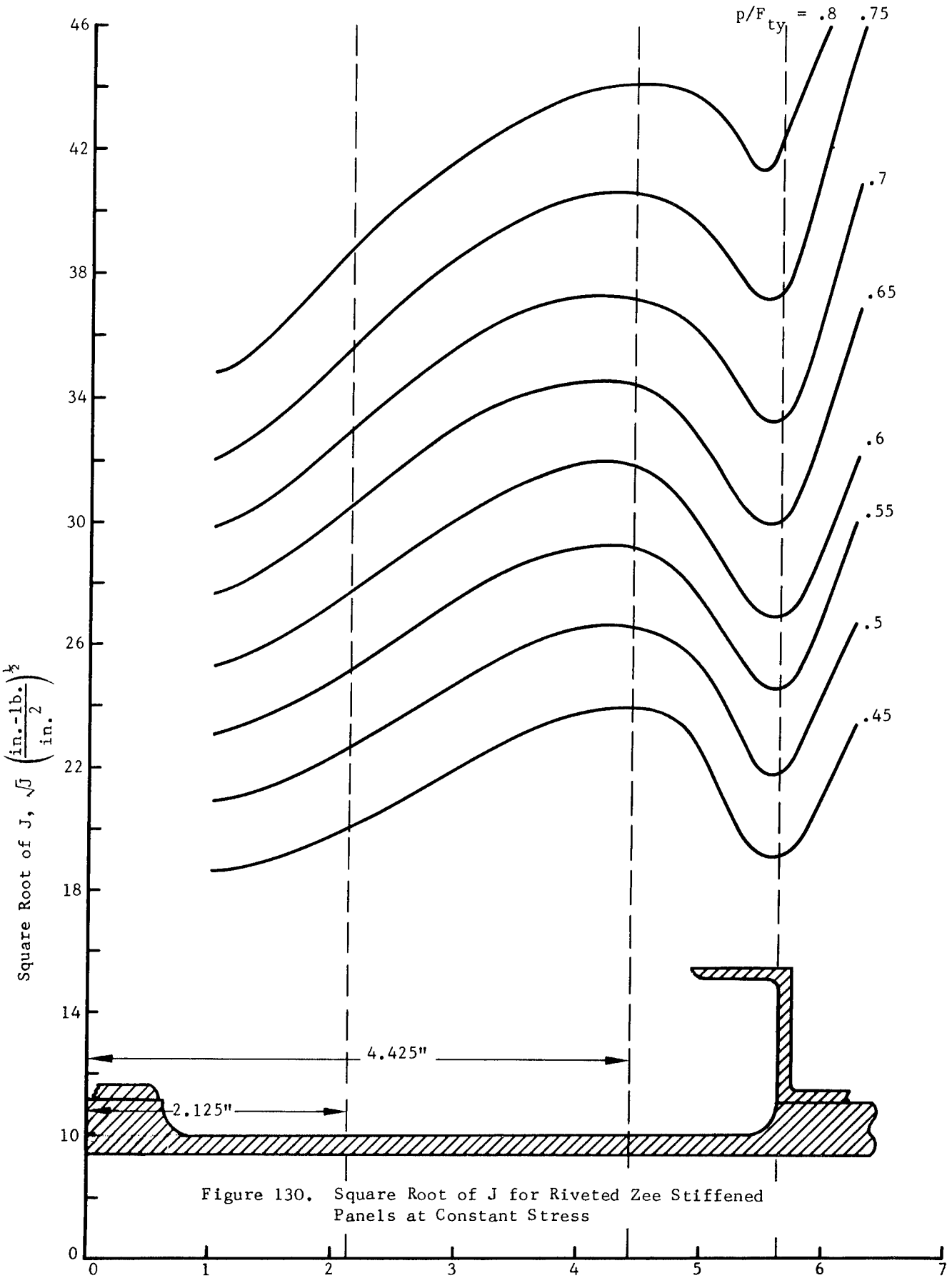

Figure 130. Square Root of J for Riveted Zee Stiffened Panels at Constant Stress

to the influence of land and stiffener. The value of the square root of J decreases to a half crack length of 5.625 inches or up to the point when the crack tip reaches the edge of the land. With further increase in crack length the value of square root of J increases. The curves shown in Figure 130 in combination with the $\sqrt{J_R}$ resistance curve for the material form the basis for the residual strength prediction procedure discussed in Section VIII.

Prandtl-Reuss elasto-plastic material behavior assumptions were made and the analysis carried out for one value of half crack length, 2.125 inches. The variation of $\sqrt{J}$ with applied normalized stress p/F_{ty} was compared for elastic, Prandtl-Reuss, and Dugdale behavior and is shown in Figure 131. At an applied stress of 75 percent of the yield strength Prandtl-Reuss values are approximately 13 percent higher than elastic values whereas those values based on Dugdale assumptions are 17 percent higher than corresponding elastic values. The Dugdale model results are very close to those based on Prandtl-Reuss material behavior. The Prandtl-Reuss results are between elastic and assumed Dugdale values to an applied stress of 80 percent of yield. Thus, if J critical were used as a fracture criterion, assumed Dugdale and Prandtl-Reuss behavior would predict conservative values of residual strength which will be shown to be within 4 to 5 percent of those obtained experimentally using Dugdale $\sqrt{J}$ values.

7.1.4 Comparison of Experimental and Analytical Results of Riveted, Zee Stiffened Panel

Table XVI shows the location of strain gages and deflection gages on the two riveted, zee stiffened panels. Also tabulated are the strain gage readings for various applied loads at half crack lengths of 2.125 inches and 4.425 inches. Figure 132 shows the experimental and analytical variation of strain in the central stringer with increasing distance from the crack for a half crack length of 2.125 inches. Good correlation was obtained between analytical and experimental strains near the crack surfaces (e.g. gages 9 and 6). However, further away from the crack surfaces, analytical strains are about 16 percent higher. A similar plot of strains for a half crack length of 4.425 inches is shown in Figure 133. In this case there is considerable difference between predicted and experimental strains. There are several factors which may cause this discrepancy:

1. Inplane buckling around the crack due to the presence of the large crack.

2. Bending in the experimental setup. It can be noted that the strain data away from the crack are smaller than the analytical strains. At a distance of 5 inches away from the crack surface the analytical strains reduce to the strains corresponding to applied gross area boundary stresses. It would be anticipated that the experimental strains would be equal to these values at that point; however, since the experimental strains are lower it would indicate that some slight bending occurred in the experimental setup which was not accounted for in the analysis.

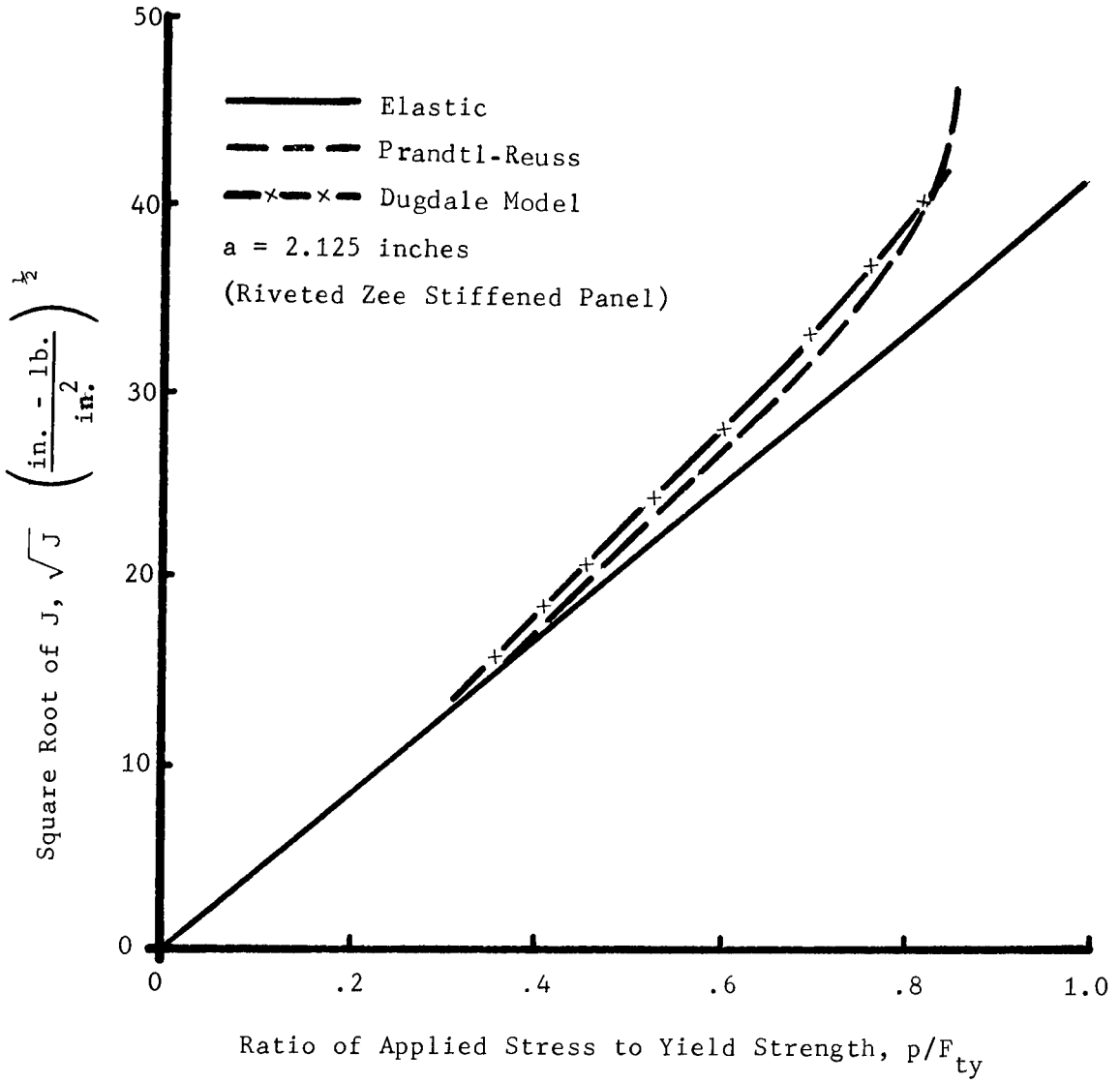

Figure 131. Comparison of Elastic, Prandtl-Reuss and Dugdale Calculated $\sqrt{J}$ Values for Riveted Zee Stiffened Panel - a = 2.125 Inches

TABLE XVI. RIVETED ZEE STIFFENED PANEL STRAIN GAGE DATA

PANEL NUMBER	LOAD	GAGE LOCATION AND STRAIN inches/inch X10^3																					
	(KIPS)	①	②	③	④	⑤	⑥	⑦	⑧	⑨	⑩	⑪	⑫	⑬	⑭	⑮	⑯	⑰	⑱	⑲	⑳	㉑	㉒
3-2-1	ZERO	0	0	0	0	0	0	0	0	0	.10	0	0	.012	.016	.017	.014	.051	.032	.016	.091	.059	.014
(a = 2.15")	5.24	.10	.20	.19	.20	.25	.24	.15	.20	.32	.10	.20	.20	.172	.134	.136	.149	.152	.154	.168	.223	.696	.165
	9.98	.20	.35	.35	.30	.35	.46	.20	.40	.63	.25	.30	.35	.337	.260	.264	.290	.289	.297	.325	.361	.335	.312
	14.98	.40	.55	.52	.40	.55	.68	.35	.60	.95	.40	.45	.50	.504	.394	.400	.438	.438	.448	.490	.501	.477	.467
	20.0	.55	.70	.70	.55	.75	.92	.40	.80	1.25	.50	.60	.65	.681	.526	.537	.592	.590	.606	.658	.640	.617	.622
	24.96	.60	.85	.88	.65	.90	1.10	.55	1.00	1.55	.70	.75	.80	.846	.662	.673	.747	.743	.763	.825	.773	.758	.777
	30.0	.85	1.05	1.08	.80	1.10	1.32	.70	1.20	1.80	.85	.95	1.00	1.021	.799	.817	.908	.907	.925	.989	.907	.898	.934
	35.2	.95	1.20	1.20	1.00	1.30	1.50	.80	1.40	2.02	.95	1.05	1.15	1.189	.939	.958	1.065	1.064	1.086	1.124	1.041	1.035	1.085
	40.0	1.15	1.40	1.38	1.15	1.50	1.65	1.00	1.65	2.20	1.10	1.20	1.30	1.352	1.070	1.093	1.213	1.223	1.248	1.300	1.171	1.169	1.227
	45.0	1.30	1.60	1.50	1.35	1.70	1.80	1.15	1.90	2.42	1.30	1.40	1.50	1.517	1.203	1.232	1.356	1.387	1.411	1.450	1.301	1.303	1.370
	50.0	1.45	1.85	1.60	1.50	1.95	1.90	1.25	2.10	2.53	1.50	1.60	1.60	1.676	1.330	1.364	1.498	1.551	1.579	1.593	1.428	1.438	1.510
FRACTURE	110.0	4.95	4.70	2.20	8.85	9.80	2.95	5.60	+10	4.75	+10	10.0	4.45	-	-	-	-	-	-	-	-	-	-
3-2-2	ZERO	0	0	.05	0	.05	0	.05	0	0	0		0	.002	.007	-.015	.010	-.013	-.014	.008	-.020	-.007	-.013
(a = 4.425")	5.40	.05	.15	.20	.05	.10	.35	0	.2	.55	.10		.20	.186	.118	.144	.167	.105	.164	.191	.152	.148	.194
	10.0	.10	.30	.50	.05	.35	.70		.35	.90	.20		.30	.383	.225	.271	.322	.263	.334	.387	.268	.272	.360
	15.0	.20	.50	.75	.05	.55	1.00		.60	1.30	.35		.45	.573	.379	.421	.537	.396	.470	.568	.376	.403	.496
	20.0	.30	.70	.95	.15	.75	1.40		.85	1.70	.50		.70	.756	.501	.576	.725	.561	.657	.745	.518	.546	.648
	25.0	.40	.85	1.15	.20	.95	1.75		1.10	2.00	.65		.85	.951	.640	.727	.922	.729	.836	.917	.655	.693	.801
	30.0	.50	1.05	1.30	.25	1.15	2.00		1.35	2.35	.80		1.05	1.140	.886	.875	1.081	.889	1.029	1.098	.800	.834	.956
	35.0	.60	1.30	1.45	.35	1.45	2.20		1.60	2.70	1.00		1.25	1.326	.911	1.037	1.229	1.084	1.231	1.274	1.068	1.000	1.125
	40.0	.75	1.50	1.55	.40	1.65	2.40		1.80	3.05	1.15		1.40	1.480	1.028	1.170	1.365	1.256	1.420	1.418	1.081	1.124	1.271
	45.0	.85	1.75	1.70	.50	1.90	2.60		2.05	3.40	1.35		1.60	1.639	1.168	1.306	1.487	1.454	1.606	1.572	1.223	1.276	1.414
	50.0	1.00	1.95	1.85	.60	2.15	2.80		2.30	3.80	1.50	BAD GAGE	1.70	1.783	1.289	1.422	1.618	1.640	1.800	1.720	1.377	1.430	1.552
	55.0	1.15	2.15	2.05	.65	2.40	3.05		2.60	4.20	1.70		1.90										
	60.0	1.25	2.40	2.20	.70	2.65	3.30		2.90	4.55	1.90		2.05										
	65.0	1.40	2.50	2.30	.80	3.05	3.45		3.40	4.70	2.10		2.20										
	70.0	1.60	3.00	2.35	.90	3.50	3.50	0	4.20	4.80	2.15		2.45										
	73.0	1.80	3.20	2.35	1.10	3.80	3.45	.10	4.60	3.10	2.35		2.70										
	* 73.8	2.30	3.10	.85	2.10	2.85	1.05	1.75	3.35	1.30	2.30		3.20										
	70.5	2.40	2.45	.80	2.20	2.80	.95	1.80	3.30	1.20	2.30		3.25										
	72.5	2.55	2.40	.70	2.40	2.70	.75	2.05	3.10	1.15	2.40		3.60										
	75.0	2.65	2.35	.60	2.55	2.55	.70	2.30	2.80	1.05	2.60		4.05										
3-2-2	77.0	2.80	2.30	.55	2.80	2.50	.60	2.65	2.70	1.00	3.30		4.75										

* CRACK RAN & ARRESTED @ EDGE ZEE STIFFENERS - READINGS AFTER ARRESTMENT

TABLE XVI. RIVETED ZEE STIFFENED PANEL STRAIN GAGE DATA (CONTINUED)

PANEL NUMBER	LOAD (KIPS)	GAGE LOCATION AND STRAIN inches/inch X10^3					
		(23)	(24)	(25)	(26)	(27)	(28)
3-2-1	ZERO	-.009	.084	.054	.014	.006	.016
(a = 2.15")	5.24	.148	.205	.185	.156	.135	.158
	9.98	.294	.338	.326	.296	.280	.300
	14.98	.449	.475	.467	.444	.434	.450
	20.0	.606	.608	.609	.590	.590	.599
	24.96	.767	.741	.750	.739	.748	.748
	30.0	.929	.874	.896	.888	.910	.900
	35.2	1.097	1.004	1.033	1.033	1.075	1.047
	40.0	1.257	1.100	1.169	1.171	1.233	1.185
	45.0	1.425	1.260	1.310	1.315	1.397	1.322
	50.0	1.593	1.390	1.448	1.453	1.563	1.450
3-2-2	ZERO	.010	.014	-.003	-.007	-.026	.010
(a = 4.425")	5.40	.148	.085	.146	.136	.181	.155
	10.0	.318	.239	.245	.302	.347	.312
	15.0	.461	.349	.361	.436	.481	.465
	20.0	.623	.458	.505	.592	.648	.639
	25.0	.762	.604	.651	.738	.791	.765
	30.0	.916	.733	.805	.882	.881	.946
	35.0	1.087	.894	.924	1.046	1.104	1.110
	40.0	1.248	1.025	1.078	1.194	1.238	1.251
	45.0	1.383	1.178	1.206	1.325	1.397	1.377
3-2-2	50.0	1.537	1.324	1.362	1.476	1.562	1.518

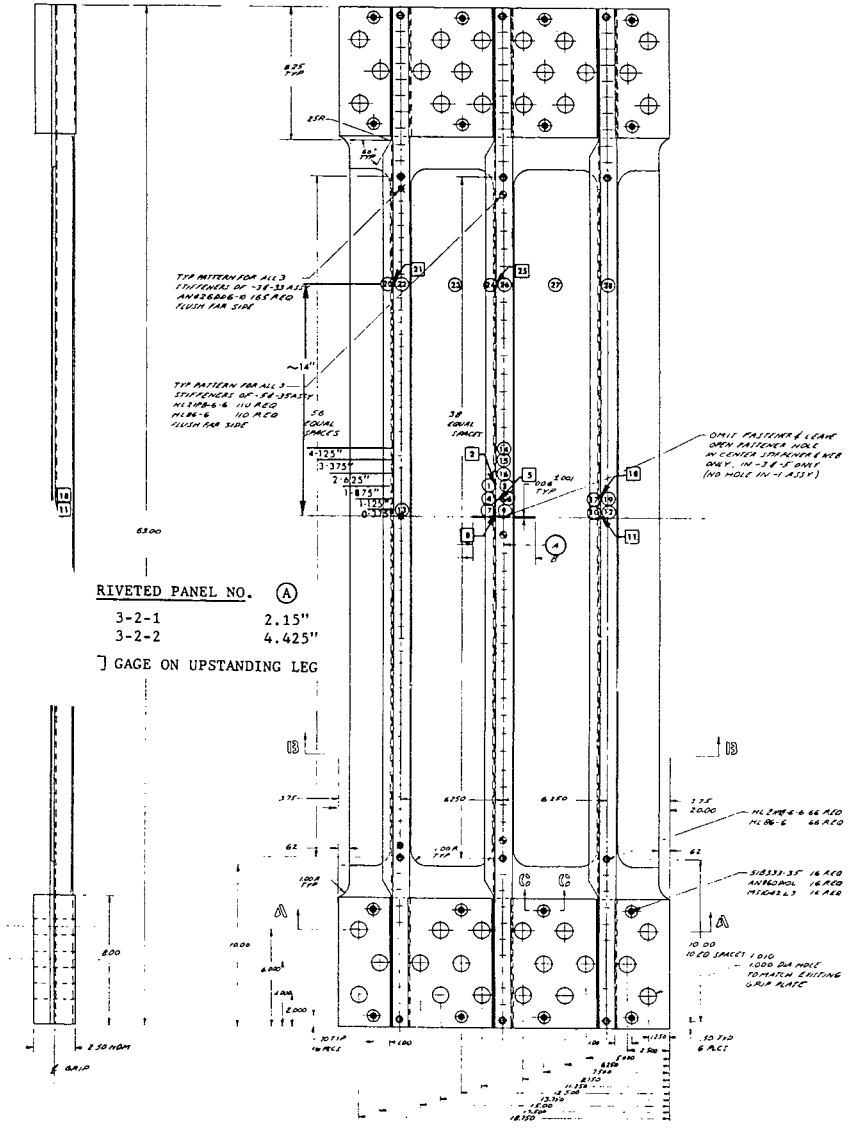

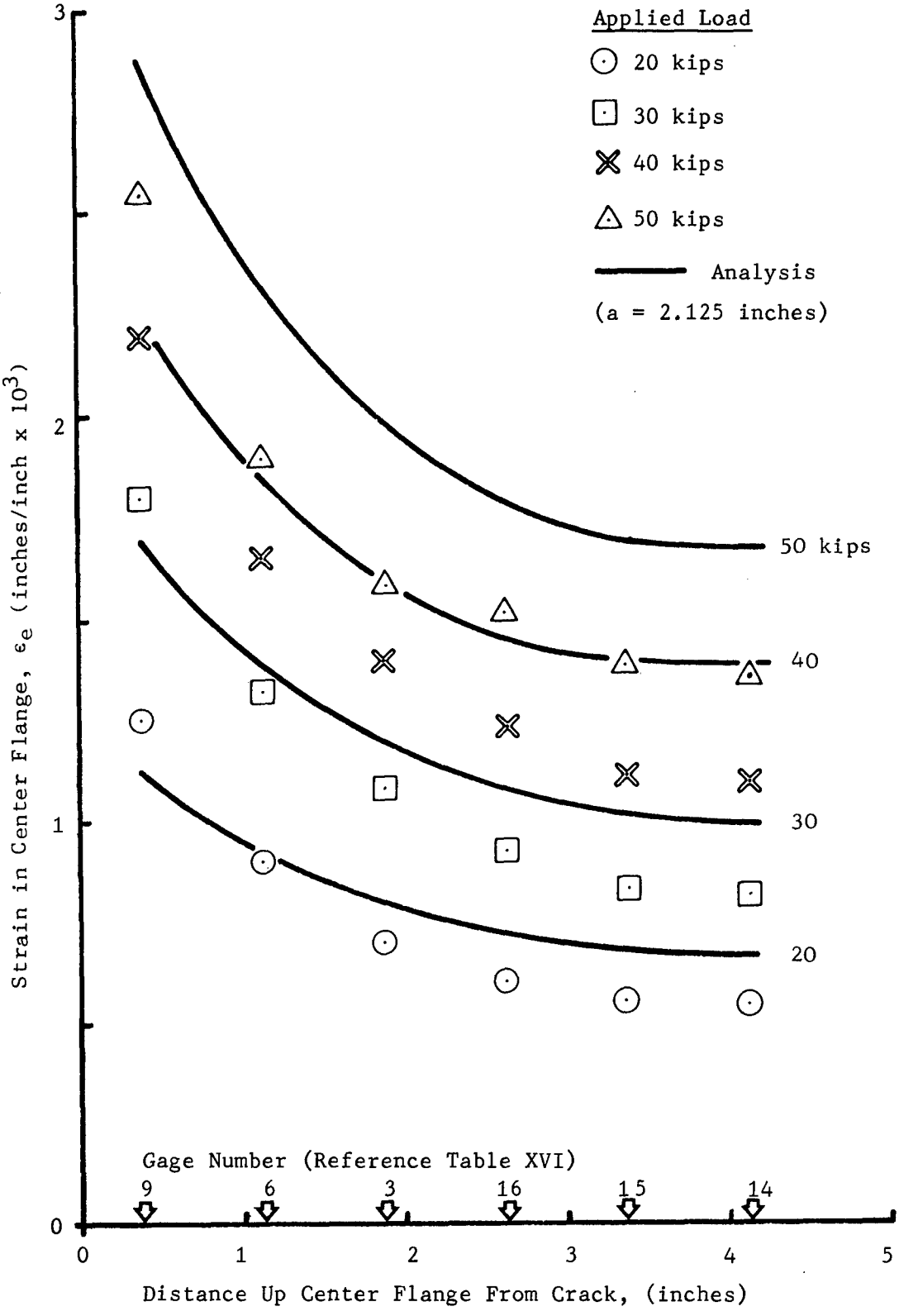

Figure 132. Strain in Central Stringer for Riveted Zee Stiffened Panel - a = 2.125 Inches

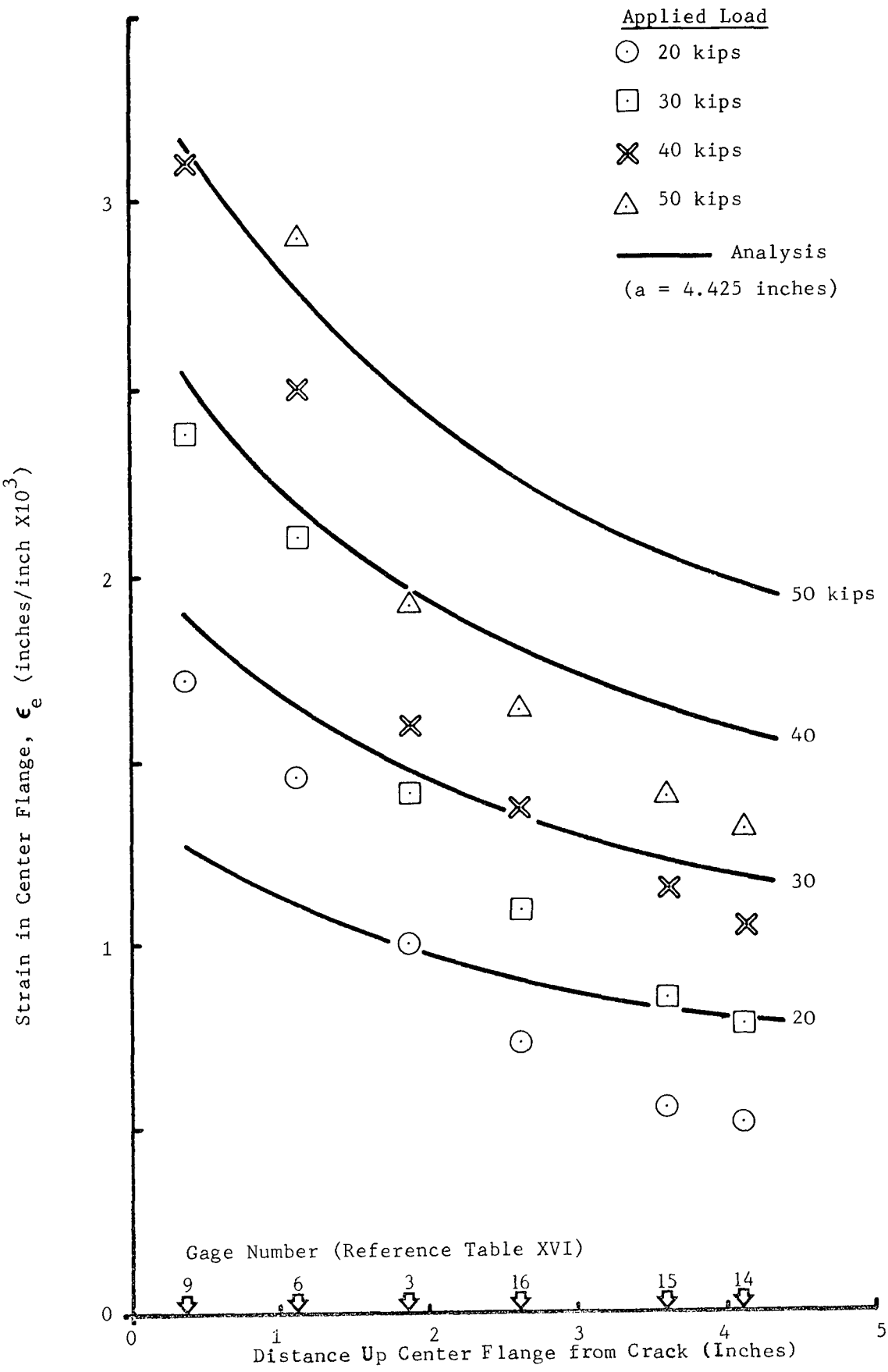

Figure 133. Strain in Central Stringer for Riveted Zee Stiffened Panel - a = 4.425 Inches

The variation of strains in the central and outer stringers, at the panel centerline is shown as a function of applied stress in Figures 134 and 135. Also shown are the elastic analytical strains in the stringers and strains based on a Dugdale type elastic-plastic analysis. At a half crack length of 2.125 inches the Dugdale type analysis gives very good correlation with experimental strains in the central stringer to an applied stress of 16 ksi. Beyond this stress experimental data is not available as the load was not recorded on tape for this one panel. However, a good correlation was obtained between experimental strain at failure (peak load) and strain obtained from Prandtl-Reuss assumptions. It should be noted however, that the half crack length at failure will be longer than 2.125 inches due to slow crack extension; hence, this correlation between experimental and analytical strains may be fortuitous.

For the 2.125 inch half crack length, the strain data from the outer stringer (Figure 135) show good correlation with analytical results based on assumed Dugdale and Prandtl-Reuss material behaviors. This is due to the elastic behavior of the outer stringer up to failure as indicated by the experimental data and similar assumption in the analysis.

For a half crack length of 4.425 inches (see Figure 134) the strains in the central stringer (again at the centerline of the crack) show good correlation between experimental and analytical results, using the Dugdale model, up to an applied stress of 20 ksi. At higher stresses there is considerable slow crack growth which renders further use of the Dugdale analysis invalid. At an applied stress of 24.8 ksi the central stringer broke and the crack ran. The strains in the outer stringer (Figure 135) show a good correlation with Dugdale type analysis to an applied stress of 24.5 ksi or the stress at which the central stringer broke. As the central stringer breaks, the outer stringer strains increase rapidly (see Figure 135). Note that in the outer stringer even the elastic analytical strains for the broken central stringer analysis are considerably higher than the strains for the intact stringer case. Further increase in load results in the outer stringer undergoing large plastic deformation and it fails at an applied stress of 25.98 ksi.

7.2 BOLTED ZEE STIFFENED PANEL

The bolted panel was analyzed assuming both elastic and elastic-plastic behavior. The analysis and experimental data of this panel is discussed in the following subsections.

7.2.1 Finite Element Modeling of Bolted Zee Stiffened Panel

The only difference in the finite element modeling of riveted and bolted panels was the spacing of the fasteners. In this case the pitch of the HI-LOKS was 1.105 inches. The HI-LOKS were modeled as shear elements and provided in the finite element analysis at every HI-LOK location. The flexible fastener model was used to model these shear elements. In the model the shear element representing the HI-LOK was assumed to have the same flexibility as in the previously studied riveted panel. The finite element model of this bolted, zee stiffened panel is shown in Figure 136.

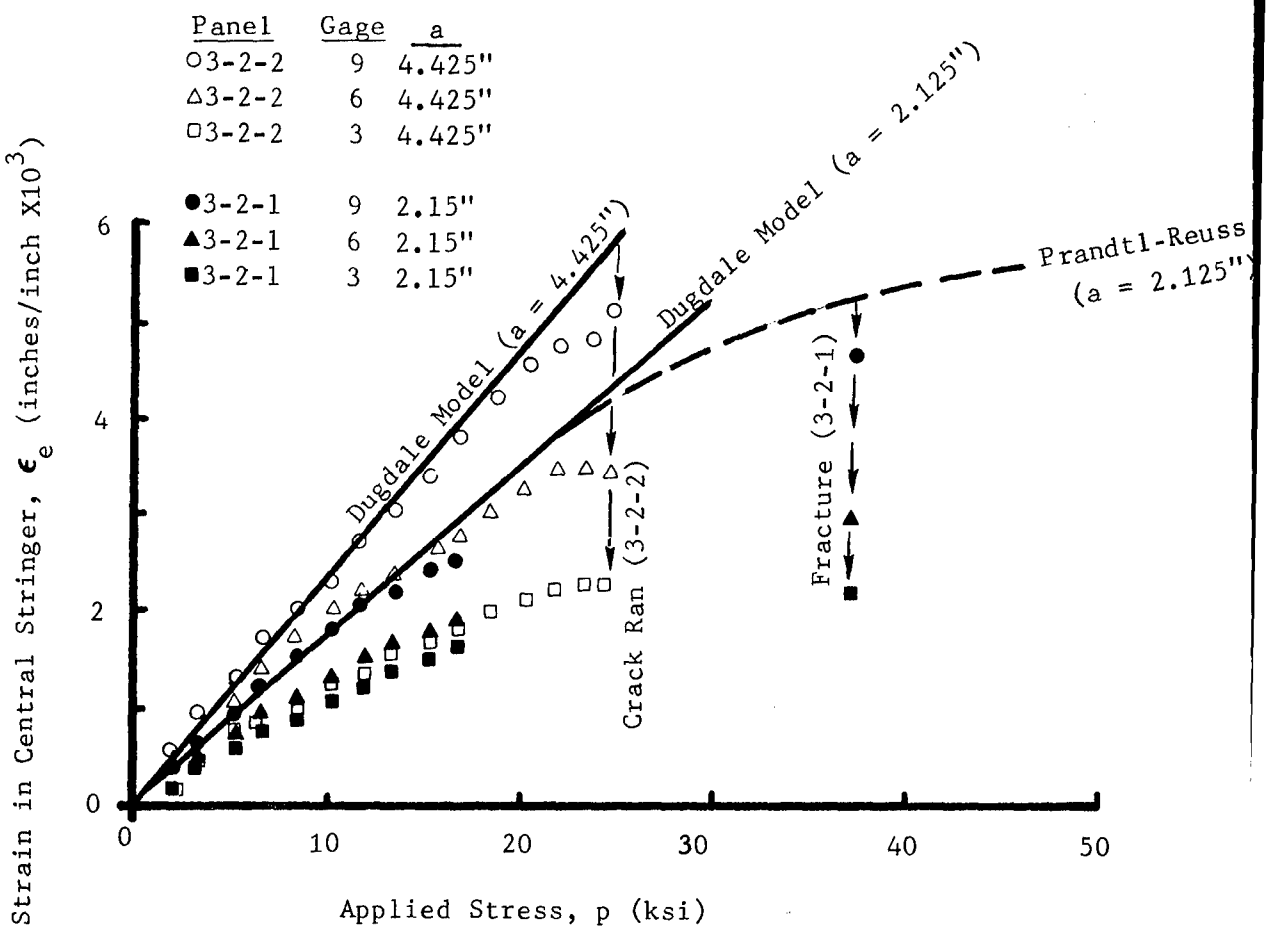

Figure 134. Strain in Central Stiffener as Function of Applied Stress, Riveted Zee Stiffened Panels

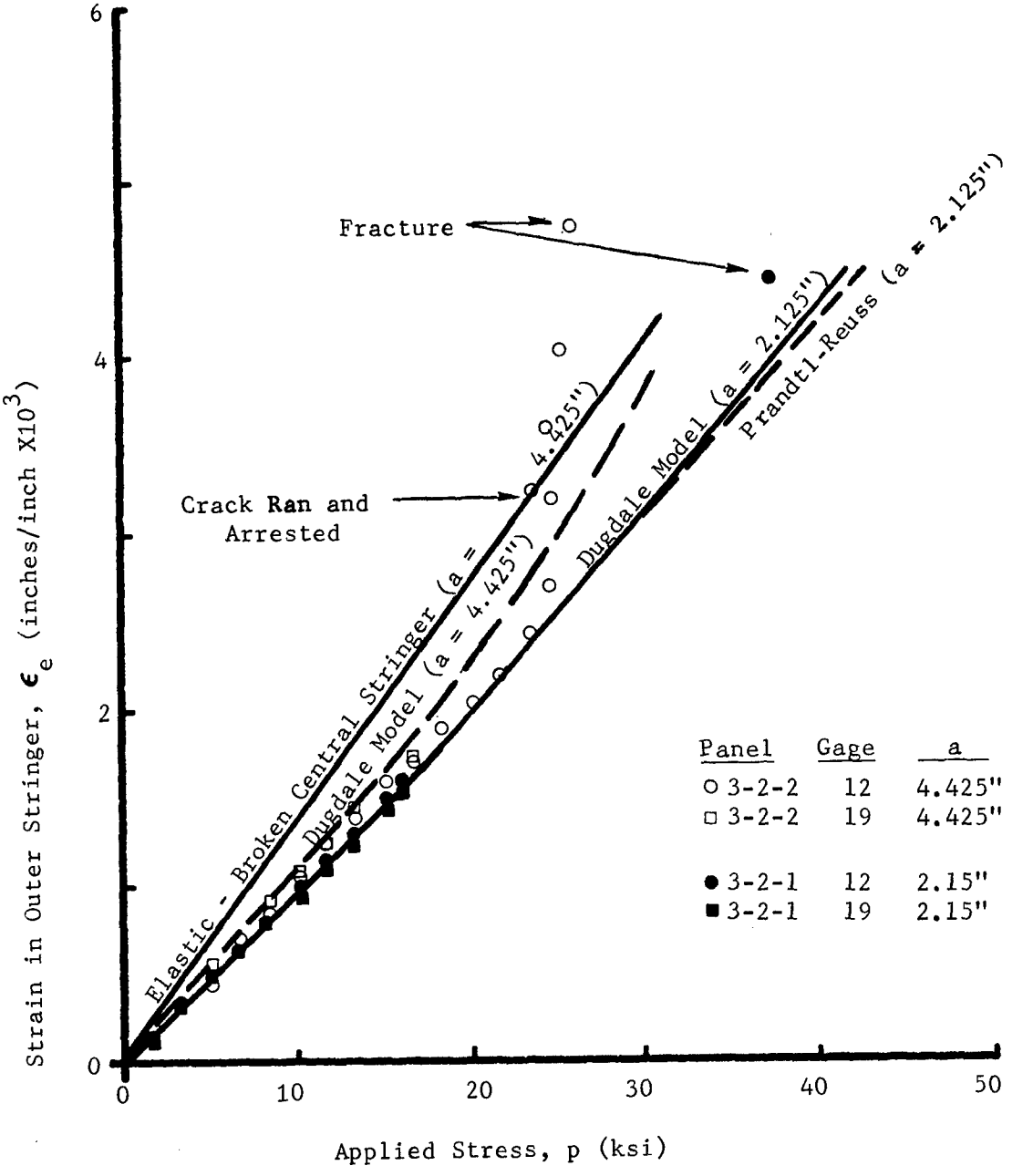

Figure 135. Strain in Outer Stiffener as a Function of Applied Stress, Riveted Zee Stiffened Panels

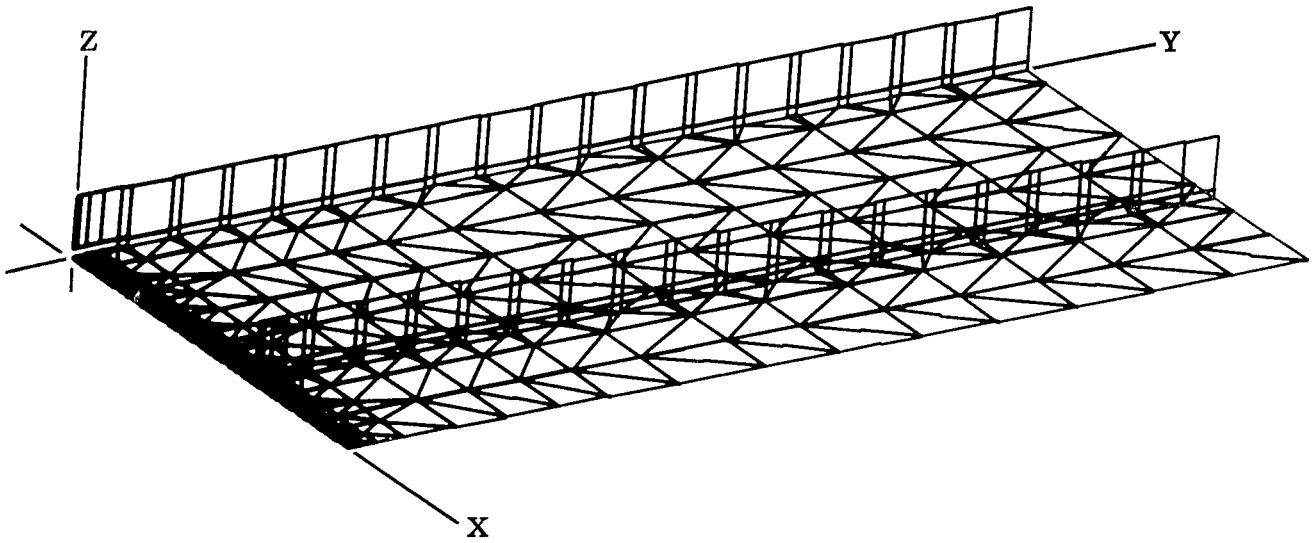

Figure 136. Finite Element Model of Bolted Zee Stiffened Panel

7.2.2 Analysis of Bolted Zee Stiffened Panel

The elastic analysis of the bolted panel was carried out for half crack lengths of 2.125 and 4.625 inches. A comparison was made of the elastic analysis for the riveted and bolted panels at a half crack length of 2.125 inches. This comparison showed a variation of less than 2 percent in square root of J; thus an elastic-plastic analysis of the bolted panel was not felt warranted for this crack length, and it was assumed that the analysis would be the same as for the riveted panel. However, due to additional fatigue precracking a half crack length of 4.625 inches was obtained for the longer crack length bolted panel. The corresponding riveted panel elastic-plastic analysis was not available at this crack length; therefore, the bolted panel was analyzed using the tested half crack length of 4.625 inches assuming a Dugdale type elastic-plastic analysis. Figure 137 shows the variation of $\sqrt{J}$ with normalized applied stress ratio (p/F_{ty}) for elastic and Dugdale behavior. Dugdale $\sqrt{J}$ values differ slightly from computed elastic values which is primarily due to the crack tip being in proximity to the land (within one inch). Figure 137 also shows the $\sqrt{J}$ values for the riveted panel with half-crack length of 4.425 inches. These values are only slightly lower than the bolted panel (half crack length of 4.625 inches). Thus, the elastic-plastic analysis for riveted and bolted panels may be assumed to be similar.

7.2.3 Comparison of Experimental and Analytical Results of Zee Stiffened Bolted Panel

The location of strain gages for the bolted zee-stiffened panels is shown in Table XVII. Also indicated are the strain values in the central and outer stringers at several locations for various applied loads. Figures 138 and 139 show the variation of experimental and analytical strain with applied stress for the central and outer attached flange of the zee stiffeners. Good correlation is obtained between Dugdale analytical and experimental strains for a half crack length of 2.125 inches to an applied stress of 20 ksi. (A difference of 0.075 inches occurs between actual and analytical crack size which is not considered important for this short crack length.) At higher applied stresses the experimental strains are smaller than those given by the Dugdale type analysis. For longer crack lengths an excellent correlation is obtained between experimental and analytical central stringer strains up to panel failure. The outer stringer strains (Figure 139) show a considerable variation from the predicted strain values. It can also be noted that the experimental data for a half crack length of 2.05 inches is displaced at a constant value from the Dugdale analytical results to an applied stress of approximately 25 ksi. A linear curve drawn through the experimental data does not pass through the origin therefore it would appear that there was some error in recording the output strain data on tape. At the longer crack length (4.625 inches) the outer stringer strain gages show good correlation with Dugdale analytical results to a stress of 10 ksi. At 10 ksi and beyond the experimental results show a larger data scatter. This panel was inadvertently placed in compression loading prior to fracture which could explain this large data scatter at higher loads.

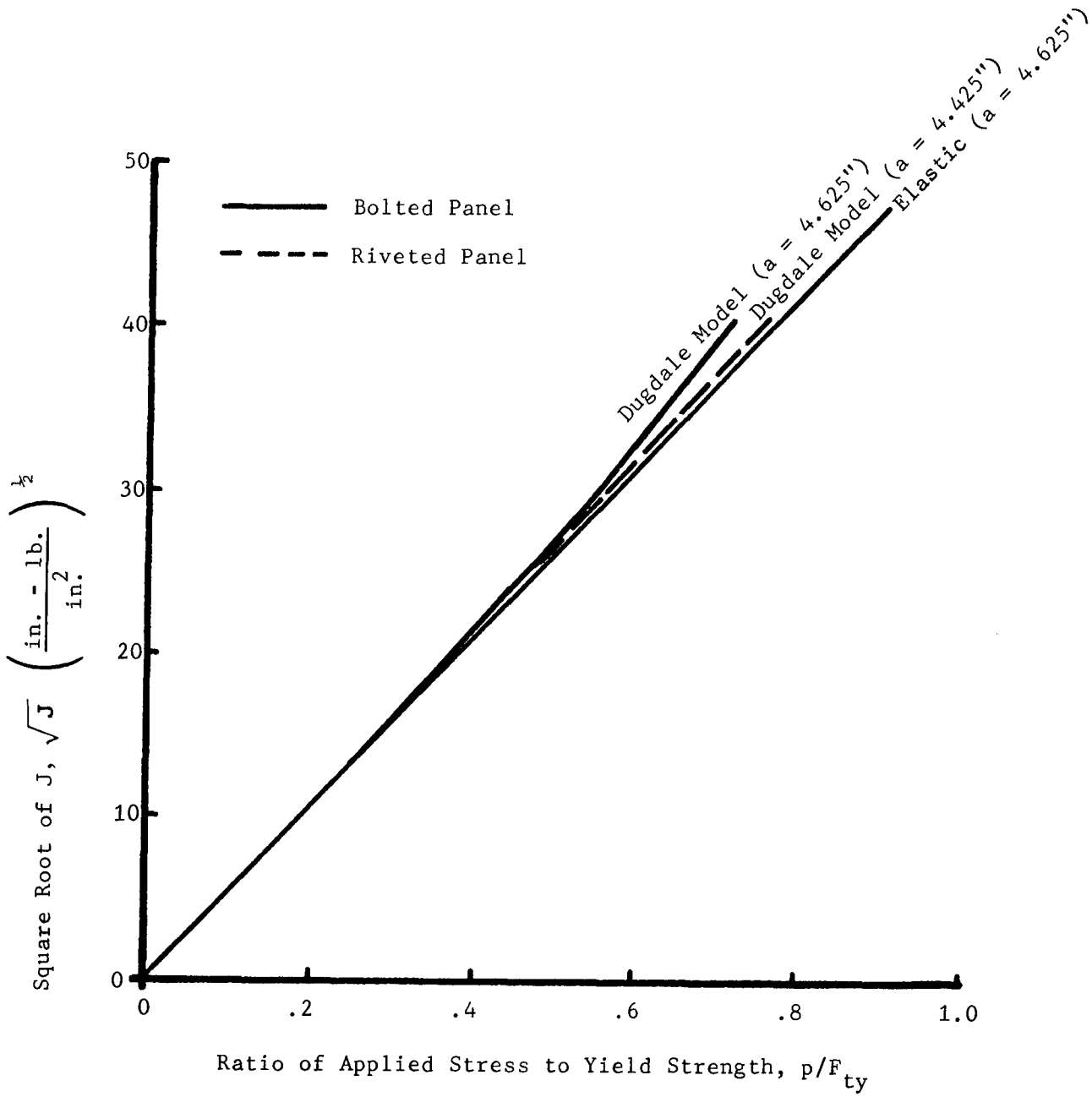

Figure 137. Comparison of Riveted and Bolted Elastic and Elastic-Plastic Square Root of J Values

TABLE XVII. BOLTED ZEE STIFFENED PANEL STRAIN GAGE DATA

PANEL NUMBER	LOAD (KIPS)	GAGE LOCATION & STRAIN X10^3 inches/inch																					
		①	②	③	④	⑤	⑥	⑦	⑧	⑨	⑩	⑪	⑫	⑬	⑭	⑮	⑯	⑰	⑱	⑲	⑳	㉑	㉒
3-3-1	ZERO	0	0	.05	0	0	.05	0	0	.05	0	0	.05	.015	-.006	-.002	.005	-.008	-.010	0	.007	.002	.016
(a = 2.05")	5.0	.28	.20	.10	.20	.15	.15	.15	.10	.15	.20	.20	.15	.114	.143	.154	.146	.153	.185	.164	.162	.154	.164
	12.0	.70	.35	.15	.50	.40	.25	.40	.20	.35	.45	.20	.35	.338	.330	.340	.350	.374	.446	.374	.370	.360	.386
	17.6	1.05	.55	.35	.70	.65	.45	.55	.20	.55	.70	.40	.55	.486	.479	.482	.500	.550	.615	.556	.520	.509	.564
	20.0	1.18	.60	.35	.80	.60	.55	.60	.45	.60	.80	.25	.60	.589	.564	.570	.596	.647	.732	.665	.616	.602	.649
	25.4	1.50	.80	.50	1.05	.80	.60	.78	.60	.80	1.15	.45	.80	.746	.700	.699	.742	.805	.904	.835	.750	.741	.797
	30.0	1.78	1.05	.65	1.20	1.00	.80	.90	.75	.95	1.40	.60	.90	.888	.830	.830	.902	.955	1.047	1.006	.882	.869	.925
	35.0	2.05	1.20	.80	1.40	1.20	.95	1.05	.95	1.10	1.75	.80	1.10	1.055	.960	.968	1.090	1.139	1.196	1.176	1.023	1.016	1.093
	40.0	2.30	1.45	.95	1.58	1.40	1.10	1.20	1.10	1.25	2.20	.95	1.20	1.234	1.111	1.118	1.236	1.324	1.365	1.356	1.178	1.176	1.251
	50.0	2.80	1.90	1.25	1.88	1.85	1.45	1.45	1.55	1.60	3.40	1.35	1.55										
	60.0	3.25	2.35	1.55	2.10	2.30	1.75	1.72	1.90	1.95	5.90	1.65	1.90										
	70.0	3.70	2.85	1.90	2.25	2.70	2.10	1.92	2.30	2.25	9.30	1.90	2.25										
	80.0	3.95	3.40	2.20	2.35	3.20	2.40	2.08	2.75	2.60	14.8	2.20	2.65										
	90.0	4.15	4.10	2.45	2.45	3.70	2.75	2.20	3.20	2.90	-	2.50	3.05										
	100.0	4.35	5.10	2.75	2.60	4.30	3.20	2.32	3.65	3.20	-	2.80	3.55										
3-3-1	107.0	5.05	8.75	2.75	3.18	5.10	3.50	2.90	4.35	4.05	-	3.90	8.00										
3-3-2	ZERO	-.002 / 0	0	0	-.002 / 0	0	0	.004 / 0	0	.02	0	0	0	.001	-.006	.052	-.005	.002	.005	0	-.003		.024
(a = 4.625")	5.0	.571 / .58	-.18	-.12	.390 / .50	-.15		.105 / .10	-.15	.18		.10		-.754	-.006	-.010	-.632	-.318	.135	-.742	-.357		.109
	5.4	.607 / .58	-.18	-.12	.411 / .52	-.15		.129 / .12	-.15	.18		.12		-.257	.007	.003	-.641	-.323	.144	-.760	-.348		.128
	10.2	.980 / .98	-.18	-.15	.742 / .85	-.15		.306 / .28	-.15	.38		.30		-.829	.096	.077	-.665	-.253	.322	-.808	-.115		.293
	15.2	1.383 / 1.32	-.10	-.15	1.089 / 1.20	-.12		.519 / .52	-.05	.58		.50		-.763	.213	.255	-.585	-.114	.514	-.757	.112		.451
	20.0	1.684 / 1.68	.07	-.12	1.395 / 1.52	.06		.746 / .75	.10	.78		.68		-.670	.326	.315	-.477	.040	.693	-.687	.305		.587
	24.8	2.008 / 2.00	.25	-.12	1.699 / 1.80	.25		.959 / .98	.28	.98		.88	0	-.557	.445	.454	-.366	.201	.870	-.600	.504	N	.741
	30.0	2.366 / 2.36	.45	-.12	2.030 / 2.15	.45		1.169 / 1.18	.98	1.16		1.05	.12	-.430	.562	.702	-.234	.367	1.052	-.507	.701	O	.904
UNLOAD	50.0	4.080 / 4.10	1.42	-.12	3.178 / 3.32	1.35		1.931 / 2.05	1.30	1.90		1.78	.92	.195	1.097	1.273	.371	1.127	1.764	.051	1.431	D	1.518
	ZERO	.037 / .02	-.05	0	-.016 / .10	-.05	0	-.022 / 0	0	.02	0	-.02	0	.008	.001	.013	.004	.003	-.014	.005	-.001	A	-.078
																						T	
2ND LOADING	ZERO	.004 / .05	-.06	-.08	.008 / .05	-.05	0	.047 / 0	.08	.02	0	.05	0	0	.002	0	.002	-.001	.001	0	.006	A	.053
	5.4	.596 / .56	-.22	-.20	.424 / .41	-.20		.088 / .12	-.07	.18		.05	0	-.708	.007	.030	-.592	-.383	.161	-.688	-.297		-.182
	15.2	1.309 / 1.23	-.11	-.20	1.071 / 1.05	-.07		.498 / .54	0	.58		.43	0	-.728	.218	.254	-.556	.0310	.523	-.708	.162		-.093
	40.0	3.149 / 3.13	.96	-.20	2.620 / 2.80	1.01		1.628 / 1.58	.90	1.52		1.35	.52	-.088	.828	.973	.092	.775	1.428	-.200	1.139		1.130
UNLOAD	50.0	4.056 / 4.00	1.56	-.18	3.180 / 3.15	1.47		1.900 / 1.95	1.30	1.88		1.78	.90	.240	1.094	1.271	.407	1.160	1.788	.111	1.515		1.350
	ZERO	-.035 / .05	-.12	-.12	.020 / .10	-.08		-.023 / 0	.08	.02		.05	0	-.005	-.001	.021	0	.004	.003	-.011	.005		-.153
3RD LOADING	50.0	4.065 / 4.00	1.56	-.12	3.181 / 3.10	1.47		1.892 / 1.92	1.40	1.88		1.70	.95	.242	1.098	1.281	.409	1.163	1.776	.123	1.526		1.413
	60.0	5.00	2.22	-.12	3.70	2.06		2.25	1.66	2.20		2.00	1.30										
	70.0	5.43	3.12	-.12	4.08	2.61	0	2.60	2.32	2.78	0	2.57	1.92										
	77.0	6.55	7.06	-.12	4.26	3.67	1.82	2.75	3.07	3.60	.08	3.70	>5.3										
3-3-2	ZERO	1.910 / 1.88	3.12	OUT	1.015 / 1.05	.18	0	.822 / .80	-.03	.18	-.20	-.15	OUT	1.093	.145	.232	.050	1.857	-1.052	-.430	-.027		.065

TABLE XVII. BOLTED ZEE STIFFENED PANEL STRAIN GAGE DATA (CONTINUED)

PANEL NUMBER	LOAD (KIPS)	GAGE LOCATION & STRAIN X10^3 inches/inch								
		(23)	(24)	(25)	(26)	(27)	(28)	(29)		
3-3-1	ZERO	.009	-.007	-.007	.010	-.012	.016			
(a = 2.05")	5.0	.160	.162	.167	.165	.157	.168			
↓	12.0	.365	.366	.353	.393	.386	.414			
↓	17.6	.528	.512	.510	.569	.570	.571			
↓	20.0	.619	.601	.596	.659	.643	.679			
↓	25.4	.784	.760	.746	.832	.818	.826			
↓	30.0	.935	.904	.904	.984	.993	.981			
↓	35.0	1.092	1.070	1.057	1.155	1.147	1.128			
3-3-1	40.0	1.284	1.229	1.225	1.332	1.325	1.283			
3-3-2	ZERO	-.005		-.001	-.006	.002	.002	-.004		
(a = 4.625")	5.0	.217		-.152	.088	.207	.109	.445		
↓	5.4	.224		-.138	.095	.214	.115	.472		
↓	10.2	.354		.035	.239	.345	.276	.785		
↓	15.2	.497		.211	.388	.489	.436	1.115		
↓	20.0	.632		.372	.539	.625	.591	1.414		
↓	24.8	.761		.538	.675	.760	.738	1.706		
↓	30.0	.905		.701	.820	.903	.887	2.019		
UNLOAD	50.0	1.494		1.354	1.374	1.479	1.484	3.540		
↓	ZERO	-.004		.006	-.009	.003	-.001	.020		
2ND LOADING	ZERO	-.001		.001	.003	.002	.002	-.003		
↓	5.4	.229		-.122	.099	.214	.116	.458		
↓	15.2	.479		.239	.445	.480	.442	1.071		
↓	40.0	1.183		1.069	1.099	1.174	1.197	2.725		
UNLOAD	50.0	1.470		1.396	1.378	1.463	1.498	3.522		
↓	ZERO	.009		.008	-.036	.003	-.001	-.046		
3RD LOADING	50.0	1.467		1.408	1.374	1.462	1.497	3.516		
3-3-2	ZERO	-.014		.015	.050	.002	-.049	1.150		
	DATRAN DATA / TAPE DATA									

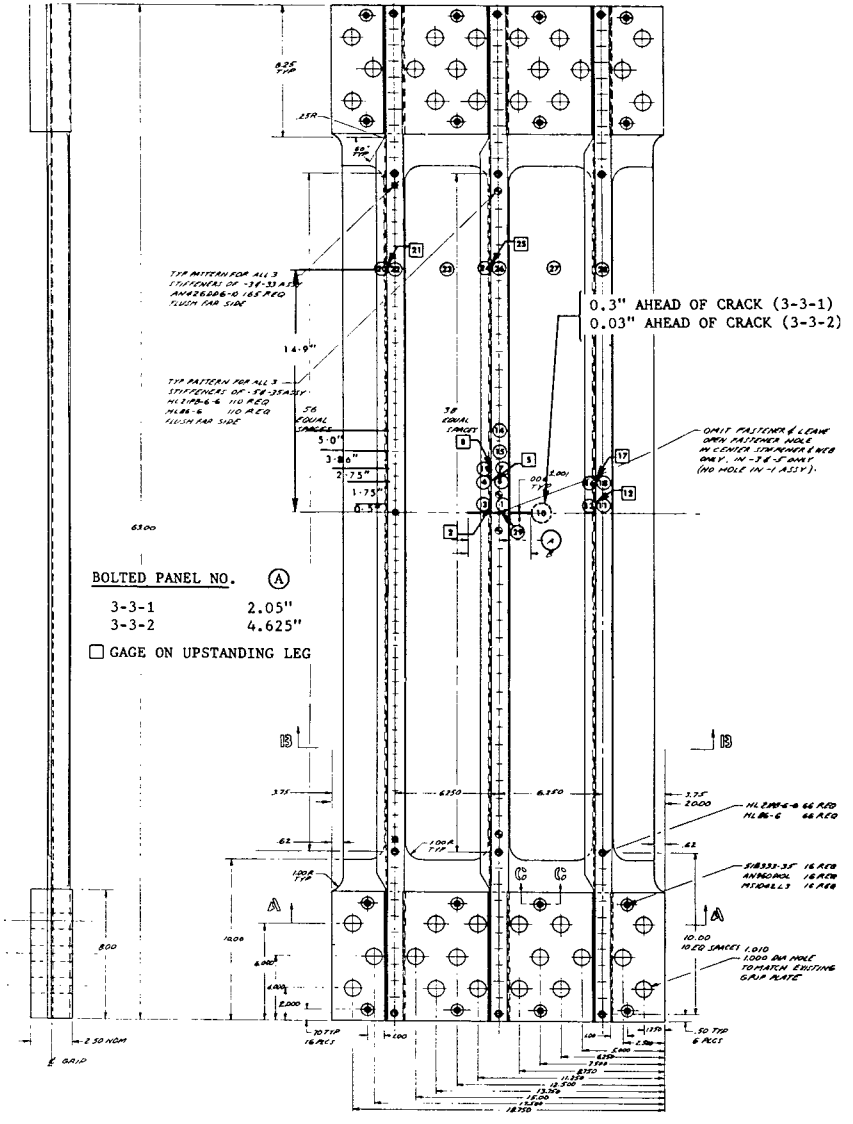

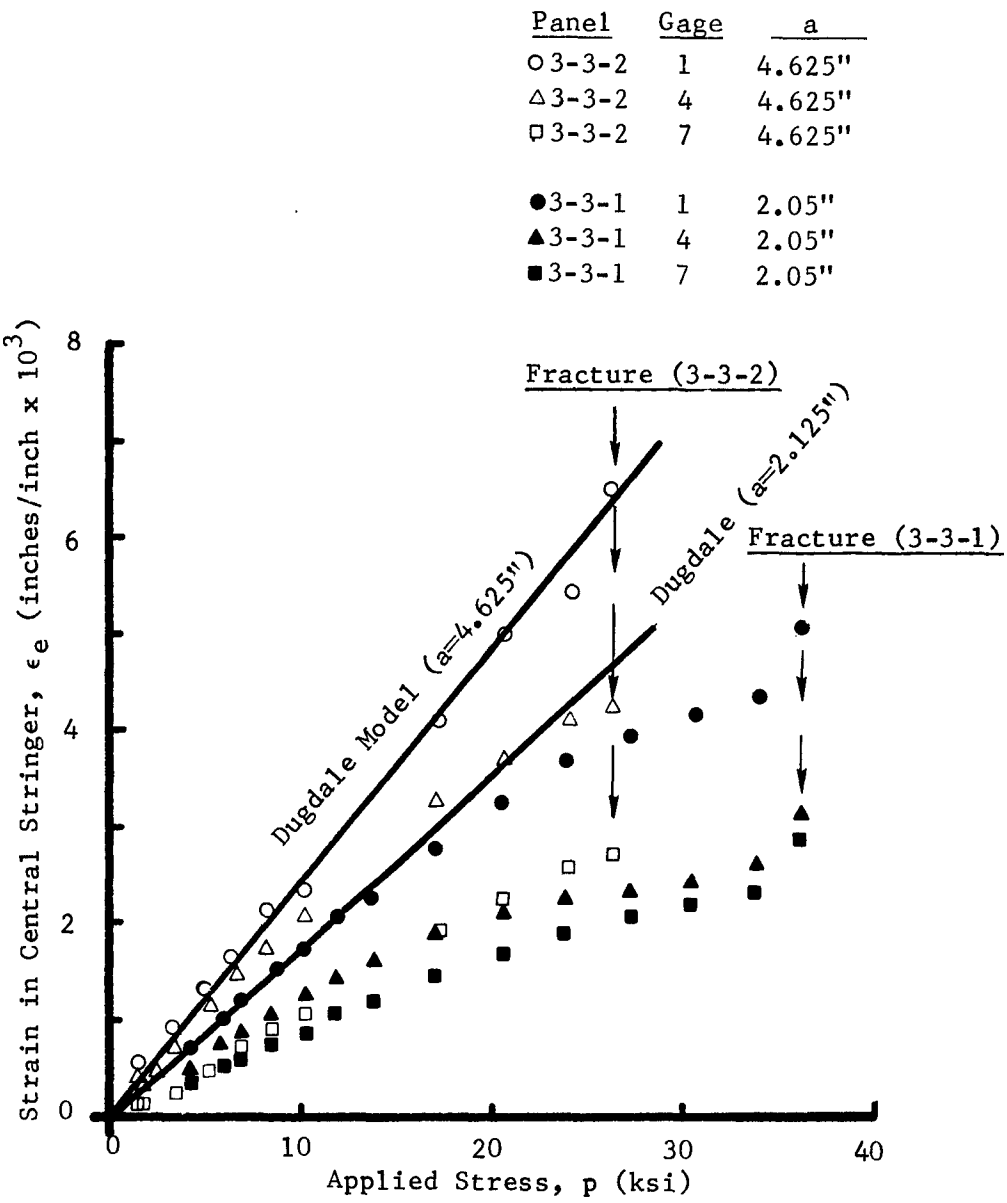

Figure 138. Strain in Central Stiffener as Function of Applied Stress, Bolted Zee Stiffened Panels

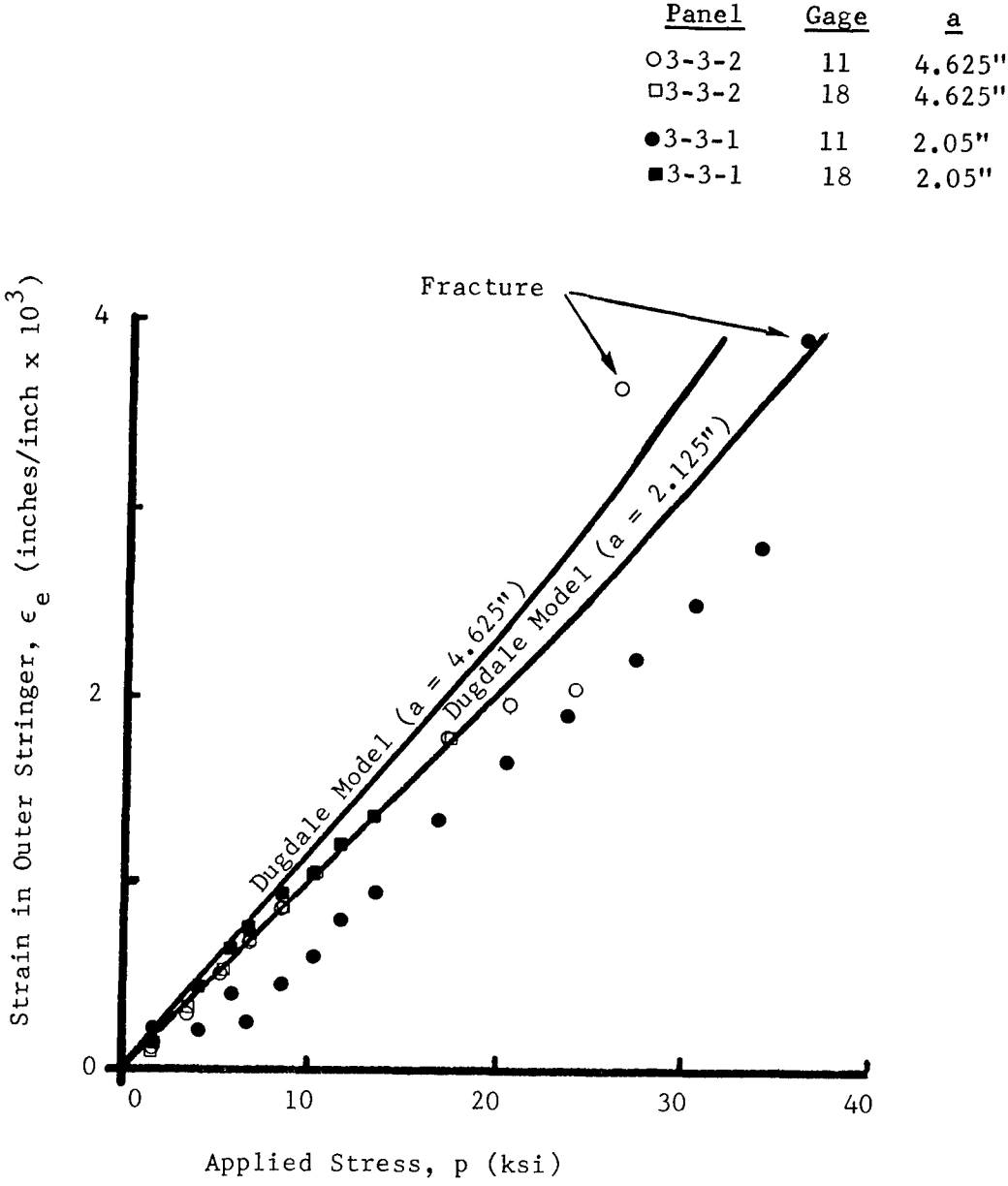

Figure 139. Strain in Outer Stiffener as Function of Applied Stress, Bolted Zee Stiffened Panels

7.3 BONDED ZEE STIFFENED PANEL

In the analysis of this panel certain simplified assumptions had to be made in the finite element modeling to account for the continuous adhesive bonding of the stringers. Elastic and elastic-plastic analysis, based on Dugdale type plastic zone assumptions were carried out for this panel. The modeling, analysis and experimental data of the bonded panel are discussed in the following subsections.

7.3.1 Finite Element Modeling of a Bonded Zee Stiffened Panel

For the bonded panel, the sheet was modeled exactly like the riveted and bolted panel, however some changes were made in the modeling of stiffeners and method of attachment. In this case since the stringer is bonded it is assumed to be continuously attached, therefore the connected leg of the stringer could not be modeled as a rod element. For this panel the connected leg (flange) and vertical web of the zee section are modeled as membrane plate elements. The top flange of the zee is modeled as a rod element. To account for the continuous bonding of the stringer, across the width of the zee section, it is assumed that the zee section is connected to the sheet by three shear elements (shear springs) as shown in Figure 140. The shear elements are assumed to be continuous along the length of the panel and are proportioned so that the central element (shear element 2 in Figure 140 (b)) transfers half of the total load and each of the outer shear elements (elements 1 and 3 in Figure 140 (b)) transfers one-fourth of the total load. The shear elements are assumed to have the same modulus as the modulus of the adhesive. Using these three shear elements avoids modeling the panel in three dimensions. The finite element modeling of one quarter of the bonded zee stiffened panel is shown in Figure 141.

Varying the proportioning of shear element load by assuming that all three shear elements (elements 1, 2 and 3 of Figure 140 (b)) take a load equal to 1/3 p, did not significantly alter the analytical results.

7.3.2 Analysis of the Bonded Zee Stiffened Panel

The adhesively bonded panel was analyzed assuming elastic and elastic-plastic behavior for half crack lengths of 2.125 inches and 4.225 inches. The comparison of elastic and the Dugdale type elastic-plastic analysis is shown in Figure 142 where the variation of $\sqrt{J}$ is shown with applied stress (p/F_{ty}). For small crack lengths (a = 2.125 inches) the Dugdale values are considerably higher than those obtained by assuming elastic behavior. At an applied stress of 75 percent of yield the Dugdale values are about 17 percent higher than elastic $\sqrt{J}$ values. However at a half crack length of 4.225 inches Dugdale $\sqrt{J}$ values are only slightly higher than elastic values which is primarily due to the influence of stringers and lands on the crack tip stresses. For comparative purposes Figure 142 shows the results obtained for the riveted zee stiffened panels using Dugdale type elastic-plastic analysis. It can be noted that at the same applied load (stress) and half crack length (2.125 inches) the riveted panel results are considerably higher than corresponding adhesively bonded $\sqrt{J}$ values. For example at an applied stress of 75 percent of the yield $\sqrt{J}$ values for the riveted panel are about 12 percent higher than

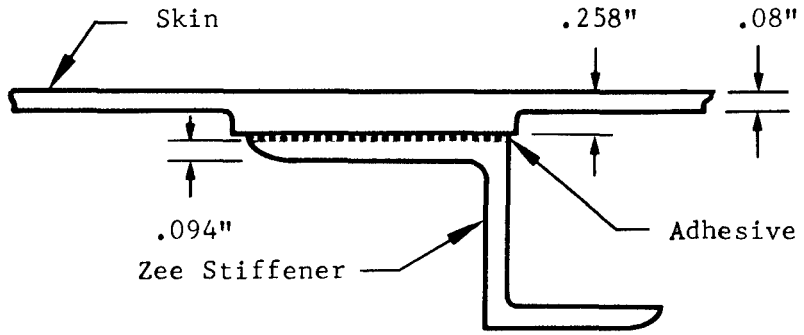

(a) Cross-Section of Adhesive Bonded Panel at Stringers

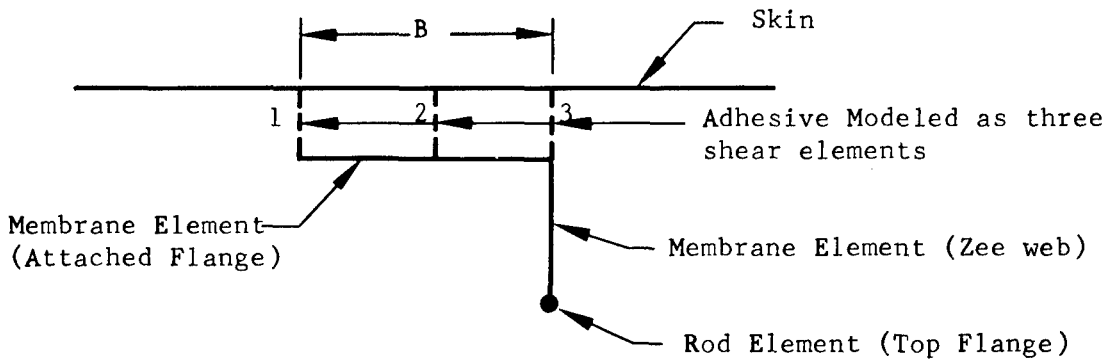

(b) Finite Element Modeling of (a)

Figure 140. Finite Element Representation of Adhesive Bonded, Zee Stiffened Panel - Stiffener Area

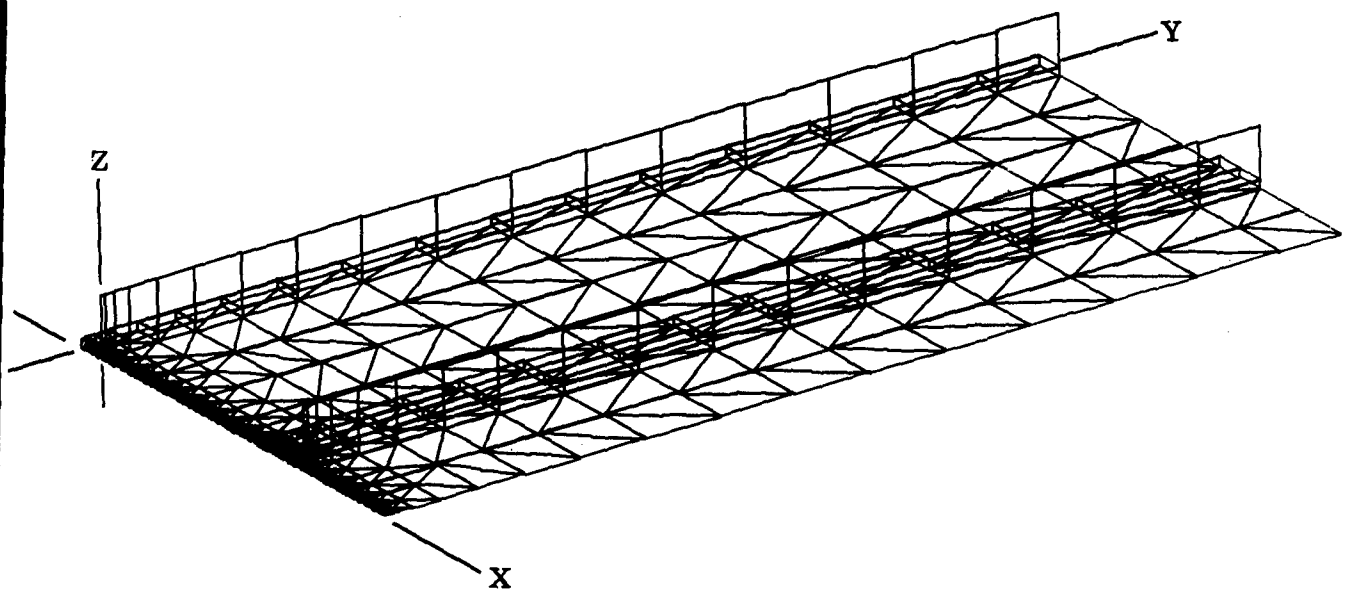

Figure 141. Finite Element Model of Adhesive Bonded Zee Stiffened Panel

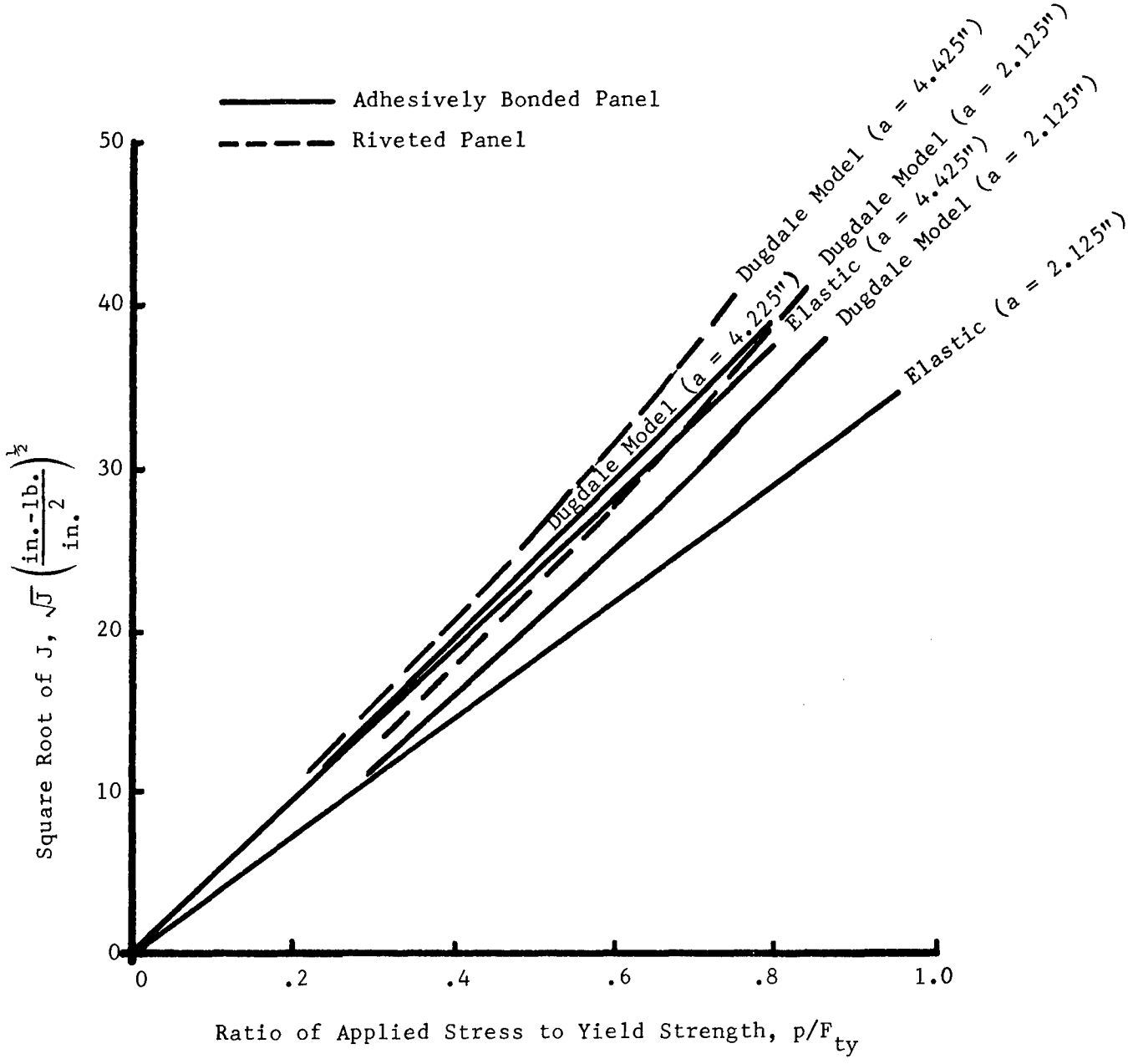

Figure 142. Comparison of Elastic and Dugdale Model Analyses for Bonded and Riveted Zee Stiffened Panels

those for the adhesively bonded panel. At a longer crack length, the riveted panel (crack length a = 4.425 inches) is only 0.2 inch longer than the crack length for the bonded panel. The $\sqrt{J}$ values are considerably higher for the riveted panel at any value of applied stress. For example at an applied stress of 60 percent of yield the riveted panel $\sqrt{J}$ values are approximately 10 percent higher than those for the adhesively bonded panel. Thus if J critical were used as a failure criterion the adhesively bonded panel would be able to carry more load compared to either the riveted or bolted panel at the same crack length.

7.3.3 Comparison of Experimental and Analytical Results of Zee-Stiffened Bonded Panel

The strain gages were located on the bonded panels as shown in Table XVIII. Also indicated are the strain readings to failure for a half crack length of 2.03 inches and 4.22 inches. The comparison of analytical and experimental strains for central and outer stringers is shown in Figures 143 and 144. At a half crack length of 2.03 inches, the correlation between analytical and experimental strains in the bonded leg of the central stringer is excellent to a stress of 12 ksi at stresses beyond this value, the experimental strains are considerably higher than the analytical. This indicates that some small, stable slow crack growth occurred at this stress. For an applied stress greater than 17 ksi the strains in the stringer increase rapidly due to stringer yielding.

For the short crack length the correlation between analytical and experimental strains in the outer stringer (Figure 144) is excellent to an applied stress of about 37 ksi, although some slow stable crack growth occurred at lower stresses. The reason for the good agreement between the experimental and analytical strains is due to the stresses in the outer stringer not being significantly affected by small amounts of slow crack growth for this crack length. It may be noted that similar behavior was observed in the elastic analysis of the wing channel panel of Figure 144 where stresses in the stringer are plotted as a function of crack length for a fixed applied load (stress). For a half crack length of 4.22 inches, the central stringer strains (Figure 143) show very good agreement with analytical results to an applied stress of 14 ksi. Beyond this stress experimental strains are considerably higher than analytical strains due to slow stable crack growth which increases the physical crack length. For stresses greater than 17 ksi, the central stringer strains increase very rapidly. These data indicate that the central stringer has undergone very large plastic deformations, thus this case is likely to be stringer critical case. The outer stringer experimental strains (Figure 144) show a very good correlation with analytical predictions based on Dugdale and Prandtl-Reuss material behaviors to panel failure. This is an indication that there was very little slow stable crack growth prior to panel failure.

The good correlation between experimental strains and analytical predictions using this simplified finite element model (where the adhesive was replaced by three shear elements) indicates that this model can be used for prediction of both residual strength and load transfer for adhesive bonded skin/stiffener construction.

TABLE XVIII. BONDED ZEE STIFFENED PANEL STRAIN GAGE DATA

PANEL NUMBER	LOAD (KIPS)	GAGE LOCATION & STRAIN X10^3 inches/inch																					
		①	②	③	④	⑤	⑥	⑦	⑧	⑨	⑩	⑪	⑫	⑬	⑭	⑮	⑯	⑰	⑱	⑲	⑳	㉑	㉒
3-3-4	ZERO	.006 / .02	0	0	.005 / 0	0	.02	0	0	0	0	.02	0	.003	0	.006	.002	-.004	-.002	.001	-.014	.006	.002
(a = 2.03")	5.0	.356 / .40	.02	.03	.273 / .28	.18	.06	.18	.15	.05	.20	.13	.25	.127	.144	.139	.168	.166	.169	.145	.095	.119	.153
	10.0	.721 / .76	.20	.08	.536 / .53	.35	.18	.33	.30	.23	.40	.30	.25	.287	.290	.284	.330	.334	.332	.288	.260	.264	.301
	15.0	1.050 / 1.08	.35	.14	.789 / .80	.53	.28	.50	.50	.40	.60	.48	.40	.437	.424	.424	.489	.492	.491	.422	.391	.393	.447
	20.0	1.380 / 1.42	.52	.20	1.053 / 1.06	.70	.42	.68	.68	.42	.82	.63	.60	.603	.566	.565	.654	.656	.658	.568	.484	.539	.600
	25.0	1.732 / 1.78	.70	.25	1.324 / 1.32	.90	.56	.85	.85	.68	1.05	.78	.75	.764	.705	.699	.807	.821	.823	.709	.662	.677	.745
	30.0	2.123 / 2.18	.90	.30	1.595 / 1.58	1.08	.68	1.05	1.05	.82	1.30	.98	.90	.928	.840	.840	.966	.992	1.014	.848	.800	.823	.900
	35.0	2.623 / 2.66	1.08	.38	1.866 / 1.88	1.28	.80	1.20	1.25	1.00	1.52	1.13	1.10	1.094	.979	.977	1.127	1.157	1.160	.990	.934	.959	1.045
	40.0	3.234 / 3.26	1.32	.45	2.137 / 2.12	1.45	.93	1.40	1.42	1.12	1.80	1.28	1.25	1.254	1.111	1.109	1.287	1.320	1.325	1.127	1.071	1.099	1.195
	45.0	3.926 / 3.92	1.58	.50	2.401 / 2.40	1.62	1.03	1.55	1.62	1.28	2.08	1.46	1.40	1.417	1.244	1.233	1.452	1.486	1.490	1.260	1.205	1.235	1.341
	50.0	4.758 / 4.76	1.82	.60	2.657 / 2.65	1.82	1.16	1.72	1.85	1.45	2.40	1.63	1.58	1.589	1.378	1.363	1.619	1.661	1.662	1.395	1.343	1.377	1.489
	60.0	7.38	2.30	.80	2.90	2.30	1.50	1.95	2.20	1.80	3.28	1.93	1.92										
	69.6	11.58	2.90	.95	3.15	2.80	1.78	2.20	2.75	2.15	6.28	2.38	2.32										
	80.0	5.58	4.08	1.20	3.30	3.35	2.08	2.40	3.20	2.25	10.00	2.68	2.60										
	90.0	5.58	5.28	1.35	3.40	3.80	2.32	2.55	3.60	2.80	17.40	3.03	3.00										
	100.0	5.26	8.00	1.65	3.60	4.40	2.63	2.80	4.05	3.20	5.92	3.48	3.52										
	110.0	4.78	10.72	2.05	3.90	4.95	3.03	3.00	4.65	3.70	5.20	4.08	4.20										
	122.0	4.78	9.60	5.15	4.60	7.50	7.73	3.80	8.00	4.30	4.00	9.88	13.00										
3-3-4	ZERO	3.360 / 3.58	4.20	3.40	1.662 / 1.75	3.75	4.58	1.90	4.75	1.40	3.20	4.08	1.04	2.075	3.535	1.719	7.389	OUT	1.676	-.028	.033	.016	.009
3-3-3	ZERO	.003 / .04	0	-.04	-.007 / 0	0	-.04	0	0	0	0	0	0	.001	.007	.009	.001	0	.005	-.001	-.007	.001	-.001
(a = 4.22")	5.0	.409 / .40	.20	-.04	.437 / .40	.20	.04	.35	.20	.20	.35	.20	.20	.161	.182	.140	.186	.193	.196	.131	.273	.200	.168
	10.0	.888 / .92	.40	-.04	.880 / .80	.40	.04	.70	.40	.30	.65	.40	.40	.284	.369	.280	.373	.389	.392	.258	.324	.300	.315
	15.0	1.354 / 1.36	.70	-.04	1.302 / 1.30	.60	.04	1.00	.55	.40	.95	.60	.55	.447	.560	.420	.548	.575	.580	.379	.464	.444	.470
	20.0	1.845 / 1.86	.90	-.04	1.736 / 1.70	.90	.04	1.35	.80	.60	1.35	.80	.75	.624	.774	.578	.744	.775	.786	.514	.615	.593	.627
	25.0	2.325 / 2.32	1.20	.04	2.186 / 2.00	1.10	.08	1.75	1.00	.80	1.70	1.00	.95	.806	1.024	.727	.947	.983	1.000	.646	.762	.750	.786
	30.0	2.760 / 2.80	1.40	.14	2.578 / 2.50	1.30	.14	2.00	1.20	.95	2.10	1.15	1.10	.981	1.243	.872	1.128	1.179	1.174	.769	.895	.875	.929
	35.0	3.243 / 3.32	1.64	.24	3.002 / 3.00	1.60	.14	2.25	1.40	1.10	2.60	1.35	1.30	1.177	1.516	1.036	1.333	1.398	1.412	.903	1.045	1.031	1.097
	40.0	3.96	1.92	.24	3.40	1.92	.19	2.20	1.65	1.25	3.36	1.60	1.50										
	50.0	6.76	2.64	.44	4.00	2.20	.24	2.80	2.20	1.65	6.00	2.00	2.00										
	60.0	11.80	3.68	.59	4.60	2.60	.39	3.12	2.90	2.10	14.80	2.40	2.55										
	70.0	18.20	5.40	.66	5.92	3.25	.44	3.36	3.60	2.60	4.00	2.88	3.10										
	80.0	13.72	8.32	1.04	8.12	4.40	.74	3.60	4.30	3.10	3.84	3.80	3.90										
	84.5	12.16	15.80	4.50	11.80	7.65	5.10	4.80	9.90	3.65	3.84	14.80	9.30										
3-3-3	ZERO	9.974 / 10.20	7.00	3.60	4.533 / 4.60	OUT	2.60	20.8	4.95	1.00	1.60	4.60	.80	1.884	1.836	1.132	4.542	3.876	1.160	.680	.808	1.582	.693

DATRAN DATA / TAPE DATA

TABLE XVIII. BONDED ZEE STIFFENED PANEL STRAIN GAGE DATA (CONTINUED)

PANEL NUMBER	LOAD (KIPS	GAGE LOCATION & STRAIN X10^3 inches/inch					
		(23)	(24)	(25)	(26)	(27)	(28)
3-3-4	ZERO	-.002	-.012	-.002	-.002	.005	.002
(a = 2.03")	5.0	.160	.163	.151	.155	.166	.161
	10.0	.318	.298	.293	.308	.331	.319
	15.0	.463	.429	.429	.451	.488	.466
	20.0	.620	.570	.571	.602	.652	.621
	25.0	.777	.705	.711	.751	.813	.777
	30.0	.936	.844	.856	.906	.982	.936
	35.0	1.091	.986	1.000	1.060	1.143	1.086
	40.0	1.244	1.125	1.142	1.208	1.304	1.236
	45.0	1.397	1.263	1.285	1.359	1.464	1.374
	50.0	1.558	1.405	1.431	1.512	1.629	1.541
	60.0						
	69.6						
	80.0						
	90.0						
	100.0						
	110.0						
	122.0						
3-3-4	ZERO	-.026	.085	.036	-.019	-.010	.036
3-3-3	ZERO	0	-.010	-.002	.004	-.001	-.004
(a = 4.22")	5.0	.132	.250	.202	.155	.152	.172
	10.0	.305	.318	.305	.297	.330	.325
	15.0	.449	.462	.447	.436	.482	.486
	20.0	.607	.616	.600	.587	.653	.650
	25.0	.765	.772	.749	.745	.819	.812
	30.0	.916	.918	.895	.882	.975	.973
	35.0	1.073	1.078	1.053	1.040	1.144	1.134
	40.0						
	50.0						
	60.0						
	70.0						
	80.0						
	84.5						
3-3-3	ZERO	-.023	OUT	1.343	1.401	-.013	2.546

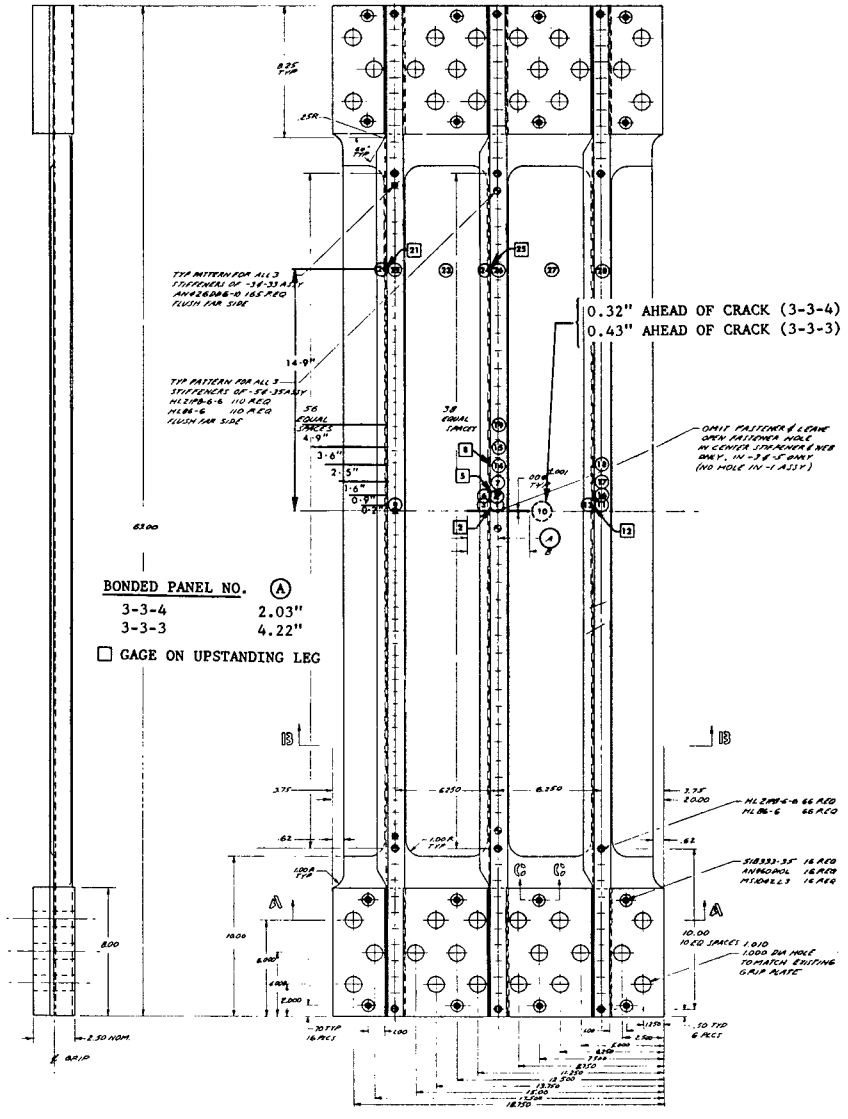

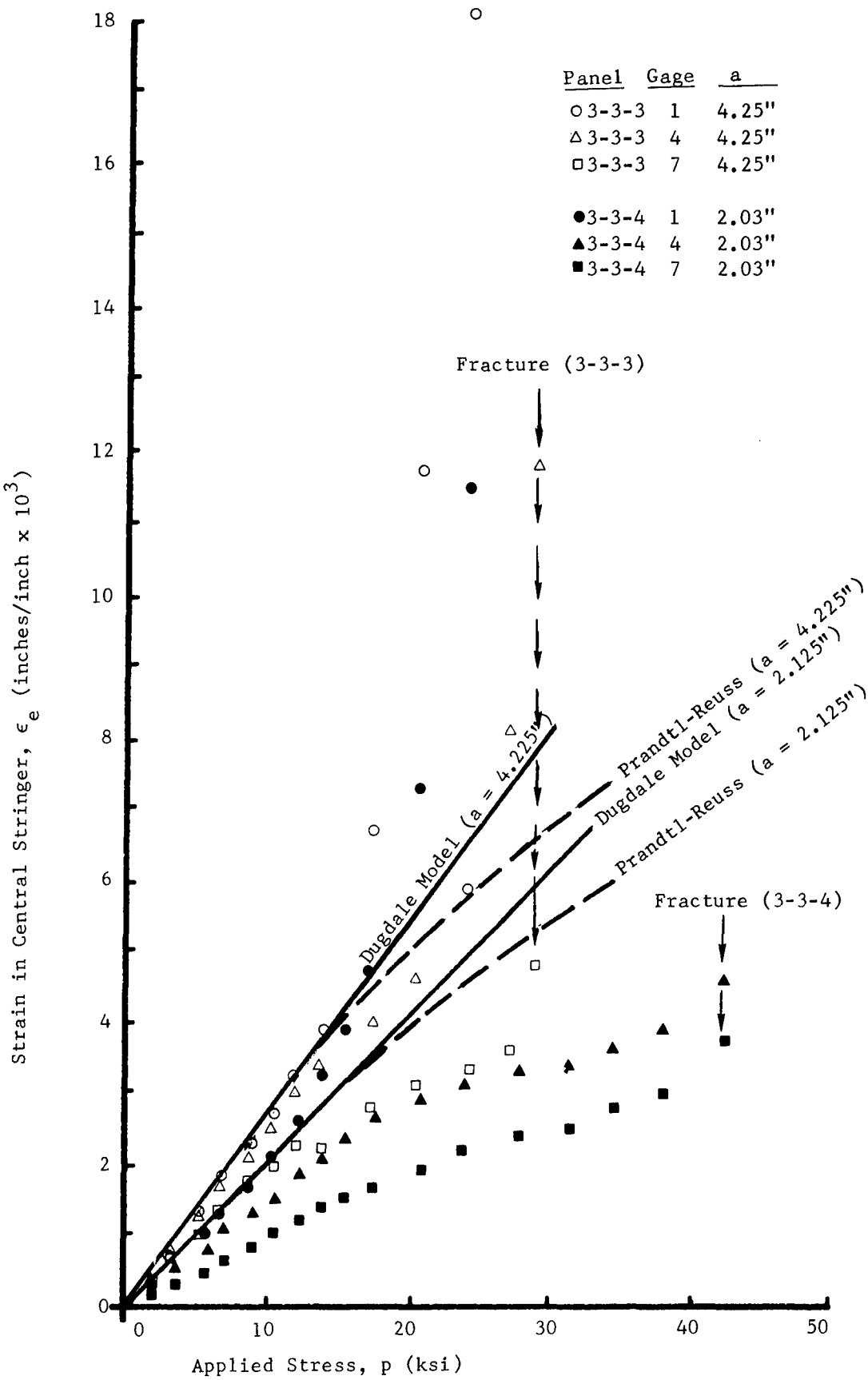

Figure 143. Strain in Central Stiffener as Function of Applied Stress, Bonded Zee Stiffened Panels

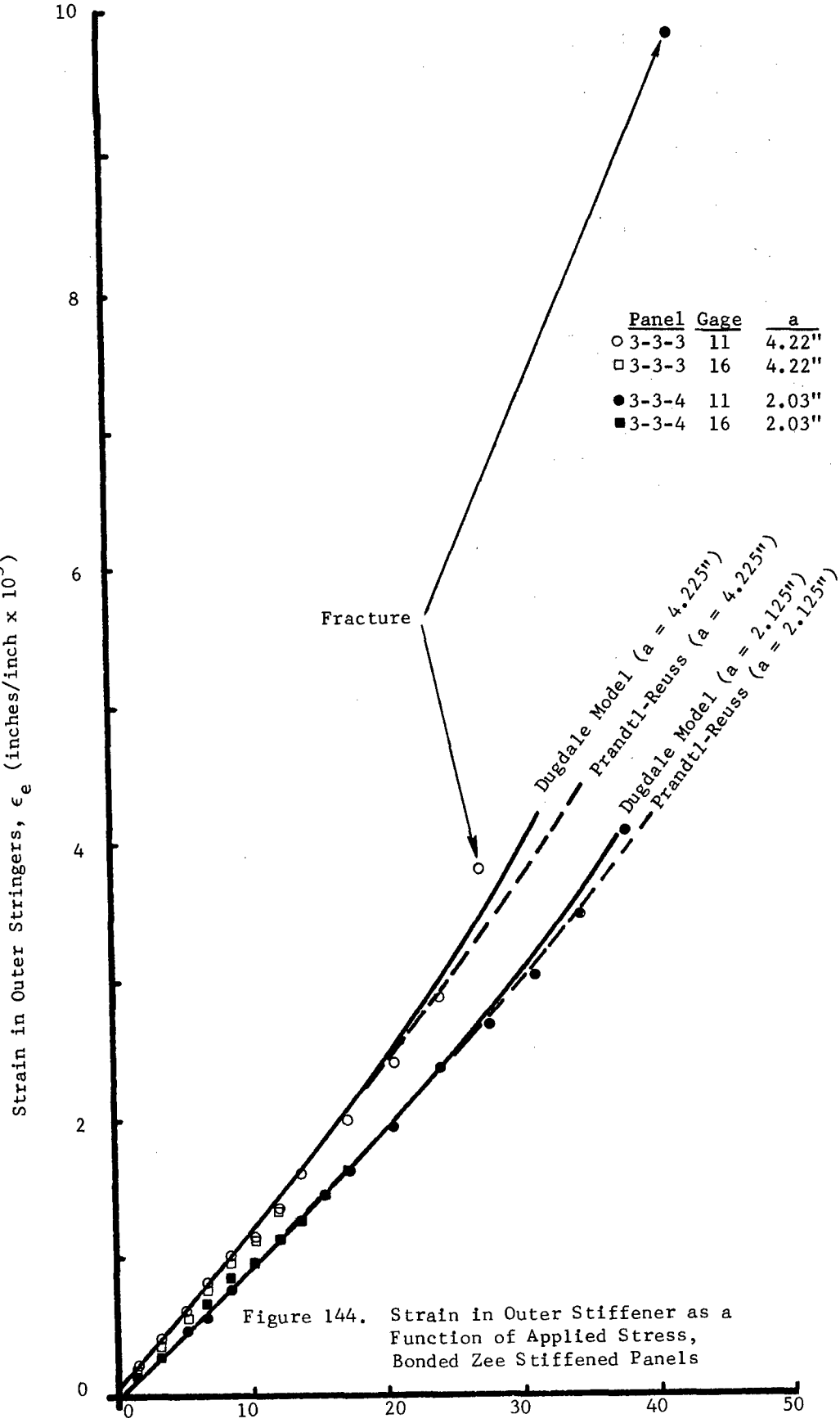

Figure 144. Strain in Outer Stiffener as a Function of Applied Stress, Bonded Zee Stiffened Panels

7.4 AN INTERCOMPARISON OF DATA

A comparison of analytical and experimental crack surface displacement (COD) and strains between the various zee stiffened panels will be presented next with a discussion of other relevant data.

7.4.1 Panel Fracture

A view of the pre and post fracture condition for a typical riveted, zee stiffened panel (a = 4.425", panel No. 3-2-2) is shown in Figures 120 and 145 for the skin and stringer side. This arrangement of clip gages (Figure 120) was used throughout the panel tests. One gage was located on the panel centerline and the remaining two gages at 1.8 inches from the panel centerline - straddling the crack. The fracture appearance for the riveted and HI-LOKED (or bolted) panels were similar in that the crack ran through the outer stringers fastener holes, without being arrested. Figure 146 is typical of the stiffener side fracture for both riveted and bolted panels. The adhesively bonded stiffener panels exhibited increasing amounts of delamination of the zee section with increasing stress which progressed from panel centerline to grip end as shown in Figure 147.

For the shorter crack lengths (a = 2.125 inches) little slow tear occurred prior to fracture whereas for the longer crack length (a = 4.425 inches) a larger amount of slow tear was observed, prior to fracture.

7.4.2 Comparison of Crack Opening Displacement

The crack openings (δ) for all riveted panels at half crack lengths of 2.125 and 4.425 inches is shown in Figures 148 to 151. For the short crack length the crack openings given by the central and outer gages is a linear function of load to an applied load of approximately 30 kips. Beyond 30 kips the openings become a nonlinear function of applied load due to plasticity and slow tear developing at the crack tips. Approaching the point of fracture, the clip gage data of the outer gages cross each other due to unsymmetrical buckling of the sheet in the cracked region (see Figure 148). For long crack lengths (Figures 150 and 151) crack openings are a linear function of applied load to approximately 25 kips, beyond this load crack openings become a nonlinear function of applied load.

Figures 152 to 155 show the crack openings at the two gage locations for two crack lengths in the HI-LOKED panels. At short crack lengths the behavior of crack openings is similar to the riveted panel. For long crack lengths the crack openings are a nonlinear function of applied load even at very small loads. The traces of the two clip gages cross at smaller applied loads than that of the riveted panel. This is primarily caused by an inadvertent compressive load placed on panel 3-3-2 prior to fracture testing. The panel was buckled considerably at that time.

The crack openings for the two bonded panels are shown in Figures 156 to 159. The behavior noted in the data of these curves is similar to the data obtained for the riveted panel.

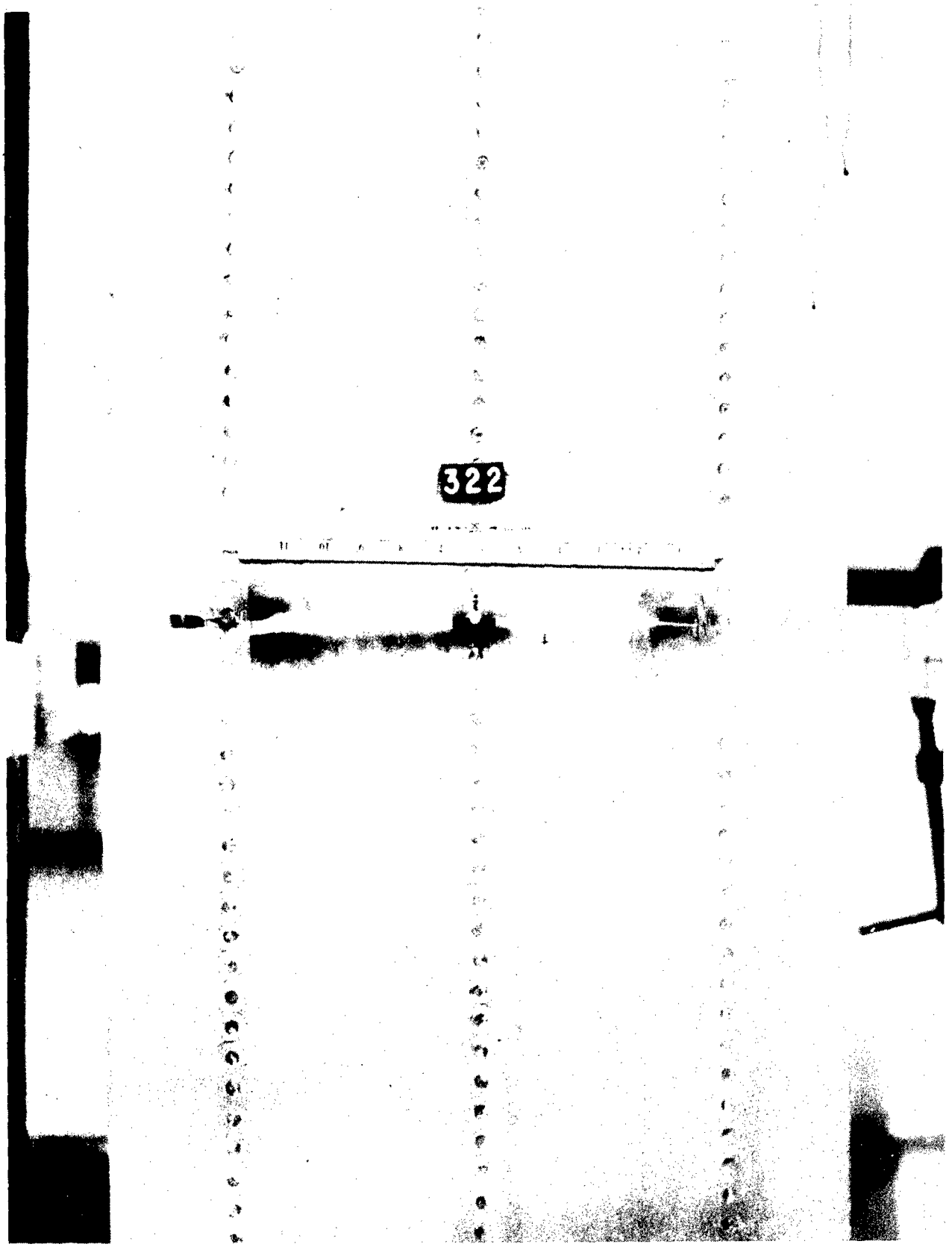

Figure 145. Typical Fracture of Riveted and Bolted Zee Stiffened Panel - Skin Side

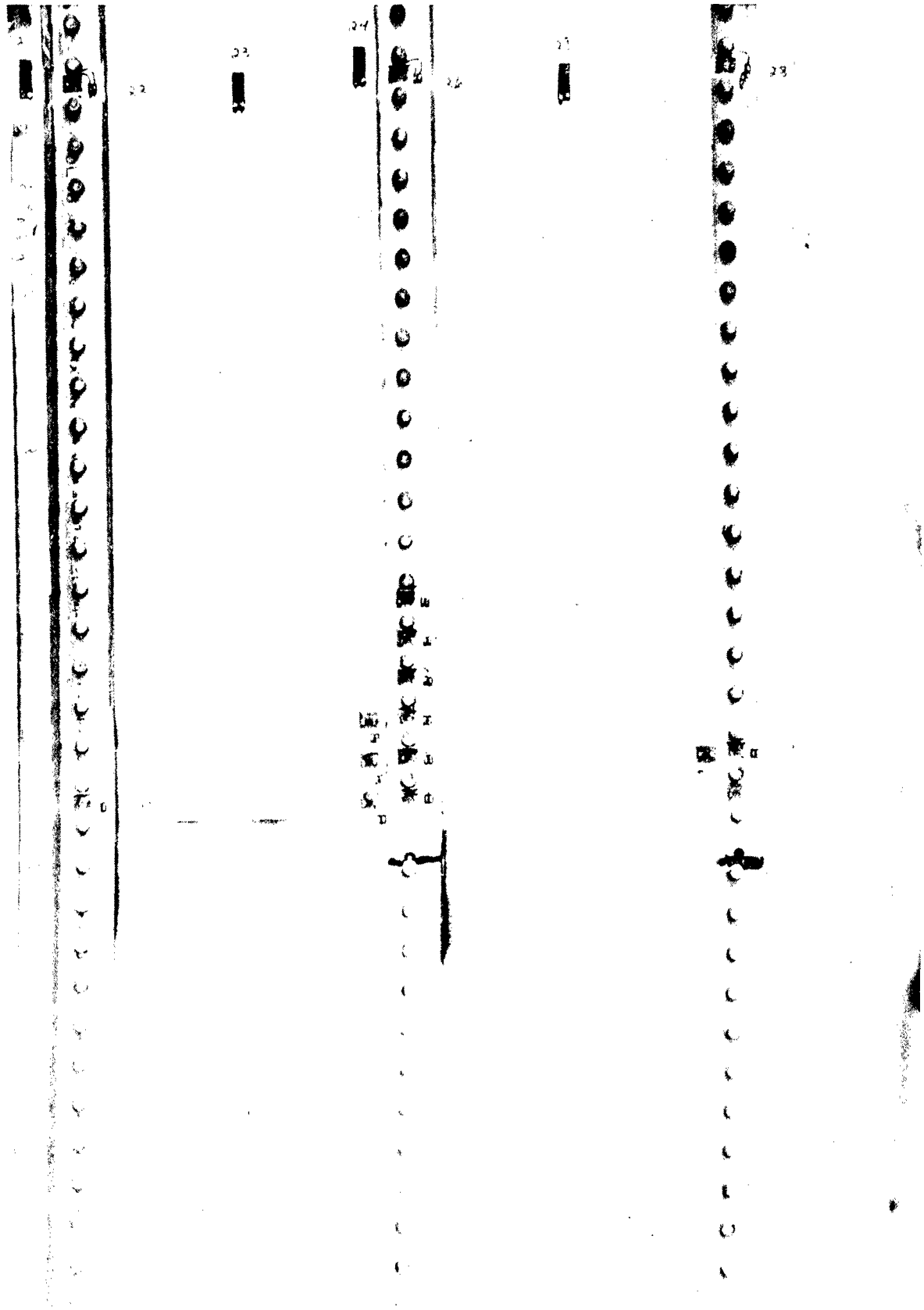

Figure 146. Typical Fracture of Riveted and Bolted Zee Stiffened Panel - Stiffener Side

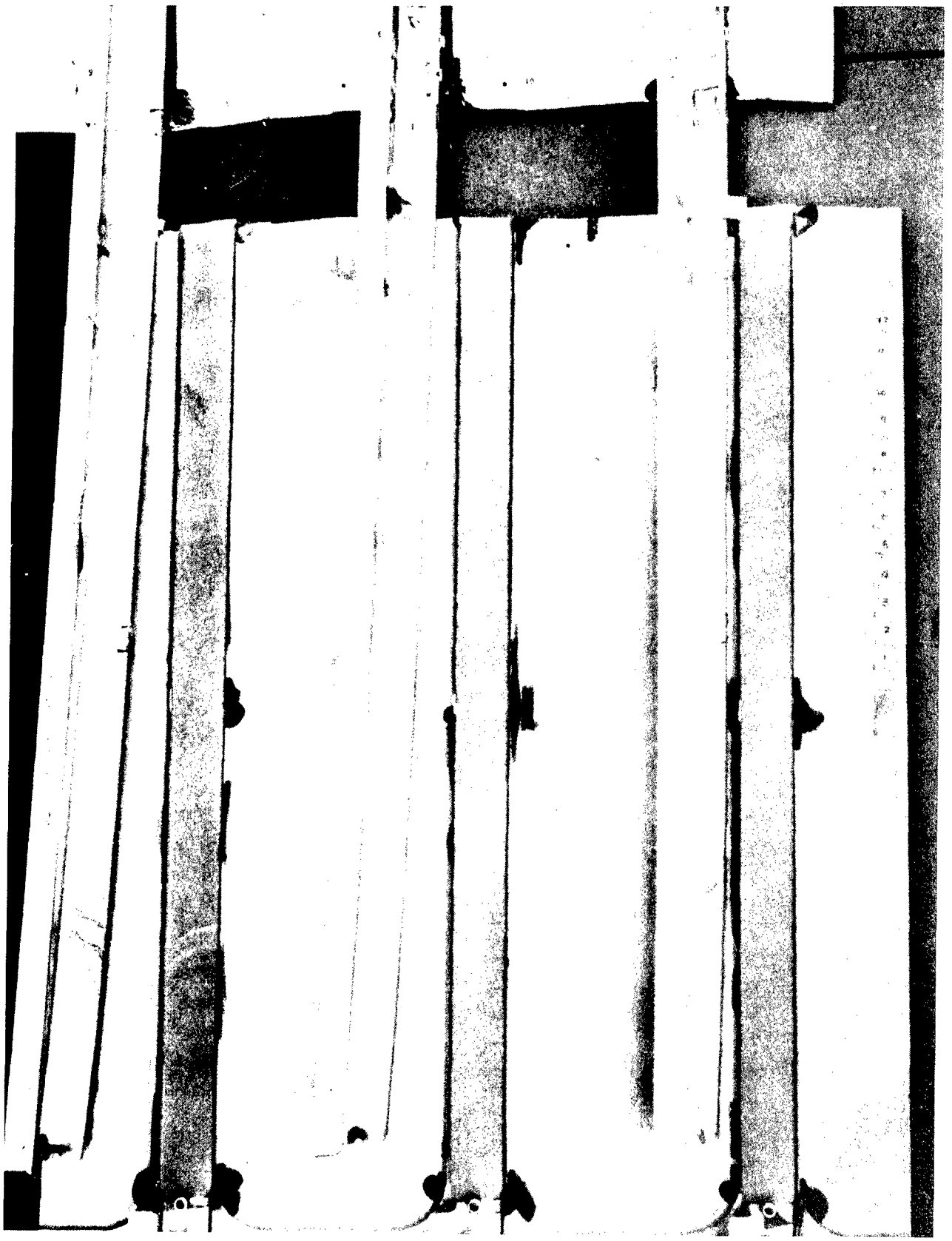

Figure 147. Typical Fracture, Stiffened Side - Bonded Panels

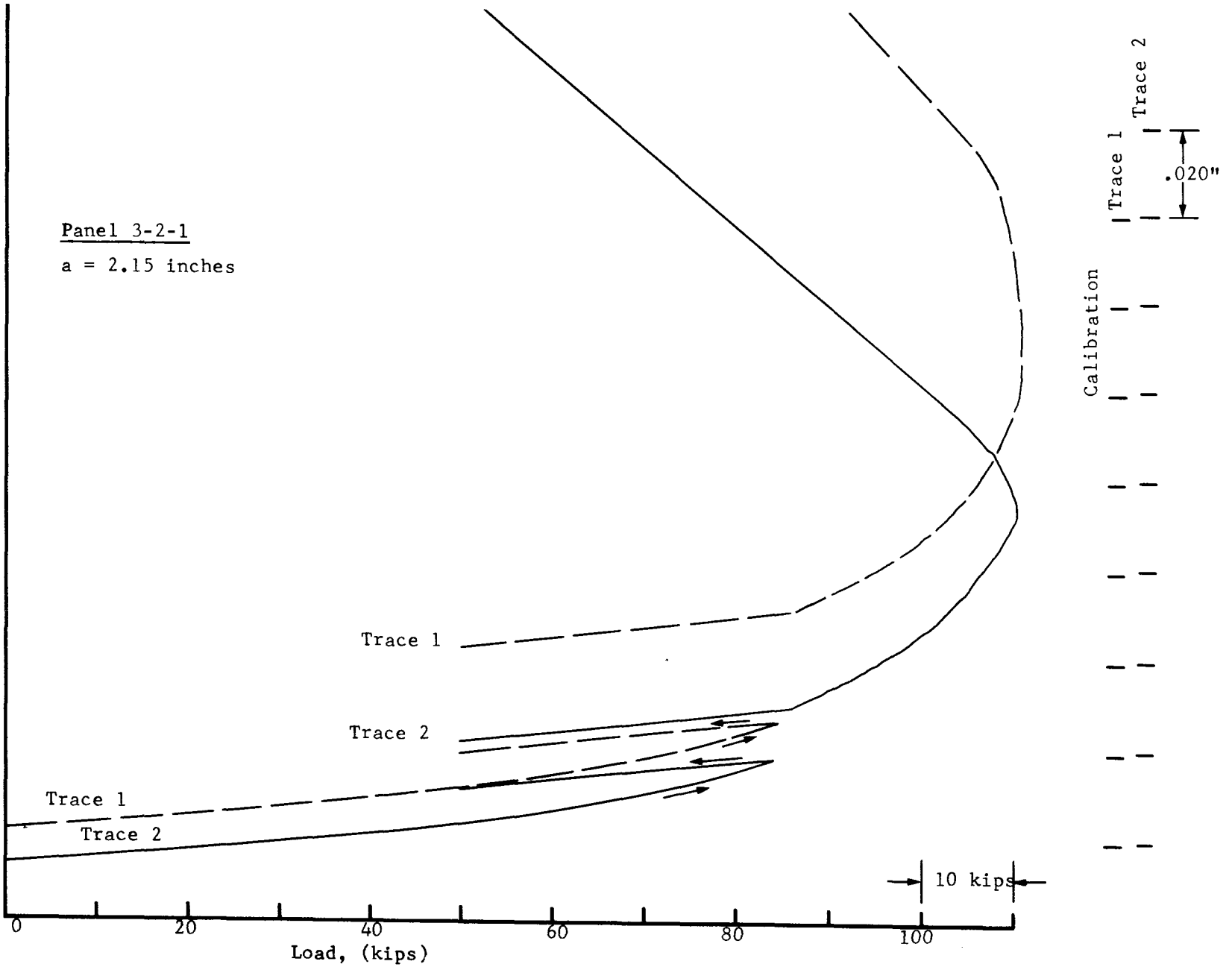

Figure 148. Load-Crack Displacement Curves - Riveted Panel 3-2-1, 1.8 Inches from Panel Centerline

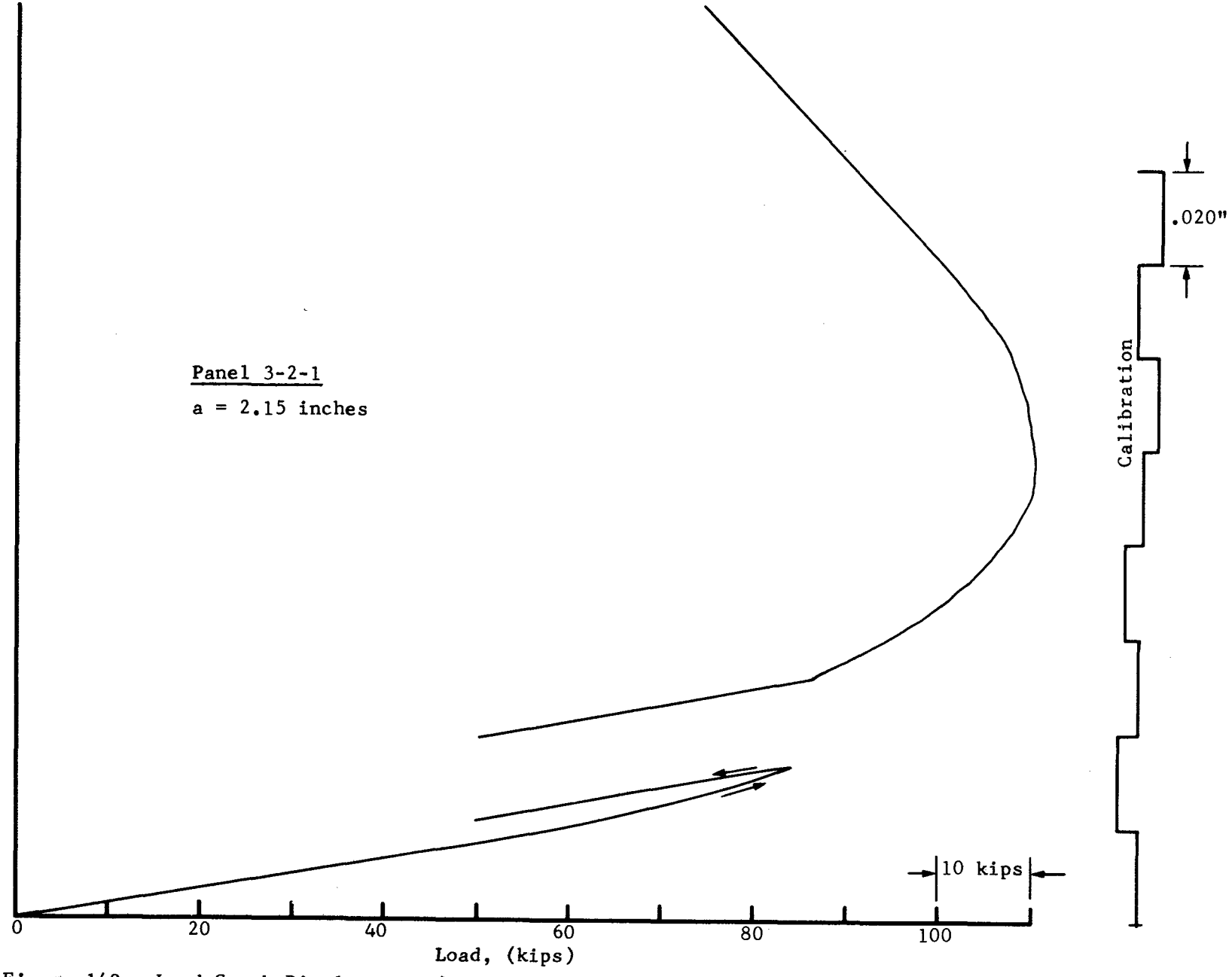

Figure 149. Load-Crack Displacement Curve - Riveted Panel 3-2-1, Panel Centerline

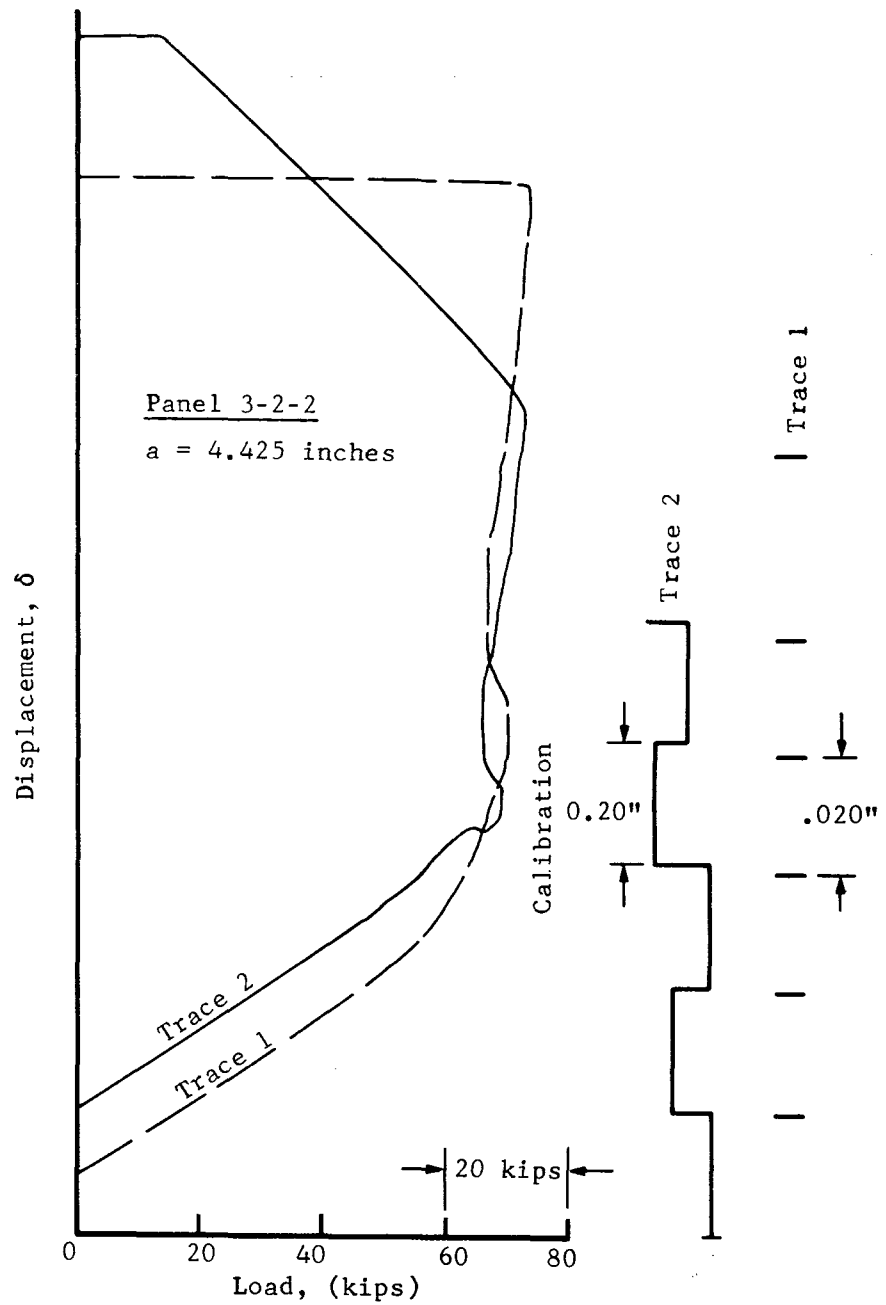

Figure 150. Load-Crack Displacement Curves - Riveted Panel 3-2-2, 1.8 Inches from Panel Centerline

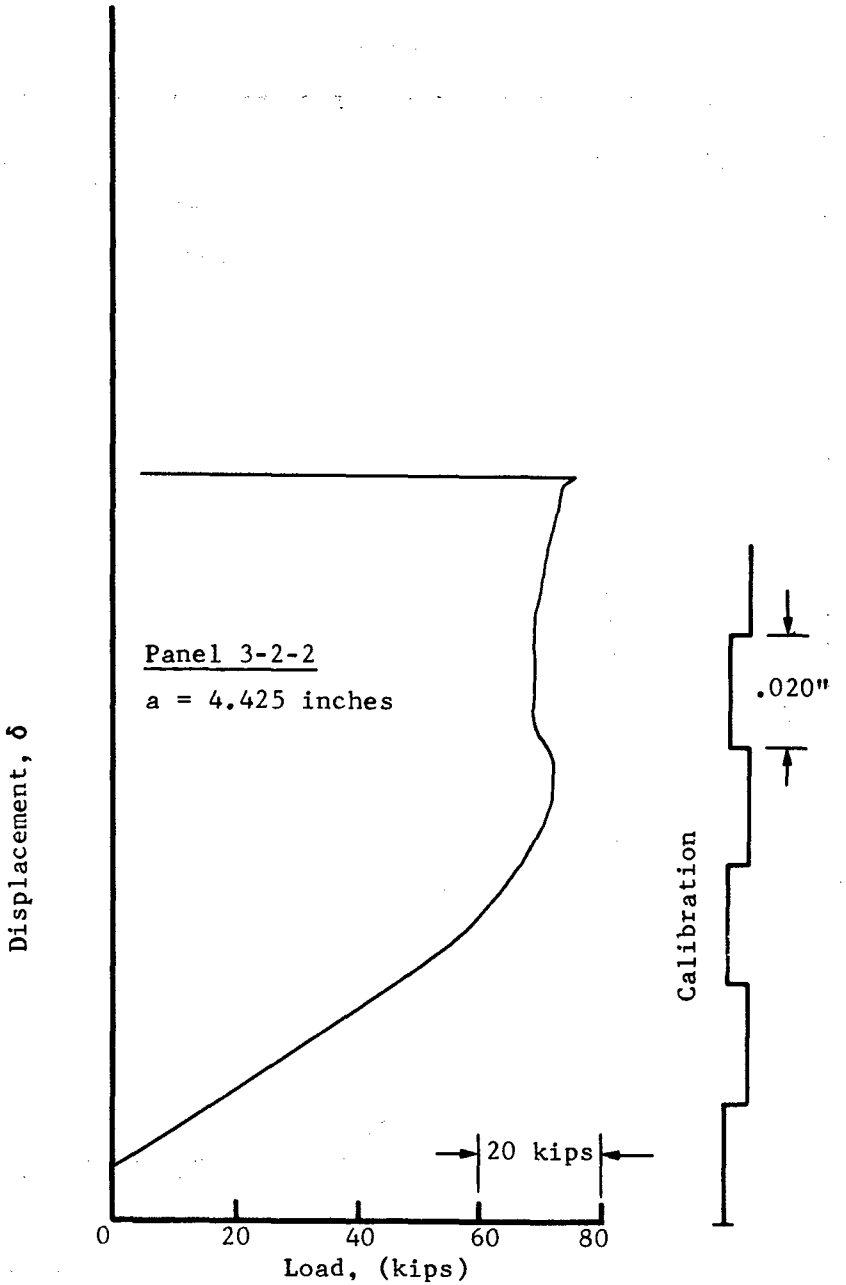

Figure 151. Load-Crack Displacement Curve - Riveted Panel 3-2-2, Panel Centerline

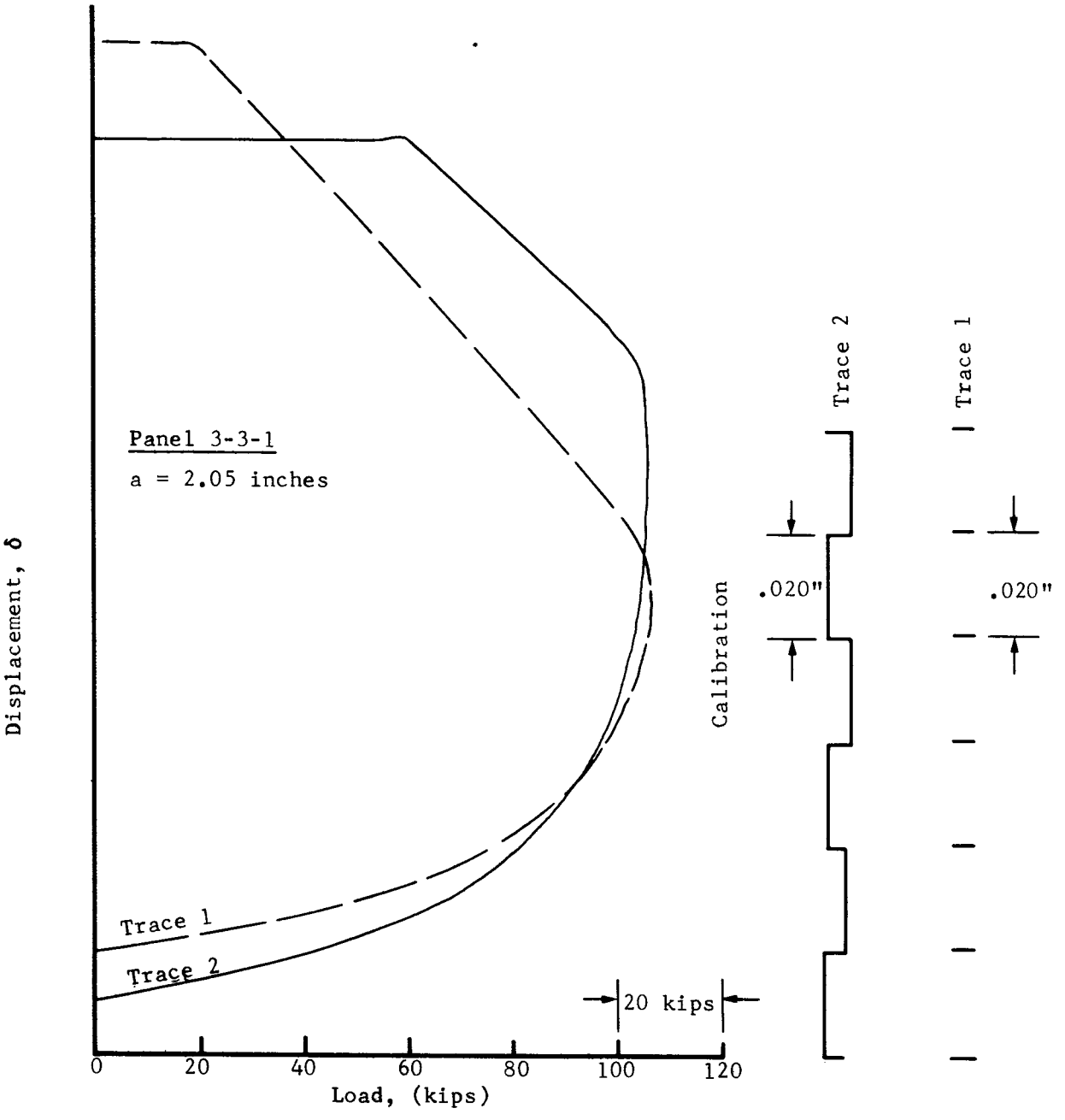

Figure 152. Load-Crack Displacement Curves - Bolted Panel 3-3-1, 1.8 Inches from Panel Centerline

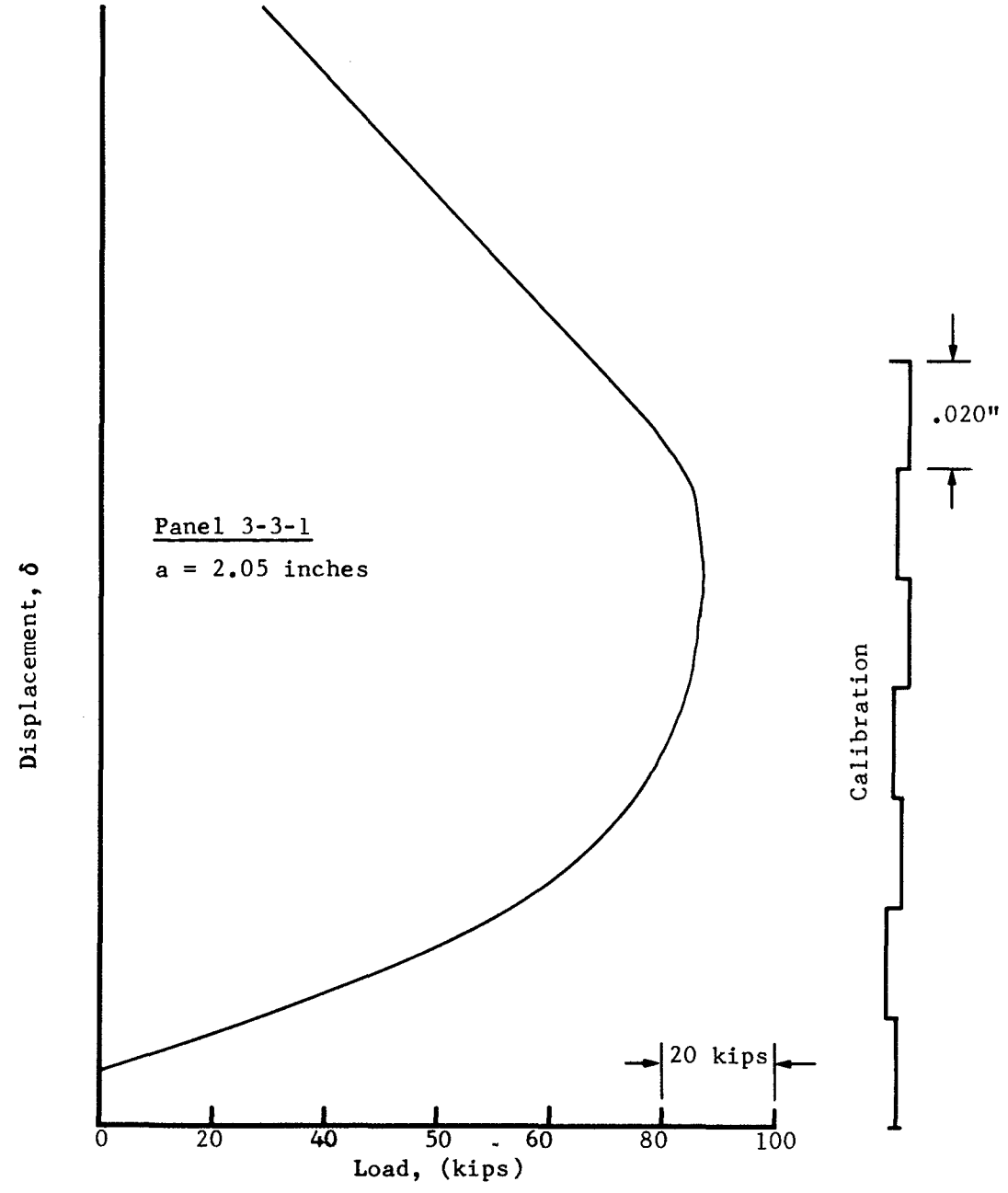

Figure 153. Load-Crack Displacement Curve - Bolted Panel 3-3-1, Panel Centerline

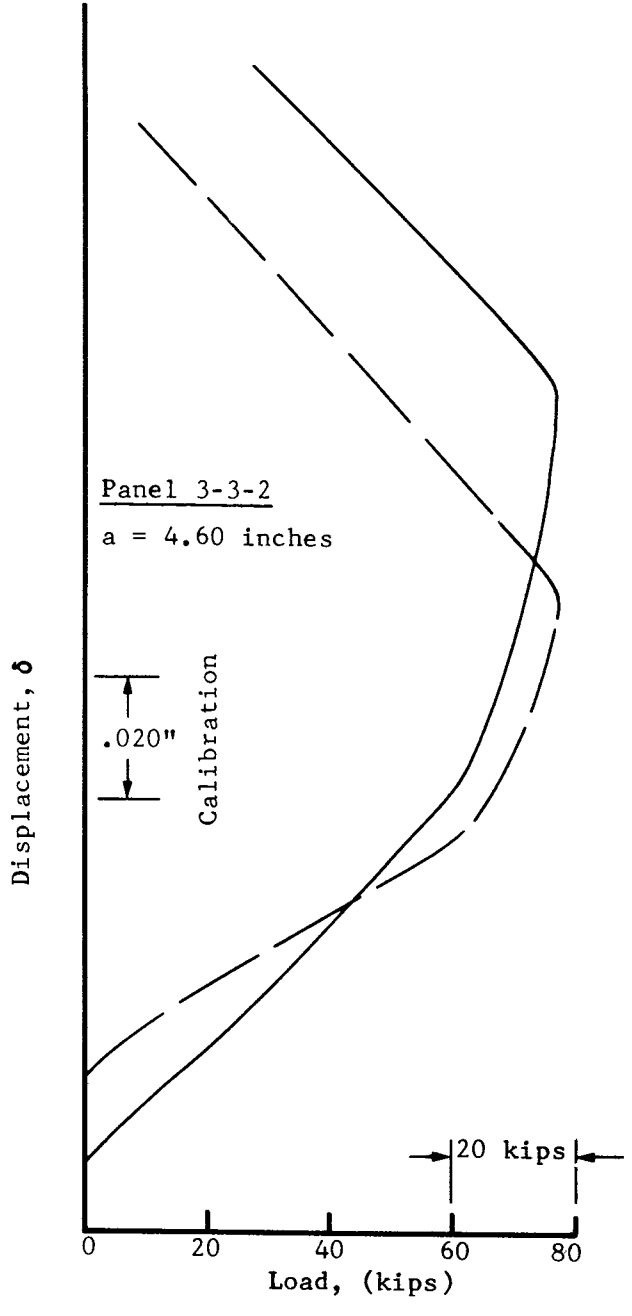

Figure 154. Load-Crack Displacement Curve — Panel

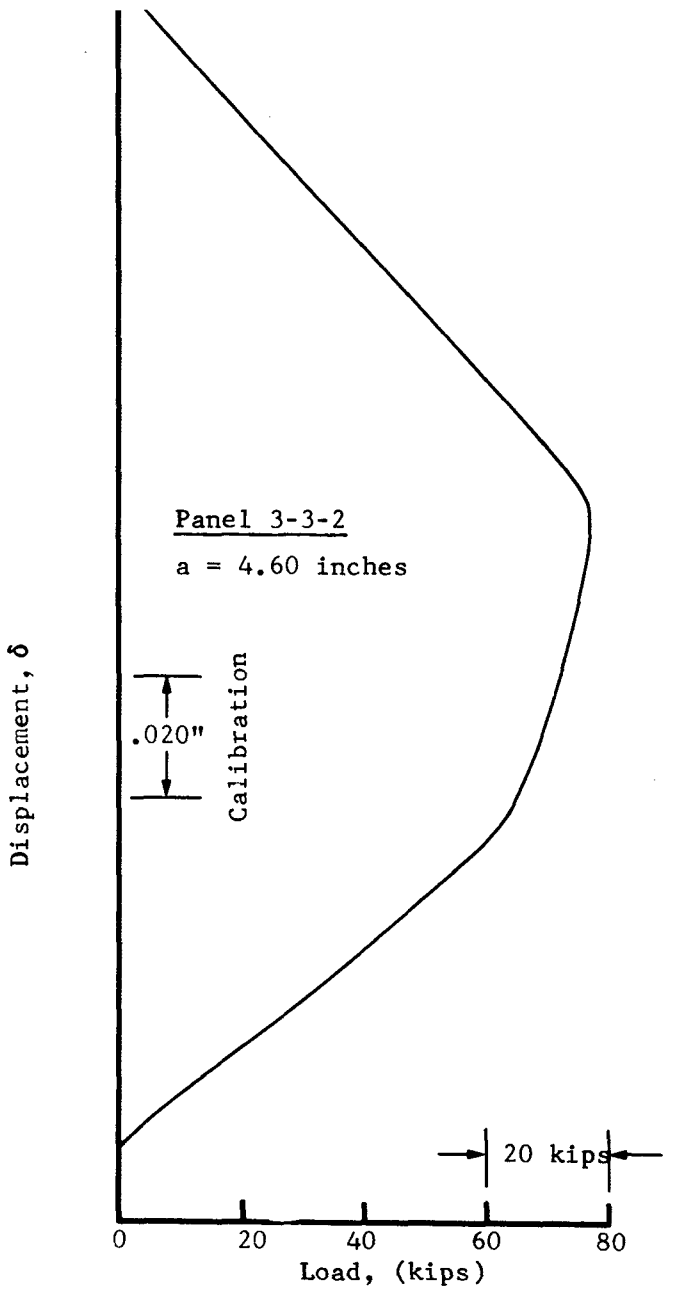

Figure 155. Load-Crack Displacement Curve - Bolted Panel 3-3-2, Panel Centerline

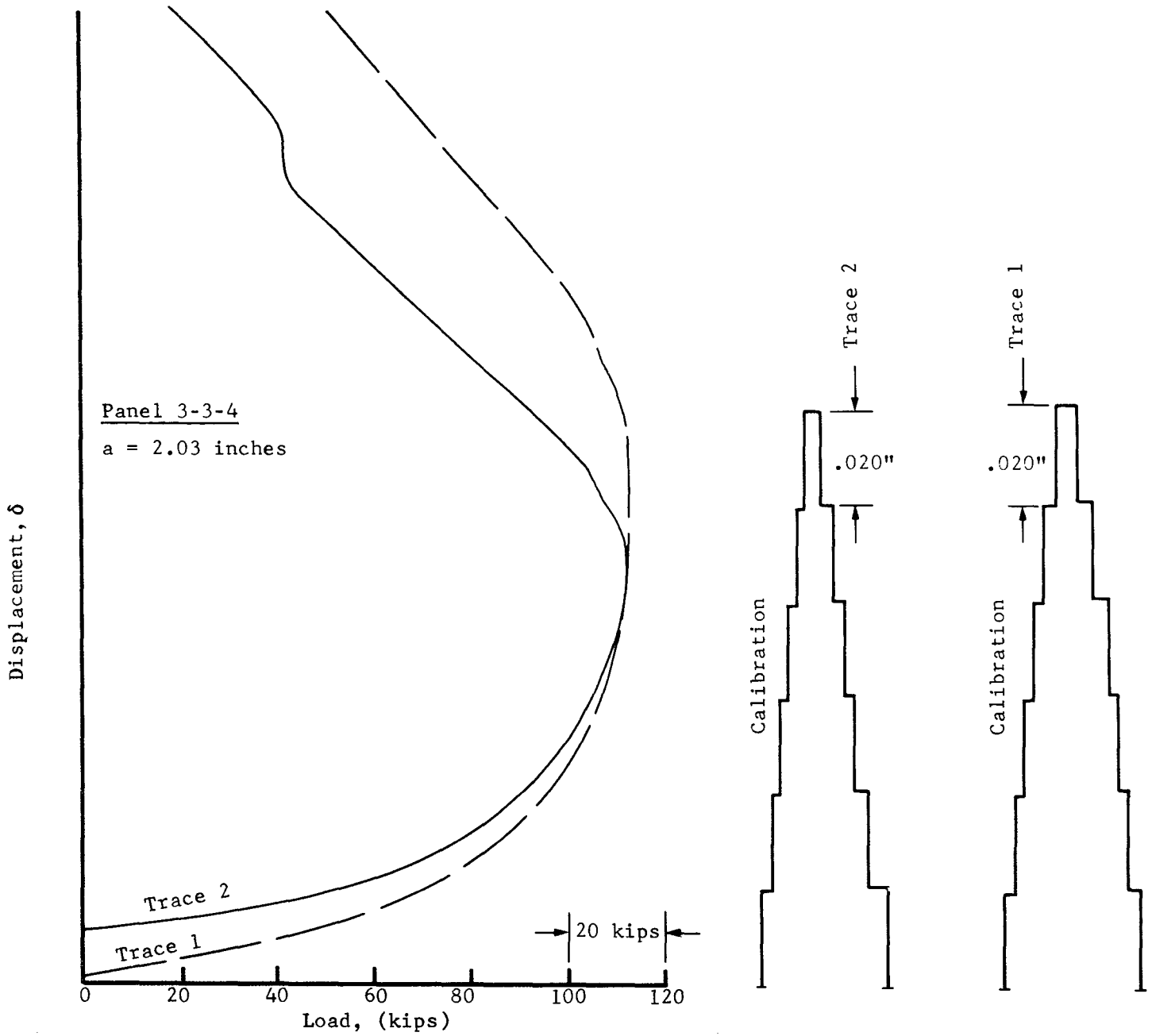

Figure 156. Load-Crack Displacement Curves -- Bonded Panel 3-3-4, 1.8 Inches from Panel Centerline

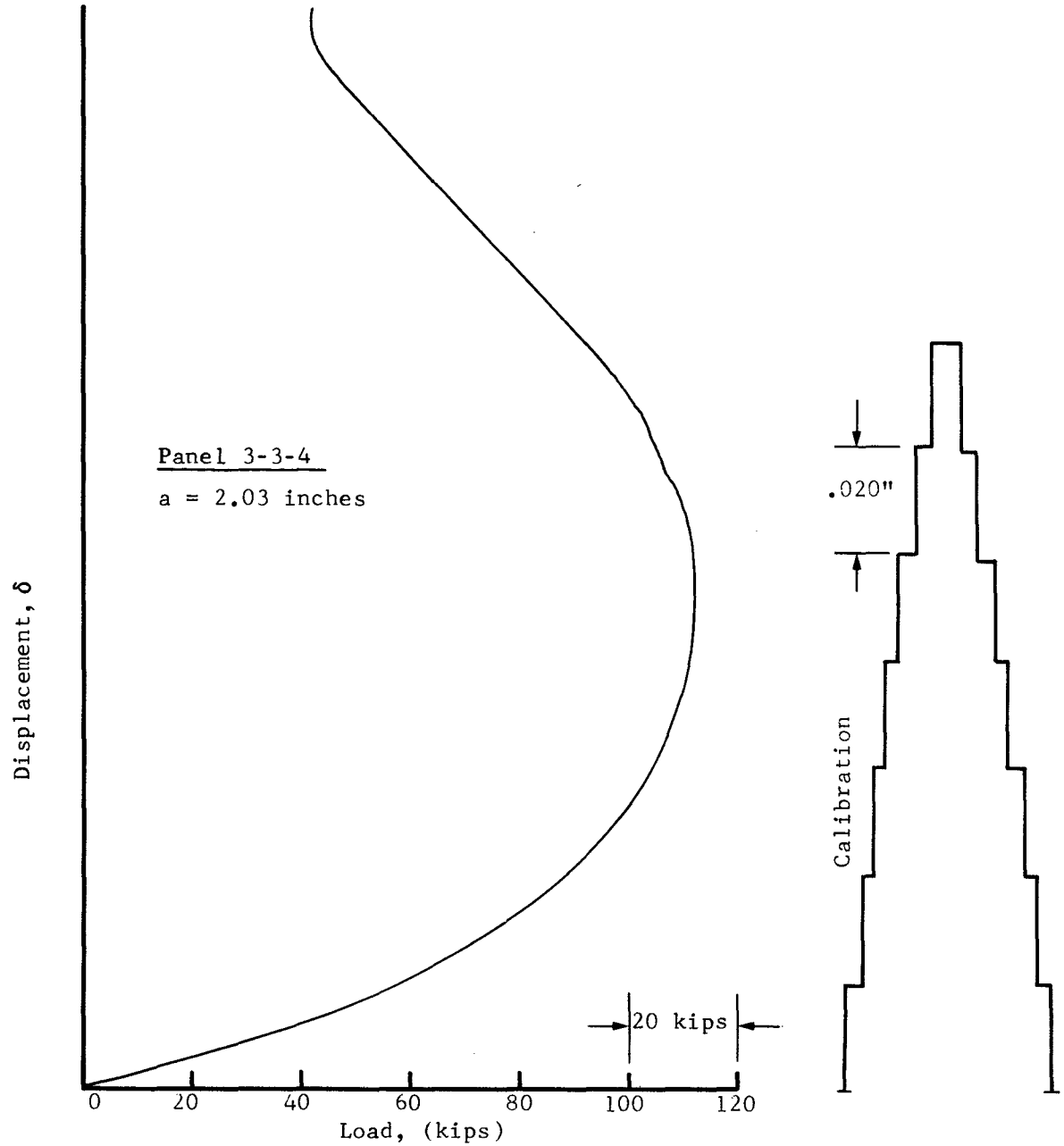

Figure 157. Load-Crack Displacement Curve - Bonded Panel 3-3-4, Panel Centerline

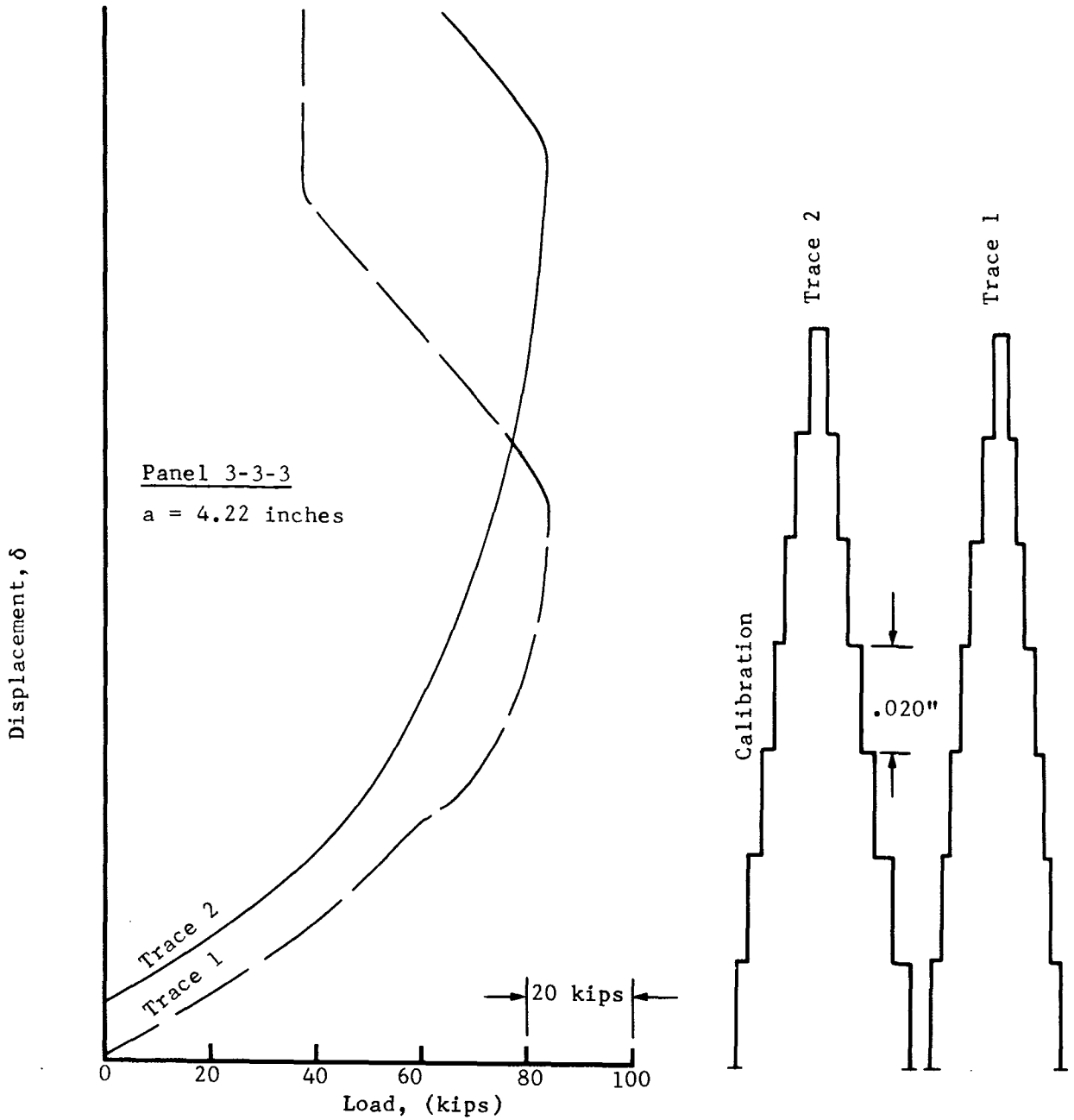

Figure 158. Load-Crack Displacement Curves - Bonded Panel 3-3-3, 1.8 Inches from Panel Centerline

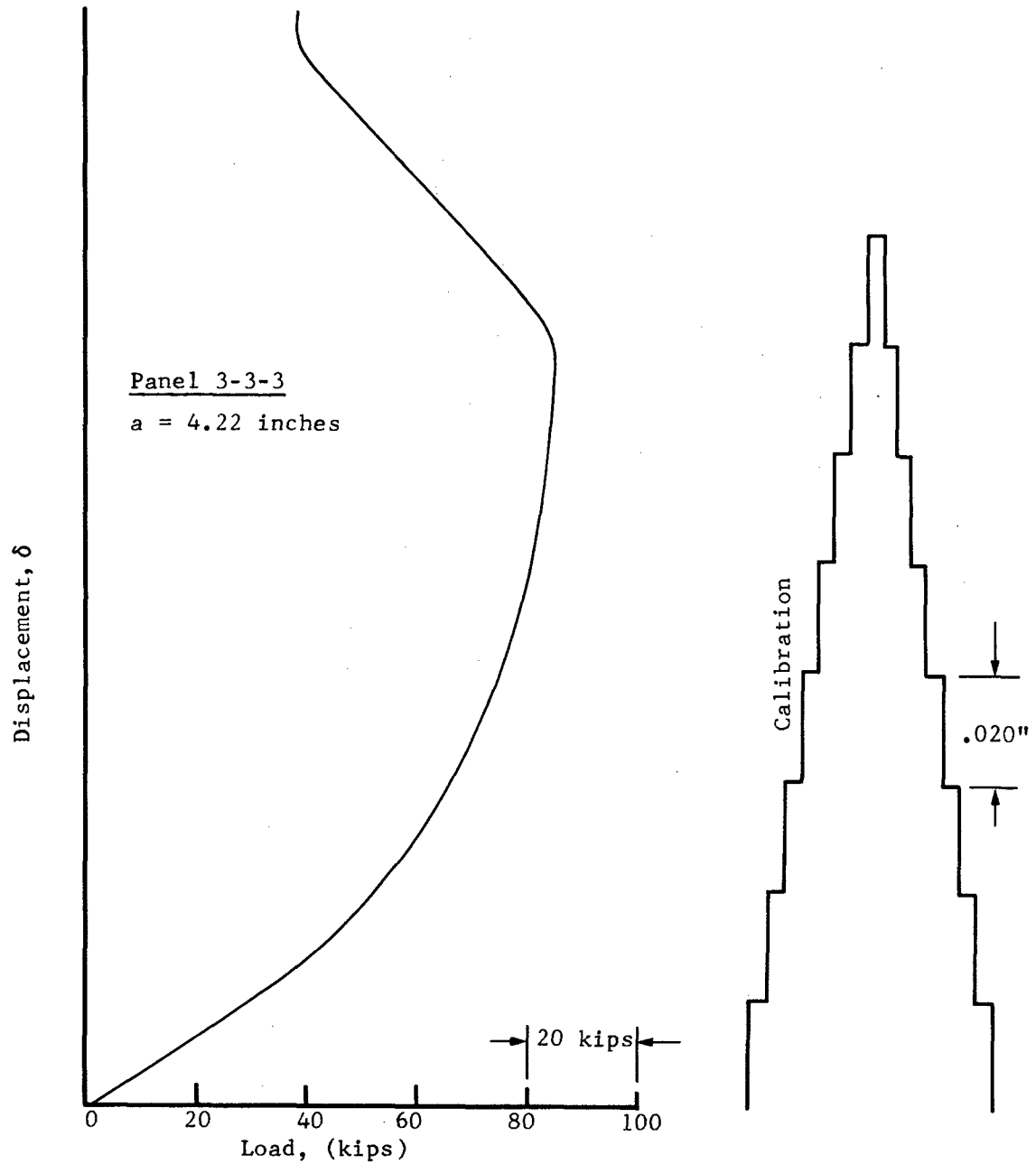

Figure 159. Load-Crack Displacement Curve - Bonded Panel 3-3-3, Panel Centerline

Crack openings were computed for each panel from the linear portions of the load versus displacement curve, at an applied load corresponding to a stress of 15 ksi. These experimental values of crack opening were compared with analytical values obtained from the elastic analysis and are shown in Table XIX. The central crack openings for the bonded panel are smaller than those for a bolted panel. For small crack lengths the correlation between analytical and experimental COD values at the panel centerline is good for all three panel types. However at longer crack lengths experimental values of δ are considerably higher than corresponding analytical values. This increase in δ can best be explained by increased inplane panel bending at longer crack lengths.

7.4.3 Comparison of Strain Data

The comparison of strain data for the central stringer attached flange for the three types of panels is shown in Figures 160 and 161. The strains are plotted as a function of distance from the crack surface (toward the grip end of the panel). For the short crack length, the strains away from the crack surface in both bonded and bolted panels are smaller than the strains in the riveted panel. However, central stringer strain near the crack surface is highest for the bonded panel. The bolted and riveted central stringers have almost identical strains near the crack surface. For an applied load of 40 kips, strains in the bonded panel are considerably higher near the crack surface which indicates that there is large load transfer to the central stringer in the bonded panel. This is primarily due to the continuous bonding of the stringer along the entire width and length of the land unlike the riveted or bolted panel where load transfer is only through the attachment(s). In a bonded stringer there is a steeper decay in strains (Figure 160) away from the crack surface, compared to either the bolted or riveted panel.

For the long crack length (Figure 161) and an applied load of 20 kips the strains in the central stringer of a bolted panel are slightly higher than corresponding strains in a riveted panel (up to 3 inches away from crack surface) caused by the slightly larger crack in the bolted panel. The central stringer strains of the bonded panel are higher than corresponding strains in a riveted panel at an applied load of 20 kips. For applied loads of 30 and 40 kips, attached flange strains of the bonded panel are higher than corresponding strains in either riveted or bolted panels irregardless of the smaller crack length of the bonded panel. From these data it is evident that the strains in the central stringer near the crack surface are similar in riveted and bolted panels; however, the central stringer in a bonded panel shows higher strains. The adhesively bonded flange also shows a faster decay of strains away from the crack surface.

TABLE XIX. COMPARISON OF ANALYTICAL AND EXPERIMENTAL CRACK OPENINGS

(Applied Stress = 15 ksi)

PANEL NO.	HALF CRACK LENGTH a(inches)	TYPE	EXPERIMENTAL	ANALYTICAL	EXPERIMENTAL			ANALYTICAL
			δ CENTRAL (inches)	δ CENTRAL (inches)	δ OUTER GAGE I (inches)	δ OUTER GAGE II (inches)	AVG. δ OUTER GAGES (inches)	δ OUTER GAGE (inches)
3-2-1	2.125	Riveted	.0136	.0118	.0067	.0071	.0069	.0058
3-2-2	4.425	Riveted	.0275	.0181	.0278	.0273	.0275	.0181
3-3-1	2.125	Bolted	.0152	.0128	.0091	.0091	.0091	.0061
3-3-2	4.625	Bolted	.333	.212	.308	.0359	.0334	.0201
3-3-4	--	Bonded	.012	.0095	.0065	.0081	.0073	.0051
3-3-3	4.225	Bonded	.0257	.0138	.0252	.0266	.0259	.0146

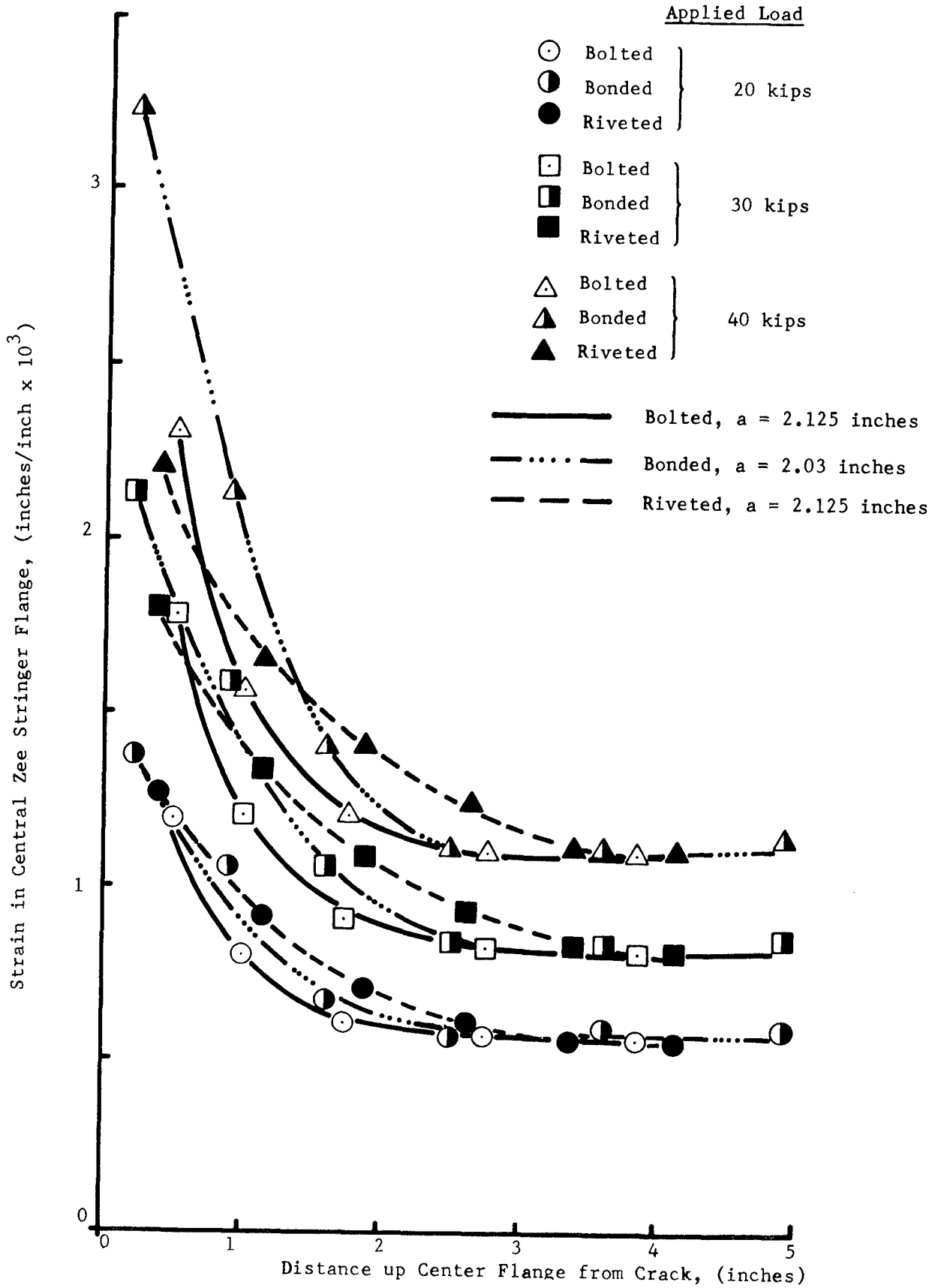

Figure 160. Comparison of Analytical and Experimental Strains in Central Zee Stringer - a ≃ 2.1 Inches

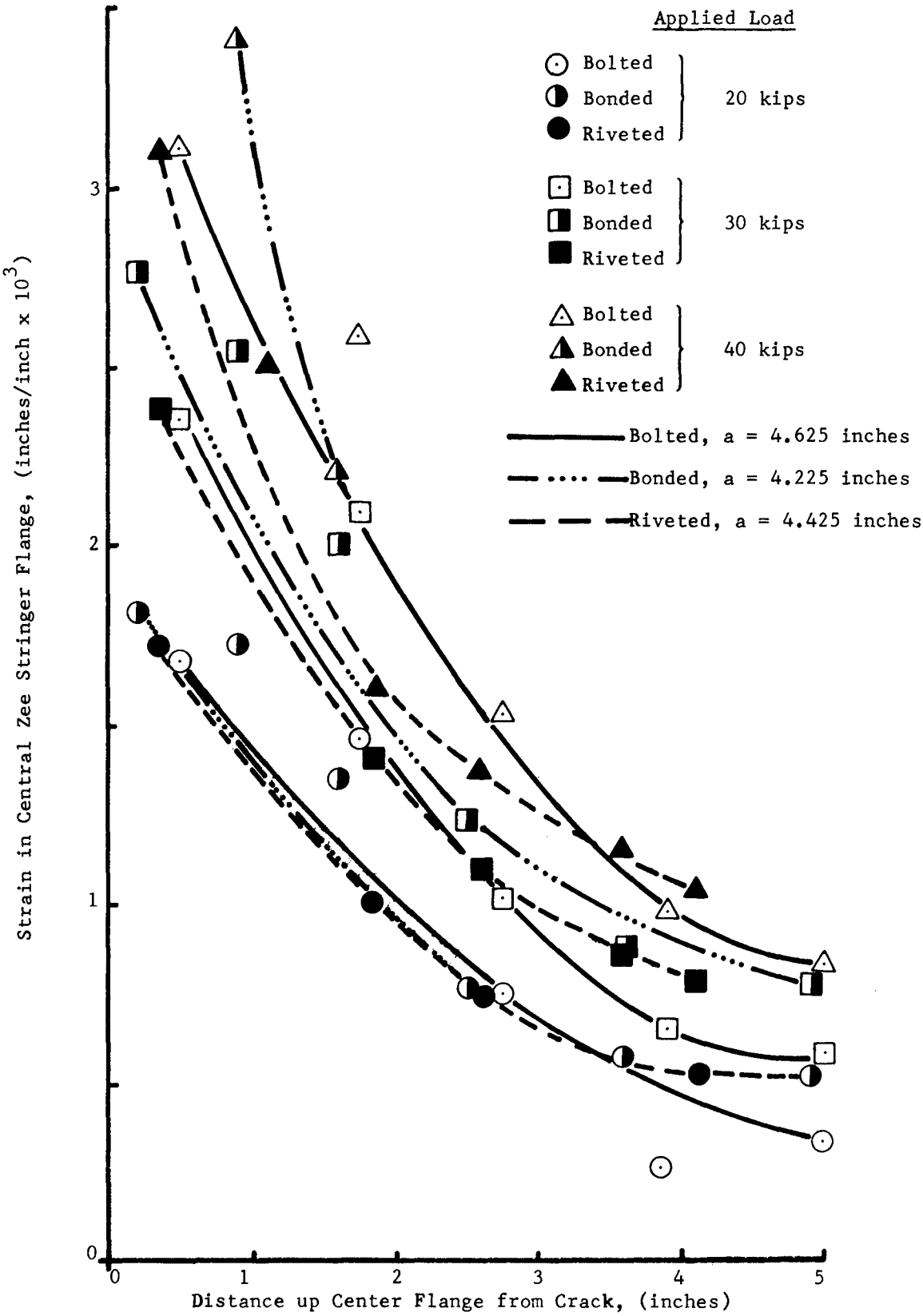

Figure 161. Comparison of Analytical and Experimental Strains in Central Zee Stringer - a $\simeq$ 4.4 Inches

VIII. RESIDUAL STRENGTH PREDICTION

The detailed step by step procedure required to perform a structural residual strength prediction is presented in this Section. Residual strength and slow tear predictions will be made for all zee stiffened panels and compared with experimental results. The application of this procedure to the more complex Phase III test panels will also be outlined.

8.1 PROCEDURE

NOTE: The intent of presenting this residual strength prediction procedure in a brief general outline is to show step by step the required data and analysis. It should not be assumed by reading this step by step procedure that the uninitiated can perform a residual strength prediction. It is strongly recommended that the details of all preceding sections be examined prior to attempting a structural residual strength analysis following these ten procedural steps.

STEP 1. Model the structure for finite element analysis or use an existing finite element model remembering -

a) Two dimensional structural idealization (see Section 3.1)

b) No out-of-plane bending permitted

c) Use proper fastener model, flexible fastener model for riveted or bolted structure (Section 3.1.3) or the shear spring model for bonded structure (Section 7.3.1)

d) Use material property data for skin and substructure of interest (i.e. E, F_{ty} and F_{tu})

e) Select most critical location for crack (normally highest stressed area)

f) Take advantage of structural symmetry.

STEP 2. Select one crack length (2a or a) of interest (based on inspection capability or detailed damage tolerance requirement). Based on this "standard" crack length, five other crack lengths are selected for Dugdale type elastic plastic analysis. These crack lengths should be selected such that crack length to stiffener spacing a/s ratios vary between 0.15 to 1.1 remembering -

a) That the greatest variation is $\sqrt{J}$ values will take place near reinforcements

b) To select at least one crack size shorter than "standard".

STEP 3. With finite element model (from Step 1) and assumed crack lengths (from Step 2) perform analysis assuming Dugdale type plastic zones for each crack size remembering -

a) To select first increment of plastic zone length at 0.2 inches and sufficient successive increments (normally 6) to reach Bueckner-Hayes calculated stresses up to 85 percent of F_{ty} (see Section 3.3.1.1)

b) Make judicious selection of plastic zone increments so as to take advantage of overlapping a_e values (e.g. 3.2, 3.5, 4.2, 5.0 inches for a 3 inch physical crack and 4.2, 4.5, 5.0 inches, etc., for a 4 inch physical crack). If overlapping is done those cases where the crack surfaces are loaded throughout the crack length will be common for two or more physical crack sizes hence the computer programs need be run only once (e.g. 4.2 and 5.0 inches) thus reducing computer run times.

STEP 4. From Step 3 obtain stresses in stiffeners for Dugdale analysis and elastic analysis. Plot stiffener stresses as function of applied stress. (See e.g. Figure 33, Section 3.3.3.2.)

STEP 5. From the crack surface displacement data of Step 3 plot $\sqrt{J}$ (obtained by Bueckner-Hayes approach, see Section 3.3.1.1) versus applied stress to F_{ty} ratio for each crack size. An example is shown in Figures 128 and 129, Section 7.1.3.

STEP 6. From Step 5 cross plot the data in the form of $\sqrt{J}$ versus crack size (a) at specific values of applied stress to F_{ty} ratio (see e.g. Figure 130, Section 7.1.3).

STEP 7. Employing the data of Step 4 and the "standard" crack size determine, gross panel stress to yield strength ratio, p/F_{ty} at ultimate strength (F_{tu}) for the stiffener material - assuming zero slow crack growth. This information will be used subsequently to determine if a skin or stiffener critical case is operative.

STEP 8. Obtain crack growth resistance data for skin material (see Volume II of this report) remembering -

a) To use thickness of interest (i.e. if chem milled 7075-T6 use chem milled 7075-T6 material)

b) Use proper crack orientation LT or TL or off angle to correspond to anticipated structural cracking.

STEP 9. Employing procedure of Section 6.3 plot $\sqrt{J}$ versus Δa_{PHY} curve from the data obtained in Step 8. Several examples are shown in Figures 102 through 119 for various materials, crack orientations and thicknesses.

STEP 10. Determine structural residual strength. On the $\sqrt{J}$ versus crack size (a) plots obtained in Step 6 for the structure, overlay the $\sqrt{J_R}$ versus Δa_{PHY} material plot of Step 9 at the initial crack length of interest. (This procedure is shown in the next subsection.) Determine if -

At the gross panel stress obtained from Step 7 significant slow tear ($\geq$ 0.25 inch) will occur as indicated from the intersection of the $\sqrt{J_R}$ versus $\Delta a_{PHY.}$ curve with the constant p/F_{ty} curve at stringer ultimate strength (see Step 7). Interpolation will probably be necessary between values of constant p/F_{ty}. Then proceed as follows:

- If significant slow tear occurs ($\geq$ 0.25 inches) the structure can be considered to be skin critical (at that particular crack length). Tangency of $\sqrt{J_R}$ versus $\Delta a_{PHY.}$ and $\sqrt{J}$ versus $a_{PHYSICAL}$ at constant applied stress can be used to determine extent of slow tear and residual strength at failure as a percentage of F_{ty}. (Application of this step is given in Section 8.2.)

- If significant slow tear does not occur ($\Delta a_{PHY.} < 0.25$ inch) the structure will normally be stiffener critical. To determine a conservative value of residual strength (for that crack length) use the Dugdale curve of Step 4 and stiffener ultimate strength (see Figure 65, Section 4.4 for an example of a direct application).

The most important factor to consider in residual strength prediction of a cracked structure is to decide whether the structure is skin or stiffener critical. Normally a short crack length is likely to be a skin critical case and a long one a stiffener critical case. However there is no clear cut demarcation between the two cases as factors such as percentage stiffening, spacing of stringers, lands in the structure and other structural details will influence the type of failure. Hence, a good technique is to determine the residual strength of a given structure based on both skin critical and stiffener critical cases. The minimum fracture stress of the two will then represent the residual strength of the structure and should be considered to be the governing case.

8.2 APPLICATION TO PHASE II PANELS

The procedure to be followed for residual strength prediction was outlined in Section 8.1. This procedure was used to predict the residual strength of the zee stiffened panels. The analysis of these panels has been previously discussed in Section VII. The following subsections detail the residual strength prediction of the riveted, bolted, and bonded panels using the analysis of Section VII and the $\sqrt{J_R}$ resistance curves of the material obtained in Section 6.3. The initial physical fatigue crack lengths, areas, load at failure and stresses at failure of all panels are shown in Table XX.

In performing a residual strength prediction for stiffener critical cases, it is necessary to know the ultimate strength of stringers, in this case 2024 extrusions. No material strength data were collected during the course of investigation on these extrusions. Hence, data available in the literature was used in the analysis. Available ultimate strength data for 2024 extrusions varied from 60 ksi to 70 ksi. In the present program values of 65 ksi and 70 ksi are used.

TABLE XX. FAILURE STRESSES OF PHASE II PANELS

Panel Number	Type of Panel	Gross Panel Area (Square Inches)	Half Crack Length, a (Inches)	Load at Failure (kips)	Gross Panel Stress at Failure (ksi)	Net Stress at Failure (ksi)	Predicted Failure Stress (ksi)	Square Root of J @ Failure $\left(\frac{\text{in.-lb.}}{\text{in.}^2}\right)^{\frac{1}{2}}$	Comments
3-2-1	Riveted	2.953	2.15	110	37.25	45.91	40.05	33.2	Skin Critical
3-2-2	Riveted	2.964	4.425	77	25.98	37.92	27.5	25.8	Stringer Critical
3-3-1	Bolted	2.940	2.05	107	36.39	44.72	40.05	32.4	Skin Critical
3-3-2	Bolted	2.915	4.60	77	26.41	39.09	27.0	26.4	Buckled Panel
3-3-4	Bonded	2.903	2.03	122	42.03	51.64	43.8	25.8	Skin Critical
3-3-3	Bonded	2.916	4.22	84.5	28.98	41.62	28.8	34.0	Skin Critical

8.2.1 Residual Strength Prediction of Riveted and Bolted Panels

The two half crack lengths, 2.15 and 4.425 inches, represented the skin critical and stringer critical cases. The stresses in the central (unbroken) stringer for both crack lengths are shown in Figure 162 based on elastic and Dugdale model type analysis. For the 2.15 inch half crack length stresses based on Prandtl-Reuss material behavior are also shown. If there is little or no slow stable crack growth the stringer stresses shown in Figure 162 will be valid up to panel failure. However, if there is significant stable crack growth these stresses will change considerably. For a half crack length of 2.125 inches using an ultimate strength of 65 ksi (for the extruded zee) the Dugdale, elastic, and Prandtl-Reuss material behaviors predict failure at 37.5 ksi, 40 ksi, and 47.5 ksi, respectively. For an assumed extruded zee ultimate stress of 70 ksi the three types of material behaviors predict a failure at 40 ksi, 43 ksi, and 55 ksi, respectively. If there is little or no slow crack growth prior to fracture the failure for the 2.125 inch crack is likely to occur somewhere between stresses of 37.5 to 47.5 ksi for an ultimate stress of 65 ksi and between 40 ksi and 55 ksi for an ultimate stress of 70 ksi. If the actual F_{tu} of the zee material were known it could be used rather than handbook values and naturally result in a better prediction. On the $\sqrt{J}$ versus physical crack length (a) plot of Figure 163, the $\sqrt{J_R}$ resistance curve ($\sqrt{J_R}$ versus Δa_{PHY}) is superimposed at a half crack length of 2.15 inches. At an applied stress of 37.5 ksi (the minimum predicted failure stress) corresponding to a stringer ultimate stress of 65 ksi, (see Figure 162) or $p/F_{ty} = 0.7$ there is considerable stable slow crack growth (about 1.5 inches to point A). Therefore the stresses in the central stringer for a half crack length of 2.15 inches as given by Figure 162 will not be valid at failure due to extensive slow crack growth. Failure in a panel with this crack length will be skin critical. A failure of a skin critical type structure will be given by the point of tangency between $\sqrt{J}$ versus "a" curves for the panel and the $\sqrt{J_R}$ resistance curve of the material. Note that for this panel geometry there are two material resistance curves shown, one for 0.08 inch thickness (curve R_1 taken from data of Figure 112) and the other (curve R_2 taken from Figure 114) for 0.258 inch thickness in the LT direction. With increasing load the crack tip will follow the resistance curve R_1 (since the crack tip is in the chem milled pocket) and a gradual transition will occur to resistance curve R_2 with increasing slow crack extension since the crack is approaching the 0.258 inch thick landed area. The final failure of the panel will be governed by the point of tangency between the resistance curve R_2 and the $\sqrt{J}$ versus 'a' curves. In Figure 163 this point of tangency or instability occurs between curve R_2 and the $\sqrt{J}$ versus "a" curve at $p/F_{ty} = 0.75$ or $p = 40.05$ ksi. The slow tear occurred up to a half crack length of approximately 5.5 inches, i.e., Δa_{PHY} of 3.35 inches. Thus the predicted failure stress of this panel would be 40.05 ksi and the actual failure stress from Table XX (Panel 3-2-1) is 37.25 ksi which shows a 7.5 percent variation. Notice that this residual strength prediction is based on an assumed average in material yield strength of 53,400 psi (average of 0.08 and 0.258 inch thick material in the LT direction) for Dugdale type analysis. The actual skin material yield strength values were obtained from test coupons taken from the skin material after fracture. If the panel had a different yield strength for the skin material, the predicted failure load would be different.

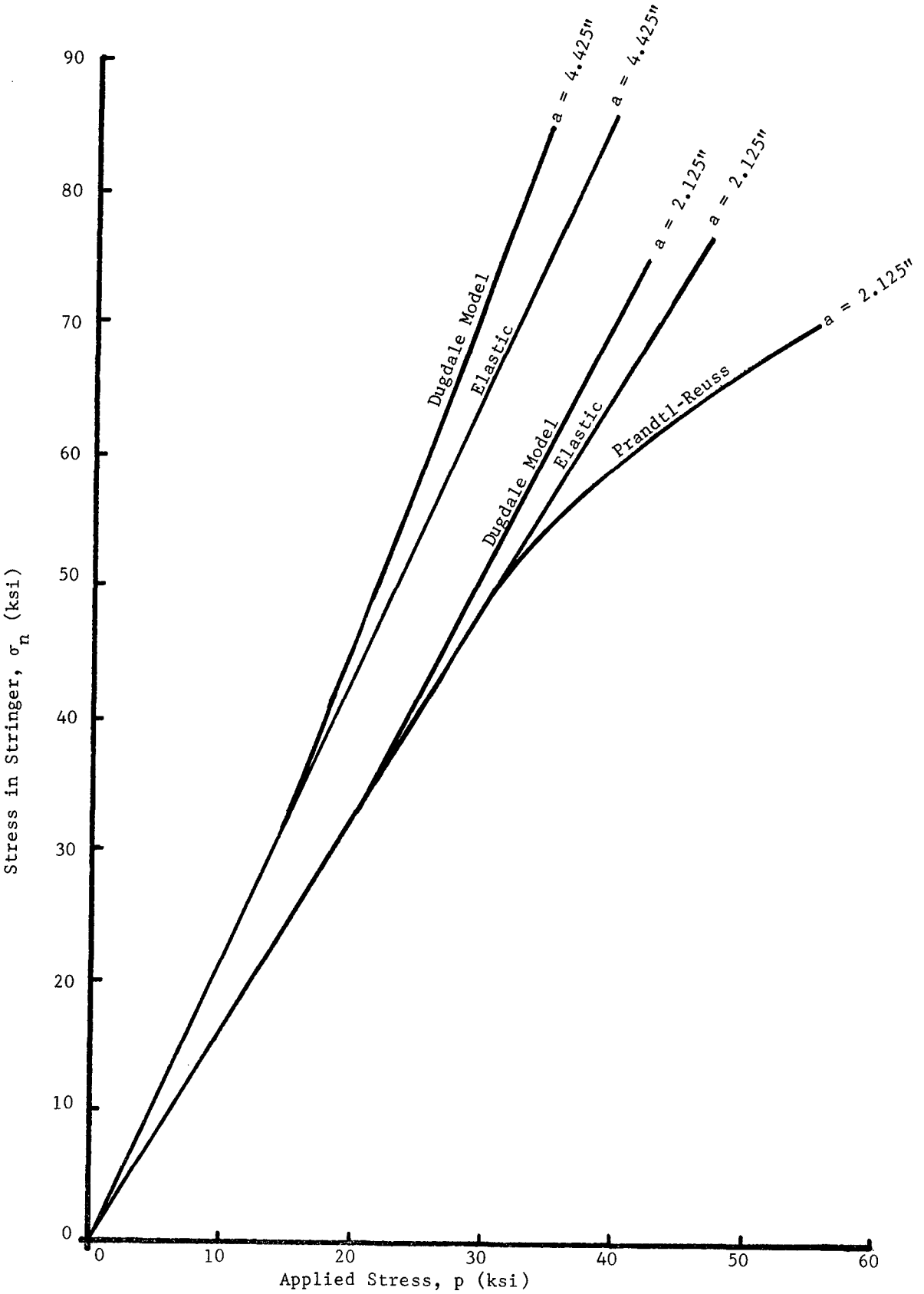

Figure 162. Comparison of Analytical Stress in Central Stringer for Riveted Zee Stiffened Panel - a = 2.125 and 4.425 Inches

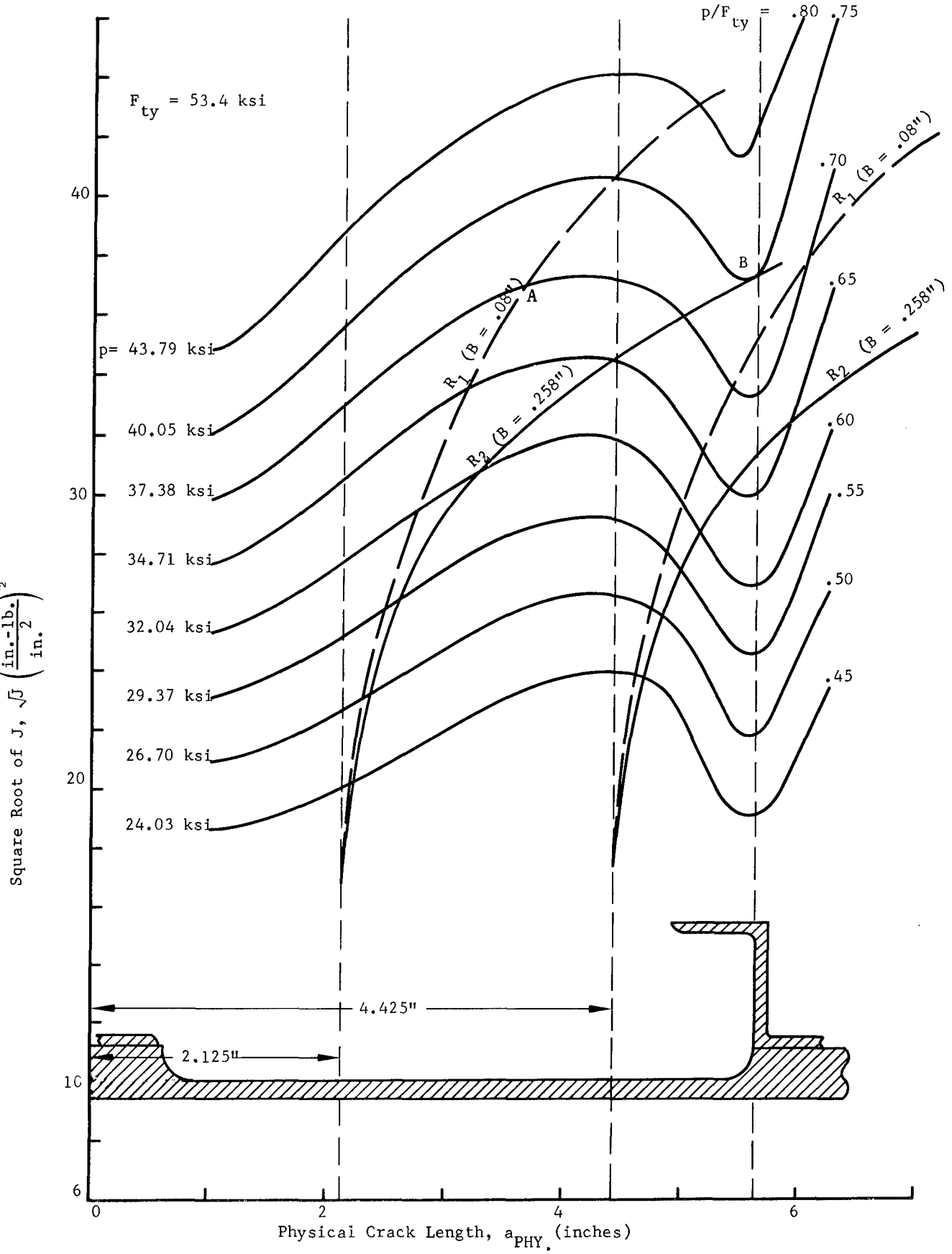

Figure 163. Superposition of $\sqrt{J}$ and $\sqrt{J_R}$ Crack Growth Resistance Curves for Zee Stiffened Panel

If the applied panel stress was less than 75 percent of the yield there would be slow, stable tear as the load increases and there would be no fast fracture. Figure 163 indicates that the point of instability (point B of Figure 163) is reached approximately 0.1 inch before the crack reaches the beginning of the land and before it reaches the centerline of stringer. At this point of instability the $\sqrt{J}$ values for the panel increase rapidly for the same applied load. However the resistance curve of the material drops lower than the crack driving force curve of the panel, hence there is no possibility of the crack arresting at the stringer. However, if the crack driving force curve were lower than the resistance curve, there will be crack arrest in the panel.

Next consider the half crack length of 4.425 inches. For a half crack length of 4.425 inches the Dugdale model analysis (see Figure 162) predicts failure at an applied stress of 27.5 ksi ($p/F_{ty} = 0.515$) and elastic analysis at an applied stress of 30 ksi ($p/F_{ty} = 0.561$). Referring to Figure 163, where the $\sqrt{J_R}$ resistance curve is superimposed at a half crack length of 4.425, it is seen that the resistance curve R_1 at an applied stress ratio of $p/F_{ty} = 0.5$ shows very little slow crack growth (approximately 0.25 inches). Hence, this case will be a stiffener critical case and the stringer stresses given in Figure 162 will be valid as the physical crack length has not changed significantly due to the small amount of slow, stable crack growth. The predicted failure stress of this panel is 27.5 ksi. The fact that this crack length represents a stringer critical case is evident from the strain data obtained for this panel as shown in Figures 134 and 135 of Section 7.1.4. Referring to these Figures it can be seen that the central stringer failed at an applied stress of approximately 24.8 ksi and overall panel failure occurred at a stress of 25.98 ksi (see Table XX). For this crack length the predicted failure stress was based on the ultimate stringer stress of 65 ksi, however, the ultimate stress of the material may vary between 60 ksi and 70 ksi. Any variation of ultimate stress would reflect in a lower failure stress of the panel.

As pointed out in Section 7.2, the finite element model and fastener model used for both riveted and bolted panels were similar, except for pitch. The HI-LOKED (bolted panel) pitch was 1.105 inches and 0.75 inches for the riveted panel. Additionally, it was determined that the analysis for a 2.125 inch half crack length was exactly the same for the two panels. Thus the $\sqrt{J}$ versus crack lengths plots of Figure 163 and stringer stresses shown in Figure 162 are valid for both riveted and bolted panels. The predicted failure load for the bolted panel with a half crack length of 2.125 inches will be 40.05 ksi for a skin critical case. The actual failure load for the panel was 36.39 ksi.

Bolted panel number 3-3-2 had a half crack length of 4.60 inches which is slightly longer than the riveted panel, therefore, the predicted failure load for this panel will be slightly lower. This is also evident from Figure 164 where the $\sqrt{J}$ versus applied stress plots are shown for bolted, riveted, and bonded panels for all tested crack lengths. The $\sqrt{J}$ values for the bolted panel with a half crack length of 4.425 inches are slightly higher than those for a riveted panel with a half crack length of 4.425 inches at the same applied stress. Therefore the failure load for the bolted panel is expected to be slightly lower. Since the two panels had almost the same crack length, the square root of J values will be similar for the two panels at the point of instability. Thus, using the predicted failure stress of 27.5 ksi for a riveted

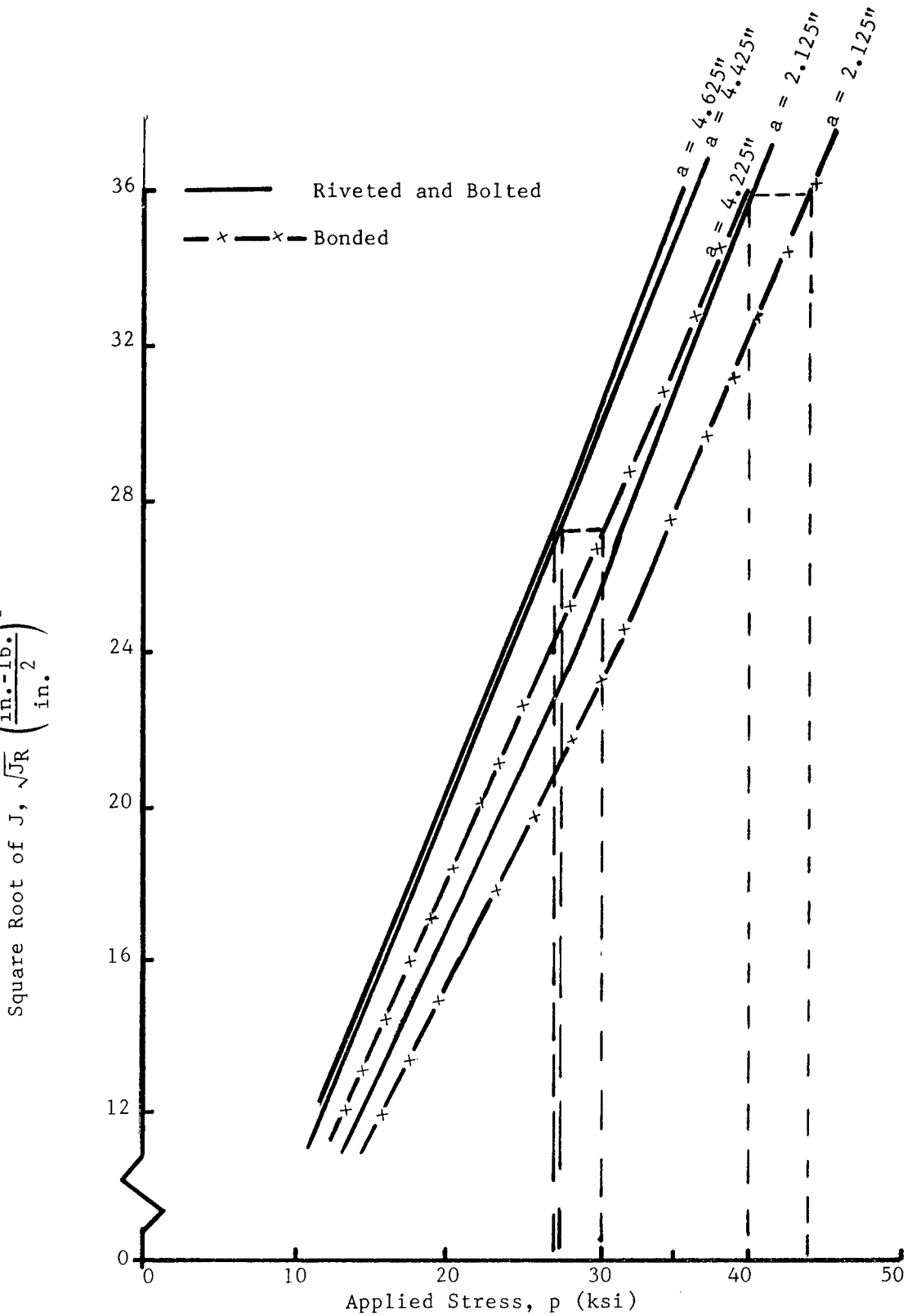

Figure 164. Square Root of J Values for Riveted, Bolted and Bonded Zee Stiffened Panels from Dugdale Model Analysis

panel and assuming that $\sqrt{J}$ values at fracture are the same in both panels the predicted failure stress from Figure 164 is 27 ksi. The actual failure stress of this panel was 26.41 ksi. It must be noted however that this bolted panel was also buckled during the fatiguing process. However, it is believed that the buckling that did occur should not significantly affect the final failure of the panel.

8.2.2 Residual Strength Prediction of Bonded Panel

The stresses in the central stringer of the bonded panel at half crack lengths of 2.125 and 4.225 inches are shown in Figure 165. The predicted failure stresses, corresponding to stringer ultimate strength of 65 ksi, are 38.7, 40 and 44 ksi for Dugdale, elastic and Prandtl-Reuss material behaviors. Predicted stringer failure stresses for a stringer ultimate stress of 70 ksi are 41.3, 43 and 50.5 ksi for the three types of material behaviors. If there were little or no slow stable crack extension the failure will be stringer critical and will occur within these stress ranges. However, as pointed out in the case of riveted and bolted panels (shown in Figure 163) there will be considerable slow crack growth for the shorter crack lengths. The curves of the type shown in Figure 163 have not been obtained for the bonded panel, but from the analytical results of the riveted panel, it can be assumed that the failure in a bonded panel at a half crack length of 2.03 inches will be skin critical. The plot of $\sqrt{J}$ versus applied stress for a half crack length of 2.125 and 4.225 inches for the bonded panel is shown in Figure 164. The tested crack lengths for bonded and riveted panels are similar; therefore, the value of $\sqrt{J}$ at fracture for these two panels would be expected to be similar. Thus using the predicted failure stress of 40.05 ksi for the riveted panel a $\sqrt{J}$ value of 36 is predicted at failure for the riveted panel from Figure 164.

The predicted failure stress for a half crack length of 2.125 inches in the bonded panel at a $\sqrt{J}$ value of 36 $\left(\frac{\text{in.-lb.}}{\text{in.}^2}\right)^{\frac{1}{2}}$ at failure is 43.75 ksi. It is interesting to note that if the actual panel failure stress of 37.25 ksi, for the riveted panel (half crack length of 2.125 inches), is used in Figure 164 to predict failure of the bonded panel, the $\sqrt{J}$ at failure is 33.2 $\left(\frac{\text{in.-lb.}}{\text{in.}^2}\right)^{\frac{1}{2}}$ and the predicted failure stress of the bonded panel is 41.25 ksi (see Table XX or Figure 165). The actual failure stress of the bonded panel was 42.03 ksi. It should be noted that an average skin yield strength of 53.4 ksi was used for all the panels.

For a half crack length of 4.225 inches the bonded stringer failure is anticipated at stresses of 28.8, 30.5 and 32.5 for Dugdale, elastic, and Prandtl-Reuss material behaviors. As mentioned in Section 8.2.1 for a riveted panel the failure of this type of panel should be stringer critical. If the least of these values is taken as the failure stress, the failure is likely to occur at an applied stress of 28.8 ksi. If the actual failure stress of 25.98 ksi (for riveted panel) and the $\sqrt{J}$ versus applied load curves of Figure 164 (bonded panel) are used for failure prediction, the failure stress for the bonded panel is 29 ksi compared to actual failure stress of 28.98 ksi (see Table XX).

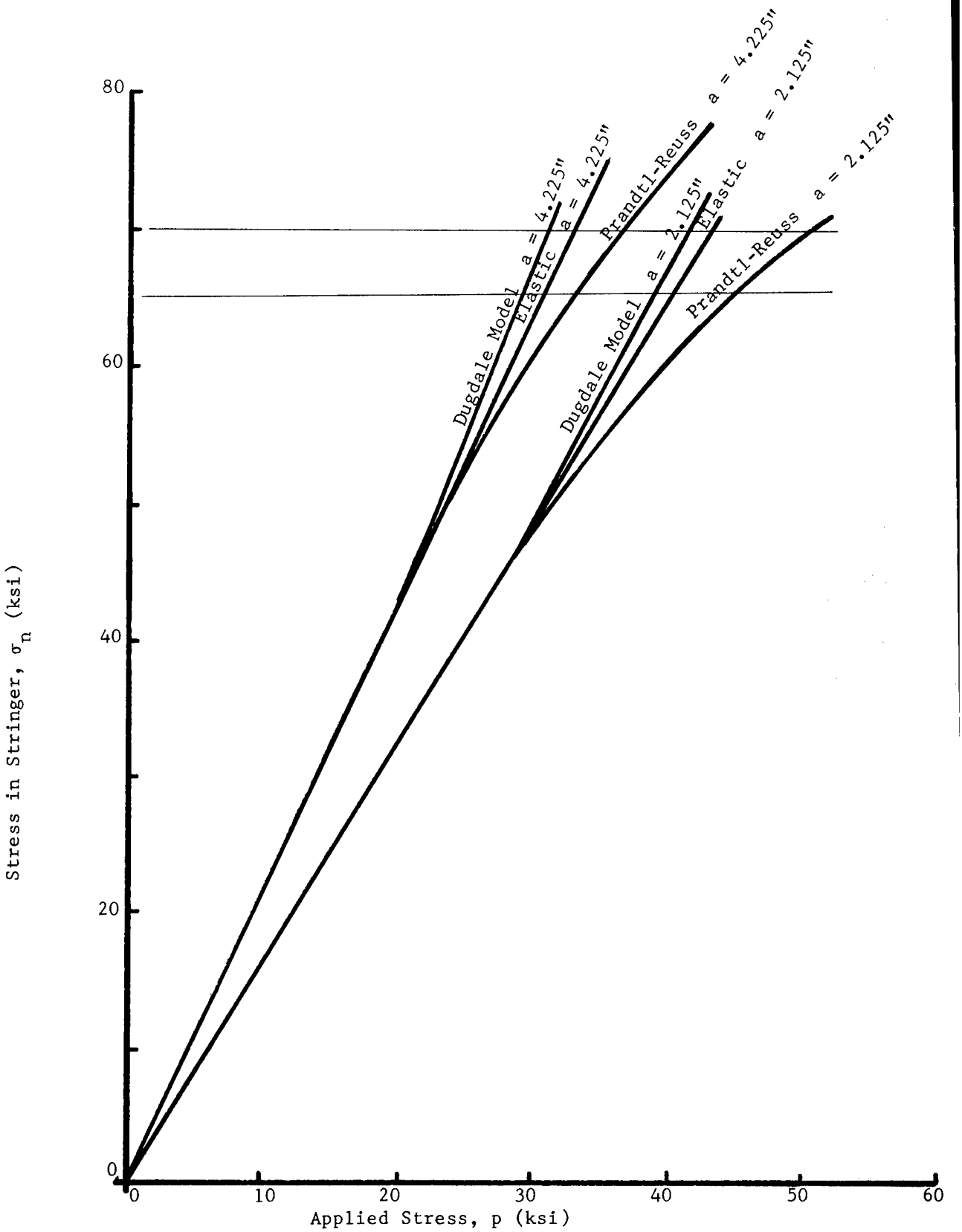

Figure 165. Stress in Central Stringer for Three Material Behavior - Bonded Panel

The fact that this crack length represented a stringer critical case is evident from the strain data of the central stringer (see Figure 143 of Section 7.3.3). From Figure 143 it is seen that the central stringer has undergone extremely high plastic strains prior to failure.

The value of $\sqrt{J}$ corresponding to actual failure stress for each of the panels is shown in Table XX. It is seen that $\sqrt{J}$ value for each of the panels is almost the same at similar crack lengths.

8.2.3 Residual Strength Prediction Based on Elastic Analysis

The residual strength predicted in Sections 8.2.2 and 8.2.3 was based on Dugdale model type elastic-plastic analysis. The residual strength prediction of these zee stiffened panels based on elastic analysis will require the calculations of elastic stress intensity factors for various crack lengths. A plot of stress intensity factors versus physical crack length at various applied loads can then be made similar to the plots of Figure 163. The variation of elastic stress intensity factors (K) with crack length for several applied stress to F_{ty} ratios is shown in Figure 166. Shown are the elastic crack growth resistance, K_R curves obtained from various width CCT (TL) specimens (Reference 57) for a thickness of 0.064 inches (2024-T3) superimposed on half crack lengths of 2.125 inches and 4.425 inches. Also shown on Figure 166 are the elastic-plastic K_R curves for 0.08 and 0.258 inch thickness from Volume II of this report. It is evident from these curves that the instability of the structure will occur at a stress much higher than the material yield strength. The K_R analysis predicts extremely small slow tear even at applied stresses of 82 percent of yield stress at a crack length of 2.125 inches. Thus for skin critical cases, the linear elastic or modified linear elastic analysis will overestimate the residual strength of the structure to an extremely high degree.

For stringer critical cases the elastic analysis for stringer stresses in Figures 162 and 165 can be used. The elastic analysis will predict stringer failure of the riveted panel (half crack length of 4.425 inches) at an applied stress of 30 ksi (assuming stringer ultimate stress of 65 ksi). The measured failure stress of the panel was 25.98 ksi. Similarly for the bonded panel with half crack length of 4.225 inches the data from Figure 165 will predict failure at an applied stress of 32.8 where the actual failure stress was 28.98 ksi. This indicates that even for stringer critical cases, the elastic analysis overestimates the residual strength of the structure. It may be remembered that even for the wing channel panel, which was stringer critical, the elastic analysis overestimated the residual strength of the structure by approximately 3.5 percent. This small overestimate in residual strength for the wing channel panel was due to a very high percentage stiffening of the structure. It is evident from these analyses that an elastic analysis will considerably overestimate the residual strength of a reinforced structure.

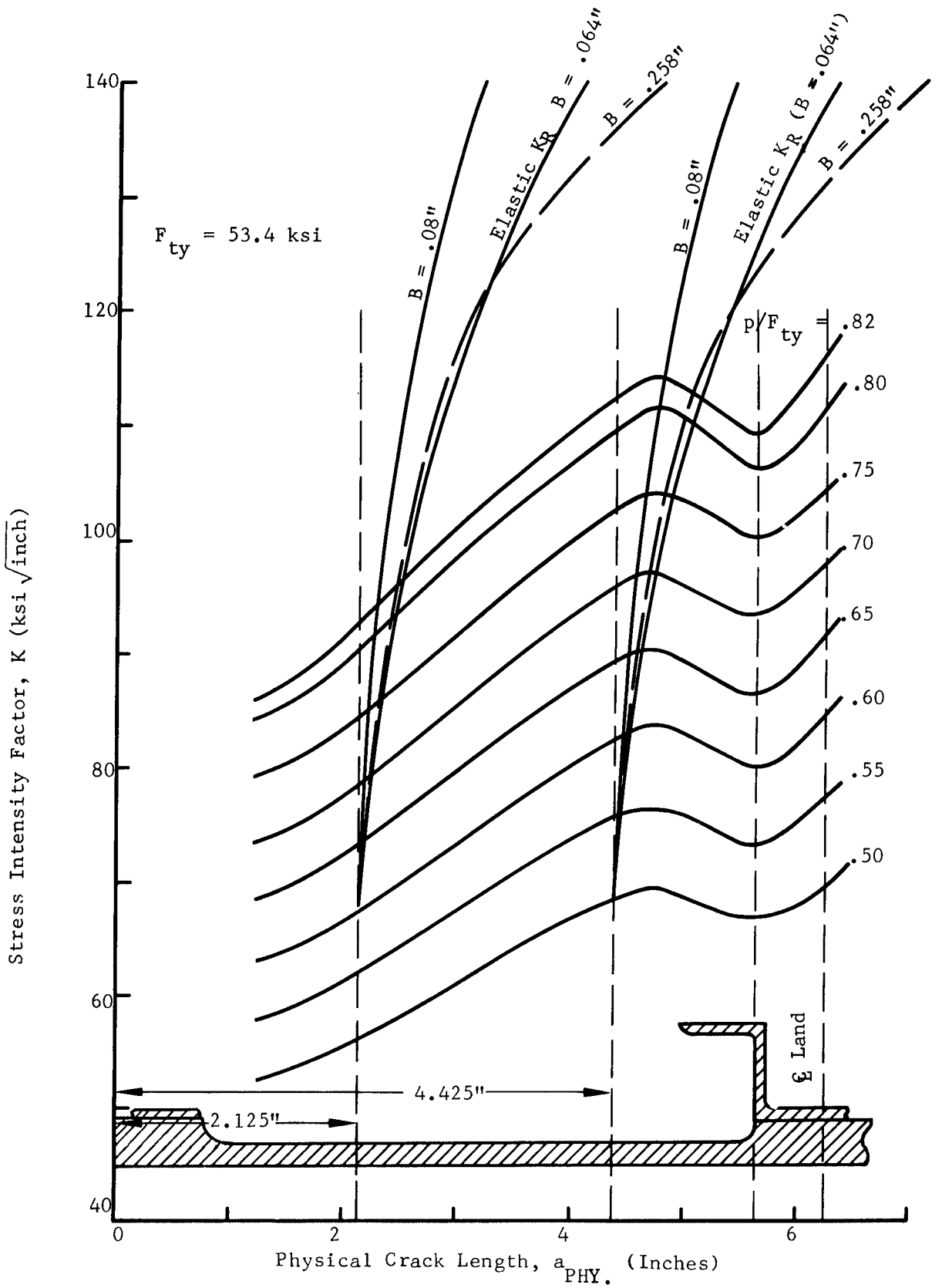

Figure 166. Elastic Stress Intensity and K_R Superposition for Zee Stiffened Panel Geometry

8.3 APPLICATION TO PHASE III PANELS

The analytical procedure presented in this report will be used to analyze the more complex structural panels of Phase III, including an initial broken stiffener case.

Skin materials will be from those materials which have already been characterized during this program Phase. It is anticipated that crack arrest will occur in these panels and predictions will be made of this behavior and residual strength.

Biaxial specimens representative of fuselage structure will also be analyzed and tested. These panels will test the generality of the $\sqrt{J_R}$ failure criterion; indications are that it can be used for this type of loading (see e.g. Section 3.4.2).

The residual strength analysis procedure outlined in Section 8.1 will be modified, if found necessary, by the results obtained during Phase III. Thus the preliminary procedure can then be presented in a general form, applicable to most structural, residual strength problems.

IX. SUMMARY AND CONCLUSIONS

A procedure for residual strength analysis of complex structure has been developed. This procedure has been tested in predicting failure stresses for several complex, riveted, bolted and adhesively bonded structural panels. This new method makes use of the material crack growth resistance curve incorporating both elasto-plastic and slow stable tear in the fracture criterion for skin critical structure. Comparisons were made with assumed Dugdale, Prandtl-Reuss, and elastic material behavior for both skin and stiffener critical structure using a J integral approach. The role of material slow tear has been examined for both linear elastic and elastic-plastic behavior. A comparison has been made which indicates the superiority of the elasto-plastic analysis to the point of stringer failure at ultimate strength.

The importance of finite element modeling of attachment and stiffener has been determined and the use of a flexible fastener model for riveted and bolted structure verified. A shear spring model was demonstrated for use with adhesively bonded stringers with excellent correlation with measured panel failure stress.

Material crack growth resistance curves have been developed using the crack line wedge loaded specimen geometry for two aluminum and titanium alloys and one high strength steel. The data necessary to develop the fracture criterion for both plane stress and mixed mode fracture have been examined and good repeatability of materials fracture data have been obtained. The resulting $\sqrt{J_R}$ resistance curve appears to possess the versatility to be used in predicting residual strength in other than uniaxial tension loading and will be examined further in Phase III.

The studies undertaken during Phase II have resulted in the following conclusions:

1) The $\sqrt{J_R}$ resistance curve of the material combined with a Dugdale type elastic-plastic analysis can predict the residual strength of a stiffened structure for skin critical cases in both plane stress and mixed mode fracture.

2) The elastic-plastic analysis of a cracked, stiffened structure using a Dugdale type plastic zone model can be employed in the residual strength prediction scheme.

3) Elastic-plastic analyses of a cracked stiffened structure based on Dugdale type plastic zone give J integral values which are very close to those which assume Prandtl-Reuss material behavior.

4) For stringer critical cases, Dugdale model type analysis predicts stringer failure within 5 percent of the actual failure load or within the anticipated materials fracture data scatter.

5) The J integral is path independent for cracked, stiffened structure, whether or not the path is taken across the stringer. At high applied loads (when the stringer yields) care is required in calculating J to show the path independence.

6) The finite element method of structural analysis can be successfully used as an analytical tool in residual strength prediction.

7) Fastener flexibility has considerable influence on the elastic stress intensity factors in a built-up structure and the residual strength predictions of a stiffened structure are influenced by the assumed flexibility of the fastener.

8) A flexible fastener model gives more realistic analytical values of crack openings in a stiffened structure.

9) For identical structural geometries the structure using adhesive bonding has a higher residual strength than either riveted or bolted structure.

10) Determination of a skin or stiffener critical fracture situation can be made using the developed residual strength procedure.

11) For stiffened panels a good correlation is obtained between Dugdale type plastic zone size and plastic zones given by Prandtl-Reuss behavior (assuming that the size of plastic zone is given by the number of elements ahead of the crack tip reaching yield stress corresponding to 0.2 percent permanent strain). However, for crack line wedge loaded (CLWL) specimens the plastic zone size given by Prandtl-Reuss behavior is considerably smaller than that given by Dugdale behavior.

12) For stringer critical cases an elastic analysis will overestimate the failure load of a cracked structure.

13) Residual strength predictions for a cracked structure based on elastic analysis considerably overestimate the residual strength of the structure for skin critical cases. Thus a K_c approach to residual strength prediction of structure appears to be of doubtful value.

14) Use of a finite element method of residual strength analysis is not recommended for use in parametric studies since the computer time involved is excessive.

15) The crack line wedge loaded specimen geometry can be used to obtain $\sqrt{J_R}$ crack growth resistance curves. However for material with preferred rolling the LT crack orientation data will be difficult to obtain and alternate specimens should be considered.

16) The finite element analysis of a crack line wedge loaded specimen requires a careful consideration of method of load application and displacement constraints provided to the loaded points.

17) The specimen independency of the crack growth resistance curve has been shown for two specimen geometries and loading conditions.

18) Slow stable crack growth in thin sections appears to occur at very low values of stress intensity or at values approaching K_{Ic}.

REFERENCES

1. Verette, R. M. and Wilhem, D. P., "Development & Evaluation of Methods of Plane Stress Fracture Analysis, Review and Evaluation of Structural Residual Strength Prediction Techniques", AFFDL-TR-73-42, May 1973.

2. Vlieger, H. and Broek, D., "Residual Strength of Built-up Sheet Structures", National Aerospace Laboratory, NLR MP 72029U, The Netherlands, Sept. 1972.

3. Kuhn, P., "Residual Strength in the Presence of Fatigue Cracks", Paper presented to AGARD, Structures and Materials Panel, 1967. (Also NASA-unpublished report), pp. 25.

4. Bloom, J. M., "The Effect of a Riveted Stringer on the Stress in a Sheet with a Crack or a Cutout", Office of Naval Research Report No. 20, June 1964 (AD603693).

5. Poe, Jr. C. C., "The Effect of Riveted and Uniformly Spaced Stringers on the Stress Intensity Factor of a Cracked Sheet", in Proceedings of Air Force Conference on Fatigue and Fracture of Aircraft Structures and Materials, AFFDL-TR-70-144, December 1969, pp. 207-215.

6. Swift, T., "Development of the Fail-Safe Features of the DC-10", Damage Tolerance in Aircraft Structures, American Society for Testing and Materials STP 486, 1971, pp. 164-214.

7. ASTM-STP 527, "Symposium on Fracture Toughness Evaluation by R-Curve Method", D. E. McCabe (Editor), American Society for Testing and Materials, 1973.

8. Rice, J. R., "A Path Independent Integral and the Approximate Analysis of Strain Concentration by Notches and Cracks", Journal of Applied Mechanics, Trans. ASME, June 1968, pp. 379-386.

9. Wilhem, D. P., "An Improved Technique for Residual Strength Prediction - A Modified Crack Growth Resistance Approach", Proceedings of an International Conference on Prospects of Fracture Mechanics, Delft University of Technology, The Netherlands, G. C. Sih, H. C. vanElst, and D. Broek, editors, June 1974, pp. 389-404.

10. Griffis, C. A. and Yoder, G. R., "Application of the J Integral to Crack Initiation in a 2024-T351 Aluminum Alloy", Naval Research Lab Report 7676, April 1974.

11. Vlieger, H., "Residual Strength of Cracked Stiffened Panels", National Aerospace Laboratory, NLR-TR 7100U, The Netherlands, January 1971.

12. Creager, M. and Liu, A. F., "The Effect of Reinforcements on the Slow Stable Tear and Catastrophic Failure of Thin Metal Sheet", AIAA Paper No. 71-113, January 1971.

13. Wells, A. A., "The Status of COD in Fracture Mechanics", Proceedings of Canadian National Congress on Applied Mechanics, Calgary, Alberta, May 1971, pp. 59-77.

14. Sih, G. C., "A Special Theory of Crack Propagation", Methods of Analysis and Solutions to Crack Problems, edited by G.C. Sih, Walters-Noordhoff Publishing 1972, pp. xxi-xlv.

15. Begley, J. A. and Landes, J. D., "The J Integral as Fracture Criterion", Fracture Toughness, Proceedings of the 1971 National Symposium on Fracture Mechanics, Part II, American Society for Testing and Materials STP 514, 1972, pp. 1-20.

16. Swift, T., "The Effects of Fastener Flexibility and Stiffener Geometry on the Stress Intensity in Stiffened Cracked Sheet", Proceedings of an International Conference on Prospects of Fracture Mechanics, Delft University of Technology, The Netherlands, G. C. Sih, H. C. vanElst and D. Broek, editors, June 1974, pp. 389-404.

17. Dugdale, D. S., "Yielding of Steel Sheets Containing Slits", Journal of Mechanics and Physics of Solids 1960, Vol. 8, pp. 100 to 104.

18. Hayes, D. J. and Williams, J. G., "A Practical Method for Determining Dugdale Model Solutions for Cracked Bodies of Arbitrary Shape", International Journal of Fracture Mechanics, Vol. 8, No. 3, 1972, pp. 239-256.

19. Isida, M. and Itagaki, Y., "Stress Concentration of the Tip of the Central Transverse Crack in a Stiffened Plate Subjected to Tension", Proceedings of the Fourth U.S. National Congress of Applied Mechanics, Vol. 2, 1962.

20. Sullivan, A. M. and Freed, C. N., "The Influence of Geometric Variables on K_c Values for Two Thin Sheet Aluminum Alloys", NRL Report 7270, June 1971.

21. Feddersen, C. E., "Evaluation and Prediction of the Residual Strength of Center Cracked Tension Panels", American Society for Testing and Materials STP 486, 1971, pp. 50-78.

22. Krafft, J. M., et al, "Effect of Dimensions on Fast Fracture Instability of Notched Sheets", in Proceedings of Crack Propagation Symposium, College of Aeronautics, Vol. 1, Cranfield England, 1961.

23. Hutchinson, J. W., "Singular Behavior at the End of a Tensile Crack in a Hardening Material", J. Mech and Physics of Solids, Vol. 16, 1968, pp. 13-31.

24. Hilton, P. D. and Hutchinson, J. W., "Plastic Stress Intensity Factors for Cracked Plates", Engineering Fracture Mechanics, Vol. 3, 1971, pp. 435-457

25. Irwin, G. R., "Basic Aspects of Crack Growth and Fracture", NRL Report 6598, 1968.

26. McClintock, F. A. and Irwin, G. R., "Plasticity Aspects of Fracture Mechanics", Fracture Toughness Testing and Its Applications, American Society for Testing and Materials STP 381, June 1964, pp. 84-113.

27. Hilton, P. D., "Plastic Intensity Factors for Cracked Plates Subjected to Biaxial Loading", International Journal of Fracture, Vol. 9, No. 2, June 1973, pp. 149-156.

28. Wells, A. A., "Application of Fracture Mechanics at and Beyond General Yielding", British Journal of Welding, November 1963, pp. 563-570.

29. Barenblatt, G. I., "Formation of Equilibrium Cracks During Brittle Fracture, General Ideas and Hypothesis, Axially Symmetric Cracks", 23, 1959.

30. Barenblatt, G. I., "On Some General Concepts of the Mathematical Theory of Brittle Fracture", PMM 28, 1964.

31. Goodier, J. N., "Mathematical Theory of Equilibrium Cracks", Fracture, An Advance Treatise, II, Editor Liebowitz, Academic Press, 1968.

32. Adams, N. J. I. and Munro, H. G., "A Single Test Method for Evaluation of the J Integral as a Fracture Parameter", Engineering Fracture Mechanics, Vol. 6, 1974, pp. 119-132.

33. Yoder, G. R., et al, "J Integral and the Initiation of Crack Extension in a Titanium Alloy", Naval Research Laboratory (AD 776 212), Feb. 1974.

34. Hayes, D. J., "Some Applications of Elastic-Plastic Analysis to Fracture Mechanics", PhD Thesis, Department of Mechanical Engineering, Imperial College, University of London, October 1970.

35. Wilson, W. K. and Thompson, D. G., "On the Finite Element Method for Calculating Stress Intensity Factors for Cracked Plates in Bending", Engineering Fracture Mechanics, Vol. 3, 1971, pp. 97-102.

36. Swift, T. and Wang, D. Y., "Damage Tolerant Design - Analysis Methods and Test Verification of Fuselage Structure", AFFDL-TR-70-144, Proceedings of Air Force Conference on Fatigue and Fracture of Aircraft Structures and Materials, December 1969, pp. 653-683.

37. Prager, W. and Hodge, P. G., Jr., "Theory of Perfectly Plastic Solids", Dover Publications Inc., New York, 1968.

38. Hayes, D. J., Private Communication, July 1973.

39. Kibler, J. J., "Cylindrical and Spherical Shells with Cracks", PhD Thesis, Lehigh University, 1969.

40. Erdogan, F. and Sih, G. C., "On the Crack Extension in Plates under Plane Loading and Transverse Shear", Journal of Basic Engineering, Transactions of ASME, December 1963, pp. 519-527.

41. Forman, R. G., "Experimental Program to Determine Effect of Crack Buckling and Specimen Dimensions on Fracture Toughness of Thin Sheet Materials", AFFDL-TR-65-146, January 1966.

42. Carlson, R. L., et al, "Buckling in Thin Cracked Sheets", Proceedings of the Air Force Conference on Fatigue of Aircraft Structures and Materials, AFFDL-TR-70-144, 1969, pp. 193-205.

43. Zielsdorff, G. F. and Carlson, R. L., "On the Buckling of Thin Tensioned Sheets with Cracks and Slots", Engineering Fracture Mechanics, Vol. 4, 1972, pp. 939-950.

44. Bucci, R. J., et al, "J Integral Estimation Procedures", Fracture Toughness, Proceedings of the 1971 National Symposium on Fracture Mechanics, Part II, American Society for Testing and Materials STP 514, 1972, pp. 40-69.

45. Irwin, G. R., et al, "Flat-Plate Testing of Part-Through Cracks in Line-Pipe Steel Plates", Lehigh University, Fritz Engineering Laboratory Report No. 373.1, March 1972.

46. Irwin, G. R. and Kies, J. A., "Critical Energy Rate Analysis of Fracture Strength", Welding Journal-Research Supplement, Vol. XIX, No. 4, April 1954.

47. Freed, C. N., et al, "Crack Growth Resistance Characteristics of High-Strength Sheet Alloys", Naval Research Laboratory Report 7374, January 1972.

48. Broek, D., "Artificial Slow Crack Growth Under Constant Stress the R-Curve Concept in Plane Stress", Engineering Fracture Mechanics, Vol. 5, 1973, pp. 45-53.

49. Heyer, R. H. and McCabe, D. E., "Crack Growth Resistance in Plane-Stress Fracture Testing", Engineering Fracture Mechanics, Vol. 4, 1972, pp. 413-430.

50. Judy, Jr., R. W., and Goode, R. J., "R-Curve Characterization and Analysis of Fractures in High-Strength Structural Metals", Metals Engineering Quarterly, November 1973, pp. 27-35.

51. Bradshaw, F. J., et al, "The Effect of Section Thickness on the Crack Resistance of Aluminum Alloy L93, with Measurement of Plastic Strain", Royal Aircraft Establishment Technical Report 72039, March 1972.

52. Wheeler, C., et al, "Some Crack Resistance Curves of Sheet Compact Tension Specimens of Aluminum Alloys 7475-T761, 2024-T3 and 2024-T81", Royal Aircraft Establishment Technical Report 74086, September 1974.

53. Kendall, D. P., "Crack Growth Resistance in Laminated, Glass-Epoxy Sheet", Journal of Materials, JMLSA, Vol. 7, No. 3, September 1972, pp. 430-434.

54. Proposed Recommended Practice for R-Curved Determination, 1974 Annual Book of ASTM Standards, Part 10 (Published for Information only, Nov. 1974).

55. Irwin, G. R., "Fracture Testing of High-Strength Sheet Materials Under Conditions Appropriate for Stress Analysis", NRL Report 5486, July 1960.

56. Kobayashi, A. S., et al, "Application of Finite Element Analysis Method to Two-Dimensional Problems in Fracture Mechanics", ASME Paper, 69-WA/PVP-12, 1969.

57. Wang, D. Y., "Plane Stress Fracture Toughness and Fatigue Crack Propagation of Aluminum Alloy Wide Panels," paper presented to Sixth National Symposium of Fracture Mechanics, Philadelphia, Pa.; also Douglas Aircraft Paper 6054, 28-30 August 1972.

☆U.S.Government Printing Office: 1977 — 757-001/99